CRANFIELD UNIVERSITY

C S PLACE

MODELLING OF MULTIPLE FAILURE MECHANISMS FOR SYSTEM RELIABILITY PREDICTION

SCHOOL OF INDUSTRIAL AND MANUFACTURING SCIENCE

PhD THESIS

CRANFIELD UNIVERSITY

SCHOOL OF INDUSTRIAL AND MANUFACTURING SCIENCE

PhD THESIS

Academic Year 2001 - 2002

C S PLACE

Modelling Of Multiple Failure Mechanisms For System Reliability Prediction

Supervisors: J E Strutt
P E Irving

January 2002

This thesis is submitted in fulfilment of the requirements for the degree of Doctor of Philosophy

Abstract

Helicopters are highly dependent on their transmission systems, which provide the vital links from the engines to the rotor and ancillary systems. Components are highly loaded and must be manufactured to a high degree of accuracy; the lack of redundancy implies that this is a 'series-chain' system. Existing techniques for calculating expected life are based upon historical data from different gearbox and helicopter types, thus limiting the confidence of the results. Design techniques may be conservative in some areas, whilst neglecting to consider different load patterns, usage, maintenance and environmental factors.

This work describes the development of probabilistic models that represent damage accumulated by fatigue, wear and corrosion of the key components with an Intermediate gearbox (IGB). The parameters of these models represent geometrical, load and material data at the design stage, and produce an output in terms of failure probability against operating hours. This allows the influential parameters to be identified before building a prototype helicopter gearbox.

The results from these models are then used to predict the upper and lower bounds of system reliability. This enables the combination of diverse failure mechanisms to be viewed to determine the relevant significance of each failure mechanisms. The effectiveness of the gearbox monitoring systems has been incorporated in the computer model by considering the probability of detection (POD) of each failure mechanism.

The work to develop models found that there is a large body of work available to describe damage accumulation due to fatigue, but far less in regard to wear and corrosion. Fatigue models are very sensitive to load and material variability, particularly tooth root bending fatigue, for which many loads are considered 'non-damaging'. Wear models are mostly affected by changes in material hardness, wear coefficient and slip amplitude; changes in load are less influential on the predicted time to failure. The results for galvanic corrosion are dominated by the corrosion rate and time to initiate. In the system reliability model, reducing gear load appears to be the simplest means to increase life; increases in material strength and reduction in material variability are less achievable without significant improvements in manufacture and/or material technology.

Acknowledgements

I wish to express my gratitude to my supervisors, John Strutt and Phil Irving, who inspired me to undertake this work and gave generously of their time and assistance.

I am also very grateful to the Research Council, EPSRC, and the Industrial sponsors of the research program upon which much of this work is based. Special thanks are due to:

Mike Stuckey and Dave Lumbard - Agusta Westland (Yeovil)
Vittorio Vaccaro and Santo Allotta - Agusta Westland (Milan)
Alan Draper - Defence Procurement Agency (MOD Abbeywood)
John Bristow and John McColl - Civil Aviation Authority

I would like to acknowledge the significant support in model and software development received from Keith Allsopp, Christophe Trille, Mark Strathern and Peter Hall.

The following have also created an excellent working environment for me at Cranfield: Daren Warburton, Jonathan Morris, Gerrie Mullen and Giancarlo Bussu.

Thanks are especially due to my parents, John and Eileen, and extended family - the Bedfords and Brays, for their constant encouragement and support. Finally I would like to record my enormous thanks to my wife and daughter, Judy and Hannah. I would not have been able to complete this work without their support for this PhD, especially through this very difficult year.

This thesis is dedicated to my wonderful wife and daughter,
Judy and Hannah

"The fear of the Lord is the beginning of wisdom,
and knowledge of the Holy One is understanding."
[Proverbs 9 v10]

CONTENTS

Table of Figures

Acronyms

AAIB	Air Accident Investigation Branch
AEW	Airborne Early Warning
AGMA	American Gear Manufacturers Association
ASW	Anti-Submarine Warfare
AZ	Azimuth (angle to wind)
BER	Beyond economic repair
BS	British Standard
CAA	Civil Aviation Authority
CD	(Magnetic) Chip detector
COV	Coefficient of Variation
DAR	Damage Accumulation Rate
DARA	Defence Aircraft Repair Agency
EDA	Engineering Data Analysis
EFD	Early Failure Detection
ESDU	Engineering Science data
ETA	Event tree analysis
FCR	Flight Condition Recognition
FF	Functional failure
FLM	Flight Load Monitoring
FLS	Flight Load Synthesis
FME(C)A	Failure Modes and Effects (Criticality) Analysis
FTA	Fault tree analysis
GAG	Ground-Air-Ground
GWHL	GKN Westland Helicopters Ltd
HARP	Helicopter Airworthiness Review Panel
HGBR	Helicopter Gearbox Reliability (software program)
HM	Health monitoring
HUMS	Health and Usage Monitoring System
IGB	Intermediate Gearbox
IGE	In Ground Effect

I/P	Input
IRAN	Inspect and repair as necessary
JAA	Joint Aviation Authorities
KCAS	Knots Calibrated Airspeed
LIFEX	Life expired
LB	Lower bound (of system failure probability)
LR	Loading Roughness
LSS	Logistics Support Services
MCD	Magnetic Chip Detector
MGB	Main Gearbox
NAML	Naval Aircraft Materials Laboratory
OGE	Out of Ground Effect
OLM	Operational Loads Measurement
O/P	Output
PCD	Probability of Correct Detection
PCS	Plain Carbon Steel
PFM	Progressive failure mechanism
PFND	Progressive failure mechanism not detected
POD	Probability of detection
NDI, NDT	Non-destructive inspection, testing
QDM™	Quantitative Debris Monitoring
RECON	Recondition(ed)
RPM	Revolutions per minute
RT	Rotor Transmission
RTB	Rotor track and balance
SAR	Search and Rescue
SM	Safety Margin
SOAP	Spectrographic Oil Analysis Program
SSI(M)	Stress-Strength Interference (Method)
TBO	Time between overhaul
TFS	Time to first spall
T/C, Trans Chip	Transmission chip warning light

T/R	Tail Rotor
TRGB	Tail Rotor Gearbox
TSN	Time since new
TSO	Time since overhaul
TTF	Time to failure
UB	Upper bound (of system failure probability)
UM	Usage monitoring
VHM	Vibration Health Monitoring

Notation

A_0	Cone distance
C_l	Dynamic rating (bearing)
C_a	Load application factor – calculation of σ_h
C_H	Hardness ratio factor – calculation of S_{AC}
C_L	Life factor – calculation of S_{AC}
C_m	Load distribution factor – calculation of σ_h
C_p	Elastic coefficient
C_R	Reliability factor – calculation of S_{AC}
C_T	Temperature factor – calculation of S_{AC}
C_v	Load dynamic factor – calculation of σ_h
d_i	Internal diameter of shaft
d_o	External diameter of shaft
d_p	Pitch diameter
D_0	Distance from apex to pitch point (pinion and gear)
f	Tooth face width
f_t	Tensile strength of the shaft material
F_T	Thrust load
F_{t1}, F_{r1}, F_{R1}	Tangential, Radial, Combined radial load for bearing 1 etc.
I	Geometry factor for Hertzian Contact stress
J	Polar moment of inertia
K_a	External dynamic factor – Gear tooth root bending
K_v	Internal dynamic factor – Gear tooth root bending
K_s	Size factor – Gear tooth root bending
K_m	Load distribution factor – Gear tooth root bending
K_x	Tooth lengthwise curvature factor – Gear tooth root bending
L_{10}	Time by which 10% of population have failed
n	Rotational speed in rpm
N	Number of cycles under oscillating load

N_f	Number of cycles to failure under constant stress range
N_p, N_g	Number of teeth on pinion, gear
p(F)	Probability of Failure
P	Dynamic equivalent radial load (bearing)
q	Nominal shear stress
S_{AC}	Allowable Hertzian contact stress
S_{WC}	Working Hertzian contact stress
T	Torque
T_1	Input (pinion) torque
T_2	Output (gear) torque
V_{NE}	V (speed) Never Exceed
V_Y	Speed for maximum rate of climb
W_{ap}, W_{ag}	Axial load on pinion, gear
W_{rp}, W_{rg}	Radial load on pinion, gear
W_t	Tangential load on pinion, same for gear
X	Radial load factor (bearing)
Y	Axial load factor (bearing)
α_i	Incremental damage per cycle at load state (torque) i
φ	Involute pressure angle of shaft coupling splines
Γ_p, Γ_g	Pitch angle for pinion, gear
ρ	Radius of shaft
σ, σ^2	Standard deviation, Variance
$\Delta\sigma_t$	Tooth root bending stress
σ_h	Hertzian Contact stress (gear teeth)
Σ	Shaft angle = $\Gamma_p + \Gamma_g$

1 Introduction

1.1 Introduction

Helicopters provide a versatile means of transporting people, material and equipment in a varied range of environments. They are totally dependent on their rotor transmission (RT) systems, which provide the critical links from the engines to the main rotor, tail rotor and ancillary systems. The premium on the overall weight of the helicopter means that components are highly loaded, high strength materials, manufactured to a high degree of accuracy.

The helicopter transmission system will encounter a wide variation in its operation, maintenance regime and loading. The physical environment for marine operations exposes the entire airframe to a potentially corrosive, salt-laden atmosphere. Helicopter usage also varies significantly, with the same type being used in the oil industry - multiple ground-air-ground (GAG) cycles and high flight hours - and Search and Rescue (SAR) operations - on stand-by, with a lower usage rate.

The transmission system is generally considered to be a single load path system, where failure of any component may cause functional failure of the gearbox to deliver torque **[Savage, 1988]**. Passenger and crew safety is of paramount importance and although great care is taken to design and manufacture helicopters to high standards of safety, the safety and reliability record of transport helicopters does not compare favourably with fixed wing aircraft **[Astridge, 1992; Wilson 1992]**.

This thesis describes the development of, and results from, a computer program – entitled HGBR - designed to predict the reliability of the intermediate gearbox (IGB). Two different helicopter types were studied, one with a long operating history and one new in service. The IGB was chosen as being relatively simple in design and function, and yet representing the loading and damage mechanisms that can occur in larger, more complex transmissions.

The program accepts data for the gearbox geometry, material strength and loading in order to calculate the failure probability of individual components and the system as a whole. Such results can be used to answer questions concerning the key parameters, or 'drivers', of reliability. While the results have been gained from the study of particular gearboxes with distinctive loading regimes, efforts have been made to identify general lessons that may be learnt for general gearbox design and operation/maintenance.

The HGBR program employs models to represent the damage accumulated due to the different degradation processes that act upon a gearbox. These damage accumulation models are grouped under the headings of fatigue, wear and corrosion and are applied to the main components in the gearbox. These are the gear teeth, the splined couplings of the input and output shafts, shaft bearings and gearbox casing.

1.2 Rotorcraft Safety and Reliability

The report of the Helicopter Airworthiness Review Panel (HARP) **[CAA, 1984]** was commissioned to investigate the background to helicopter safety and reliability. This reported that the fatal accident rate for larger helicopters (>2300 kg) is approximately five times that for public transport aircraft, when compared on hourly basis. This comparative figure is halved when considering risks per flight **[CAA, 1984];** helicopters typically take-off and land more often than fixed wing transport aircraft on a flying hour basis.

[James, 1990] quotes a fatal airworthiness accident rate of 30×10^{-7} fatalities per flying hour for large twin-engine helicopters, compared with other aircraft types in Table 1.1. Rotorcraft accidents more frequently involve aspects of airworthiness, compared with fixed wing aircraft.

Aircraft type	Fatal airworthiness rate
Light twins	16×10^{-7} per flight hour
Commuter turboprops	11×10^{-7} per flight hour
Large turboprops	6×10^{-7} per flight hour
Small jets	5×10^{-7} per flight hour
Large jets	1×10^{-7} per flight hour

Table 1.1 : Comparison of fixed and rotary wing fatal airworthiness accident rate [James, 1990]

The HARP report also highlighted differences in calculating the expected life of a gearbox. Major errors can be incurred in the estimation of fatigue safe-life due to a limited knowledge about usage **[CAA, 1984]**. Such inconsistencies are also due to the different assumptions made during the initial design of helicopters, including material variability and the manoeuvre-mix to be seen in service.

1.2.1 Design

Two different design and certification criteria are used for the assessment of new fixed and rotary wing aircraft, namely *safe life* and *damage tolerant* design. Safe life requires that a component or system of components be able to operate without failure for a pre-calculated period of time without need of inspection or repair, JAR 29 **[JAA, 1993].** The damage tolerant philosophy, widely used in fixed wing aircraft design, requires that a component or system be able to continue operating safely in a degraded state, but with a detectable level of damage **[Bristow, 1985]**.

Methods of increasing life used in the design of fixed-wing aircraft include redundant structures, multiple load paths, fatigue crack stoppers and multiplexing of essential systems **[CAA, 1984].** However, these techniques cannot generally be implemented in a helicopter transmission system because:

- High strength components are so heavily loaded that once a fatigue crack has developed, the damage propagates rapidly from initiation to failure.

- Few load paths exist for which redundancy can be applied.

- High speed of rotation implies a large number of cyclic loads per flight. A shaft rotation speed of 3000 rpm equates to 18×10^6 cycles in 100 hours of operation.

Helicopter components typically suffer from a mix of high and low cycle fatigue (HCF and LCF). LCF for a rotorcraft is similar to that found in fixed wing aircraft, and can be compensated by fail-safe, damage tolerant design. HCF is more of a problem in engine and transmission system, since high RPM can lead to rapid growth of damage **[CAA, 1984].**

A number of methods have been applied to increase the safety and reliability of transmission systems, for which refinements are still being developed. These include:

- The development of lighter and stronger materials, manufactured to greater accuracy.

- The application of standby systems, e.g. emergency lubrication for main gearbox bearings.

- The use of medium and high technology transducers to monitor the usage and condition (health) of the components within the transmission system. Monitoring systems used to record usage and condition of mechanical systems are frequently referred to as Health and Usage Monitoring Systems (HUMS).

Existing design techniques may be conservative in some areas, whilst neglecting other critical types of degradation, thus censoring the limited failure data that is available. Failures of one type may mask others, e.g. a gearbox may be removed for reconditioning due to external casing corrosion, at which time the bearings might also be replaced; damage accumulated by the latter would not be recorded. This could result in over-maintaining some components, replacing them when only a fraction of their 'life' has been consumed, while other components are neglected. One of the aims of usage monitoring (UM) is to reduce life-cycle costs by retiring components on the basis of actual usage and condition, Chapter 727 of DEF-STAN 00-970 **[MOD, 1989].** There is also an operational penalty to pay for unnecessary maintenance, with increased down time for both civilian and military operators.

1.3 Reliability Prediction

1.3.1 Reliability defined

The following definitions have been drawn from BS 4778 **[BSI, 1991]** and **[Kececioglu, 1972]**, respectively, and serve to clarify the meaning of the term reliability.

- **[BSI, 1991]**

  Reliability is the ability of an item (system) to perform a required function, under given environmental and operational conditions and for a stated period of time.

- **[Kececioglu, 1972]**

  Reliability is the *conditional numerical probability* at a given *confidence level*, that components or systems will *perform* their intended functions without failure or satisfactorily and within specified performance limits, at a given *age* for a specified length of time or *mission time*, when used in the manner and for the purpose intended while operating under the specified *application* and operation stress levels.

The reliability assessment contained in this thesis may be used to meet the requirements quoted from BS 5760 Part 2 **[BSI, 1994]:**

a) Provide early indication of whether a system will meet a stated reliability target.
b) Show aspects of design upon which the system reliability is highly dependent.
c) Help establish the reliability required of an item.
d) Provide input to studies that may influence the design of a system.
e) Establish the effect of such occurrences as production deficiencies, maintenance and operational errors on the overall system reliability.
f) Estimate the effects of design alterations on system reliability.

1.3.2 Mechanical system reliability

The transmission system is generally considered to be a single load path system **[Astridge, 1996b; Savage et al, 1988],** where failure of any component may cause functional failure of the gearbox to deliver torque. This is in contrast to fixed wing aircraft where all safety-critical systems are duplicated or triplicated. The complexity of a helicopter gearbox, the restrictions on space and weight, plus the requirement for a single load path for the transmission of torque preclude the addition of redundancy **[Astridge, 1996a].** It is therefore vitally important that each part comprising the "mechanical chain" is designed, manufactured and maintained to the highest possible standard.

Current techniques to be included as part of the certification process include Design Safety Assessment (DSA), described in Chapter 705 of DEF-STAN 00-970 **[MOD, 1989].** However, there is an increasing need for quantitative models to provide predictive capability to achieve safety and reliability targets. Numerical safety targets are

described by **[Wilson and Cortellini, 1988; Astridge et al, 1993]**. However, to date there have been few ways of linking the present failure rate analysis, Mean Time Between failure (MTBF) and the alternative design considerations **[Carter, 1997].**

Currently the main factor considered is material strength variation for fatigue, where a '3–sigma' working curve is used to give a probability of failure of 1 in 1000 **[Everett et al, 1992].** Typically, due to cost constraints, only limited fatigue tests are carried out on transmission gears. A 'factor' of 1.4 is used to reduce the measured endurance limit to a 'working curve' that is then used to calculate life. A similar safety factor of 1.2 is used on the measured loads when performing the life calculation.

The failure of mechanical systems is generally attributable to time-dependent failure mechanisms, which can be broadly categorised under the headings fatigue, wear and corrosion. The time-dependent failure mechanisms do not exhibit random-type failures. There is little information currently available to assess how these different failure mechanisms interact. This increases the difficulty of assessing the failure characteristics of such systems. **[Sheikh et al, 1995]** have described the failure of a system of components subject to fatigue; their work indicated that the failure rate for such a system of components would increase with time.

1.3.3 Stress-strength interference

The approach to be adopted in this work is that of stress-strength interference (SSI), a technique that emerged from the field of structural reliability **[Freudenthal, 1947; Melchers, 1992].** This approach has been applied in the areas of fatigue, e.g. **[Carter, 1986; Spigel, 1989]** and corrosion **[Strutt & Allsopp, 1993].**

This thesis has made use of SSI to describe the physical failure mechanisms of a transmission system. The different features of this approach include:

- The prediction of the time to failure is calculated from engineering principles rather than historical data (actuarial approach). The latter are not available for new designs. Even when failure data is available, it is often of limited use since the environmental and load factors that lead to the failure are seldom recorded. If failure data were plentiful, this would imply a weakness in design, which would have lead to design changes **[Sidaway, 1999].**

- The SSI technique is applied by relating stress to component degradation and strength to the limit of allowable damage. The mean and variance of these parameters are used to specify the certainty with which the stress and strength are known.

- The SSI models for the failure mechanisms – referred to as 'failure models' – are used to calculate an estimate for the system reliability. The latter is therefore calculated from design data before any in-service data is available.

1.4 Objectives

This thesis describes the development and application of a probabilistic model to predict the system reliability of a helicopter transmission system. This has been achieved by modelling diverse failure mechanisms, namely fatigue, wear and corrosion. This approach to the prediction of reliability allows the effects of varying material, loading and usage parameters to be investigated. Such damage models are widely used to represent fatigue damage, but are less prevalent in the fields of wear and corrosion. The application of condition monitoring is also included within the model in order to estimate its benefit. The specific objectives are:

1. To develop a computer based model to represent physical failure mechanisms in order to predict the reliability of helicopter transmission systems.

2. To apply the model by predicting the reliability of a rotorcraft transmission system to test the methods used.

3. To investigate means by which condition monitoring information from the gearbox system can be used in the quantification of system reliability.

4. To investigate the effect on reliability of the variability of material strength and input loading.

1.5 Software program HGBR

A program entitled Helicopter Gearbox Reliability (HGBR) was developed as part of this work. This is made up of models that represent the damage accumulated due to fatigue, wear and corrosion of the main components in the gearbox. These are the gear teeth, the splined couplings of the input and output shafts, shaft bearings and gearbox casing.

A probabilistic approach has been adopted to represent the variation in material and other failure model parameters. This seeks to represent variability in the former quantities by using probability distributions. The amount of damage accumulated at any given time is predicted by sampling parameters and using these within the damage accumulation model. Knowing the failure criterion then allows the calculation of the time to reach a certain failure probability. Damage models for fatigue and wear are dependent on the number of operating hours of the helicopter, while the model for corrosion damage of the casing depends on calendar time.

One hurdle to be overcome in the assessment of *system* reliability is the comparison of the probability of diverse failure mechanisms occurring. Some of the degradation processes lead to functional failure of a component, e.g. tooth root bending fatigue results in the breakage of a tooth leading to a potential loss of drive. Other failure processes, e.g. fatigue pitting of the gear teeth and bearings, are more progressive in nature and give an early warning of potential failure, detectable by health monitoring (HM) techniques.

The effectiveness of the HM system has been incorporated in the computer model by considering the probability of detection (POD) of each failure mechanism. In the case of a progressive degradation process, should the HM system fail to detect early warning signs, a functional failure could occur. For such cases, the POD is combined with the probability of degradation occurring to calculate a probability of functional failure.

The prediction of the system reliability is also complicated by the inter-dependency of the components due to the common underlying loads. The frequently used 'series' system representing a chain of independent units is not strictly valid in this situation **[Astridge, 1996b]**. Work undertaken in the field of structural design has shown that a multi-dimensional mathematical solution is required **[Ang and Tang, 1984]**. However, the upper and lower limits for such a calculation can be calculated from knowledge of the individual failure probability values. This is the approach that has been adopted in this work.

The upper reliability bound is that obtained by considering the failure of the least reliable component alone as being responsible for the system failure. The lower reliability bound is obtained from multiplying the individual reliability values, as in the case of the series chain model.

1.6 Research activity and results

1.6.1 Program Application

The HGBR program was used to investigate the relative effect of loading and material variability and how these change the overall system reliability. This shows the relative influence of certain key parameters on the failure probability, and how this may change over time. The model has been used to predict which will be the predominant failure mechanism, which may change depending on the failure probability deemed 'acceptable' for the gearbox.

In this manner the relative merit of any further refinements and improvements may be evaluated. This shows whether the system safety and reliability may be more greatly improved by increasing material strength, reducing operational loads (or their variability), or increasing the effectiveness of HM detection.

The intermediate gearbox (IGB) has been chosen due to its limited complexity compared to the main and tail rotor gearboxes. This has reduced the time spent in the calculation of component stresses, whilst still enabling all relevant damage mechanisms to be modelled. Larger and more complex gearboxes are affected by the same degradation mechanisms, and the techniques employed to model the IGB reliability may be scaled-up accordingly.

1.6.2 Thesis Layout

Chapter 2 contains a review of current literature in the field of mechanical reliability, reliability models and in particular their application to transmission systems. A description of the most widely used probability distributions is included, and standard techniques for the assessment of system safety and reliability are referenced.

Chapter 3 is a description of the intermediate gearbox (IGB), the mechanical system for which techniques in this thesis are developed. This chapter includes details of the damage mechanisms that have been reported, as found both in open literature and from the manufacturer.

Chapter 4 describes the damage accumulation models used in the prediction of reliability in this thesis. This includes detail of damage models applied to represent fatigue, wear and corrosion of the gearbox components. The method used for estimating system reliability is also described.

The current status in health and usage monitoring systems (HUMS) is reviewed in Chapter 5. This was performed to determine the applicability of HUMS to the reliability model and to estimate their effectiveness, or probability of detection (POD) of damage.

The construction of the damage models and the data (geometrical, material and loading) used in the models are described in Chapter 6. This is backed-up by Appendix E, which contains supplementary data and analysis. These are the data that are used as baseline values in the sensitivity studies in Chapters 8 and 9. A description of the HGBR program is given (amplified in Appendix A), plus a summary of the methods used in obtaining maintenance data, Chapter 7.

Chapter 7 contains analyses of the results obtained from maintenance records, to investigate potential application in the reliability prediction process. This information has been obtained from a sample study of archived records, Appendix D, and highlights the benefit and limitations of such data.

Chapter 8 contains the results for single failure mechanisms, broadly segregated into fatigue of gear teeth and bearings and spline wear. This includes graphs showing the effects of changing material and load parameters on the predicted life.

Chapter 9 contains the results from the corrosion model, plus an examination of the application of the probability of detection (POD) in quantifying failure probability. A series of graphs is then presented to give a set of examples of the lower and upper bounds for system reliability for both example gearboxes with different load and material parameters.

Chapters 10 and 11 contain the Discussion and Conclusions respectively. These have reflected on the development of the models, and results derived therefrom, by considering them against the Objectives in Section 1.4.

2 Literature Review

2.1 Introduction

There is a wide range of diverse techniques available for the assessment of reliability, both qualitative and quantitative. It is intended that this review will describe the application of techniques to the assessment of mechanical reliability, with their respective merits and limitations.

The aim of this review is to report the basis and application of models that have been used to assess and quantify reliability. Wherever such methods are based upon general principles, techniques and probability distributions, then background information of these will also be discussed. In specific cases, the results of other gearbox reliability models have been reported.

Current helicopter industry approaches to safety-critical aerospace components **[Viswanathan et al 1988; Amer, 1989]** are based on either Safe Life or Damage Tolerance concepts. The distinction between these two approaches is described by **[Bristow and Minter, 1999].** In essence, the preferred method of controlling component failures is through Damage Tolerance. In this approach, the rate of damage growth within a component is measurable and detectable over a period of time that exceeds the interval between inspections. However, in cases where rotational speed and loading are high, the rate of damage growth may be too great for detection to be guaranteed. In the latter case, a Safe Life approach is adopted, where the material properties and loading parameters are based on design assumptions. The expected life is then calculated and components are replaced at the end of this calculated life, without regard to the actual damage accumulated.

2.2 Reliability Assessment

Industry standards now stipulate that Design Safety Analysis (DSA) must be performed as part of the certification for modern helicopter types **[Astridge, 1996a]**. To date, the reliability predictions for mechanical systems have been based on Fault Tree Analysis (FTA) and Failure Modes, Effects and Criticality Analysis (FMECA) **[Astridge, 1992; Wilson, 1992]**. These techniques are described in Section 2.2.1 and 2.2.3 respectively. The application of probability distributions is less widespread, but those methods worthy of particular mention, including Probabilistic Fatigue Methodology, Weibull analysis and Stress-Strength Interference are described in Sections 2.4 to 2.6.

The employment of reliability block diagrams, fault or event tree analyses, using failure *event* data is described by **[Astridge, 1989; Wilson, 1992].** However, these tools do not easily model the time-dependent degradation processes, which lead to the eventual failure events in transmission systems, as will be highlighted.

2.2.1 Fault Tree Analysis

Fault Tree Analysis (FTA) is a cause analysis, and provides a means of identifying graphically the various possible event combinations that could lead to a single undesirable event **[Billinton and Allan, 1992; Davidson, 1994]**. It is often referred to as a "top-down" analysis since the single undesired event is at the top of the "tree". The possible combinations of sub-events are then linked together using Boolean logic, providing a graphical representation of logical relationships between combinations and sequences of undesirable events leading to system failure.

Based upon typical gearbox failure mechanisms (see Chapter 3), a Fault Tree diagram has been drawn to represent the failure of an intermediate gearbox (IGB), Figure 2.1. The top event is 'Loss of yaw control of the helicopter' and a top-down list of causal factors is shown. The top event could be chosen to represent a less severe event, for example the unscheduled removal of a component.

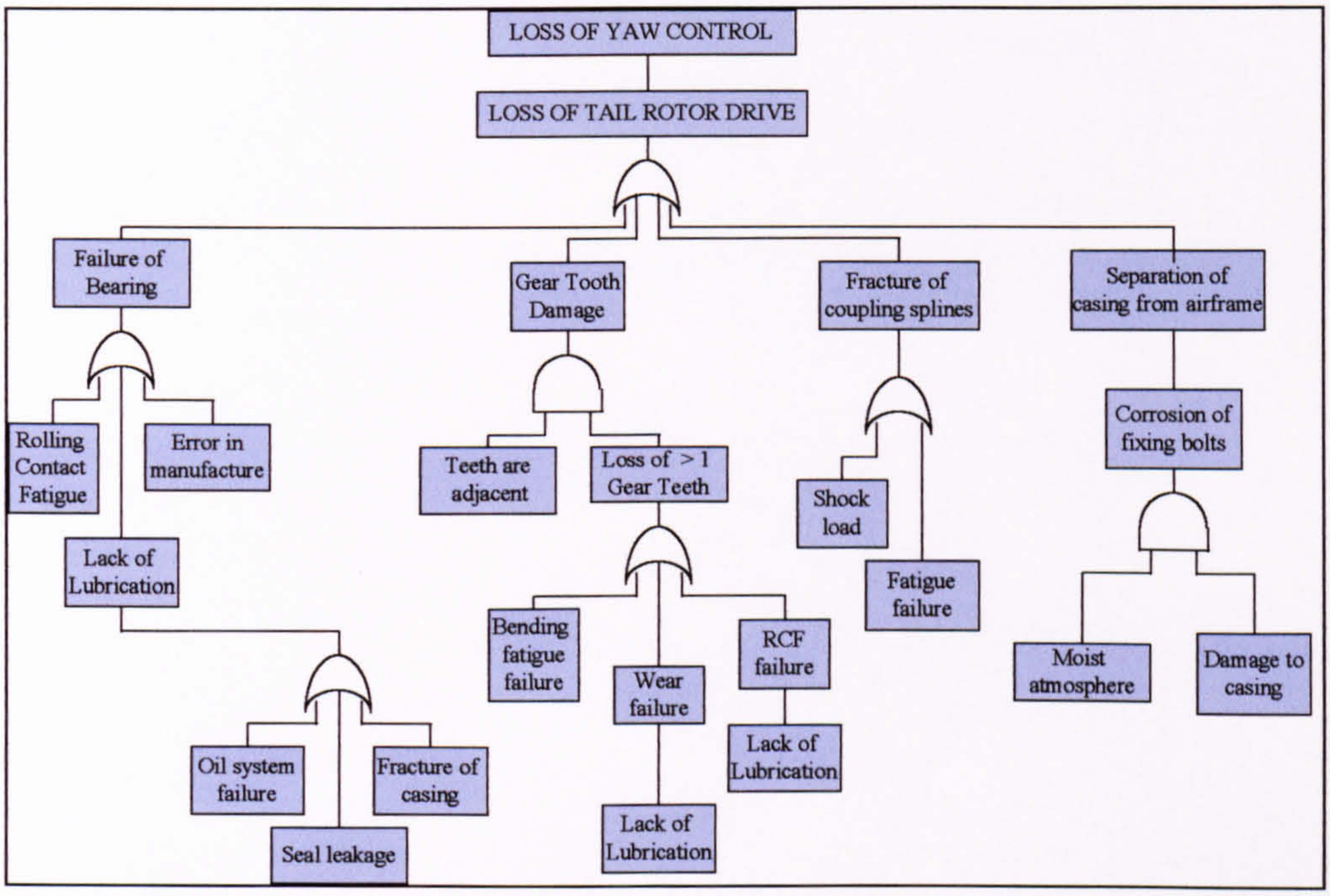

Figure 2.1 : High level Fault Tree Analysis of typical IGB

For a complex system with independent[1] components, such a Fault Tree diagram would aid the calculation of system reliability, given the failure rate of each component. However, for a transmission system, none of the degradation mechanisms can be considered as failure events, but rather as continuous processes affected by loading, material and other factors; FTA cannot easily represent these. Also, the failure mechanisms are not independent of one another; both loading and environmental conditions experienced by the components are inter-related.

[1] Components are described as independent provided they do not share the same material strength, applied loading or environment, for a mechanical transmission system.

The failure mechanisms within a gearbox are time- or cycles-dependent, requiring a "damage model" capable of accepting all these factors. In Figure 2.1 for example, the loss of lubrication does not produce an instantaneous failure, but rather increases the rate of degradation and hence the probability of failure. The FTA analysis may prove useful in describing the hierarchy of failure events that lead to failure of the gearbox. In its present form, however, it cannot accommodate diverse damage models used to represent physical degradation mechanisms.

2.2.2 Event Tree Analysis

Event Tree Analysis is an effective technique for assessing the consequences of various combinations of events, typically within a particular failure mode. It may be used in parallel with a FTA where the latter provides data for the initiating and/or subsequent events. The ETA allows the analyst to calculate the frequency of different events by identifying all possible outcomes that are initiated by a single event **[Billinton and Allan, 1992]**.

An example of an event tree is given in Figure 2.2. The initiating event A is characterised by a probability value, say p, and the corresponding event 'not A' (**A**) has a probability of (1-p). Subsequent branches of the event tree represent events B, C and D, to which probability values are assigned. In this way the probability of each branch of the tree may be calculated, based upon known values of probability. By quantifying the probability of events, an ETA enables the user to calculate the probability of the different outcomes of those events.

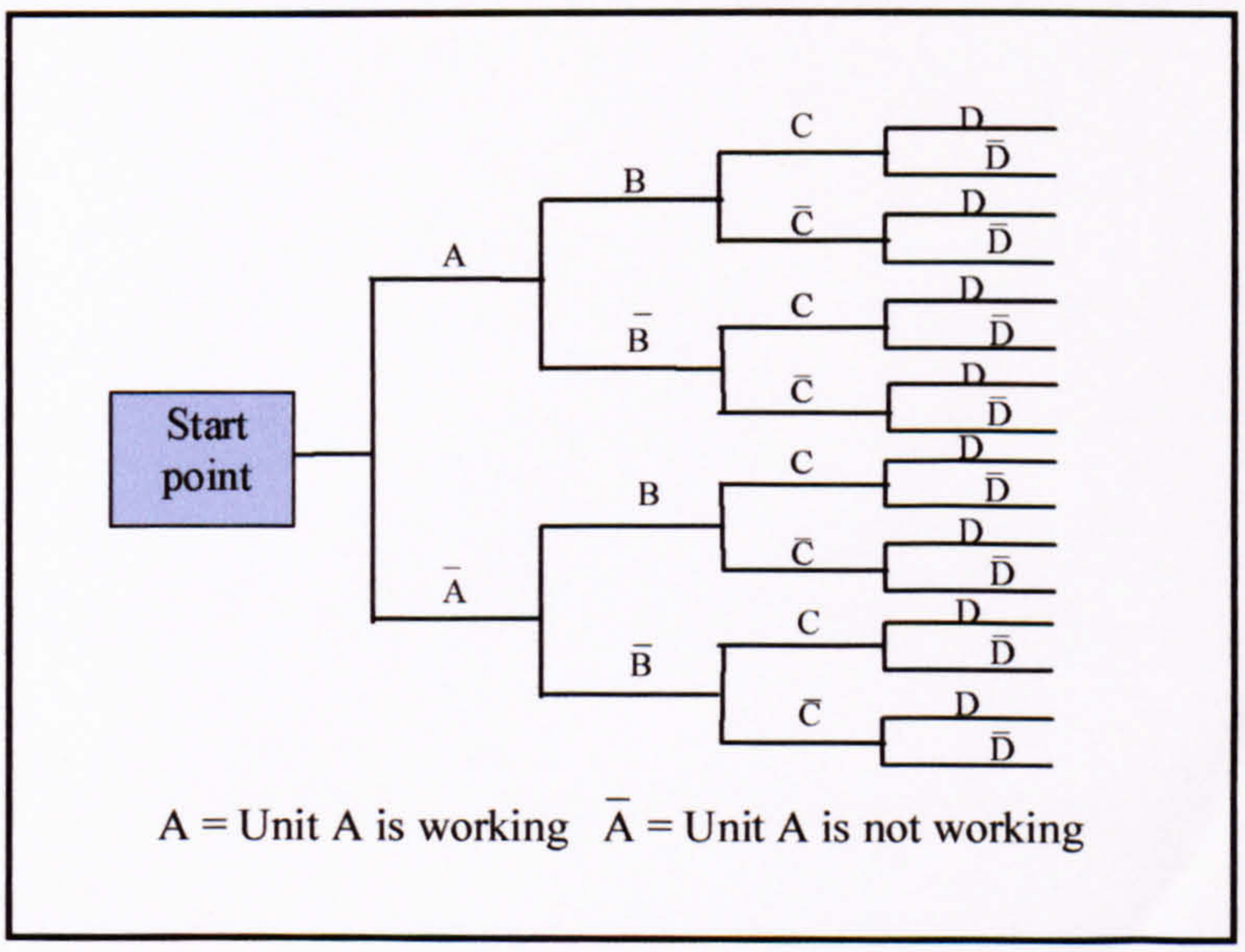

Figure 2.2 : Example of Event Tree Analysis

The ETA approach is mainly suited to discrete events rather than continuous damage processes and is often used in Quantified Risk Assessment (QRA). In QRA, the hazard (end event) frequency and consequence are multiplied together to quantify 'risk' associated with the hazard **[Billinton and Allan, 1992]**. It is therefore considered to be

inappropriate for representing the probability of gearbox failure mechanisms, which change with load, age and gearbox condition. Hence, the ETA has not been applied in the current work of reliability prediction of a transmission system.

2.2.3 Failure Modes and Effects Analysis

The Failure Modes and Effects Analysis (FMEA) is a qualitative assessment tool for listing all the possible failure modes for each and every component within a system. This can be extended to include details of the occurrence rate of the failure modes and the level of criticality in a Failure Modes, Effects and Criticality Analysis (FMECA). The performance of a FMECA is essential feature of current reliability analysis and is applied as part of Design Safety Analysis **[Astridge, 1996b]**.

BS 5760, Part 5 **[BSI, 1991]** emphasises that the FMEA and FMECA are able to show the effects of potential fault modes within a system, which take into account the possible degradation of performance and the consequences for safety. The FMEA/FMECA are also good tools for identifying the failure modes that significantly affect the availability[2], reliability, maintainability and/or safety of a system.

2.2.4 Reliability Block Diagram

The Reliability Block Diagram (RBD) is a useful technique for depicting the inter-dependencies between components within a system. RBD may be used to quantify system reliability and availability, which will depend on any redundancy in the system, depicted by components being in series or parallel, see Figure 2.3. If the random (negative exponential) model - Section 2.3.2 - is used to represent the reliability of each component, the system reliability (all components independent) is:

$$R_{sys} = \prod_{i=1}^{6} R_i = \prod_{i=1}^{6} e^{-\lambda_i t} \qquad (2.1)$$

So the system failure rate is the sum of the component failure rates:

$$\lambda_{sys} = \sum_{i=1}^{6} \lambda_i \qquad (2.2)$$

Such RBD must be drawn carefully, as they are intended to show information regarding critical components and any redundancy thereof. They are not necessarily the same as a Functional Block Diagram (FBD), which shows the physical interconnection of components making up a system, e.g. electrical circuit diagram, or mechanical load diagram. A good description of the methods available for use in calculating reliability and availability using RBD is found in **[Davidson, 1994]**.

---

[2] Availability is defined as the probability that an item, at any instant in time, will be able to perform its function **[Carter, 1986]**. This takes account of what proportion of time is spent in maintenance.

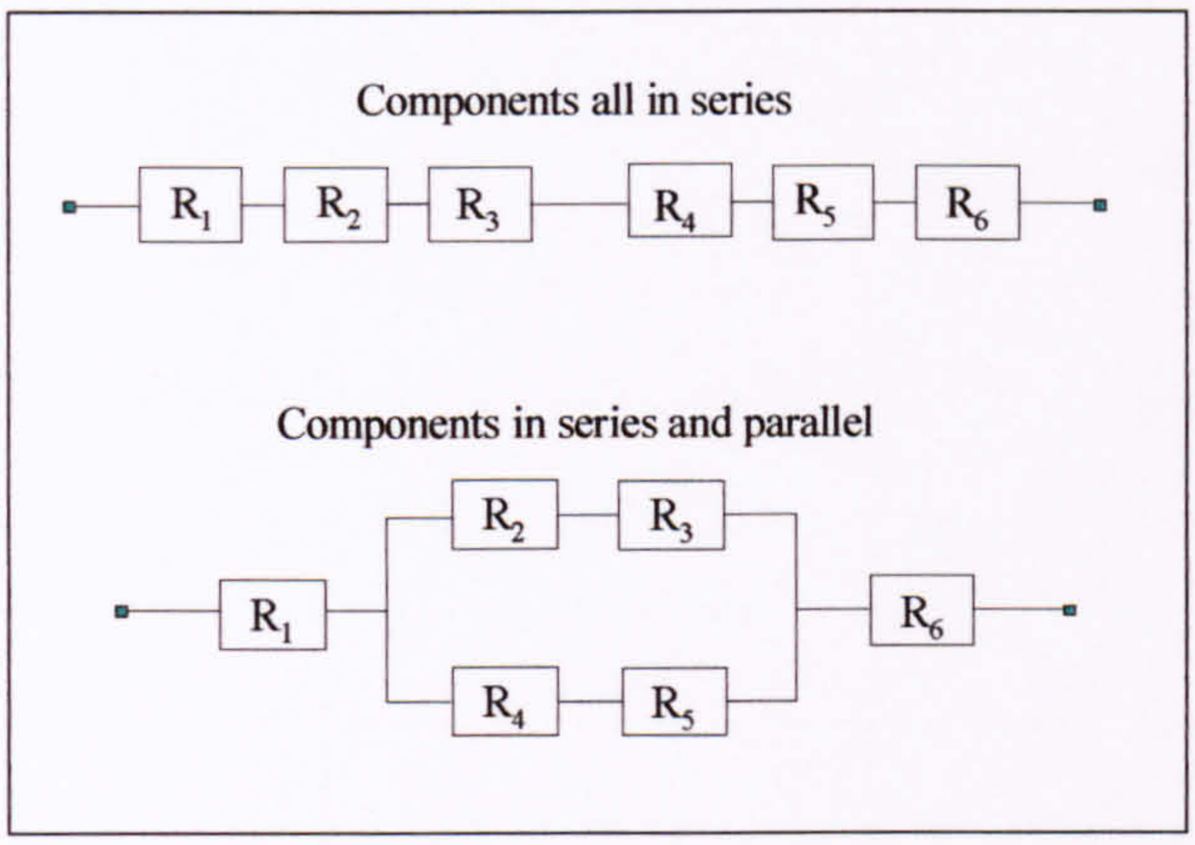

Figure 2.3 : Examples of RBD with components in series and parallel

2.3 Probability Distributions used in Reliability Assessment

Probability distributions are used regularly in the field of reliability assessment. The most widely used are considered here, namely the Normal (or Gaussian), Log-normal, Exponential and Weibull distributions. Further details regarding these distributions are given in Appendix C.

2.3.1 Normal and Log-normal Distributions

The Normal (or Gaussian) distribution is widely known and is described in many reliability texts **[Bury, 1975; Billinton and Allan, 1992]**. It is useful for describing the occurrence of any variable that is distributed symmetrically about a mean value μ. A measure of the scatter of the values, or spread of the distribution, is taken from the variance σ^2, which is the square of the standard deviation σ. The shape of the distribution is shown in Figure 2.4.

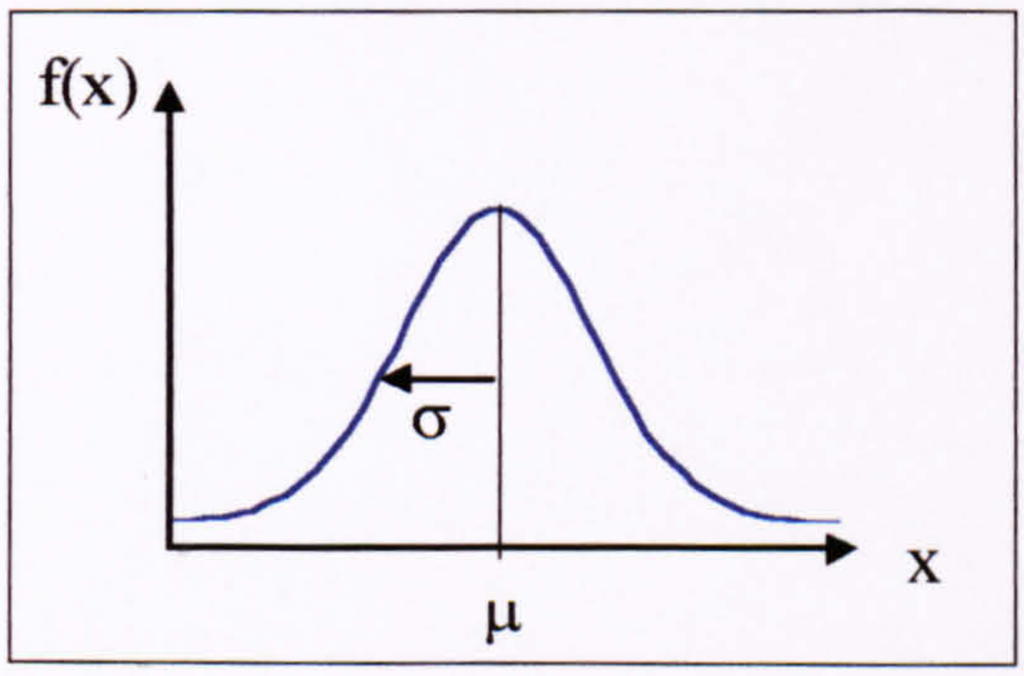

Figure 2.4 : Normal distribution with mean μ, standard deviation σ

A variation of the Normal distribution is the Log normal distribution, which is used when the variables appear 'skewed', and have no negative values, e.g. times to repair components. The variable X has a log normal distribution if ln X has a Normal

distribution, with parameters μ and σ, where the latter are the mean and standard deviation of ln X **[Billinton and Allan 1992]**. Appendix C expands upon the relationship between Normal and Log-normal distribution.

2.3.2 Exponential Distribution

The exponential distribution is used to represent events or other data that occur randomly in space or time. When applied to reliability, it may be used to represent a system or component with a constant failure rate λ. If the hazard (or failure) rate is constant, then it can be shown that the reliability, i.e. the probability of no failure, may be written **[Carter, 1986]**:

$$R(t) = e^{-\lambda t} \tag{2.3}$$

The failure function is

$$F(t) = 1 - R(t) = 1 - e^{-\lambda t} \tag{2.4}$$

The probability density function of failure is therefore:

$$f(t) = \frac{dF}{dt} = \lambda e^{-\lambda t} \tag{2.5}$$

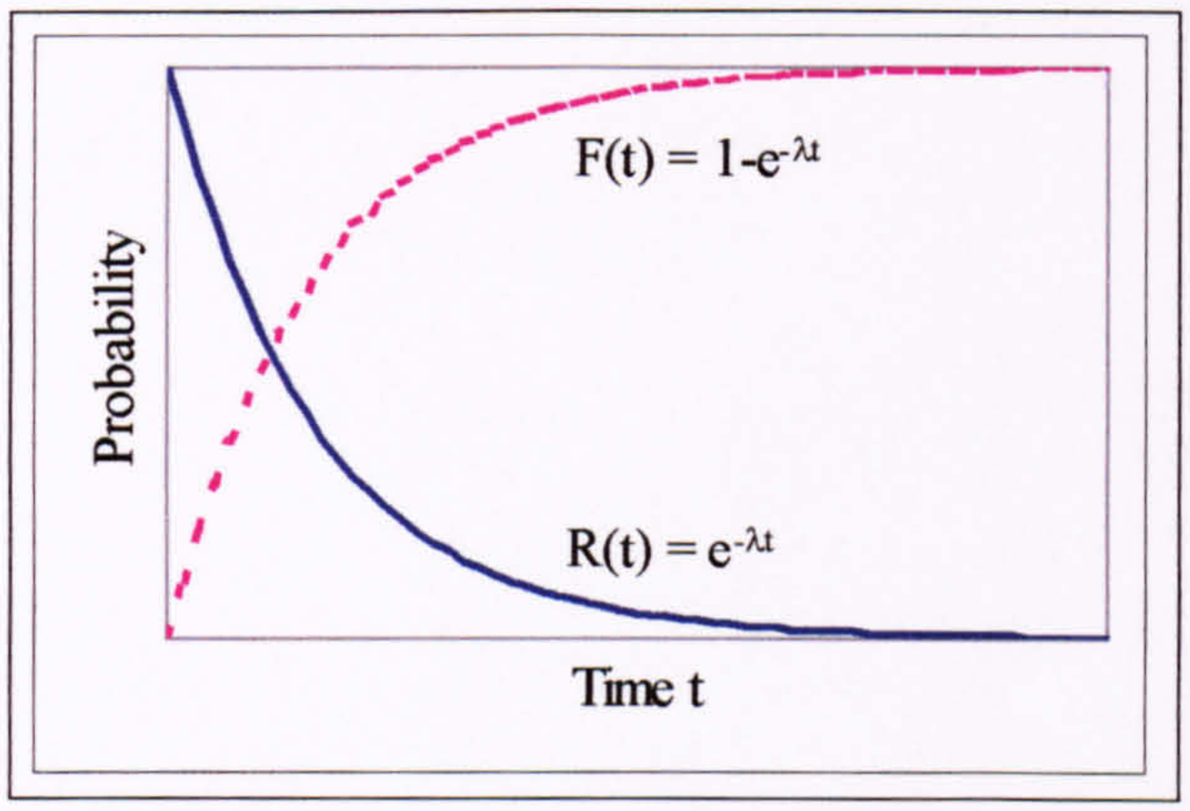

Figure 2.5 : Reliability and failure function of Exponential distribution with failure rate λ

The exponential distribution (Figure 2.5), is defined by the failure rate λ, which is the reciprocal of the mean time to failure (MTTF) or mean time between failures (MTBF). The distribution is widely used for modelling the life of components where the underlying damage mechanisms are not known.

2.3.3 Weibull Distribution

The Weibull distribution is widely used to analyse the failures of mechanical systems and is described in most reliability texts, e.g. **[Bury, 1975; Billinton & Allan, 1992]**. Specific examples are provided by **[Carter, 1986 p. 151; Hill, 1976],** who show how

to fit Weibull curves to data for geartrain failures and generator drive failures. The same technique is applied in this thesis work to fit data from oil debris analysis for gearbox bearings, see Appendix C.6.

The equation for this three-parameter distribution is shown in equation 2.6, and part of its versatility comes from the Weibull slope β, or shape parameter. A value of $\beta < 1$ indicates a decreasing failure rate, $\beta = 1$ indicates a constant failure rate and $\beta > 1$ indicates an increasing failure rate. These correspond to the three regions of the 'bath-tub' curve (Figure 2.6) where a period of 'wear-in' (decreasing failure rate) is followed by a constant failure rate, then a period of 'wear-out' (increasing failure rate).

$$F(t) = 1 - R(t) = 1 - \exp\left[-\left(\frac{t-\gamma}{\eta}\right)^{\beta}\right] \qquad (2.6)$$

where β, Weibull slope, which defines the shape of the failure distribution,
η, characteristic life (scale parameter); the life by which 63.2% of the population have failed,
γ, minimum life, or location parameter (hours).

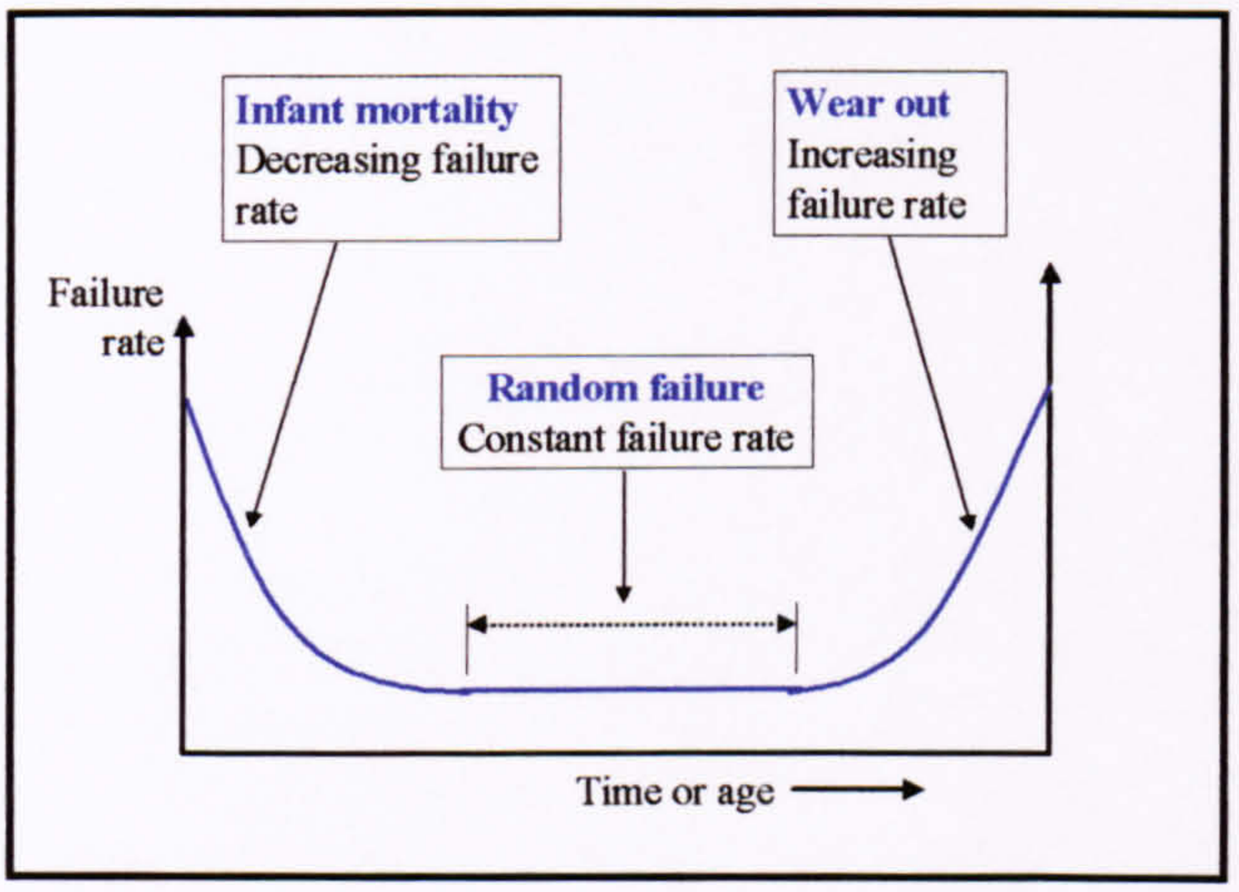

Figure 2.6 : Typical bath-tub curve showing three stages in component life

2.4 Reliability Assessment Techniques for Mechanical Systems

2.4.1 Previous work in calculating life

A number of techniques have already been employed in the modelling of gearbox reliability, and the components within. Most of the work in this area has taken place in the area of fatigue life prediction, with only limited work performed for other failure mechanisms, e.g. wear and corrosion.

The traditional approach has always been one of conservatism. The means of quantifying fatigue life is based upon material data in the form of an S-N curve. This is then combined with an assumed design load spectrum, with certain safety factors, and

an appropriate damage model applied to calculate life **[Bristow, 1985]**. The model generally used is the Palmgren-Miner linear damage rule (see Chapter 4), but other models are also used, e.g. crack growth (Paris Law).

The fatigue strength is normally based upon a failure probability of one in a 1000, but the conservatism in load and usage is not quantified **[Everett et al, 1992]**. The need to measure this level of conservatism has become apparent, and probabilistic fatigue models have evolved to fill the gap. These use probability distributions to represent variation in material strength and the load spectrum itself, and may employ simulation to generate results.

However, significant errors can be introduced in the calculation of life depending on the procedure used for the calculation. The American Helicopter Society (AHS) conducted a 'round robin' exercise to investigate the techniques used and assumptions made in calculating the probabilistic fatigue life of a helicopter pitch link. Each manufacturer was supplied with dimensions, loading and material fatigue S-N data for the pitch link **[Everett et al, 1992]**, and asked to calculate the safe life. The results gave an extremely wide range of results, which was attributed to differences in stress cycle counting techniques and the fatigue S-N curve reduction factors **[Gunsallus et al, 1990]**.

The prediction of gear life is considered in the analysis of fatigue of gears **[Coy et al, 1985]**. These workers have applied the model developed by **[Lundberg and Palmgren, 1947]** for the contact fatigue of bearings. This is described in Chapter 4, where the same model has been used to calculate the lives of bearings in the intermediate gearbox.

2.4.2 Quantitative Reliability Assessment Techniques

The modelling of mechanical failures has often been accomplished by adopting a random hazard failure model, with a constant failure rate. Historical records can give an indication of the failure/removal rate, and this can be used to calculate a Mean time to Failure (MTTF) for use in such a model. This is the basis of the Generic Parts Method, which assumes that system components fail independently of each other, and the failure rates are constant with time, DEF-STAN 00-41 **[MOD, 1993]**. It is also assumed that most parts failures cause system failures and that system failures are caused by part failures. Results from this method are therefore overly pessimistic, and this technique is inappropriate for a transmission system.

However, the assumption of a constant failure rate is not considered correct for many mechanical components, since it takes no account of the wear-out process. Research into the times to failure (TTF) of mechanical valves in process plant showed a clearly increasing failure rate **[de la Mare, 1980]**.

The Weibull distribution has been used for calculating the reliability of a general transmission system, as reported by **[Savage et al, 1994]**. The latter developed a software program called TLIFE, which predicts the reliability for spur, helical and spiral bevel transmission systems. The models within the program are based upon the two-parameter Weibull distribution for the life of the gears and bearings, which are assumed

to form part of a strict series model. The use of the Product Rule produces an overly conservative result, as discussed in Section 2.7.

The TLIFE program does not consider the effect of gear tooth root bending fatigue, wear or corrosion. This is considered to be a limitation of the technique, since other failure mechanisms are prevalent in a gearbox. However, it is useful in showing the links between the input torque and loads on the gears, shafts and bearings, according to the input geometry.

[Astridge, 1996a] has performed system reliability calculations as part of the Design Safety Analysis (DSA) required by recent changes in airworthiness regulations, JAR 29 **[JAA, 1993]**. The technique makes use of a large database of civil and military helicopter accident and incident records to perform safety analysis for new designs. The failure rate drawn from accident data is then reduced by:

- Risk Reduction Measures, e.g. new design features designed to prevent this failure mechanism, new materials with greater strength.

- Compensating provisions, e.g. condition monitoring

This technique is based on engineering judgement as to the order-of-magnitude improvement that is to be applied. As such the technique is limited by the skill of the analyst, and such factors are open to interpretation by different users. However, the work does appreciate that the application of the series 'Product Rule' may be overly pessimistic in calculating system reliability. Other benefits of this work **[Astridge, 1997]** are the compilation and analysis of failure statistics of helicopter rotor transmission systems.

[Goode and Roylance, 1999] have postulated a two-part reliability model to predict reliability, consisting of a stable zone (normal operation) and an unstable zone (pending failure). This predicts the time spent in the 'stable zone' from a Weibull failure model based on historical failure data, since condition monitoring does not offer any information about the remaining life of the bearing. Once a pre-set 'alarm level' is exceeded, the time to failure is approximated by an exponential model, followed by an exponential damage growth model.

This technique was developed for bearings in a steel processing plant, where there would be an adequate warning of bearing failure. However, it could not be appropriate for helicopter gearbox bearings; this is because once damage is detected, bearings are removed from service immediately, since further operation in service could result in total gearbox failure within the duration of one flight.

In the automotive industry, transmission reliability software has been developed using the BS/ISO standards for design purposes. This allows the design to be optimised before the gearbox is built, with a large resultant cost benefit **[James, 1998]**. However, this approach is mainly CAD design with finite-element (FE) analysis, and does not consider wear and corrosion of components.

2.4.3 Damage Models

There are a number of streams of work being carried out to model damage accumulation, also referred to as the 'Physics of failure'. Work in the related field of the physical degradation of electronic components has been conducted by **[CALCE, 1999]**. The work in this field is the most developed, in that electronic components are not subject to the same wide fluctuations in environment, load etc, as mechanical components.

Work to develop probabilistic models to represent the cumulative damage of fatigue is described in **[Bogdanoff, 1985].** This work has focussed on the development of probabilistic models related to the Paris-Erdogan equation for fatigue crack growth. However, the current work in this thesis is focused on fatigue crack initiation, and makes use of Miner's Law for linear damage accumulation, see Section 2.4.1 and Chapter 4.

Similarly, damage accumulation models have been proposed for the modelling of corrosion damage, based on research in the offshore oil and gas industry e.g. **[Strutt and Allsopp, 1993]**. This work included the application of probability distributions to parameters in the corrosion pit growth process, to assess risks throughout pipeline life.

In the field of wear, a probabilistic approach was adopted by **[Kececioglu and Koharcheck, 1983]**, who have shown the successful fitting of Normal distributions to test data for spline wear life. Other workers, notably **[Qureshi and Sheikh, 1997]** and **[Warburton, 2000]** have developed damage growth models for the wear mechanism, whose parameters are based upon probabilistic distributions.

The latter worker developed a wear model to describe the wear-in period of a subsea actuator, by analysing the design and environmental factors. A significant feature of this was the use of a Failure and Degradation Influence Diagram to distinguish the competing underlying failure processes and mechanisms. A similar approach has been adopted in this current work to identify the key components and failure mechanisms, Chapter 3.

2.5 Probabilistic Fatigue Methodology

The most extensive application of probabilistic techniques in transmission components is that of fatigue modelling and life calculation. In its most rudimentary form, probabilistic fatigue methodology may be implemented by the application of 'safety factors' to account for uncertainty in the strength, loading and usage of a transmission system. These allow for the lack of knowledge of the exact loading, strength and operation of a helicopter but will generally lead to a conservative estimate of life.

2.5.1 Material variability

Gearbox components are manufactured to a high degree of accuracy from materials of high purity. Nevertheless, variation in material properties exists between different samples of the same population due to inclusions and other micro-structural differences.

The S-N curve for such components is distributed, with an assumed Log-normal distribution for load at constant cycles, as in Figure 2.7 **[Viswanathan et al 1988, Bury 1975, Yang 1996]**. Each line shown represents the different combinations of stress and life for a particular failure probability.

The current design procedure allows for material variability by performing tests of component samples, then applying a test or safety factor to derive a 'safe' working S-N curve. In the case of high precision, high cost transmission components, the number of tests is limited; the test factor will depend on the number of samples tested.

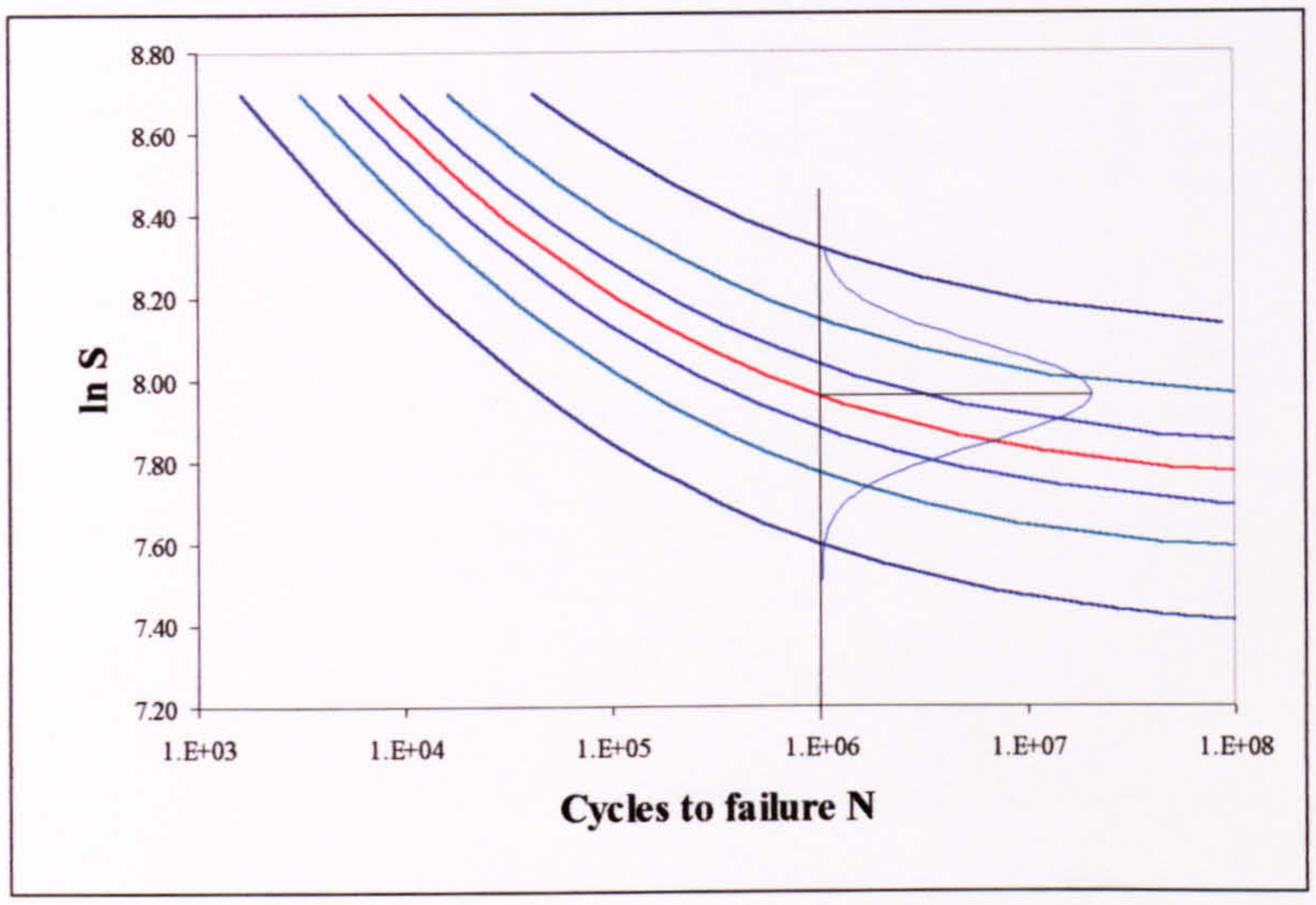

Figure 2.7 : P-N-S curve showing the distribution of ln S at constant life

If one gearbox is tested, the stress at which failure occurs is reduced by 1.4 to provide a "working" curve for determining the safe life of the gearbox **[Cansdale & Tigwell, 1987]**. If four gearboxes are tested, the factor is 1.3. This working curve is taken to be the 3σ curve, at which the probability of failure is 0.1% with a 95% confidence **[Stagg, 1976]**. These factors are derived in the Appendix C.

2.5.2 Load variability

Another source of variability is that of the loading applied to the transmission system. In each helicopter, the flying of a particular manoeuvre will entail a distribution of loads, which will vary each time it is carried out. This is due to a variety of factors, including pilot technique, wind conditions, aircraft weight and the position of the centre of gravity. In order to account for this variability a load factor 1.2 is often used when calculating the fatigue life **[Irving and Hudson, 1998]**.

This factor may lead to an overly conservative fatigue life however, and several studies to measure in-flight loads have taken place, e.g. **[Crawford, 1999]**. Such information on the variation of loads within a manoeuvre may then be used for assessing the probabilistic fatigue life, e.g. **[Viswanathan et al, 1988]**.

2.5.3 Usage variability

The third source of variability is that of the occurrence of helicopter manoeuvres. Different missions and environments will entail a different mix of manoeuvres for a fleet of helicopters. Usage variability is normally modelled by the use of probability distributions to represent the likelihood of a particular manoeuvre occurring during a flight. Examples of this include the work by **[Viswanathan et al, 1988]** and **[Moon et al, 1996]**. The latter applied Weibull distribution functions to represent strength, load and usage variability. In this technique samples of the three distributions were used to calculate the overall fatigue life using Miner's cumulative damage sum.

2.6 Stress-Strength Interference Method

2.6.1 Theory

The load, or stress, acting upon an item and the strength of that item are parameters distributed about a mean value, and are often represented by probability distributions. In order to calculate the probability of the load exceeding the strength, the stress-strength interference (SSI) method is used **[Carter, 1986]**. This represents the intersection of two such distributions, an example being Figure 2.8, which shows two overlapping Normal probability density functions (PDF), as defined in Section 2.3.1.

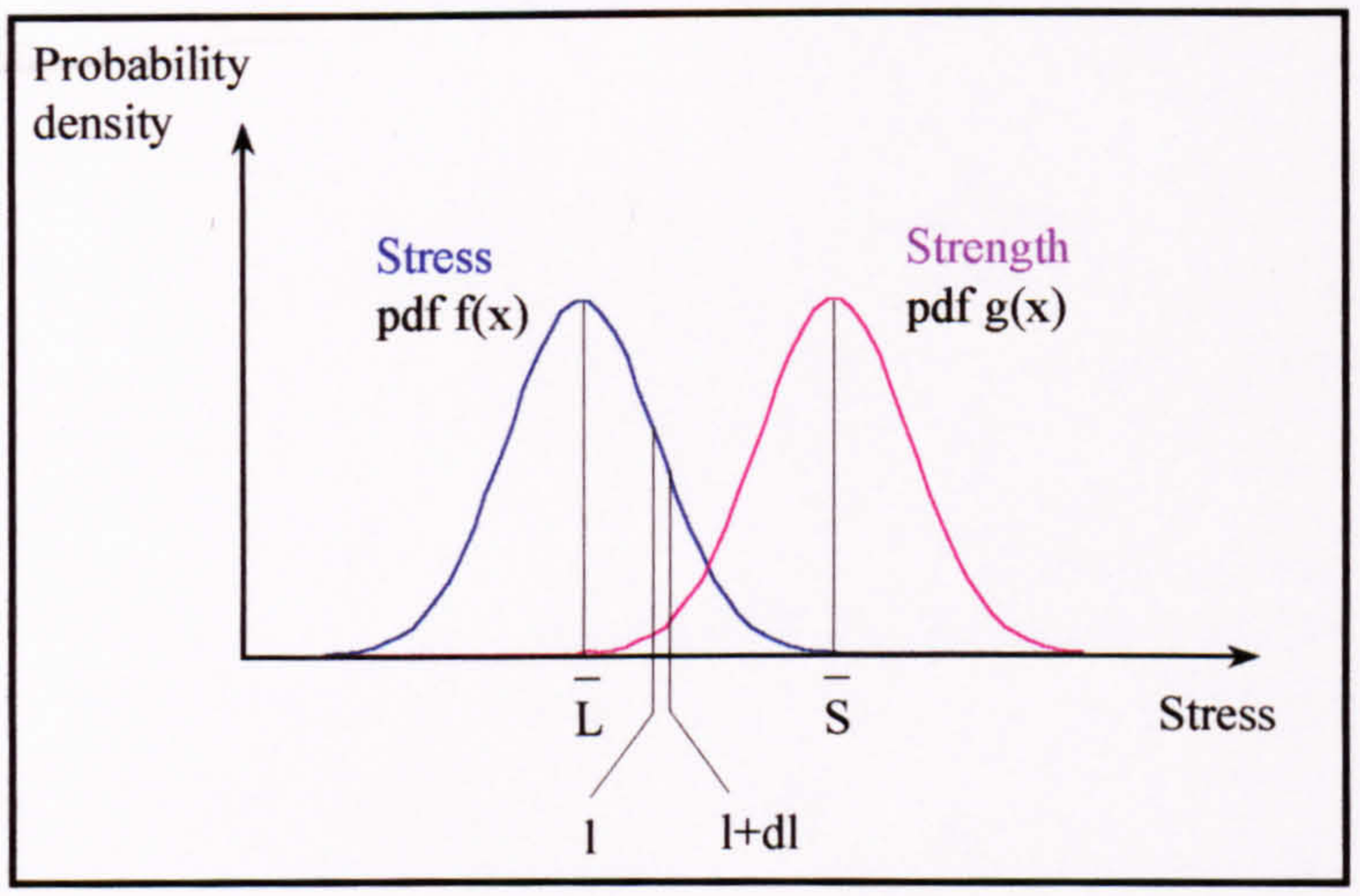

Figure 2.8 : Representation of Stress/Strength Interference

- load f(x) - the load or stress being applied to a component, and
- strength g(x) - the variation of the strengths of those components (manufacturing and/or material differences).

In this example, the load (or stress) distribution overlaps the strength distribution, which means that for *some* components at *some* loads, the stress will exceed the strength. When this occurs the item or component will fail. It can be shown that the probability of failure may be calculated **[Carter 1997, Strutt et al, 1995]** as:

$$p(F) = p(\text{load exceeds strength}) = p(l>s)$$

$$p(F) = \int_{-\infty}^{\infty} f(x)\left[\int_{-\infty}^{l} g(x)dx\right]dx = \int_{-\infty}^{\infty} f(x).G(L)dx \qquad (2.7)$$

where G(l) is the *cumulative density function* of the strength distribution.

This probability of failure may be reduced by altering the amount of overlap of the two distributions in Figure 2.8, either by further separating their means or by reducing the variance of either one or both. Two quantities which are frequently used in SSIM are the *Loading Roughness* (LR), a measure of the load variability, and the *Reliability Index* β (related to the *Safety Margin*), a measure of the amount of overlap of the distributions. These are defined as

$$LR = \frac{\sigma_L}{\sqrt{(\sigma_S^2 + \sigma_L^2)}} \qquad (2.8)$$

$$\beta = \frac{\bar{S} - \bar{L}}{\sqrt{(\sigma_S^2 + \sigma_L^2)}} \qquad (2.9)$$

$$SM = \bar{S} - \bar{L} \qquad (2.10)$$

where $\bar{S}$ and $\bar{L}$ are the mean strength and load, and
σ_S^2, σ_L^2 and the variance of the strength and load (respectively)

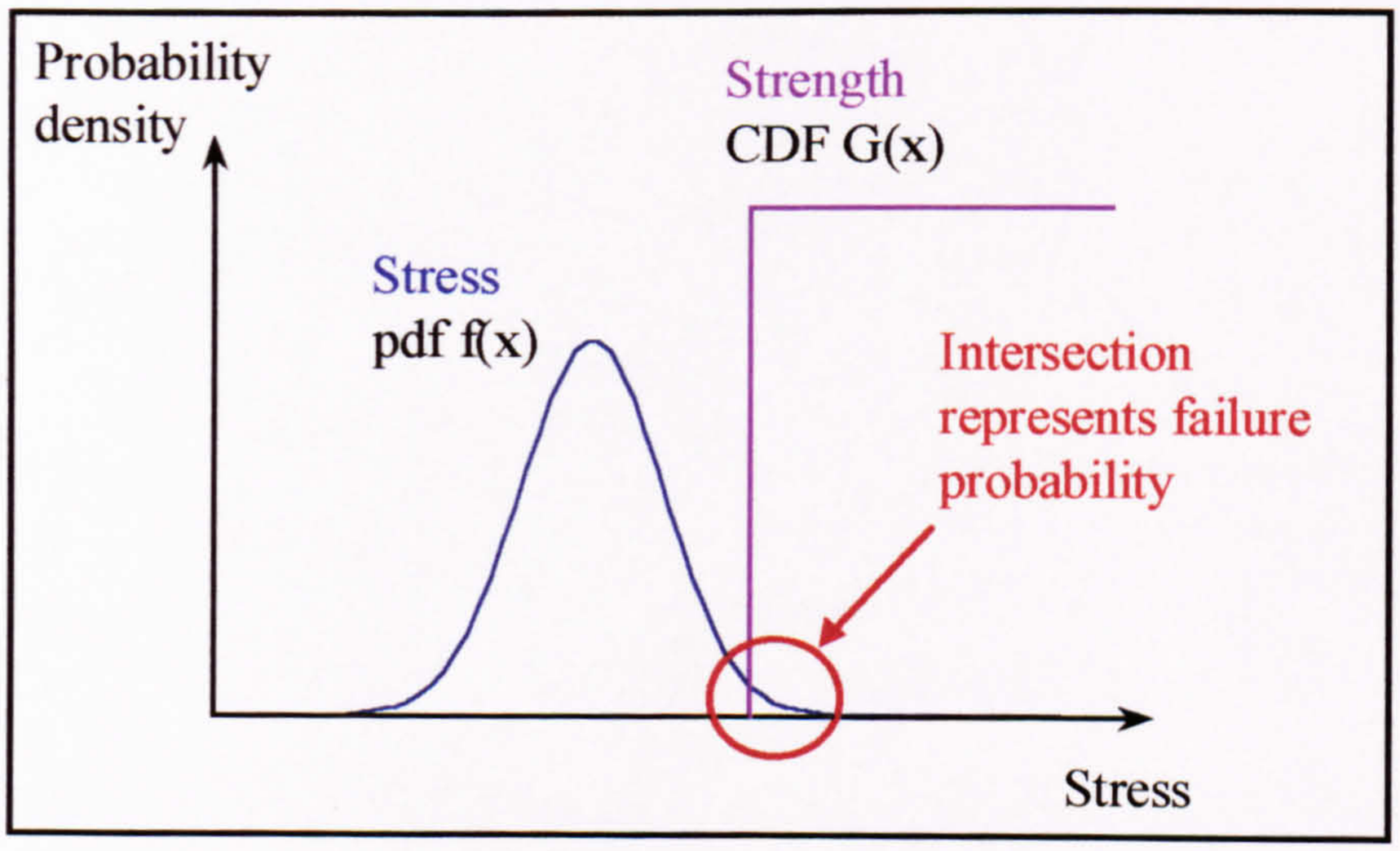

Figure 2.9 : Interference of Stress and Strength Distributions

The stress strength interference for an example damage process is depicted in Figure 2.9, which graphically represents the interference between the PDF of the stress or load f(x) (actual damage), and the CDF of the strength G(x), the allowable damage. This could represent the value of critical crack length in the case of a fracture mechanics damage model, or a certain crack depth in corrosion. Since this allowable damage level is fixed, the CDF G(x) is depicted as either 0 or 1, as in Figure 2.9.

2.6.2 Application of SSIM

The SSI method may be applied to a variety of failure mechanisms. The general principles were developed for use in structural reliability analysis **[Freudenthal, 1947; Melchers, 1987]**. The techniques developed have been applied to model degradation due to fatigue **[Carter, 1986]** and corrosion **[Strutt and Allsopp, 1993]**, where the two distributions are used to represent actual damage (stress) and allowable damage (strength). If there is no intersection, this defines a period of intrinsic reliability, where there will be no failures. The SSI method has also been applied by **[Spigel, 1991]** for the calculation of safe-life of rotorcraft components, in a technique called Stress-Strength-Time (SST). The inclusion of time allows for the degradation of strength with increase of age.

The application with the greatest potential for use in this work is that of **[Carter, 1986]**. The theory developed in **[Carter, 1997]** is applied to a series of mechanical components and distinguishes between two separate types of failure:

i. Stress-rupture, whereby the failure of a component results in a terminating event e.g. fracture. In this situation, the load and strength distributions are fixed; the loading of a component does not reduce its strength until failure occurs. When a particular stress is applied to a particular component, if failure does not occur, then it will not fail in the future, irrespective of the number of applications.

ii. Wear-out, whereby the repeated application of varying stresses to a component may cause internal damage that reduces the strength of that component without necessarily causing failure. In this case, the strength distribution will alter during the life of a component, e.g. cumulative fatigue damage at a micro-structural level.

The physical failure mechanisms to be considered for a transmission system, i.e. wear, corrosion and fatigue, belong to category **(ii)** above i.e. *wear-out* failure modes. Each of these may be represented as in Figure 2.10. This shows an example of linear damage growth against time, either calendar based (for corrosion damage) or flying hours (load cycles). This could represent damage accumulated by fatigue (proportion of fatigue life consumed), corrosion (pit depth) or wear (material loss). However, the term damage could represent anything from the alignment of a seal to accidental damage caused by human error. The distribution for the damage parameter is due to uncertainties in the model (or parameters within the model) and/or the physical variability of the material considered. Figure 2.10 shows the statistical distribution of this growth in damage at a particular time or N (number of cycles).

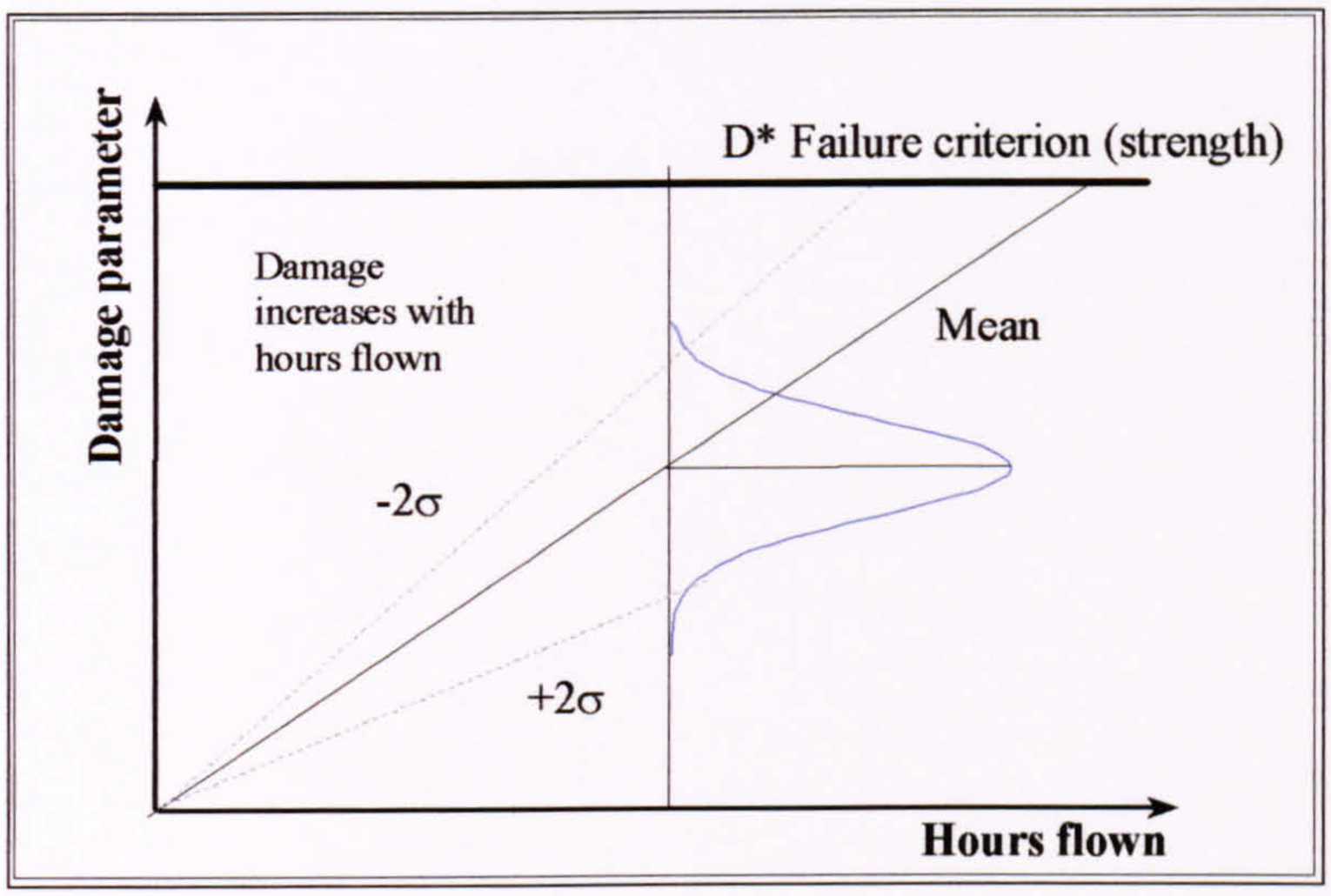

Figure 2.10 : Representation of damage growth process

As an example of a failure mechanism, the amount of fatigue damage (dependent on cycles N), will increase during a component's life - the mean damage increases and the damage variance may also change. Likewise, the residual strength distribution will also change with time - the mean could decrease with a change in variance as well. Hence the intersection of the two distributions will increase with time, and the probability of failure increases. This allows a **characteristic life (or safe life)** - the predicted time of failure at some probability of occurrence **[Strutt et al, 1995]** - to be calculated for a particular probability of failure **p***, shown in Figure 2.11.

This nomenclature will be used throughout this work, whereby **p*** is the 'acceptable' or required probability of failure for which there is a characteristic life at some confidence level. The quantity p(F), probability of failure, varies with time to failure (Figure 2.11).

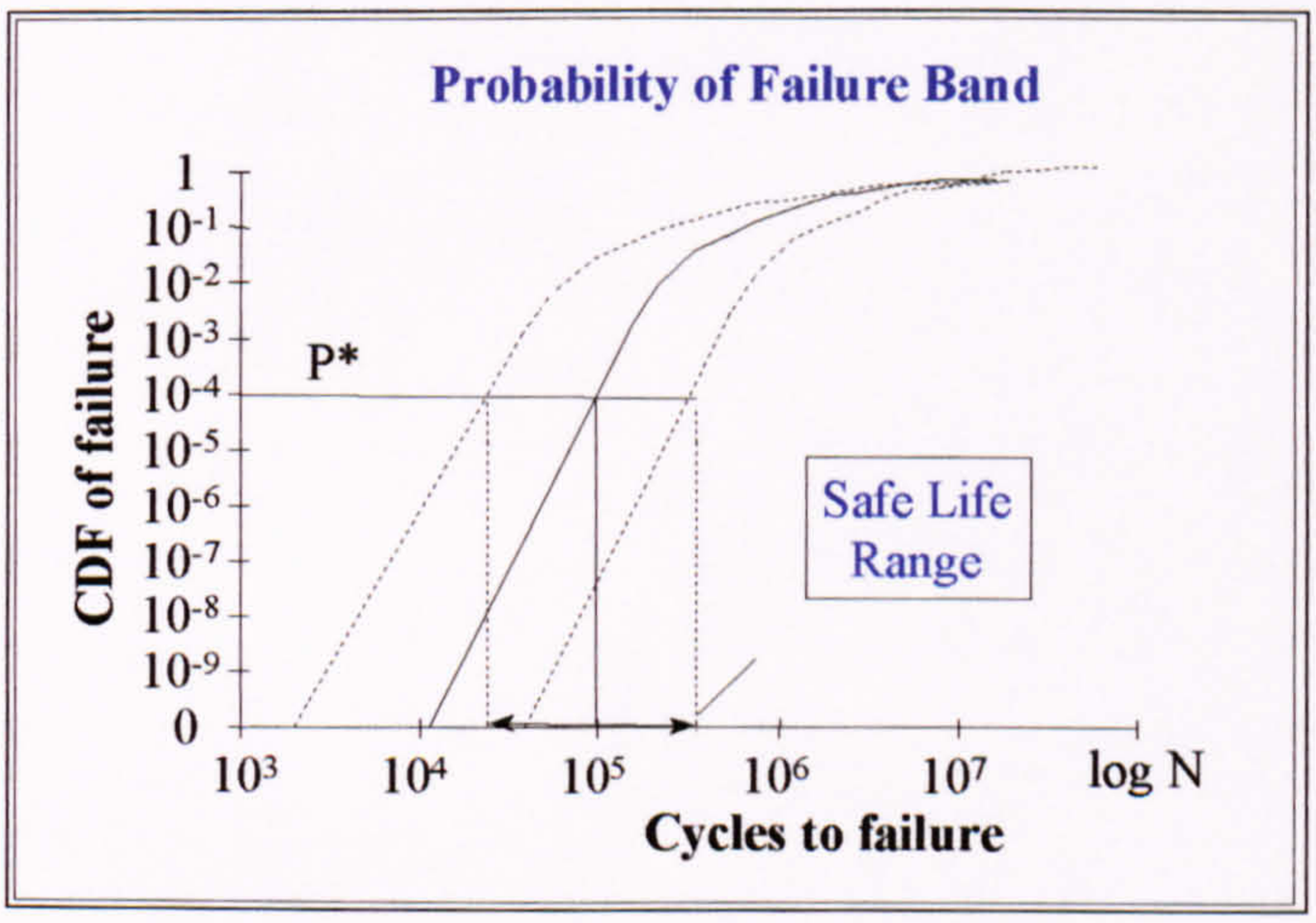

Figure 2.11 : Illustration of probability of failure bands [Strutt et al, 1995]

2.7 System Reliability

The modelling of system reliability for mechanical systems is in a less developed state than for other applications, e.g. electronics. Techniques currently in use have been described in Sections 2.4.2 and 2.4.3. Given the current lack of data with which to build accurate damage models, the most useful existing techniques are those of Astridge **[1996b]**, Savage **[1994]** and Martin **[1980a].** The latter author also considers the different types of failure **[Davies, 1972]** that may occur (Figure 2.12):

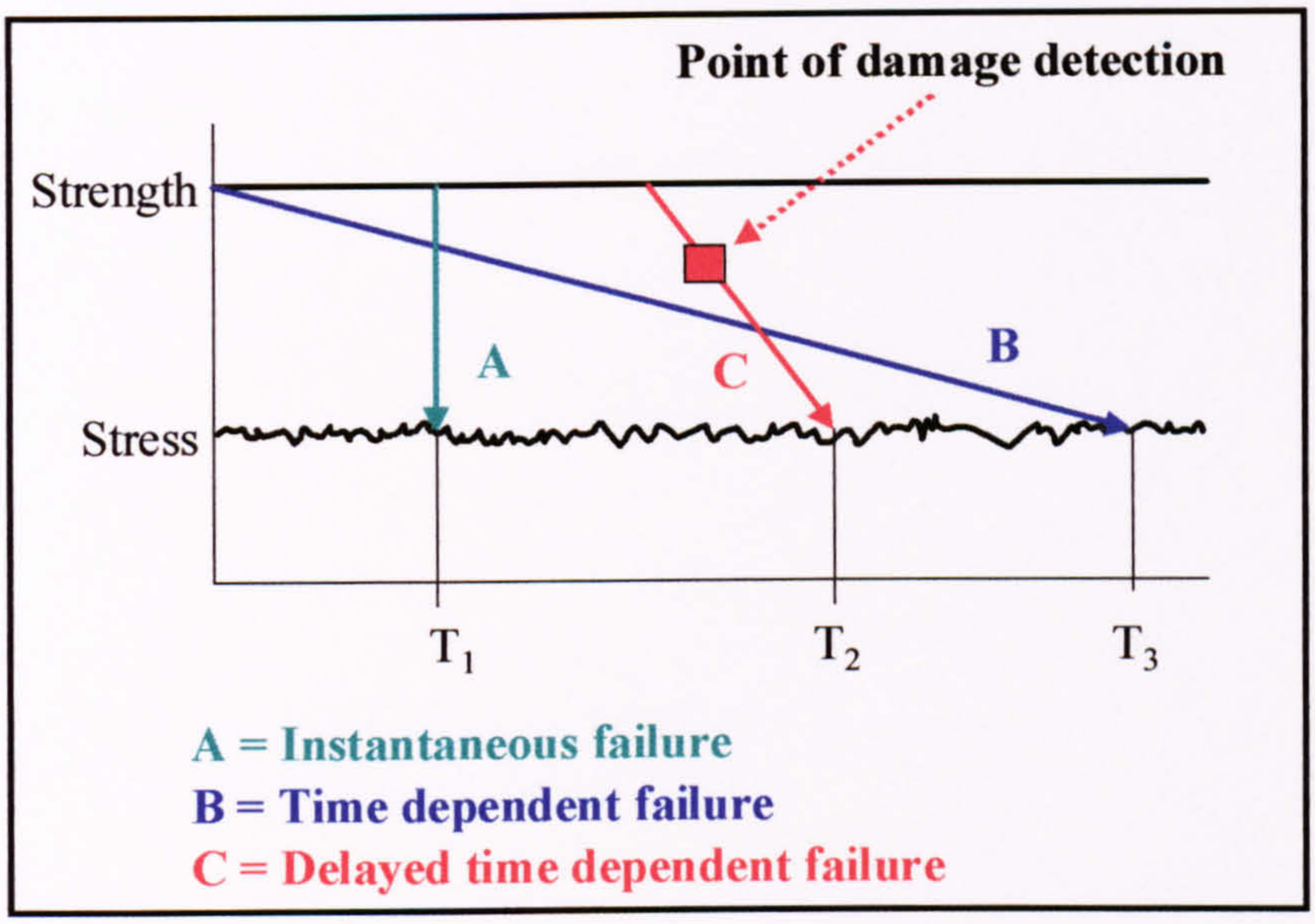

Figure 2.12 : Mechanical Failure Types
[Martin, 1980a; Davies, 1972]

a) Instantaneous – An instantaneous collapse of the margin between stress and strength, cf. Stress-rupture in Section 2.6.2

b) Time-dependent failures – A gradual reduction in the margin between stress and strength.

c) Delayed Time-dependent failures – The deterioration of the component may be detected before actual failure takes place.

The probability of the failure being detected before failure occurs may be used in order to calculate component reliability. This idea **[Martin, 1980a]** has been applied in this thesis work, by including the POD of non-instantaneous failure mechanisms in the reliability calculations, Chapter 4.

2.7.1 Failure Events for Mechanical equipment

The inter-relationships of failure events in mechanical systems can be of three different types, as summarised in Sections a) to c) **[Martin, 1980a].** His work has included the application of probability theory to the formulation of expressions for system reliability.

a) Mutually exclusive

The occurrence of any one event will cause system failure. When replaced however, the occurrence of the first event dictates that the other potential failure events will not then occur. If there are n potential failure events, F_1, F_2 etc, the system failure probability, $\mathbf{p_{sys}}^*$ may be written as:

$$\mathbf{p_{sys}}^* = p(F_1) + p(F_2) + p(F_3) + \ldots + p(F_n) \qquad (2.11)$$

b) Independent

The occurrence of any one of the potential failure events will cause system failure, and the occurrence of this failure event would have no influence on the occurrence of others. If there were two potential failure events, F_1, F_2, the system failure probability, $\mathbf{p_{sys}}^*$ may be written as:

$$\mathbf{p_{sys}}^* = p(F_1) + p(F_2) - p(F_1) \,.\, p(F_2 \mid F_1)$$

$$= p(F_1) + p(F_2) - p(F_1) \,.\, p(F_2)$$

$$= 1 - \{[1-p(F_1)].[1-p(F_2)\} \qquad (2.12)$$

If there were n independent failure mechanisms, it may be shown that

$$\mathbf{p_{sys}}^* = 1 - \prod_{i=1}^{n} \{1-p(F_i)\} \qquad (2.13)$$

which is the same as the Product Rule for reliability, written as

$$\mathbf{R_{sys}} = \prod_{i=1}^{n} R_i \qquad (2.14)$$

c) Conditional or Consequential

If the potential failure events were consequential, then the occurrence of any one event results in a 'knock-on' effect whereby all failure events occur. Failure events F_1, F_2 etc are considered as subset of failure event F_n, and system failure probability is:

$$\mathbf{p_{sys}}^* = p(F_n) \qquad (2.15)$$

2.7.2 Mechanical series Chain

In order to calculate the reliability of a mechanical system as a whole, the reliability of each component part must be calculated. The Reliability Block Diagram (RBD) for a

simple series system is shown in Figure 2.13, a series mechanical chain, where failure of one component will lead to failure of the gearbox. The reliability of such a series system is as below **[Carter, 1997]**:

$$R_{sys} = \prod_{i=1}^{k} R_i = R_1.R_2.R_3...R_k \qquad (2.16)$$

where R_{sys} is the reliability of the system,
R_1, R_2 etc. are the values for the reliability of the component parts of the system.

Figure 2.13 : Reliability Block Diagram of a Series System

As emphasised by Carter, this simple product rule is only truly valid when components are independent from each other. This is rarely the case for a mechanical system, and is certainly not true of a helicopter transmission system model **[Astridge, 1996b; Savage et al, 1988]**. In the gearbox under consideration, each component will suffer damage of a particular form which accumulates at a rate dependent on the operating environment i.e. load, temperature, lubrication. The loads experienced by each part are highly correlated, and there is also dependency due to common maintenance periods.

Equation 2.16 (the '*Product Rule*') will produce different results depending on the Loading Roughness (LR), Section 2.6.1. When the LR is zero, i.e. when the system load has one unique value, all elements of the system will contribute to the system reliability **[Carter, 1986]**. If the LR is one, when the strength has one unique value, the system reliability will equate to that of the least reliable part. With an intermediate value of loading roughness, the system reliability will lie between these two values, as follows:

$$\prod_{i=1}^{k} R_i < R_{sys} < R_{min} \qquad (2.17)$$

where $\prod_{i=1}^{k} R_i = R_1.R_2.R_3...R_k$,
R_i is the individual unit reliability and
R_{min} is the individual reliability of the first unit to fail

2.8 Analytical and Numerical Techniques

For a system of components within a system, there are two main alternatives for the solution of the reliability model. The problem may be solved either analytically, an example being FORM and SORM, or numerically using Monte-Carlo Simulation, for example. These two approaches both have their own advantages.

2.8.1 Analytical Approach

A typical analytical method for solving the problem of multi-dimensional system reliability is that of the First or Second Order Reliability Model (FORM/SORM). If the probability of system failure can be represented as equation 2.18, then the solution becomes a complex integral in multi-dimensional space.

$$f(x) = \int_{\underline{x}} \Phi(\underline{x}) \, d\underline{x} \qquad (2.18)$$

where $\underline{x}$ is a vector of design variables.

The FORM and SORM techniques were developed to give an approximation to this integral **[Ditlevsen and Madsen 1996, Ebbeler et al 1995]**, in which:

a) variables $\underline{x}$ are transformed into normal variables, thus transforming $\Phi(x)$ into a standard normal density function.

b) the area where failure is defined (or "limit state") is approximated by an area bounded by a plane (first order) or a second order surface (second order).

c) the probability of failure p_f may be computed using the newly defined $\Phi(x)$ and the transformed variables.

The FORM and SORM techniques have not been employed in this work since the failure modes have been considered as independent mechanisms as a first approximation. The techniques are also potentially unstable for complex, non-analytical failure models **[Ebbeler et al, 1995]**.

2.8.2 Numerical Approach

A typical numerical method of solving complex system problems is Monte-Carlo Simulation (MCS). The technique makes use of random number generation in order to produce artificial data for use in statistical analysis, described in BS 5760 Part 5 **[BSI, 1991]**. The main element of a Monte-Carlo simulation procedure is the generation of random numbers from a specified distribution **[Ang & Tang, 1984]**; these are then used to reproduce virtually any stochastic process and its statistical distribution.

MCS is particularly useful where there is an absence of significant test data, which would normally be used to model the reliability of a component or system. This is particularly true for the gearbox under consideration; to derive a value for the system reliability of a population of gearboxes would require years of operational experience that is clearly not available for new designs. MCS can provide a way for simulating the degradation of thousands of gearboxes subject to statistical variation in materials for the failure mechanism of corrosion, see Chapter 9.

2.8.3 Markov Analysis

Some systems may be viewed as being able to occupy one of a number of "states", which could represent functioning and non-functioning states; for a transmission system they could include load and lubrication states. The probability of the transitions between states would depend on the prior states. However, if this *transition probability* depends only on the current state then the transition process may be modelled by a *Markov* Chain **[Ang and Tang, 1984]**.

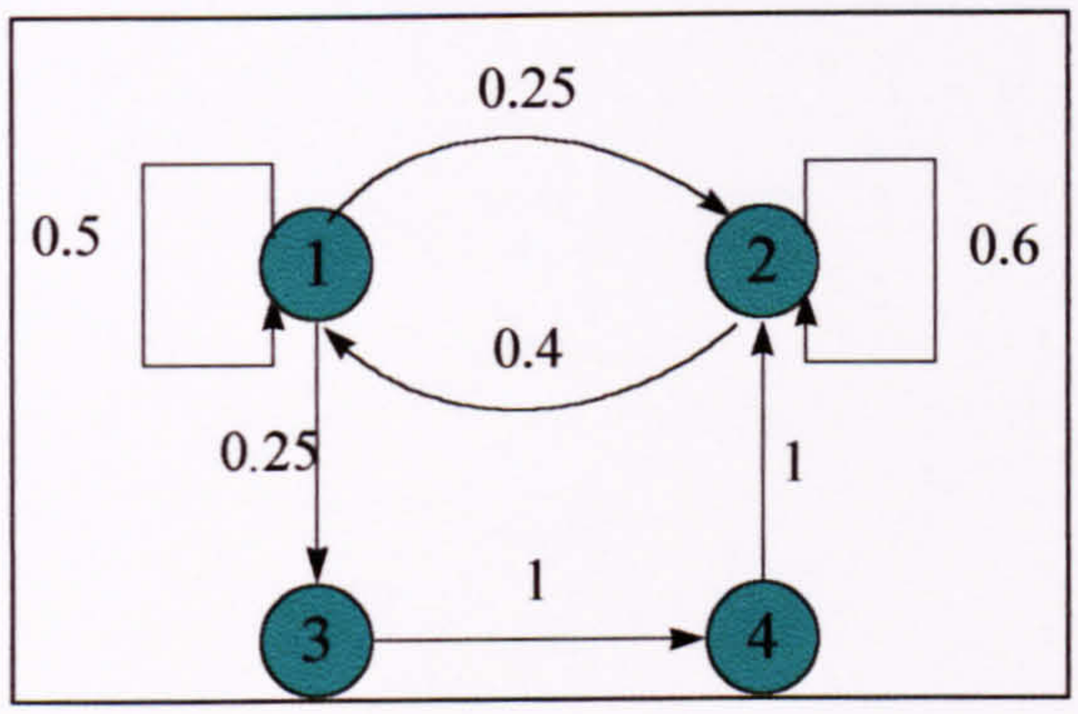

Figure 2.14 : Transitional Probabilities of Markov Chain

An example of a Markov Chain is given in Figure 2.14, where each circle is a 'state', representing a condition of a component, e.g. correct functioning, breakdown or repair. An arrow represents the probability of remaining in each state or moving to another state, with a figure for probability alongside.

Markov models may be used to represent any process that can be considered as a sequence of discrete states. This may include the analysis of machine availability or damage processes. Although mainly used for the modelling of discrete states, they may also include the effects of continuous processes, where each state describes a separate process.

2.9 Summary

The techniques currently available for the reliability analysis of a transmission system are not capable of providing a complete method of quantifying the estimated life. Most system reliability techniques rely heavily on existing data of past component failures. No details of the loads or environment are retained with such failure data, and often failures are few and far between, as should be the case for flight critical components. Nevertheless, the designer, operator and maintainer need some method of predicting system vulnerabilities. The probability functions developed so far have mainly been aimed at fatigue life prediction, although there has been limited work in the fields of wear **[Kececioglu and Koharcheck, 1983]** and corrosion **[Strutt and Allsopp, 1993]**. The system reliability models that do exist are based on fatigue only **[Savage et al, 1994]**, or are based on historical data with applied engineering judgement **[Astridge, 1999]**.

3 Description of Intermediate Gearbox and Failure Mechanisms

3.1 Introduction

This chapter will describe the object of study for which this thesis is written. Helicopter gearboxes consist of generally complex mechanisms with multiple load paths, which was one reason for choosing the intermediate gearbox. Notwithstanding this apparent simplification, the techniques employed for the analysis of the IGB could be applied equally well to a more complex transmission system. Indeed, other mechanical and electrical system could be similarly analysed.

For the purpose of this thesis, two different types of helicopter have been studied; these will be referred to as Type A and Type B for the remainder of this work. The Type A (first flight 1960s) is a military helicopter used in the Anti submarine warfare (ASW), Airborne Early Warning (AEW) and Search and Rescue (SAR) roles. A large service history exists for this helicopter. The Type B (first flight 1990s) has been designed to more recent standards. It too is a multi-role helicopter, with both civil and military variants.

The chapter provides a description of the IGB configuration, and goes on to document the principal failure mechanisms that can occur. The actual failure types that have been recorded are tabulated, from which the key models are identified. Chapter 7 also contains additional maintenance and failure data analysed for the Type A.

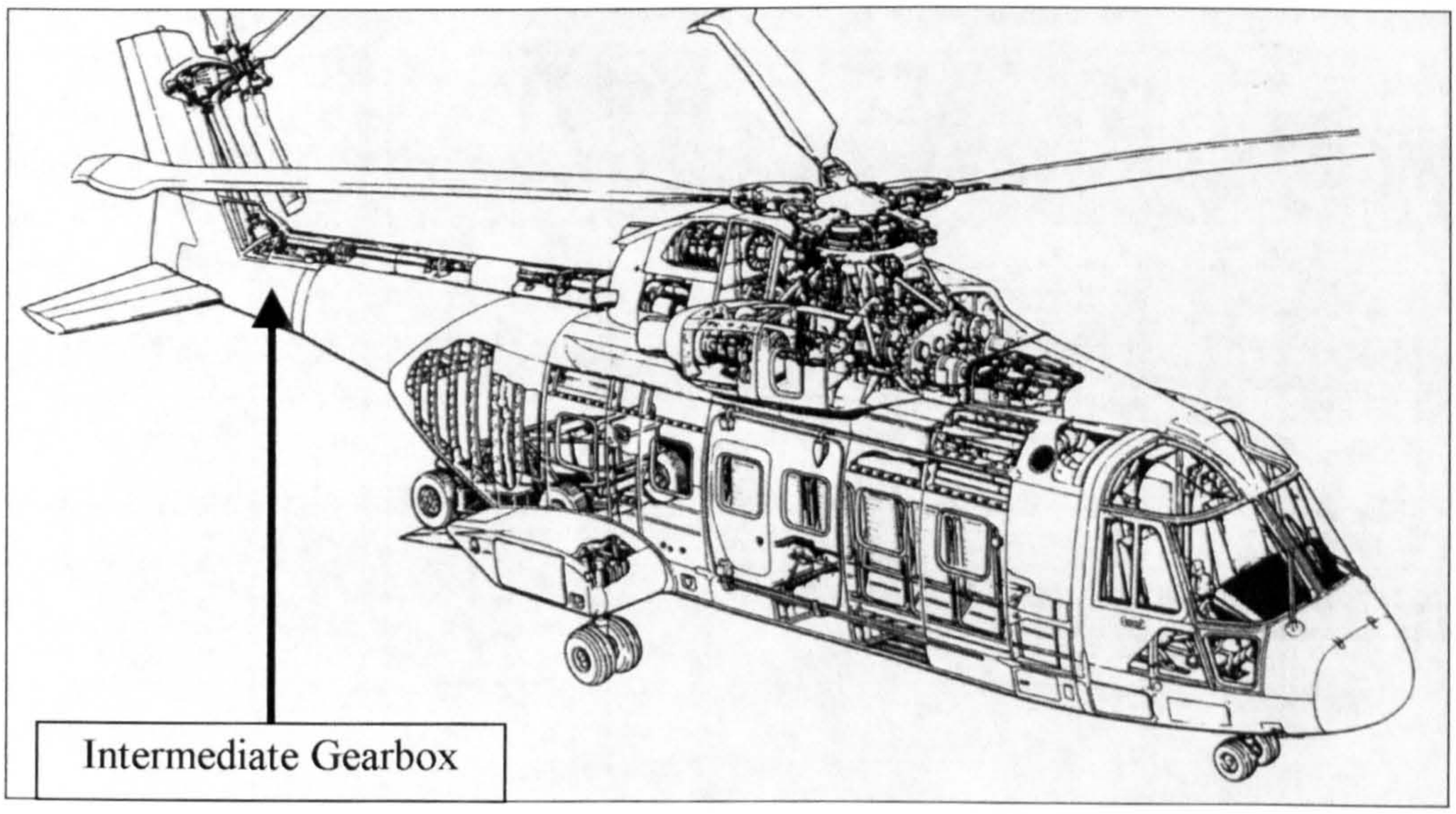

Figure 3.1 : Cutaway drawing showing location of IGB [Jane's All the World's Aircraft 1997/98[1]]

[1] Reproduced with permission from Jane's Information Group

3.2 Intermediate Gearbox

The IGB is located as shown in Figure 3.1. Its function is to transmit torque from the drive shaft leading from the main gearbox (MGB) to the tail rotor drive shaft. In both the Type A and Type B helicopters, the IGB consists of a spiral bevel gear pair, enclosed in a sealed casing. The input and output shafts are held in place by two sets of bearings. The input and output shafts within the gearbox are connected to the drive train by means of splines which form a coupling for transmission of input and output torque. In the Naval variant, where helicopter parking space is at a premium, the input shaft carries a Disconnect "dog-tooth" Coupling, which allows the tail boom to be folded. This coupling is not considered within the scope this work, since it is external to the gearbox.

The level and type of lubrication between the components influence all internal gearbox failure mechanisms. For this reason, a short description of the types of lubrication regime is given, in addition to the principal failure mechanisms.

A general schematic view has been drawn up as Figure 3.2, showing the basic components of the transmission system for both helicopter types. The main items not visible in the figure are the oil pump and filter system, plus the disconnect coupling, the latter not being within the scope of the target system.

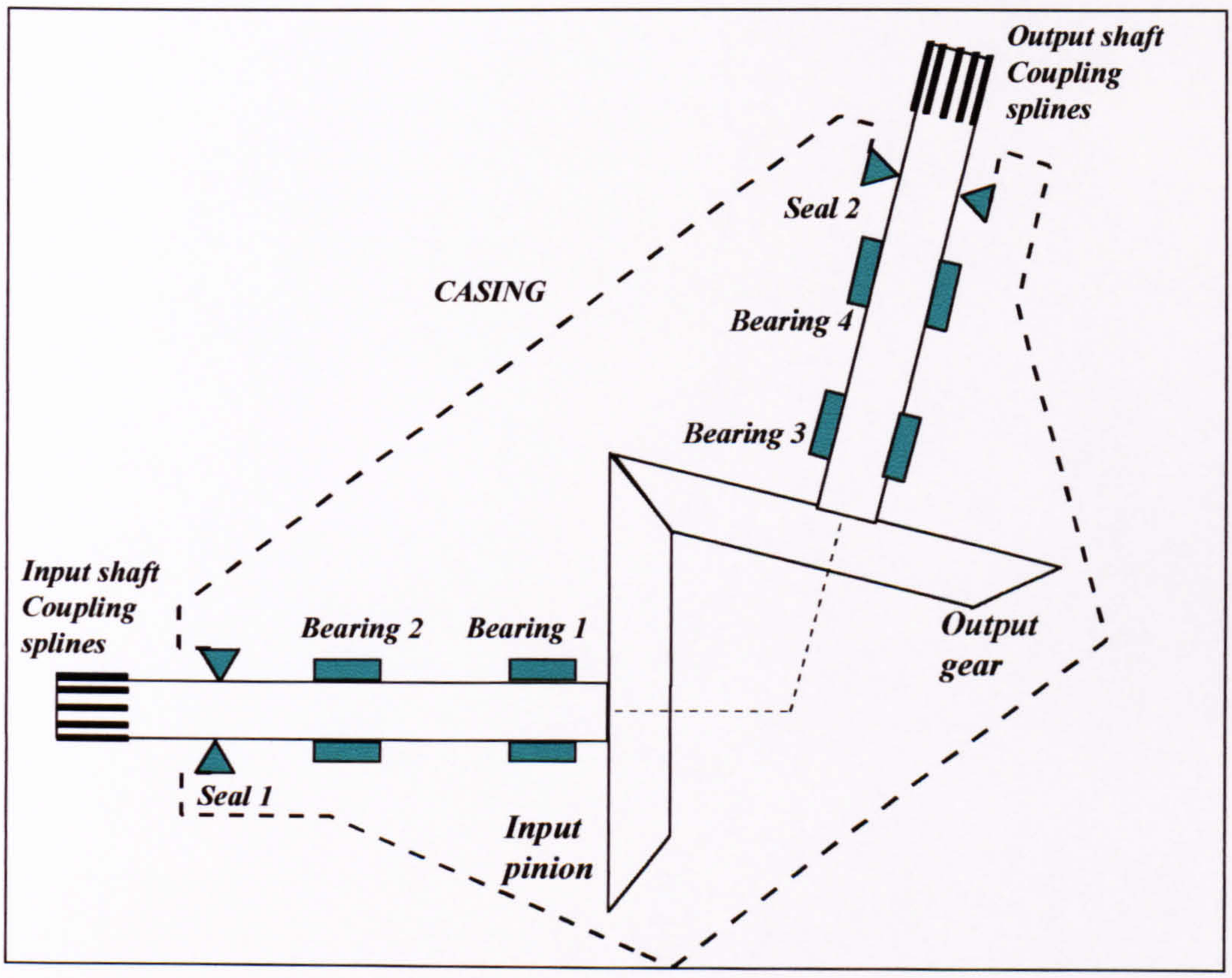

Figure 3.2 : Schematic Intermediate Gearbox

3.3 Intermediate Gearbox Components

3.3.1 Gear and shaft

The input shaft and pinion (driver) are manufactured from a single forging, as are the output shaft and gear (driven). They are both high-grade steel, S156 steel in the case of the Type A, AISI 9310 for the Type B IGB. The steel for both components is manufactured by the Vacuum Induction Melt - Vacuum Arc Remelt (VIM-VAR) process to ensure the highest level of purity and homogeneity **[Astridge, 1989]**.

The surface of the teeth are case-carburised to give enhanced durability against wear, as are certain areas of the shaft, in particular the area in contact with the bearings and the male coupling splines.

3.3.2 Bearings

The bearings used in the IGB provide axial and radial support to the input and output shafts and gears. The Type A IGB has four taper-roller bearings; the Type B IGB has angular contact ball bearings outboard on both shafts, and plain roller bearings inboard. The rolling elements are made from high quality alloy steel, typical examples being SAE8719, SAE8119 and SAE8019.

3.3.3 Seals

Radial lip seals are used on both input and output shafts to prevent oil leakage from around the rotating shaft and bearings. They also function to guard against contamination from outside sources e.g. dust, sand etc. Typical materials are of a fluoro-elastomeric material (e.g.VITON^{TM}) or silicone rubber. A garter spring is used to maintain radial pressure of the seal on the shaft to prevent oil leakage.

3.3.4 Casing

The Type A casing is made from magnesium casting alloy (AZ91C), to provide a light yet rigid containment for the transmission. It must also be able to react the forces from the gears within the casing. As will be described in Section 3.9 however, the casing is retained to the airframe by means of steel bolts, raising the prospect of galvanic corrosion. The casing has a chromate conversion coating and epoxy resin sealers **[Astridge, 1989]** that serve to guard against corrosion in the atmospheric conditions likely to be encountered e.g. marine air.

An alternative casing material for the Type A is magnesium alloy WE43, which is studied in this work to compare its performance from a system reliability stand-point. The Type B gearbox casing is made from aluminium casting alloy (A357), with steel bolts used for fixing to the airframe.

3.3.5 Lubrication System

Lubrication of all the moving parts is vital to the gearbox operation. The gearbox lubrication system is designed to prevent premature component failure, assure reliable operation, and increase the service life of the transmission **[Brink et al, 1993]**. Various methods of oil circulation are used for different transmission systems, and the oil normally contains an Extreme Pressure (EP) additive. This provides emergency lubrication between components in the case of oil system failure/loss.

The Type A gearbox is lubricated by the action of the gear teeth dipping into the oil at the bottom of the gearbox housing - *splash lubricated* type. Oil is circulated by the rotating shafts and gears without a pump or filter system and is channeled by oil ways that ensure that oil is fed to bearings. The output shaft includes a spiral ring that operates on an 'Archimedes screw' effect to feed oil to the uppermost (outboard) bearing.

The Type B gearbox is lubricated by a more complex oil circulating system, with an oil pump driven by the one of the gears. This ensures that the oil circulates via ducts in the casing and oil jets aimed at critical components such as gear contact areas and bearings. The temperature and pressure of the oil is monitored constantly during flight, and an oil level transducer measures the quantity of oil before and after flight.

The most common causes of lubrication-induced failure are contamination, incorrect oil/additives or loss of oil from the system. The condition and quantity of the oil is therefore monitored in order to detect the onset of damage to any of the gearbox components. In the Type A gearbox, a Magnetic Chip detector (MCD) is fitted, which detects the presence of magnetic debris (e.g. from wear) in the oil and feeds a warning lamp in the cockpit. The detector is combined with a magnetic plug, which serves to attract ferrous debris; this is removed and analysed at regular intervals. The Type B IGB has a more advanced sensor system and is fitted with a detector which can estimate the quantity of metallic contamination in the oil; a quantitative debris monitor (QDM^{TM} - see Section 5.2.2).

3.4 Loading of Components

The transmission shafts connected by the IGB rotate at constant speed. The requirement to change the turning moment provided by the tail rotor is achieved by changing the pitch angle of the tail rotor blade. The torque transmitted via the IGB is proportional to the turning moment that the tail rotor must provide to:

a) balance the turning moment of the main rotor, and

b) yaw the helicopter about the vertical axis when required for a manoeuvre, e.g. spot turn when in the hover.

The torque is transmitted from the input to the output shaft via the spiral bevel gear pair (Figure 3.2), so that each tooth is subject to both tooth root bending and Hertzian

Contact stresses. These values can be calculated using standard texts and industry standards such as **[Shigley, 1986; AGMA, 1986]**, as shown in Appendix B.

The geometry of the spiral bevel gearing is such that the tooth stresses will be reacted by radial and axial forces in the gears, and hence the shafts. This will induce additional stresses in the bearings and in turn the gearbox casing, which are used both to support and locate the gears. The stresses experienced by the gears, shaft, bearings and casing are therefore directly related to the level of torque transmitted through the IGB.

All helicopter gears are designed using a '*design spectrum*', a given set of torque values that are a conservative estimate of loads to be experienced in service. This normally takes the form of a spectrum of transmitted torque values, each with an associated percentage of time. This design spectrum is correlated with the manoeuvres that the helicopter is expected to perform. The number, type and sequence of these manoeuvres depend to a large extent on the role for which the helicopter is designed.

Additional loads over and above the design spectrum are referred to over-torque or shock loads. These are normally attributed to operational errors in which the pilot may have been forced to perform an emergency manoeuvre that produces a large step change in torque transmitted to the tail rotor. Other causes are tail strikes in which the tail rotor may inadvertently come into contact with the ground, trees etc. It is also possible for the tail rotor to be struck by loose debris if the helicopter is operating at low level or on deck.

3.5 Lubrication Regime

There are three types or regimes of lubrication that may be present within a transmission system **[Drago 1988, Ku 1980, Gohar, 1988]**; hydrodynamic, elasto-hydrodynamic (EHD) and boundary lubrication (BL). These regimes refer to the ratio of composite surface roughness to the lubricant film thickness that separates the moving components, a ratio defined as the specific roughness, $1/\Lambda$ **[Dawson, 1965]**.

The rotating gears and bearings within the transmission system are designed to operate within the EHD regime, as described in Section 3.5.2. However, the boundary lubrication regime, described in Section 3.5.3, may be encountered during the following events:

- Engine start-up, when the oil is cold and there may be little or no layer of lubricant between components. This is particularly so in the case of the Type A IGB, which is "splash-lubricated".

- Times of heavy and/or possibly shock loading, when the high loading on components will increase the lubricant temperature, hence reducing its viscosity. This means that there will be a reduction in the thickness of the lubricant layer and therefore a greater degree of wear and fatigue damage.

- High operating temperatures, which cause the oil viscosity to decrease so reducing the separation between rotating components.

3.5.1 Hydrodynamic lubrication

For Hydrodynamic lubrication (HD) a fully developed lubrication film exists, which separates the surfaces of the gear teeth, or other components. The surfaces are assumed to remain undeformed under the load applied, and wear is negligible (Figure 3.3).

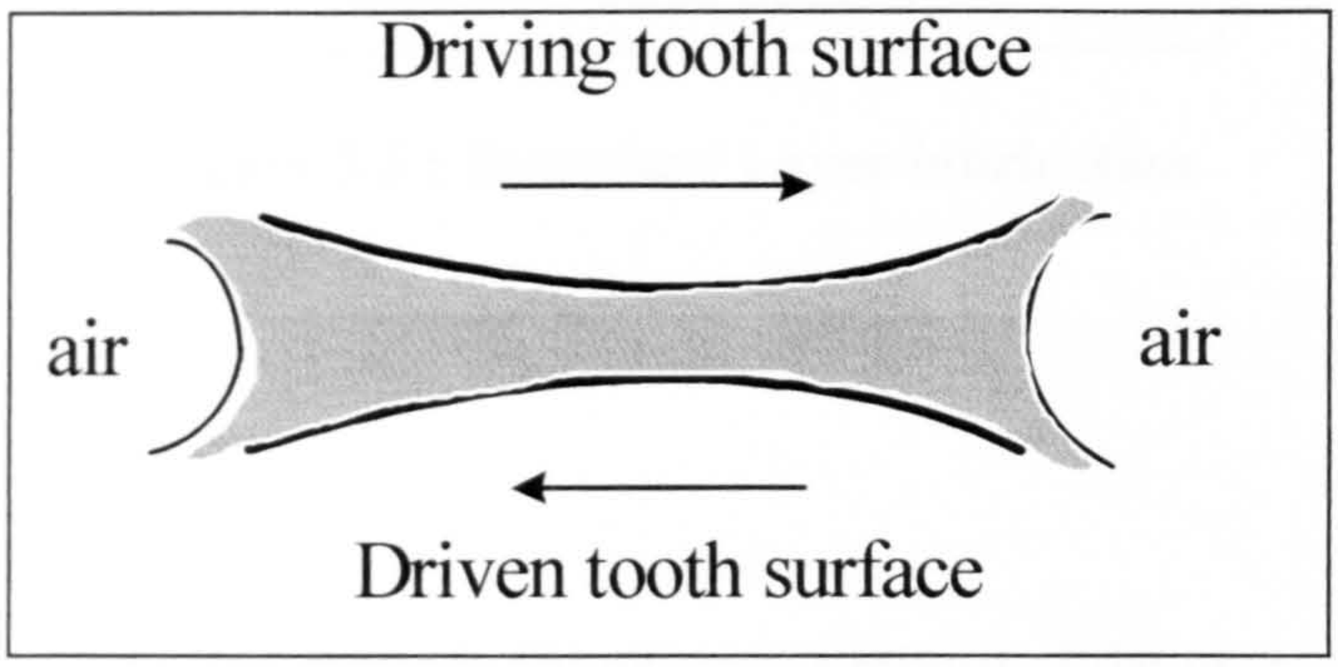

Figure 3.3 : Hydrodynamic lubrication

3.5.2 Elasto-hydrodynamic Lubrication

Under an elasto-hydrodynamic lubrication (EHD) regime, both the fluid properties of the oil and the elastic properties of the gears influence the width of the film separating the gear surfaces. This is the most common, and best attainable, lubrication regime for highly loaded gearing (Figure 3.4). A 'good' film thickness is typically a few microns, with a value for Λ of 2 to 3 **[Ku, 1980]**.

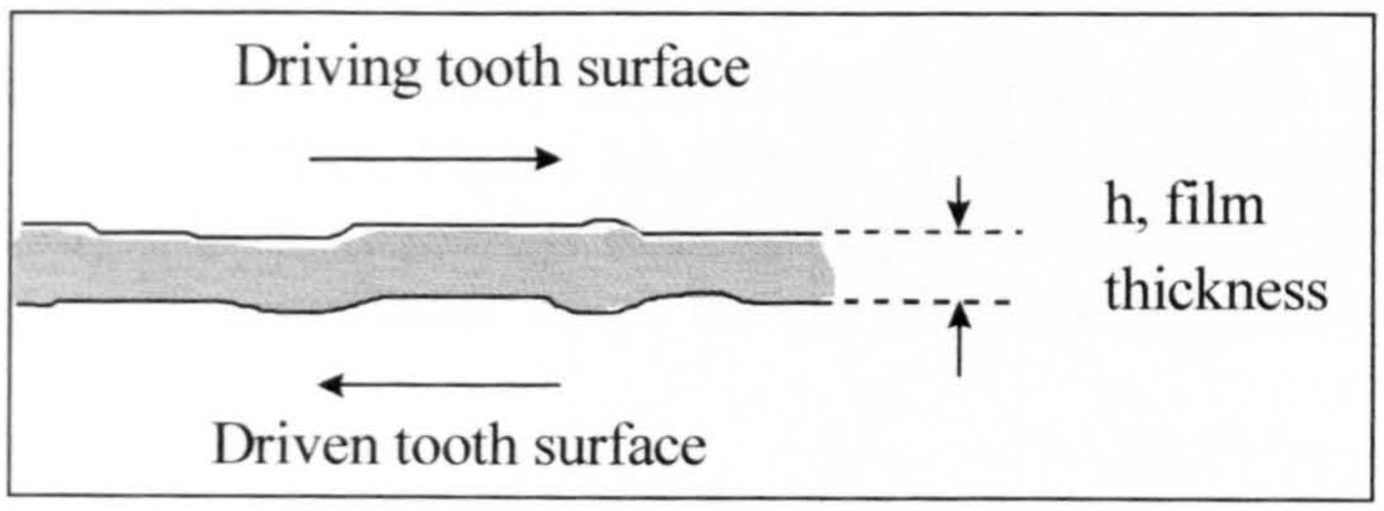

Figure 3.4 : Elasto-hydrodynamic lubrication

3.5.3 Boundary Lubrication

For boundary layer lubrication (BL) the layer of lubrication separating the surfaces breaks down and allows metal to metal contact (Figure 3.5). This may occur when high temperatures reduce the viscosity of the lubricant, and results in progressive wear or in extreme cases, scuffing.

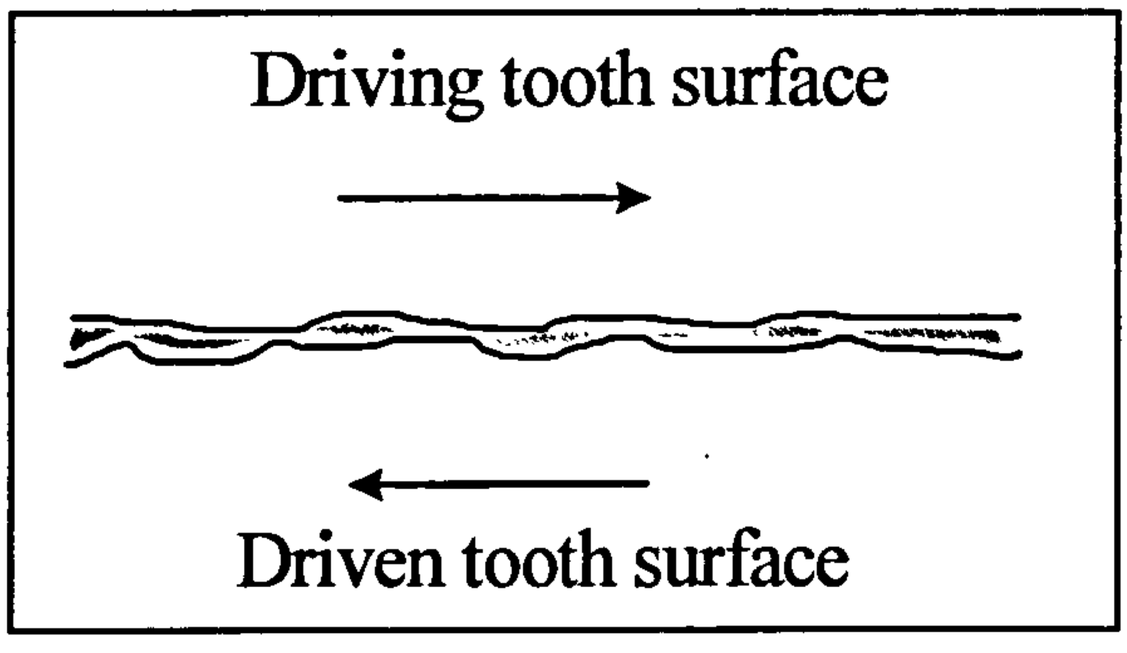

Figure 3.5 : Boundary Layer lubrication

3.6 Tooth Fracture

3.6.1 Overload fracture

Any extra-ordinary load that exceeds the ultimate strength of the gear tooth material can cause failure by overload fracture. This would lead to the static failure at the tooth root, which could occur suddenly and without warning. The likely causes of this event would be a tail-strike, where the impact of the tail rotor would send an abnormally high torque through the helicopter tail rotor drive-train.

In the case of the IGB, it is more likely that a tail-strike would cause an 'over-torque', a short period of time in which tail rotor torque exceeds the maximum value for any other manoeuvre. This would have the effect of increasing the rate of fatigue damage accumulation.

3.6.2 Tooth root Bending Fatigue

Failure by bending fatigue is normally initiated in the critical section near the tangency point between profile and fillet, Figure 3.6 **[Drago, 1980]**. Local stresses in excess of the material endurance limit, coupled with possible presence of non- metallic inclusions, lead to the initiation of microcracks within the slip planes of the gear surface **[Schijve, 1990]**.

The time for fatigue crack growth from the first appearance of a macro crack, quoted as 1mm **[Schijve, 1990],** to full failure is a small proportion of the total tooth life **[Drago, 1980]**. Gears are therefore normally designed with a fatigue life representing the crack initiation phase only. One characteristic of this failure mechanism is the lack of debris produced, in contrast to surface fatigue. Hence, there is little 'telltale' evidence of impending failure by bending fatigue **[Astridge, 1989].**

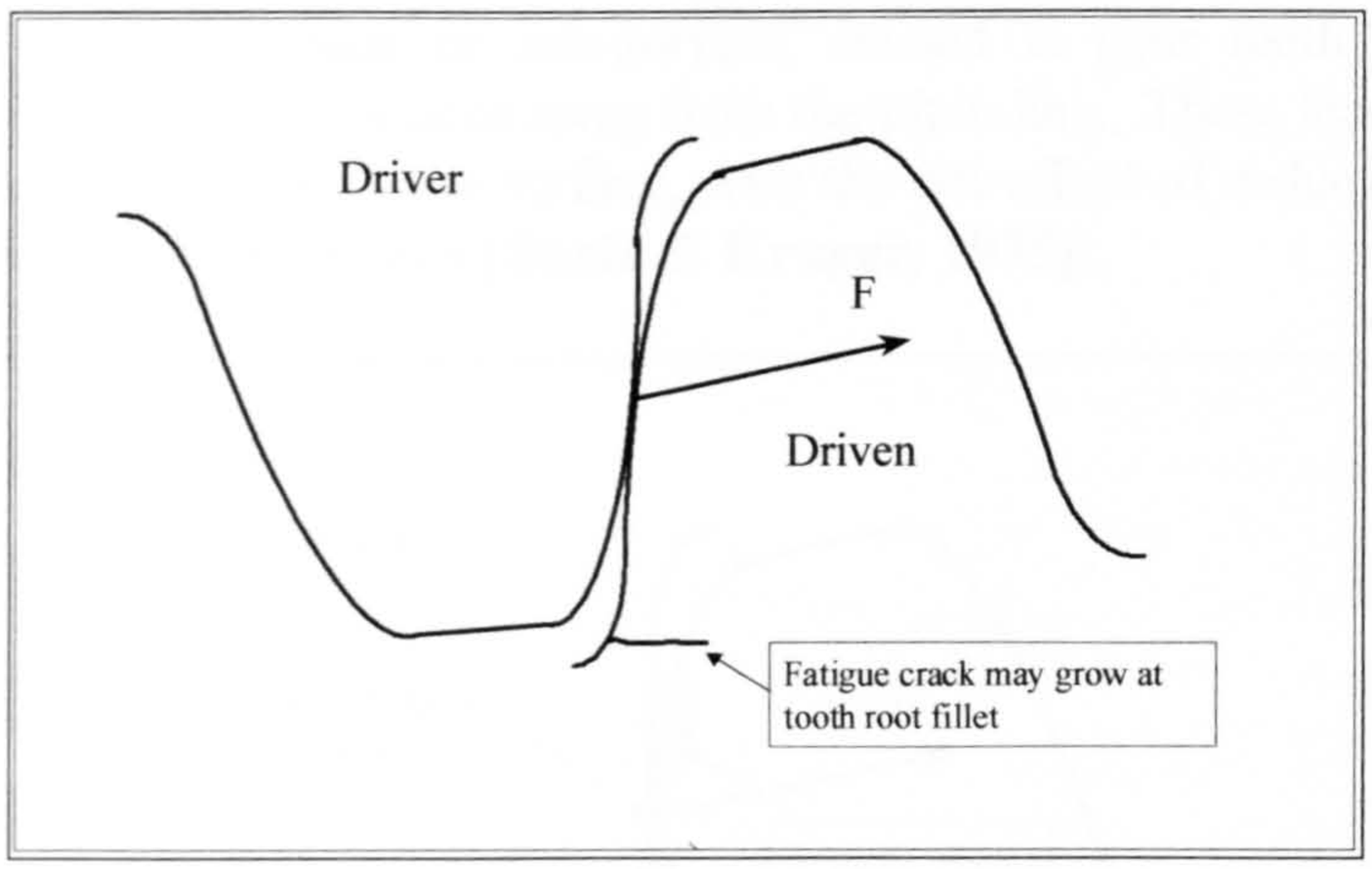

Figure 3.6 : Region where tooth root fatigue crack may grow

3.7 Surface Fatigue

Surface fatigue is a distinct type of damage separate from wear and is defined by BS7848/ ISO 10825 **[BS/ISO, 1995]** as "Material damage due to surface and subsurface stresses produced by the repeated application of forces. It is characterised by removal of metal and the formation of cavities". This failure mechanism may occur in both gear teeth and bearings and is frequently referred to as rolling contact fatigue (RCF).

This failure mechanism is caused by the cyclic nature of loading during the contact of two rolling parts, e.g. gear teeth rotating and meshing with each other. It is dependent on the number of load applications and is thought to be caused by the combination of the following stress fields exceeding the endurance limit of the material:

a) Repeated rolling (Hertzian) contact that develops a semi-circular pressure distribution and an induced reaction stress beneath the contact surface **[Bartz & Kruger, 1975]**. Cracks preceding pitting fatigue are controlled by shearing stresses which reach a maximum at a depth of **0.78a** where **a** is the smaller radius of the flattened area. In the case of gear teeth in mesh, the stress field so described exists only at the pitch line.

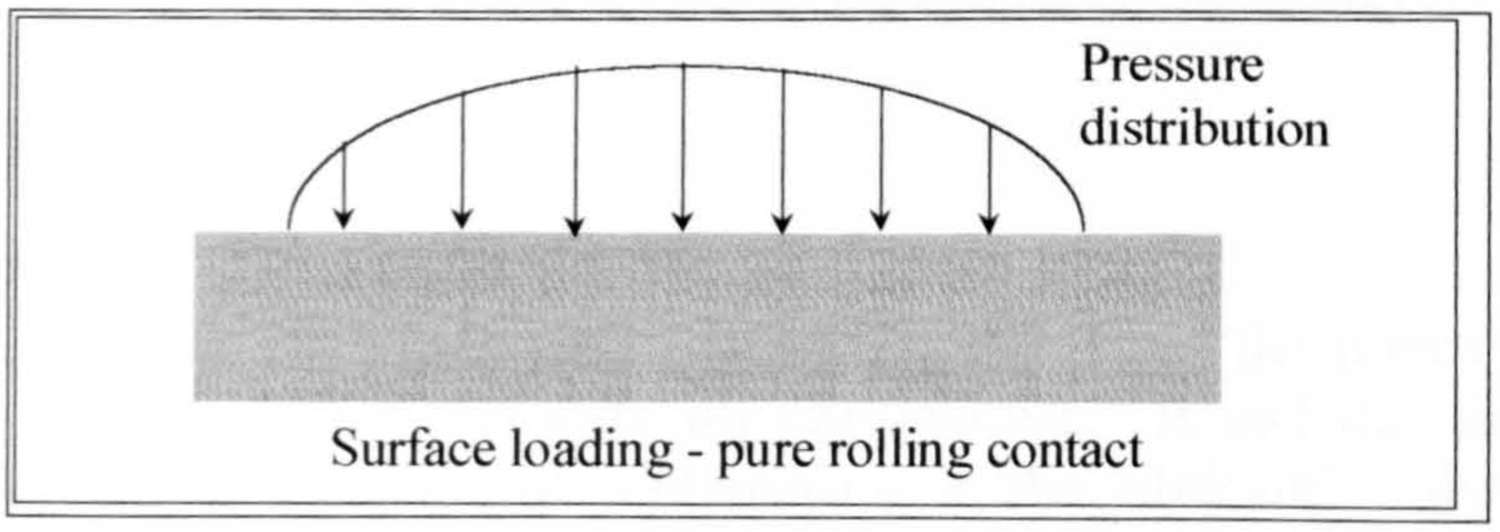

Figure 3.7 : Pressure distribution of gear teeth in pure rolling contact

b) Sliding stresses, surface or sub-surface, caused in gear teeth by the relative motion of contacting surfaces away from the pitch line. These lead to normal and shear stresses parallel to the surface, with the net effect of reducing the depth of the maximum shear stresses **[Bartz & Kruger, 1975]**.

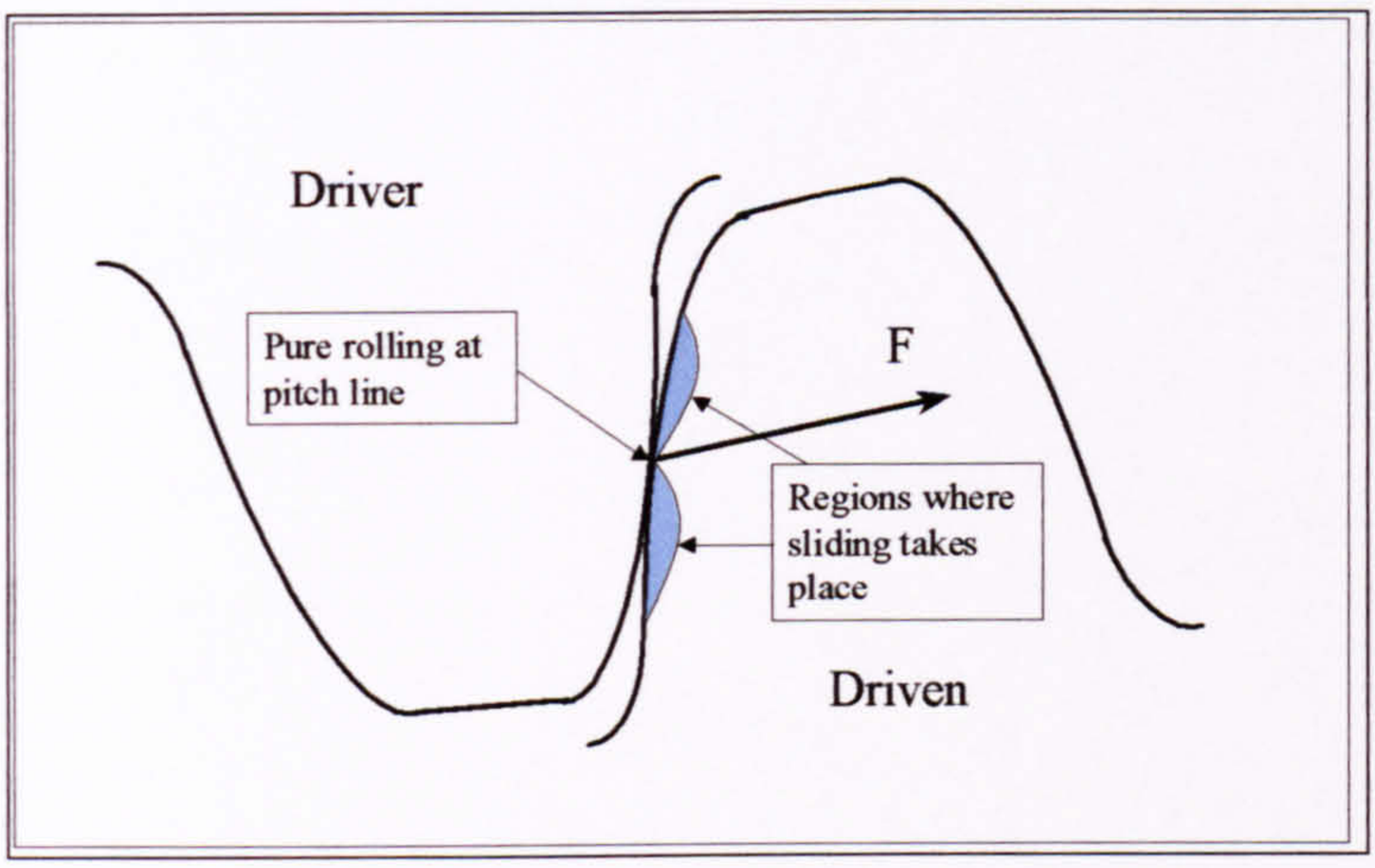

Figure 3.8 : Regions of gear teeth where rolling contact fatigue may occur

The combined effect of the above two types of relative motion (Figure 3.8) may cause the initiation of a fatigue crack; this may then propagate parallel to the surface under the influence of further application of loads from the repeated meshing process. When such cracks meet they isolate and remove a piece of surface material called a pit or spall **[Venkatesh & Krishnamurthy, 1980]**.

[Drago, 1988] distinguishes between the two terms *pitting* and *spalling*. Pitting is caused by sub-surface stresses (set up by pure rolling) exceeding the fatigue limit. Spalling may be caused by a higher level of sliding causing the maximum shear stress to occur at a point closer to the surface. The failure then occurs at or near the surface, which produces a spall of debris.

The surface fatigue mechanism is not immediately catastrophic in nature, but in the later stages metallic chips large enough to be detected by magnetic chip detector (MCD) will be present in the lubricant **[Drago, 1988]**. If left unchecked, this damage will spread across the entire contacting surfaces, and could lead to functional failure.

3.8 Wear

Wear is defined by BS7848/ISO 10825 **[BS/ISO, 1995]** as "the removal of material which occurs when two surfaces slide on one another. It includes the removal of material as a result of the action of contaminants in the lubricant". Wear may occur between gear teeth, interconnecting splines or between rotating parts of a bearing, and may be categorised as follows.

3.8.1 Adhesive wear.

Adhesive wear may occur between gear teeth, splines or within a bearing, and may be sub-divided into a number of stages.

a) Initiation. When two components (e.g. gear teeth) come into contact during the boundary lubrication regime, the initial contact occurs away from the pitch line and gives rise to a relative sliding velocity between the teeth. The local temperature over the area of contact is proportional to the sliding velocity and wear is initiated when local asperities on each tooth are momentarily welded together. Since the relative velocity is zero at the pitch line, adhesive wear is more prominent at the extremes of contact.

b) Progressive. Adhesive wear occurs mainly when the gears operate in the boundary lubrication state, which does occur at infrequent intervals during the life of a gearbox. Such wear normally occurs at a slow rate without significantly affecting the efficiency of the gears, and may be designated as *progressive wear* **[Fillion, 1996]**. It is also referred to as *moderate wear* or *polishing* **[Drago, 1988]**.

c) Scuffing. Scuffing is an extreme form of adhesive wear which can be caused by gear loading beyond design limits and/or a loss of lubrication, for example. A high load will lead to higher lubricant temperature and thus a reduced viscosity, and thus increase the amount of direct metal-to-metal contact. This exacerbates the effect of local welding of the tooth surface and causes an extremely high rate of tooth profile loss.

Adhesive wear could be caused by a lack of lubrication between the gear teeth, splines or bearings causing high local loading and metal to metal contact. In the case of a bearing, continued shortage of lubrication could result in overheating and disintegration.

3.8.2 Abrasive wear

Abrasive wear is defined by BS7848/ISO 10825 **[BS/ISO, 1995]** as "the removal or displacement of material due to the presence of hard particles (e.g. metallic debris, scale, rust, sand, abrasive powder or the like) suspended in the lubricant or embedded in the flanks of the mating teeth". Abrasive wear will only occur if the lubricant is contaminated with particles that are larger than 30 microns **[Lorick, 1970]**. Such particles could originate from contamination in the lubricant, metal debris from surface (pitting) fatigue or metal lost through adhesive wear for example.

An oil filtration system will reduce the effect of abrasive wear considerably by filtering out any particles below a size determined by the filter used. The use of fine filtration (e.g. 3μm oil filter) will delay the onset of abrasive wear and rolling contact fatigue **[Astridge, 1989]**. Also widely used is the Magnetic Chip Detector (MCD) which will provide a warning when there is a significant build up of metallic debris in the circulating lubricant, see Section 5.2.1.

3.8.3 Corrosive wear

Corrosion of the gear teeth damages the finish on the teeth and reduces the area in contact, thus increasing the loading and accelerating the wear rate **[Drago, 1988]**. Such corrosion can be caused by a number of factors, for example:

a) Chemical effects of the breakdown of Extreme Pressure (EP) additives in the oil.

b) The presence of a corrosive atmosphere, e.g. air containing (sea) water moisture entering via breather hole in the gearbox casing.

c) Contamination of oil - with water (if lubricant is hydroscopic), or surface treatments (if held in storage).

3.9 Corrosion

Gearbox casings have frequently been constructed from Magnesium alloy, in particular AZ91 and ZE41. Owing to its relative reactivity in relation to the steel mounting bolts, galvanic corrosion in the presence of moisture is a significant factor in calculating gearbox reliability **[Drago & Lenski, 1984]**. All casings are protected from both galvanic and plain corrosion by coatings, e.g. chromate conversion coatings, which serve to prevent the initiation of corrosion. Nonetheless, the coating may be penetrated by accidental damage, e.g. during maintenance.

Externally, the main type of corrosion to affect the IGB is galvanic corrosion, where two dissimilar alloys are coupled in the presence of an electrolyte **[Jones, 1992]**. The more reactive of the two metals will be corroded to a greater degree, while the other is protected from corrosion. The rate of corrosion damage depends upon:

a) Difference in corrosion potential between the two metals in the galvanic series, the scale measuring the re-activity of a material in a particular electrolyte. The galvanic series indicates a qualitative difference that will give a predicted corrosion rate.

b) Extent of the contact area between the two metals, i.e. the relative area of the anode and cathode.

c) Presence of an electrolyte, e.g. sea water.

Helicopter transmission casings make use of chromium conversion coatings and epoxy resin sealant to provide protection against corrosion **[Astridge, 1989]**. Despite such protection, in the case of the Type A IGB, corrosion often occurs between the magnesium alloy casing and the steel bolts that are used to mount the gearbox on the airframe. Localised damage to the protective coating is likely to initiate corrosion of the casing. Magnesium alloy is in fact one of the most active materials in the presence of sea

water, and is therefore particularly susceptible to corrosion; the casing will therefore corrode in preference to the steel bolts if the protective coating is damaged.

3.10 Reported Failure Mechanisms and Causes

3.10.1 Failure mechanisms identified

Data on the failure mechanisms reported for the Type A gearbox have been supplied by the manufacturer **[Agusta Westland, 1997]**, see Table 3.1. This contains a mixture of information concerning mechanical defects and events, upon which the reliability analysis has been based. A survey of literature and consultation with Repair and Overhaul (R & O) organisations (Chapter 7) has also played a part in determining important failure mechanisms.

External Mechanisms	Likely Cause
Casing Corrosion (from scratches/damage)	Build/maintenance – error in protection
Galvanic corrosion (steel bolt/washer, Magnesium alloy interface)	Build/maintenance – error in protection
Shock Load	Pilot induced
Coupling Spline Wear	Lack of lubrication
Disconnect coupling dog tooth wear/ damage/disengagement	Under/over lubrication

Internal Mechanisms	Likely Cause
Gear tooth pitting	Lack of lubrication / poor tooth contact geometry / foreign particle damage / overtorque
Bearing pitting	Foreign particle damage / Lack of lubrication / overtorque
Bearing geometry stress concentration fatigue (e.g. banded pitting)	Build error (misalignment)
Shaft fretting	Tolerance error
Bearing race fretting	Tolerance error
Seal damage/wear	Foreign particle ingress/installation
Bearing overheat damage/staining	Low/excessive lubrication level
Internal corrosion	Incorrect storage

Table 3.1 : Reported Defects for Type A gearbox [AgustaWestland, 1997]

The types of damage have been categorised into three groups as follows. This thesis started by studying the failures that occur due to category **(a)**, but this also led to the inclusion of categories **(b)** and **(c)**. Categories **(b)** and **(c)** will either initiate and/or accelerate the classical failure mechanisms in category **(a)**.

a) 'Classical' failure mechanisms, i.e. wear, corrosion and fatigue.

b) Defects introduced by assembly/overhaul activities, routine maintenance and inspection.

c) External loads outside the normal operating spectrum e.g. over-torque, tailstrike.

3.11 Failure mechanisms to be modelled

The data from Table 3.1 have been combined with information regarding potential failure mechanisms in the literature **[Astridge, 1989]** to define a list of failure processes that are to be represented by damage models, see Chapter 4. Insufficient information was found upon which to base a model for seal failure **[Horve, 1974]**, giving rise to oil leakage. Hence this failure mechanism has been omitted; it is assumed that oil leakage is detected during maintenance, and will not be considered as a failure mechanism in its own right, see Section 10.2.2.

Despite this omission, the range of failure mechanisms selected is sufficiently diverse to demonstrate the technique for modelling multiple failure mechanisms. For this thesis, the following components and failure mechanisms have been represented. They are also presented in matrix form in Table 3.2.

i. Gear teeth - Tooth root bending fatigue

ii. Gear teeth - Rolling contact fatigue (RCF)

iii. Bearings - Rolling contact fatigue

iv. Splines on input and output shafts – Wear

v. Corrosion of casing

While it appears that these all come under the heading of 'classical' failure mechanisms **(a)**, it should be stated that assembly and maintenance errors **(b)** may initiate and/or accelerate damage accumulation in certain cases. Spline wear and casing corrosion are two examples where this could occur, and model parameters must reflect such errors (Chapter 4). Over-torque events **(c)** will cause high levels of torque within the gearbox, which will increase the damage accumulation rate for wear and fatigue mechanisms.

Component/ Failure mechanism	**Gear teeth**	**Bearings**	**Shaft splines**	**Casing**
Wear	-	-	X	-
Rolling contact fatigue (RCF)	X	X	-	-
Tooth root bending fatigue	X	-	-	-
Corrosion				
Plain	-	-	-	X
Galvanic	-	-	-	X
Maintenance errors	-	-	X	X
Over-torque	X	X	-	-

Table 3.2 : Matrix of Failure Mechanisms and Components chosen for modelling

4 Damage models for failure mechanisms and Calculation of System Reliability

4.1 Introduction

This chapter describes the steps taken to develop models that will represent failure mechanisms. These are to be used in the calculation of the failure probability due to each damage mechanism as a function of time. The development of models to represent damage caused by physical failure mechanisms is a central part of the approach taken in the prediction of the system reliability.

In this work, damage models have been applied to represent the physical damage processes that can and do occur within the transmission system. These have been grouped into three broad categories, namely:

- Fatigue - Tooth root bending fatigue (gear teeth) & rolling contact fatigue (gear teeth and bearings)
- Wear of coupling splines
- Corrosion of casing – Plain and Galvanic corrosion

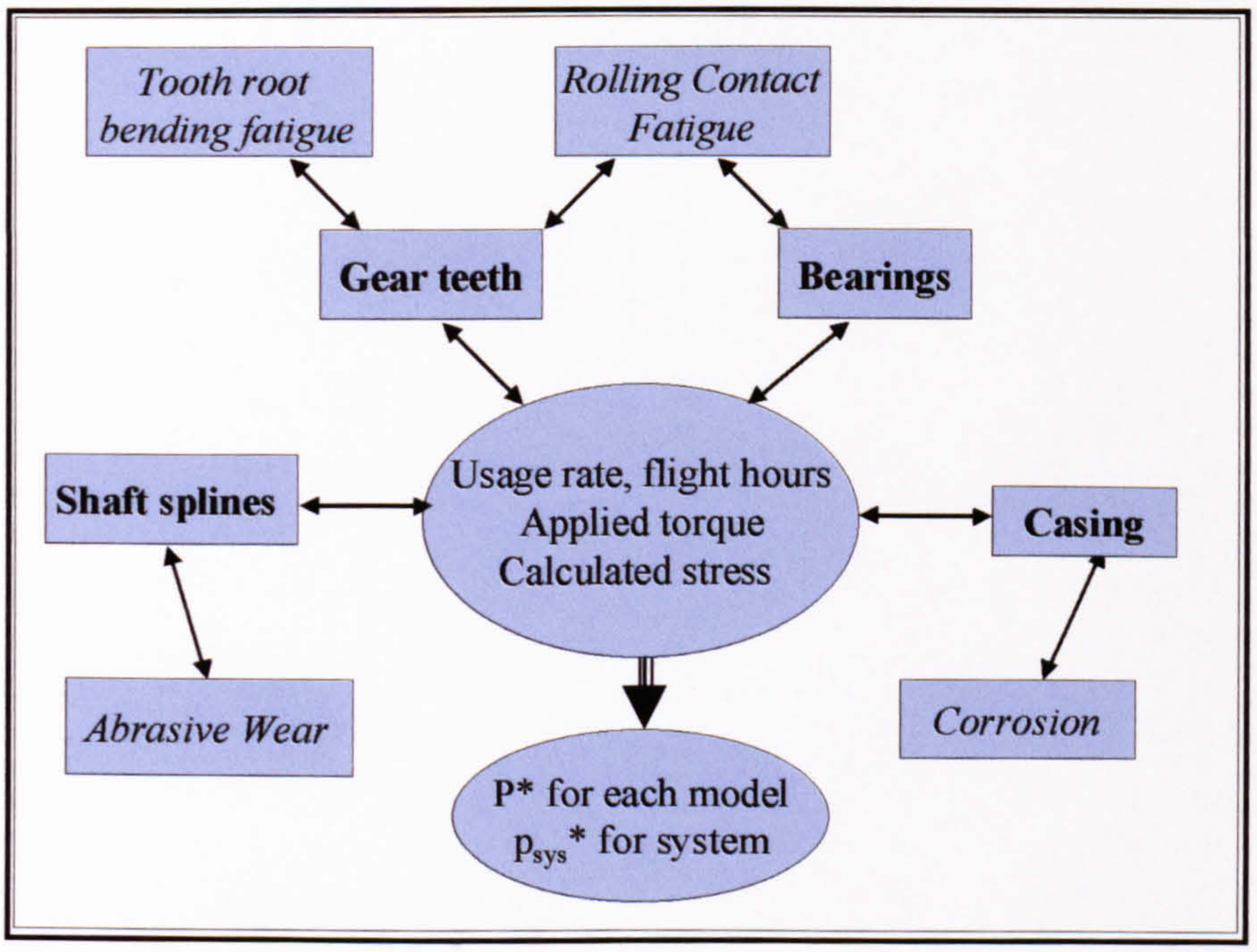

Figure 4.1 : Models used in calculating component and system reliability

Figure 4.1 represents the failure mechanisms contained within the software program, referred to hereafter as the HGBR program, and indicates the data flow between the models. Essentially, each failure process is modelled separately using loading and material data supplied from a centrally held database. The objective is to calculate the

time to failure at discrete values of probability. The individual results are then combined in order to quantify the upper and lower bounds on system reliability, as in Section 4.7.

The phrase 'cumulative damage' will also be used in its various forms and for fatigue and wear is taken to mean: *'The irreversible accumulation of damage in mechanical components under cyclic mechanical usage.'* **[Bogdanoff, 1985]**. In the reliability models, the reliability of each component is calculated using stress-strength interference, together with appropriate damage models to represent each failure mechanism. These are combined to calculate a figure for the system reliability as a whole, with upper and lower bounds derived in Section 4.8. Figure 4.2 shows the inputs required.

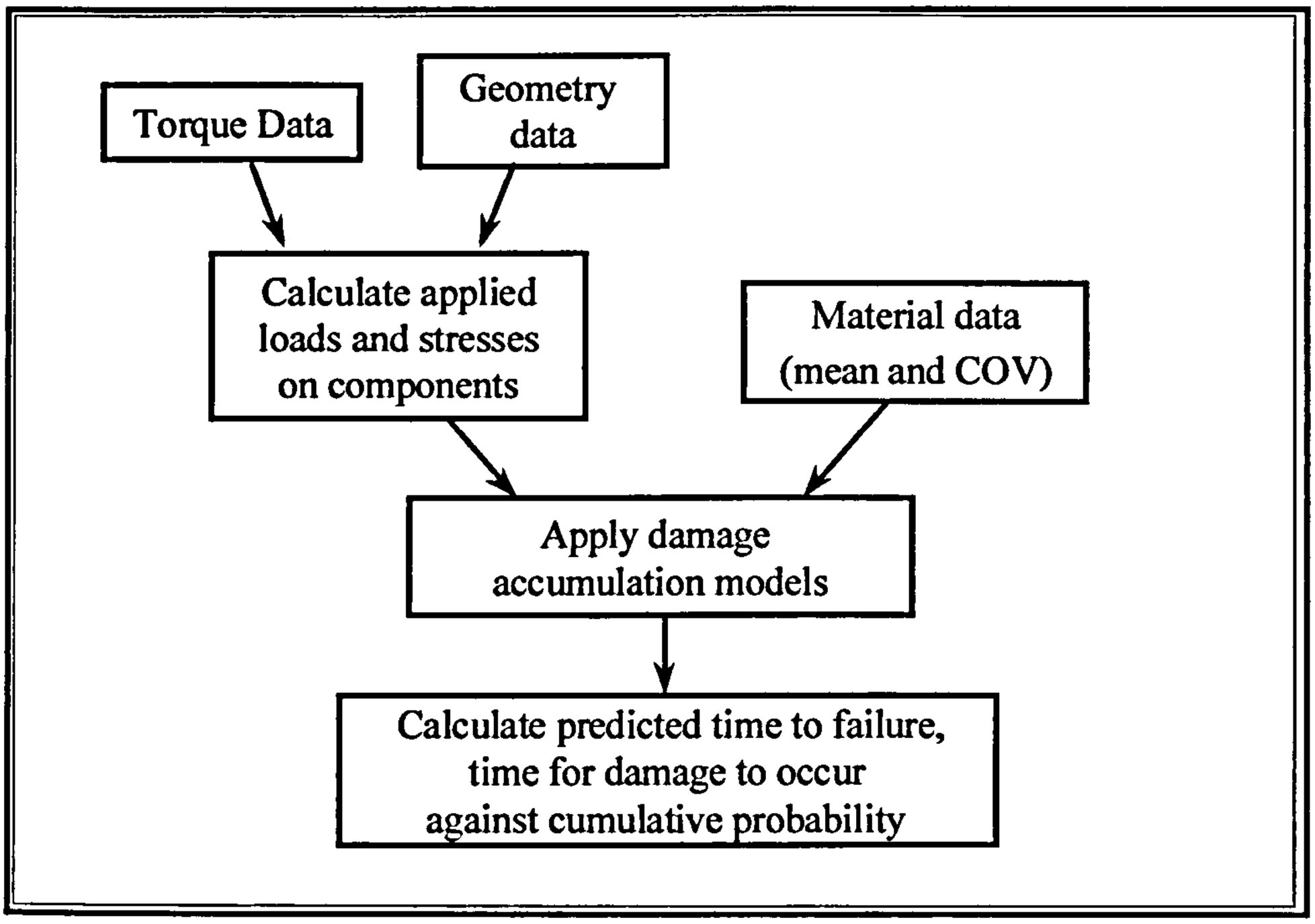

Figure 4.2 : Procedure for calculating gearbox component reliability

The time to failure (TTF) at each failure probability p(F) is calculated individually for each failure mechanism using a probability distribution for the material parameters. In the case of fatigue, it is assumed that the S-N curve is distributed log-normally about the mean on cycles, see Appendix C **[Carter, 1986]**. For other damage models, probability distributions are also used to represent the uncertainty in the knowledge of parameters.

Sections 4.2 to 4.5 describe the models used to represent the above mechanisms of degradation and the parameters used in each one. The models operate independently of one another, and there are therefore no effects of interaction between them. Chapter 6 gives details of the data used in the sensitivity studies reported in Chapters 8 and 9. This includes a description of the material and loading parameters that are varied in each of the models.

The procedures for calculating the time to failure for fatigue and wear models use the same time base, since all depend on the number of shaft rotations; damage is only accumulated when the tail rotor is rotating. However, corrosion of the casing occurs on a calendar time basis, and damage is therefore calculated on a monthly time scale, depending on the environment in which the helicopter is based, e.g. marine, land etc.

4.2 S-N based Fatigue Model

4.2.1 General

Fatigue damage models are generally used to predict either crack initiation time or crack propagation time. Models already exist which aim to represent each of the two stages, the best known being Miner's Law for crack initiation, and the Paris Law for crack propagation **[Suresh, 1991]**. Owing to the high cycle loading on the gearbox components, the time for a crack to propagate is proportionately much shorter than the time to initiate. The damage accumulation model used for fatigue is therefore based on Miner's Law for linear fatigue damage summation.

The time to failure (TTF) is the point when the damage exceeds a nominal 1mm crack, equated here to Miner's sum of unity. If n_i is the number of cycles of constant stress amplitude $\Delta\sigma_i$ in a sequence of m blocks, and N_{fi} is the number of cycles to failure at $\Delta\sigma_i$ then the Palmgren-Miner (P-M) model is written:

$$\sum_{i=1}^{m} \frac{n_i}{N_{fi}} = 1 \qquad (4.1)$$

Using material property data (e.g. the fatigue S-N curve) and the loading on the component in question, the damage accumulation rate can to be determined for all fatigue damage models. The models accept S-N data in the form of a three-parameter curve:

$$\Delta\sigma = S_{inf}\left(1 + A.N_f^{-\gamma}\right) \qquad (4.2)$$

where $\Delta\sigma$ is the applied stress range
S_{inf} is the endurance limit
A and γ are material constants
N_f is the number of load cycles to failure

The same equation has been applied to gear tooth root bending fatigue and gear tooth rolling contact fatigue, with a different S-N curve used in each case. Equation 4.2 is used to represent alternating load against N_f for tooth root bending fatigue (TRBF), Section 4.2.3, and gear tooth rolling contact fatigue (RCF), Section 4.2.4.

From this stress vs life (cycles to failure) data the incremental damage factor α_i can be determined for each load state[1]. For Miner's Law this is the reciprocal of the cycles to failure for each stress range; α_i is constant when the cyclic stress range per cycle is constant:

$$\alpha_i = 1/N_{fi} \qquad (4.3)$$

The number of load cycles N for tooth root bending and gear teeth RCF is determined from knowledge of the shaft rpm, since each tooth experiences one load cycle per shaft revolution. The applied torque determines the stress range at the time of tooth engagement.

4.2.2 Application of S-N based fatigue models

The calculation of the TTF for different values of failure probability is achieved by considering the probability distribution of the S-N curve. Instead of one S-N curve, a family of curves is plotted to give the so-called PNS (probability-cycles-stress) curves **[Chapter 16 - Bury, 1975]**. The shape of the probability distribution for stress at constant N may be approximated to Log-normal distribution **[Bury, 1975, Yang, 1996]**, which appears as a Normal distribution when plotted for ln (S), Figure 4.3.

A new factor (δ) is introduced which is varied to find the S-N curve for the respective p*. The value of δ is calculated from the standard deviation of the fatigue curves probability distribution and the desired failure probability; see Figure 4.3.

$$\delta = \sigma_{ln} \times n_{stdev} \qquad (4.4)$$

σ_{ln} = standard deviation of the Log-normal distribution
n_{stdev} = number of standard deviations to meet p*, e.g. 3.09 for p* of 10^{-3}.

Parameter σ_{ln} is calculated in equation 4.5 from the coefficient of variation for the fatigue curve, derived in Appendix C.2. If COV is the coefficient of variation of the corresponding *normal* distribution, then

$$\sigma_{ln} = \sqrt{\ln(1+(COV)^2} \qquad (4.5)$$

The fatigue model is based upon equation 4.2 for the S-N curve, which is re-arranged in terms of α_i, the incremental damage factor. The equation is amended to include δ and α in the following manner. This is to be used in the calculation of the incremental damage factor at each load state and required probability p*:

---

[1] Load state is defined as a period of time during which the applied torque and load remain constant. Note that manoeuvres may contain different levels of torque/stress and therefore consist of more than one load state.

$$\alpha^{\gamma} = N_f^{-\gamma} = \frac{(\Delta\sigma.e^{-\delta} - S_{inf})}{A.S_{inf}} \qquad (4.6)$$

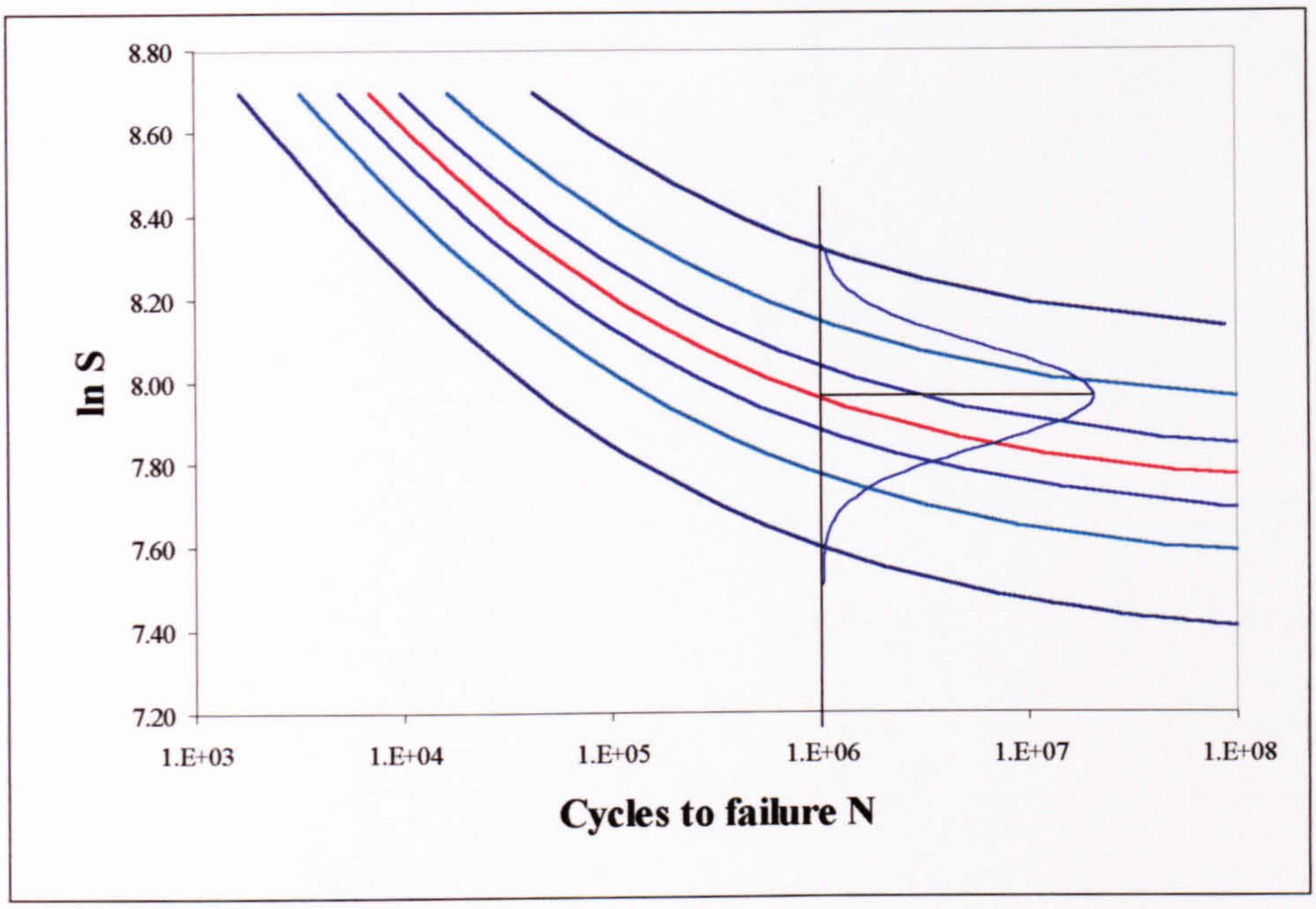

Figure 4.3 : P-N-S curve showing the distribution of Ln S at constant life

The calculation of TTF for fatigue mechanisms is performed using a loading history or spectrum that contains values for torque/loads and the duration of these torque/loads, together with material data. The calculations of predicted life for TRBF and gear RCF models are performed in the following steps 1 to 5, Figure 4.2. The exception to this sequence is the damage model for bearing contact fatigue, which is described in Section 4.3.

1. Knowing the mean S-N fatigue curve and variance, one S-N curve is chosen from the probability distribution of curves. Steps 2 – 5 are then performed in sequence for each value of probability **p*** from 10^{-9} to 0.5, by applying equation 4.6.

2. For each load state within the load sequence or spectrum, the S-N curve is used to calculate the number of cycles to failure, N_f, at that stress range.

3. The incremental damage factor α_i is calculated using the relationship between , N_f, and α_i (equation 4.3).

4. The amount of damage accumulated at each load state is calculated. Damage is assumed to occur at a (fixed) linear rate at each loading state; Figure 4.4 shows a diagrammatic representation of 4 load states.

$$D_{tot} = \sum_{i=1}^{k} D_i = \sum_{i=1}^{k} (n_i . \alpha_i) \qquad (4.7)$$

D_{tot}	Total amount of damage which occurs over all load states
D_i	Amount of damage accumulated at each of the k load states
α_i	Incremental damage factor at each of the k load states
n_i	Number of load cycles contained in each of the k load states

5. The time to failure (TTF) at the failure probability in question is then the time taken for the actual damage to reach the failure point, which is unity for fatigue damage models using Miner's law:

$$TTF = \frac{1}{D_{tot}} . T_{spec} \qquad (4.8)$$

where T_{spec} = time corresponding to the damage D_{tot}

As an example, if D_{tot} is calculated to be Miner damage sum 0.1, calculated from load states representing 100 hours, the predicted TTF is:

$$TTF = \frac{1}{0.1} . 100 = 1000 \text{ hours} \qquad (4.9)$$

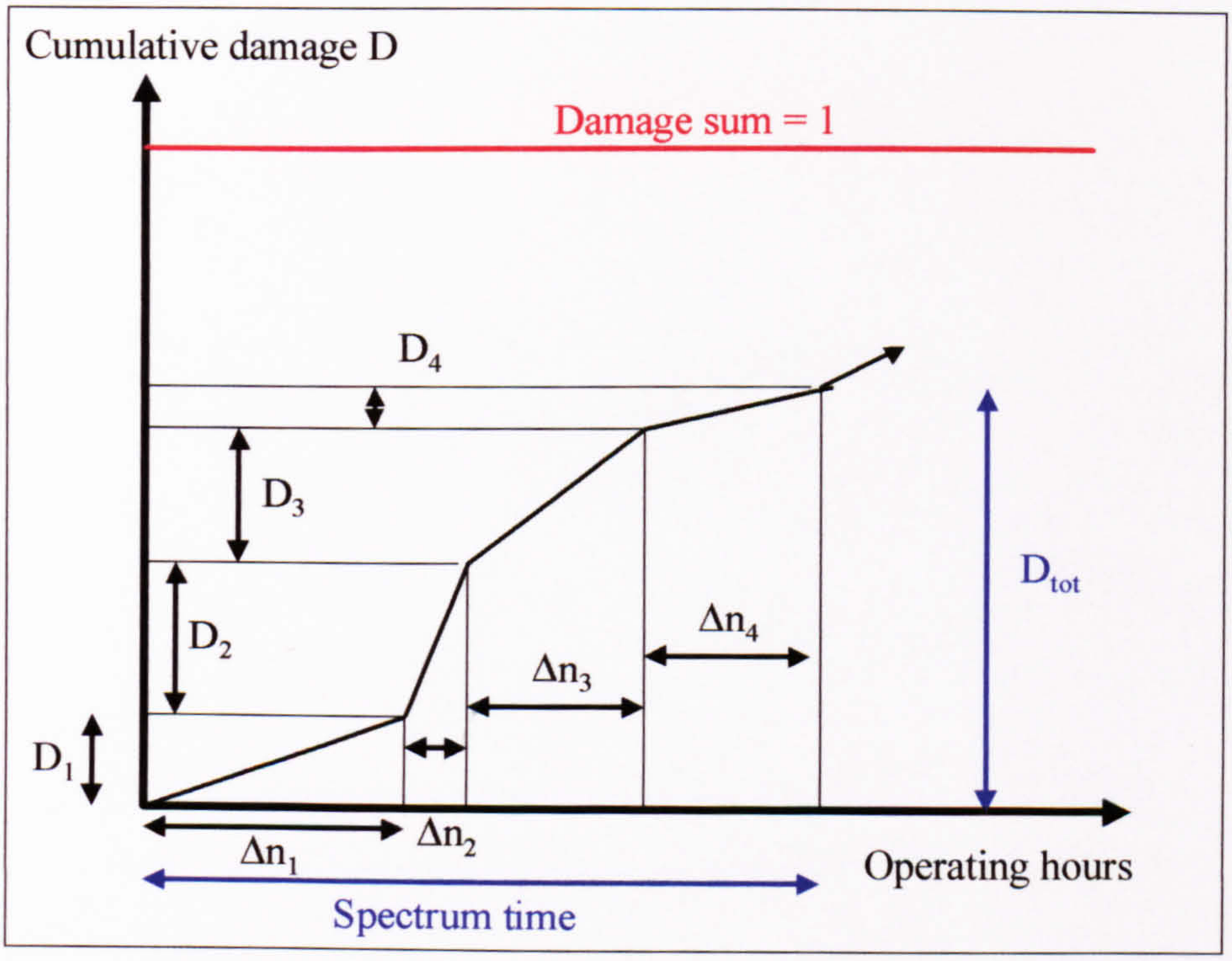

Figure 4.4 : Summation of cumulative damage

4.2.3 Tooth Root Bending Fatigue

The S-N curve equation given in equation 4.2 has been modified to replace $\Delta\sigma$ with T the input torque (equation 4.12). This substitution is justified since during the meshing of the gear teeth, the applied torque is directly proportional to the bending stress range at the tooth root from zero to peak stress and back to zero, equations 4.10 **[AGMA, 1986]** and 4.11. Gearbox fatigue tests also generally record torque rather than bending stress at the tooth root. N_f is the number of load cycles to initiate a 1mm crack in the tooth root.

$$\Delta\sigma_1 = \frac{2TK_a}{K_v}.\frac{P_d}{Fd}.\frac{K_sK_m}{K_xJ} \qquad (4.10)$$

$$\Delta\sigma_1 \propto T \qquad (4.11)$$

where $\Delta\sigma_1$ is tooth root bending stress in GPa.
T is torque in N m
P_d is the transverse diametral pitch at the outer end of tooth in mm^{-1}.
F is the net face width in mm.
d is the outer pitch diameter of the pinion in mm.
J is the geometry factor for bending strength.
Factors K are engineering factors as below.

K_a	External dynamic factor
K_v	Internal dynamic factor
K_s	Size factor
K_m	Load distribution factor
K_x	Tooth lengthwise curvature factor

The relationship between torque versus cycles to failure (T-N curve) is presented in equation 4.12, and displayed in Figure 4.5, and is assumed to be the same for the two gearbox types, as supplied by the two manufacturers.

$$T = T_{inf}\,(1 + A.N_f^{-\gamma}) \qquad (4.12)$$

where T, T_{inf} are the input torque and endurance limit, respectively.
A is a material constant
N_f is the number of load cycles to failure

Numerical values for all the constants used in the above equation are contained in Chapter 6, which gives data for both Type A and Type B gearboxes.

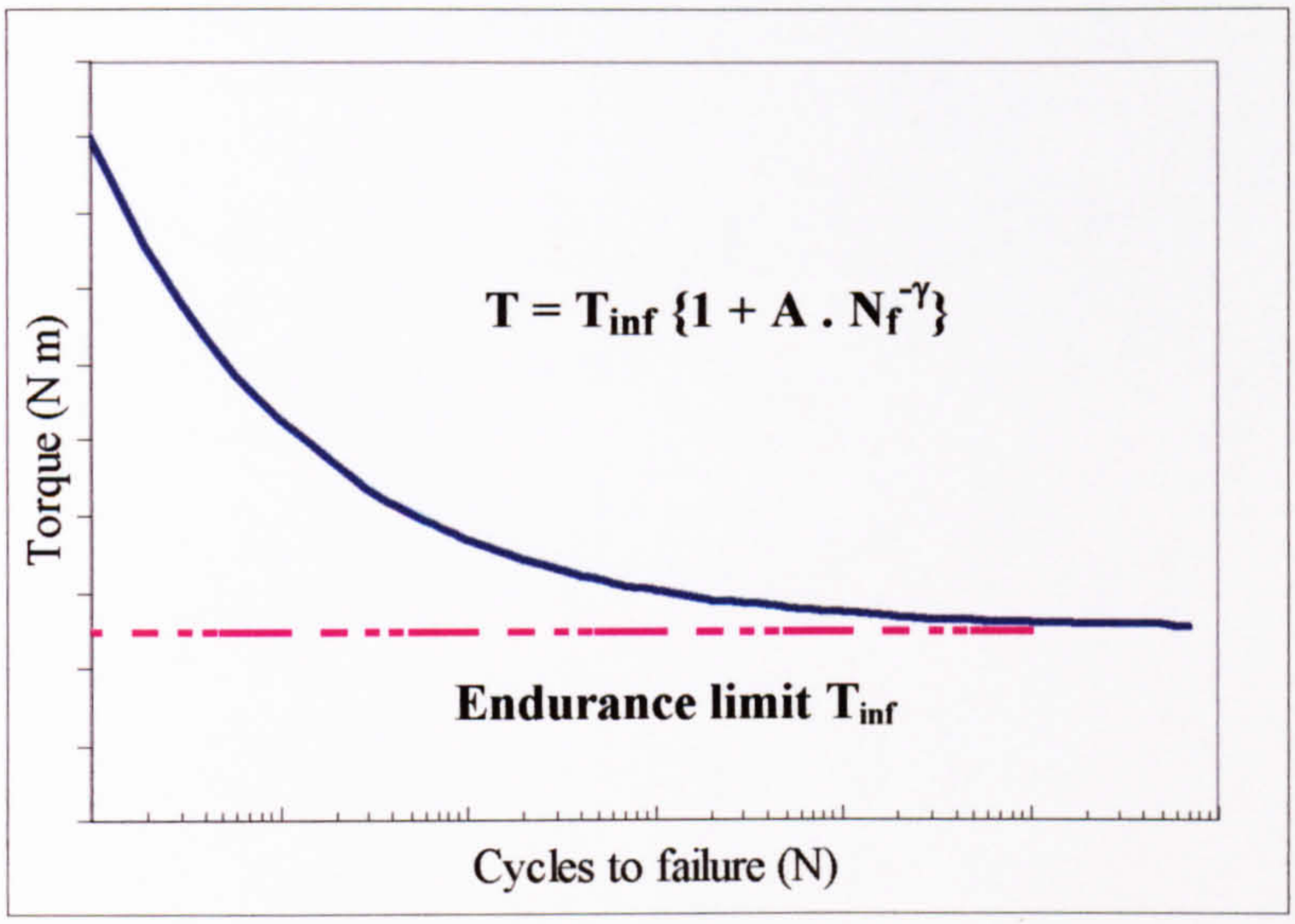

Figure 4.5 : T-N Plot for Tooth root bending fatigue

4.2.4 Gear Teeth Rolling Contact Fatigue

For gear tooth rolling contact fatigue, equation 4.2 has again been employed. In this case, the applied stress range is the working Hertzian contact stress (S_{WC}) and N_f is the number of gear meshing cycles for a pit of at least 1.58mm diameter by 0.2mm depth to develop **[AGMA, 1986]**.

Experimental data in the form of Hertzian contact stress versus cycles to pit formation are not widely available. With most test data this failure mode is presented in the form of a Weibull plot for tests at a particular contact stress level. For variable amplitude loading as required in the helicopter gearbox model, a load versus life curve has been plotted using industry standard AGMA 2003 **[AGMA, 1986]**. This load/life curve has been drawn using information provided by the design standards due to the lack of test data for the particular gear set in question.

The damage model employed for reliability prediction makes use of an S-N curve, calculated from equation 4.13, using the Life factor C_L (Figure 4.6). A curve of the S_{WC} against N may then be plotted, and is shown in Chapter 6. S_{WC} is alternating Hertzian working contact stress in MPa and N is the number of cycles for a spall or pit of at least 1.58mm diameter by 0.2mm depth to develop **[AGMA, 1986]**. The Hertzian contact stress on the gear teeth has been calculated from knowledge of the gear geometry, Appendix B.

This has been used to produce a family of curves for different failure probabilities distributed log-normally about the mean **[Bury, 1975]**. The working contact stress (S_{WC}) is taken as **[AGMA, 1986]**:

$$S_{WC} = \frac{S_{AC}.C_H}{C_T.C_R}.C_L \qquad (4.13)$$

where S_{AC} the allowable contact stress taken as 1.726 GPa, for carburised and case hardened bevel gears **[Drago, 1988]**
C_H, C_T, C_R, C_L are factors used to calculate working stress S_{WC} **[AGMA, 1986]**

C_H Hardness ratio factor that accounts for different hardness between the gear and pinion; when of equal hardness, as in this gearbox, $C_H = 1.0$.

C_T Temperature factor that accounts for high gear operating temperature; $C_T = 1.0$ for temperatures less than 120^O C.

C_R Reliability factor that accounts for the probability of a spall occurring. For probability < 0.01, $C_R = 1.0$; for probability = 0.5, C_R is 0.87.

C_L Life factor, based on the number of cycles N for a pit of minimum 1.58mm diameter by 0.2mm depth to develop, see equation 4.14

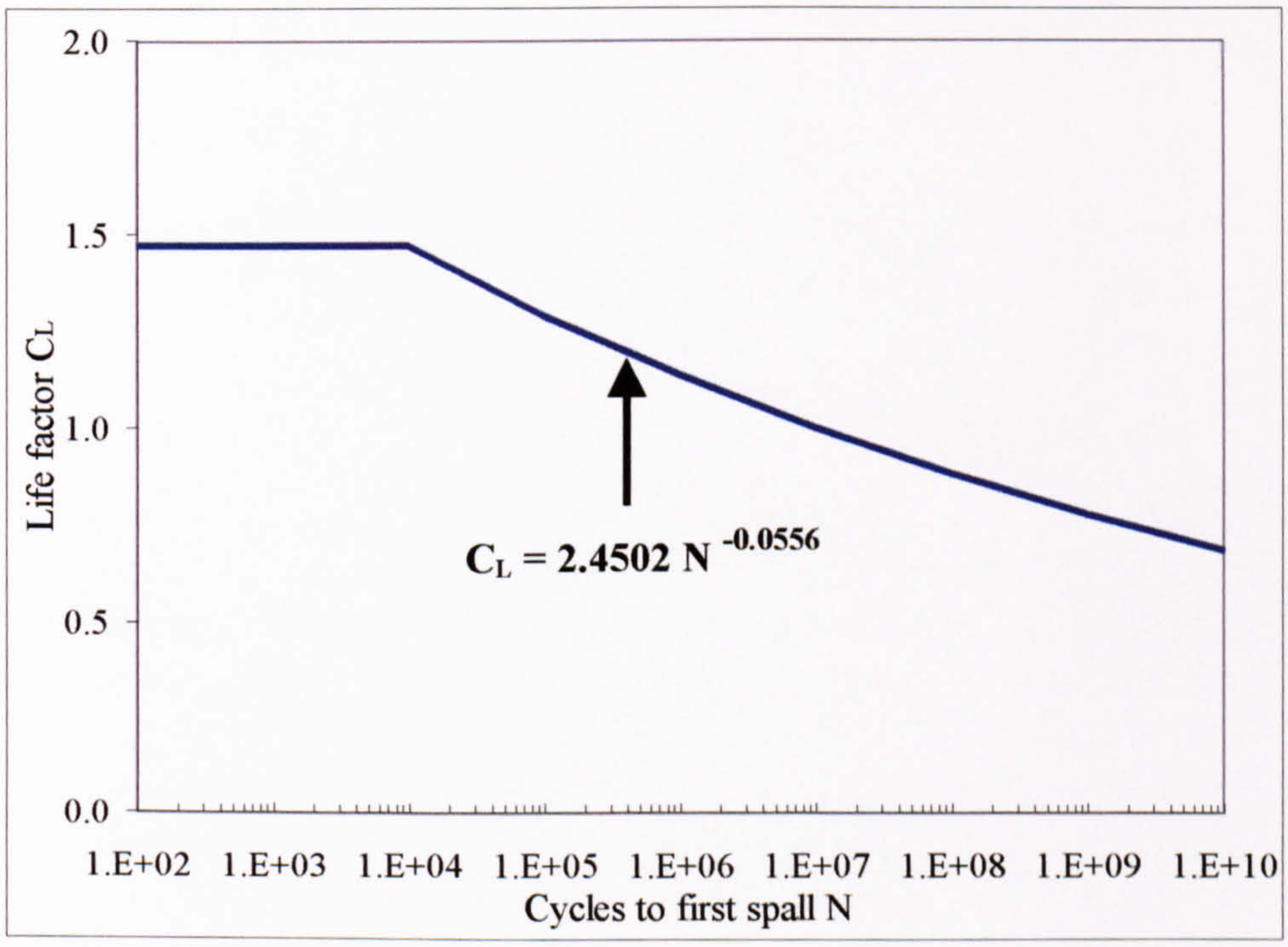

Figure 4.6 : Life Factor for Pitting Resistance (carburised, case-hardened steel bevel gears [AGMA, 1986]

The Life factor used in the calculation of the allowable contact stress is taken from **[AGMA, 1986]**, see equation 4.14 and Figure 4.6.

$$C_L = 2.4502\, N^{-0.0556} \tag{4.14}$$

Substituting in equation 4.13

$$S_{WC} = \frac{S_{AC}.C_H}{C_T.C_R}.\,(2.4502\, N^{-0.0556}) \tag{4.15}$$

The distribution of stress at constant life has been assumed to be the same as that described for the general fatigue model operation (Section 4.2.2). The predicted time to first spall (TFS) was therefore calculated for each probability value based on the assumption that S_{WC} is described by a Log-normal distribution at constant N.

Numerical values for all the constants used in the above equation are contained in Chapter 6. Geometrical data are different for Type A and Type B gearboxes, but material data is the same for both.

4.3 Bearing Contact Fatigue Model

4.3.1 General

For the contact fatigue of ball and rolling element bearings, the Lundberg-Palmgren **[Lundberg and Palmgren, 1947]** model for L_{10} life has been adopted. This indicates the number of cycles (or operating hours) at which 10% of a population of bearings will have developed a spall of a specified size (equations 4.16 and 4.17). This damage limit, is specified as a spalled area of $6mm^2$ by one manufacturer **[TIMKEN, 1994]**.

The L_{10} life forms a point on a Weibull distribution, and the life for other failure probabilities can be derived if the Weibull slope β is known; typical values are 1.5 for roller bearings and 1.1 for ball bearings **[Coy et al, 1985]**. The life may be quoted in units of shaft revolutions, which are the same as cycles N, or hours of operation. These are related by the (constant) rotational speed of gear shaft.

$$L_{10} = \left(\frac{C_1}{P_0}\right)^p . 10^6 \quad \text{revolutions} \tag{4.16}$$

$$\text{or} \qquad L_{10} = \left(\frac{C_1}{P_0}\right)^p . \frac{10^6}{60n} \quad \text{hours} \tag{4.17}$$

where C_1 is the bearing dynamic rating in kN. This is defined as the load that would result in an L_{10} life of 10^6 cycles.
n is the bearing rotation speed in rpm
Exponent p is $^{10}/_3$ for roller bearings and 3 for ball bearings
P_0 is the dynamic equivalent radial load, in kN, calculated as:

$$P_0 = X.F_R + Y.F_a \tag{4.18}$$

where X and Y are the radial and axial load factors, respectively
F_R and F_a are the radial and axial loads, respectively, in kN

The L_{10} life is the time at which the probability of failure p(F) is 10%, or 0.1. Below or above this value, the time to failure for different values of p(F) can be estimated using a Weibull plot of bearing lives, equation 4.19 **[Bompas-Smith, 1973]**.

$$F(t) = 1 - R(t) = 1 - \exp\left[-\left(\frac{t-\gamma}{\eta}\right)^{\beta}\right] \tag{4.19}$$

where R(t) is reliability as a function of time
β is Weibull slope
η is characteristic life (scale parameter)
γ is minimum life (hours).

Figure 4.7 shows an example of a Weibull plot that could be used to represent the life of bearings. The added lines are defined as:

A - Two parameter Weibull plot with minimum life of zero
B - Three parameter Weibull plot with minimum life of 10 hours
C - Minimum life equals 5% of L_{10} life at 0.1% quantile, i.e. $p(F) = 10^{-3}$

Below the 5% quantile, there are two theories for calculating the time to failure. **[Tallian, 1982; Harris 1991]** quote a minimum bearing life (L_{min}) equal to 5% of the L_{10} life, at which p* is taken as 10^{-3}, see Figure 4.7 line C. Laboratory tests **[Tallian, 1962]** have shown that there were no failures before this point. This approach differs from a three-parameter Weibull plot with a non-zero minimum life, which takes the form of line B.

Alternatively, a two-parameter Weibull function, with minimum life of zero (Figure 4.7 line A) is employed. This is the approach of **[TIMKEN, 1994; Hoeprich, 1998]**, who do not quote a minimum life, but instead use a reliability factor based upon a Weibull slope of 1.5, to calculate life at much lower values of p*, see equation 4.22 and Appendix B.4.

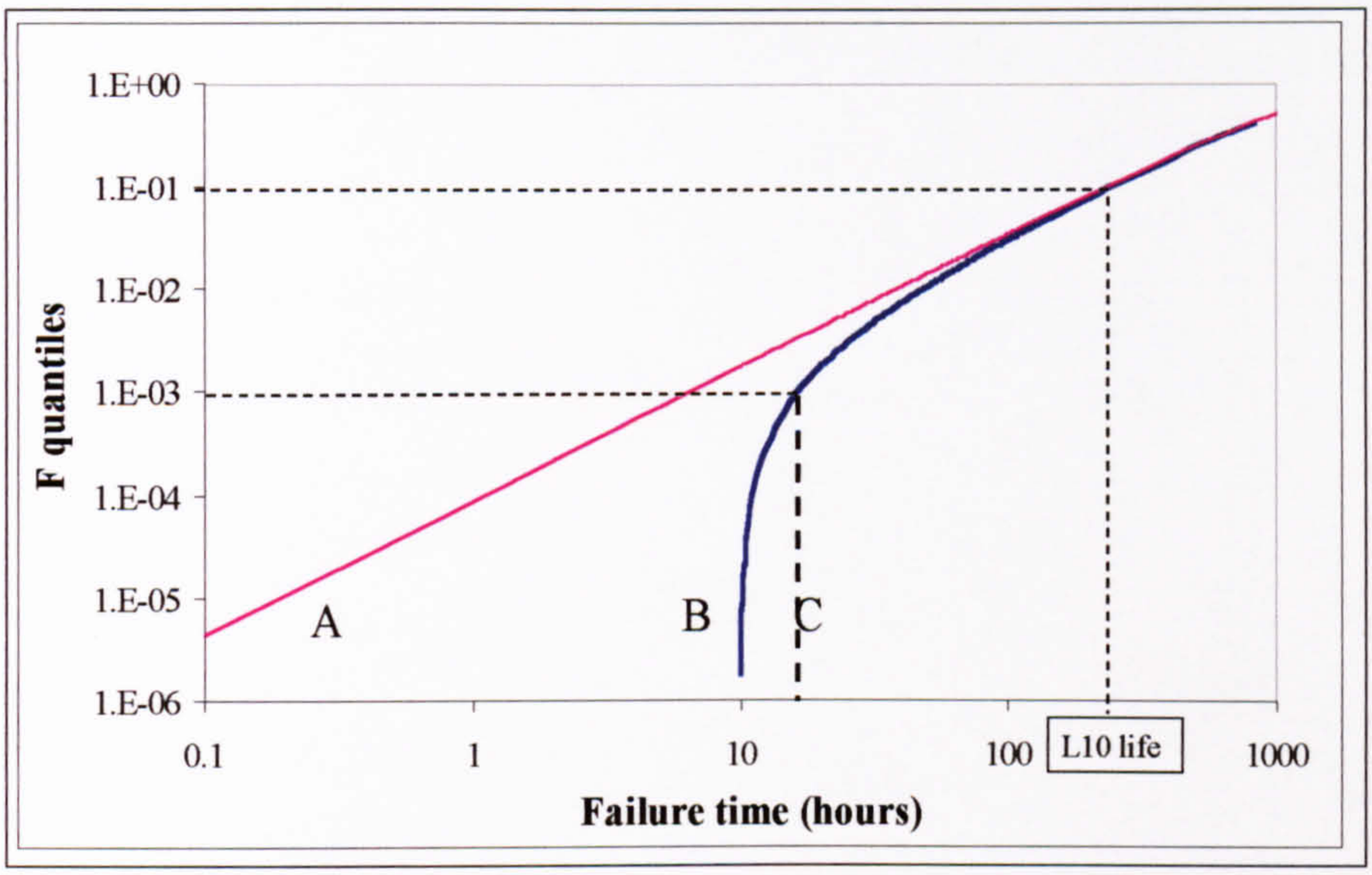

Figure 4.7 : Weibull plots ($\beta = 1.3$, $\eta = 1300$ hours, $\gamma = 10$ hours (B), $\gamma = 0$ (A)

4.3.2 Application of Bearing Contact fatigue model

The bearing contact fatigue model has been applied to calculate the life of each of the four bearings within the gearbox. For variable amplitude loading, rather than calculate the L_{10} life at each load state individually, it is possible to calculate the *root mean cube* of a series of loads P_{rmc} as in equation 4.20 **[Harris, 1991]**. P_{rmc} is the load which when applied for the total number of cycles N_{tot}, will cause the same damage as all the individual loads applied separately. The cube factor is due to the cube-law relationship between load and life, equation 4.17. This is the model that has been used in the HGBR software program.

$$P_{rmc}^{3.33} . N_{tot} = \sum_{i=1}^{k} P_i^{3.33} . n_i \qquad (4.20)$$

$$P_{rmc} = \left[\frac{\sum_{i=1}^{k} P_i^{3.33} . n_i}{N_{tot}} \right]^{0.3} \qquad (4.21)$$

where n_i = number of cycles in each torque state
N_{tot} = total number of cycles

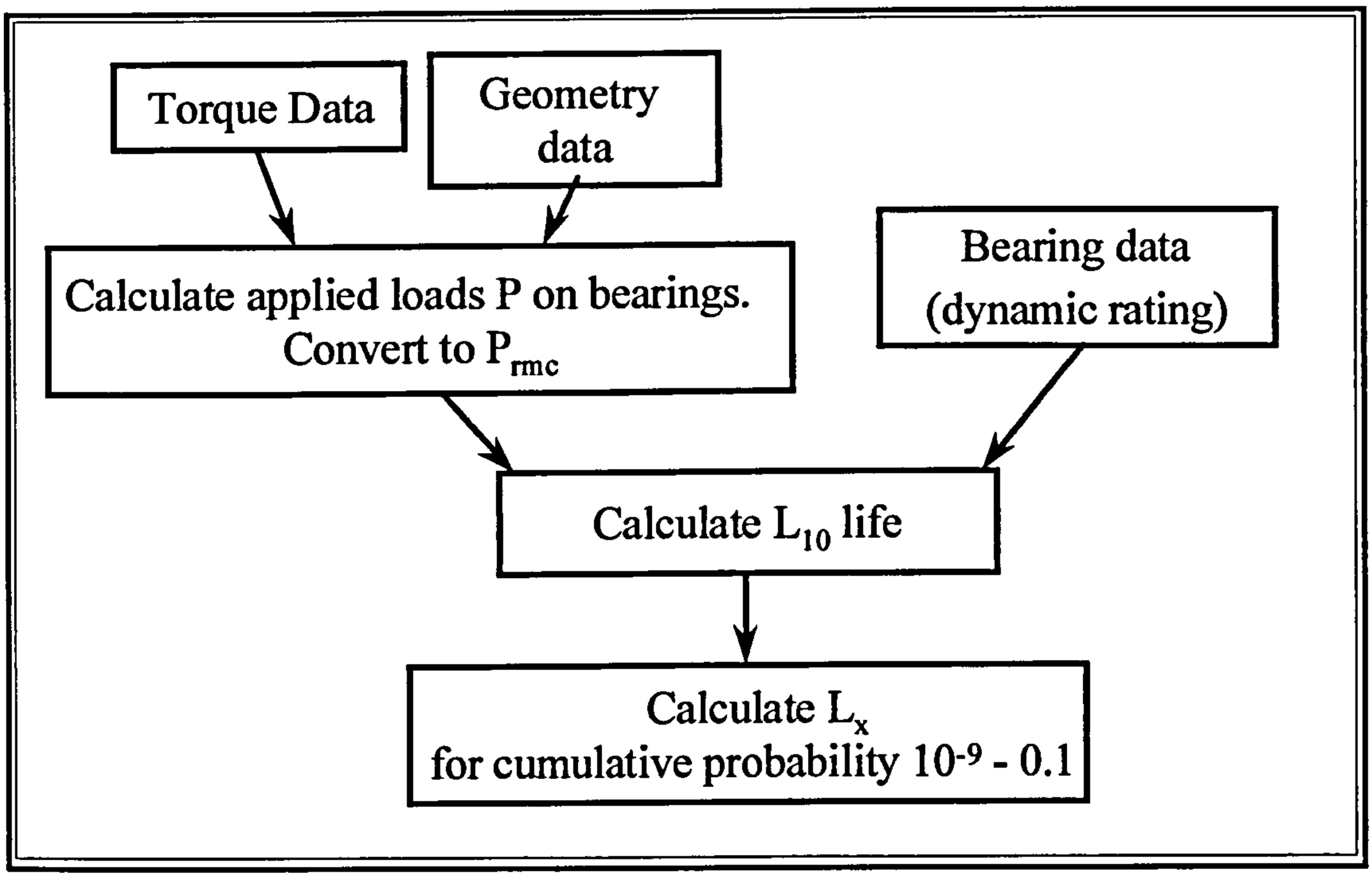

Figure 4.8 : Sequence for calculating bearing TFS by Contact Fatigue

The sequence of the calculation is illustrated in Figure 4.8. The bearing life model used in the prediction of reliability makes use of the two-parameter Weibull curve, with a minimum life of zero. From manipulation of the L_{10} life equation in Appendix C, equations 4.22 and 4.23 allow the mean time to first spall for bearings to be estimated at failure probabilities down to 10^{-9}.

$$L_x = a_1 \, . \, L_{10} \qquad (4.22)$$

where
$$a_1 = 4.48 \left(\ln \frac{100}{R} \right)^{\frac{2}{3}} \qquad (4.23)$$

The values for a_1 for bearing lives less than L_{10} were calculated from equation 4.23, and are given in Table 4.1.

The confidence bands at such low failure probabilities are wide, given the lack of sufficient test data. However, the low theoretical values of p* are nonetheless extrapolated in order to account for the finite probability of failure in the harsh operating environment. Predicted lives below one hour are not considered in the overall calculation.

Failure probability p* (1-R)	Log p*	Reliability factor a_1
10^{-9}	-9	0.000 004 5
10^{-8}	-8	0.000 021
10^{-7}	-7	0.000 096
10^{-6}	-6	0.000 45
10^{-5}	-5	0.002 08
10^{-4}	-4	0.009 65
10^{-3}	-3	0.045
0.01	-2	0.209
0.1	-1	1.0

Table 4.1 : Reliability factor a_1 for bearing lives below L_{10}

4.4 Damage Model for Shaft Wear

4.4.1 General

Previous theoretical and experimental work on the wear of splines due to misalignment was carried out by **[Weatherford et al, 1966]**. Further work to analyse the wear mechanism which occurs in splined couplings was undertaken by **[Newley, 1978]**. Recently, additional work to study and model this degradation mechanism has begun **[Adey et al, 1999; Davies et al, 1999; Baker et al, 1997]**.

There is only a limited range of models capable of predicting the failure point for shaft couplings that suffer wear. One such model is given by **[Calistrat, 1980; Rabinowicz, 1995]**, which describes the wear process caused by the angular misalignment between the mating shafts, see Figure 4.9.

The following wear equation was proposed by **[Archard, 1953]** and described by **[Halling, 1983]**, equation 4.24. This states that the amount of material lost due to the contact of two surfaces in relative motion is directly proportional to the normal load applied and the distance moved, and inversely proportional to the hardness of the softer material.

$$\text{Wear volume } \alpha \frac{\text{Load . distance moved}}{\text{hardness}}$$

or
$$\text{Wear volume} = \frac{K}{H} \text{. Load . distance moved} \qquad (4.24)$$

where K is the wear coefficient
H is the indentation hardness

The constant K represents the likelihood of a wear particle forming at each asperity interaction **[Halling, 1983]**, and quoted values are to be found in the literature e.g. **[Rabinowicz, 1980]**. However, these parameters should be treated as stochastic variables for a model such as is required here e.g. **[Qureshi and Sheikh, 1997]**.

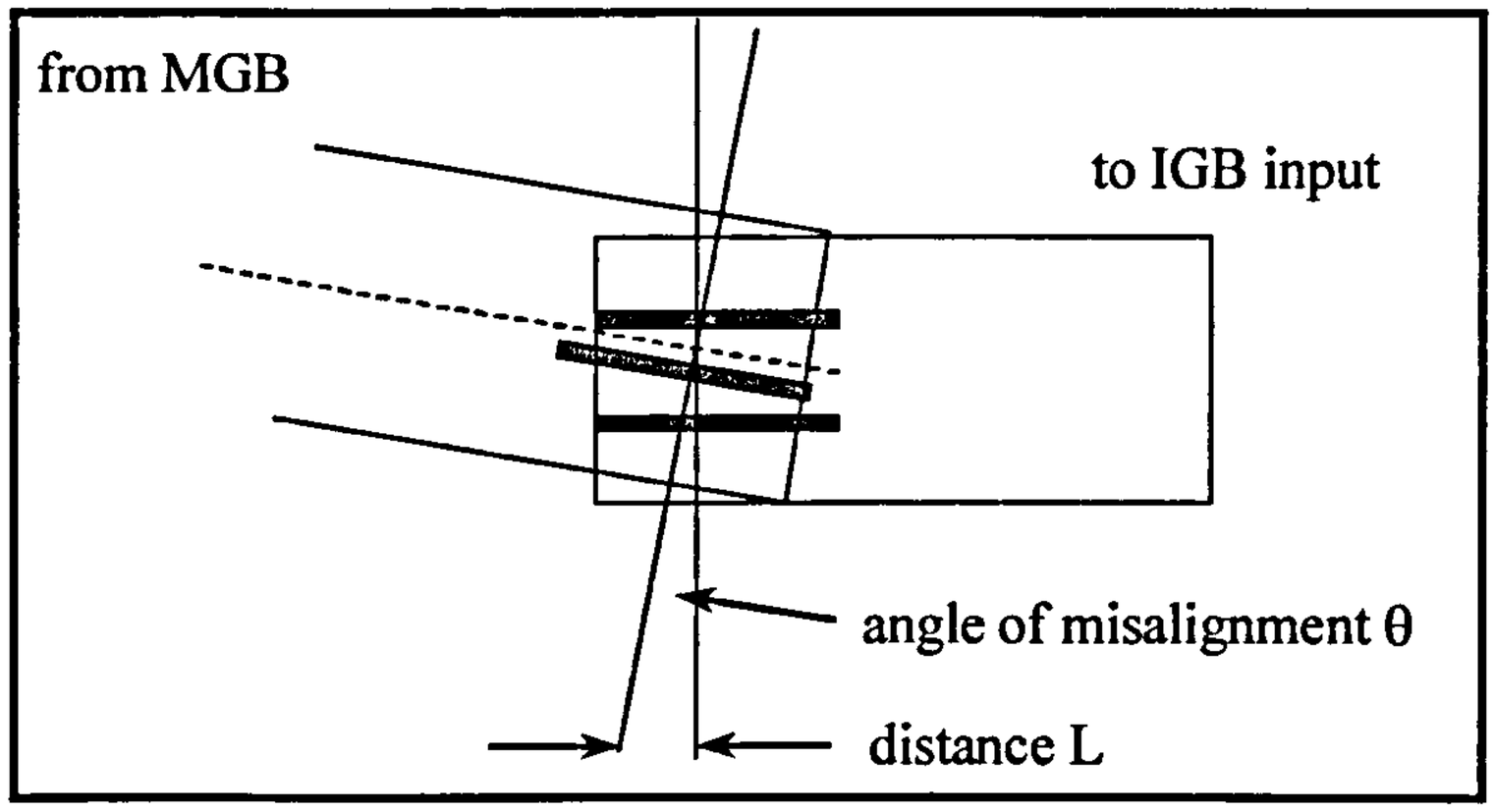

Figure 4.9 : View of misalignment of coupling splines [Calistrat, 1980]

For the shaft splines, wear may be caused by the relative metal-to-metal movement of the interconnecting couplings and/or by angular misalignment; if the far two ends of the mating shafts are fixed, there will be a relative movement between the splines as the shafts rotate. Any relative axial movement may also cause wear, whenever there is metal-to-metal contact with poor lubrication.

For the misalignment case, Archard's equation for shaft spline wear may be written as **[Calistrat, 1980]**, see Appendix B.4:

$$\text{Wear volume} = \frac{K}{H}.2\frac{PD}{2}\theta.\frac{2T}{PDn\tan\varphi} \quad \text{per revolution} \qquad (4.25)$$

where the parameters are defined as:

K	Wear coefficient
H	Indentation hardness (units of load/area)
T	Transmitted torque (Nm)
n	number of splines
φ	Involute pressure angle of the splines
PD	Pitch diameter of the splines (mm^{-1})
θ	Angle of misalignment in radians

If all the parameters in equation 4.25 and the failure limit are known, or can be modelled by distributions, then the time to reach the failure criterion can be calculated, as in section 4.4.2.

4.4.2 Application of wear model

The wear model uses the same torque input loads as do the fatigue damage models, and requires all the parameters in equation 4.25 in order to run. For each failure probability (Figure 4.10), the distance moved is calculated based a log-normal distribution defined by a mean and COV. This is justified since such a distribution applies to positive random variables, which is the case for the wear model, with positive slip distances and misalignments.

The log-normal distribution is also positively skewed, which would be expected with the expected value being close to zero. The standard deviation of the distribution may be written as (Appendix C.1):

$$\sigma_{ln} = \sqrt{\ln\left(1 + (\text{spline COV})^2\right)} \qquad (4.26)$$

The relative movement between the splines is calculated in one of two ways. In the case of relative movement, e.g. torsional backlash, between the mating splines, the slip amplitude is the 'Distance moved' in equation 4.28. If the mating shafts are misaligned, the 'Distance moved' is a function of the misalignment angle, and is derived in equation 4.29. Since the principal causes of spline wear are shaft misalignment/relative movement and poor lubrication, the model is largely controlled by potential errors made during maintenance.

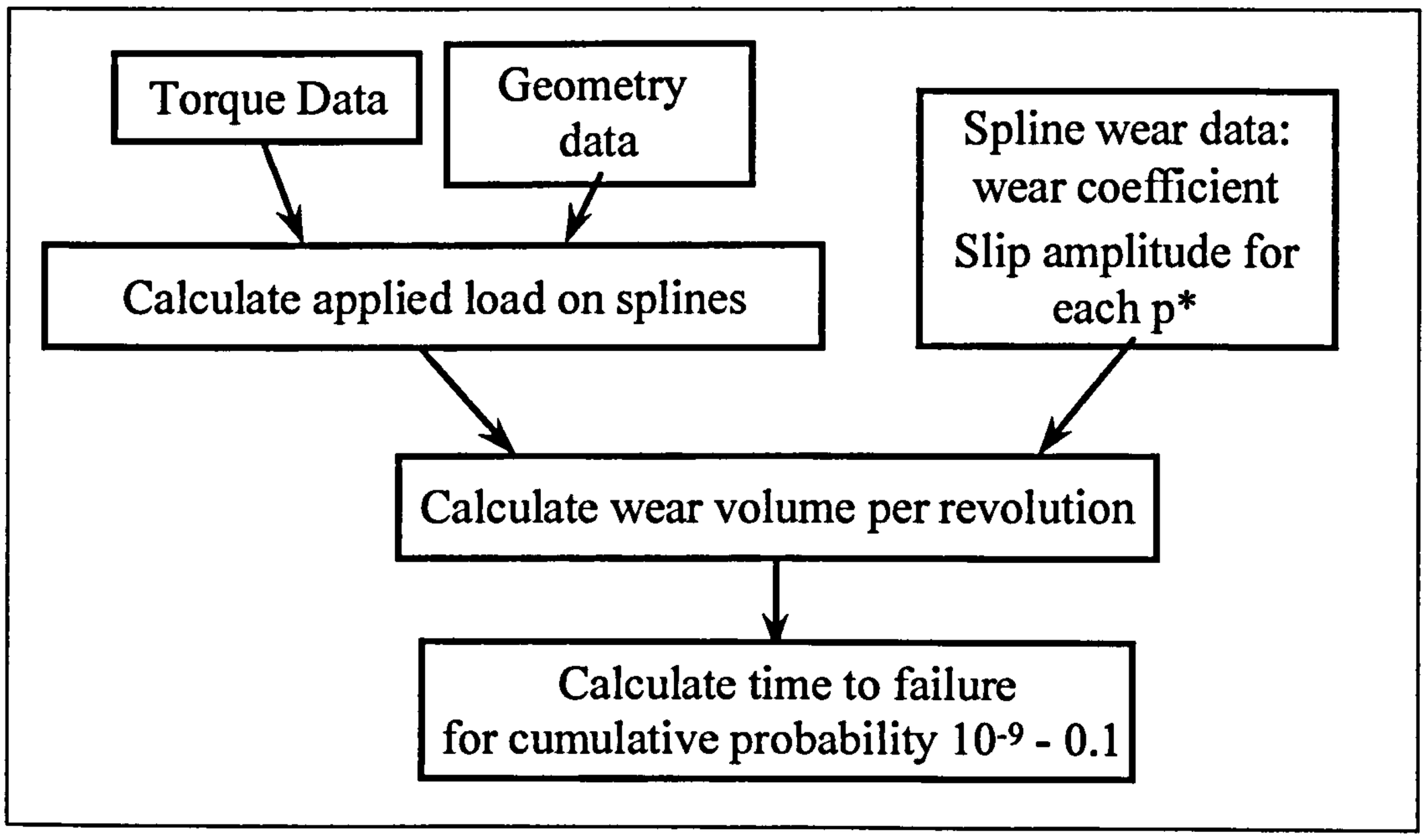

Figure 4.10 : Sequence for calculating spline wear TTF

The factor δ is used to find the misalignment angle or slip amplitude for each failure probability (10^{-9} to 0.5), and is calculated as:

$$\delta = \sigma_{ln} \times n_{stdev} \quad (4.27)$$

where n_{stdev} Number of standard deviations for the desired failure probability
σ_{ln} Standard deviation of the distribution of wear cycle amplitude

Axial movement

$$\text{Distance moved} = \text{Mean amplitude} \cdot e^{-\delta} \quad (4.28)$$

Angular Misalignment

$$\text{Distance moved} = 2L = 2\,\frac{PD}{2}\,\theta \quad (4.29)$$

where θ Angle of misalignment in radians $= \theta_{mean} \cdot e^{-\delta}$ (4.30)

The calculation of TTF for wear is performed using a loading history or spectrum containing values for torque/loads and the duration of these torque/loads. Data for geometrical and wear parameters are also required. The calculations of predicted life wear are performed in the following steps 1 – 5, (Figure 4.10). The model allows the use of either shaft misalignment or axial slip amplitude as an input parameter.

1. Knowing the mean slip amplitude and variance, the slip amplitude is chosen from the Log-normal probability distribution. Steps 2 – 5 are then performed in sequence for each value of probability p* from 10^{-9} to 0.5, by applying equation 4.27.

2. The value for wear coefficient is the mean value from a Normal distribution, based on values entered by the program user.

3. For each value of slip amplitude chosen at (1) above, equation 4.25 is used to calculate the amount of wear material removed at each load state. Damage is assumed to occur at a (fixed) linear rate at each loading state.

4. The amount of damage accumulated at each load state is summed to calculate the total worn volume for the entire load spectrum/history.

5. The time to failure (TTF) at p* in question is the time taken for the actual damage to reach the failure point, W_{tot}, the limit of acceptable damage.

$$TTF = \frac{W_{tot}}{D_{tot}} \cdot T_{spec} \quad (4.31)$$

where W_{tot} = maximum allowable damage (worn volume)
D_{tot} = wear volume for all load states
T_{spec} = time corresponding to the damage D_{tot}

As an example, if D_{tot} is calculated to be 1 mm^3, calculated from load states representing 100 hours and the maximum allowable damage is 30 mm^3, the predicted TTF is:

$$TTF = \frac{30}{1}.100 = 3000 \text{ hours} \quad (4.32)$$

4.4.3 Wear model Confidence limits

For each value of failure probability, the 2 sigma (95%) confidence limits on TTF are calculated using the upper and lower limits of the wear coefficient, K. The upper and lower limits on the time to failure are then obtained using equation 4.25 with the following values of wear coefficient:

Upper TTF limit $K_{2\sigma} = K_{mean} - 2K_{\sigma}$ (4.33)

Lower TTF limit $K_{+2\sigma} = K_{mean} + 2K_{\sigma}$ (4.34)

where K_{mean} and K_{σ} are the mean and standard deviation of the wear coefficient.

In most of the sensitivity studies however, the confidence limits have not been plotted. This is to achieve more clarity and also because most of the analysis has been conducted to view changes in the mean value.

4.5 Casing Corrosion

The corrosion model adopted in the current modeling approach is based upon a Monte-carlo Simulation in order to provide an estimation of life for the required failure probability p*. The key parameters which are to be included are those which represent:

a) The environment in which the helicopter operates.

b) Corrosion rates of the different materials (mean and coefficient of variation).

c) The mean time for corrosion to initiate (MTTI).

d) The maximum acceptable loss in section of gearbox casing (mean and coefficient of variation).

The corrosion model developed in this work is based on a random (exponential) model

for initiation, followed by a linear model to represent plain and galvanic corrosion after initiation. These two phases represent the probability of the corrosion protection being penetrated, followed by a period of corrosion during which the effective section of the gearbox casing is reduced.

4.5.1 Plain and galvanic corrosion

The main cause of corrosion of the gearbox casing is the galvanic action between the mounting bolts (steel) and the gearbox casing. However, plain corrosion, where no dissimilar metals are involved, may still occur and is therefore part of the model. The Type A gearbox casing is magnesium alloy, while that of Type B is aluminium alloy, A357. The same model, with different parameters, has been developed to represent the plain corrosion and galvanic corrosion of the casing material.

Corrosion rates have been taken from published data for magnesium and aluminium alloys **[Sims and Railton, 1951; Geary, 1990]**. These include data for galvanic and plain corrosion rates, plus details of the protective schemes and coatings used **[Geary, 1996; Danford et al, 1997]**.

The casing is assumed to have failed when the total section loss, M, rises above a predetermined threshold M* specified by the analyst. M is calculated from the different corrosion rates that apply in each environment – see section 4.5.3. The following three environments have been applied in the model:

- Marine; moist air with saline content - sea-borne or shore based helicopters, North Sea operations, Naval ASW and SAR roles.

- Land - inland bases with normal variations in humidity, but little salt content in air, e.g. transport role.

- Dry - hot/arid operating base, e.g. desert, low humidity.

4.5.2 Corrosion Initiation

The model for random initiation may be derived as follows in equations 4.35 and 4.36. The mean time to initiate (MTTI) is the reciprocal of λ, the number of initiating events per month. The random distribution represents the likelihood that the protective coating is damaged or penetrated in some manner, e.g. by an error during routine maintenance. The time for initiation (T_{init}) is sampled using a random, equal-chance model:

$$\text{Prob (initiation)} = p_{init} = 1 - e^{-\lambda t}$$
$$1 - p_{init} = e^{-\lambda t} \qquad (4.35)$$

Taking natural logs of both sides,

$$\ln (1 - p_{init}) = -\lambda t$$

$$T_{init} = \frac{-\ln(1-p_{init})}{\lambda} = -\ln(1-p_{init}).MTTI \qquad (4.36)$$

4.5.3 Corrosion growth

The rate of corrosion is assumed to be linear, an approximation justified by the lack of appropriate models for casing corrosion. Research work on the corrosion of gearbox casing materials gives constant values for corrosion rates **[Geary, 1996]**, which depend on the environment, e.g. humidity, salt content of the air. The proportion of time spent in each environment (marine, land, dry) is used to calculate the total section loss for critical sections of the gearbox casing.

The corrosion rate for each environment is assumed to be Normally distributed, with mean and COV used to describe the variation in corrosion rate. The effective corrosion rate R may be calculated as **[Mansfeld, 1982]**:

$$R = r_m.\frac{p_m}{100} + r_l.\frac{p_l}{100} + r_d.\frac{p_d}{100} \qquad (4.37)$$

where r_m, r_l, r_d — Corrosion rate for the respective environment in mm/year
p_m, p_l, p_d — Percentage time spent in marine, land, dry atmosphere.

4.5.4 Total time to reach corrosion limit

The predicted time to failure is calculated as the point when $M > M^*$, where M^* is the maximum allowable section loss due to corrosion. M^* is also taken from a normal distribution, with estimated mean and variance. The time to reach the unacceptable corrosion limit, T, is calculated as follows:

$$T = T_{init} + \frac{M^*}{R} \qquad (4.38)$$

where T_{init} — Time for corrosion to initiate in years
M^* — Metal loss limit due to corrosion in mm
R — Effective corrosion rate in mm/year

4.5.5 Application of Corrosion model

The corrosion model makes use of Monte Carlo simulation (described in Chapter 2) to draw samples from the distributions for corrosion rates, time to initiate and maximum allowable damage, M^*. A total of 10000 trails are run each time the programme is run, according to the following sequence (Figure 4.11):

1. Sample to obtain T_{init} from a negative exponential distribution based on the mean time to initiate (MTTI) supplied by the user. This is the time at which the corrosion is assumed to begin due to penetration of the protective coating.

2. Sample from normal distributions to obtain corrosion rates in the marine and land environments, using values for the mean and COV supplied by the user. The program samples from the probability distributions that represent the variability of the corrosion rates.

3. Sample from normal distribution to obtain the failure limit M*. The COV allows for the variability in inspection regularity and in the success of detecting corrosion.

4. Calculate time to reach corrosion limit from equation 4.38. The results of the 10000 tests are then ranked in order of time to reach corrosion limit, T. This allows the probability of failure to be estimated with the corresponding time in months.

5. With knowledge of the flying rate in hours per year, the time to reach the corrosion limit is directly compared with the cycles-base damage models for wear and fatigue.

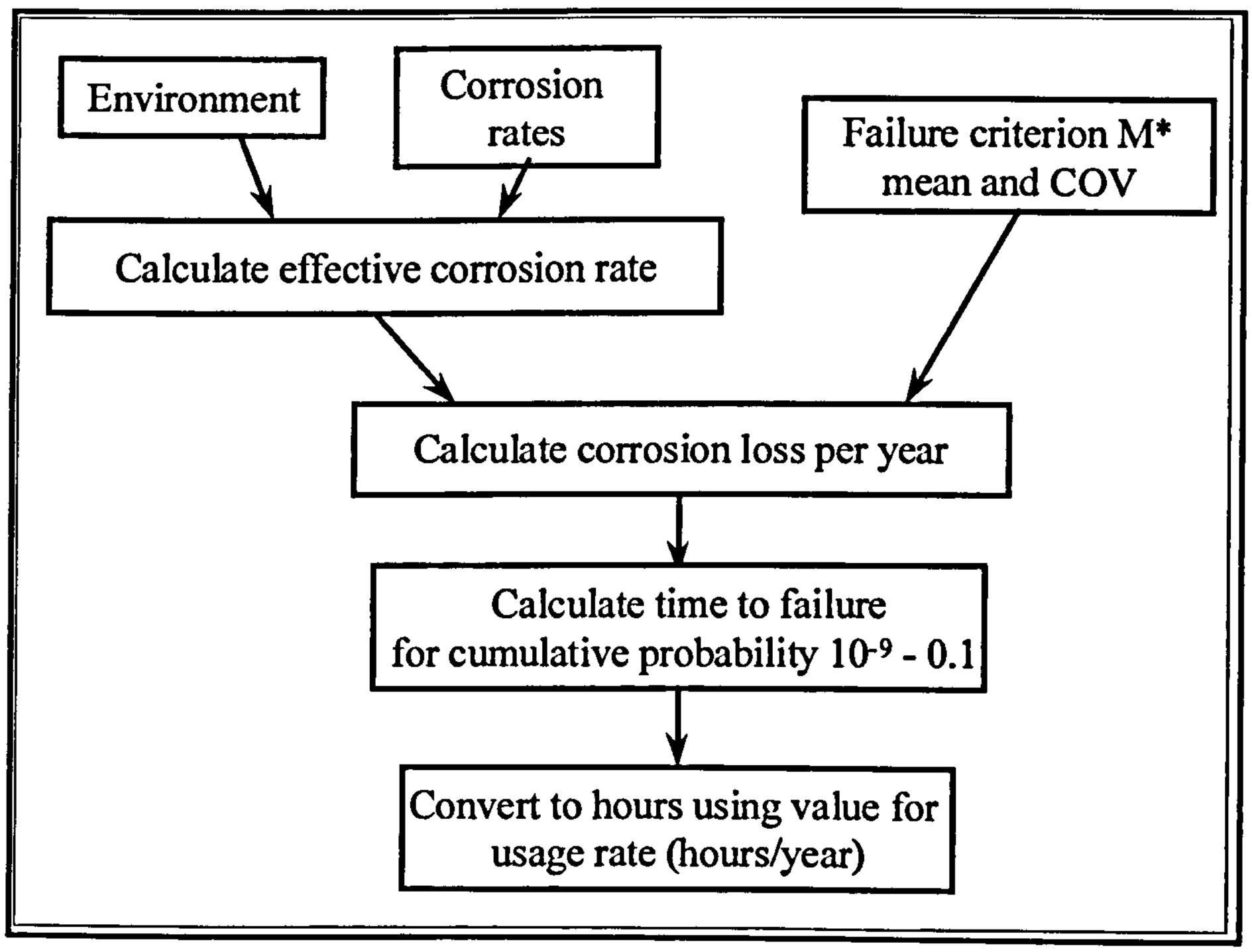

Figure 4.11 : Sequence for calculating corrosion TTF

4.6 Maintenance Errors

The introduction of errors during initial assembly, overhaul and/or routine maintenance is an ever-present possibility throughout the service life of a gearbox **[Astridge, 1996a]**. Those errors that have been considered have been listed in Table 4.2.

Without test data, it is very difficult to accurately assess the correlation between the angle of misalignment and the reduction in the endurance limit. Hence, the maintenance errors considered are those that affect, or initiate, spline wear and casing corrosion. This assumption is justified by considering the failure mechanisms observed in service.

Part	Description of Error	Effect of Error
Coupling splines	Inadequate lubrication	Increased wear coefficient
Coupling splines	Shaft misaligned or not adjusted correctly	Increased relative displacement
Casing (external)	Mechanical damage to casing and/or protective coating	Initiates corrosion

Table 4.2 : Summary of maintenance errors represented [Astridge 1996a, 1997]

Although such maintenance errors would reduce the expected reliability of rotating components, i.e. gears, shafts and bearings, no data are available with which to quantify this reduction in component life. Maintenance procedures dictate extremely accurate tolerances for gear tooth meshing, such that examples of gear misalignment are rare. The parameters studied for gear fatigue are therefore limited to material and load variability.

4.7 Combination of diverse failure mechanisms

In order to calculate a value for the system reliability, it was first necessary to combine the failure probability values for the separate failure mechanisms. The program is able to predict the probability of diverse failure mechanisms occurring individually. However, up to this point 'failure' has been defined differently for each mechanism so a simple 'Time to failure' (TTF) does not indicate the severity of the failure process.

Some of the degradation processes lead to functional failure of a component, e.g. tooth root bending fatigue results in the breakage of a tooth leading to a potential loss of drive. Other failure processes, e.g. fatigue pitting of the gear teeth and bearings, are more progressive in nature and may give an early warning of potential failure, detectable by health monitoring (HM) techniques. Multiple failure mechanisms have been combined by considering the effectiveness of the HM system in the computer model. This has two major benefits since:

a) diverse failure mechanisms may be combined, and

b) detection capability of the HM may be included in the reliability prediction and hence its effectiveness can be evaluated.

The above has been accomplished by considering the probability of detection (POD) of each failure mechanism **[Martin et al, 1983]**. In the case of a progressive degradation process, should the HM system fail to detect early warning signs, a functional failure could occur. For such cases, the POD is combined with the probability of degradation occurring to calculate a probability of functional failure:

$$p(FF) = p(PFM) \,.\, p(PFND) = p(PFM) \,.\, (1 - POD) \qquad (4.39)$$

where

p(FF)	Probability of functional failure
p(PFM)	Probability that progressive failure mechanism occurs
p(PFND)	Probability that a progressive failure mechanism is not detected by the health monitoring system.
POD	Probability of detecting damage caused by failure mechanism = 1 - p(PFND)

The significance of POD will be evaluated for the failure mechanisms described by the reliability models. This relates to the condition monitoring provisions within the gearbox as described in Chapter 5, and also to the likelihood of successful damage detection by other means, e.g. inspection.

Since the probability of successful damage detection is related to the amount of damage, the POD may be varied depending on the threshold of allowable damage **[Harlow and Wei, 1999]**. In the case of TRBF the POD was related to the Miner damage sum (DS), with increasing POD for increasing DS. The values used were POD 0% at DS 0.8, 50% at DS 0.9 and 90% at DS 1.0 **[Irving et al, 2000]**

4.8 Calculation of System Reliability

4.8.1 Background

The common underlying loads that affect all failure mechanisms (except corrosion) complicate the prediction of the system reliability. The frequently used 'series' system representing a chain of independent units (Figure 4.12) is not strictly valid in this situation **[Astridge, 1996b]**. Chapter 2 introduced the concepts of loading roughness (LR), reliability index β and safety margin (SM) as applied to system reliability.

Figure 4.12 : Reliability Block Diagram of a Series System

4.8.2 Method of Calculation

Work undertaken in the unrelated field of structural design has shown that a multi-dimensional mathematical solution is required **[Ang and Tang, 1984]**. This was discussed in Chapter 2. However, the upper and lower limits for such a calculation can be calculated from knowledge of the individual failure probability values. **[Ang and Tang, 1984]** state that the two bounds of R_{sys}, the system reliability, are given by the following two cases:

a) All components are independent, there is no 'spread' on the load distribution – smooth loading (LR is zero):

$$R_{sys} = 1 - p_{sys} = \prod_{i=1}^{k} (1 - p_i) \qquad (4.40)$$

where p_i is the probability of failure for each of the k components

b) All components interact, there is no 'spread' on the strength distribution – rough loading (LR is 1):

$$R_{sys} = 1 - p_{sys} = 1 - p_{max} \qquad (4.41)$$

where p_{max} is the highest failure probability at a given time.

With an intermediate value of loading roughness, the system reliability will lie between these two values, as follows:

$$\prod_{i=1}^{k} R_i < R_{sys} < R_{min} \qquad (4.42)$$

where $\prod_{i=1}^{k} R_i = R_1.R_2.R_3...R_k$, R_i is the individual unit reliability and R_{min} is the individual reliability of the first unit to fail

4.8.3 Calculation of failure probability from TTF

The HGBR program was written on the basis that the material properties of the relevant component and the applied load history were known. A Log-normal distribution was assumed for the S-N curve, or its equivalent, and a particular S-N curve selected for the

failure probability desired. These parameters were then used to calculate a predicted time to failure, or time to first spall. This produced a failure probability curve in the form of Figure 4.13, where p_1 - p_4 are pre-defined, and values for time to failure t_{F1}, t_{W1} etc. are calculated by the respective model.

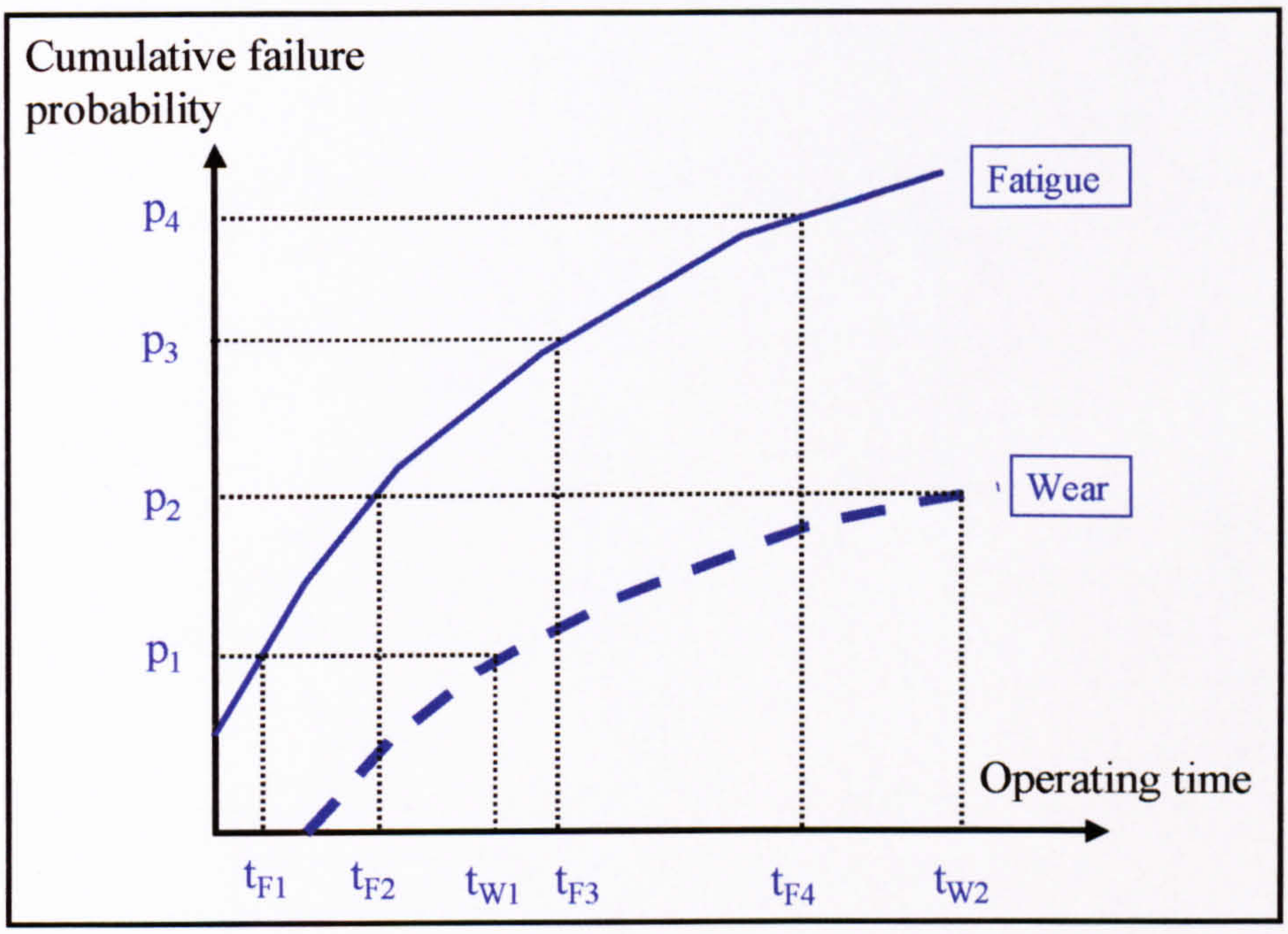

Figure 4.13 : Illustration of calculation of TTF (t_{F1} etc) at discrete values of p*

A different approach was taken to combine the different failure results in order to determine bounds for the system reliability. Values for the latter quantity must be calculated at discrete points of time, at intervals determined by the range of interest, in order to allow equations 4.40 and 4.41 to be employed.

This method is shown schematically in Figure 4.14, where values for T1 - T3 are pre-defined, and the requirement is to calculate p_{1W}, p_{1F} etc. The failure probabilities thus calculated are then used to calculate the upper and lower bounds for system reliability at these points, chosen in this case between 1 and 10^5 hours.

The method of calculation adopted allows the time to failure (TTF) to be specified, which is followed by the calculation of the cumulative probability for this TTF. The mathematical expression used in Section 4.2.2 is reversed in order to determine the values of p* at a particular TTF for a given set of material and loading parameters, see Appendix C.4. The procedure is straightforward for certain models, in particular:

- Bearing contact fatigue, where p* may be calculated by re-arranging the L_{10} life equation for different values of TFS.

- Spline wear, where a Log-normal distribution is used for slip amplitude, allowing p* to be determined from knowledge of the worn volume.

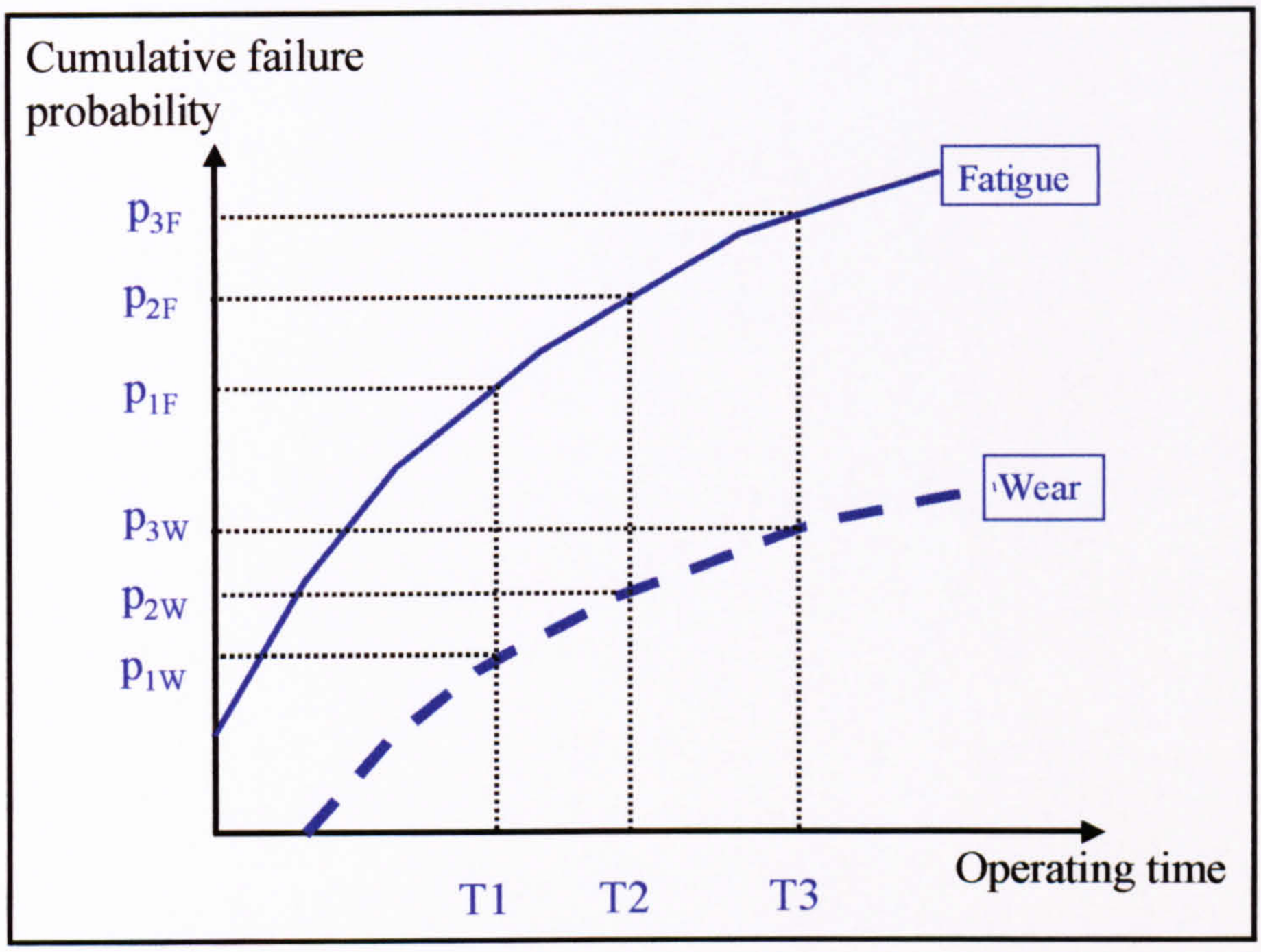

Figure 4.14 : Illustration of calculation of p* (p_{1F} etc) at discrete lives T1 etc

For gear TRBF and RCF, the use of the S-N curve required an iterative solution to be adopted. This was coded in Visual Basic™, as an addition to the HGBR program, and is explained in Appendix C.

The corrosion model presented certain different features due to the use of a Monte-Carlo routine to generate simulated test results. As explained in Section 4.5.5, a total of 10,000 results are calculated and then ranked in order to produce a cumulative density function (CDF). From this it is possible to derive the TTF for particular values of p*.

A difficulty arises however when it is required to find p* for particular values of TTF. Unlike the other models where the formulae applied to calculate life may be re-arranged, the corrosion model does not enable the user to do the same. The solution in this case is to apply an interpolation routine to the 10,000 data points within the corrosion CDF. For each required TTF, the routine searches for the corrosion results closest to and on either side of this value. By linear interpolation, an approximate value for p* is found in every case where the TTF falls within the band of 1 to 10^5 hours.

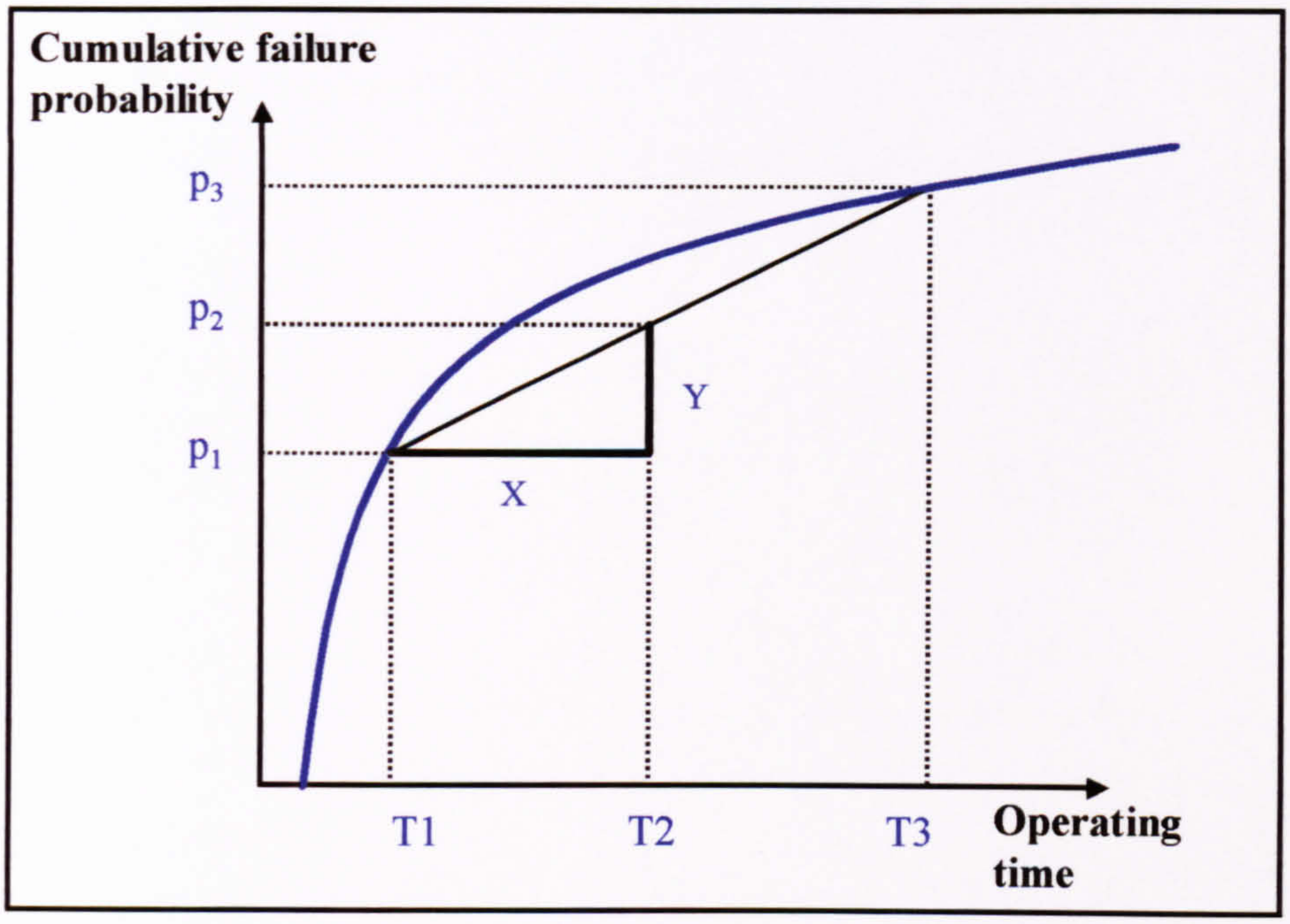

Figure 4.15 : Schematic of interpolation routine for Corrosion model

Referring to Figure 4.15, the values of p1 and p3 are known, corresponding to T1 and T3 respectively. It is required to find the value of p* at T2, in this case, which is achieved as follows.

Gradient of straight line is $$\frac{Y}{X} = \frac{p_3 - p_1}{T3 - T1} \tag{4.43}$$

Value of p_2 is calculated approximately,

$$p_2 \approx p_1 + (T2 - T1) \cdot \frac{(p_3 - p_1)}{(T3 - T1)} \tag{4.44}$$

5 Health and Usage Monitoring Techniques in Helicopter Transmission Systems

5.1 Introduction

A key development in the pursuit of improved safety and reliability in helicopter transmissions is the introduction of health and usage monitoring systems (HUMS). The monitoring techniques have been reviewed to describe their effectiveness in monitoring the condition and usage of the gearbox. The particular aim is to determine their relevance to the system reliability prediction for the gearbox.

The report of the Helicopter Airworthiness Review Panel (HARP) made a total of 15 recommendations for improving the safety and reliability of helicopter design and operation **[CAA, 1984]**. Three of these 15 recommendations made direct reference to the application of condition monitoring to helicopter systems, which lead to the increased application of health and usage monitoring systems (HUMS). The term HUMS is used to encompass a wide range of monitoring techniques and functions, including fatigue and creep life usage, performance and status monitoring of all mechanical systems and subsystems **[Astridge, 1996a]**.

Helicopter HUMS provide discrete and continuous monitoring of parameters that describe, directly or indirectly, the condition (health) and the loads imposed (usage) on the engine, rotor and transmission components (gears and shafts). At the most basic level, condition monitoring includes sensors to measure oil temperature and pressure, ranging up to techniques for diagnosing gear and bearing defects and quantifying the amount of contaminated lubricant.

Health monitoring (HM) is a technique that provides a means of determining the continued serviceability of components, systems, or structures, without the need for component removal for inspection **[MOD, 1989]**. Its purpose is to improve flight safety, rotorcraft availability, maintainability, reduce life cycle costs and provide the ability to complete a flight. Health monitoring is provided by a number of systems and techniques, which will be described in Sections 5.2 to 5.4.

Usage monitoring (UM) is a technique that assesses the life consumption of life-limited components, systems, and structures by monitoring the actual load, rpm, engine and oil temperature etc. This allows an estimate to be made of the damage accumulated by the component or system **[MOD, 1989]**. Usage monitoring and the benefits therefrom are described in Section 5.6.

Operational trials of HM systems, to evaluate vibration health monitoring (VHM) techniques, were carried out by two operators from 1987 to 1991, a review of which was published by the CAA **[CAA, 1993]**. HUMS is now widely used by all North Sea operators, and is being installed or retrofitted to new and existing medium to heavy rotorcraft. The importance of HUMS is reflected both in airworthiness regulations, e.g.

JAR-29 **[JAA, 1993]** and in accident and incident reports **[AAIB, 1988, 1997]**. HUM systems have also made a significant impact with regard to maintenance credits and the adoption of on-condition maintenance strategies **[CAA, 1992; MOD, 1989]**.

5.2 Oil debris monitoring

Oil Debris monitoring is used to detect damage to the gears (scoring, pitting, wear) and bearings (pitting, retention failure) **[Augustin, 1998]**. These failure processes generate debris with a distribution of size, shape and number. The analysis of oil debris provides a qualitative and quantitative analysis of the size, number, morphology and origin of metal released by these failure processes. However, the quantity of debris detected may represent only a proportion of the actual metal lost from the surface of the bearing, due to inefficiency in the detection (Section 5.2.1). Examples of oil debris analysis applied to the Type A gearbox are given in Section 5.2.4.

The onset of fatigue and/or wear of gearbox components could be due to any number of factors e.g. shaft misalignment, stress concentrations or contamination of the lubricant. Debris may be released in any combination of size, shape and rate, and there are a number of different techniques applied to detect particles. The sensitivity of a number of techniques to particle size is portrayed in Figure 5.1.

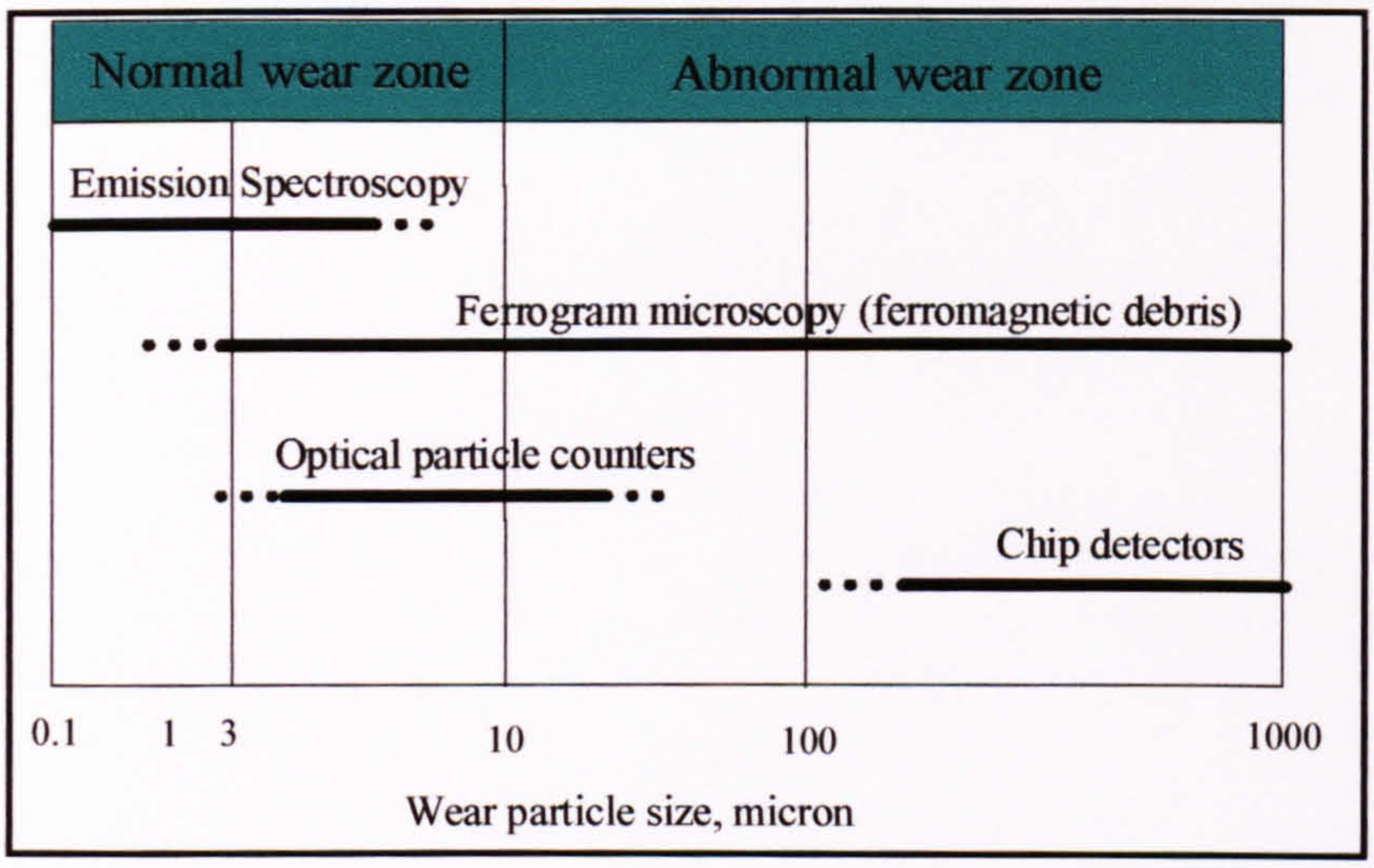

Figure 5.1 : Particle size sensitivities of wear particle technologies [Fitch, 1999]

5.2.1 Magnetic Chip Detector

The Magnetic Chip Detector (MCD) is normally located in the lower part of a gearbox, and works by attracting magnetic particles that may be present in the circulating lubricant. During flight, if enough debris is attracted to the plug, the gap between two contacts may be bridged, so providing an indication to the pilot - called a 'Trans-chip' (Transmission chip) warning.

The performance of oil debris monitoring is dependent on the debris detection efficiency, which is influenced by the effectiveness and location of the device. It is extremely important to place the debris monitor in a location where it will detect the debris released from a damaged component. The debris detection efficiency is the ratio of product of the number of particles indicated by the detector to the number of particles released by wear, fatigue etc. It is the product of the three efficiencies listed below **[Howard, 1987]**:

- Transport efficiency - the number of particles which travel past the detector (n_p) as a proportion of the number of particles released by wear, fatigue etc (n_r).

- Capture efficiency - the number of particles caught by the detector (n_c) as a proportion of the number of particles that travel past the detector (n_p).

- Indication efficiency - the number of particles indicated by the detector (n_i) as a proportion of the number of particles that are caught by the detector (n_c).

$$\text{Debris detection efficiency} = \frac{n_i}{n_r} = \frac{n_p}{n_r} \cdot \frac{n_c}{n_p} \cdot \frac{n_i}{n_c} \qquad (5.1)$$

5.2.2 Quantitative Debris Monitoring

Development of the MCD has led to the ability to quantitatively assess the number and sizes of particles in the oil system, a technique termed Quantitative Debris Monitoring (QDM). Such a sensor has a coil assembly with a fixed magnetic field **[Howard, 1987]**. When ferrous debris is attracted by the magnetic pole of the sensor, it creates a disturbance in the magnetic field proportional to the mass of debris captured **[ibid]**.

The sensor is calibrated to register different particle sizes, sometimes in two categories (small and large) and provide a count of each. The criteria for the rejection (removal from service) of a gearbox by QDM are based upon the detection of distinct sizes of debris. Once a pre-determined threshold is exceeded, based on the cumulative number of particles generated and/or the rate of particle generation, an alert to the pilot or maintenance staff will be generated.

5.2.3 In-line oil debris monitor

Another device that may be used in the lubrication circuit is the in-line oil debris monitor (ODM). This uses a series of coils in which an alternating magnetic field exists. Metallic debris passing by the monitor alters the magnetic field, resulting in a characteristic output signature **[Goddard and MacIsaac, 1995; Muir and Howe, 1997]**. This technique is capable of estimating the size and number of ferrous and metallic non-ferrous particles, in the range from 135 to 630 μm **[Goddard and MacIsaac, 1995]**.

5.2.4 Oil Debris Analysis

In many engines and gearboxes, oil debris analysis is one of the techniques employed to measure the quantity of wear debris produced, which may originate from the gears, shafts or bearings. Regular oil samples are subjected to spectrographic analysis (see Section 5.2.5) in order to determine which contaminating elements (if any) are present in the lubrication system, up to a maximum particle size of approximately 10 μm.

Above this size of particle, the primary method of detecting and measuring ferrous debris wear is to examine the residue from the Magnetic Chip Detector (MCD) using an optical microscope. If debris is present, further analysis is undertaken using Scanning Electron Microscopy (SEM) and Energy Dispersive X-ray Analysis (EDAX).

The magnetic plug may be removed and checked at regular intervals, e.g. every 50 hours of operation, within 30 minutes of engine shutdown. Ferrous debris that has been attracted to the plug is wiped on to a piece of adhesive card, which is then sent for laboratory examination **[Hunter, 1975]**. In the laboratory, the 'plug wipe' is examined first under the optical microscope, then with a SEM, with EDAX. EDAX is capable of identifying the composition of the metallic debris, and hence the source of the debris, since different bearing steels are often used in each of the four bearings. The number and size of particles, composition and morphology are studied as in the example SEM image, Figure 5.2.

The debris detected give some indication of the amount of material lost by wear on the bearings and/or gears in the gearbox. This indication will depend on the efficiency of the chip detector (Section 5.2.1) since often **[Cooper, 1989]** only a proportion of the material removed by the fatigue or wear process will reach the sensor.

On the basis of the oil debris analysis, a gearbox may be removed from service if there is enough concern about its condition. However, there is little information available to correlate the quantity and type of debris with the actual extent of damage to a component. Recent work has been carried out with a view to automating the diagnostic process using particle recognition software **[Farrant, 1999]**. Work is also underway in the development of wear debris identification software that will help to identify the failure mechanism from the size and shape of the debris particles **[Barraclough et al, 1999; Price & Roylance, 1998]**.

Figure 5.3 presents the results from the EDAX for a typical sample of bearing debris, showing the relative proportion of each element in the material. Knowledge of the types of steel used within the gearbox components should then allow the user to pinpoint the source of the debris, even to distinguish between bearing rollers, cage and race.

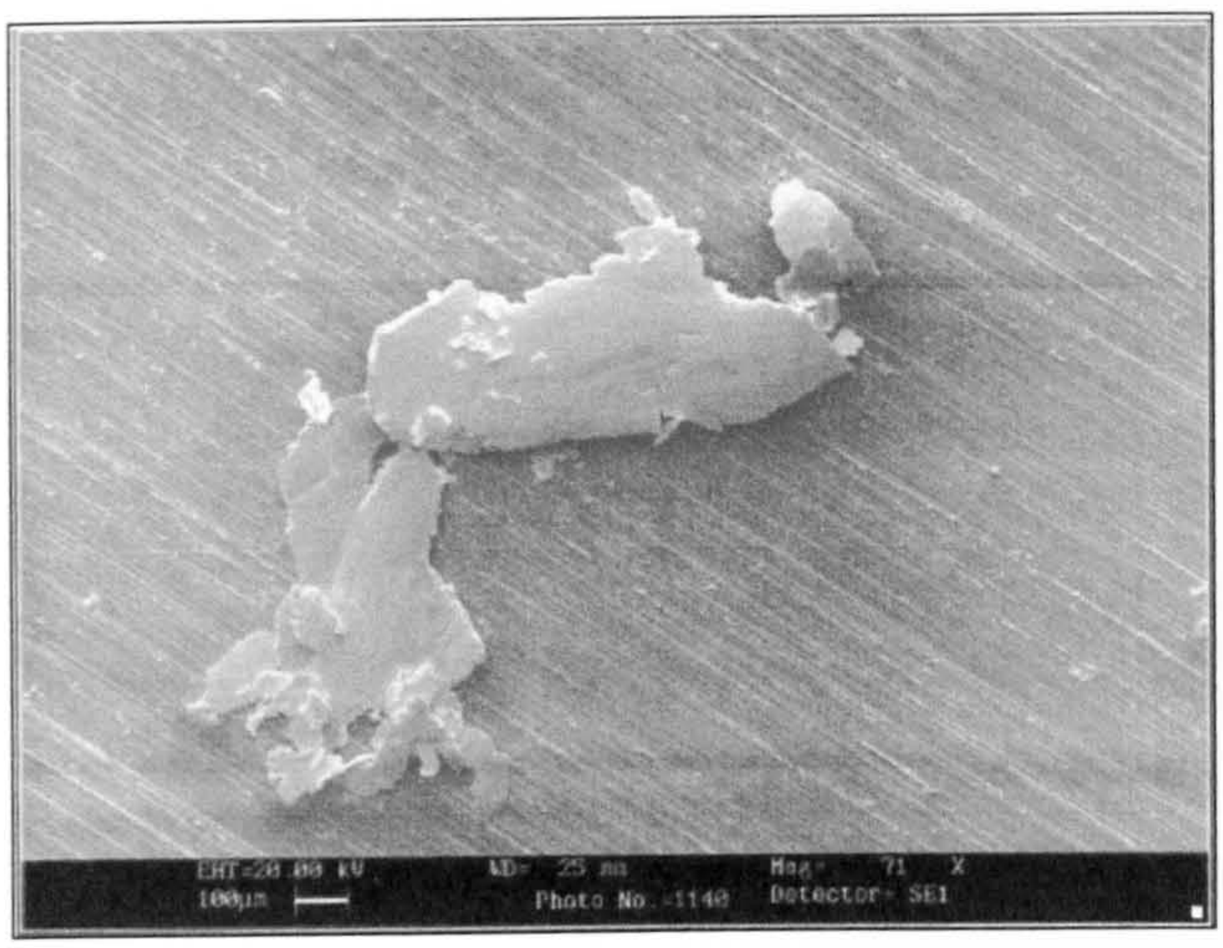

Figure 5.2 : SEM image of debris from bearing steel [1]

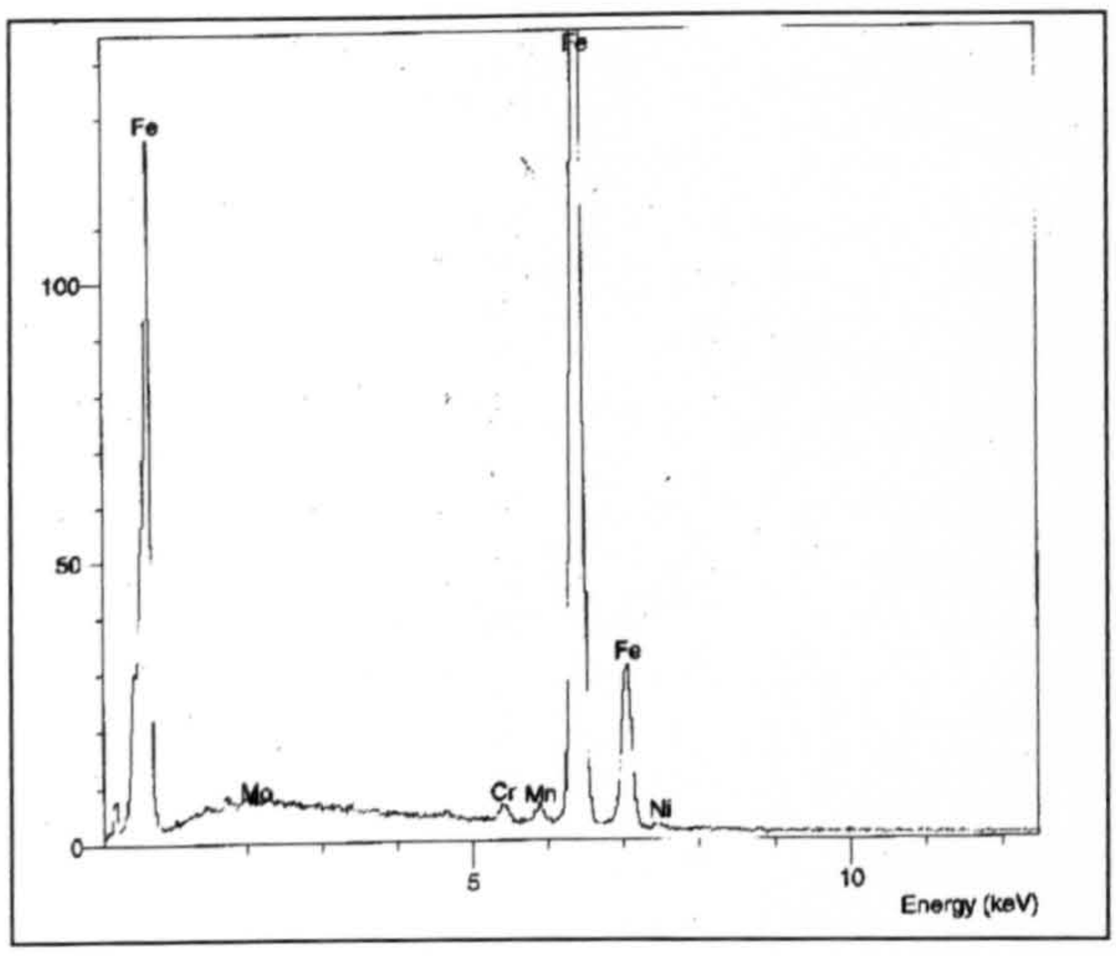

Figure 5.3 : EDAX analysis of Wear Debris [1]

5.2.5 Spectrographic Oil Analysis Program

The Spectrographic Oil Analysis Program (SOAP) is widely used for both ferrous and non-ferrous particles of up to 5-7 µm. Oil samples are taken from the gearbox at regular intervals (e.g. 50 hours) and analysed using either atomic absorption or optical emission techniques. A minute quantity is vaporised using an electric arc, and the resulting wavelengths of emitted light are measured **[Hunter, 1975]**. Each wavelength corresponds with a particular element, allowing a measure in parts per million (*ppm*) to be made.

---

[1] SEM/EDAX images supplied by Naval Aircraft Materials Laboratory

The results give the number of *ppm* of each element contained in the oil, and given certain knowledge of the alloys present in the oil it is possible to determine which components are producing material **[Collier-Marsh and Astridge, 1985]**. The drawback with SOAP analysis is that it is off-line and can be slow (since laboratory facilities are necessary), and it is often difficult to detect a trend of deterioration. SOAP analysis is useful for detecting particles too small to register from the analysis of magnetic plug debris.

5.3 Vibration monitoring

Vibration health monitoring (VHM) is among the most widely used form of HM for all types of rotating equipment. For the helicopter transmission system, VHM is provided by a series of accelerometers positioned at strategic positions on the gearbox casings and shaft housings. The accelerometers measure the vibration of the shafts and gears, the data for which is then processed to enable any abnormal trends to be recognised and, if possible, pinpointed to the relevant component. Typical locations for the accelerometers are shown in Figure 5.4, an example of a typical medium to heavy twin-engine helicopter.

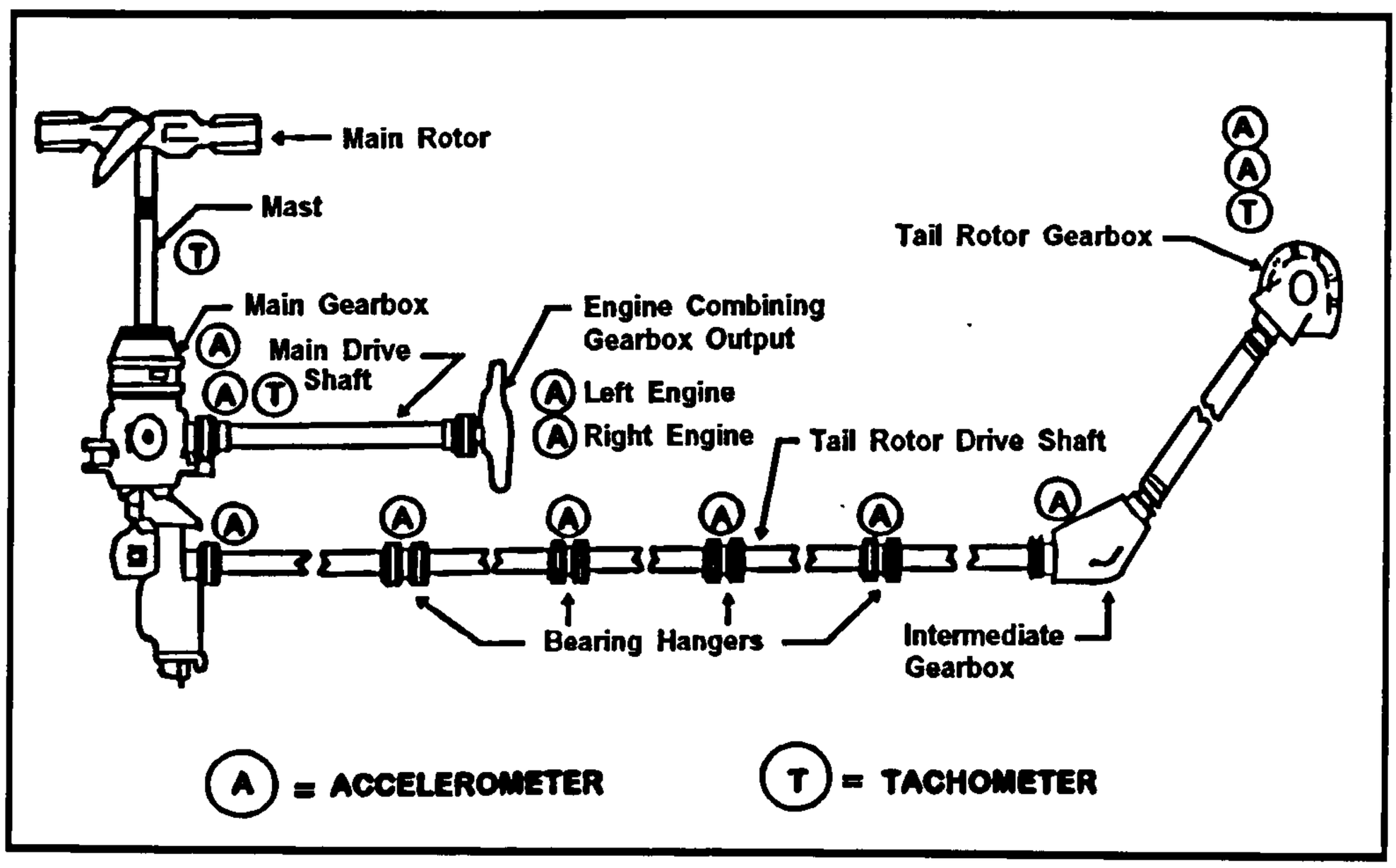

Figure 5.4 : Drive train vibration sensors [Augustin, 1998]

Deliberate tests to failure in gearbox test rigs have shown that impending fractures seldom cause tell-tale debris to be released. The only method of detection is vibration analysis, which has greater sensitivity than visual inspection **[Collier-Marsh and Astridge, 1985]**. Information on techniques used to process the vibration data and the correlation with gearbox component damage may be found in **[Gadd and Mitchell, 1984; Cameron and Stuckey, 1994]**.

The detection and diagnostic capability of VHM is crucial if it is to provide early warning of impending component failure. Not only must the vibration sensors be optimised for location and sensitivity, but the output in terms of vibration levels and trends must be analysed correctly. The diagnostic ability of the system will depend largely on the acceptable threshold levels set by the user; if too low there will be too many 'nuisance alerts'. If set too high then there is a significant risk that an accident could occur.

Work is still ongoing to build up experience of diagnosing gearbox failure mechanisms from both in-service components and seeded fault trials **[Hess et al, 1998]**. There is also potential for the fusion of data from both oil debris monitoring (Section 5.2) and VHM to provide an enhanced diagnostic capability **[Howard and Reintjes, 1999; Byington et al, 1999]**.

5.4 Application of HM data

The HM data available for the two types of helicopter considered differ in respect of the number of parameters available for inspection. The Type A gearbox was designed in the 1960s before significant development of health and usage monitoring. Most modern transmission systems have HUMS as an integral part of the design. Table 5.1 contains a summary of the different HM sensors and techniques and the parameters measured.

Monitoring technique	Parameter measured
Magnetic chip detector	Presence of debris caused by wear and/or fatigue
Oil sampling	Size, shape, morphology of debris in oil
SOAP test	Type of material present in oil, e.g. removed by wear and/or fatigue
QDM debris monitor	Number of ferrous particles generated by wear and/or fatigue and rate of generation
Accelerometer/ azimuth sensor (vibration health monitoring)	Acceleration due to vibration
Oil level sensor (on ground)	Oil quantity remaining
Temperature sensor	Oil temperature
Pressure sensor	Oil pressure

Table 5.1 : HM parameters measured in typical transmission system

The effectiveness of vibration health monitoring in use with commercial operators is exemplified in **[Kershner et al, 1997]**, which shows its ability to correctly identify the

onset of failure mechanisms. This is based on a total of 210 000 flying hours amassed by 43 Sikorsky S-61 and 23 S-76 from 1993 to 1996. Data from the North Sea operators has also been collected and assessed by the CAA **[McColl, 1997]**. The latter represents data from 160+ aircraft which accumulated in excess of 500 000 flying hours over the reported period.

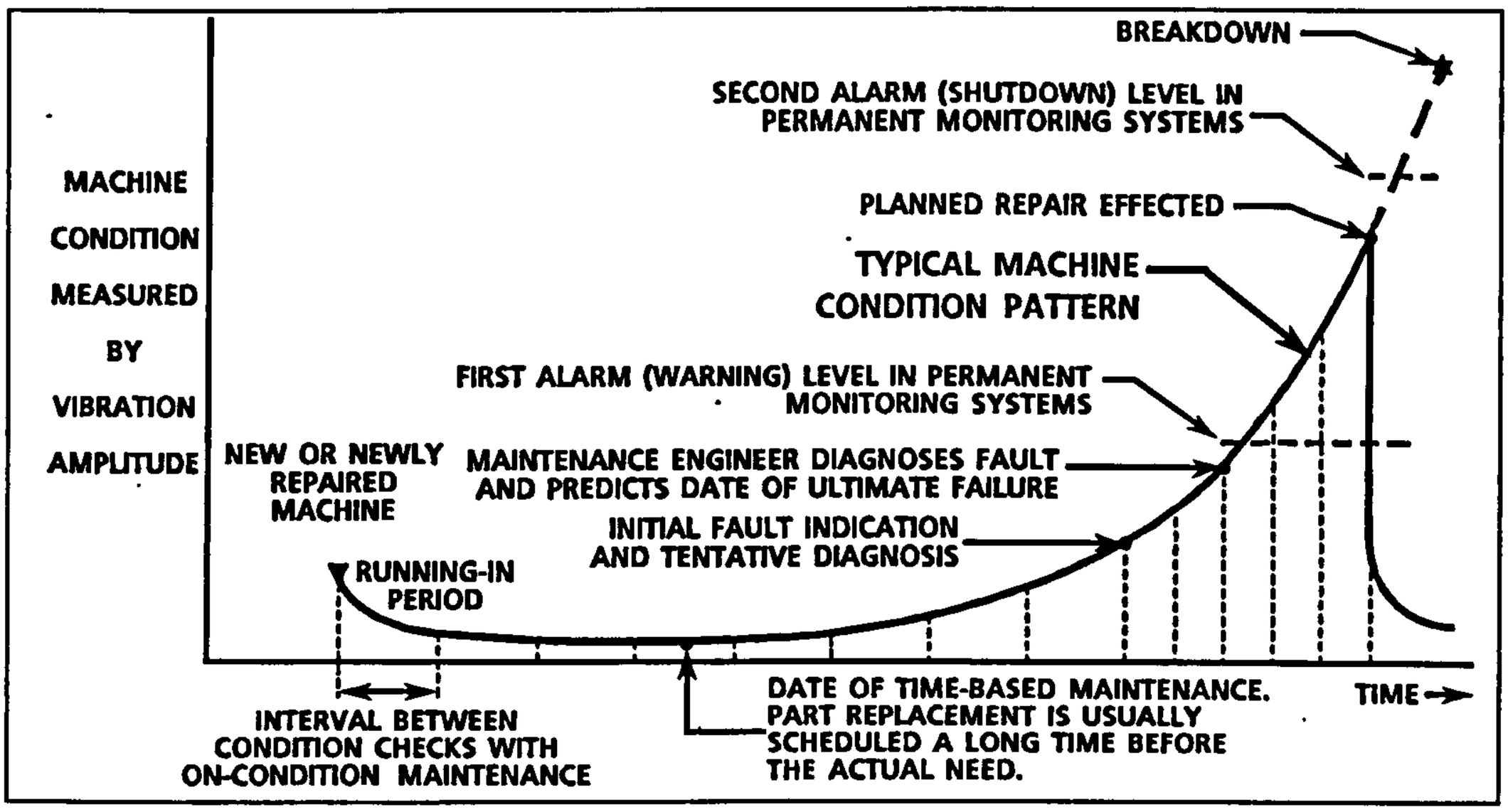

Figure 5.5 : Machine Wear out Pattern [Augustin, 1998]

The influence on life prediction of HM data may be considered based upon the data provided. HM systems indicate the presence or absence of a developing failure mechanism (see Figure 5.5), and ideally the extent and location of the fault. However, no data are provided with which to assess the remaining useful life, unless evidence of failure is detected. This means HM is a failure warning device rather than a means of calculating the eventual point of failure.

An incident with G-PUMH highlights this, where post-incident analysis revealed that the first indication could be seen just 50 hours before component fracture, in Figure 5.6 **[AAIB, 1997]**. This is due to the high cyclical loading and speed of rotation of critical components (approximately 3000 rpm).

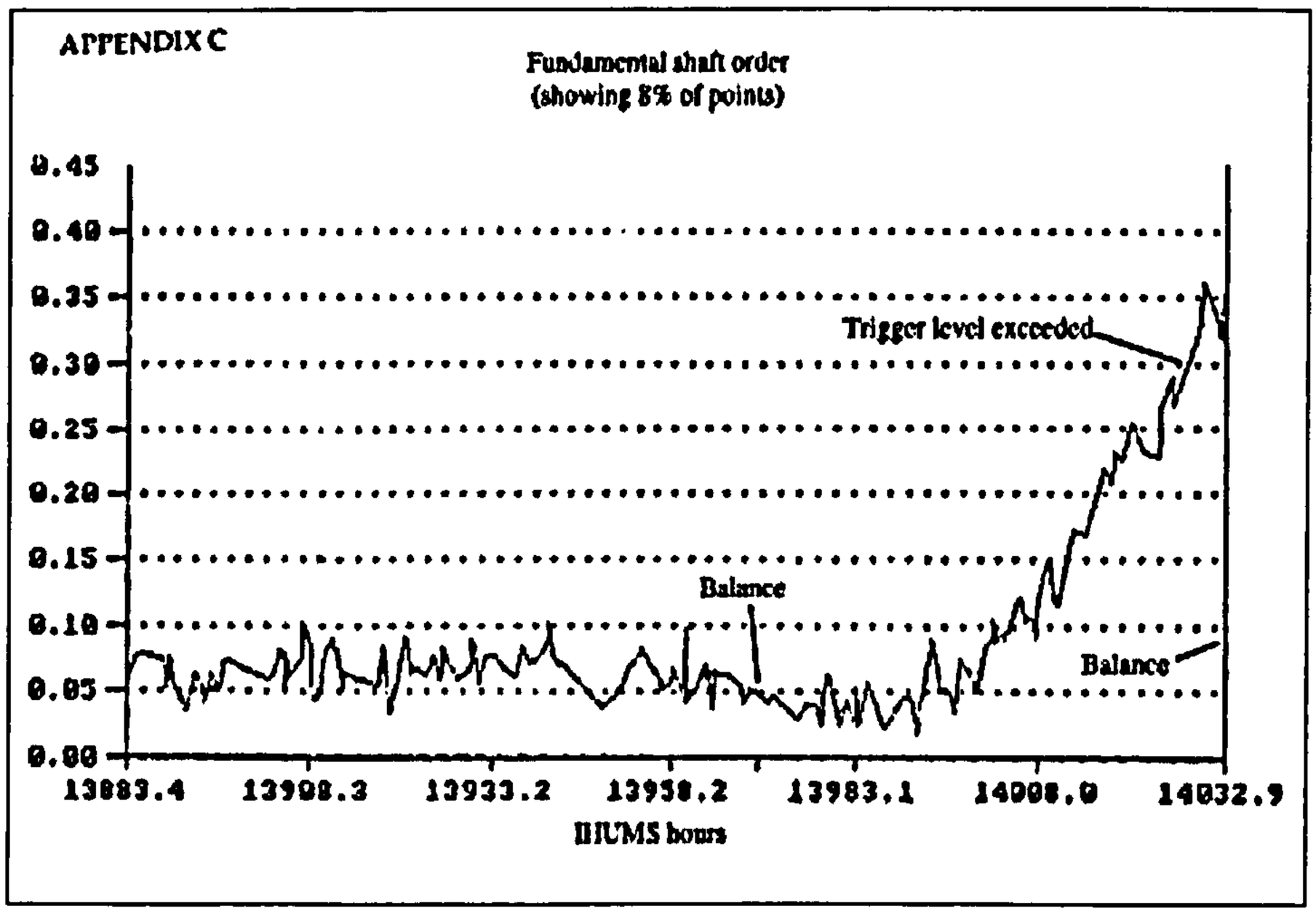

Figure 5.6 : IHUMS trace from TRGB of helicopter G-PUMH before incident [AAIB, 1997]

5.4.1 HM Probability of Detection

The accuracy and sensitivity of HM systems may be considered in terms of the probability of detection (POD) and the probability of correct diagnosis (PCD) **[Fillion, 1996]**. The POD of a HM system is a means to quantify the reliability of that system in detecting a failure mechanism before failure occurs; the PCD is a measure of the likelihood that the location and extent of the fault will be correctly identified. Both quantities are normally quoted as a percentage, together with an associated level of confidence, e.g. 95% **[Heida, 1984]**.

It is essential that the cumulative POD be as high as possible since certain failure mechanisms progress rapidly, as depicted in Figure 5.5 and Figure 5.6. The POD will generally depend however on the size of defect, or extent of damage, to be detected, as illustrated in Figure 5.7.

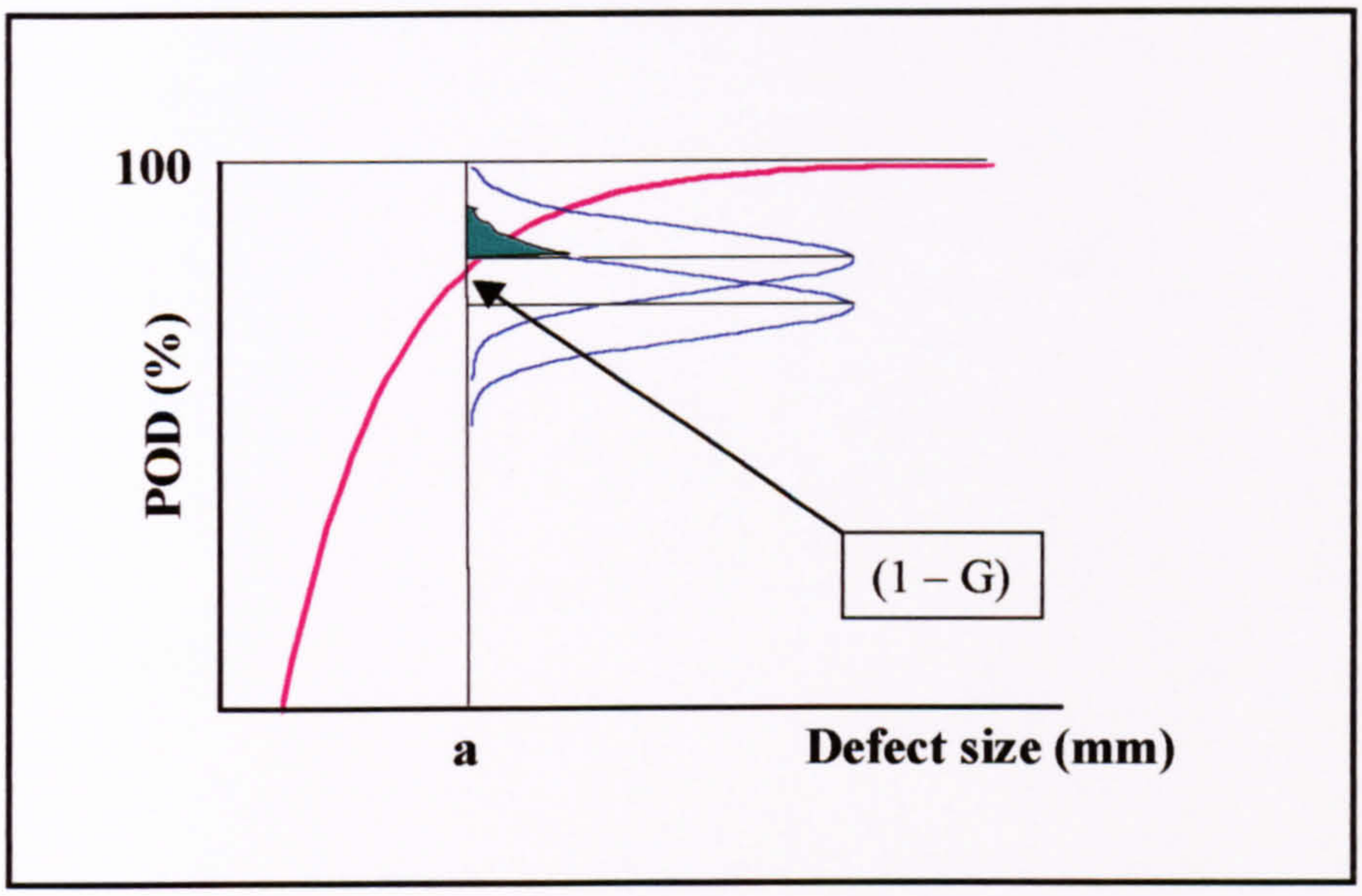

Figure 5.7 : Graph of POD against defect size, showing the representation of specified confidence level G [Heida, 1984]

The POD for vibration health monitoring has been estimated in Section 5.5, which provides an example using in-service detection data. Quantifying the POD also provides a means of combining diverse failure mechanisms, as described in Chapter 6.

5.5 Calculation of Probability of Detection

A method for evaluating the detection capability of HM systems has been applied by **[Fillion, 1996]** using data provided by the CAA from North Sea helicopter operators. This featured the application of a technique for calculating the reliability of a discrete detection system (Non-Destructive Inspections, NDI) to a continuous condition monitoring system (HUMS).

Type	HM detection	No	Potentially catastrophic or hazardous	Major	Minor
1	Successful detection by HM	43	6	24	13
2	Fault evident from HM data after arising *	11	2	9	
3	Fault not detected by HM	9	2	7	
	Total arisings	**63**	**10**	**53**	

Table 5.2 : Detection figures for HM systems [McColl, 1997]

Updated HM data was recently published by **[McColl, 1997]**, representing over 500 000 hours of accumulated flight data. The HM techniques were all based on vibration monitoring and rotor track and balance (RTB) and did not include oil debris monitoring. The data showed a total of 72 arisings, where an arising is defined as an event that led to a significant maintenance action. Of this figure, 63 were related to airworthiness, categorised in Table 5.2.

Type 2 marked * can be considered as HM system success in detecting but failure to correctly diagnose the fault **[Fillion, 1996]**. The numbers of occurrences in Type 1 and 2 were therefore added together to obtain a total of 54 detected faults from 63 possible cases, or 85.7%. The POD of the HM system can be calculated by applying the following equation **[Heida, 1984]**:

$$P_L = \frac{n}{n + (N - n + 1).F_G(f_1, f_2)} \qquad (5.2)$$

where P_L is the lowest confidence limit, or the POD
N is the number of inspections in a test
n is the number of detections

F_G (f_1, f_2) is the appropriate percentile of the F distribution with a specified level of confidence G and degrees of freedom f_1 and f_2, and may be found in tables **[Heida, 1984]**, where

$$f_1 = 2\,(N - n + 1) \qquad (5.3)$$

$$f_2 = 2\,n \qquad (5.4)$$

With the current data, the number of detections (n) is 54 out of total (N) 63. Therefore, using equations 6.3 and 6.4, $f_1 = 20$ and $f_2 = 108$. For a confidence level of 95%, the percentile of the F distribution is estimated as $F_{0.95}(f_1, f_2) = F_{0.95}(20, 108) \cong 1.68$ **[Heida, 1984]**. Substituting in equation 5.2:

$$P_L = \frac{54}{54 + (63 - 54 + 1).(1.68)} = 0.763 \qquad (5.5)$$

Hence the cumulative POD for the HM system results in Table 5.2 is 76.3% with a confidence level of 95%.

5.6 Usage Monitoring

The UM data provided by the helicopter operator is extremely useful in supporting or changing the basis upon which life limited components are assessed. As illustrated in Figure 5.8, a vital component will be assigned a service limit, or 'life', based on an

assumed usage spectrum. If the actual loading in service were less severe than the design loading, then the component would be removed with only a proportion of its useful life consumed. If the service loading was more severe then there is a risk that the component could fail before reaching its service limit. If the loads were known exactly by UM, it is therefore possible to reduce the cost of unnecessary maintenance and the risk of premature failure.

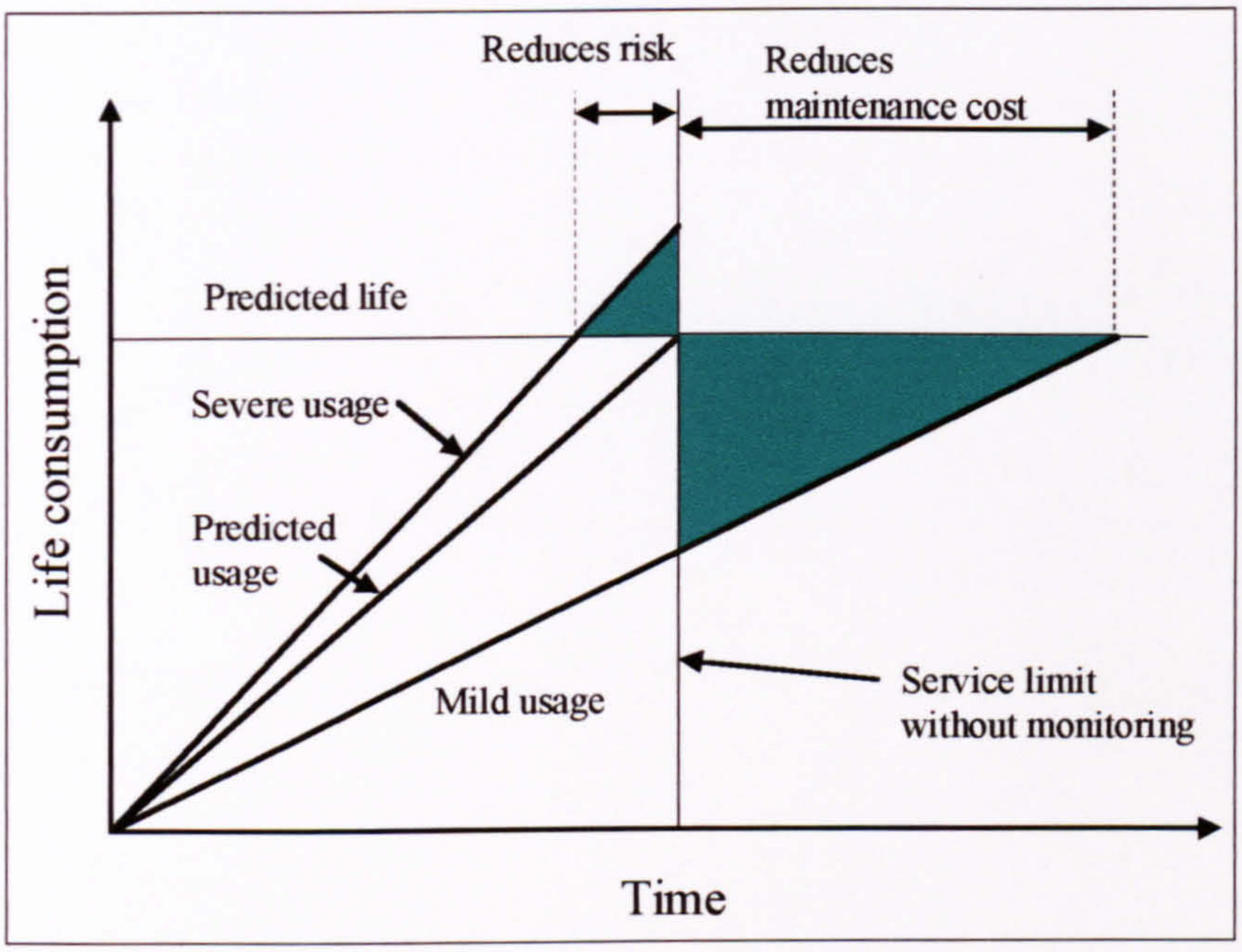

Figure 5.8 : Potential benefits of usage monitoring [Dickson et al, 1996]

The two main methods applied in usage monitoring are flight condition recognition (FCR) and flight load synthesis (FLS) as described in **[Dickson et al, 1996]**. Both methods have the end goal of accurately quantifying the loads imposed on the gearbox (or other helicopter components). Using material data, e.g. S-N curves, the predicted life of a component may then be recalculated using real rather than assumed design data.

The application of usage monitoring techniques to the calculation of more accurate fatigue lives is also discussed by **[Irving and Hudson, 1998]**. The latter shows that the variability for non-zero damage levels for nominally identical manoeuvres is between 100 and 1000; this may result in significant differences in life calculations.

5.7 Summary

A review of the current HUMS methodologies has been carried out with a view to evaluating the effectiveness of the different techniques with regard to reliability prediction. The results of the investigations have shown that there is a substantial

literature concerned with techniques for health monitoring, mainly in the areas of vibration health monitoring and oil debris monitoring. Work is also being carried out to investigate the 'fusion' of these two techniques to provide a more comprehensive diagnostic capability **[Howard and Reintjes, 1999; Byington et al, 1999]**.

Little information was available with which to correlate the HM indication with particular damage levels, e.g. spalled area of gears and bearings in the gearbox. This makes it difficult to incorporate HM data in models of damage accumulation, and limits their usefulness to that set out below.

The reliability and confidence level of HM techniques applied by civilian North Sea operators has been estimated from a limited data-set **[McColl, 1997]**. The cumulative probability of detection (POD) was calculated as 76.3% with 95% confidence base on data supplied by the CAA **[ibid]**. The POD for oil debris monitoring is difficult to quantify owing to the lack of detailed information with which to calculate the debris detection efficiency.

HUMS may extend gearbox life in two ways, described below, the first of which has been tested in this thesis (Chapters 4 – model, Chapter 9 - results).

- The POD of health monitoring techniques may be applied in the calculation of the failure probability of the system. By considering the POD for each failure mechanism, diverse failure criteria may be aligned to one standard – functional failure. The latter will occur if the damage accumulated reaches its limit and the HM system fails to detect and indicate that damage has occurred.

- The data from usage monitoring may be used for updating the predicted failure probability of the fatigue models. Accurate knowledge of the loads applied to the gearbox, compared to the initial design spectrum, allows damage to be recalculated using Bayesian techniques **[Irving et al, 1998]**. The data from HM cannot be used in this manner since current technology will only provide a 'failure warning' system. Bayesian updating would require data throughout the life of the gearbox.

6 Model Construction and Input Data

6.1 Introduction

This chapter gives details of the data used for the sensitivity studies that are reported in Chapters 8 and 9. The program software has been used to generate results from both the Type A and Type B gearboxes, and seeks to establish patterns from the results that could be applicable to any design of gearbox. Where appropriate, comparisons have been made between the two different designs.

The two types of helicopter gearbox have been used in the generation of results in order to provide confidence in the operation of the damage models, and the results therefrom. One of the aims of this work however has been to develop the capability of analysing a generic transmission system of single input-single output configuration.

6.2 Geometrical Data

The gearbox geometrical data used for the models is listed in two parts. The first describes the pinion and gear in detail (Figure 6.1 and Appendix E.1.1), giving information on the number and geometry of the teeth. The second part gives information on the shaft and bearing configuration (Figure 6.2 and Appendix E.1.2), which also includes data for the coupling splines. The data has been taken from drawings supplied by the manufacturer or estimated from open literature e.g. **[Drago, 1988]**. Both the Type A and Type B gear-sets are of the spiral bevel type, and are made from S156 and AISI9310 respectively.

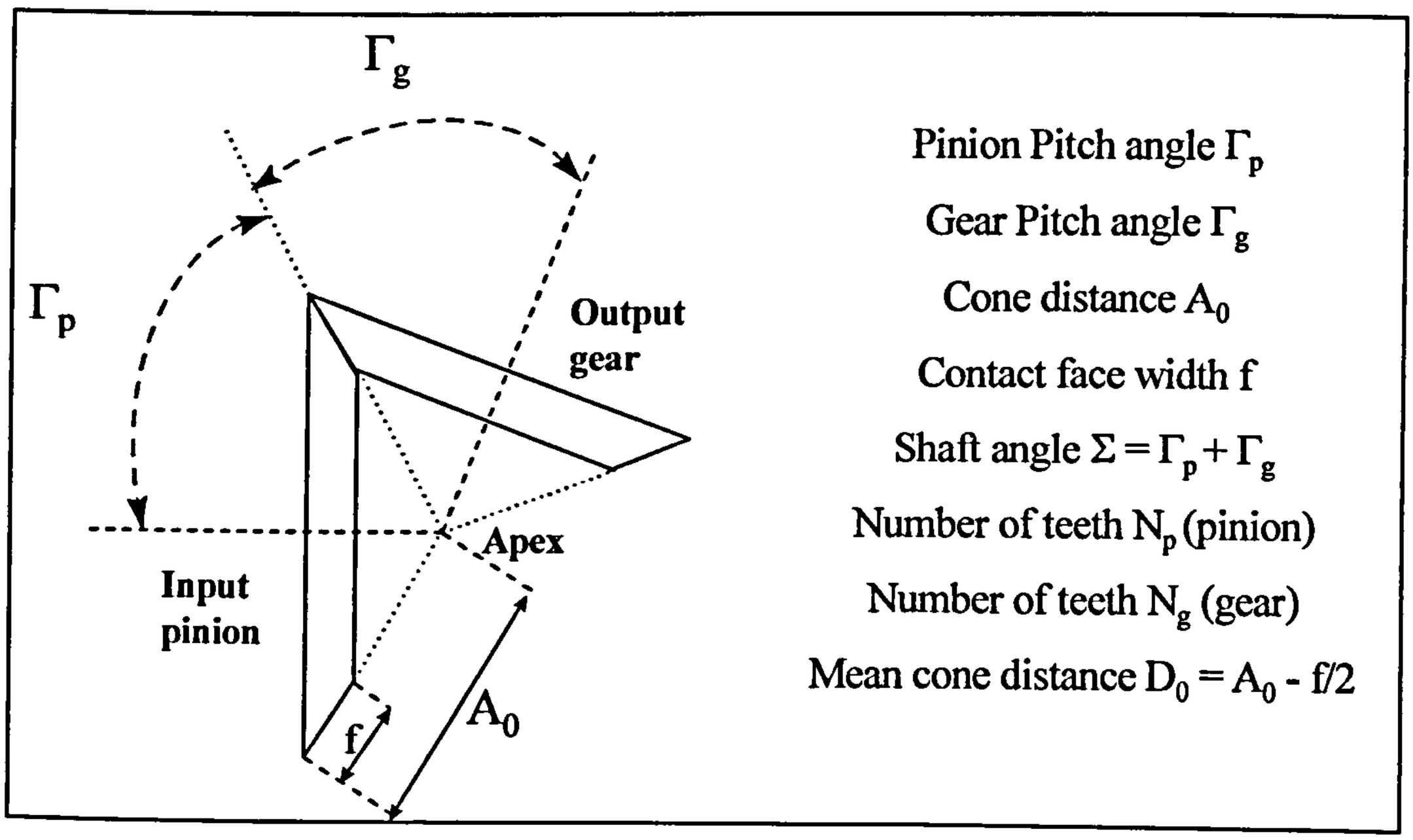

Figure 6.1 : Geometry of the IGB Gear-set

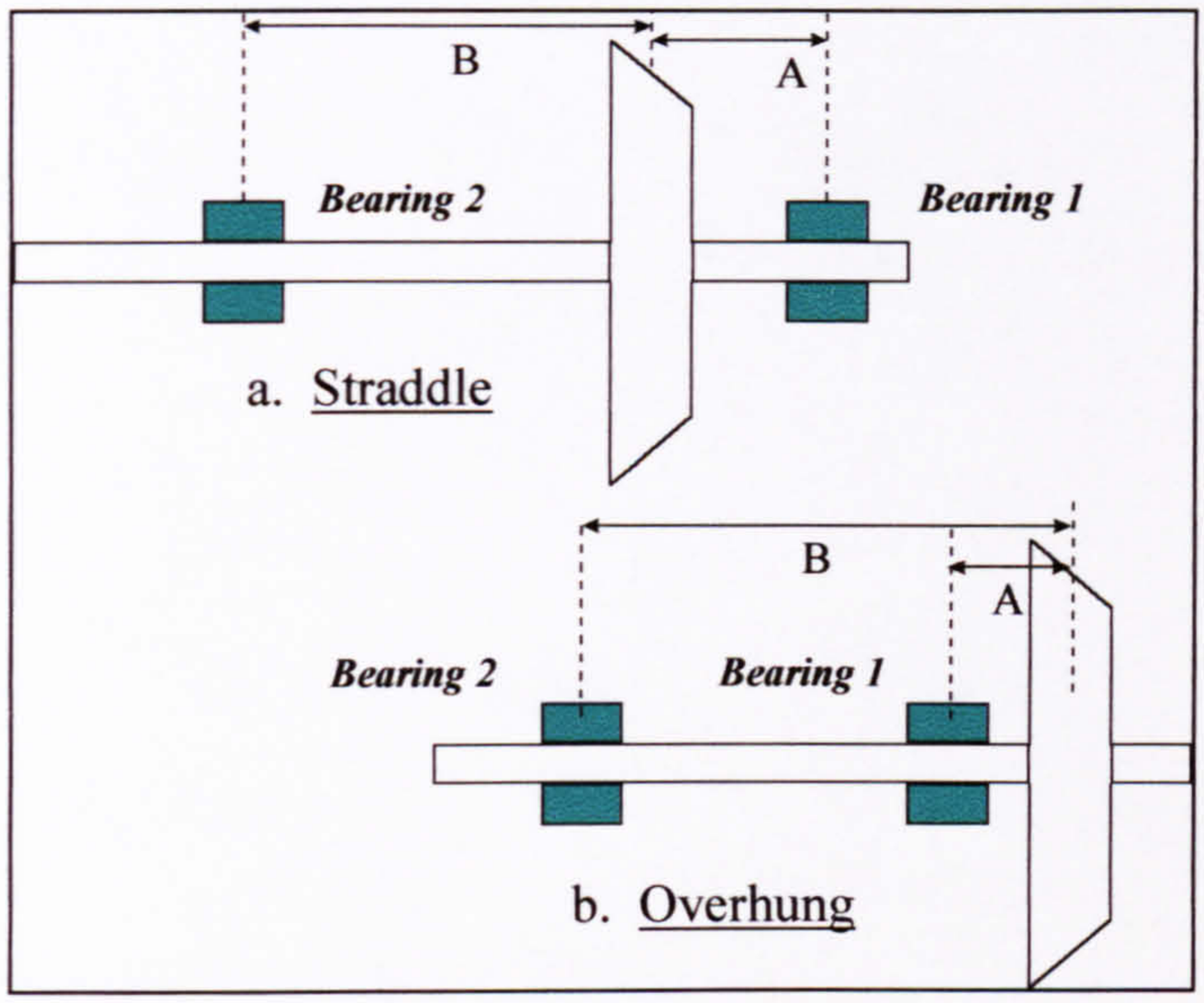

Figure 6.2 : Two configurations of bearing and shaft assembly [Savage and Brikmanis, 1986]

6.3 Material Data

The following sections provide greater detail of the data employed in the damage accumulation models described in Chapter 4. Numerical data for the parameters used are given in Appendix E.

6.3.1 Tooth root bending fatigue data

Industry practice for calculating the endurance limit (T_{inf}) is to test a sample gearbox, which provides one sample value. A working value is then calculated by reducing the T_{inf} value by 1.4, the 'safety factor' used to obtain a three-sigma (3σ) curve, representing a failure probability of approximately 10^{-3}. This factor is derived using the method described in Appendix C.2.1. A lower safety factor of 1.3 may be applied if the test sample size is increased to four **[Cansdale & Tigwell, 1987].**

For the HGBR models, the next step was to derive a value for the mean T_{inf}, as illustrated below. This was carried out using an indicative value for coefficient of variation of 6%, calculated from test data **[Cansdale & Tigwell, 1987]**. A similar value (7%) was used in the AHS 'round-robin' investigation into fatigue calculation methods **[Everett et al, 1992].**

$$COV = \frac{\sigma_T}{T_{mean}} = 0.06 \qquad (6.1)$$

and $$T_{-3\sigma} = T_{mean} - 3\,\sigma_T = T_{mean} - 3\,(0.06\,T_{mean})$$

$$T_{mean} = T_{-3\sigma} + 0.18\ T_{mean} \quad (6.2)$$

$$0.82\ T_{mean} = T_{-3\sigma} \quad (6.3)$$

For Type A and Type B, the values for three-sigma endurance limit ($T_{-3\sigma}$) are quoted as follows, from manufacturers' data. Beside these are the calculated values of T_{inf}, which will be used as baseline values for the sensitivity studies to follow.

Gearbox	$T_{-3\sigma}$ (Nm)	T_{inf} (Nm)
Type A	1005	1226
Type B	1850	2256

The sensitivity of the calculated life to loading and material variability at different values of probability of failure p(F) has been investigated, see the results in Chapter 8. The influence of material variability on the predicted Time to Failure (TTF) was investigated by varying the following parameters:

- Endurance limit of the gears (T_{inf}). This has the effect of shifting the T-N curve up or down and represents a variation in the mean strength of the gear material.

- Coefficient of variation (COV) for the T-N curve. This has the effect of narrowing or widening the distribution for the T-N curve and represents a variation in the data scatter for the gear material. For these studies COV was varied from 0 - 18%.

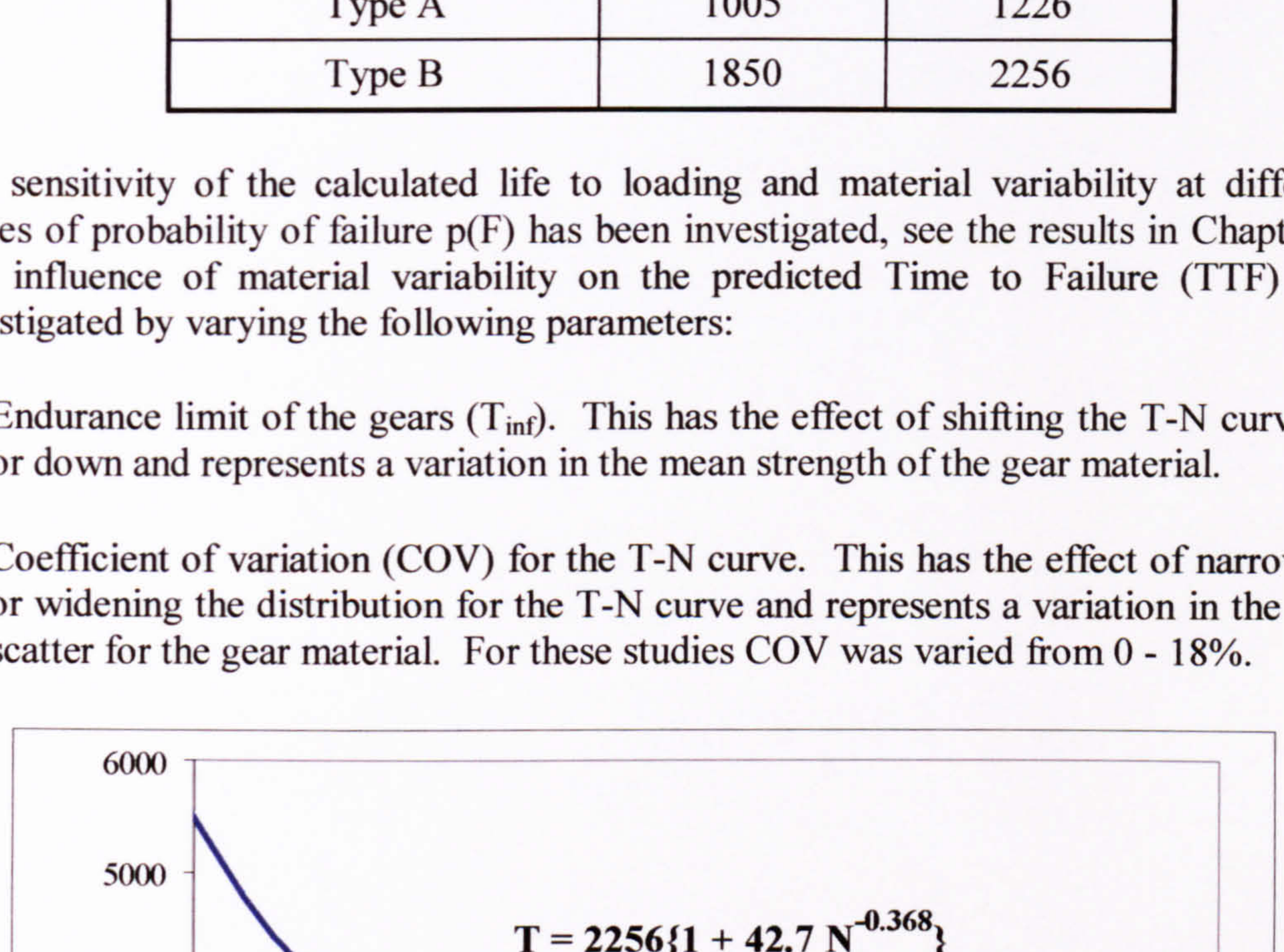

Figure 6.3 : T-N Plot for Tooth root bending fatigue (Type B gearbox data)

The form of the T-N curve used was supplied by the manufacturer and is presented as:

$$T = T_{inf} \left\{1 + 42.7\, N^{-0.368}\right\} \qquad (6.4)$$

where T is the input torque in Nm.
T_{inf} is the endurance limit of the gear concerned in Nm.
N is the number of gear tooth meshing cycles to failure.

6.3.2 Gear tooth rolling contact fatigue data

The damage model data has been based on the equation for the working contact stress allowable for gear tooth rolling contact fatigue (equation 6.5). An indicative value for S_{AC} for carburised and case hardened bevel gears is 1.726 GPa **[Drago, 1980]**.

$$S_{WC} = \frac{S_{AC}.C_H}{C_T.C_R}.C_L \qquad (6.5)$$

where S_{AC} the allowable contact stress
Factors C_H, and C_T are 1.0, C_R is 0.87
Factor C_L depends on cycles, according to equation 6.6.

$$C_L = 2.4502\, N^{-0.0556} \qquad (6.6)$$

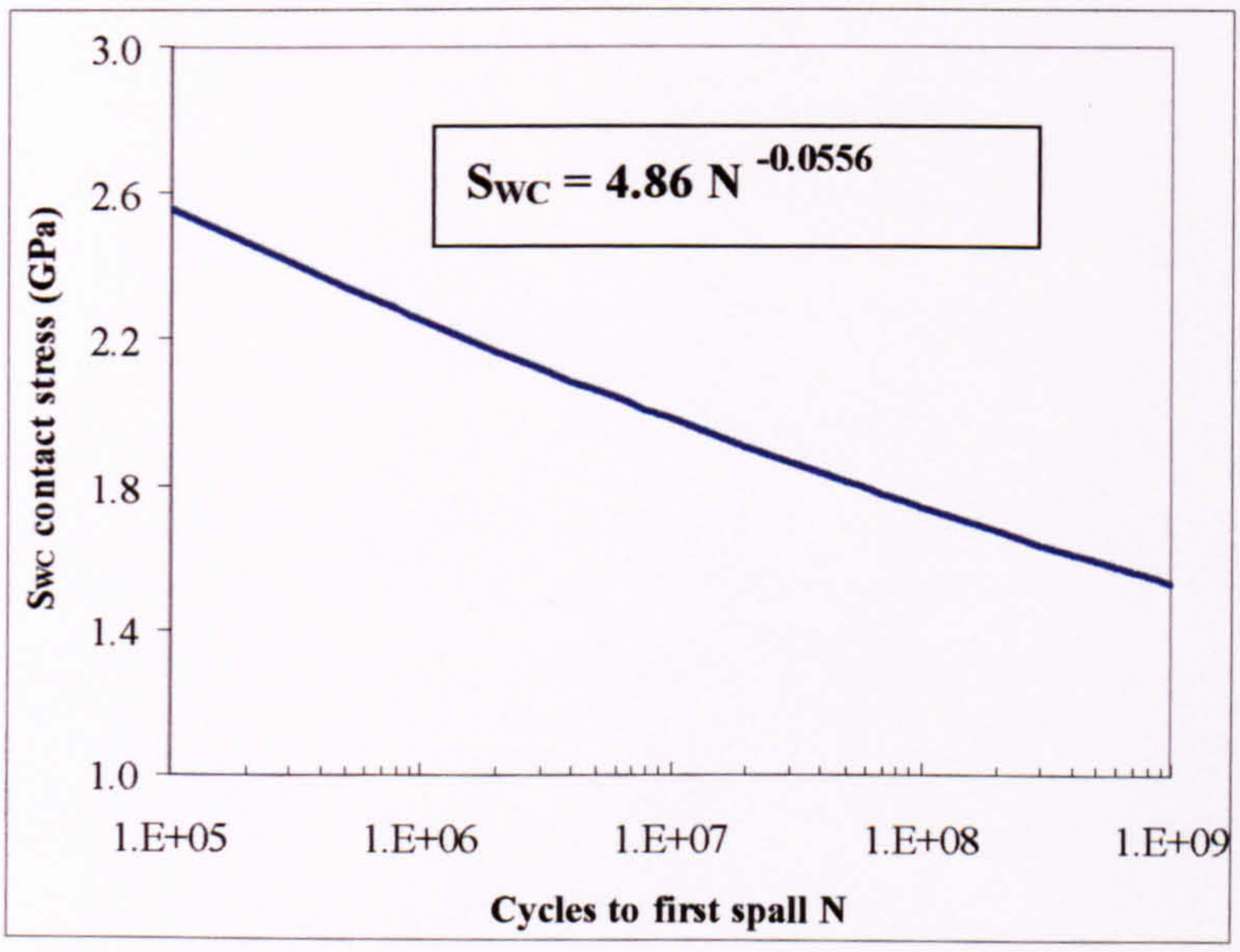

Figure 6.4 : S-N curve for Gear Rolling contact fatigue, based on data from [AGMA, 1986]

Combining equations 6.5 and 6.6 yields the mean working curve for Hertzian contact stress, based on standards **[AGMA, 1986]**, see Figure 6.4:

$$S_{WC} = 4.86\ N^{-0.0556} \qquad (6.7)$$

where S_{WC} is the Working stress in GPa
N is the number of gear tooth meshing cycles to the formation of the first spall or pit size minimum 1.58mm diameter by 0.2mm depth

The influence of material variability on the predicted time to first spall (TFS) was investigated by varying the following parameters:

- Allowable contact stress S_{AC} around the baseline value of 1.726 GPa, from 1.2 to 2 GPa.

- Coefficient of variation (COV) for the S-N curve - the variation in the data scatter used in calculating the time to first spall (TFS). A COV of 15% was used for the initial study, due to the lack of experimental data for the particular gearbox; for later studies COV was varied from 0-20%.

6.3.3 Shaft spline wear data

The model was run with values for the slip amplitude taken from a normal distribution, with loading from the input torque spectrum. The time to failure was found by calculating the time taken for a certain wear volume (failure point) to be reached. In this case the failure criterion was chosen as 25 mm^3 of worn material; this could be increased or decreased depending on the maximum acceptable shaft tolerance.

Parameter	Values used
Wear coefficient (K) - mean	10^{-8} to 10^{-4}
Wear coefficient (K) COV	0 to 30%
Slip amplitude mean (micron)	50, 100
Slip amplitude COV	0 to 30%

Table 6.1 : Parameter values used for spline wear model

The tests in Chapter 8 were run with the parameter values given in Table 6.1, using the confidence limits of the wear coefficient K to define the confidence limits for the predicted TTF results. The value of the wear coefficient K depends on the type of contact and the lubrication present between the male and female splines. Typical wear coefficients were taken from published literature **[Rabinowicz, 1980]**, see Table 6.2.

Contact	Lubrication state	Wear coefficient
Metal on metal (like)	Clean	1.7×10^{-3}
	Poor	6.7×10^{-5}
	Average	3.3×10^{-6}
	Excellent	3.3×10^{-7}

Table 6.2 : Typical wear coefficients [Rabinowicz, 1980]

6.4 Torque Loading Data

The reliability model requires knowledge of the input torque in order to calculate the stresses on each component, which help define the damage accumulation rate for each damage model. If the input torque is known, then the loading on the gear teeth, shaft and bearings can be calculated provided the geometry of the components is known. This is accomplished using formulae obtained from standard mechanical engineering texts e.g. **[Shigley, 1986]** and applied by other workers in this field **[Savage and Brikmanis, 1986]**, see Appendix B.2.

A total of four torque data files, two for each gearbox type, have been used to generate results for all fatigue and wear models, see Appendix E.3. One of these data files is a torque-time history (Section 6.4.1), and the others are torque spectra composed of design and recorded values, as described in Sections 6.4.2 to 6.4.4:

- ASW loading – based upon Type A design data
- Flight 110 – recorded data from Type A
- Prototype Spectrum - based upon Type B prototype (design) data
- Civil spectrum – recorded data from Type B

6.4.1 Torque Loading Data – ASW loading

Only limited design information was available with which to generate a torque-time history for the Type A model, so a simulated sortie sequence was created using the HELIX sortie pattern **[Edwards and Darts 1984]**. This was accomplished by using estimated design values for torque in each manoeuvre, and designing an ASW sortie profile assuming a constant torque in each flight condition, using data in Appendix E, Section E.3.1 (see Figure 6.5).

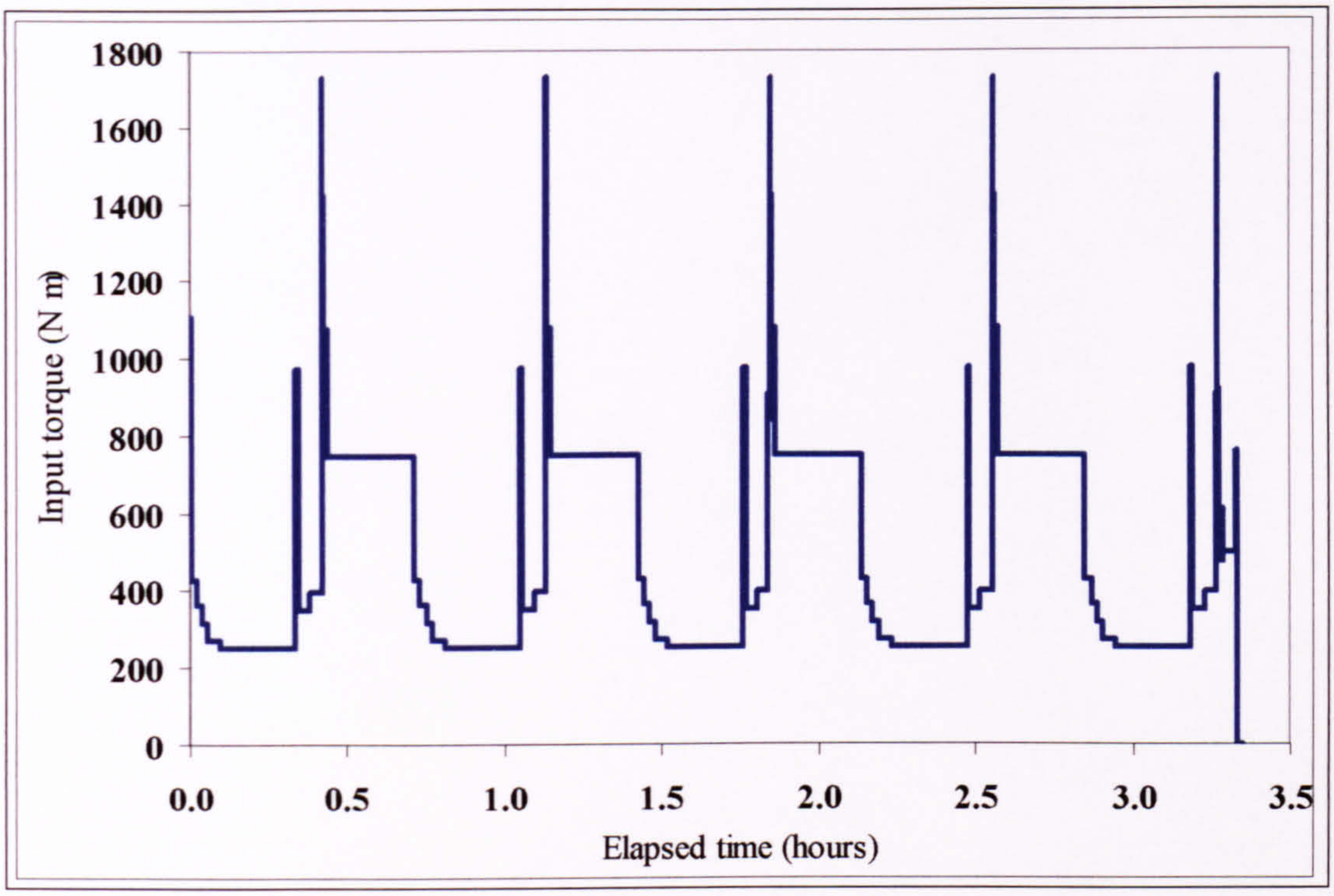

Figure 6.5 : Simulated ASW sortie torque-time history for Type A gearbox

The sequence of manoeuvres was created from the HELIX ASW sortie, which featured a mission lasting 3 hours 20 minutes. The percentage occurrences of each manoeuvre in Appendix E are used to determine the duration of each flight condition. For example, the hover manoeuvre (ref no 10) represents 33.01% of the torque-time history or 66 minutes, split into four separate periods of 16.5 minutes during the ASW mission. Other manoeuvres are similarly distributed, with auto-rotation and recovery (ref no 21 and 22) inserted once each (see Appendix E.3.1).

Difficulties emerged due to the lack of torque design data for the Type A manoeuvres. When the ASW torque-time history, designed according to the values in Appendix E, was employed to perform a Miner's damage summation, the calculated life was very low; 158 hours at p* of 10^{-3}. This was due to the assumption that the torque value was constant for the whole of each manoeuvre. In reality this peak may only be reached for a low number of cycles (1-2% of the manoeuvre), with the remaining proportion being at lower values. To achieve a more realistic life, the seven most damaging manoeuvres had their peak torque reduced by 25%. The resulting data file is referred to the 'ASW torque history (75% Peaks)', designated as 'ASW loading', (see Figure 6.5).

6.4.2 Torque Loading Data – Type A Flight 110

Recorded tail rotor torque data has been obtained from DERA, taken from a total of 98 flights of Type A helicopter. The data provides the torque in Nm, sampled 4 times per

second. A sample of the time history is shown in Figure 6.6, which shows the sequence of torque values for flight reference number 110. The total flight history, representing 2.25 hours, is given in Figure 6.6.

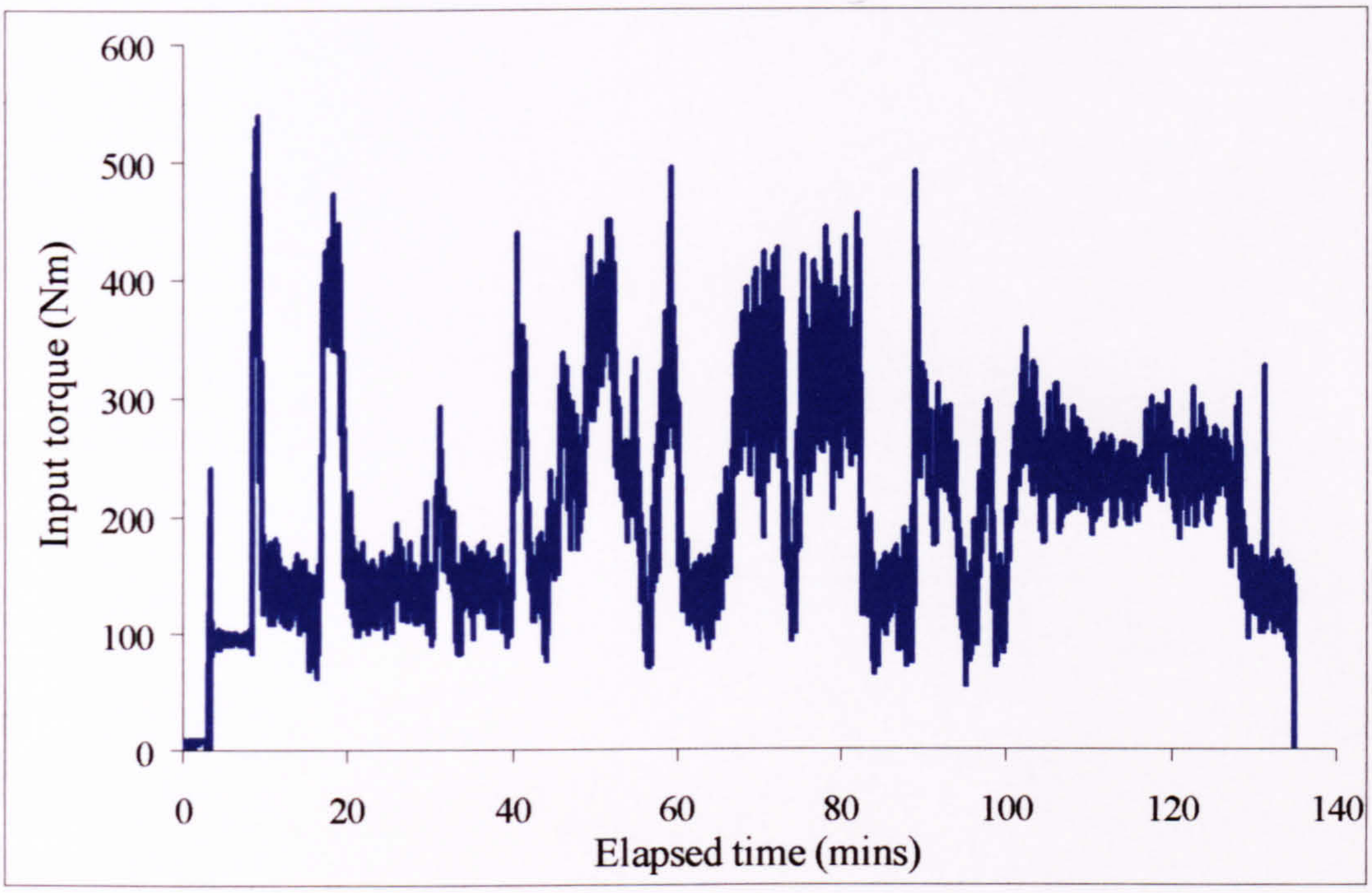

Figure 6.6 : Torque Loading Data – Type A Flight 110[1]

Owing to the number of data points, 32365 torque values for flight 110, the torque-time history was converted to a torque spectrum for use in the reliability model software. The torque data points were sorted by magnitude to determine the 'time at level' for each input value (see Appendix E.3.2). One data point was assumed to represent 0.25 sec at a particular constant torque. By manipulating the data to form a spectrum, as in Figure 6.7, the recorded loading information can be used as the input for the damage models. The torque spectrum yields the same results in the reliability model as the torque-time history it replaces because the fatigue and wear models used in this work are insensitive to the sequence of load cycles.

The recorded flight has been used for comparison with the other input torque data. However, its shortcomings arise from a lack of information with which to correlate the tail rotor torque to individual flight manoeuvres. No recorded data were available to help ascertain which manoeuvres caused which torque loading, so it is not possible to build-up different sortie profiles as attempted in the ASW torque-time history described in Section 6.4.1.

[1] Type A torque data supplied by QinetiQ

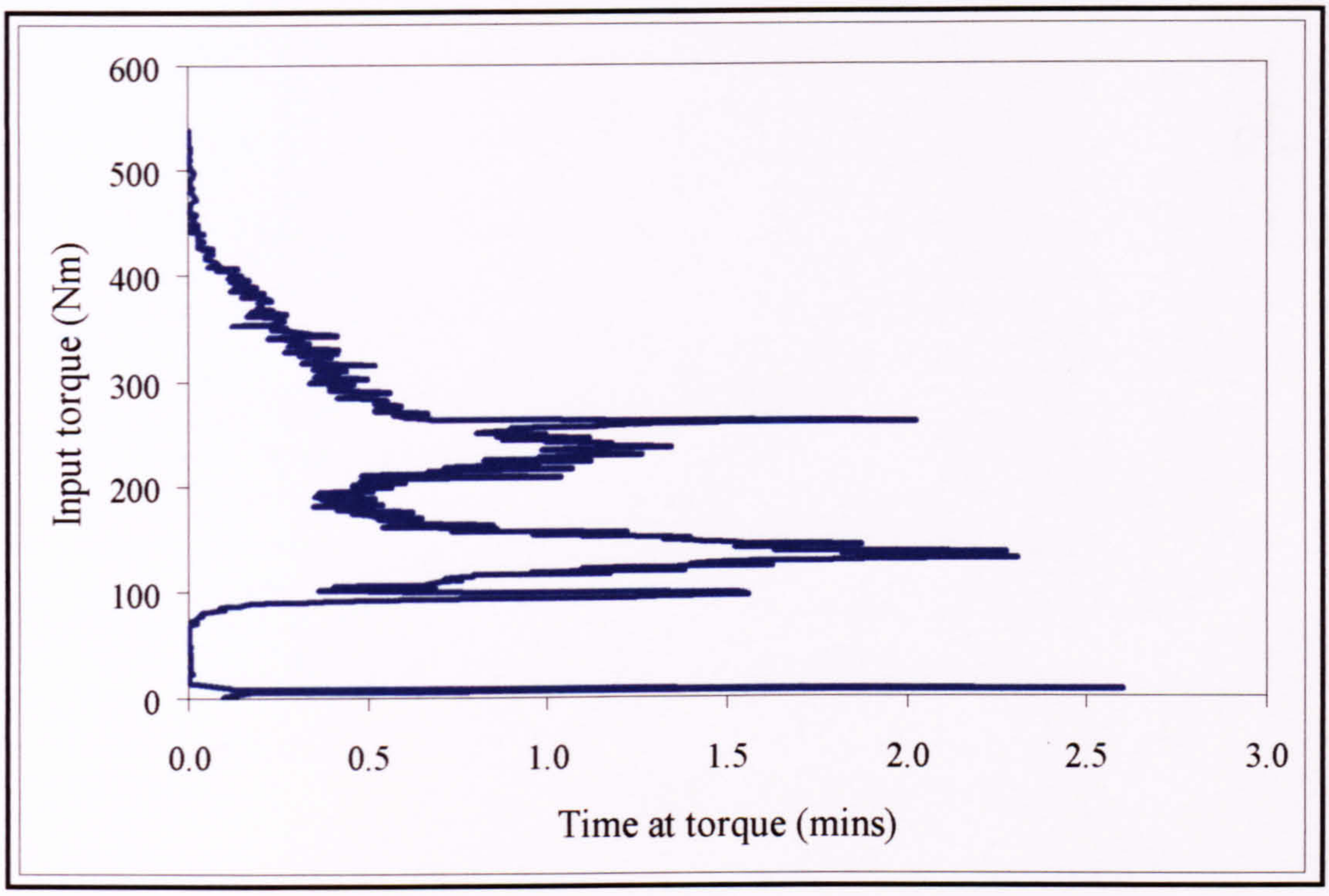

Figure 6.7 : Type A gearbox input torque spectrum (Flight 110)[3]

6.4.3 Torque Loading Data – Type B Prototype Spectrum

The first example of torque data for the Type B gearbox was a spectrum for the prototype design consisting of 22 different torque levels, each with an associated percentage (see Appendix E.3.3). This data was used to create an input file for the HGBR software model by calculating the time (and cycles) spent in 100 hours, e.g. 100 Nm for 0.5% becomes 100 Nm for 0.5 hour within the 100 hour period. Most of the spectrum (98.83%) consists of constant torque at 60% of T_{max}, with higher values lasting for very short periods

The spectrum was used in initial calculations of the gear life, but is not representative of actual in-service loads. However, it is useful in this context of reliability prediction by providing an example of heavy gearbox loading. Sensitivities to such loading can therefore be identified.

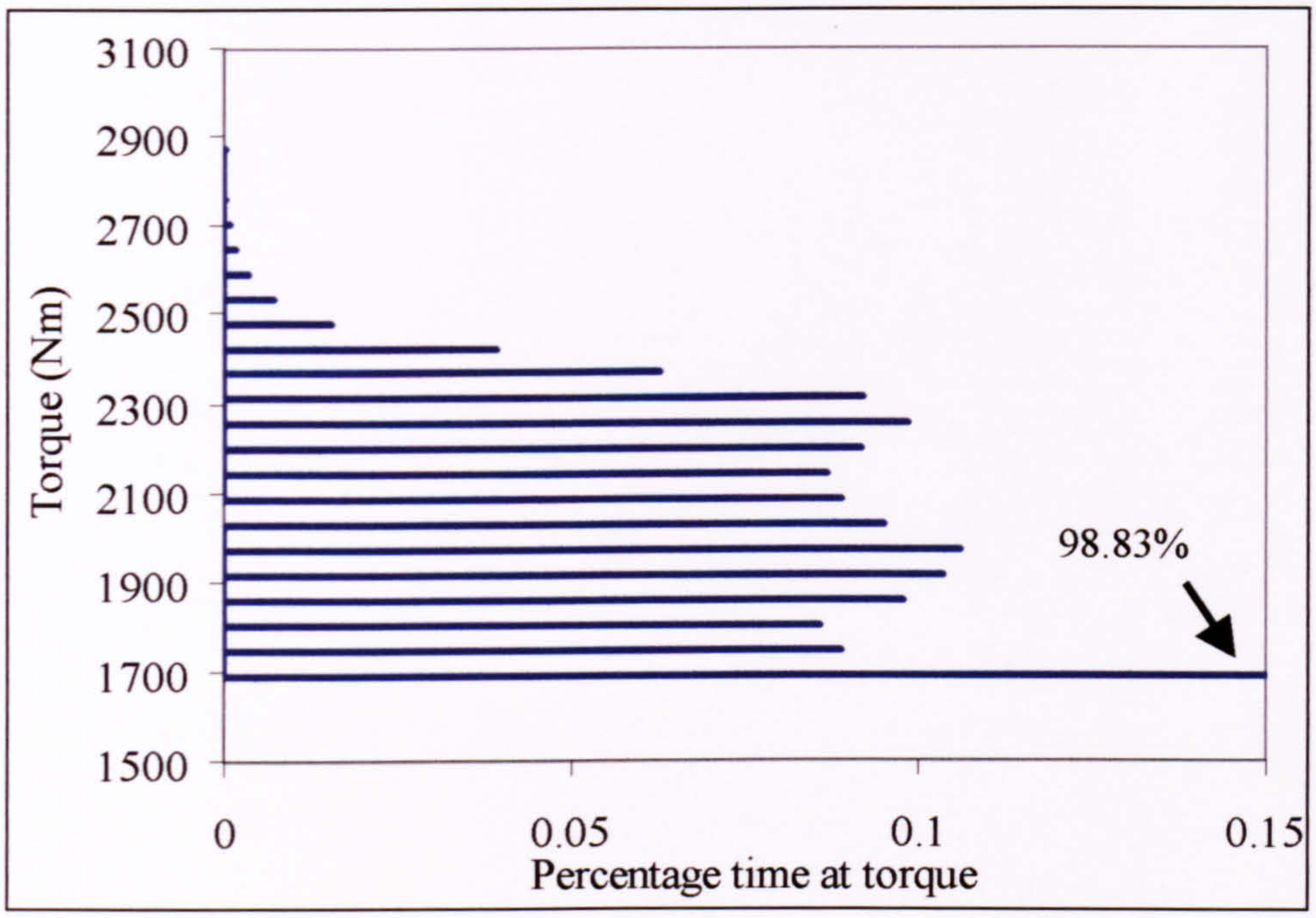

Figure 6.8 : Type B gearbox prototype torque spectrum[2]

6.4.4 Torque Loading Data – Type B Recorded data

In the case of the Type B, far more information is available regarding the actual torque transmitted via the IGB, and how this is related to the manoeuvres or flight regime. The civil torque spectrum for Type B contains 1650 different load states, each lasting for a percentage of the total operating time.

The torque data for each load state have been gathered into each of the 35 manoeuvres shown in Appendix E.3.4, where the entry to and exit from each manoeuvre are considered together with the steady state. In order to provide input for the damage models, the percent values were converted to times at torque by assuming a 100-hour flight history (see Appendix E.3.4). The total spectrum for all the manoeuvres showing the percentage time at each value of torque, is given in Figure 6.9.

[2] Type B torque data supplied by Agusta Westland

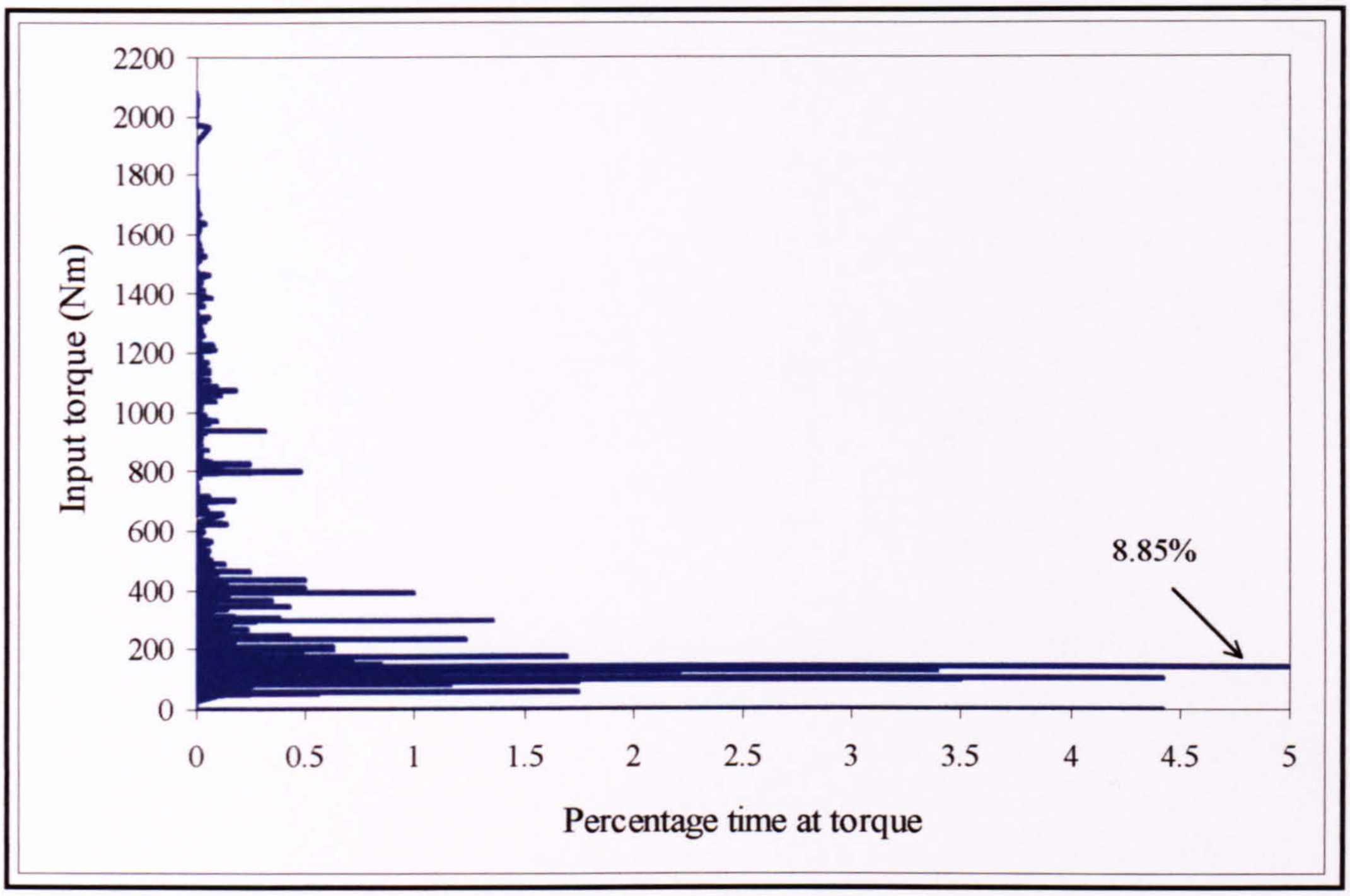

Figure 6.9 : Type B IGB input torque spectrum[3]

6.4.5 Loading variability

Within each flight condition there is a variation of torque due to changes in the helicopter weight, position of the centre of gravity (CG), and additional load factors on the tail rotor. In the Civil spectrum, each manoeuvre contains between 12 and 70 torque values, each with an assigned percentage of occurrence; a Magnitude Occurrence Spectrum (MOS). In this work, load variability has been introduced by changing the content of the Type B spectrum applied to the damage accumulation models.

The most damaging manoeuvres with the highest torque values were selected by examining the highest torque values within the Civil spectrum. These manoeuvres are Sideways flight 60° (ref 12), Sideways flight 90° (ref 13) and spot turn port (ref 5), with reference numbers shown in Appendix E.3.4. The MOS of these manoeuvres, plus the take-off manoeuvre (ref 2), are shown in Figure 6.10.

[3] Type B torque data supplied by Agusta Westland

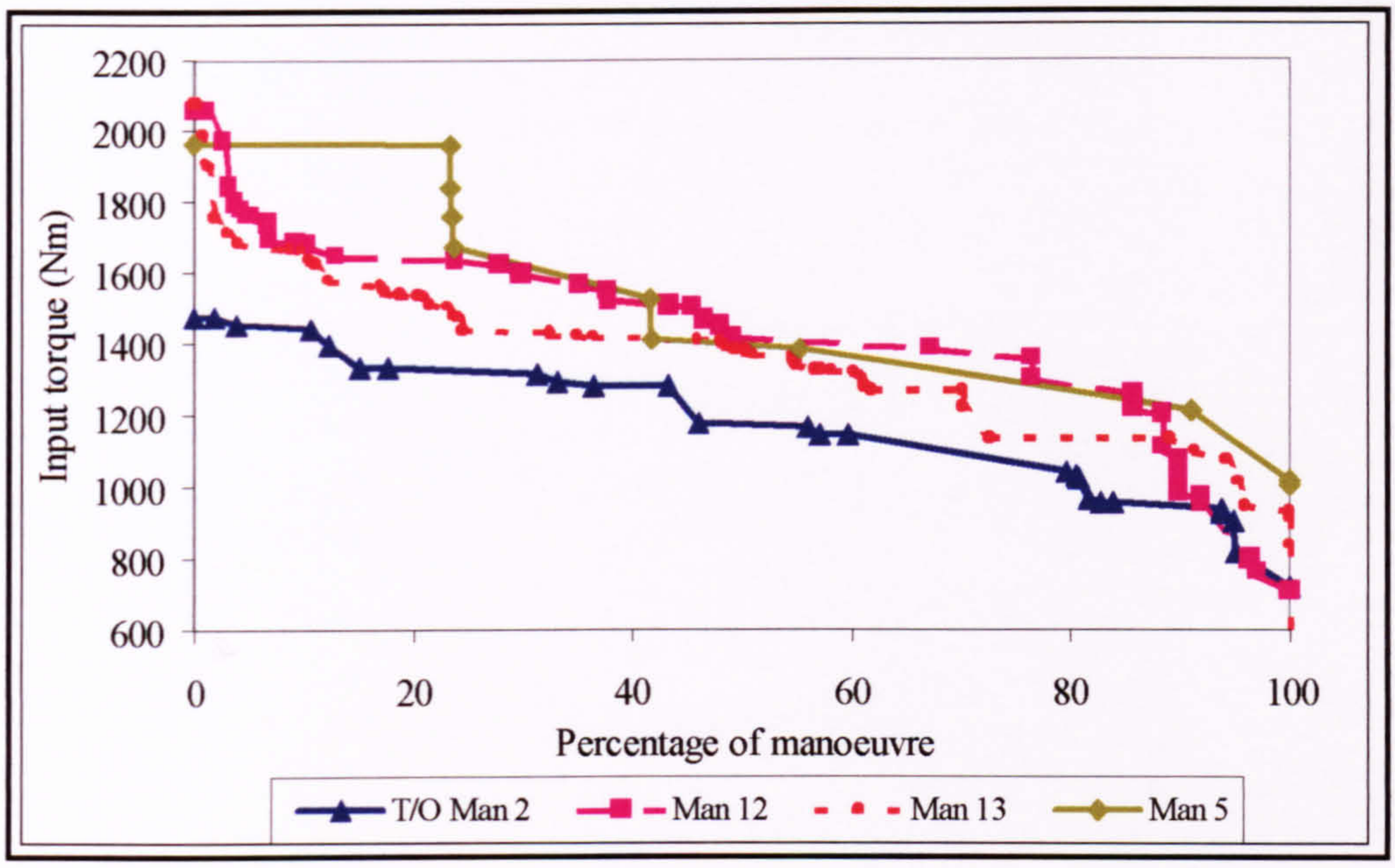

Figure 6.10 : MOS for Damaging Manoeuvres 2, 12, 13, 5

Loading variability was then introduced to the model by varying the percentage occurrence of these damaging manoeuvres, within the total flight spectrum. The take-off manoeuvre was included for comparison, as given in Table 6.3. Such variation of the load input data has allowed the effect of load variability on the individual damage models to be investigated.

Manoeuvre number	Manoeuvre	Design spectrum occurrence (%)	Range of values used (% of total flight)
2	Take off	0.43	0.1 – 5
12	60deg sideways flight	0.372	0.1 – 2
13	90deg sideways flight	0.372	0.1 – 2
5	Spot turn port	0.25	0.1 – 2
-	Over-torque 2200 Nm	-	0.0006
-	Over-torque 2400 Nm	-	0.0028
-	Over-torque 2600 Nm	-	0.0056
-	Over-torque 2800 Nm	-	
-	Over-torque 3000 Nm	-	

Table 6.3 : Loading variability introduced to Civil spectrum by variation of MOS and addition of over-torques

The occurrence of over-torques was also included as an additional load state, the proportion for which was varied from 0.0006 to 0.0056%. These percentage values represent one over-torque event of two second duration, which occurs once per 100 hours (0.0006%) and once per 10 hours (0.0056%).

6.5 Casing Corrosion data

The models for plain and galvanic corrosion of the gearbox casing have been supplied with data for three different materials (see Table 6.4), described below. The results obtained for two of these materials (AZ91C and WE43) are shown in Chapter 8.

- Magnesium alloy AZ91C, a typical material for helicopter gearboxes.
- Magnesium alloy WE43; new material used in Type A gearbox casing, with lower demonstrated corrosion rate for plain corrosion, similar corrosion rate for galvanic corrosion **[Geary, 1990, 1996]**.
- Aluminium alloy A357; typical material for Type B gearbox casing.

	Environment (units)	Casing material		
		AZ91C	**WE43**	**A357**
Plain corrosion rate mean	Marine (mm/year)	6	0.76	0.125
	Land (mm/year)	2	0.2	0.05
Plain corrosion rate COV	Marine	0.05	0.05	0.1
	Land	0.05	0.05	0.1
Galvanic corrosion rate mean	Marine (mm/year)	76	76	0.25
	Land (mm/year)	5	5	0.1
Galvanic corrosion rate COV	Marine	0.1	0.1	0.1
	Land	0.1	0.1	0.1
Plain corrosion M* mean	Mm	5	5	5
Plain corrosion M* COV	-	0.05	0.05	0.2
Galvanic corrosion M* mean	Mm	5	5	5
Galvanic corrosion M* COV	-	0.05	0.05	0.2

Table 6.4 : Data for models for Plain and Galvanic Corrosion [Geary, 1990 and 1996]

6.6 HGBR Program Software

The HGBR program created for the purpose of this work has been written in Borland Delphi™, an object oriented version of Pascal computer language. The program contains the theoretical models that have been described in Chapter 4, together with loading, geometry and material data for the Type A and Type B gearboxes.

The program is made up of a number of program *units*, each of which has an associated *form*. The forms represent the graphical user interface (GUI), which contain graphs, edit boxes, buttons, tables etc. The units contain the Pascal code to allow the program to run, see Appendix A. The pairs of units and associated forms have the same name; the key sections of the program are listed in Table 6.5.

Unit name	Content/Function
mathlib	Definitions of functions used to calculate loads, plus procedures for calculating the fatigue life for the gear teeth and bearings. This applies geometrical formulae to calculate component stresses from input torque.
System Modelling	Calculation and output display section of the program. It controls the graphical output and contains the damage models for casing corrosion and shaft spline wear.
Gearbox Parameters DBAccess	This is the part of the program that controls the data file used for each set of experiments.
Torqbands	Gearbox loading section, which controls the load spectrum used by the program. This part of the program is used for selecting the load file or torque spectrum to be used.

Table 6.5 : Names and functions of HGBR software units and forms

A flowchart of the program operation is shown in Figure 6.11, which gives a summary of the key stages in the operation of the model. Data for the geometrical, material and loading parameters have already been discussed in Sections 6.2, 6.3 and 6.4. All data pertinent to the gearbox and loading spectrum are loaded from a database selected at the start of the program. Any changes made are then saved to a new database, so that a record of the different parameter values used in experiments can be retained. The program then calculates the loading of each component in turn, before using material data to calculate the expected life at different probability values. Further details of the program, with the input screen displays presented to the user are given in Appendix A.

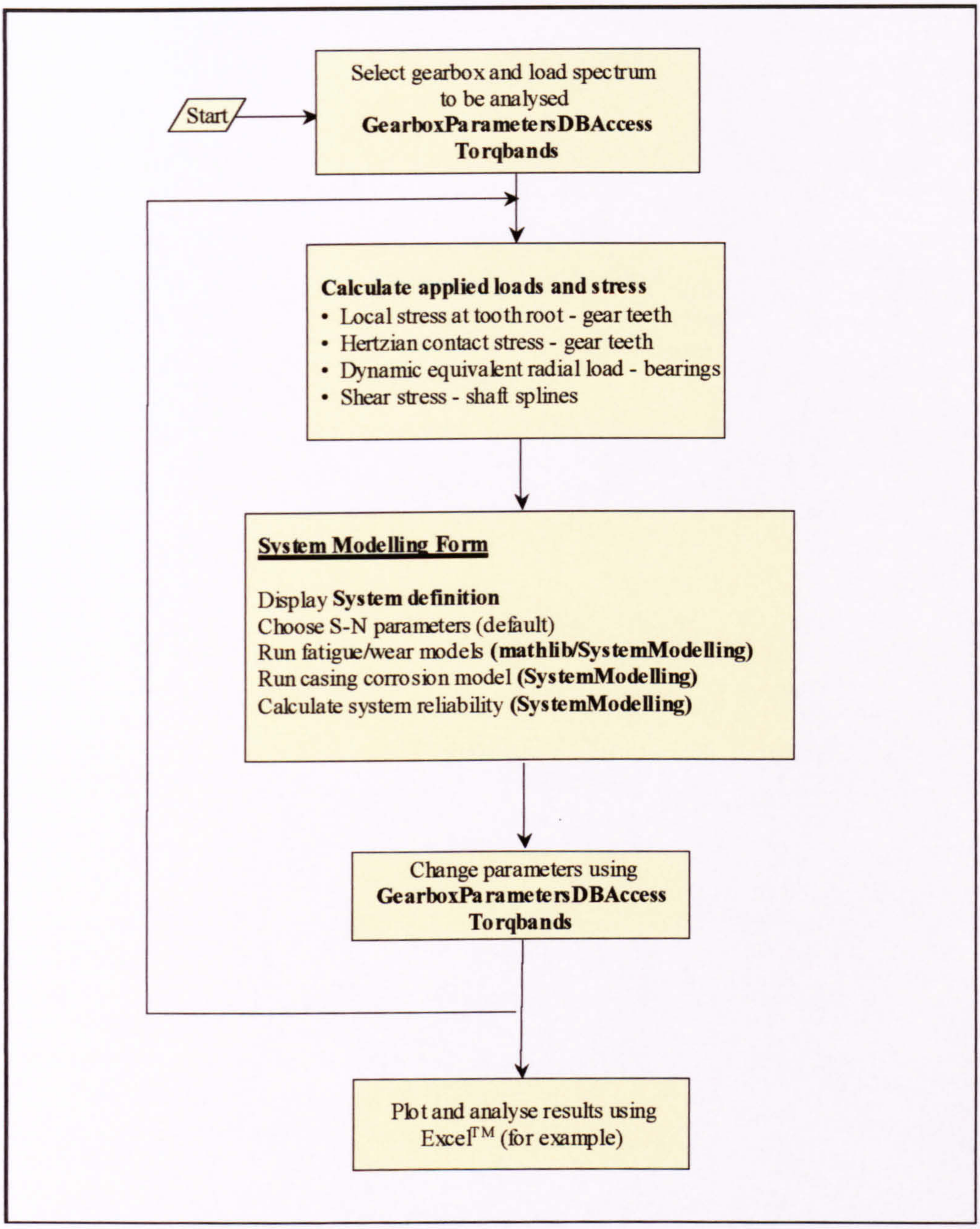

Figure 6.11 : Program Flowchart for Reliability Prediction

6.7 Analysis of Maintenance Data

As an additional step to the development of the theoretical models for the reliability prediction, a survey was conducted of the various sources of maintenance data of the Type A gearbox. Samples of maintenance records from three separate sources (Table 6.6) have been studied, to establish the periodicity of, and reasons for, maintenance of the Type A gearbox. Results from the analysis of the maintenance data are presented in Chapter 7.

Source	Acronym (in data)	Data obtained
Naval Aircraft Materials Laboratory, Fleetlands, Portsmouth	NAML	Details of all records for gearbox removals due to oil debris analysis 1980-1998. See Appendix D.1
Defence Aviation Repair Agency, Perth	Perth	Sample of archived work records for strip and recondition of gearbox 1974-1998. See Appendix D.2
EDA4, Logistic Support Services, RAF Wyton	EDA	Summary of all job cards raised for 1st and 2nd line maintenance over 1982-1998. See Appendix D.3

Table 6.6 : Sources of data for study of maintenance records

The data obtained from NAML were provided in summary form, derived from internally held records. They contain details of the hours at which a gearbox 'rejection' (removal for overhaul) takes place, based upon oil debris analysis. In most cases for the Type A, debris is due to bearing wear and fatigue, and the records suggest reasons for this degradation in certain cases, e.g. excessive axial loading. A total of 77 records are listed in Appendix D.1.

The data from Perth are the most detailed and were obtained from a manual examination of archived work records. The activity consisted of a search through all 'job-cards' raised on each gearbox to record all relevant maintenance activities conducted during overhaul. Only a limited sample of records was studied, 118 sets of documents for separate overhauls of 67 gearboxes over the period 1974 to 1998. As implied, some of the records covered more than one overhaul of the same gearbox – indicated by shading in Appendix D.2.

The data obtained from EDA were provided in summary form, based upon internally-held records, listed in Appendix D.3. These 704 records were sorted by Access™ and Excel ™, but do not accurately record failure mechanism, or gearbox hours.

7 Analysis of Helicopter Transmission Maintenance Data

7.1 Introduction

A study was made of the records kept by the maintenance organisations for the Type A gearbox, for which a large body of historical data exists. Such records provide information of how often the gearboxes are repaired and reconditioned, and certain data of the faults found. This study was carried out to seek to confirm the faults reported in the literature so that the reliability model might truly represent failure mechanisms seen in practice, as well as those considered in design.

The operators' maintenance records for transmission systems show that gearboxes are often taken out of service for reasons other than that expected from the original design criteria. For example, the TBO period for some gearboxes is dictated by the predicted limit of fatigue damage. However, a gearbox may be removed from service in order to repair corrosion damage many hours before the fatigue damage limit is reached. **[Drago & Lenski, 1984]** reported that over 40% of gears and bearings for the US Navy CH-46 helicopter were discarded or re-worked due to corrosion alone. A summary of the types of defects and faults that can occur is given by **[Astridge, 1989]**.

The data have been studied in order to assess the extent and frequency of occurrence of actual failure mechanisms and also to test the viability of using historical data in the prediction of future reliability. The specific aims were:

- Comparison of faults found in service with the failure mechanisms considered at the design stage.
- Comparison of faults found in service with table of failure types for the Type A gearbox **[Agusta Westland 1997]**, Chapter 3, Table 3.1.
- Assistance to the modelling process by quantifying the frequency of occurrence of in-service damage mechanisms for comparison with results from damage models.

The types of maintenance records from the three sources are given in Table 7.1, and the raw data from NAML and Perth are given in Appendix D.1 and D.2 respectively. The data generally contain the type of failure or degradation (e.g. spline wear, casing corrosion) and the number of hours for which the gearbox has operated when it is repaired. The latter quantity is not always known accurately, since records often contain only the number of hours flown by the helicopter itself, rather than the hours operated by the gearbox. In some cases these quantities will be the same (where a new gearbox has been fitted to a new airframe), but often a reconditioned gearbox will be fitted to a different airframe so that the number of hours on the gearbox will be different. This chapter will distinguish clearly between the following quantities:

- Airframe hours - the cumulative number of hours for which the helicopter has operated since initial build.

- Gearbox hours - the cumulative number of hours for which the gearbox has operated, either time since new (TSN) or time since overhaul (TSO).

Organisation	Acronym (in data)	Data obtained
Naval Aircraft Materials Laboratory, Fleetlands, Portsmouth	NAML	Records for gearbox removals due to oil debris analysis.
Defence Aviation Repair Agency, Perth	Perth	Sample of archived work records for gearbox strip and recondition.
EDA4, Logistic Support Services, RAF Wyton	EDA	Summary of all job cards raised for 1st and 2nd line maintenance.

Table 7.1 : Sources of data for study of maintenance records

7.2 Data from Naval Aircraft Materials Laboratory (NAML)

Details were obtained of 77 cases of gearboxes being removed from service due to warnings received from oil debris monitoring, between 1980 and 1998. These records are given in full in Appendix D.1. In all cases the debris that gave rise to these warnings was found to originate from the fatigue or wear of the bearings. The most reliable method used for detecting the source of the debris is that of scanning electron microscopy (SEM) linked to energy dispersive analysis by X-ray (EDAX); other techniques include the spectrographic oil analysis program (SOAP). These techniques are described, together with their benefits and limitations in Chapter 5.

The records obtained from NAML report the presence of flakes of bearing steel, identified from the SEM/EDAX analysis. Only in 16% of cases (12 out of 77) however, was there any record of the likely cause of the debris being produced. When mention is made, the primary causes are:

- Misalignment of the bearing, leading to stress concentration (6 cases).

- Excessive axial pre-load, during (re-) assembly (5 cases).

- Lack of lubrication of the bearing, which can be caused by:

  – Debris in the oil ways which normally ensure that oil is fed to bearings (Appendix D.1, NAML data serial no 22).

– Ineffective operation of the spiral on the output shaft which feeds oil to the outboard bearing on the output shaft (Appendix D.2, Perth data serial no 1).

More detailed analyses of the manifestations and causes of the bearing debris are given in the listing of rectification work carried out at DARA, Perth, listed in Appendix D.2. These causes will be discussed in Section 7.3.

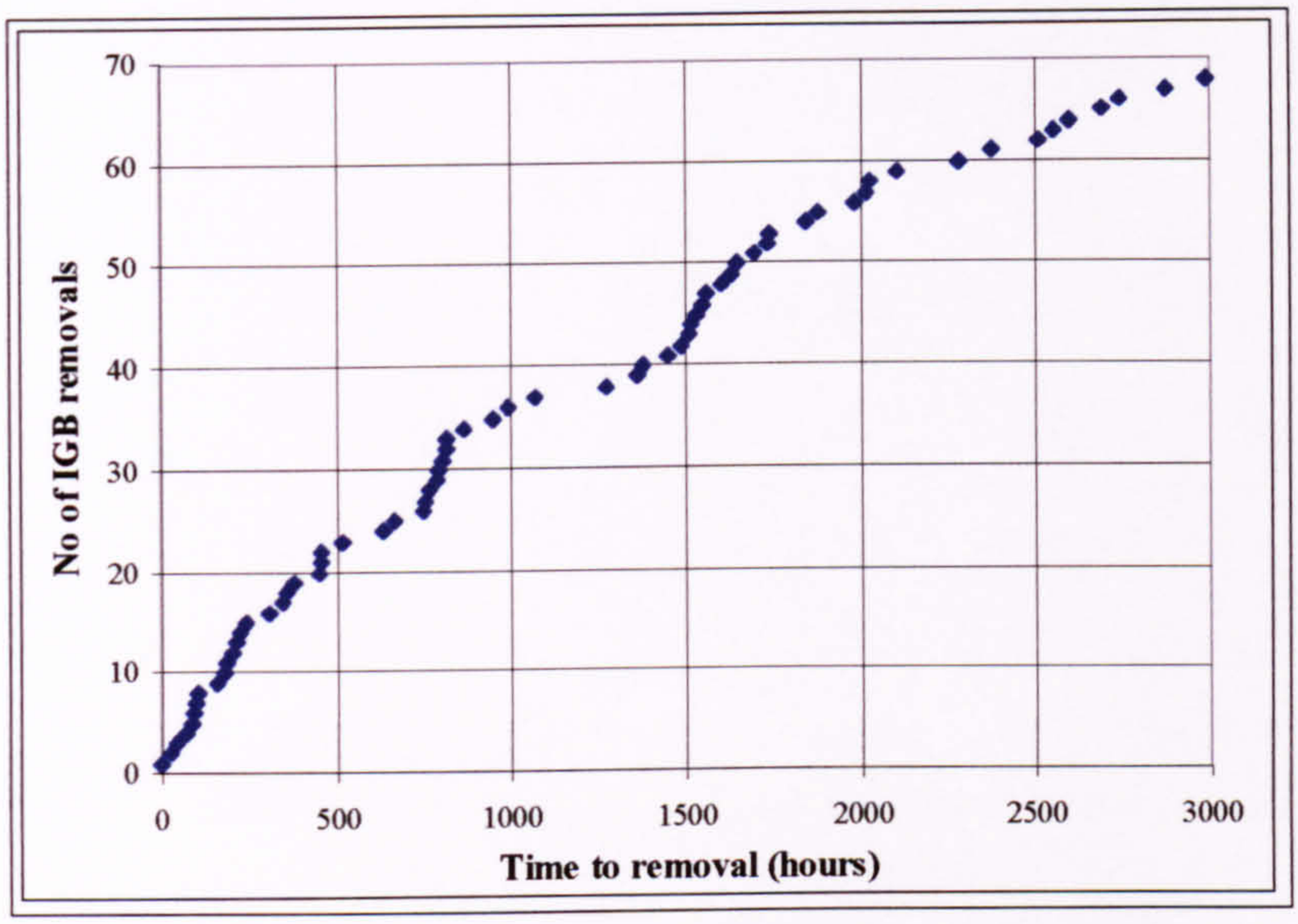

Figure 7.1 : Cumulative number of removals of Type A gearbox for bearing wear debris (total 68)

Figure 7.1 shows the cumulative number of removals of Type A gearboxes due to the presence and detection of oil debris, plotted against the number of hours operated. The records for the times to removal are gearbox hours, but do not distinguish between TSN and TSO; this is an important distinction since bearings are most often replaced at overhaul. The times to removal greater than 3500 hours are likely to be the TSN hours, and have been removed from the following analyses. Hence the graph shows data from 68 of the 77 gearboxes initially considered.

The times to removal were then ranked in order of time to rejection and plotted as in Appendix C.5 to determine whether a Weibull distribution could be fitted to the failure data. To establish the percentage of gearboxes that have failed, a total population of 140 gearboxes has been assumed, based upon the fleet size in service. Figure 7.2 shows the Weibull distribution fitted to the NAML data.

The value of Weibull slope β describes the failure rate for the failure mechanism under investigation. A value less than one implies that the failure rate is decreasing with time, β equal to one means a constant failure rate (random or exponential model), and β greater than one means that the failure rate is increasing, the wear-out mode **[Carter, 1986]**.

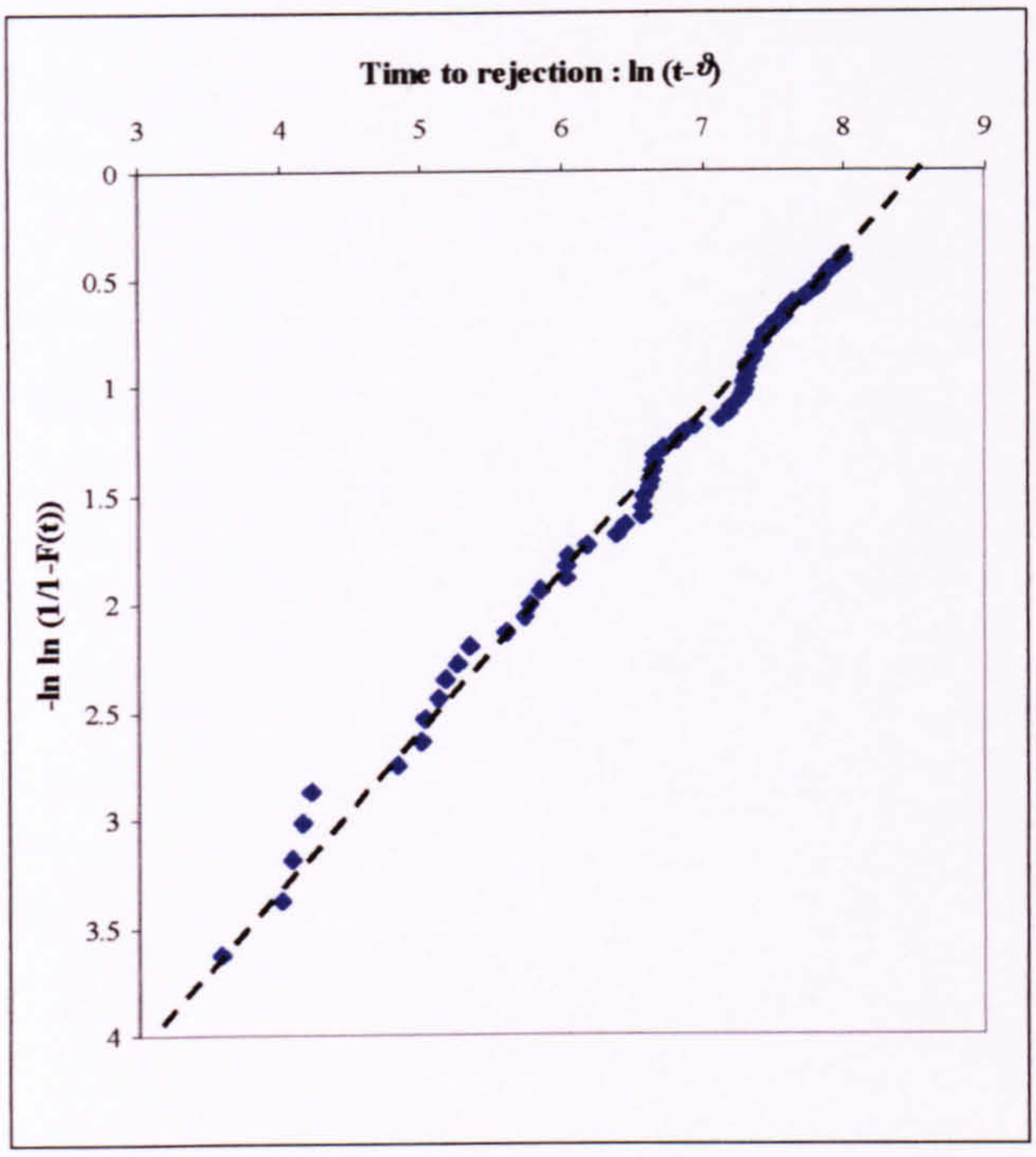

Figure 7.2 : Weibull plot of removals of Type A gearbox for bearing wear debris (assumed population of 140 IGB)

The Weibull analysis (Appendix C.6) performed yielded the following parameters, based on the distribution shown in Figure 7.2:

β, Weibull slope = 0.73
η, characteristic life = 4950 hours
γ, minimum life = 35 hours

A minimum life $\gamma > 0$ implies that the failure rate is virtually zero before 35 hours, referred to as intrinsic reliability **[Carter, 1986]**. After this time, some bearings will fail, but the Weibull slope β of 0.73 implies that the failure rate will decrease with time. The failure rate is the number of gearbox removals per unit time (hours) arising from bearing fatigue and wear; the decreasing trend is shown in Figure 7.3. The characteristic life η of 4950 implies that 63.2% of the population of gearboxes will have been removed due to bearing fatigue and wear by this time. The complete fitted Weibull equation for the NAML bearing data is therefore:

$$F(t) = 1 - \exp\left[-\left(\frac{t-35}{4950}\right)^{0.73}\right] \qquad (7.1)$$

The slope of less than one is significant, since bearing manufacturers often quote a Weibull slope of between 1.1 and 1.5, i.e. an *increasing* failure rate for the calculation of bearing lives **[TIMKEN, 1994]**. The latter represents tests conducted under controlled laboratory conditions where bearing installation, loading and lubrication are

strictly controlled. The Weibull slope of greater than one indicates a 'wear-out' type failure mechanism as would be expected due to rolling contact fatigue of the rollers and raceways (Chapter 3). **[Carter, 1986]** suggests that a Weibull slope of $\beta \sim 0.7$ indicates fatigue failure.

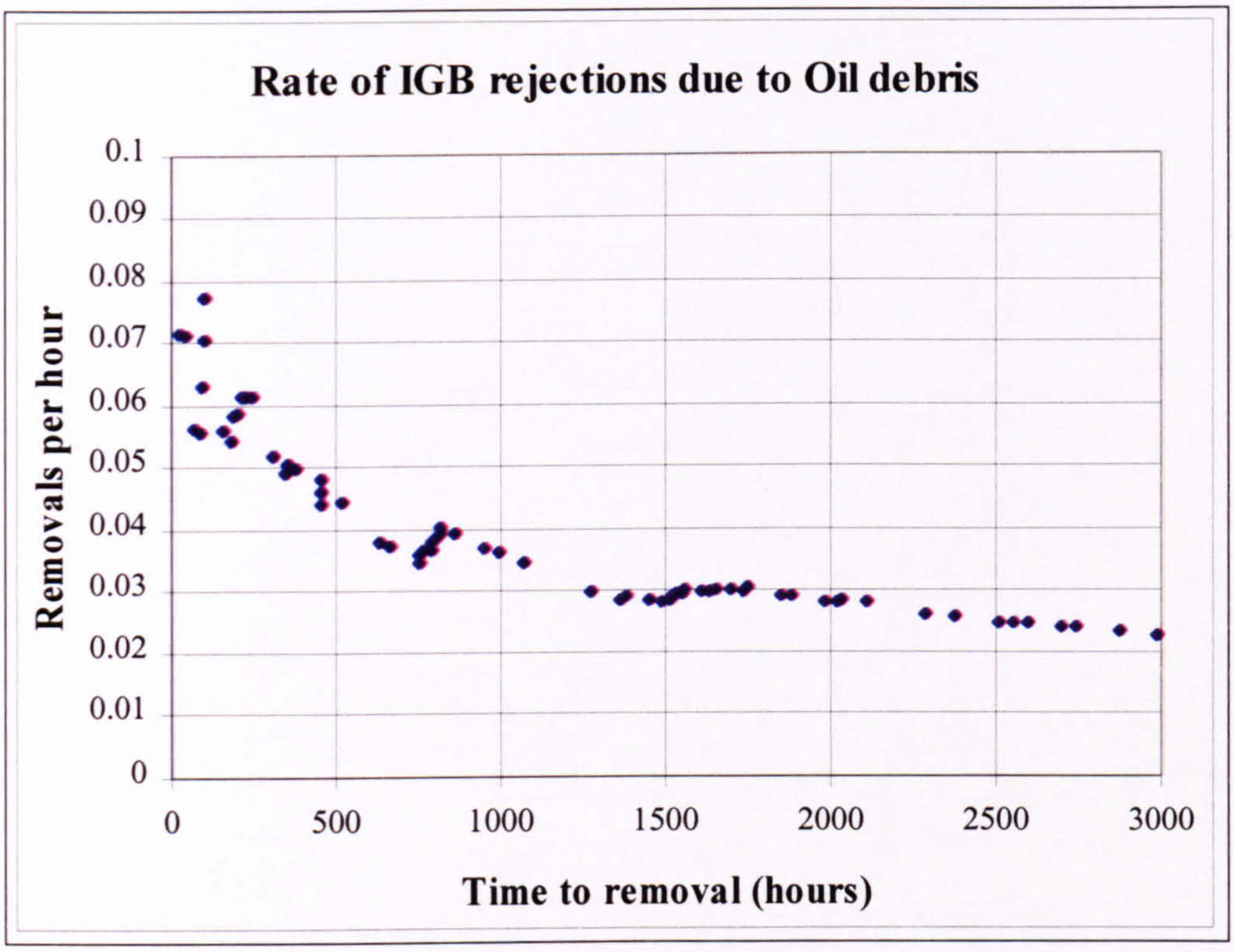

Figure 7.3 : Rate of IGB removals due to bearing wear debris

The Weibull slope of 0.73 calculated for the NAML data implies that bearings are not reaching their expected fatigue life, but are failing due to other reasons. Typical among these are incorrect installation and inadequate lubrication, which would explain the *decreasing* failure rate, as those bearings with defects were detected and rectified in the early stages of life. Other workers, e.g. **[Reed, 1998]**, have highlighted such premature failures that arise from causes other than fatigue. Figure 7.3 shows that the removal rate approaches a constant value (between 0.02 and 0.03 removals per hour) after 2000 hours of gearbox operation.

7.3 Defence Aviation Repair Agency, Perth

The archived records of "work packs" of the Type A gearbox were examined to record data from the overhaul of this particular IGB. Records are filed by gearbox reference number, and in some cases there are details of a gearbox which was rectified/overhauled at Perth a number of times. When this is the case, the records are grouped together in a shaded block.

A sample of the records was studied, which produced 118 entries for separate workshop visits of 67 gearboxes over the period 1974 to 1998. These records are given in full in Appendix D.2, and the main categories of damage are listed in Table 7.2. Note that the total adds to more than 118 since gearboxes often have a combination of damage e.g. corrosion and spline wear.

Recorded damage	Number of cases	Percentage
Bearing defect	46	39%
Spline wear	39	33%
Corrosion – External	24	20%
Corrosion – Internal	11	9.3%
Seal leakage	9	7.6%
LIFEX components	6	5%

Table 7.2 : Defects from 118 records from maintenance of Type A gearbox (Perth)

These data are the most detailed of all maintenance records analysed in this work. The most pertinent information that can be gained from the Perth data is the time since overhaul (or since new) for a fault to develop and be detected. Although the descriptions of the damage are qualitative only, the time for the failure mechanism and possible cause are normally quoted.

A significant number of the Perth records give details of spline wear, bearing damage and corrosion. Those referring to bearing damage may be cross-referenced to NAML data, since oil debris detection reported by NAML normally leads to a requirement for the gearbox to be overhauled.

7.3.1 Bearing defects

The most frequently mentioned items (46) in the Perth data are the bearings, of which there are four per gearbox; this includes fatigue spalling, pitting and scoring of the bearing rollers and cages. Figure 7.4 shows a plot of the number of gearboxes for which bearing damage was recorded, against the time since last overhaul (TSO) or time since new (TSN).

The data show that there is an initially increasing rate of occurrence of bearing defects in the first 1000 hours, from 0.019 to 0.025 occurrences per hour. This is followed by a steady decrease from 0.025 to 0.014 occurrences per hour over the interval 1000 to 3000 hours. The most likely reason for these results is that any errors in assembly and/or defects in the bearings will become apparent after an initial period of operation, in this case up to 1000 hours. The rate thereafter decreases since gearboxes will generally be removed for reconditioning for other reasons, rather than bearing damage.

These figures bear some resemblance to the maintenance data obtained from NAML, which showed a decreasing rate of occurrence for bearing debris, see Figure 7.3. The actual rate of occurrence per hour is less for the Perth data compared to NAML since only a limited sample was taken in the former case (118 records). The NAML data by contrast contain records of all gearboxes in service over the time period concerned.

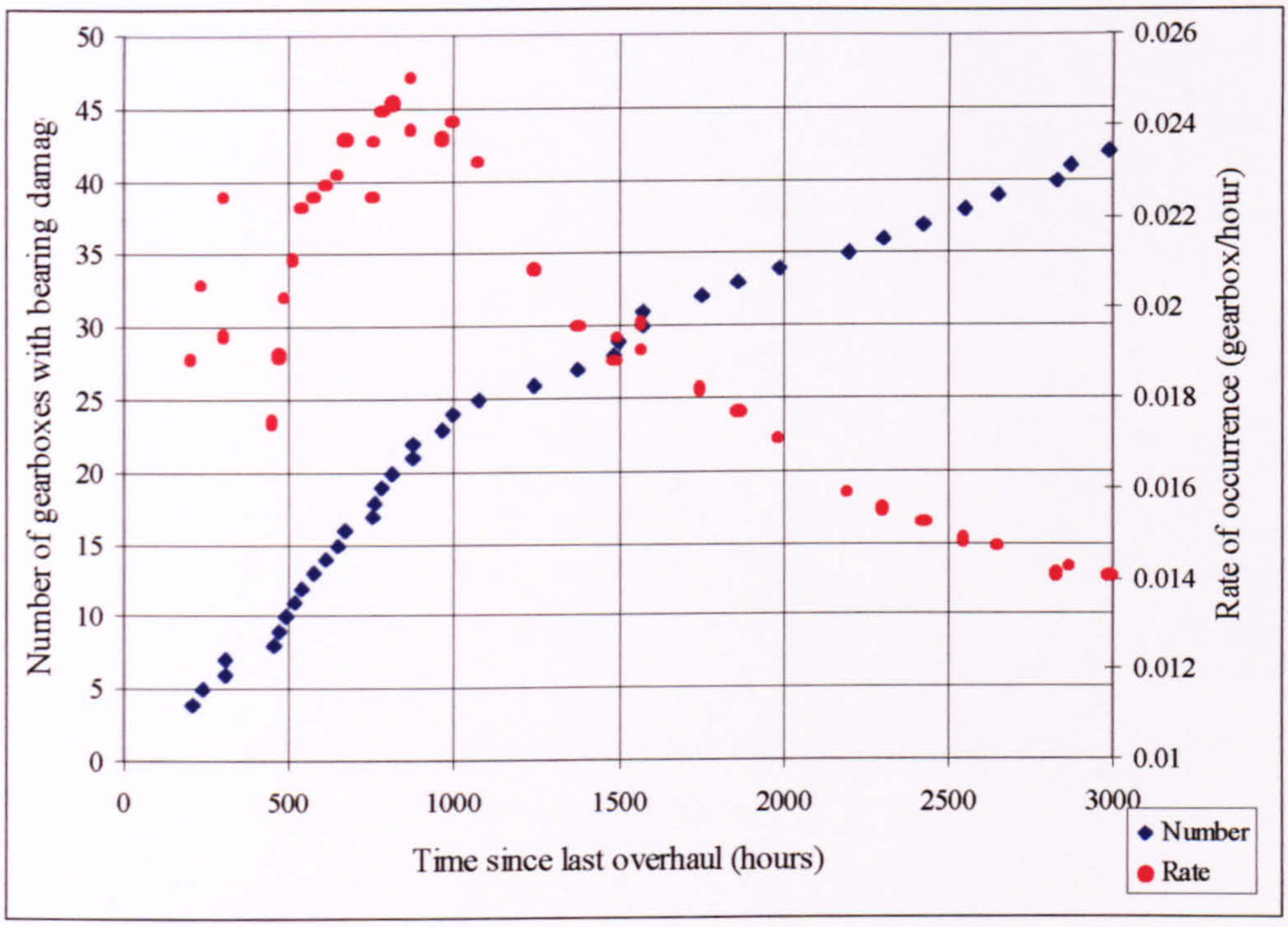

Figure 7.4 : Reported occurrences of bearing damage at overhaul of Type A gearbox (total 46)

7.3.2 Spline wear

A large proportion of overhauled or reconditioned gearboxes had suffered from some degree of wear on the coupling splines. Figure 7.5 shows a plot of the number of gearboxes for which spline wear was recorded, against the time since last overhaul (TSO) or time since new (TSN). The graph shows that spline wear occurs at an almost linear rate over much of the period of interest. The rate increases from 0.005 to 0.008 occurrences per hour over the first 1000 hours, then increases gradually from 0.008 to 0.01 occurrence per hour up to 3000 hours.

The records do not attribute any causal factors to the occurrence of this wear, but lack of lubrication between the mating splines is thought to be one of the primary causes **[Agusta Westland, 1997]**. Other potential problems may be caused by corrosion of the splines leading to profile loss, which results in a fretting action between the components **[Agusta Westland, 1995]**.

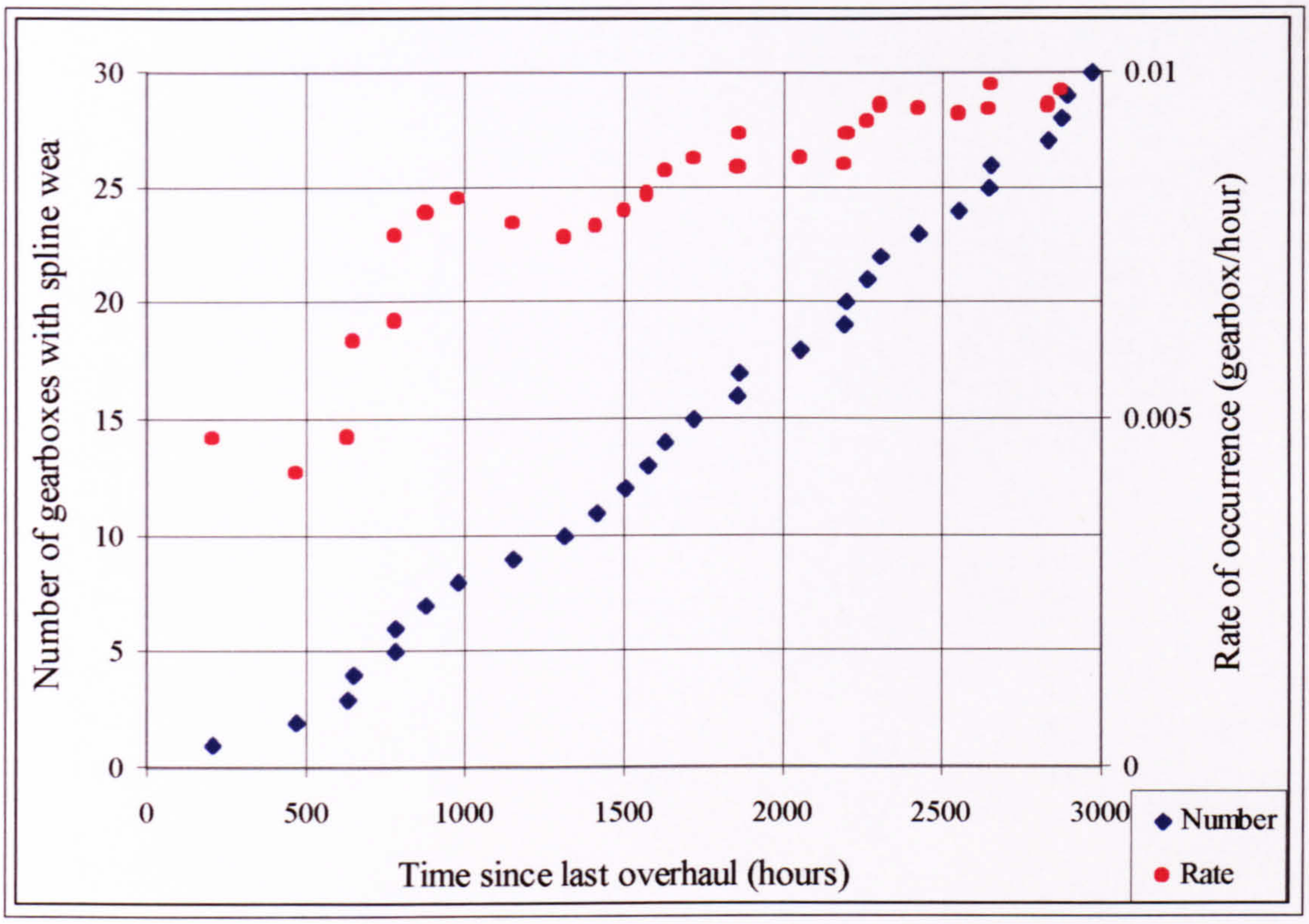

Figure 7.5 : Reported occurrences of spline wear at overhaul of Type A gearbox (first 30 shown)

7.3.3 Corrosion

The number of gearboxes with corrosion is plotted against time since overhaul in Figure 7.6. Both external and internal corrosion of the IGB are reported, but the former is more prevalent; 24 cases of external corrosion, 11 cases of internal. The data do not indicate how many cases of external corrosion were detected during routine maintenance, e.g. before and after each flight, while the helicopter was on the front line Unit.

Damage due to external corrosion is frequently repaired in situ, as part of the maintenance strategy for the IGB. The analysed cases reported in the Perth data may therefore be considered to represent a significant level of corrosion damage. The graph shows that there are few reported cases of external corrosion below 1000 hours, but there is then a linear increase in the reported cases, with an observed rate of 0.007 occurrences per hour.

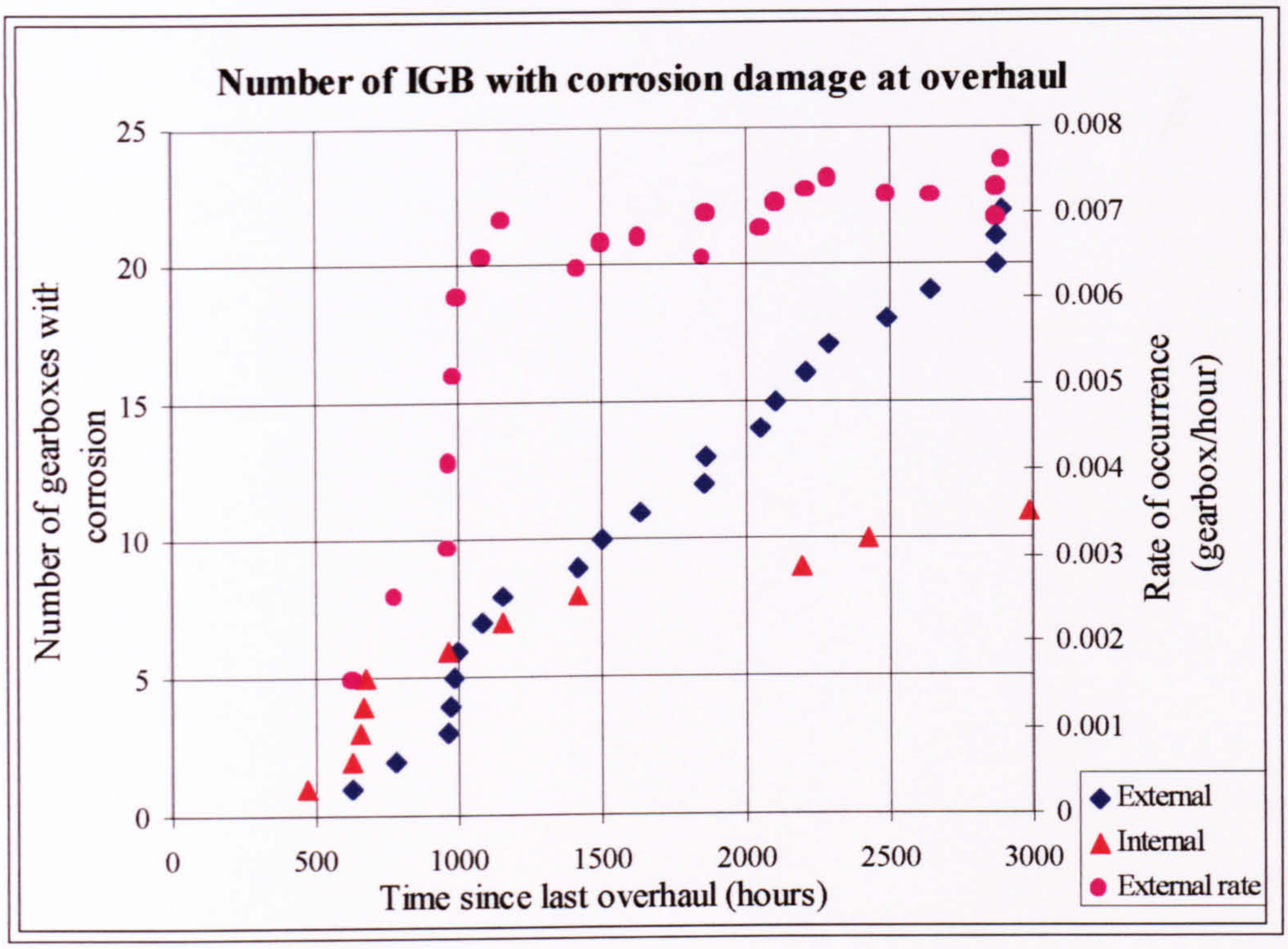

Figure 7.6 : Reported occurrences of corrosion at overhaul of Type A gearbox (total 24 external, 11 internal)

7.4 Data from EDA4 - Logistics Support Services

EDA4 (part of LSS, RAF Wyton) collect all documentation of all maintenance operations performed on military aircraft, in this case the Type A gearbox. Data were obtained from searches against part numbers for the individual components and for the complete IGB assembly. Altogether 704 records were detailed, from 1982 to 1998, listed in Appendix D.3. The data entries were sorted and checked for duplicate records, and the main categories of damage recorded were grouped as follows (see Table 7.3):

a) Defective item – component within gearbox

b) Symptom – the manner in which the defect was discovered.

c) Fault – a description of the fault itself.

Of the 704 records, the categories of fault recorded do not always indicate the type of damage or degradation that has occurred. The drawback with this data is the one word type description of faults, an acronym, e.g. **CMTNMTSWARF** is shorthand for 'contamination by swarf' against the relevant component. The records contain the helicopter airframe hours, which provides no indication of the number of hours accumulated by the IGB.

A significant proportion of records, 30 per cent, did not even indicate which component was at fault. However, by studying the records it has been possible to build up a picture of the relative occurrence of the different failure mechanisms that are reported.

Table 7.3 shows that of those records for which details were available, "Seal wear/Oil leakage" was the most commonly recorded fault, with 15% of all reported maintenance actions. This significant proportion is not reflected in the data from Perth, Section 7.3, since this is a fault that might be rectified in-situ at first line, without returning the gearbox for overhaul.

Recorded damage	Number of cases	Percentage
Seal wear/Oil leakage	105	15 %
Contamination & Magnetic Chip Detector warnings	85	12 %
Robbed	59	8.4 %
Corrosion	59	8.4 %
Worn - component not specified	52	7.4 %
Bearing damage	44	6.3 %
Shaft/spline wear	28	4 %
LIFEX components	26	3.7 %
Misaligned/Out of alignment	14	2 %
Disconnect coupling – Worn - Corroded	14 4	2 % 0.6 %
No failure mechanism specified	214	30 %

Table 7.3 : Recorded defects from Type A gearbox (EDA)

The next most commonly reported fault is that of contamination and magnetic chip detector (MCD) warnings (12%). A proportion of these cases may be reflected in the data from NAML (Section 7.2), although a simple oil change may be all that was required in a number of cases.

After this, corrosion and "robbing" (transferring a gearbox from one helicopter to another) are the next most frequently reported maintenance arisings, both 8.4%. Corrosion may frequently be rectified in situ, but could also require the gearbox to be removed for reconditioning. The catchall word "Wear" is used without any reference to component for 7.4% of the records. It is probable that these refer to either the spline wear (4%) or the disconnect-coupling (2%). The faults involving misalignment (2%) may also be attributable to wear, giving a potential proportion of spline wear of 13.4%. Bearing damage is also reported in 6.3% of the records, and is often associated with contamination and MCD warnings. In every case, this type of damage would require the gearbox to be stripped and the bearings replaced.

A plot of failure types is given in Figure 7.7 that shows the relative occurrence of the different failure mechanisms as a proportion of the total number of defined faults. This excludes the fault categories for which the component and/or the type of defect are unknown. The total under the category "spline wear" has been obtained assuming that the shaft misalignment has led to wear, and that half of the general "Wear" references pertain to the splines.

A useful comparison may be made between the proportion of faults recorded in Figure 7.7 and the data obtained from Perth (Table 7.2). The most common type of fault, seal wear and oil leakage, appears only in the data from EDA, since the rectification work would be carried out at first line in most cases. However, if the two categories of fault, "Contamination" and "Bearing damage" are taken together, the combined proportion (33%) is of the same order of magnitude as the records from Perth (39%). Similarly, external corrosion, reported as 15.2% above, compares with 20% recorded at Perth.

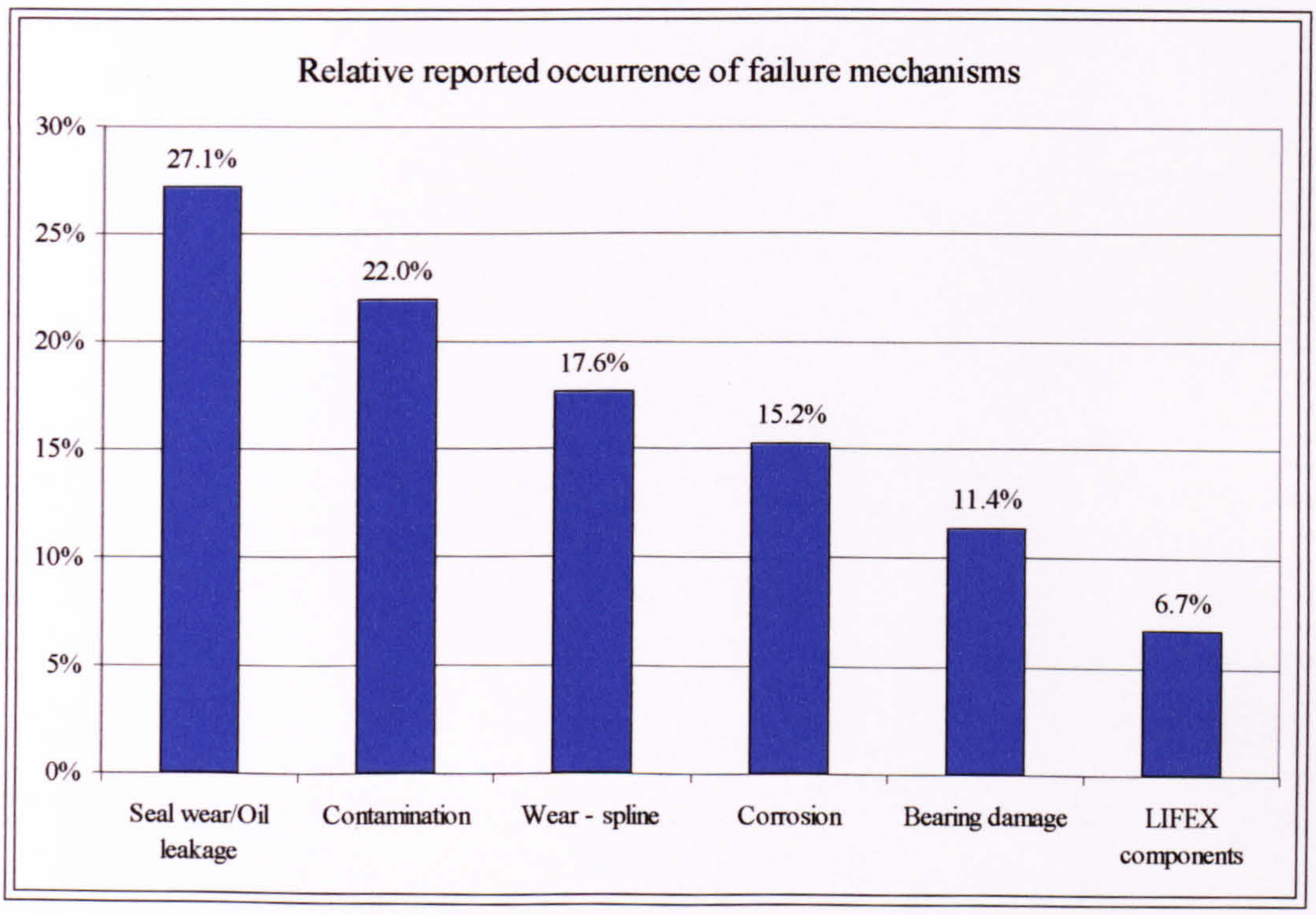

Figure 7.7 : Relative occurrence of failure types (EDA)

The proportion of spline wear differs between the two sets of data, 17.6% in Figure 7.7 (EDA) and 33% in Table 7.2 (Perth). This is due most likely to the fact that some instances of spline wear may only become apparent when the gearbox is stripped completely. The proportion in the Perth data is therefore higher than the EDA data, based on first and second line maintenance records.

The data from three maintenance organisations has been analysed to discover the main types of failure mechanism seen in practice. The data shows the relative frequency of occurrence of the various failure types, together with an indication of the number of operating hours at the time of the discovery of the fault. No data were available on the actual quantity of damage on the relevant component, e.g. depth and extent of corrosion pits, amount of material removed by wear.

7.5 Summary and Conclusions

The data from three maintenance organisations has been analysed to discover the main types of failure mechanism seen in practice. The data shows the relative frequency of occurrence of the various failure types, together with an indication of the number of operating hours at the time of the discovery of the fault. No data were available on the actual quantity of damage on the relevant component, e.g. depth and extent of corrosion pits, amount of material removed by wear. The main conclusions from this study are:

- The Type A gearbox seldom reaches the quoted Time between Overhaul (TBO) period, determined by its tooth root bending fatigue life.

- The most frequently observed failure mechanisms are bearing fatigue/wear, spline wear and casing corrosion. The occurrence rates obtained from Perth data were 0.015, 0.009 and 0.007 occurrences per hour at the 2000-hour point respectively. However, these figures were obtained from a sample of 120 records from maintenance archives and are therefore only useful for comparative purposes.

- The occurrence rate for bearing fatigue/wear from NAML data was observed to be 0.02 occurrences per hour at the 2000-hour mark. This is greater than the figure from Perth since the latter was taken from a limited sample size.

- The NAML bearing data showed a removal rate which decreased with time (Weibull slope $\beta = 0.73$). This could be related to the installation and initial operating environment of the bearings. A classical fatigue type failure, based on a wear-out type mechanism ($\beta > 1$) would have been expected from the manufacturers data.

- Oil leakage and seal wear is frequently observed at first line; this fault may be corrected in-situ.

8 Results from Fatigue and Wear Models

8.1 Introduction

The reliability prediction models developed for this work have been implemented in Delphi™ software entitled HGBR. This program has been employed to investigate the relative impact of loading, material and geometrical parameters with reference to the intermediate gearbox. Data for the models are given in Chapter 6 and Appendix E, which contain geometrical, material and load information for the two example gearboxes. The four torque data sets are split equally, two spectra for each gearbox. However, wherever possible, general rather than specific conclusions have been drawn.

Results are presented from HGBR version 3.0, and individual models within the program have been applied to generate results. These are the output of models for fatigue and wear (Sections 8.2 to 8.4) that are dependent on operating hours (cycles). Results from the corrosion and system reliability models are presented in Chapter 9.

The results are organised in order of components and failure mechanism as given in Table 8.1. Within each section, the results of sensitivity studies are presented graphically in order to convey the relative influence of certain model parameters.

Component	Failure mechanism	Analysis	Section
Gear teeth	Tooth root bending fatigue	Material variability	8.2
Gear teeth	Rolling contact fatigue	Material variability	8.3
Gear teeth	Tooth root bending fatigue	Loading variability - Variation of percentage occurrence of manoeuvres	8.4
Gear teeth Bearings	Rolling contact fatigue		
Gear teeth	Tooth root bending fatigue	Over-torque - Variation of proportion of over-torque	8.5
Gear teeth Bearings	Rolling contact fatigue		
Gear teeth	Tooth root bending fatigue	Comparison between loading and material variability	8.6
Shaft splines	Wear	Variation in slip amplitude and wear coefficient	8.7
Shaft splines	Wear	Variation in loading and over-torque	8.8

Table 8.1 : Results presented using Individual Failure Models

Model results consist of graphs of calculated values of failure probability p(F) against time to failure (TTF) for each failure mechanism. When describing results, the value of p* is quoted, which is a discrete value of cumulative failure probability p(F), Figure 8.1.

The curves show the mean expected value of TTF and the confidence limits are not shown. This is because the models aim to demonstrate the effect of changing material and load parameters. The relative change in the results, which is the object of the testing, is not affected by confidence limits.

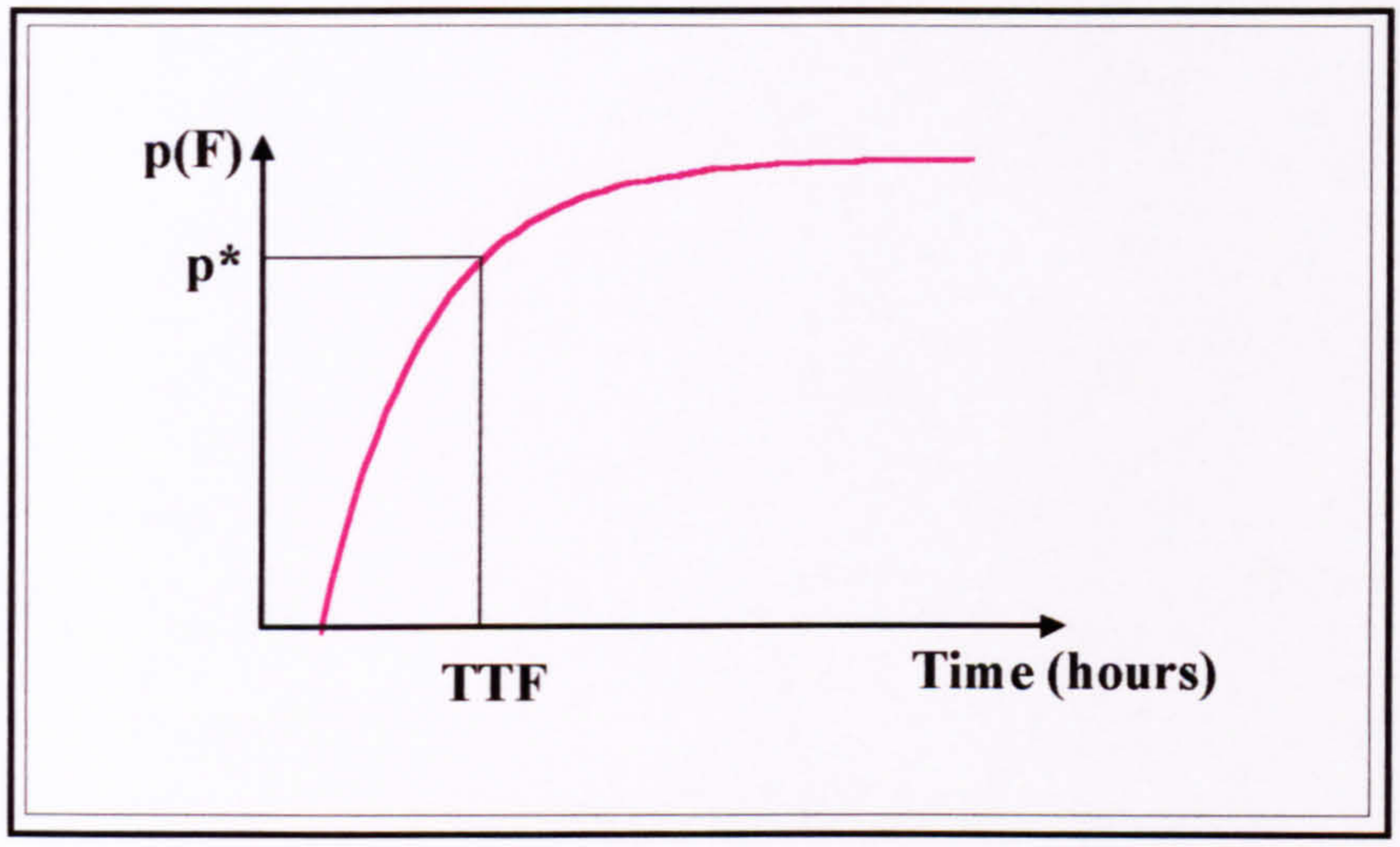

Figure 8.1 : Nomenclature for results

Results are also presented showing time to failure values at a particular value of **p***, in order to illustrate the influence of key parameters. When the value of **p*** is 10^{-6}, this corresponds to 'six-nines' reliability, often used in the helicopter industry **[Everett, Bartlett and Elber, 1992]**. Where appropriate, a different value of **p*** is used, e.g. 10^{-3}, in order to allow a clearer comparison of the results to be made, or where lower failure probability could not be calculated.

8.2 Tooth root Bending Fatigue - Material variability

The effect of material variability on gear tooth root bending fatigue has been investigated by quantifying the change in time to failure/spall with a change in model parameters. The method chosen was to vary the position of the T-N curve by changing the endurance limit T_{inf} and using different values for the coefficient of variation (COV). The predicted failure probability has been calculated using the model described in Section 6.2.3.

8.2.1 Type A Gearbox – ASW loading

Figure 8.2 shows a plot of failure probability p* against predicted time to failure due to tooth root bending fatigue for the Type A gearbox. There are five curves drawn, each representing a different combination of mean T_{inf} and COV, using the ASW torque-time history described in Appendix E.3.1. The failure curves converge at the mean failure probability **p*** = 0.5.

The design T-N curve (mean T_{inf} 1226 Nm, COV 6%) yields a predicted life of the order of 2500 hours for a failure probability **p*** of 10^{-3}. This is the usual criterion to which gears are designed, that calculated using the 'Mean minus 3-sigma' curve for material variability (Appendix C.2.1). The value of life calculated is lower than would be expected – typical gearboxes have TRBF lives in excess of 5000 hours. This is due to the overly conservative loading (ASW history) applied, compared to the actual spectrum used for design, as explained in Section 7.4.1.

Reducing the mean T_{inf} from 1226 Nm to 1100 Nm (for constant COV 6%) decreases the TTF from 2500 to 250 hours (factor of 10), at p* of 10^{-3}. If the mean T_{inf} is maintained constant and the COV increased, the effect is to shift the failure curve to the left and to reduce the gradient, due to the increasing uncertainty in T_{inf}. An increase in COV from 6% to 10% (for constant T_{inf} 1226 Nm) causes the predicted TTF at p* of 10^{-3} to reduce from 2500 to 600 hours, a reduction factor of 4.2. This factor changes with the required value of p*; a lower value of failure probability implies that changes in COV would have a greater impact, since it determines the 'spread' of the probability distribution.

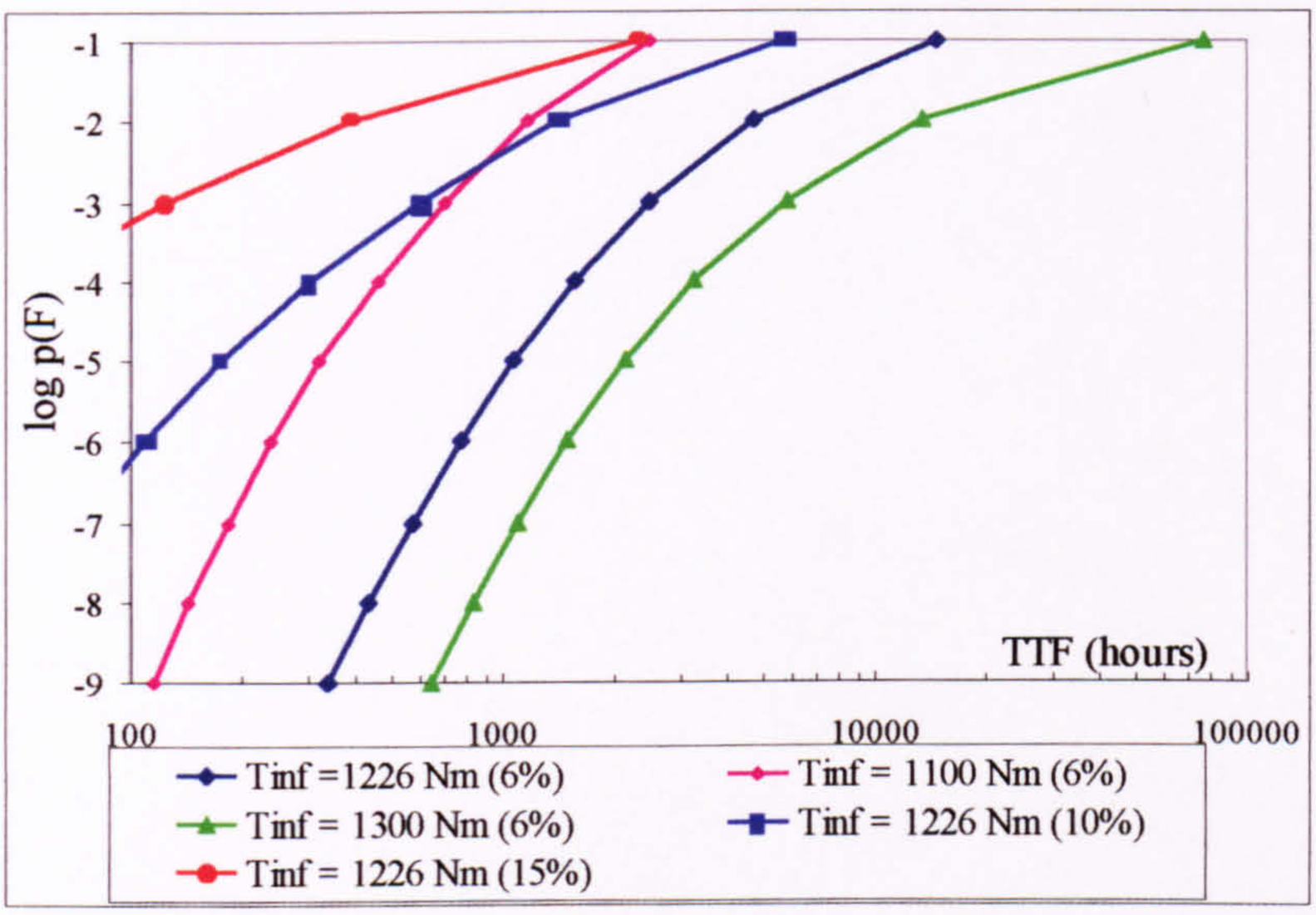

Figure 8.2 : TTF by tooth root bending fatigue for different values T_{inf} and COV for Type A Gearbox – ASW history

The graph shows how large changes in estimated life can be achieved by altering the mean and COV of the endurance limit. Such changes may be difficult to achieve with existing materials and proven manufacturing methods, but may be achievable when designing a replacement part. There could be a difference in the cost of manufacture, or weight, which is a function of endurance limit and/or material scatter. Such studies would yield the optimum solution, and the trade-off between T_{inf} and COV is shown in Section 8.2.3.

8.2.2 Type B Gearbox – Civil Spectrum

For the purpose of comparison Figure 8.3 shows a plot of failure probability against predicted time to failure due to tooth root bending fatigue for the Type B gearbox. There are five curves drawn, each representing a different combination of mean T_{inf} and COV, using the Civil torque spectrum (Appendix E.3.4). The normal T-N design curve (mean T_{inf} 2256 Nm, COV 6%) yields a predicted life of 25250 hours at **p*** 10^{-6} and > 10^5 hours at **p*** of 10^{-3}. The times to failure (TTF) are higher than the typical values for the Type A, Figure 8.2, due to the greater material strength (T_{inf}) of the more recent Type B design.

Reducing the mean T_{inf} (at constant COV 6%) from 2256 to 2000 Nm has the effect of decreasing the times to failure, from 25250 to 4000 hours (factor of 6.3) at **p*** of 10^{-6}. The net effect of increasing COV is the same as that in Section 8.2.1. An increase in COV from 6% to 10% (at constant T_{inf} 2256 Nm) causes the predicted TTF at p* of 10^{-6} to reduce from 25250 to 1690 hours, a reduction factor of 15.

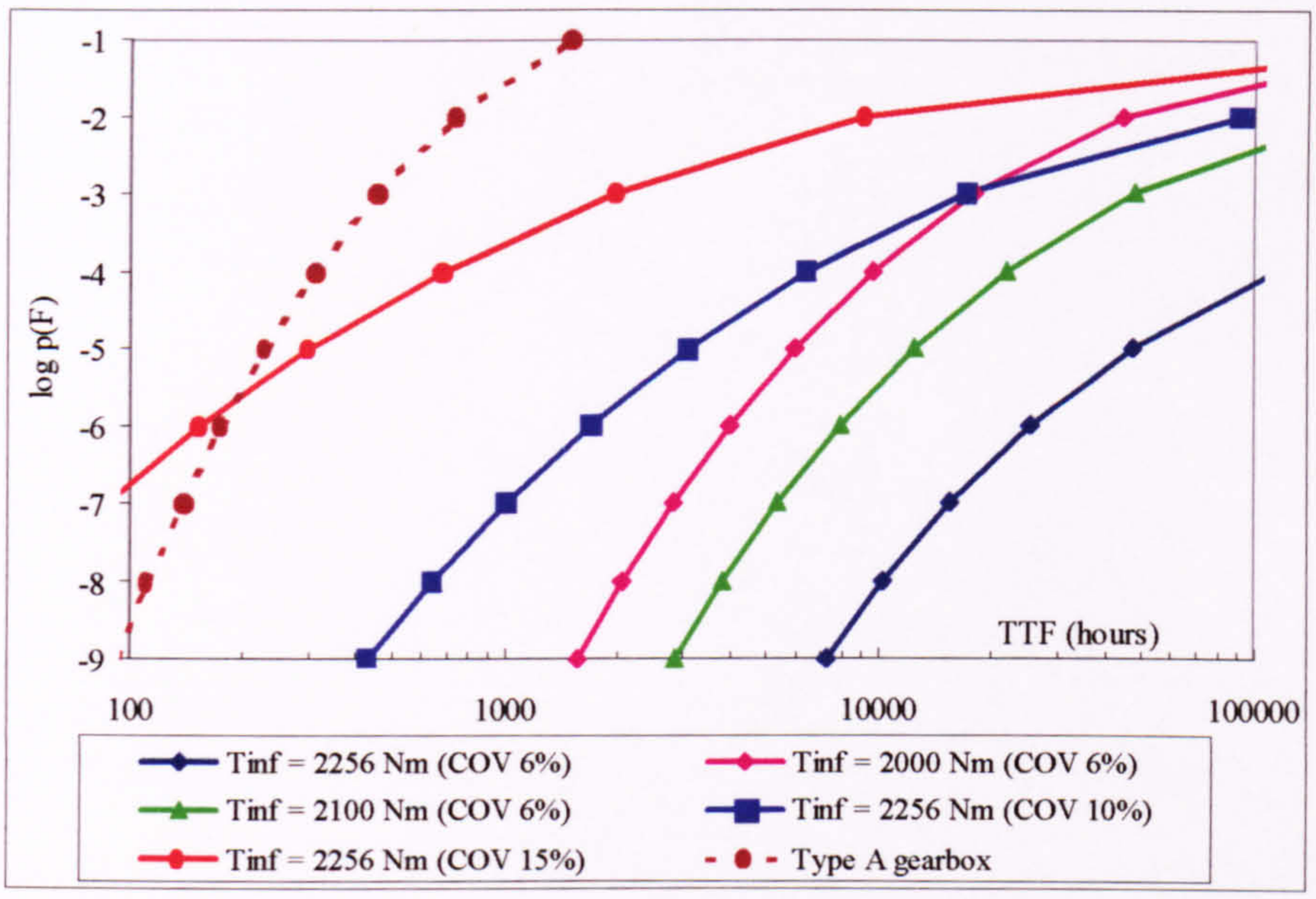

Figure 8.3 : TTF by Tooth root Bending Fatigue for different values T_{inf} and COV for Type B gearbox – Civil spectrum

8.2.3 Variation of endurance limit (T_{inf}) and COV

Figure 8.4 and Figure 8.5 show the plots of T_{inf} (endurance limit) versus the calculated TTF at constant p* of 10^{-6}. Each graph contains the results of calculations for a range of COV between 0 - no scatter - and 16% - average to poor scatter. Figure 8.4 is for Type A gearbox with ASW loading and Figure 8.5 is for Type B gearbox with Civil spectrum.

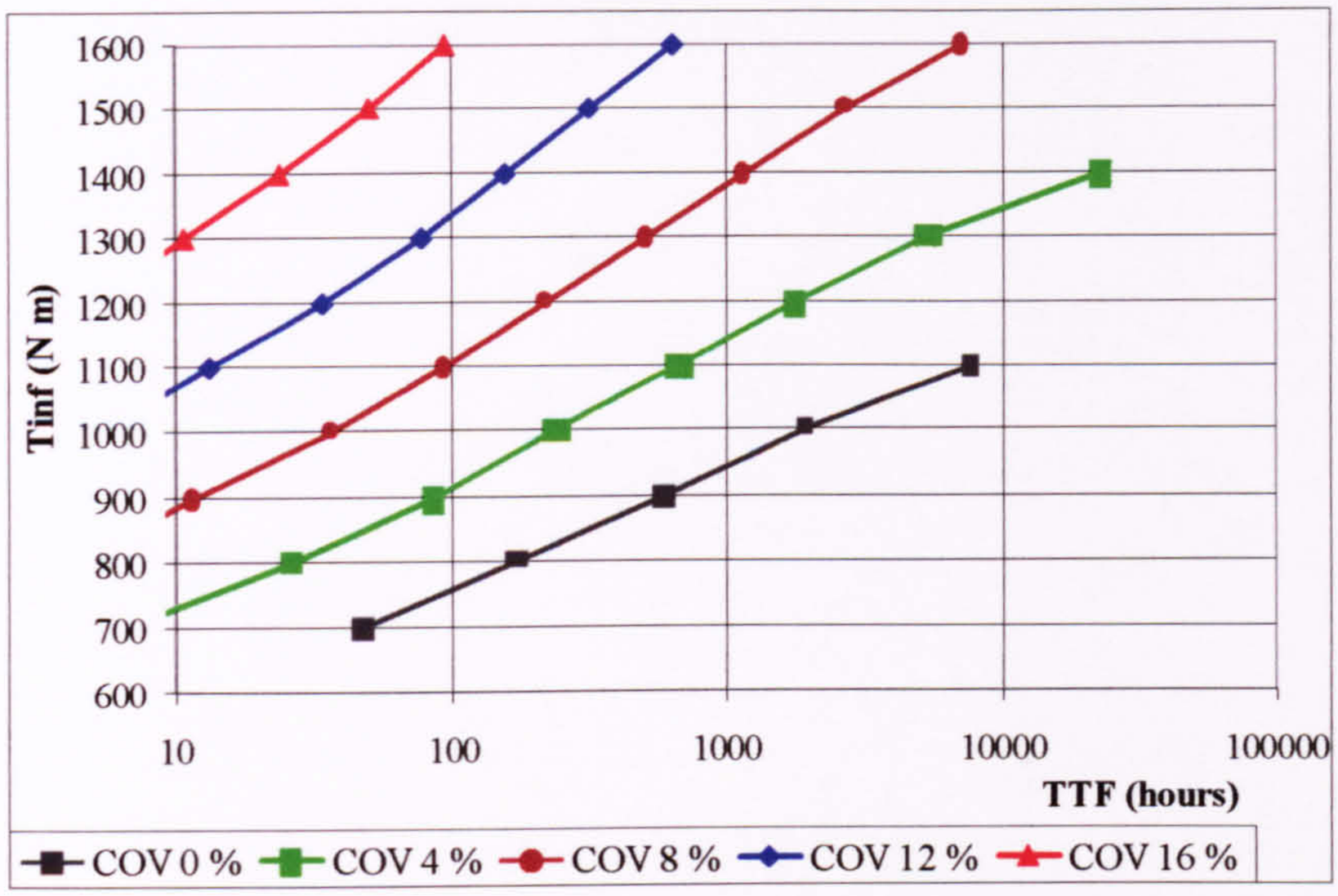

Figure 8.4 : Plot of T_{inf} versus TTF by tooth root bending fatigue for COV 0 – 16%, Type A gearbox, ASW Loading at $p^* = 10^{-6}$

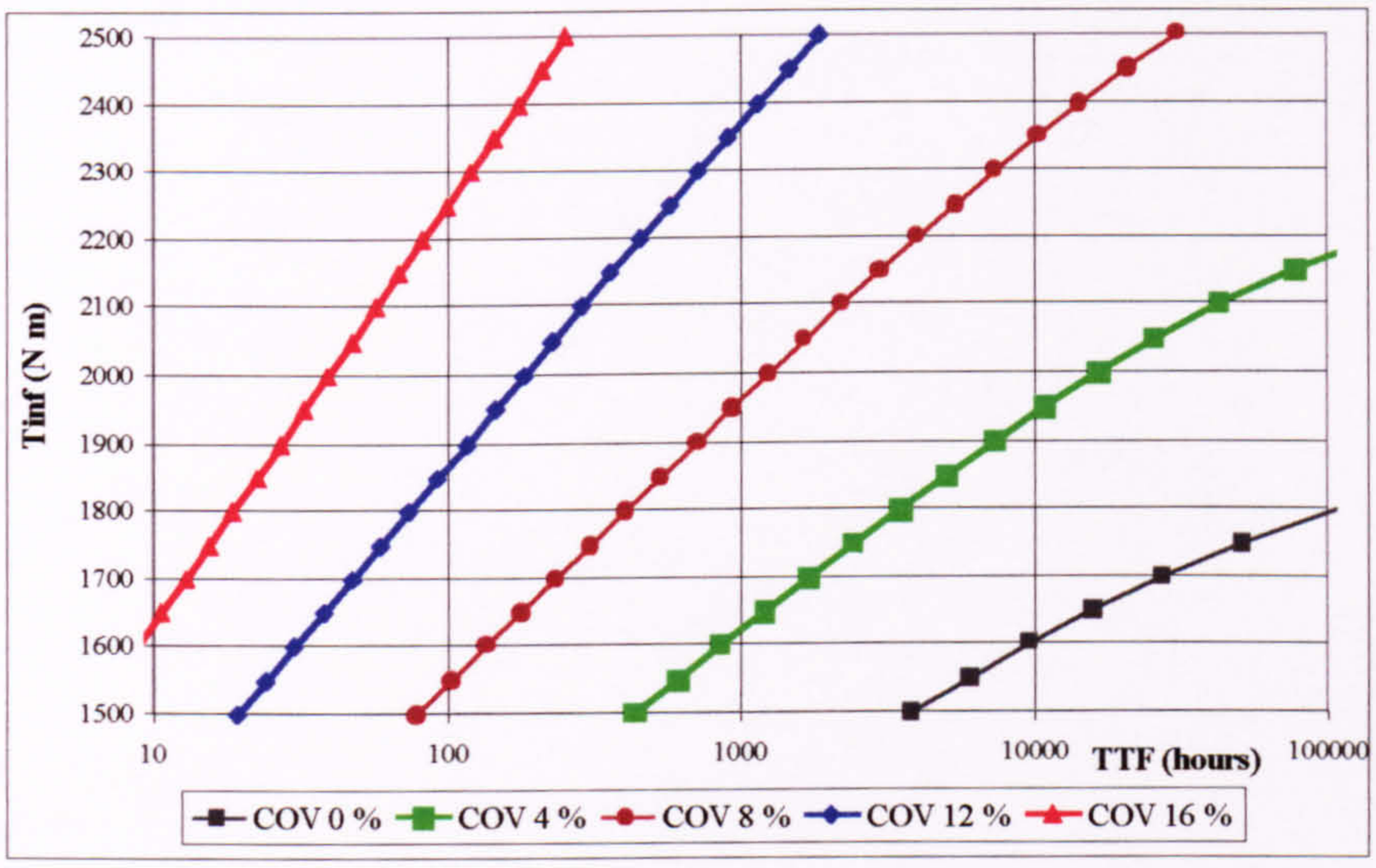

Figure 8.5 : Plot of T_{inf} versus TTF by tooth root bending fatigue for COV 0 – 16%, Type B gearbox, Civil spectrum at $p^* = 10^{-6}$

The curves for both gearboxes show the expected increase in life with increasing T_{inf} - this would be expected on a non-probabilistic analysis. However the role of increasing COV at a constant value of T_{inf} may be seen in each case. For Type A, at constant T_{inf} - for example 1100 Nm – the increase in COV causes a reduction in life from 7900 hours for zero scatter to 13 hours for COV of 12% for p^* of 10^{-6} (Figure 8.4). For p^* of 10^{-3}, the TTF is the same at zero COV, but at COV of 12%, the life reduces to 10^6 hours.

For Type B, at constant T_{inf} - for example 1700 Nm – the increase in COV causes a reduction in life from 27380 hours for zero scatter to 48 hours for COV of 12% for p* of 10^{-6} (Figure 8.5). For p* of 10^{-3}, the TTF is the same at zero COV, but at COV of 12%, the life reduces to 257 hours.

8.2.4 Trade-off between endurance limit and COV

For typical gearbox lives in the region of 10000 – 20000 hours, and realistic COVs of 8% - 16%, there is a sensitive interaction between T_{inf} and the COV values. Slight changes in either can drastically influence the life obtained. This is demonstrated in Table 8.2, in which COV is reduced from 12 to 4% in 2% steps at constant T_{inf}, and T_{inf} is increased from 1000 to 1500 Nm at constant COV. The table shows the factor by which the estimated life is increased by a decrease in COV or an increase in T_{inf}; this is for the Type A gearbox, with ASW history. Results are shown for p* of 10^{-6} and 10^{-3}.

$p^* = 10^{-6}$	COV (%) 12-10	COV (%) 10-8	COV (%) 8-6	COV (%) 6-4
T_{inf} = 1000 Nm	2.50	3.13	2.85	2.84
T_{inf} = 1250 Nm	2.68	3.05	3.65	4.23
T_{inf} = 1500 Nm	3.60	4.08	11.38	
$p^* = 10^{-6}$	T_{inf} (Nm) 1000-1050	T_{inf} (Nm) 1050-1100	T_{inf} (Nm) 1100-1150	T_{inf} (Nm) 1150-1200
COV = 4%	1.86	1.89	1.86	1.83
COV = 6%	1.66	1.71	1.76	1.78
COV = 8%	1.79	1.61	1.59	1.63
$p^* = 10^{-3}$	COV (%) 12-10	COV (%) 10-8	COV (%) 8-6	COV (%) 6-4
T_{inf} = 1000 Nm	1.96	1.87	2.04	2.23
T_{inf} = 1250 Nm	2.31	2.35	2.73	4.39
T_{inf} = 1500 Nm	4.24	18.80		
$p^* = 10^{-3}$	T_{inf} (Nm) 1000-1050	T_{inf} (Nm) 1050-1100	T_{inf} (Nm) 1100-1150	T_{inf} (Nm) 1150-1200
COV = 4%	1.97	1.91	1.97	2.26
COV = 6%	1.87	1.89	1.86	1.84
COV = 8%	1.74	1.79	1.82	1.81

Table 8.2 : Reduction in TTF for changes in T_{inf} and material COV (Type A gearbox, ASW history)

Corresponding results are shown in Table 8.3, which is for the Type B gearbox, with Civil spectrum. Different values are used for T_{inf} in this case. The tables present the analyst with options for either increasing T_{inf} or reducing COV in order to increase the TTF. Realistic increases in T_{inf} may be more achievable for TRBF, given that the baseline COV is 6% for this work.

$p^* = 10^{-6}$	COV (%) 12-10	COV (%) 10-8	COV (%) 8-6	COV (%) 6-4
T_{inf} = 1500 Nm	2.00	2.08	2.24	2.46
T_{inf} = 1750 Nm	2.17	2.36	2.64	3.00
T_{inf} = 2000 Nm	2.46	2.76	3.20	4.12
$p^* = 10^{-6}$	T_{inf} (Nm) 1900-1950	T_{inf} (Nm) 1950-2000	T_{inf} (Nm) 2000-2050	T_{inf} (Nm) 2050-2100
COV = 4%	1.48	1.52	1.57	1.66
COV = 6%	1.38	1.39	1.40	1.41
COV = 8%	1.33	1.33	1.33	1.34
$p^* = 10^{-3}$	COV (%) 12-10	COV (%) 10-8	COV (%) 8-6	COV (%) 6-4
T_{inf} = 1500 Nm	1.67	1.74	1.82	1.92
T_{inf} = 1750 Nm	1.86	1.96	2.08	2.26
T_{inf} = 2000 Nm	2.10	2.29	2.65	3.68
$p^* = 10^{-3}$	T_{inf} (Nm) 1900-1950	T_{inf} (Nm) 1950-2000	T_{inf} (Nm) 2000-2050	T_{inf} (Nm) 2050-2100
COV = 4%	1.68	1.81	2.03	2.43
COV = 6%	1.49	1.53	1.59	1.68
COV = 8%	1.41	1.43	1.44	1.47

Table 8.3 : Reduction in TTF for changes in T_{inf} and material COV (Type B gearbox, Civil spectrum)

8.3 Gear tooth rolling contact fatigue - Material variability

Tests were carried out into the effect of material variability for gear tooth rolling contact fatigue (RCF) on predicted failure probability. The two parameters changed for the sensitivity studies were the allowable contact stress S_{AC} and the COV of the S-N curve, with data given in Chapter 6.

8.3.1 Type A Gearbox – ASW loading

Figure 8.6 shows a plot of failure probability against predicted TFS due to gear tooth rolling contact fatigue for the Type A gearbox. There are five curves drawn, each representing a different combination of mean S_{AC} and COV, using the ASW torque-time history. The S-N design curve (mean S_{AC} 1.726 GPa, COV 15%) yields a predicted life of 430 hours for a p* of 10^{-3}. This low value is due to the uncertainty on the S-N curve and the conservative values of torque contained in the ASW history. A sixth curve has also been plotted showing the design failure curve for Type B gear RCF, with different geometry.

Reducing the mean S_{AC} at constant COV has the effect of shifting the failure curve to the left, with a predicted life of 110 hours at p* of 10^{-3} for S_{AC} of 1.6 GPa (COV 15%). If the mean S_{AC} is maintained constant and the COV decreased, the effect is to shift the failure curve to the right and to increase the gradient. This is due to the decreasing uncertainty as to the value of the allowable contact stress. For S_{AC} of 1.726 GPa, a decrease in COV from 15% to 10% causes the predicted TFS at p* of 10^{-3} to increase from 430 to 6950 hours, a factor of 16.

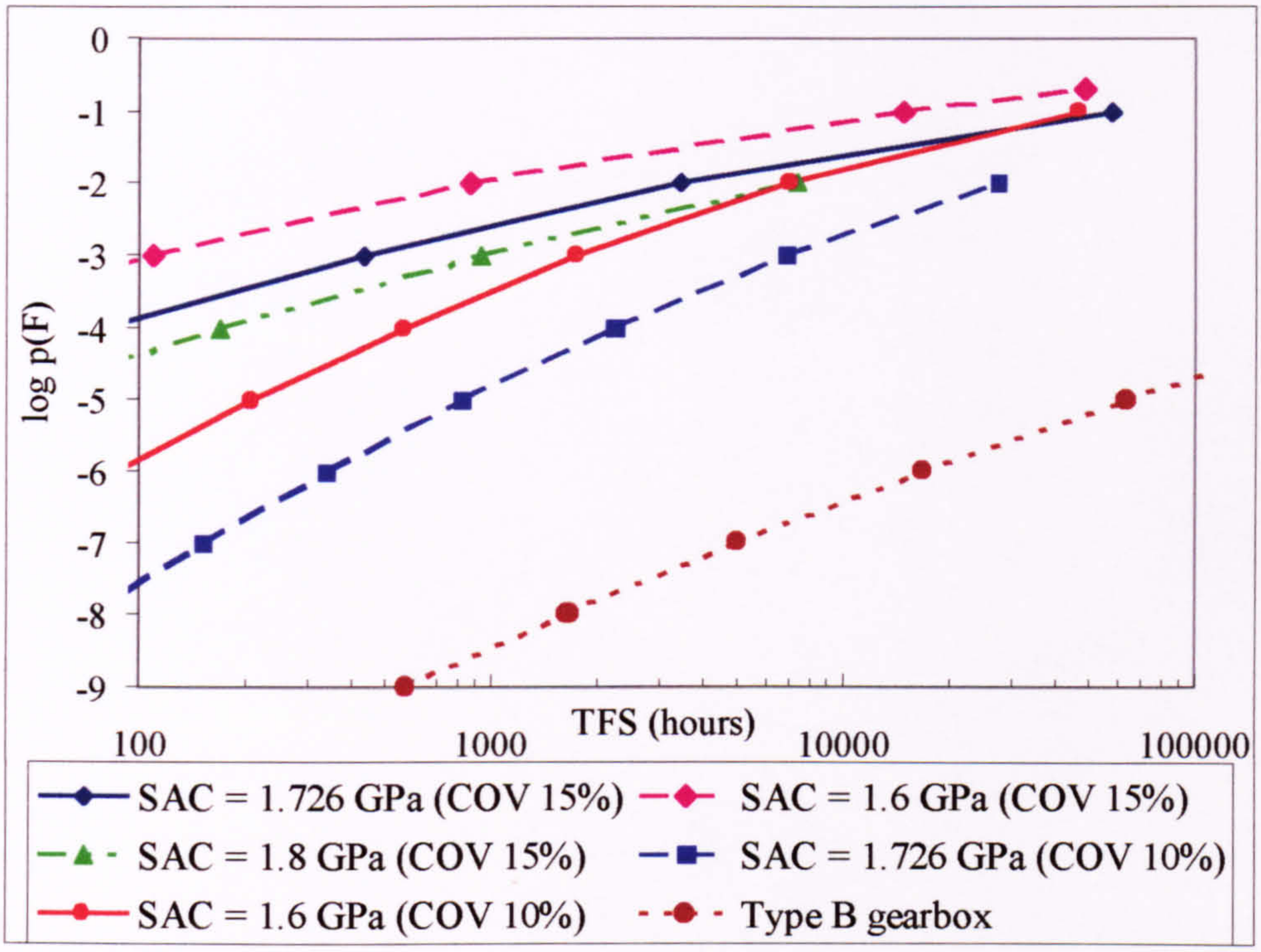

Figure 8.6 : Plot of TFS by gear teeth RCF for different values of S_{AC} and COV for Type A gearbox, ASW Loading

8.3.2 Type B Gearbox – Civil Spectrum

Figure 8.7 shows a plot of failure probability against predicted TFS due to gear tooth rolling contact fatigue for the Type B gearbox. There are five curves drawn, each representing a different combination of mean S_{AC} and COV, using the Civil spectrum. The S-N design curve (mean S_{AC} 1.726 GPa, COV 15%) yields a predicted life of 1210 hours for a p* of 10^{-6}. A sixth curve has also been plotted showing the design failure curve for Type A gear RCF, taken from Figure 8.6.

Reducing the mean S_{AC} at constant COV is again seen to shift the failure curve to the left, with a predicted life of 306 hours at p* of 10^{-6} for S_{AC} of 1.6 GPa. For S_{AC} of 1.726 GPa, a decrease in COV from 15% to 10% causes the predicted TFS to increase from 1210 to 86500 hours, a factor of 72, at p* of 10^{-6}. This large decrease is due to the relatively benign torque spectrum used for the Civil spectrum.

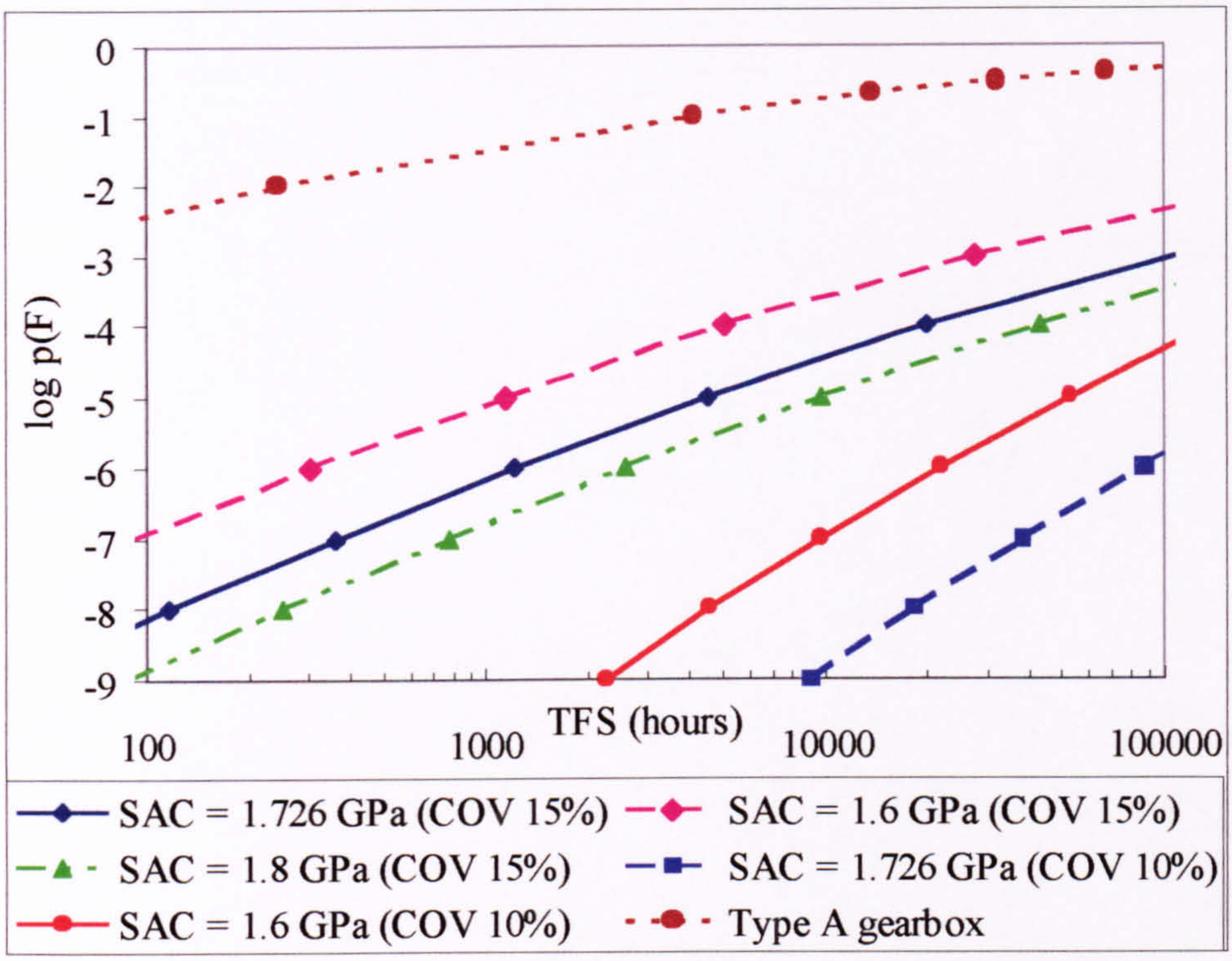

Figure 8.7 : Plot of TFS by gear teeth RCF for different values of S_{AC} and COV for Type B gearbox, Civil spectrum

8.3.3 Variation of allowable contact stress and COV

Figure 8.8 shows the plot of the allowable contact stress S_{AC} versus the calculated time to first spall at p* of 10^{-6}. The graph has been obtained using data for the Type B gearbox, with the Civil torque spectrum. Results are shown for a range of coefficient of variation (COV) values between 4% and 20%. The curves show the increase in time to first spall (TFS) with increasing S_{AC} and again display the important role played by the COV.

For a constant value of 1.6 GPa for S_{AC} and failure probability of 10^{-6} (Figure 8.8) the predicted TFS reduces from in excess of 120 000 hours to 130 hours as COV increases from 8% to 16%. For the same conditions at a higher p* of 10^{-3} (not shown) the TFS is reduced from in excess of 10^6 hours to 15 000 hours.

As existed for tooth root bending fatigue, there is a sensitive interaction between S_{AC} and the material COV parameters. However, for RCF the effect of the degradation is a progressive deterioration of the gear surface rather than a functional failure. It is suggested that reducing the COV from 15% would be the most practical measure to increase predicted life, especially at low p* values.

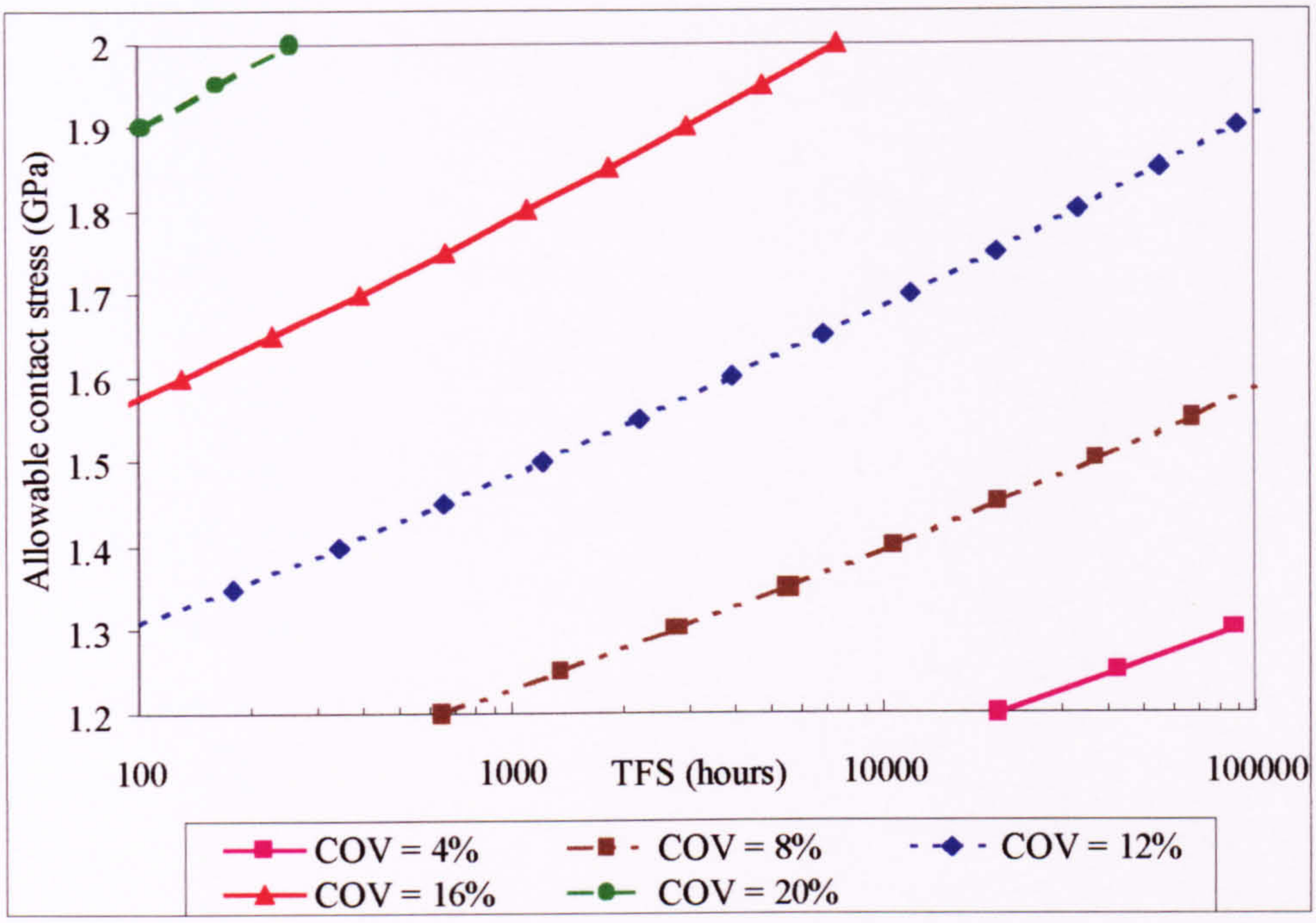

Figure 8.8 : Plot of S_{AC} versus TFS by Gear Tooth RCF for COV 0 – 16%, Type B gearbox, Civil spectrum at p* 10^{-6}

8.4 Loading Variability for Fatigue Models

8.4.1 Results presented

All of the damage models applied thus far have used fixed loading data. The effect of load variability has been studied to determine its significance in the calculation of reliability. Load variability has been introduced in two particular ways:

(a) Variation in the content of the torque spectrum by altering the proportion of damaging manoeuvres in the Civil torque spectrum (Sections 8.4.2 to 8.4.5).

(b) Inclusion of Over-torques, values of torque over and above the highest torque value within the data set. This has been achieved by adding additional load states to the Civil torque spectrum (Section 8.5).

Tests have been conducted on the effect on predicted failure probability of loading variability for different failure mechanisms. This was performed using the damage models for tooth root bending fatigue (gear teeth) and rolling contact fatigue (gear teeth and bearings) and spline wear. These were carried out for the Type B gearbox, using the Civil torque spectrum as a basis for testing. This is because this particular load spectrum contains the most detailed information regarding the load condition associated with different manoeuvres.

The variation of particular manoeuvres has therefore been carried out to examine the effect of helicopter usage. The manoeuvres considered are listed in Table 8.4. The proportional influence of each manoeuvre on TTF/TFS is the same at all p*, and the results are presented at $p^* = 10^{-6}$.

Ref	Manoeuvre description	Baseline (Civil spectrum)	Variation studied
2	Take-off	0.43 %	0.1 – 2%
5	Spot turn port - hover OGE	0.37 %	0.1 – 2%
12	60 degrees Sideways flight	0.37 %	0.1 – 2%
13	90 degrees Sideways flight	0.25 %	0.1 – 2%

Table 8.4 : Manoeuvres considered in load variability (Sections 8.4.2 to 8.4.5)

8.4.2 Influence of Take-off Manoeuvre (Ref 2)

The percentage occurrence of the take off manoeuvre was varied from 0.1 to 2% to ascertain its effect on fatigue damage. As shown in Figure 8.9, a reduction in the proportion of take-offs from 0.43% (the baseline value) to 0.1% results in an corresponding 3% increase for the time to first spall (TFS) for gear tooth RCF, and a 6% increase in bearing life. An increase in the proportion of take-offs from 0.43% to 2% gives a reduction in gear tooth and bearing TFS of 13% and 21% respectively.

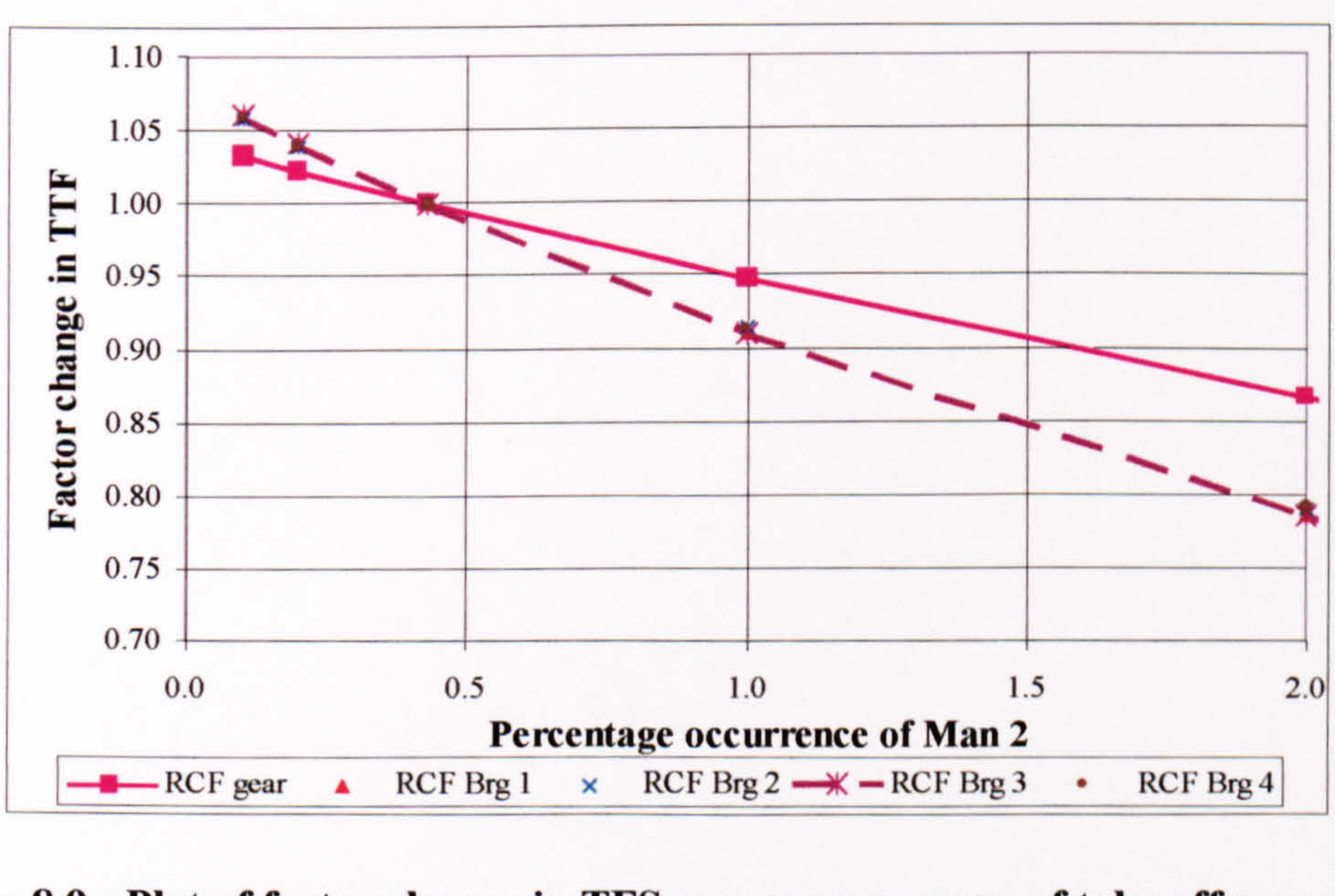

Figure 8.9 : Plot of factor change in TFS versus occurrence of take off manoeuvre

Tooth root bending fatigue does not feature in the graph since the torque values within the take off manoeuvre lie below the endurance limit for this failure mechanism; calculated times to failure therefore do not change with a variation in the proportion of this manoeuvre.

Figure 8.9 shows that the take off manoeuvre contain loads that have a larger proportional effect on the time to first spall (TFS) for the bearings than for TFS of the gear teeth RCF. This is due entirely to the composition of the manoeuvre in terms of torque values and their duration. Other manoeuvres may in fact contain torque values that reverse the order of damage influence, i.e. that have a bigger impact on gear RCF than bearing fatigue, see Section 8.4.3.

8.4.3 Influence of 60 degrees Sideways Flight Manoeuvre (Ref 12)

The percentage occurrence of manoeuvre 12 was varied from 0.1 to 2% to ascertain the effect on fatigue damage. As shown in Figure 8.10, a reduction in the proportion of this manoeuvre from 0.37% (baseline) to 0.1% results in increases of 19% for the tooth root bending TTF, 24% for gear tooth TFS, and 10% for the bearing TFS. An increase in the manoeuvre from 0.43 to 2% gives a reduction in tooth root bending TTF, gear and bearing TFS of 49%, 54% and 35% respectively.

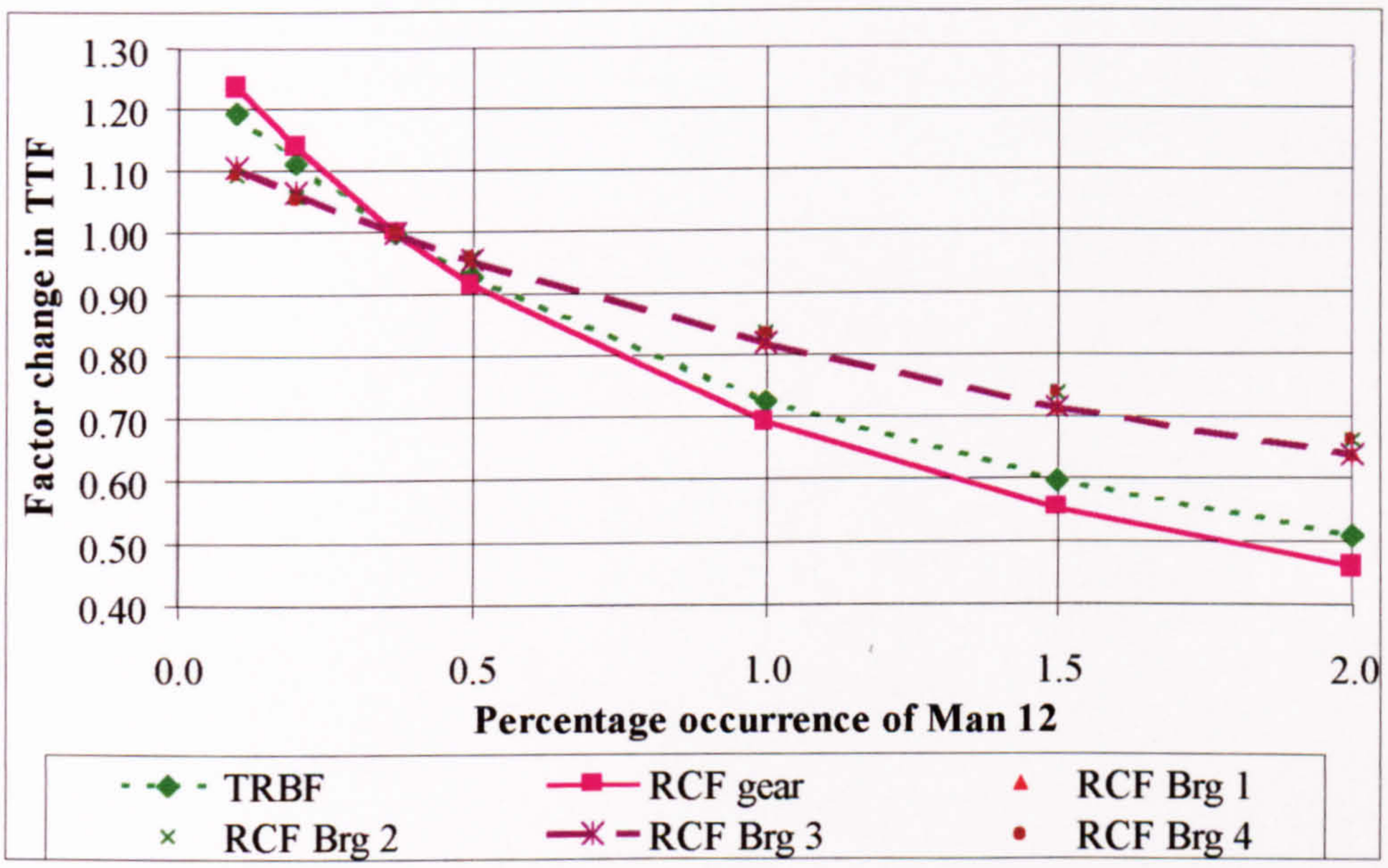

Figure 8.10 : Plot of factor change in TTF/TFS versus percentage occurrence of 60 deg sideways flight

Figure 8.10 differs from Figure 8.9 in showing that manoeuvre 12 contains loads that have a larger proportional effect on gear teeth TFS than on bearing TFS. The TTF for tooth root bending fatigue is also more sensitive to manoeuvre 12 than are the TFS of bearings 1 to 4.

8.4.4 Influence of 90 degrees Sideways Flight Manoeuvre (Ref 13)

The percentage occurrence of manoeuvre 13 was varied from 0.1 to 2% to ascertain the effect on fatigue damage. As shown in Figure 8.11, a reduction in the proportion of this manoeuvre from 0.37% (baseline) to 0.1% results in increases of 5% for the tooth root

bending TTF, 12% for gear tooth TFS, and 8% for the bearing TFS. An increase in the proportion of manoeuvre 13 from 0.43 to 2% gives a reduction in tooth root bending TTF, gear and bearing TFS of 22%, 40% and 30% respectively.

Figure 8.11 shows that manoeuvre 13 contains loads that have a larger proportional effect on gear teeth TFS than on bearing TFS. However, unlike manoeuvre 12, the TTF for tooth root bending fatigue is less sensitive to torques within the manoeuvre than are the TFS of bearings 1 to 4. This is due to the varied make-up of each manoeuvre, which contain different torque levels applied for different proportions of the manoeuvre.

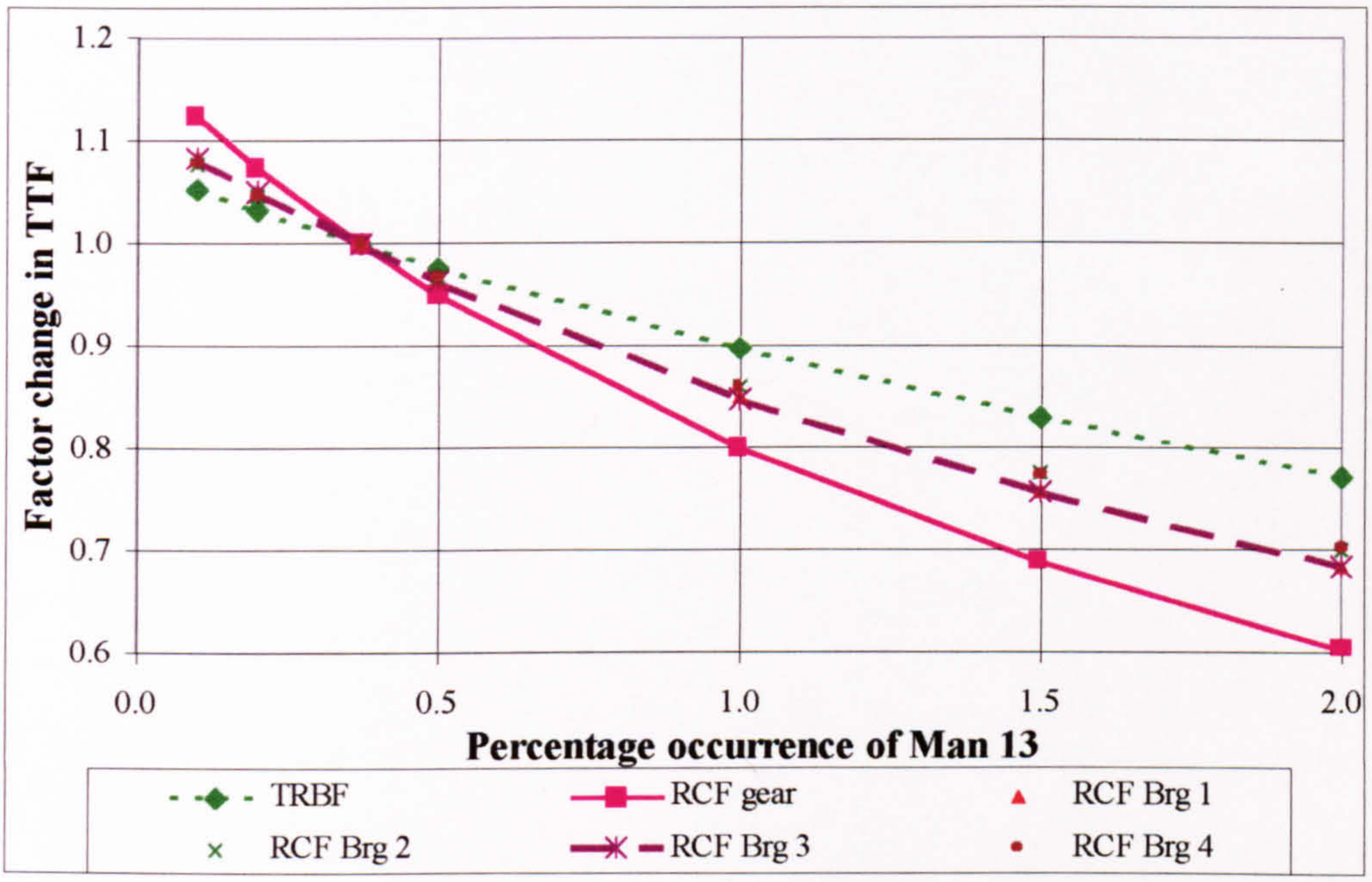

Figure 8.11 : Plot of factor change in TTF/TFS versus percentage occurrence of 90 deg sideways flight

8.4.5 Influence of Spot turn port - hover OGE Manoeuvre (Ref 5)

The percentage occurrence of manoeuvre 5 was varied from 0.1 to 2% to ascertain the effect on fatigue damage (Figure 8.12). A reduction in the proportion of this manoeuvre from 0.25% (baseline) to 0.1% results in increases of 74% for the tooth root bending TTF, 27% for gear tooth TFS and 6% for the bearing TFS. An increase in the proportion of manoeuvre 5 from 0.25 to 2% gives a reduction in tooth root bending TTF, gear and bearing TFS of 83%, 72% and 40% respectively.

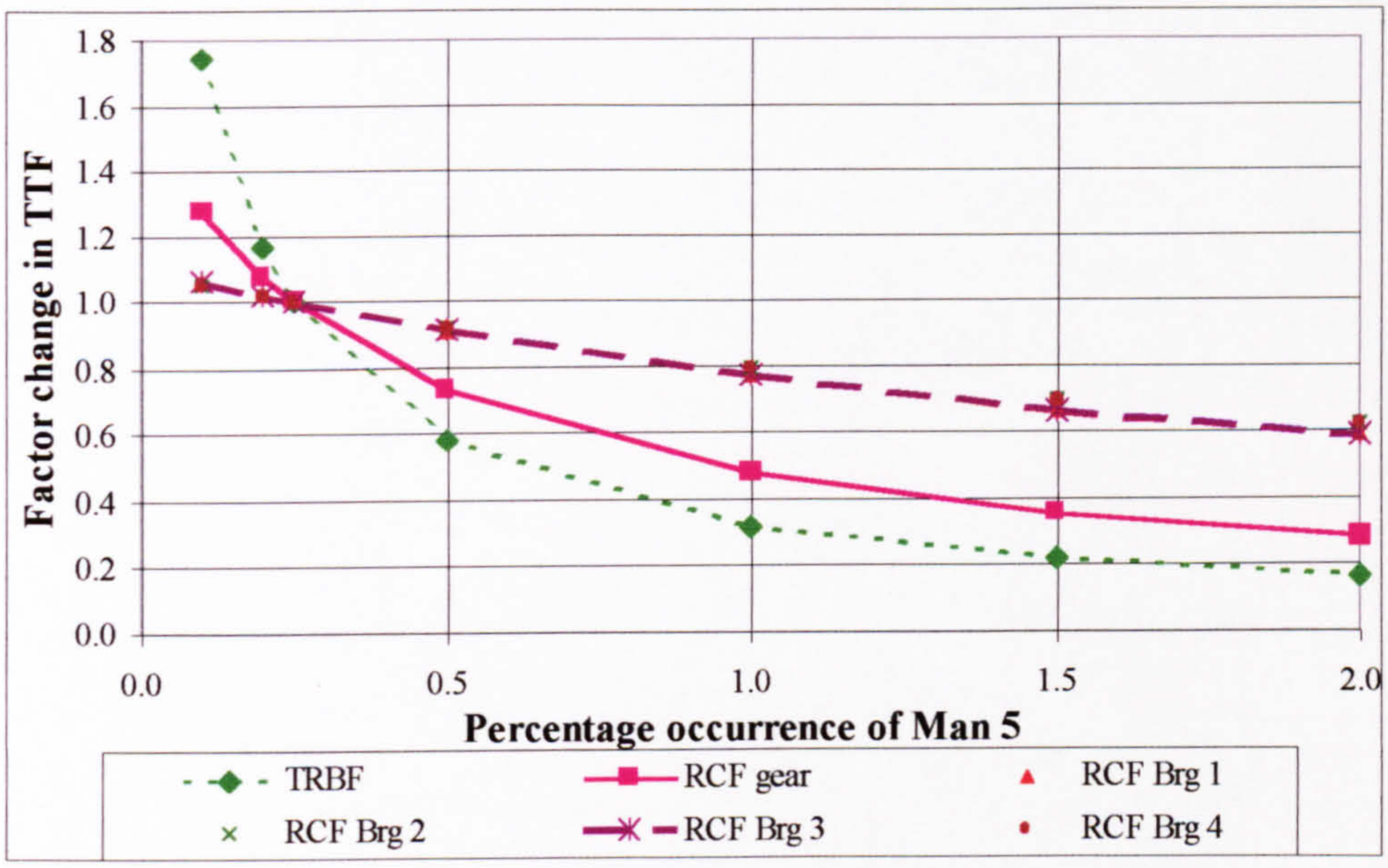

Figure 8.12 : Plot of factor change in TTF/TFS versus percentage occurrence of Spot turn port (hover OGE)

Figure 8.12 shows that manoeuvre 5 contains loads that have the largest proportional effect on the TTF for tooth root bending fatigue. The gear teeth TFS is also more sensitive to manoeuvre 5 than are the TFS of bearings 1 to 4.

8.4.6 Magnitude Occurrence Spectrum

The above differences may be explained by considering the Magnitude Occurrence Spectrum (MOS) for manoeuvres 2, 12, 13 and 5 which is shown in Figure 8.13. Manoeuvre 5 (spot turn port) contains torque values in excess of 1900 Nm for more than 20% of the manoeuvre, which explains the large influence on the time to failure by tooth root bending fatigue. Manoeuvres 12 and 13 contain torque values that are above 2000 Nm, but these make up less than 3% of the total spectrum. The effects are highlighted by calculating the actual damage content of each manoeuvre as a proportion of the flight spectrum as a whole in Table 8.5.

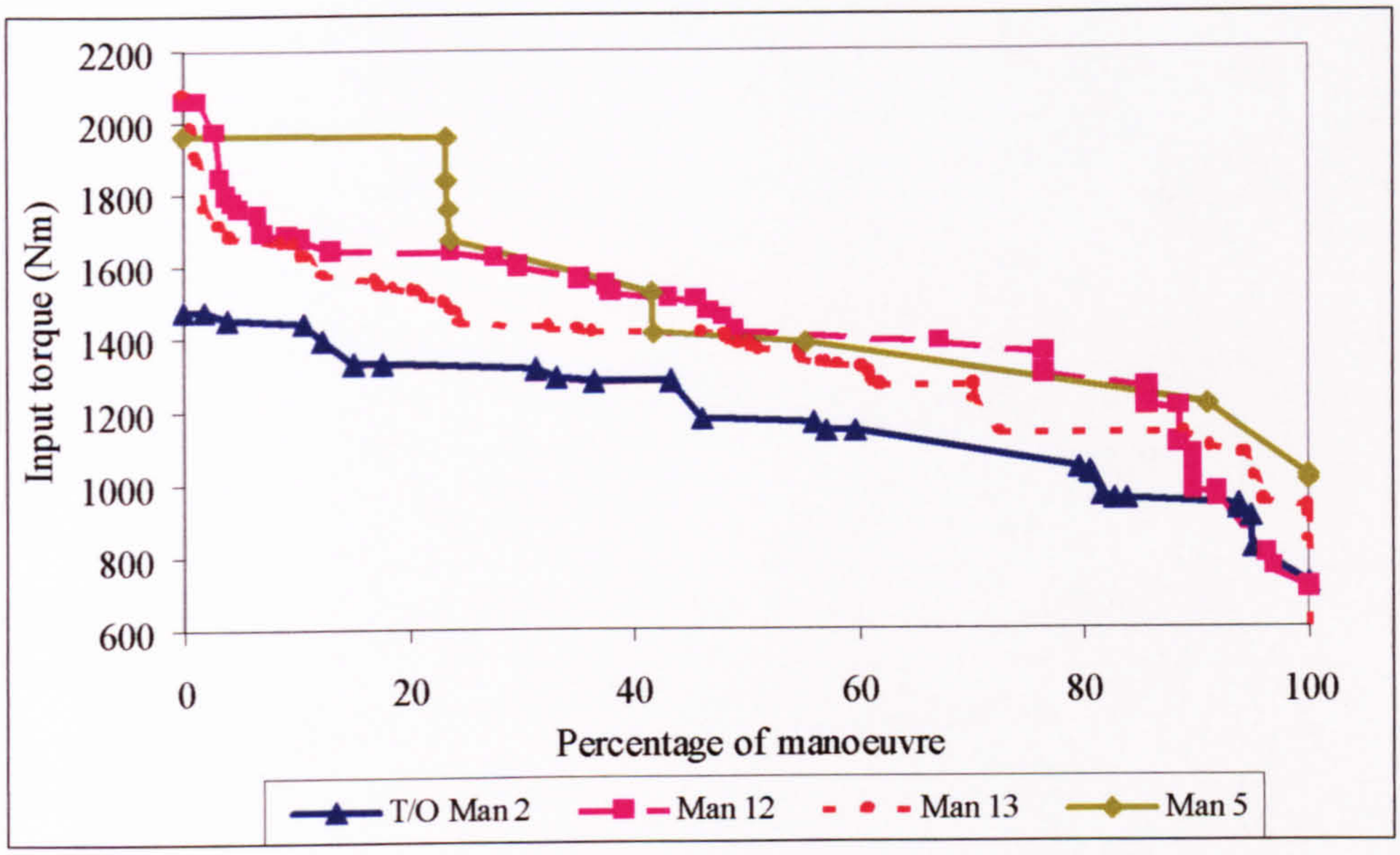

Figure 8.13 : Magnitude Occurrence Spectrum for damaging manoeuvres 2, 12, 13, 5

Table 8.5 shows the results from analysis of the individual manoeuvre at p* of 10^{-6}, see Appendix E.3.5. Manoeuvre 5 contributes 71% of the total tooth root bending damage for the spectrum. This explains why it has such a large influence on the TTF. Manoeuvres 12 and 13 are responsible for 22.2% and 6.8% of the total tooth root bending damage respectively. Figure 8.13 shows that Manoeuvre 5 has a large section (>20%) at a torque of 1880 Nm; this is the reason for its effect on the TTF.

		Damage per manoeuvre as percentage of total damage due to flight spectrum (%)			
Ref no	Manoeuvre	**TRBF**		**Gear RCF**	**Bearing RCF**
		10^{-6}	10^{-3}		
2	Take off	0	0	4.2	7.5
12	60deg sideways flight	22.2	38.7	26.5	13
13	90deg sideways flight	6.8	9.3	14.9	10.6
5	Spot turn port	71	52	35.9	10
	TOTAL	**100**	**100**	**81.5**	**41.1**

Table 8.5 : Contribution to fatigue damage by manoeuvres from Type B Civil Spectrum

At a p* 10^{-3}, manoeuvre 5 contributes 52% of the total tooth root bending damage for the spectrum. This is a smaller proportion than at 10^{-6}, because the position of the S-N curve at this probability means that a greater number of other manoeuvres also cause damage. Hence the proportion of damage contributed of manoeuvre 5 reduces. Manoeuvres 12 and 13 contribute 38.7% and 9.3% of the total tooth root bending damage, respectively at p* of 10^{-3}.

The dominance of manoeuvres 5, 12 and 13 for tooth root bending fatigue is due to the fact that these are the only manoeuvres with torque above the endurance limit at p* values considered. In the case of gear tooth RCF and bearing contact fatigue, all loads cause a finite amount of damage, as shown in Figure 8.14. Manoeuvre 12 is more influential on predicted bearing life than Manoeuvre 5 due to the power law used in the Lundberg-Palmgren model for bearing life.

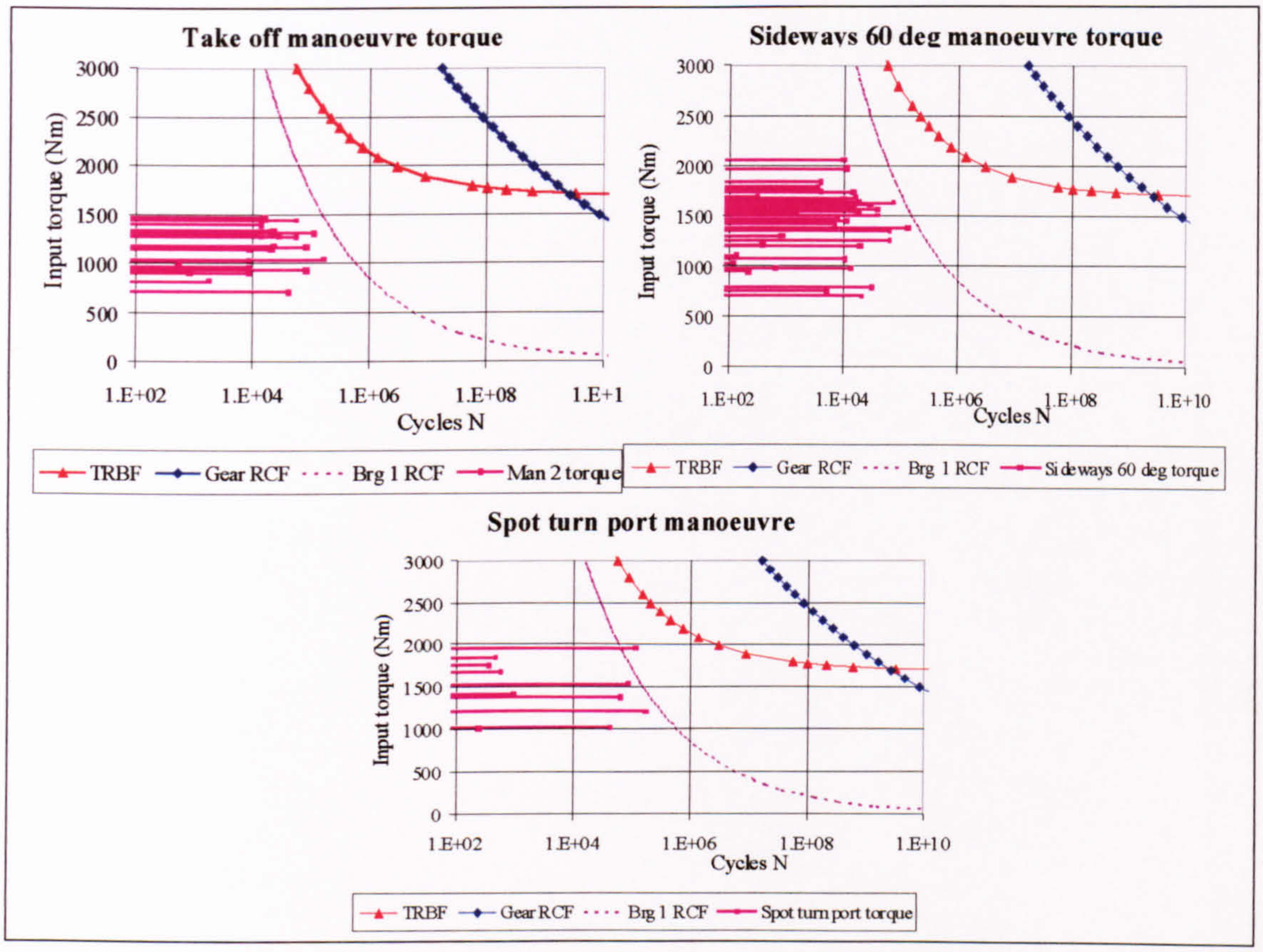

Figure 8.14 : S-N curves and torque spectra for take-off, sideways flight 60 degrees and spot turn port ($p^* = 10^{-6}$)

8.5 Over-torque Influence on Fatigue Models

8.5.1 Influence of Over-torque on Tooth Root Bending Fatigue

Figure 8.15 shows a plot of failure probability against predicted time to failure due to tooth root bending fatigue for the Type B gearbox. In addition to the baseline, three other curves are shown, each of which represents the predicted times to failure for different proportions of over-torque of size 2600 Nm within the civil spectrum. The value of 2600 Nm was chosen after examination of the Civil spectrum, within which the largest value is 2080 Nm. The baseline curve represents the torque spectrum with no over-torques, which is the same as the curve in Figure 8.3.

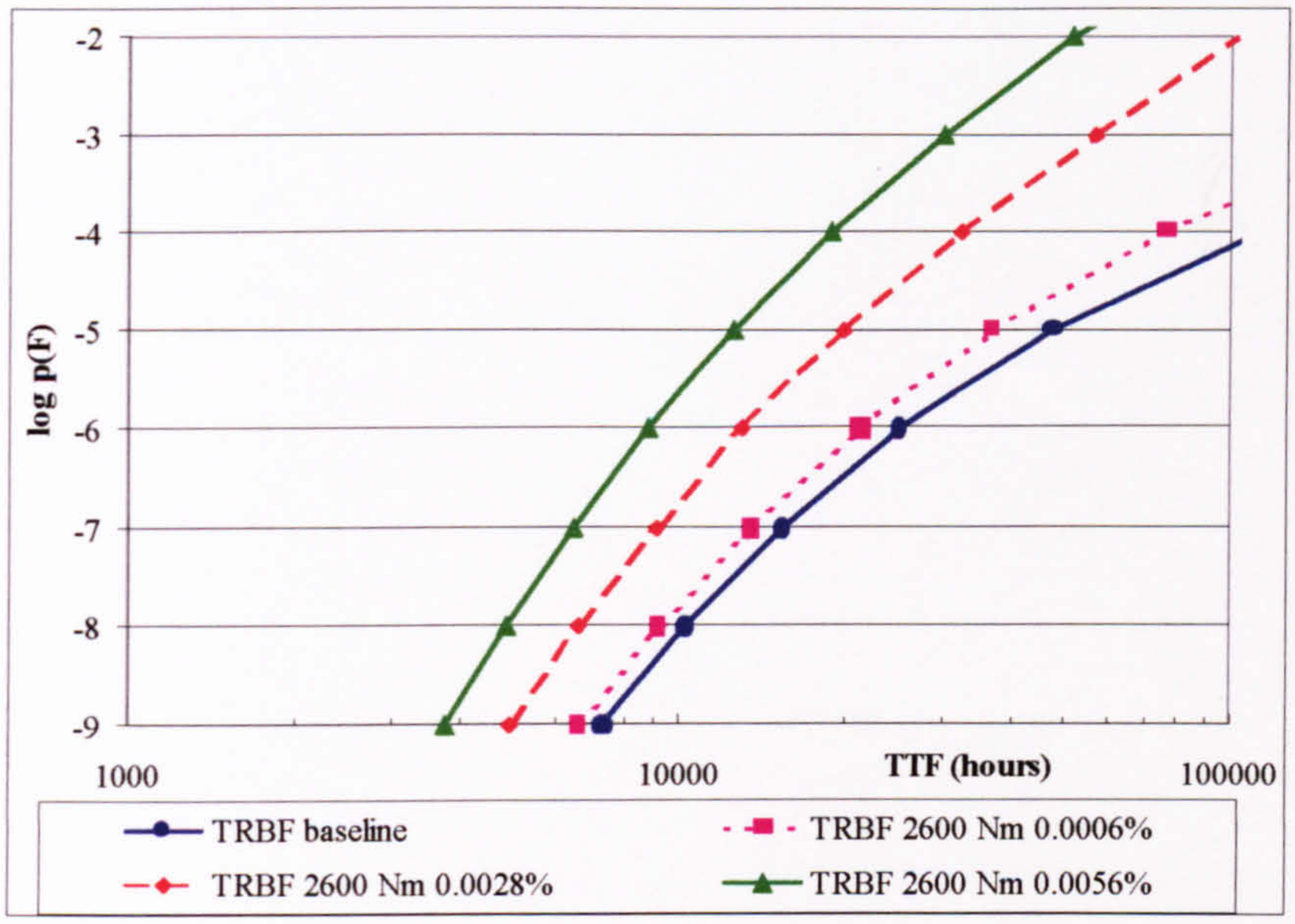

Figure 8.15 : Probability of failure by tooth root bending fatigue for different occurrence of over-torque

The curves show that there is a significant reduction in time to failure as the proportion of over-torques increases. At p* 10^{-6}, the TTF reduces from 25250 hours (baseline) to 21 300 hours (a reduction of 16%) for a 2600 Nm over-torque percent occurrence of 0.0006%. The latter percentage represents one over-torque of two-second duration every 100 hours. If this is increased to one over-torque of two seconds per 10 hours (0.0056%), the TTF at p* of 10^{-6} reduces to 8800 (a factor of 2.9 from the baseline value).

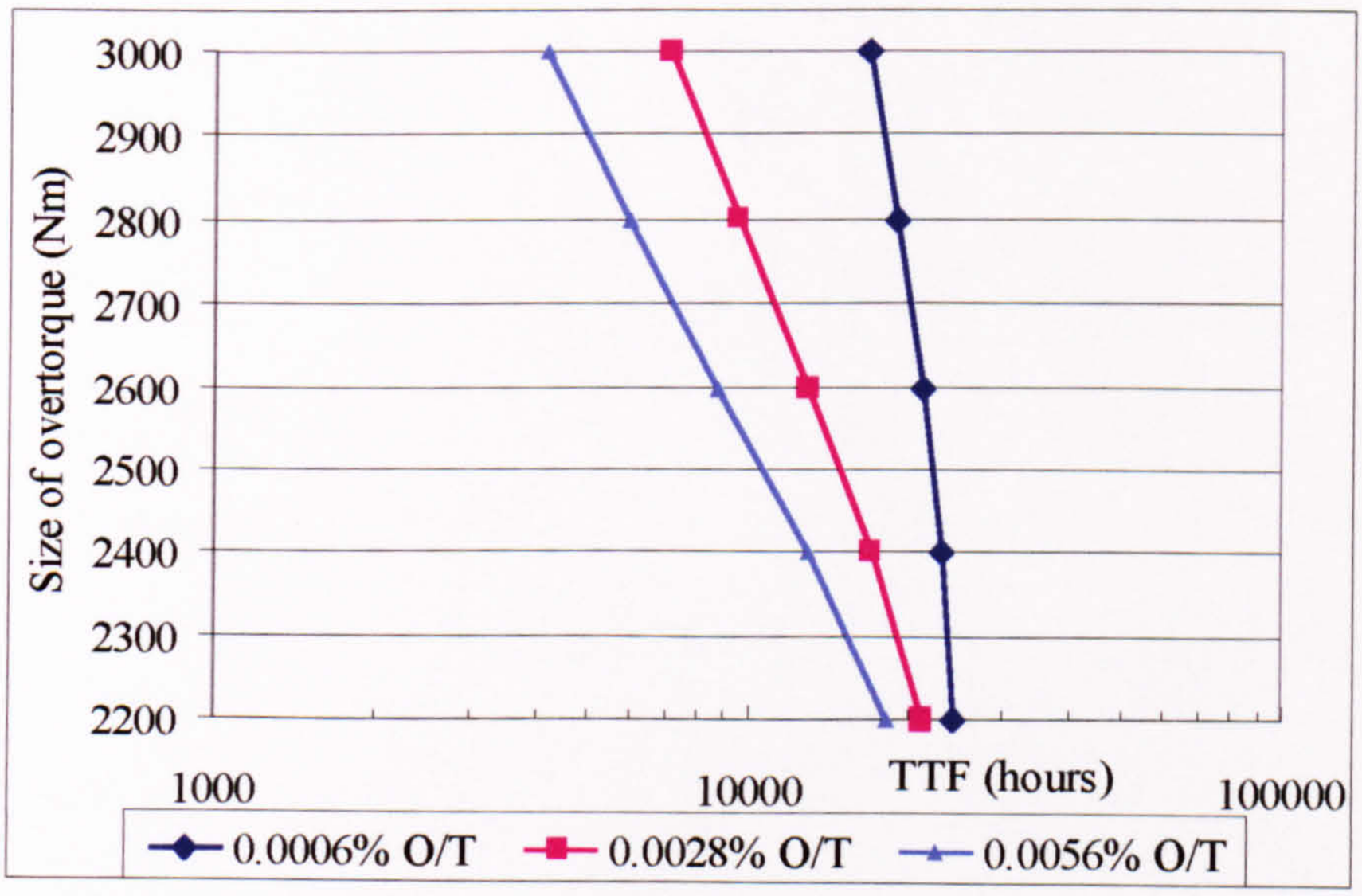

Figure 8.16 : Variation in TTF by tooth root bending fatigue for different size and percentage occurrence of over-torque at p* = 10^{-6}

Figure 8.16 shows how the predicted TTF varies in relation to the size and number of over-torques, for a p* of 10^{-6}. The graph shows that with an over-torque proportion of 0.0006%, the TTF reduces from 25330 to 16800 hours (factor of 1.5) as the size of the over-torque increases from 2200 to 3000 Nm. As the proportion of over-torques increases, so the reduction factor for TTF increases. The corresponding reduction values are 3 (0.0028% over-torque), and 4.4 (0.0056% over-torque)

8.5.2 Influence of Over-torque on Gear Tooth RCF

The same experiments with over-torque size were also conducted for gear RCF. Figure 8.17 shows how the predicted TFS varies in relation to the size and number of over-torques, for a p* of 10^{-6}. The graph shows that with an over-torque proportion of 0.0006%, the TFS reduces from 1200 to 1056 hours (factor of 1.14) as the size of the over-torque increases from 2200 to 3000 Nm. As in Section 8.5.1, the reduction factor for TFS increases as the proportion of over-torques increases. The corresponding reduction values are 1.66 (0.0028% over-torque), and 2.26 (0.0056% over-torque).

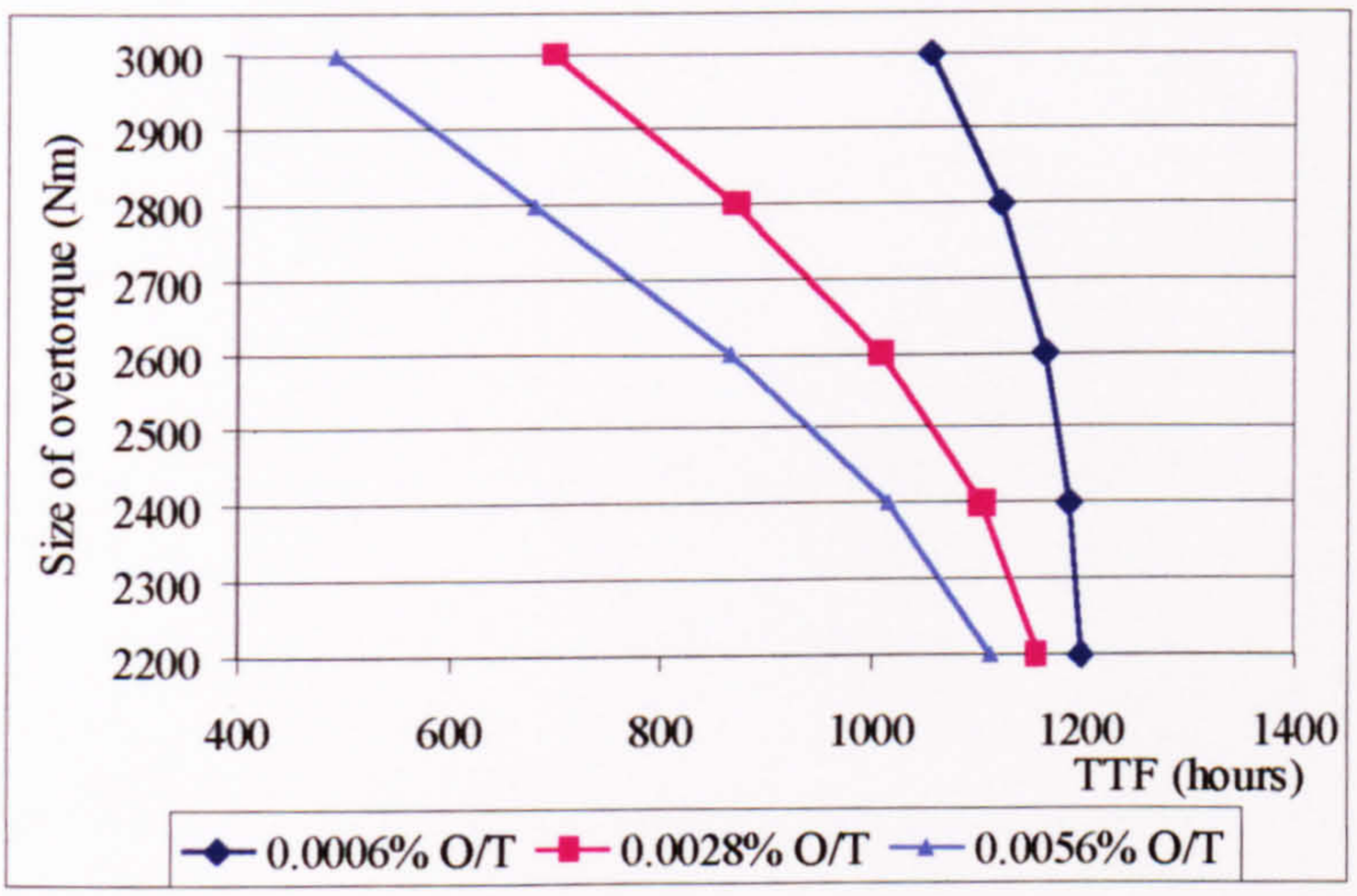

Figure 8.17 : Variation in TFS by gear tooth RCF for different size and percentage occurrence of over-torque at p* = 10^{-6}

8.5.3 Influence of Over-torque on Bearing Contact Fatigue

Figure 8.18 shows how the predicted TFS for Bearing 1 (Type B gearbox) varies in relation to the size and number of over-torques, for a failure probability of 10^{-3}. The graph shows that with an over-torque proportion of 0.0006%, the TFS reduces only slightly from 3057 to 3053 hours as the size of the over-torque increases from 2200 to 3000 Nm. As the proportion of over-torque increases, so the reduction factor for TFS increases; the factors concerned are small however showing that bearing life is unaffected by the size and occurrence of over-torques in this study. For an over-torque proportion of 0.0028%, TFS reduces from 3048 to 3027 hours as the over-torque increases from 2200 to 3000 Nm; at 0.0056%, TFS reduces from 3037 to 2997 hours.

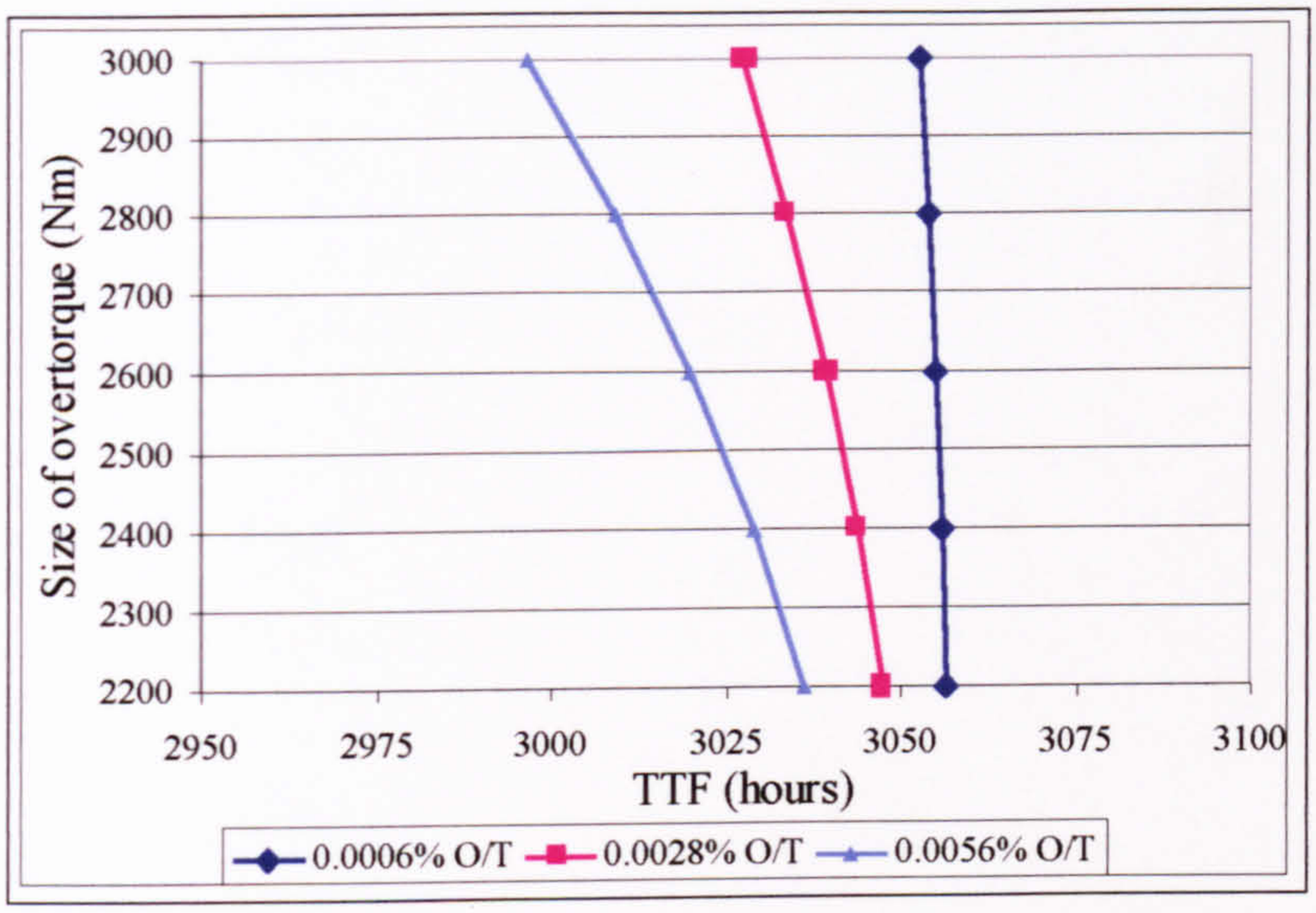

Figure 8.18 : Variation in TFS by bearing 1 for different size and percentage occurrence of over-torque $p^* = 10^{-3}$

8.5.4 Over-torque summary

The size and occurrence rate of over-torques have a significant effect on the predicted fatigue lives for tooth root bending and gear tooth RCF. In comparison, only small changes in bearing life were observed.

Manoeuvre 5 spot turn port Occurrence (%)	**Over-torque 2600 Nm** Occurrence (%)	Damage due to manoeuvre due to flight spectrum		
		TRBF (% of total damage)	**Gear RCF (% of total damage)**	**Bearing RCF (% of total damage)**
	0.0006	16.79	3.68	0.13
	0.0028	48.50	16.04	0.65
	0.0056	65.32	27.65	1.29
0.25		71	35.93	9.95

Table 8.6 : Damage contributed by over-torques compared to Spot turn port at p* of 10^{-6}

The variation in the size and occurrence rate of over-torques has a greater proportional effect on TRBF than on gear and bearing RCF. This is because for TRBF, many loads contained in the spectrum will fall beneath the endurance limit (T_{inf}). This is in contrast to RCF, where all loads contribute a finite amount of damage (Chapter 4), since no endurance limit exists. Hence an over-torque will form a larger proportion of the total damaging loads for TRBF, than it would for RCF.

Table 8.6 shows the comparative contribution of over-torque damage to the total damage content of the spectrum, together with the results for manoeuvre 5, copied from Table 8.5. The effect of the over-torque frequency on tooth root bending fatigue can be seen clearly; a frequency of 0.0056% (one over-torque of two second duration every 10

hours) contributes 65% of the total damage, close to the 71% proportion of damage contributed by spot turn port. The proportional effect of over-torques is far less marked for gear tooth RCF and bearing contact fatigue.

8.6 Loading vs Material variability

Sensitivity studies were conducted to investigate the effects of altering the percentage occurrence of the two most damaging manoeuvres for tooth root bending fatigue within the Type B Civil spectrum, compared to altering the material COV. Results are presented for Manoeuvre 12 (60-degree sideways flight) and Manoeuvre 5 (spot turn port).

8.6.1 Variation in material COV – Type B Civil spectrum

Table 8.7 presents the results of varying the material COV, whilst maintaining the proportion of Man 12 and Man 5 at the baseline values (0.43% and 0.25% respectively). This is shown at p* of 10^{-6} and 10^{-4} since the TTF values are within realistic limits (10^3 to 10^5 hours) at these probability values. If the proportion of manoeuvre 12 is held constant at 0.43% and the COV increased from 6 to 8%, the predicted TTF increases by factors of 4.5 and 5.5 at the respective p* values. If the COV is increased from 8 to 10%, the predicted TTF increases by factors of 3.4 and 3.3 at the respective p* values.

Failure probability p*	Material COV	Predicted TTF (hours)	Decrease in TTF (factor)
1e-06	6%	25260	
	8%	5670	4.5
	10%	1690	3.4
1e-04	6%	114060	
	8%	21000	5.5
	10%	6400	3.3

Table 8.7 : Predicted TTF by Tooth root bending fatigue with Civil spectrum (Manoeuvre 12 = 0.43%, Manoeuvre 5 = 0.25%)

8.6.2 Manoeuvre 12 – Material COV values 6-10%

Tests were conducted using the model for COV values in the range 6-10%, with the proportion of manoeuvre 12 varied from 0.1 to 2%; this range includes the value of 0.43%, which is used in the Civil spectrum. The results are presented in Figure 8.19 and Table 8.8.

Table 8.8 presents the results of varying the proportion of Man 12 at constant COV at p* = 10^{-6} and 10^{-4}. For a COV of 6%, increasing the percentage of manoeuvre 12 from 0.43% to 2% causes the predicted TTF to reduce by a factor of 1.97 at p* = 10^{-6} and a factor of 2.2 at p* = 10^{-4}. If the material scatter is greater, in this case a COV of 8%, the same increase in Manoeuvre 12 causes the predicted TTF to decrease by a factor of 2 at p* of 10^{-6} and by a factor of 1.96 at p* of 10^{-4}.

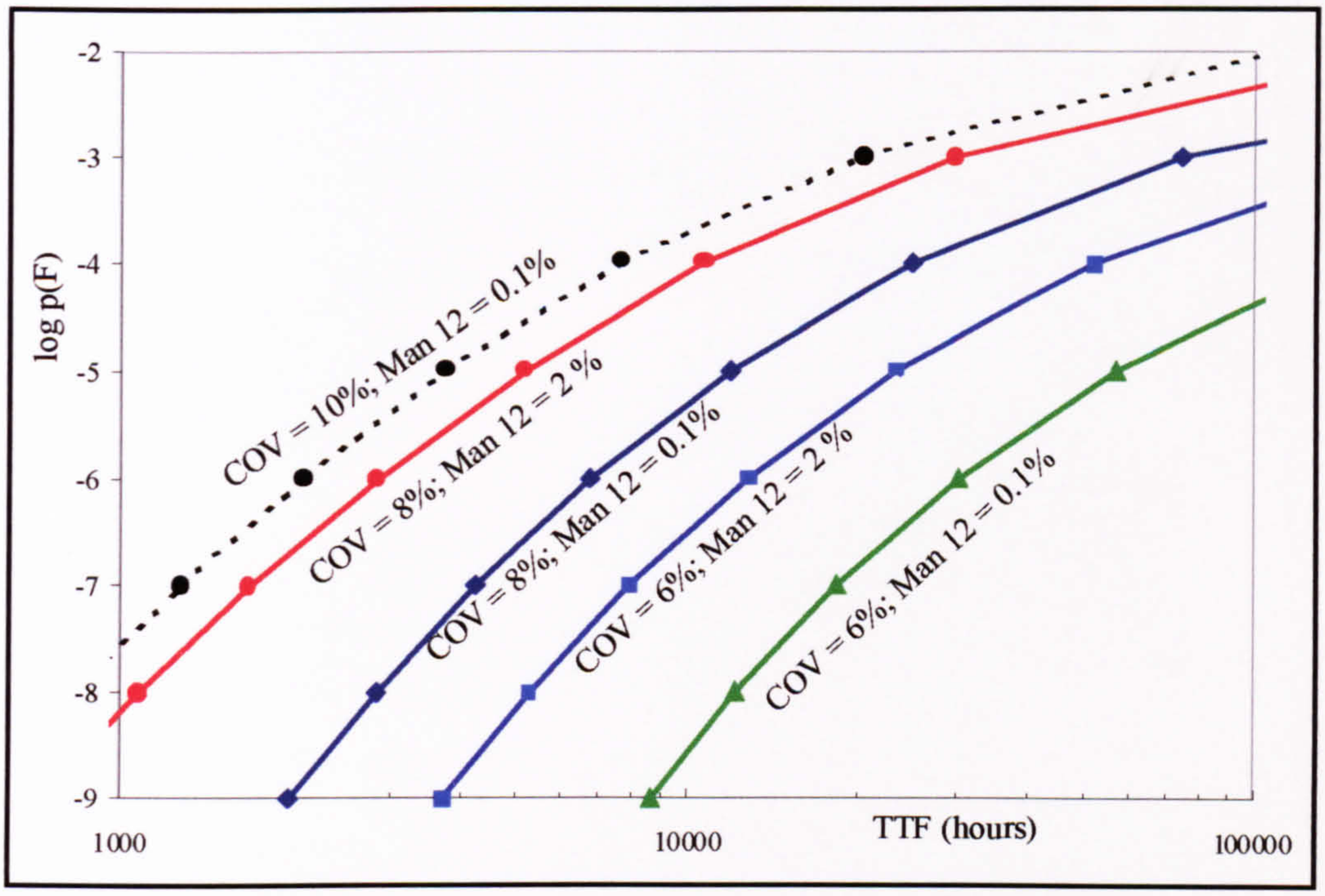

Figure 8.19 : Comparison of Type B TRBF results to show influence of Manoeuvre 12 and Material COV from 6 – 10%

Figure 8.19 shows the variation in predicted TTF as both the material COV and proportion of manoeuvre 12 are varied. It is clear that an increase in manoeuvre 12 from 0.1 to 2% has less effect than if the COV were increased by 2%. This is also seen by comparing Table 8.7 with Table 8.8. These results should be compared with those in Section 8.6.3, which are the equivalent for manoeuvre 5.

Failure probability p*	Material COV	Manoeuvre 12 proportion	Predicted TTF (hours)	Decrease in TTF (factor)
1e-06	6%	0.43%	25260	
	6%	2%	12820	1.97
	8%	0.43%	5670	
	8%	2%	2850	2
1e-04	6%	0.43%	114060	
	6%	2%	52000	2.2
	8%	0.43%	21000	
	8%	2%	10684	1.96

Table 8.8 : Predicted TTF by Tooth root bending fatigue with variation in Material COV and Civil spectrum (Manoeuvre 12)

It may therefore be summarised that in the suggested achievable range of 6 to 10% for tooth root bending fatigue **[Cansdale and Tigwell, 1987]**, the COV has a greater effect on the predicted TTF than does a variation of manoeuvre 12. This is based on a 2%

reduction in COV compared with a reduction in Manoeuvre 12 from 2% to 0.1%. The proportional change in TTF for a change in COV from 6 to 8% is greater than that from 8 to 10%.

It is also noted that the reduction factor varies depending on the desired value of p* and value of COV; at 10^{-6}, the factor is 4.5, whilst at 10^{-4} it is 5.5 for a change in COV from 6 to 8%, with a fixed load spectrum. However, as COV increases from 8 to 10%, the factor is 3.4 at 10^{-6} and 3.3 at 10^{-4}.

8.6.3 Manoeuvre 5 – Material COV values 6-10%

Manoeuvre 5 contributes 71% of TRBF damage (see Table 8.5), more than that due to Manoeuvre 12 for Type B gearbox. Tests were conducted using the gear TRBF model for COV values from 6-10%, with the proportion of manoeuvre 5 varied from 0.25% (Civil spectrum) to 2%; this produced the results in Figure 8.20 and Table 8.9.

For a COV of 6%, increasing the percentage of manoeuvre 5 from 0.25% to 2% causes the predicted TTF to reduce by a factor of 6 at $p^* = 10^{-6}$ and by a factor of 5.6 at $p^* = 10^{-4}$. For a COV of 8%, increasing the percentage from 0.25% to 2% causes the predicted TTF to reduce by a factor of 5.8 and 6 at corresponding values of p*.

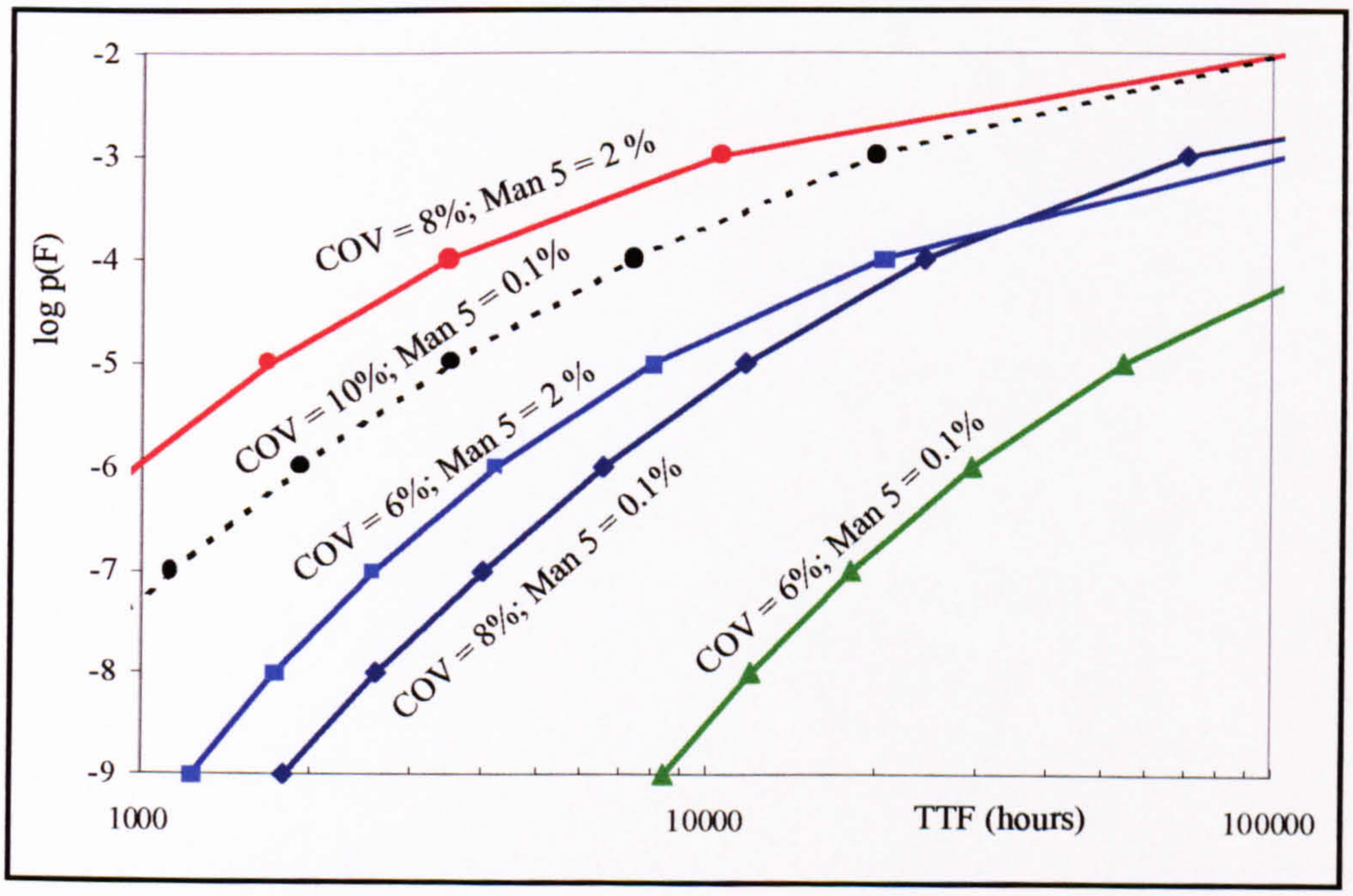

Figure 8.20 : Comparison of Type B TRBF results to show influence of Manoeuvre 5 and Material COV from 6 – 10%

It may therefore be summarised that in the achievable range of 6 to 10% for tooth root bending fatigue, a 2% change in COV has less effect on the predicted TTF than does a variation of manoeuvre 5 from 0.25 to 2%. The proportional change in TTF given by a change in COV from 6 to 8% is greater than that from 8 to 10%. However, across the

range of COV values, the effect of manoeuvre 5 is proportionately larger, with a reduction in TTF of approximately 6.

Failure probability p*	Material COV	Manoeuvre 5 proportion	Predicted TTF (hours)	Decrease in TTF (factor)
1e-06	6%	0.25%	25260	6
	6%	2%	4230	
	8%	0.25%	5670	5.8
	8%	2%	980	
1e-04	6%	0.25%	114060	5.6
	6%	2%	20454	
	8%	0.25%	21000	6
	8%	2%	3490	

Table 8.9 : Predicted TTF by Tooth root bending fatigue with variation in Material COV and Civil spectrum (Manoeuvre 5)

It is also noted that the factor varies depending on the desired value of p* and value of COV; at 10^{-6}, the factor is 6, whilst at 10^{-4} it is 5.6 for a change in manoeuvre 5 from 0.25 to 2%, with COV fixed at 6%. However, with COV fixed at 8%, the factor is 5.8 at 10^{-6} and 6 at 10^{-4}.

These differences are due to the different S-N curve chosen according to the value of p* required. The spread of S-N curves about the mean (Figure 4.3) is determined by the COV – the larger the COV, the further apart are the S-N curves at the discrete p* values.

8.7 Shaft spline wear - Influence of Slip amplitude and Wear coefficient

The spline wear model has been used to determine the significance of slip amplitude, wear coefficient and loading, using data from Chapter 6 and Appendix E. The parameters changed for the initial sensitivity studies were the mean and COV of the slip amplitude and wear coefficient. The wear coefficient K is a function of the material and lubrication of the coupling, a parameter about which little data exists for this specific case. A wide range of values for K from 1E-08 to 1E-04 was therefore studied.

Confidence limits of the wear coefficient K were used to define the confidence limits for the predicted TTF results. The slip amplitude is assumed to follow a log-normal distribution, the COV for which is used to generate the curve of p(F) against TTF. Figure 8.21 and Figure 8.22 show the mean curves for the time to failure by spline wear for a range of slip amplitude values. The log-normal distribution has been used because it is considered to be an appropriate representation for a variable (Slip amplitude) which is non-zero and whose distribution is skewed towards low values, i.e. an asymmetric distribution is expected.

8.7.1 Type A Gearbox – ASW loading

Figure 8.21 shows a plot of failure probability against the mean predicted TTF for the Type A gearbox. There are three curves drawn, each representing a different combination of mean slip amplitude and COV, using the ASW loading. The wear coefficient for all tests was 1E-06. If the mean slip amplitude were 100 microns, with COV 10%, the mean predicted TTF is 645 hours for a p* of 10^{-3}.

Reducing the mean slip amplitude has the effect of increasing the times to failure, with a predicted life of 1290 hours at p* of 10^{-3} for mean slip amplitude of 50 microns (COV 10%). If the mean slip amplitude is fixed and its COV increased, the effect is to shift the failure curve to the left and to decrease the gradient. This is due to the increasing uncertainty in the value of the slip amplitude. At 100 micron, an increase in COV from 10% to 20% causes the predicted TTF at p* of 10^{-3} to decrease from 645 to 475 hours, a factor of 1.35.

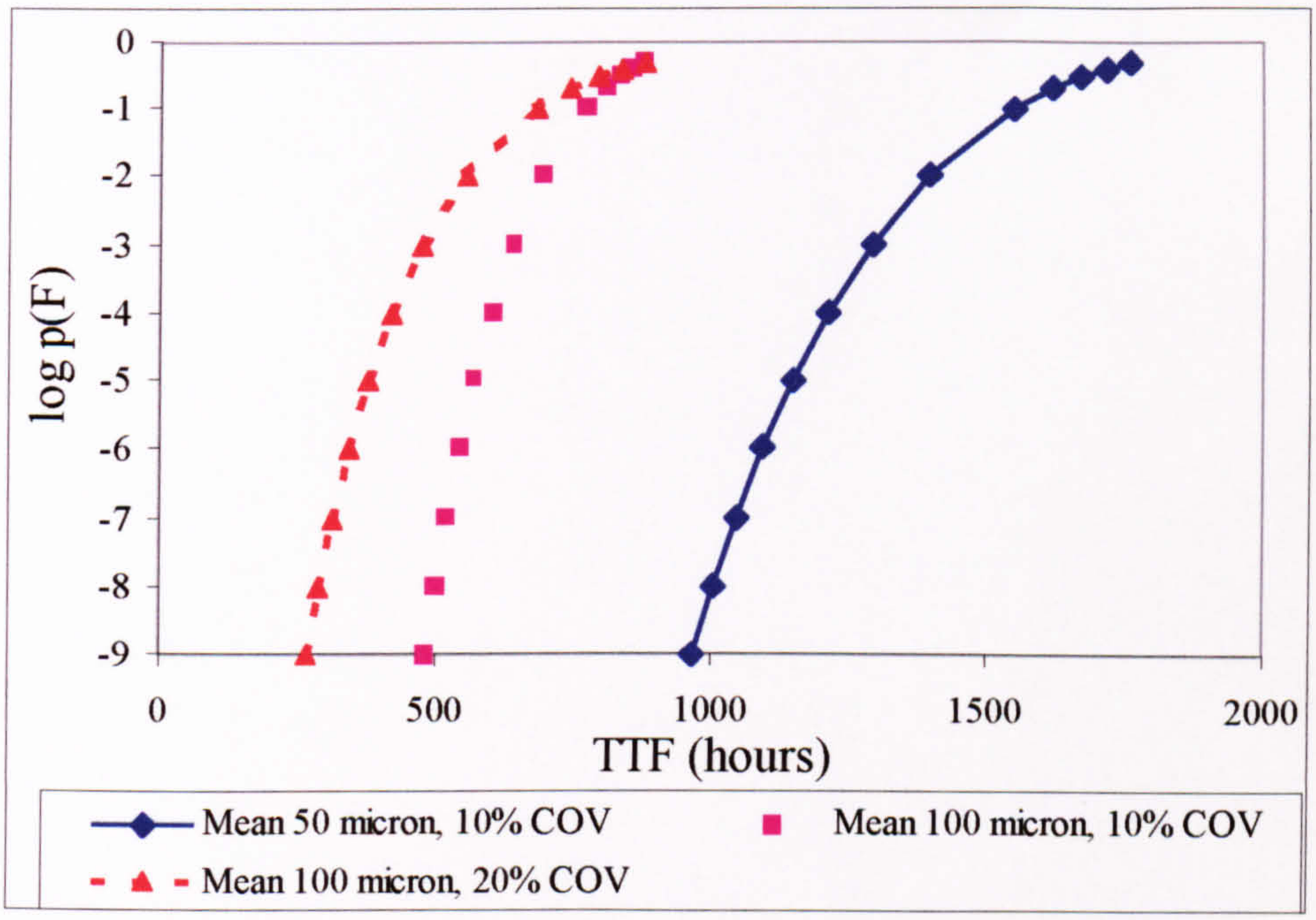

Figure 8.21 : Probability of failure vs. time to failure for different mean slip amplitudes, wear coefficient 1E-06, ASW loading (Type A)

8.7.2 Type B gearbox – Civil Spectrum

Figure 8.22 shows a plot of failure probability against the mean predicted TTF due to shaft spline wear for the Type B gearbox. There are three curves drawn, each representing a different combination of mean slip amplitude and COV, using the civil torque spectrum. The wear coefficient for all tests was 1E-06. If the mean slip amplitude were 100 microns, with COV 10%, the mean predicted TTF is 2150 hours for a p* of 10^{-3}.

Reducing the mean slip amplitude has the effect of increasing the times to failure, with a predicted life of 4300 hours at p* of 10^{-3} for mean slip amplitude of 50 microns (COV 10%). Fixing the mean slip amplitude whilst the COV increased has the same effect on the failure curve as for Type A.

At 100 microns, an increase in COV from 10% to 20% causes the predicted TTF at p* of 10^{-3} to decrease by a factor of 1.35 (2150 to 1590 hours), as for Type A, section 8.7.1. The reduction factor is the same due to the linear damage accumulation model used for spline wear.

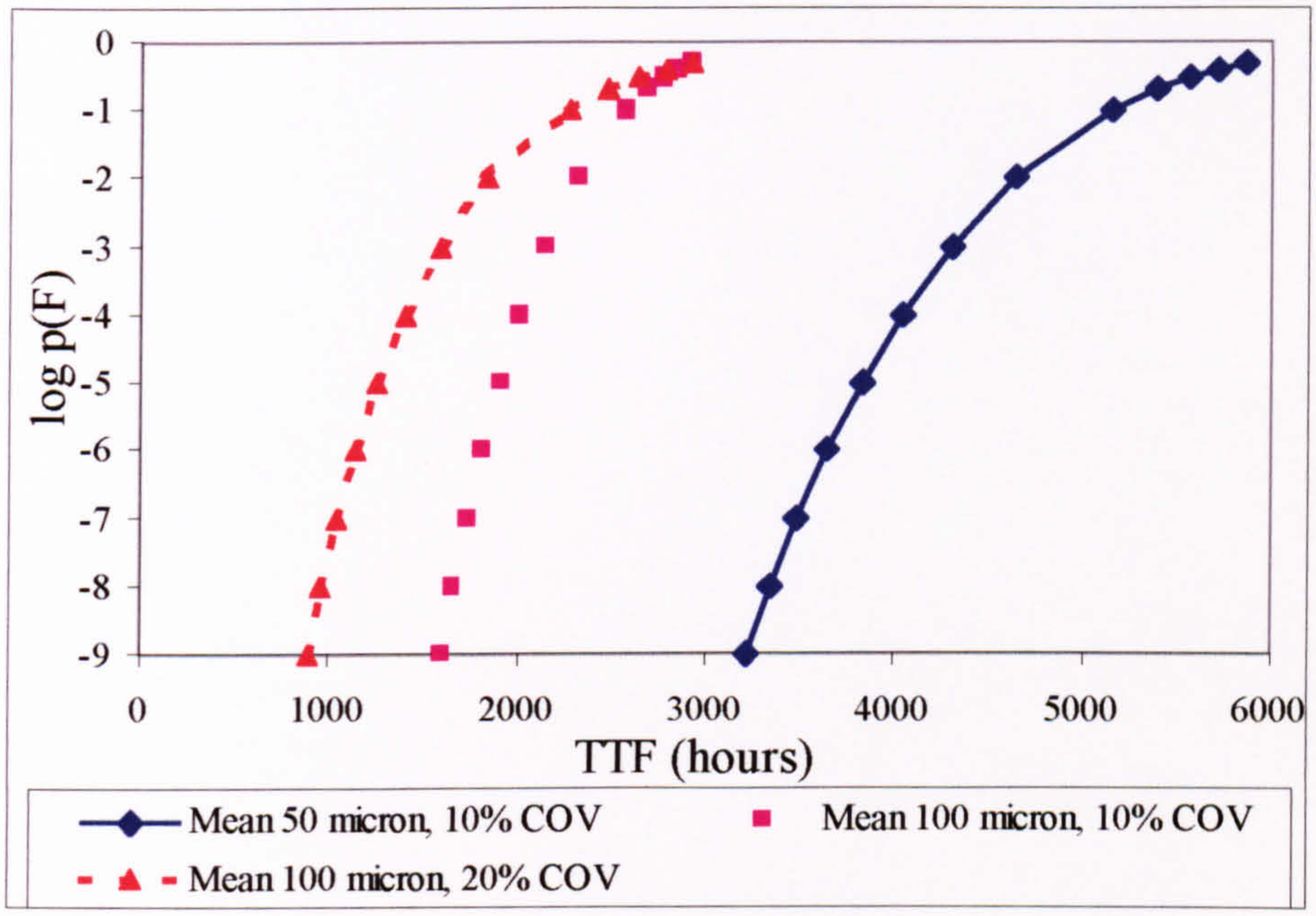

Figure 8.22 : Probability of failure vs. time to failure for different mean slip amplitudes, wear coefficient 1E-06, Civil load spectrum (Type B)

8.7.3 Variation of mean wear coefficient

Figure 8.23 shows a plot of failure probability against the mean predicted TTF due to shaft spline wear for the Type B gearbox using the Civil spectrum. There are two sets of three curves drawn, which represent the mean, with upper and lower bounds (+/- 2 sigma) for the predicted TTF. The curves are shown for two values of mean wear coefficient, each with COV 30%, for mean slip amplitude of 50 microns (COV 30%).

The confidence limits of the wear coefficient K have been used to define the confidence limits for the predicted TTF results. The distance between the upper and lower confidence limits is dependent on the knowledge of K, which is a COV of 30% in this case. For a mean K of 1E-06, the lower, mean and upper values for TTF are 1430, 2290 and 5720 hours respectively at p* of 10^{-3}. For a value of K (mean) of 1E-04, the corresponding values are directly related by a factor of 100, since the damage accumulation model is linear; 14, 23 and 57 hours.

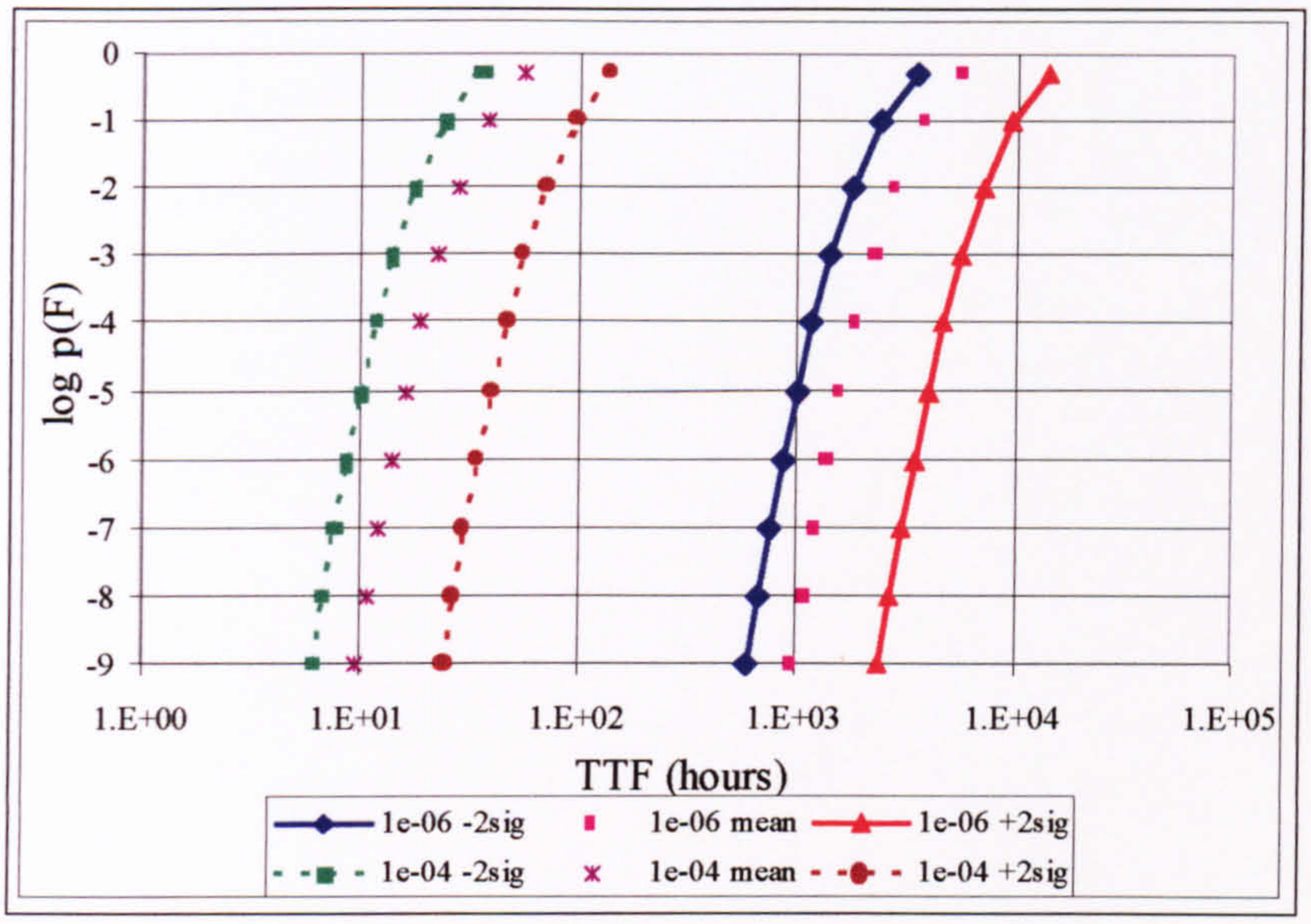

Figure 8.23 : Probability of failure vs. time to failure for different mean wear coefficient K, Type B gearbox, Civil spectrum

The same linear dependence on K can be seen in Figure 8.24, which shows the variation in predicted TTF at different values of wear coefficient from 1E-08 to 1E-05 for failure probability of 10^{-6}. The tests were run with fixed mean slip amplitude of 50 microns, with COV 30%, using the Type B data and Civil spectrum. As the value of K was increased from 1E-08 to 1E-05, the mean TTF reduced from 140300 to 140 hours, as expected a factor of 1000.

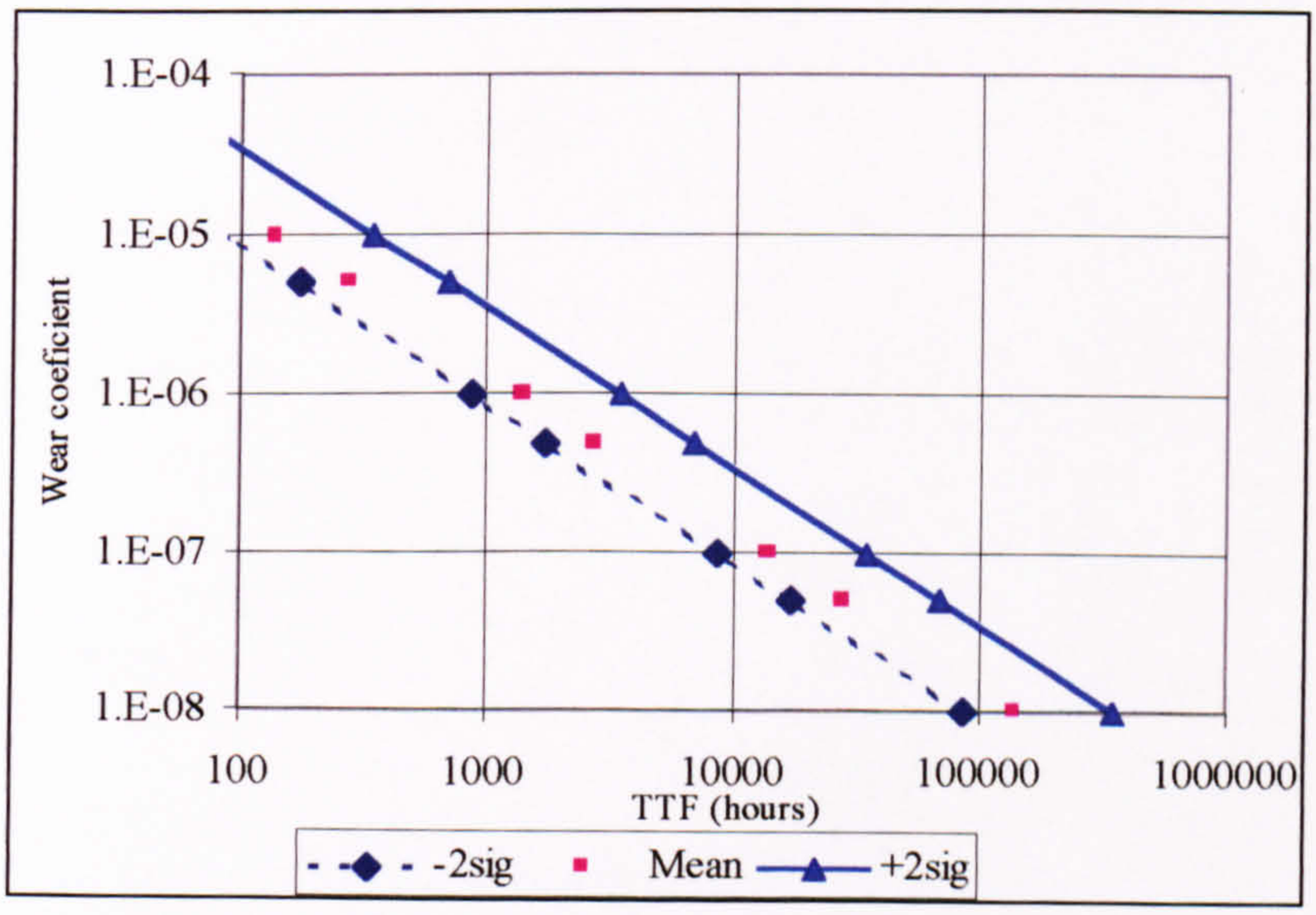

Figure 8.24 : Variation of mean wear coefficient (COV 30%), slip amplitude mean 50μm (COV 30%), Type B gearbox, Civil spectrum

8.7.4 Variation of scatter of wear coefficient

Figure 8.25 shows a plot of the variation of predicted TTF (at p* of 10^{-6}) with the variation in the scatter of wear coefficient, with a fixed mean K of 1E-06. The graph shows the lower, mean and upper values of the TTF, with zero spread for COV of 0 and the widest spread for COV of 30%. In the latter case, the predicted TTF values are 880 hours (lower bound), 1400 hours (mean) and 3500 hours (upper bound). This shows the large influence of the wear coefficient and its variability on the bounds of the TTF.

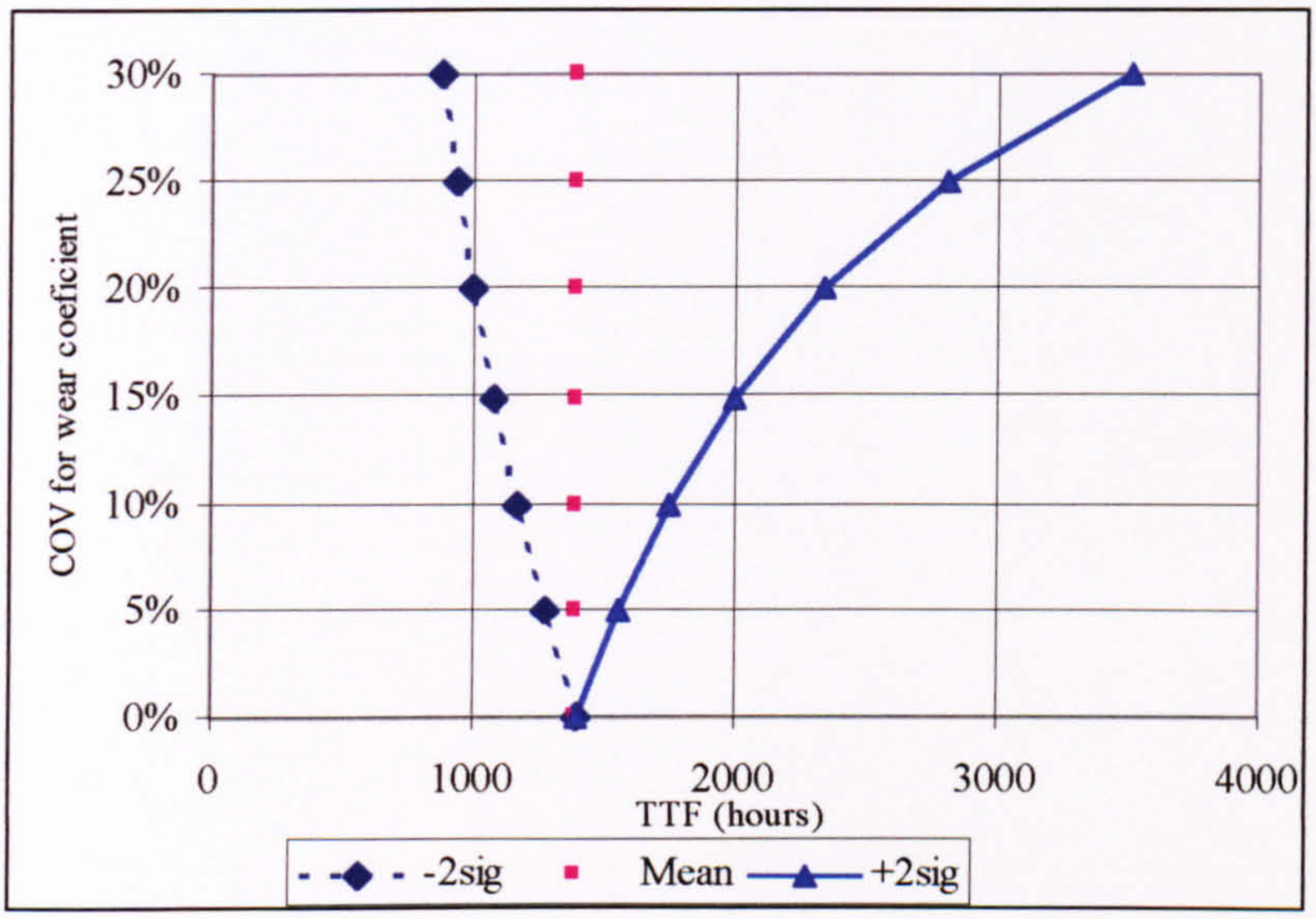

Figure 8.25 : Variation of wear coefficient scatter (mean 1E-06), slip amplitude mean 50μm COV 30%, Type B gearbox, Civil spectrum

8.8 Loading Variability for Wear Model

8.8.1 Variation in Load Spectra

Experiments were also carried out with the wear model on the effect of changing the load input data. As shown in Figure 8.26, changes to the torque spectra will directly affect the time to failure because the wear volume removed is directly proportional to load in the damage model (Section 4.4). The tests were conducted using the geometry for the Type B splines, with a mean slip amplitude of 100 microns (COV 10%). The wear coefficient was taken to be 1E-06.

The curves for Civil spectrum show the increase in life of 12 % (1640 to 1840 hours at p* 10^{-6}) when the proportion of manoeuvre 5 is reduced from 2% to 0.1% (design value is 0.25). This is the same at all values of p*, and is further examined in Section 8.8.2. The other curves show the effect of significant changes in load, with Flight 110, ASW history and Prototype spectrum, in ascending order of severity.

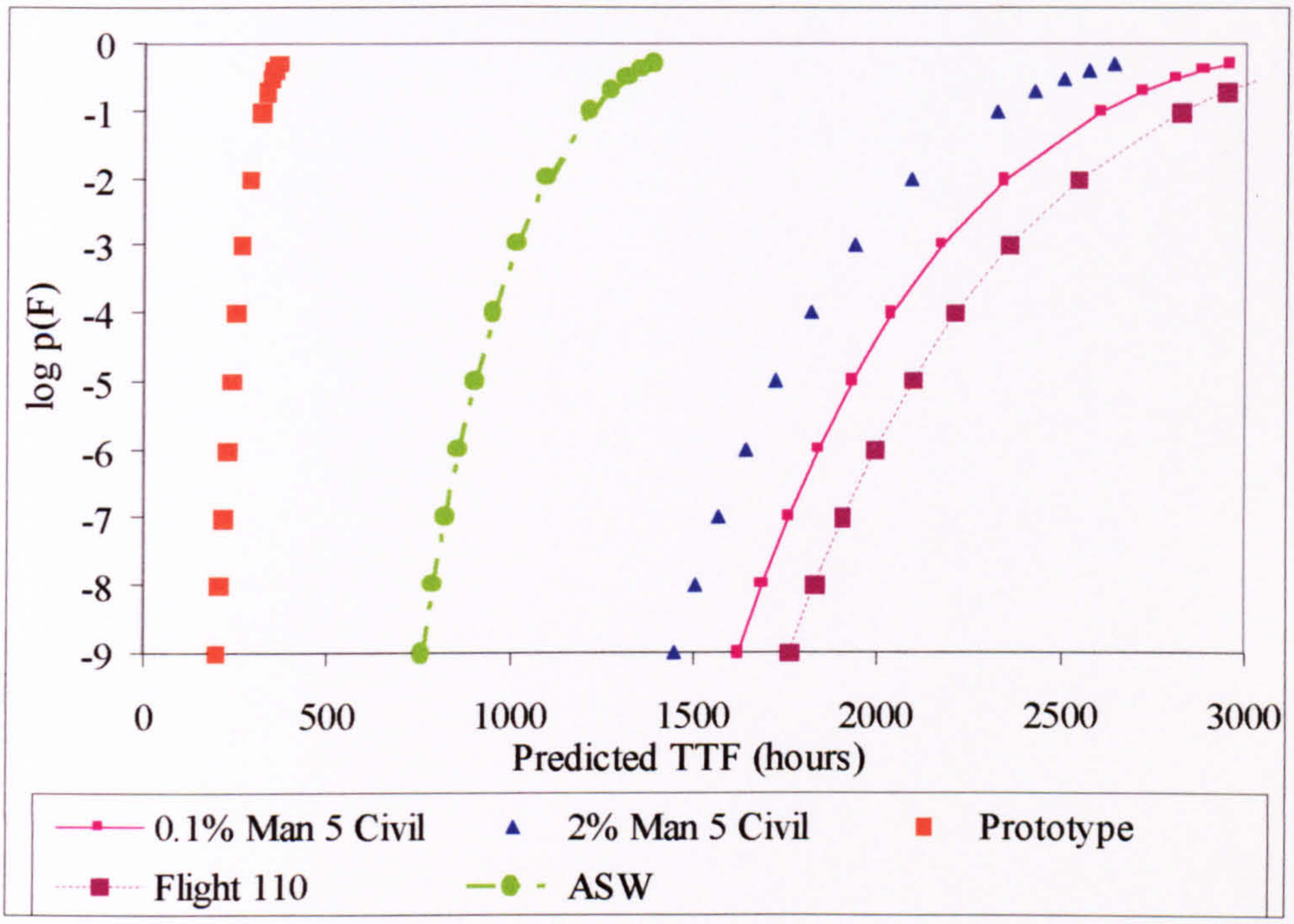

Figure 8.26 : Plot of TTF by spline wear for different load spectra (Type B, mean slip amplitude 100 micron, COV 10%, K = 10^{-6})

The variation in position and gradient of the failure curves may be viewed as being significant, but the TTF values do not vary as greatly with changes in load as do those for fatigue. Such a comparison is more easily made in Sections 9.5 and 9.6, which includes spline wear amongst the other failure mechanisms included in the system model.

8.8.2 Variation in Damaging Manoeuvres

Results are presented to provide a means of comparison between loading variability for fatigue models and the spline wear model. For this reason, the same four manoeuvres have been used here as were employed in Section 8.4, that is:

- Manoeuvre 2 - Take-off
- Manoeuvre 5 - Spot turn port (hover OGE)
- Manoeuvre 12 - 60 degrees Sideways flight
- Manoeuvre 13 - 90 degrees Sideways flight

The graph presented (Figure 8.27) shows the effects of variation of TTF when the proportion of these manoeuvres varies between 0.1% and 2%. As can be seen, the factors range from 0.9 to 1.02. This should be compared with the corresponding results for fatigue. The manoeuvre that gave the smallest variation in results for fatigue was manoeuvre 2 (Table 8.5). This caused the factor for the change in TFS for bearing contact fatigue to be 1.03 at 0.25% and 0.87 at 2%, based upon the baseline spectrum of

0.43%, Figure 8.9. It is therefore concluded that changing the proportion of the most damaging manoeuvres (for fatigue) has a far smaller effect on spline wear life.

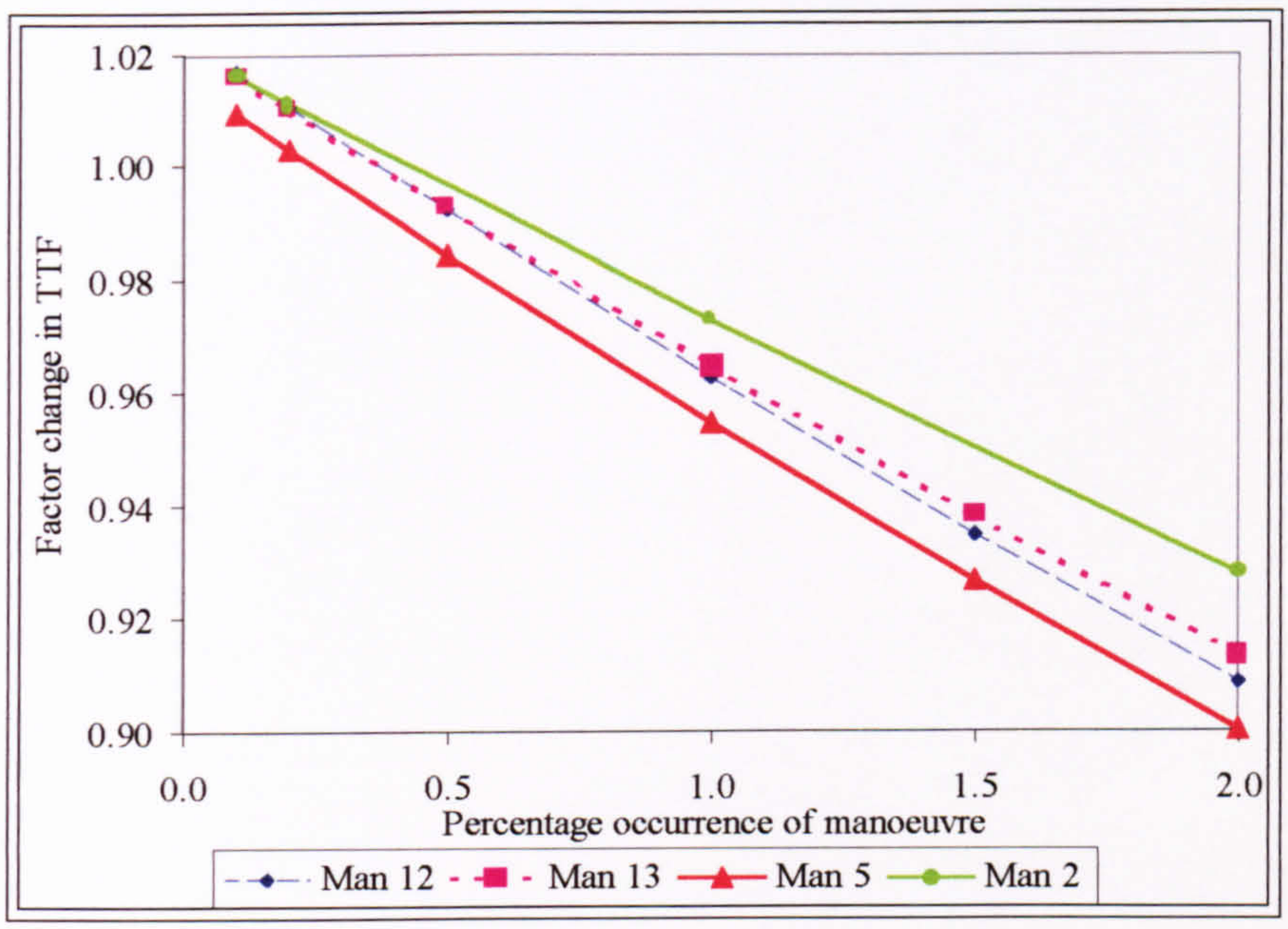

Figure 8.27 : Influence of damaging manoeuvres on spline wear (Type B, mean slip amplitude 100 micron, COV 10%, K = 10^{-6})

8.8.3 Influence of Over-torque on Spline wear

The calculation of time to failure by spline wear showed that the addition of over-torque had little effect on shaft spline wear. The results are shown in Table 8.10, which should be compared with those for fatigue in Section 8.5. The over-torque has been added to the Civil spectrum as an additional load state with a high torque value of short duration.

The spline wear failure mechanism would therefore appear to be dominated by the slip amplitude and wear coefficient K. This is chiefly because all loads contribute to the wear during each shaft rotation, so that small, brief changes of high torque, have less proportional effect than do changes in slip amplitude and wear coefficient K.

Occurrence (%)	Over-torque (N m)	TTF (hours)
0.0006	2200	1822.9
	3000	1822.87
0.0056	2200	1822.04
	3000	1821.66
Nil	0	**1823**

Table 8.10 : Variation in TTF by spline wear for different size and percentage occurrence of over-torque at p* = 10^{-6}

9 Results from Corrosion and System Reliability Models

9.1 Introduction

Chapter 8 gave results for the fatigue and wear models, which are all based upon cycles, i.e. the operating time for the gearbox. By way of contrast, a distinguishing feature of the corrosion model is the dependence on calendar time. This second Results chapter contains the output from the corrosion model (Section 9.2), which are then combined with fatigue and wear model results in the system reliability model (Section 9.4).

The system reliability model requires that all failure mechanisms be plotted on the same axis. Hence, the cycles based (fatigue, wear) and time based (corrosion) models have been combined on the same time base by assuming knowledge of the helicopter usage rate, i.e. hours flown per year, taken as 500 hours/year. By dividing the calendar TTF by corrosion (months) by the number of hours flown in one month, the equivalent TTF by corrosion may be written in hours and thus plotted on the same scale as fatigue and wear based results.

The results from each damage model have been combined in order to investigate the influential parameters for the reliability of the system. Data for the models are again taken from Appendix E, for two gearboxes (Type A and Type B) and four torque data sets, two for each gearbox.

Section 9.3 shows results from tests carried out by altering the POD of the various forms of health monitoring to investigate its impact on reliability. The value of POD has been assumed to be constant from the moment that damage becomes detectable, until the moment of eventual failure.

9.2 Corrosion Model

9.2.1 Results to be presented

Both galvanic and plain corrosion of the gearbox casing were studied by varying the input model parameters to determine their relative influence. These include the environment, type of material, corrosion rate and failure limit. The two materials considered are Magnesium casting alloys AZ91C and WE43.

The corrosion model described in Chapter 4 has been employed to estimate the time for the gearbox casing to reach a maximum section loss. Data for the casing corrosion models is given in Chapter 6, and studies of both magnesium alloys AZ91C and WE43 have been carried out. Since the galvanic corrosion rates of AZ91C and WE43 are similar **[Geary, 1990]**, only one curve is drawn to represent these results.

An alternative material, Aluminium alloy A357, has not been analysed since both plain and galvanic corrosion rates are significantly lower than those for magnesium alloys. The A357 plain corrosion rate is less than 0.25 mm/year, compared to WE43 estimated

0.76 and AZ91 estimated 6 mm/year. The A357 galvanic corrosion rate is less than 0.5 mm/year, compared to WE43 and AZ91 estimated 76 mm/year **[ibid].** However, results for A357 are included in the calculation of system reliability for Type B gearbox, see Sections 9.6.1 and 9.6.2.

The results are deliberately focused on operation in a marine, salt-laden, environment. Not only is this the most likely operating regime for most UK-based helicopters (e.g. Naval, shore-based and North Sea operations), but it also provides the worst-case scenario in which to assess corrosion.

Parameter varied	Section	Figure
Proportion of time in marine environment	9.2.2	Figure 9.1
Variation in mean corrosion rate - marine environment	9.2.3	Figure 9.2
Mean time to initiate corrosion	9.2.4	Figure 9.3
Mean limit of metal loss M*	9.2.5	Figure 9.4
COV of limit of metal loss M*	9.2.6	Figure 9.5

Table 9.1 : Results presented for Plain and Galvanic Corrosion models of AZ91C, WE43

The results from both plain and galvanic corrosion models are presented in the same figures to provide a comparison between the two types. The time to initiate corrosion (T_{init}) and the corrosion rates (k) are assumed to be independent of the torque transmitted by the IGB. This allows the corrosion models to be run independently of those for fatigue and wear.

The principal corrosion parameters have been varied in turn, as shown in Table 9.1. The results are values for the time to reach the corrosion limit, T_{limit}, in units of calendar time. All results are given for a failure probability p* of 10^{-3}, due mainly to the limitations from the Monte-carlo simulation. The number of samples was limited to 10^4, hence the minimum failure probability was 10^{-4}.

9.2.2 Variation in percentage marine environment

Figure 9.1 shows the predicted time to reach corrosion limit, T_{limit}, for an exposure proportion of 0 to 90% in the marine environment. The figures show the reduction in T_{limit} as the proportion of time in the salt-laden marine environment increases. This reduction is more marked for galvanic corrosion than for plain corrosion, because of the high value of k in the marine environment. Increasing the percentage time in marine environment from 0 to 90% reduces the predicted life by a factor of 13.4 for galvanic corrosion (both materials), 2.9 (AZ91C) and 3.7 (WE43) for plain corrosion.

For both casing materials, AZ91C and WE43, T_{limit} is much shorter for galvanic corrosion than for plain corrosion; both alloys experience similar galvanic corrosion rates, but WE43 has a much lower plain corrosion rate than AZ91C.

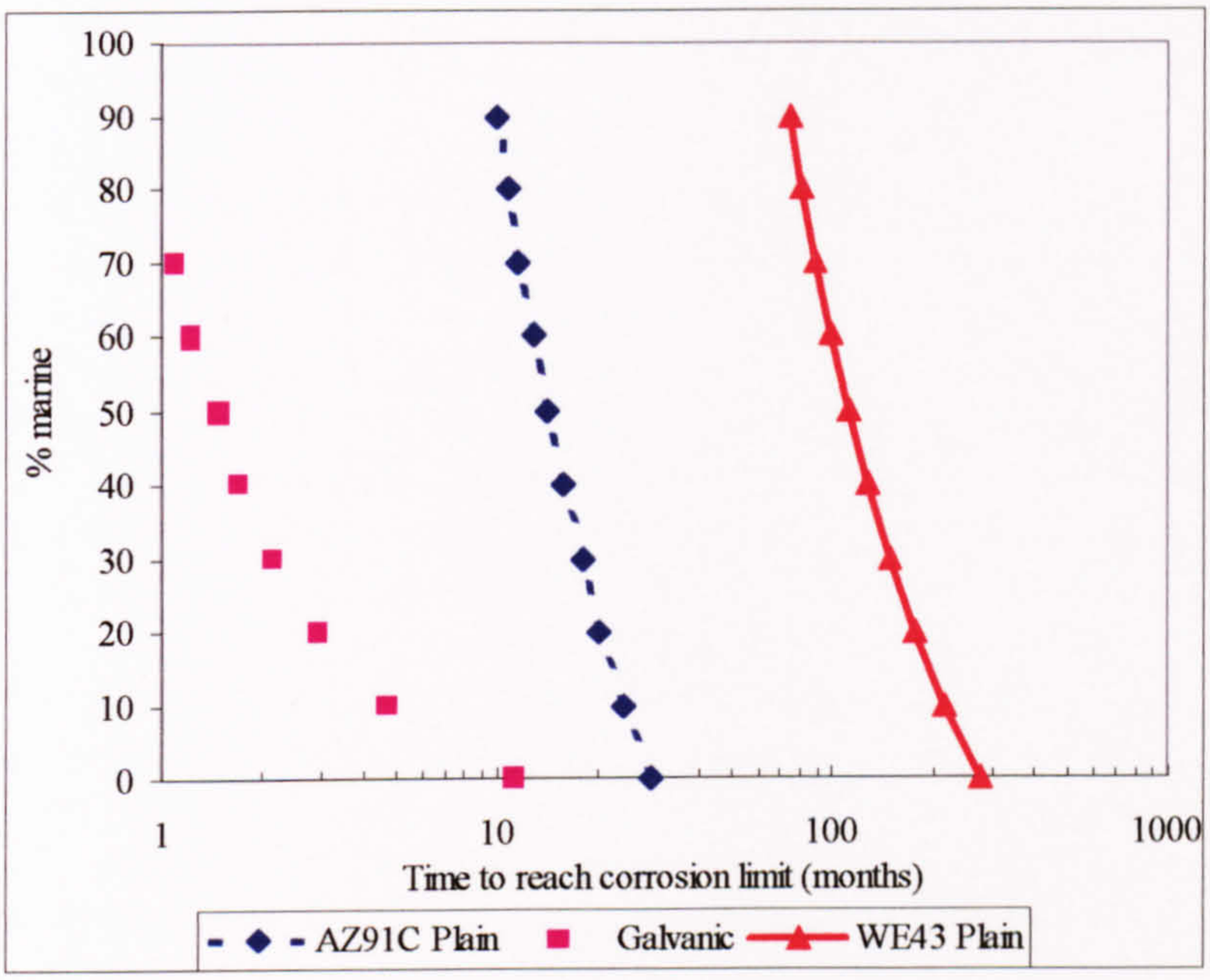

Figure 9.1 : Corrosion TTF vs Percentage time spent in marine environment at $p^* = 10^{-3}$

9.2.3 Variation in mean corrosion rate for marine environment

Figure 9.2 shows the predicted time to reach corrosion limit, T_{limit}, for different mean values of the corrosion rate (k_{mar}) in marine environment. The mean rate of galvanic corrosion was varied from 60 - 100 mm/year for both casting alloys, and the mean rate of plain corrosion was varied from 0.2 - 2 mm/year (WE43) and from 2 - 20 mm/year (AZ91C). The COV for each rate was 5% for plain corrosion and 10% for galvanic corrosion; a larger scatter was chosen for galvanic corrosion due to the increased uncertainty in local corrosion rates.

The results show how T_{limit} is affected as the mean corrosion rate changes, with the greatest proportional decrease being for WE43 plain corrosion. This is because it has the lowest range of k_{mar} (0.2 - 2 mm/year), and the TTF increases dramatically at low values. For an increase in k_{mar} of 0.2 to 2 mm/year, T_{limit} reduces from 278 to 32 months (factor of 8.7) at p^* of 10^{-3} level. For the plain corrosion of AZ91C, the larger corrosion rate leads to a shorter T_{limit}. An increase in k_{mar} from 2 to 20 mm/year gives rise to an increase from 29 to 3.5 months (factor of 8.4).

In contrast, variation in the mean rate of galvanic corrosion between 20 and 100 mm/year do not greatly effect T_{limit}, since the corrosion rates are so large. Once the corrosion has initiated, the time to exceed the corrosion limit is relatively short. A corrosion rate of 20 mm/year results in a time to failure of the order of 3 months.

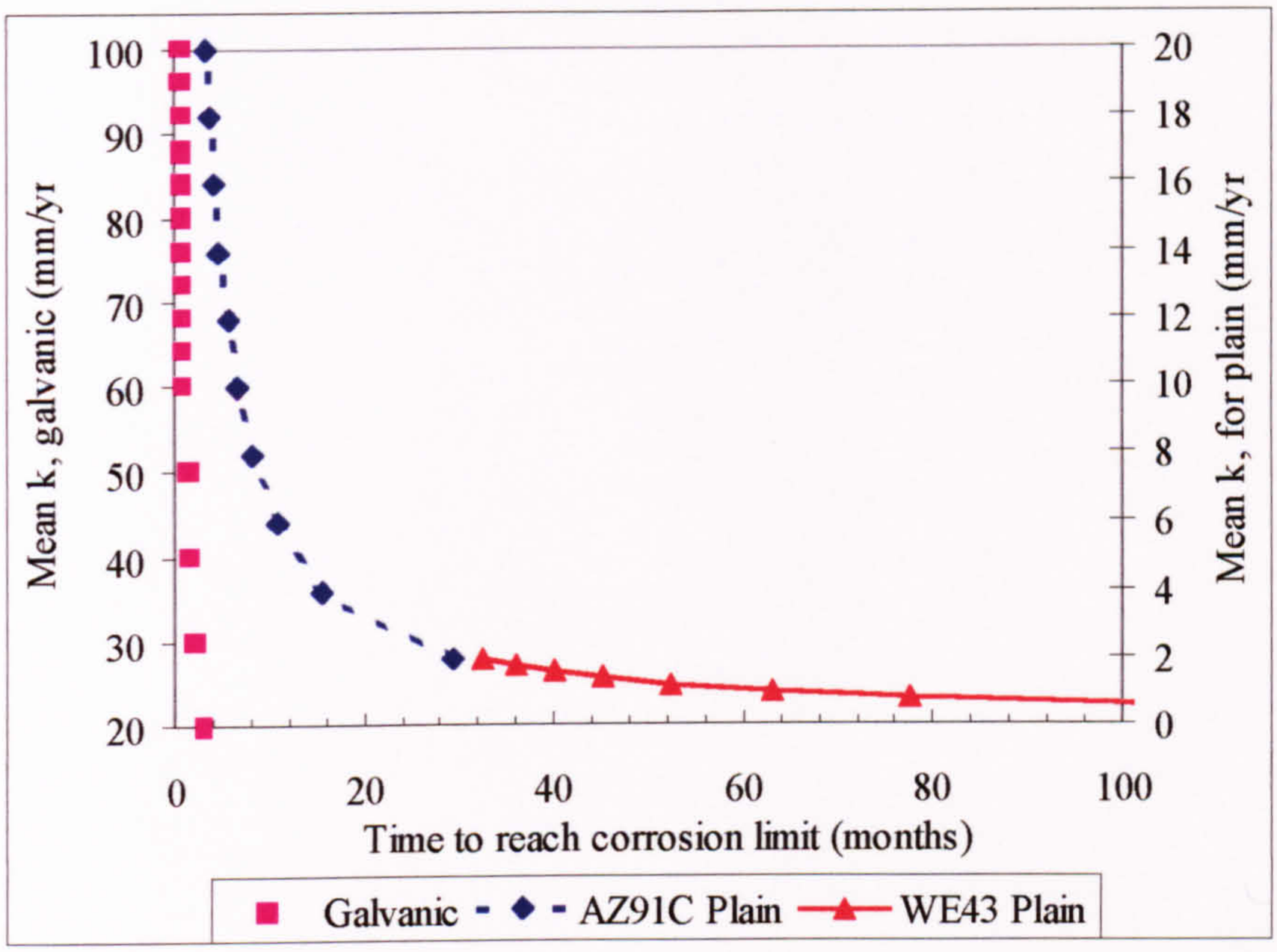

Figure 9.2 : Corrosion TTF vs Mean corrosion rate (k_{mar}) at $p^* = 10^{-3}$

9.2.4 Variation in Mean Time to Initiate Corrosion

Figure 9.3 shows the predicted time to reach corrosion limit, T_{limit}, for mean time to initiation (MTTI) values between 0 and 36 months. The figures show the expected increase in T_{limit} with the increase in MTTI. However, the proportional increase depends on the failure probability p* required; the larger p*, the more marked the increase in T_{limit}.

Failure probability p*	**Corrosion type**	**Increase in T_{limit} for increase in MTTI from 0 to 36 months**
10^{-3}	WE43 plain corrosion	6% (77.4 to 82 months)
	AZ91 plain corrosion	14% (9.7 to 11 months)
	Galvanic corrosion	36% (0.7 to 0.97 months)
10^{-1}	WE43 plain corrosion	12% (87 to 98 months)
	AZ91 plain corrosion	44% (11 to 16 months)
	Galvanic corrosion	x 5.3 (0.86 to 4.6 months)

Table 9.2 : Results from variation of MTTI

Table 9.2 shows the summary of the effect of increasing mean time to initiate. The results show that the faster corrosion mechanisms are affected more by an increase in MTTI than the slower mechanisms. This is explained since T_{corr} is shorter for the

higher corrosion rates, so that the total time to failure is more dependent on T_{init} than is the case for lower corrosion rates, see equation 9.1.

Time to reach corrosion limit = Time to initiate + Time for casing to corrode

$$T_{limit} = T_{init} + T_{corr} \qquad (9.1)$$

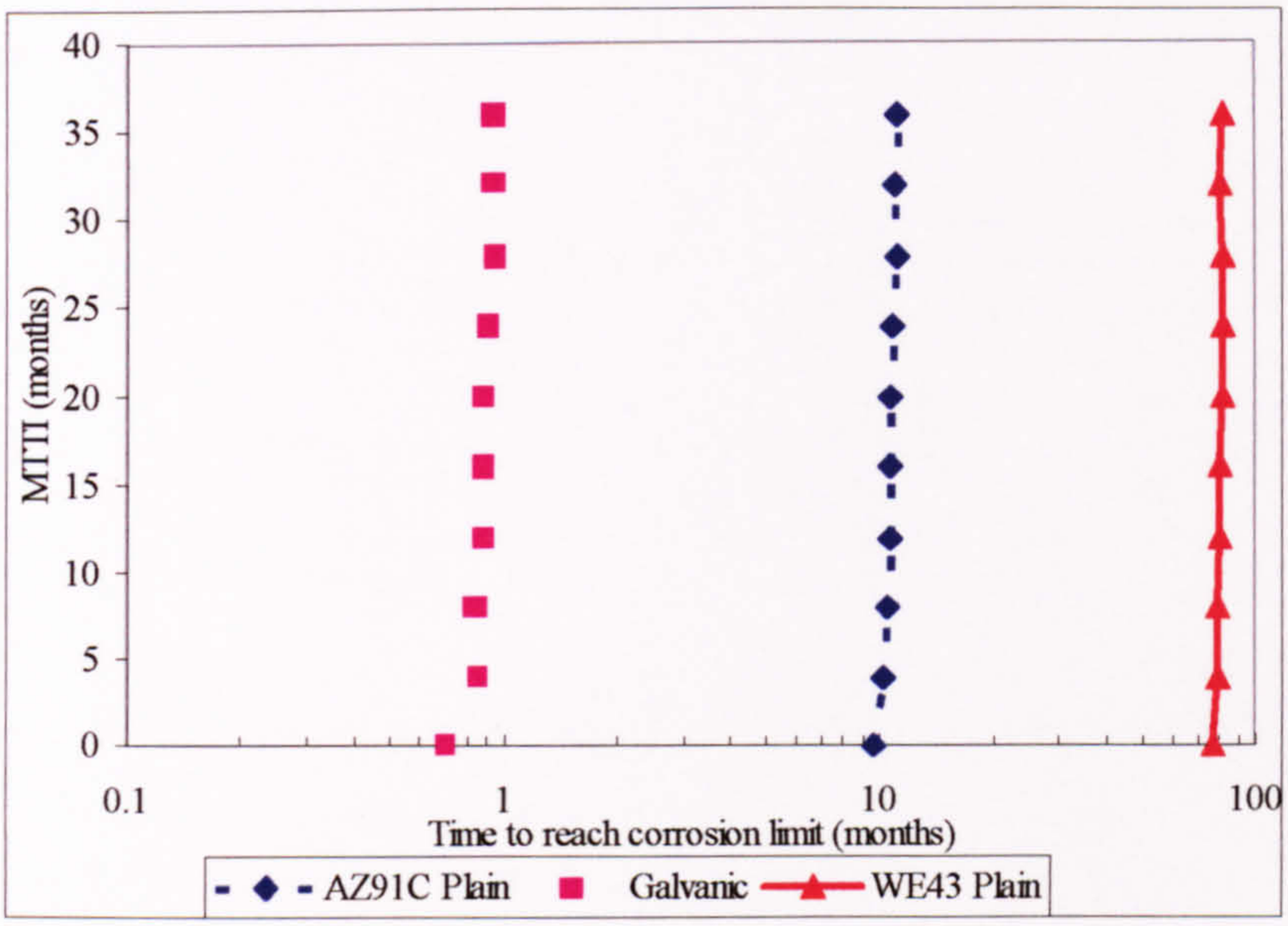

Figure 9.3 : Corrosion TTF vs MTTI at $p^* = 10^{-3}$

9.2.5 Variation in mean metal loss limit M*

Figure 9.4 shows the predicted time to reach corrosion limit, T_{limit}, for mean values of the metal loss limit M* from 1 to 10 mm. The figures show how T_{limit} increases with the increase in the mean M*, as expected. The proportional increase varies according to the failure probability required. At p^* 10^{-3} T_{limit} increases by a factor of 7.8 (0.23 to 1.8 months) for galvanic corrosion as M* increases from 1 to 10 mm; at p^* 10^{-1} (not shown) the factor is 1.5.

This effect is more marked for plain corrosion; the factor of increase is 9.3 at $p^* = 10^{-3}$ (17 to 158 months) for WE43 and 9.1 (2.3 to 21 months) for AZ91. Hence the lower the corrosion rate, the greater the proportional effect of changing the mean metal loss limit M*.

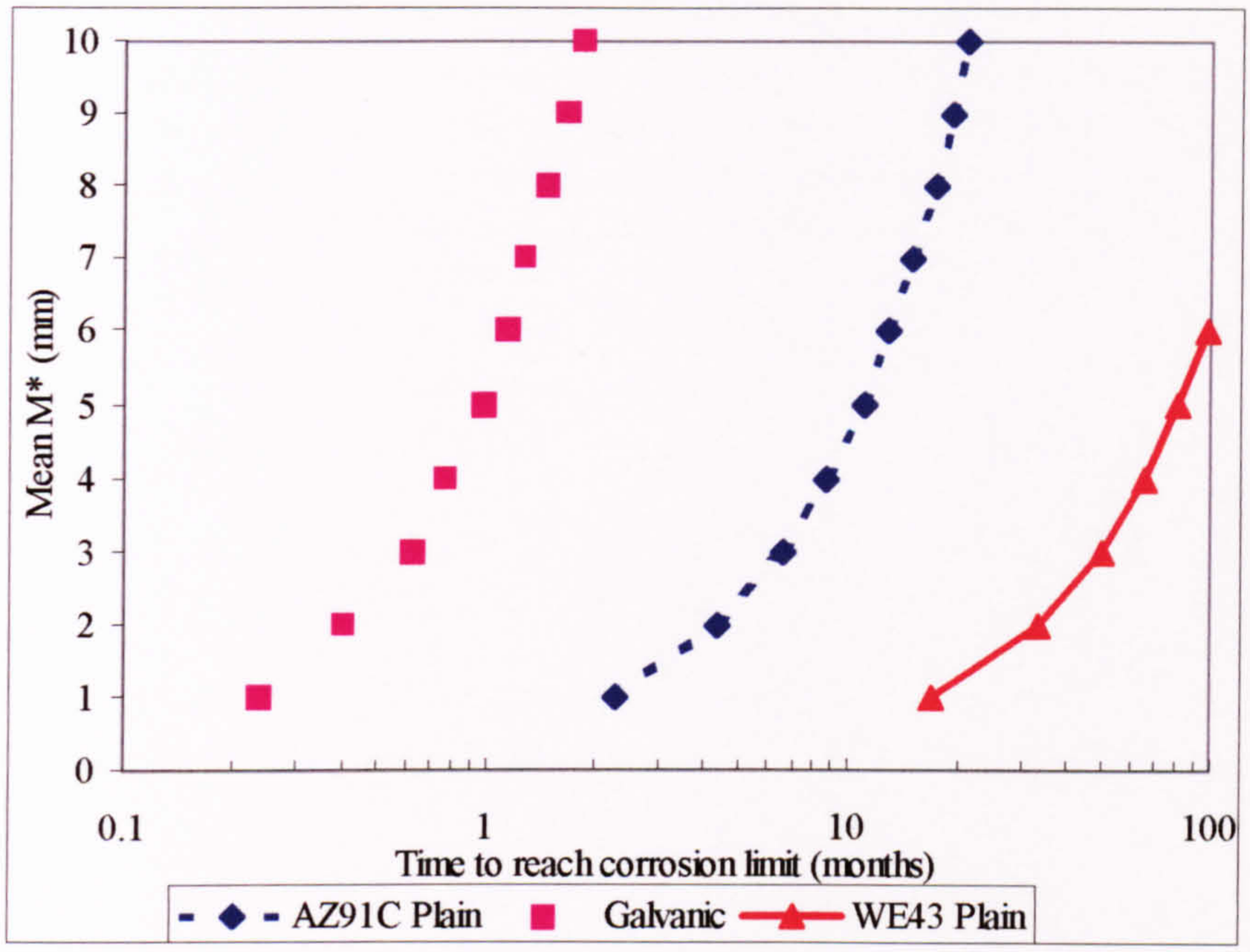

Figure 9.4 : Corrosion TTF vs Mean M* at $p^* = 10^{-3}$

9.2.6 Variation in COV for metal loss limit M*

Figure 9.5 shows the predicted time to reach corrosion limit, T_{limit}, for values of COV from 0 to 20% for the corrosion rate (k_{mar}) in marine environment. The figure shows that there is a greater variation in T_{limit} for plain corrosion than for galvanic corrosion - a variation that reduces with increasing failure probability.

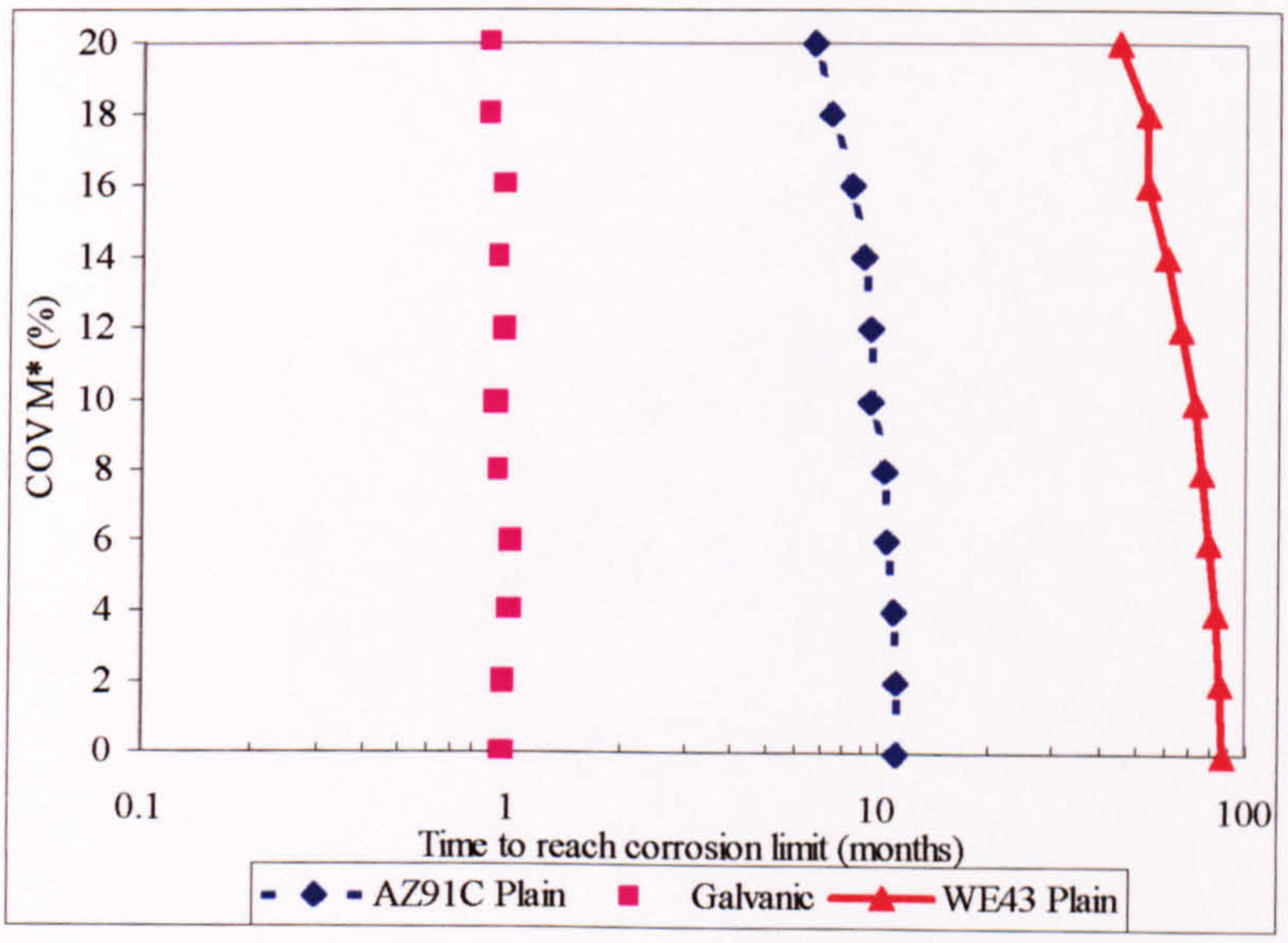

Figure 9.5 : Corrosion TTF vs COV of M* at $p^* = 10^{-3}$

At p* of 10^{-3}, T_{limit} for WE43 plain increases by a factor of 1.9 (45 to 86 months) for a change in M* COV of 20% to 0; for AZ91 plain the corresponding factor is 1.7 (6.7 to 11.3 months). At p* 10^{-1} (not shown), the corresponding factor reduce to 1.15 (WE43) and no change (AZ91C). There is virtually no variation in values of T_{limit} for galvanic corrosion.

9.3 Probability of Detection Results

The HGBR software provides the analyst with the opportunity to investigate the influence of the probability of detection (POD) on the overall time to failure in each failure model. As described in Section 6.7 and 6.8, the POD for each failure mechanism is applied to the respective model in order to work to a common failure condition (functional failure). This is an essential part of calculating the bounds of system reliability. This section consists of results gained from varying the POD for tooth root bending fatigue using the Type B gearbox and Prototype spectrum.

9.3.1 Influence of POD

Figure 9.6 shows the failure probability curves for tooth root bending fatigue for the Type B gearbox, using the Prototype spectrum, at a selection of POD values. The results are shown for calculations of fatigue life using a Miner damage sum of unity, which has been used for all studies up to this point.

Results for a detection probability of zero are the same as the basic output of the TRBF model. The failure curve represents the probability at which a crack of 1mm is predicted to occur at the gear tooth root. The Miner damage sum of unity is used to represent the cumulative damage of the 1mm micro-crack, and is the basis for calculating the time for a crack to initiate. Due to the high loading of the gears, the time between crack initiation and functional failure is deemed to be short, in the order of <10 hours. This curve is thus considered to be the time to functional failure of the gear due to TRBF.

The remaining three curves in Figure 9.6, for POD values of 50%, 90% and 99%, also represent the time for the gear to fail by tooth root bending fatigue. A functional failure is considered to occur if:

(a) A gear tooth root crack occurs, AND

(b) The crack is undetected by condition/health monitoring

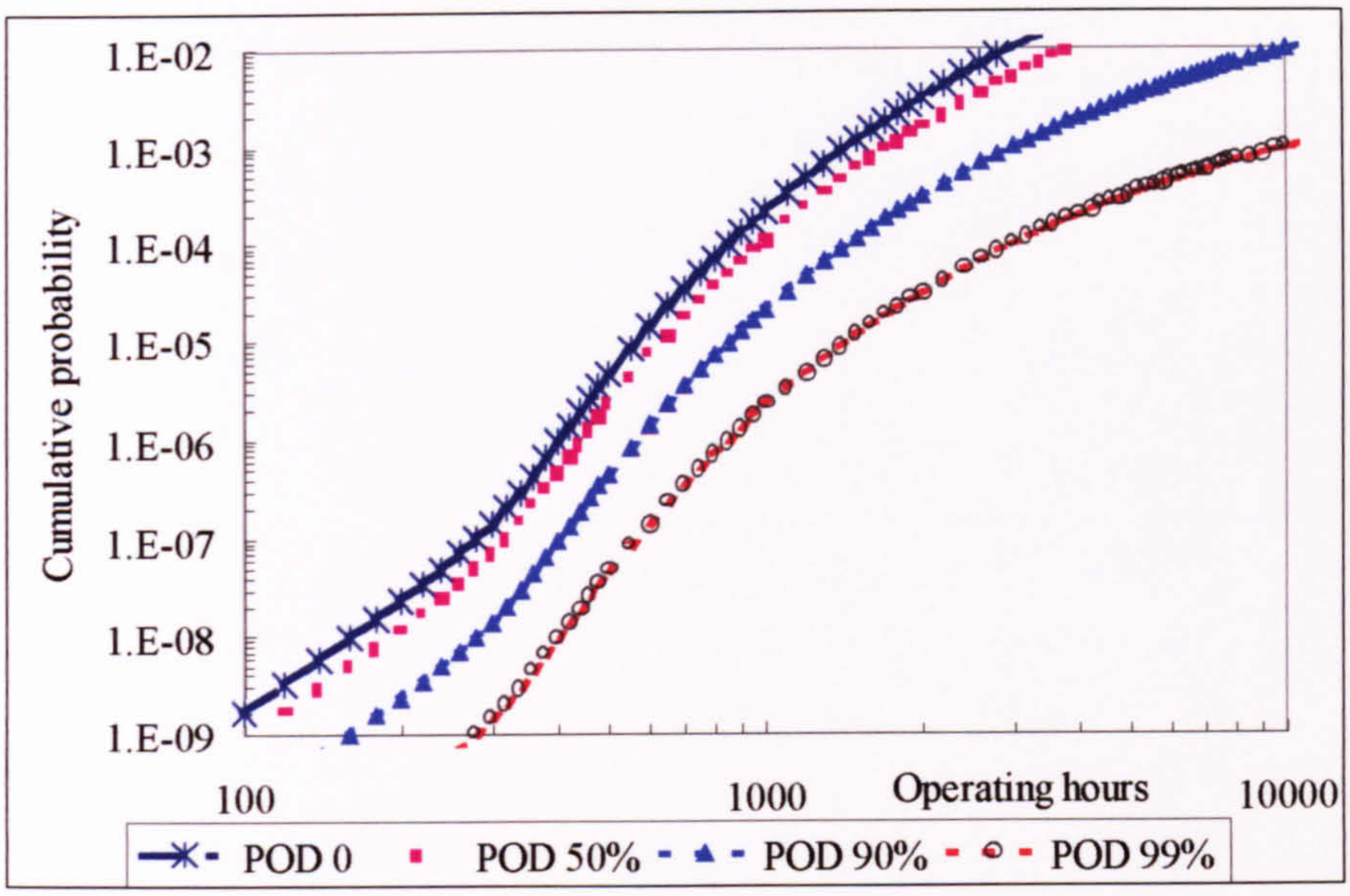

Figure 9.6 : Influence of health monitoring for TRBF (Type B gearbox, Prototype loading)

The values of failure probability have been calculated as in equation 9.2, and plotted in Figure 9.6, where p(FF) is the probability of functional failure.

$$\begin{aligned} p(FF) &= p(\text{tooth root crack initiation}) \times p(\text{crack undetected}) \\ &= p(\text{TRBF occurs}) \times (1 - POD) \end{aligned} \qquad (9.2)$$

The failure probability for TRBF at 1000 hours is predicted as 2.2E-04 with a POD of zero; this is clearly reduced by the application of condition monitoring. For the POD values illustrated (50%, 90% and 99%), failure probability is reduced by a factor of 2, 10 and 100 respectively. This is to be expected from inspection of equation 9.2.

9.3.2 Influence of POD and Miner damage sum

Figure 9.7 shows the results of changing the Miner damage sum, in addition to the POD for the detection of damage. It is likely that as damage is accumulated, the likelihood of detection will increase, see Section 5.4 **[Heida, 1984; Irving et al, 2000]**. This increase in damage towards the point of failure is represented in the case of tooth root bending by the use of a Miner damage sum (DS) less than unity. In this example, the POD is assumed to be zero, 50% and 90% at a DS of 0.8, 0.9 and 1, respectively.

The three curves (labelled 1-3 below) illustrate the occurrence of damage caused by TRBF. Only in Curve 3, for a DS of 1 however, does the curve represent functional failure.

Curve 1 {Damage sum = 0.8 and not detected} =
POD 0% {p(DS is 0.8) x (1 – POD)} = p(DS is 0.8)

Curve 2 {Damage sum = 0.9 and not detected} =
POD 50% {p(DS is 0.9) x (1 – POD)} = {p(DS is 0.9) x (1 – 0.5)}

Curve 3 {Damage sum = 1 and not detected} =
POD 90% {p(DS is 1) x (1 – POD)} = {p(DS is 1) x (1 – 0.1)}

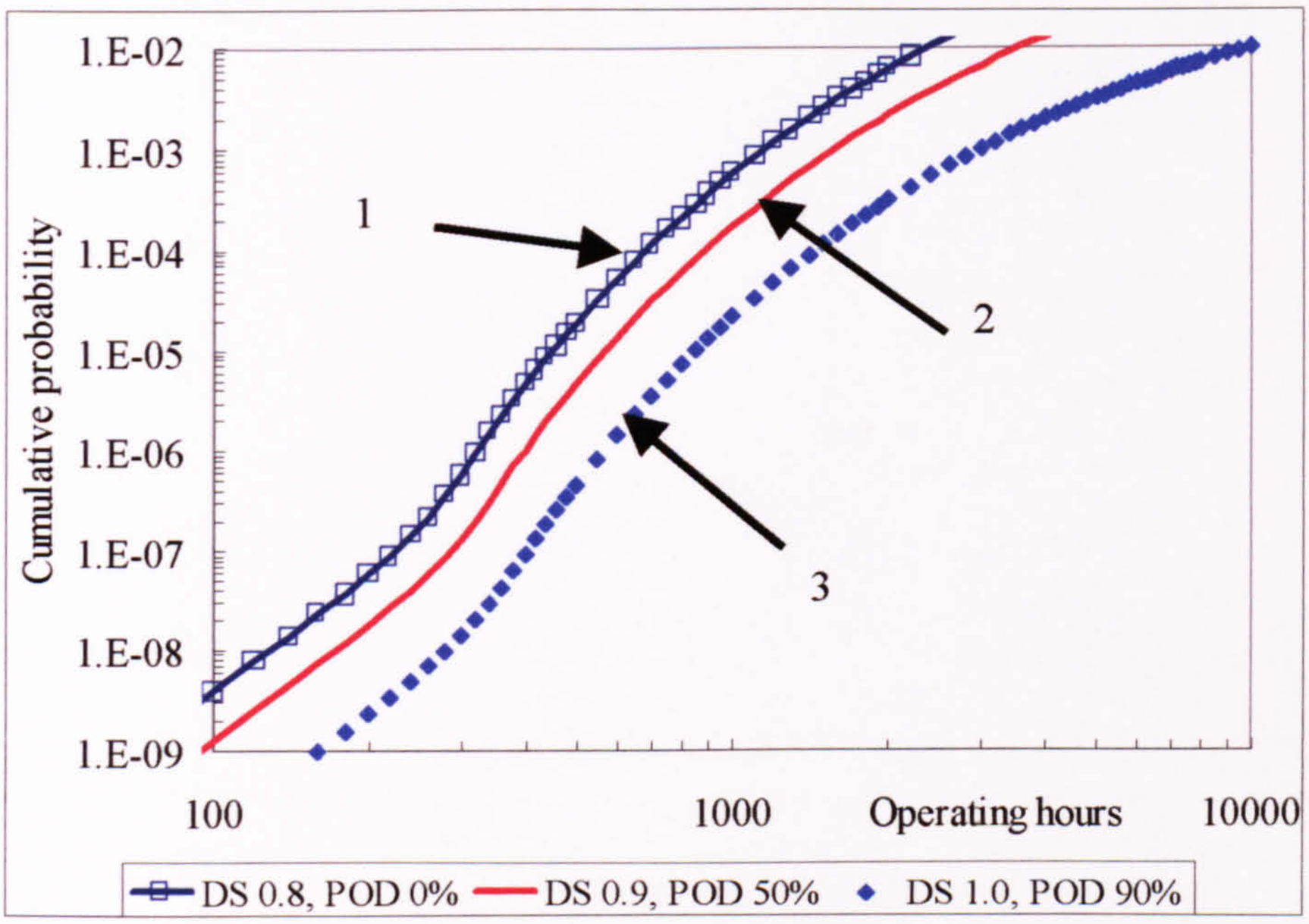

Figure 9.7 : Influence of POD and Miner Damage Sum for TRBF (Type B gearbox, Prototype loading)

By comparison with Figure 9.6, it may be seen that at 1000 hours, the probability of DS 0.8 existing undetected (5.85E-04) is approximately 2.5 times the probability of DS 1.0, with a POD of zero (2.21E-04). Condition monitoring reduces the likelihood of such damage occurring undetected; at 1000 hours, the respective values of p(F) are 1.77E-04 and 2.21E-05 for curves 2 and 3.

Results for other failure mechanisms using different load data yielded similar results, and highlight similarly the benefit of condition monitoring systems. However, the advantage of condition monitoring may be assessed more properly when set against the system reliability as a whole (Section 9.5 onwards).

The difference between the failure mechanisms should be re-stated to highlight the difference in model output. The TRBF model predicts the time at which the damage sum reaches unity according to Miner's damage summation, considered as the point of functional failure. The other damage models provide predictions of the time for a threshold of damage to be reached, e.g. a spall of a certain size, or a certain amount of metal lost by wear.

9.4 System Reliability

System reliability has been estimated using results from the failure probability of the individual damage models, which is one of the reasons for conducting the tests in Chapter 8. For failure mechanisms that are capable of detection by health monitoring, the values of failure probability have been combined with the POD (see Section 9.3). Certain assumptions have been made in the calculation of system reliability of the transmission system as a whole, as will be discussed in Section 10.7.

These assumptions have been made in order to simplify the task of combining the failure mechanisms, whilst not adversely affecting the results produced:

a) The time between the onset of degradation and its detection is a small proportion of the total time to failure. This means that the probability of detection (POD) of the damage will not change significantly after initial detection.

b) The interaction of separate failure mechanisms does not significantly alter the time to failure by those mechanisms.

The calculation of system reliability enables the dominating factors to be identified and highlights the influence of the acceptable risk of failure (p_{sys}*) may have on the dominance of these factors. The relative significance of health monitoring (HM) detection systems is also indicated. Example questions to be asked are:

1. Which failure mechanisms dominate the system reliability for low values of p_{sys}*, as compared to high p_{sys}* values?

2. What effect does the accuracy of health monitoring have on system reliability across the spectrum of p_{sys}* values?

9.4.1 System Results to be presented

Those model parameters that have a large effect on the individual failure models may be varied in order to determine their impact on the system results. It is also possible to select an appropriate interval upon which to perform maintenance, when the system reliability figure decreases below a pre-set threshold. The output from the combination of the models may be used to highlight the significance of:

- Load parameters and variability
- Material parameters and variability
- Probability of detection by health monitoring.

Tests were run for the combinations of gearbox, loading and POD values as shown in Table 9.3. While the results have been gained from the study of particular gearboxes with distinctive loading regimes, efforts have been made to identify general lessons that may be learnt for general gearbox design and operation/maintenance.

Description of Figure	Features of input data	Figure
System Reliability - Type A, ASW loading	Baseline data, AZ91C casing, POD of 90% applied	Figure 9.8
Lower bound for System failure probability - Type A, ASW loading	Variation in time to initiate and mean galvanic corrosion rate	Figure 9.9
System Reliability - Type A, Flight 110 data	Baseline data, WE43 casing, POD of 90% applied	Figure 9.10
System Reliability - Type B, Prototype spectrum	Baseline data, A357 casing, POD of 90% applied	Figure 9.11
System Reliability – Type B, Civil spectrum	Baseline data, A357 casing, POD of 90% applied	Figure 9.12

Table 9.3 : Summary of System Reliability Results

Calculated values for system failure probability (p_{sys}*) are presented as lower and upper bounds. The lower bound of p_{sys}* is calculated from the component most likely to fail at any particular time, which assumes that all the failure mechanisms are interacting (Loading Roughness = 1). The upper bound is calculated by considering all failure mechanisms for all components together, which assumes that all components and failure mechanisms are independent (Loading Roughness = 0), the Product Rule.

9.5 System Reliability of Type A gearbox

Results are presented for the Type A gearbox, using two load data files, namely ASW history and Flight 110, both defined in Appendix E. A value of 90% POD has been applied to all failure mechanisms.

9.5.1 Baseline results Type A gearbox – ASW history

Figure 9.8 shows the increase in failure probability with time for all failure mechanisms present in the Type A gearbox with AZ91C magnesium alloy casing. Results have been calculated using baseline parameters (Appendix E), under loading of ASW history. To help achieve clarity, only one failure curve is shown for bearing contact fatigue, since similar lives were calculated for each bearing; the failure curve for bearing 4 is shown, which has the lowest L_{10} life.

The figure shows that there are considerable differences between the predicted time to failure of the different failure mechanisms included in the model. Calendar-based results from the corrosion models have been included on the same time base as fatigue and wear models by applying a usage rate of 500 hours/year.

From initial operation up to 40 hours, the system reliability is dominated by the four taper-roller bearings, of which bearing 4 is predicted to fail first. After the 40-hour mark, galvanic corrosion of the AZ91C casing becomes the most likely cause of failure.

This failure mechanism continues to dominate up to 800 hours after which the highest failure probability is that of spline wear.

Spline wear is the most likely failure mechanism to occur from 800 up to 1500 hours. At this point the cumulative failure probability reaches an asymptote of 0.1. This maximum reflects the fixed probability of detection of 90%; the probability of failure is given by the probability of the damage being undetected, 10% in this case.

The failure curve for plain corrosion appears from 400 hours and has a steep gradient for the first three decades (400-600 hours). This equates to approximately 10-14 months calendar time, based upon a usage rate of 500 hours/year. The COV of the corrosion rate is set at a low level, 5% in this model, which is the reason for the small 'spread' of predicted results.

The failure curve for gear tooth RCF is present at all stages, but has a small gradient due to the high value (15%) assumed for material variability. TRBF appears at 1000 hours, and increases with time to exceed 10^{-3} at 3500 hours, allowing for POD. Thereafter it is still less likely to occur than all other failure mechanisms considered, except gear RCF. However, were it not for the POD (set to 90%), gear TRBF would play a far greater role in limiting the system reliability. It should be re-stated that this failure mechanism is one the most difficult to detect, as it produces no 'tell-tale' debris during crack initiation **[Drago, 1988]**.

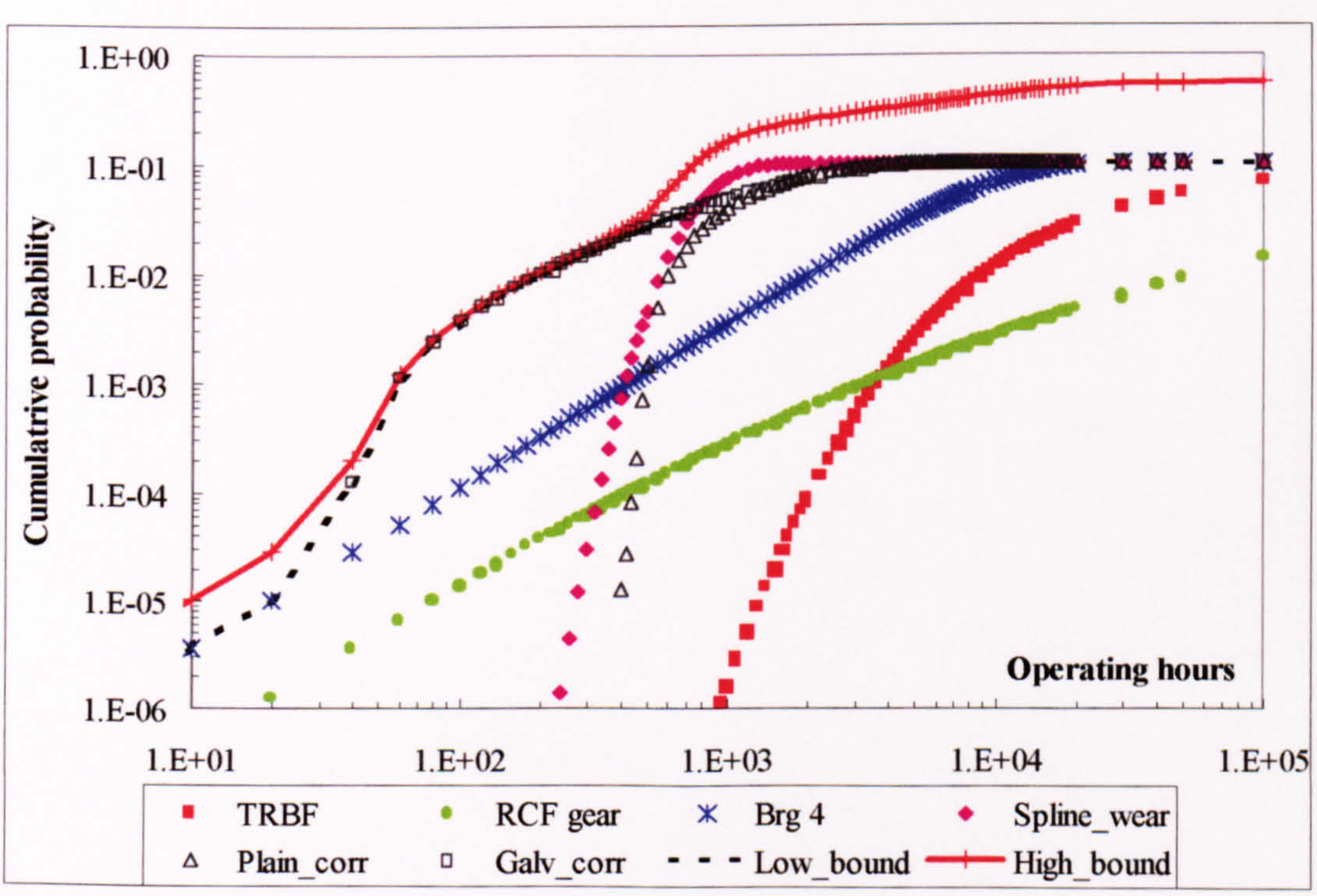

Figure 9.8 : Summary of system failure probability for Type A gearbox, with ASW history and AZ91 casing

It was observed that the lower and upper bounds (LB and UB) of the system failure probability are in close proximity for much of the region of interest (system failure probability 10^{-4} to 10^{-2}). The main distinction between the two bounds is at lives of less than 60 hours, and above 500 hours.

The reason for the convergence and divergence of the two bounds is explained by considering the method of calculating system reliability. The lower bound of $\mathbf{p_{sys}}$ equates to the highest value of p(F) at any point in time – bearing 4 at 20 hours (1.02E-05), galvanic corrosion at 60 hours (1.11E-03). The upper bound of $\mathbf{p_{sys}}$ is calculated from the 'Product Rule' that considers the results from every individual failure model. Since the value of p(F) for galvanic corrosion is significantly greater than values for gear RCF and bearing fatigue, the results converge between 20 hours (UB is a factor of 2.9 greater than LB) and 60 hours (factor is 1.1).

Above 500 hours, the contributions of spline wear and plain corrosion increase the gap between upper and lower bounds. This is also due to the incorporation of POD, such that rather than having an asymptote of 1 (as is usual for a CDF), the individual failure curves tend to 0.1, for a POD of 90%.

The lower bound of $\mathbf{p_{sys}}$ is equal to the most unreliable component, 90% reliability ($\mathbf{p_{sys}}$ = 10%). The upper bound of $\mathbf{p_{sys}}$ is calculated by considering all failure mechanisms; if there were four failure mechanisms, all with POD of 90%, the upper bound would be calculated as:

$$p_{sys}\,(UB) = 1 - \Sigma\,(1\text{-}p_i)$$

$$p_{sys}\,(UB) = 1 - \{(1\text{-}0.1)(1\text{-}0.1)(1\text{-}0.1)(1\text{-}0.1)\} = 0.343 \qquad (9.3)$$

The greater the number of potential failure mechanisms therefore, the larger the difference between the upper and lower bounds.

9.5.2 Influence of Galvanic corrosion parameters

It is apparent from Figure 9.8 that galvanic corrosion dominates the failure probability between 40 and 800 hours. For this reason it was decided to investigate the effect of varying galvanic corrosion parameters alone as in Figure 9.9, variation in the lower bound of $\mathbf{p_{sys}}$.

The lower bound is calculated from the system component most likely to fail (i.e. the largest value of p*), and follows the failure curve for galvanic corrosion for the range 40 to 800 hours. This implies that any measures that can be taken to control and reduce galvanic corrosion will have the greatest impact on $\mathbf{p_{sys}}$. Figure 9.9 shows that the largest $\mathbf{p_{sys}}$ values are obtained with a mean time to initiate corrosion of 36 months, with a mean corrosion rate of 76 mm/year, based upon 80% exposure to marine environment.

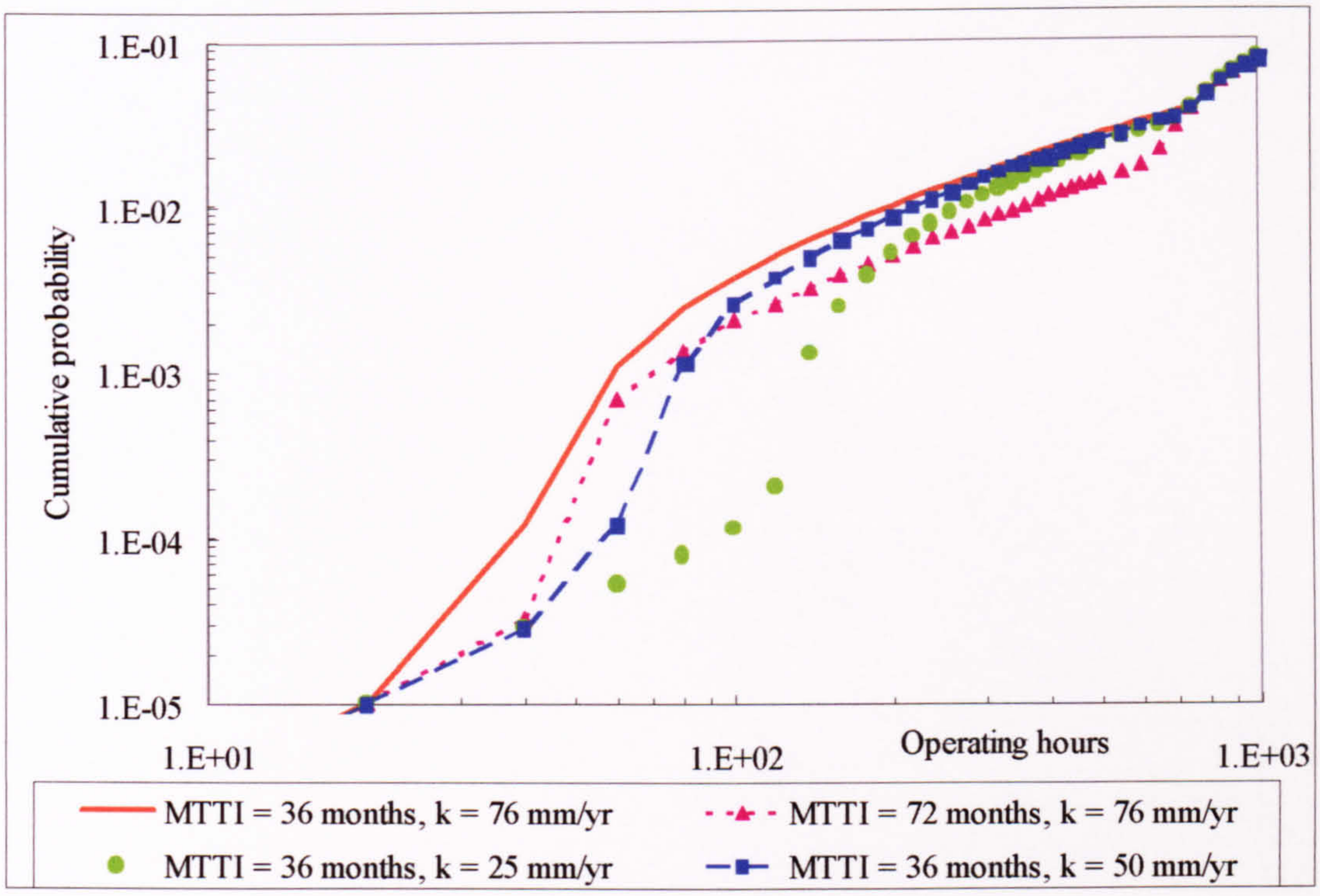

Figure 9.9 : Variation in Lower bound for System failure probability, as parameters of galvanic corrosion model vary (based on 500 hours/year)

It is interesting to note the effect of changing k_{mar} and MTTI at different $\mathbf{p_{sys}}$ values. Reducing k_{mar} (at fixed MTTI) has a greater effect in increasing life at lower $\mathbf{p_{sys}}$ values than does increasing MTTI. At higher values of $\mathbf{p_{sys}}$ (above 2E-03) the effect is reversed, see Table 9.4.

Failure probability p*	**Corrosion parameters**	**Increase in TTF**
10^{-4}	Reduce k_{mar} from 76 to 50 mm/year, MTTI = 36 months	50% (40 to 60 hours)
	k_{mar} = 76 mm/year, increase MTTI from 36 to 72 months	25% (40 to 50 hours)
10^{-2}	Reduce k_{mar} from 76 to 50 mm/year, MTTI = 36 months	10% (200 to 220 hours)
	k_{mar} = 76 mm/year, increase MTTI from 36 to 72 months	100% (200 to 400 hours)

Table 9.4 : Results from variation of Corrosion parameters

This is significant as it will indicate what effort should be made to increase MTTI or reduce k_{mar}, dependent on the required $\mathbf{p_{sys}}$*. Improvements in predicted life at lower $\mathbf{p_{sys}}$* values ($<10^{-3}$) are best obtained by reducing MTTI, whereas above 10^{-3}, reduction in k_{mar} have greater effect, for the values illustrated. However, a reduction in k_{mar} is only possible by changing materials for the gearbox casing, an effective but costly action, at least in the short term. Increasing the MTTI by the use of greater, or more effective, protective coatings, improved maintenance techniques, may be a more achievable aim.

9.5.3 Baseline results Type A gearbox – Flight 110 spectrum

Figure 9.10 shows the increase in failure probability for the failure mechanisms in Type A gearbox with WE43 magnesium alloy casing. The results presented have been calculated using baseline parameters (Appendix E), under Flight 110 loading. As in Figure 9.8 a value of 90% POD has been used in order to plot all failure mechanisms on the same time axis. The only failure curve for bearing contact fatigue shown is that for bearing 4, that with the lowest L_{10} life.

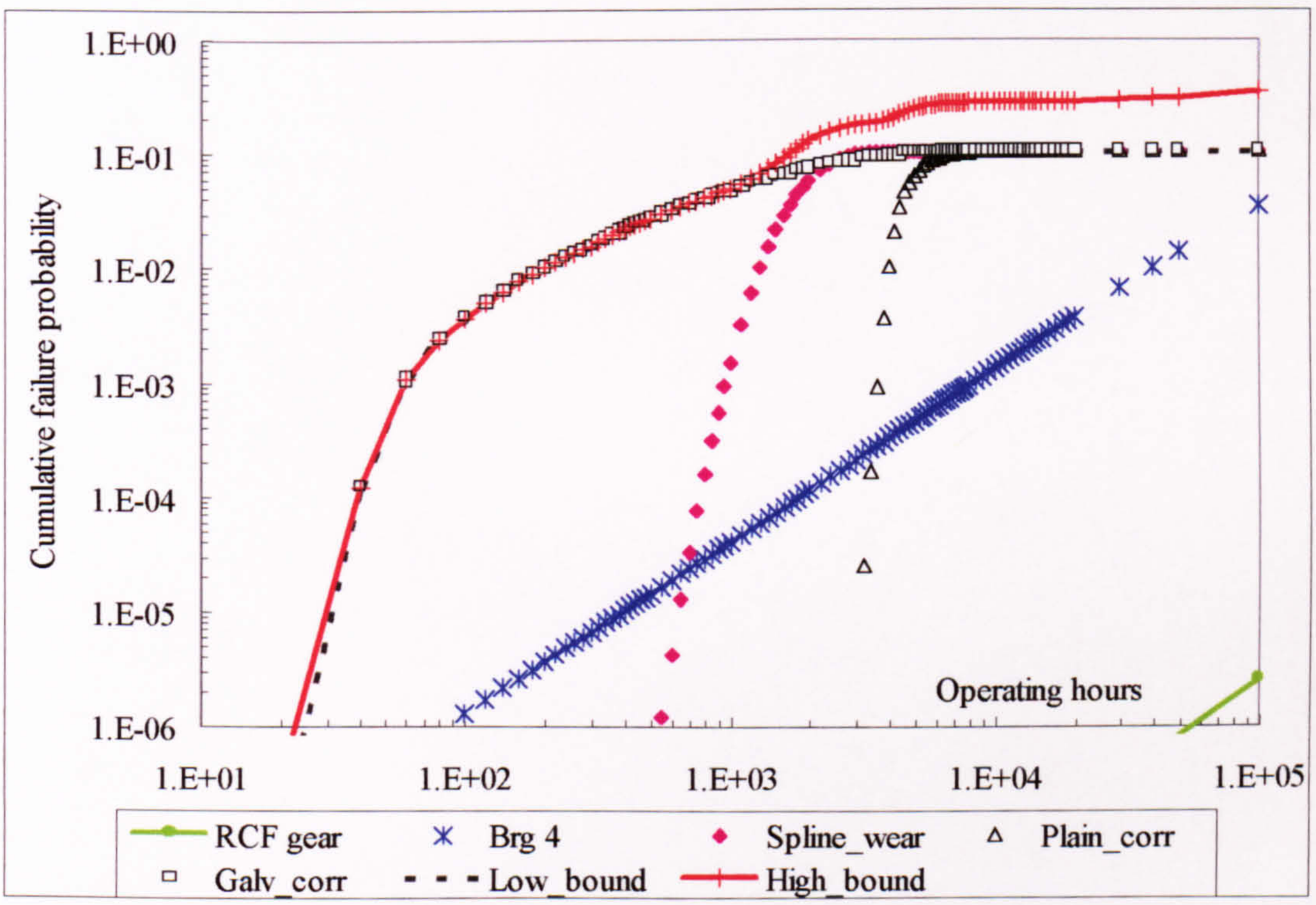

Figure 9.10 : Summary of system reliability for Type A gearbox, with Flight 110 spectrum and WE43 casing

By comparison with Figure 9.8, the first point to note is that the curve for tooth root bending fatigue does not feature on the new graph. This is because the loading in Flight 110 is less severe than ASW history, and the resultant torque values lie beneath the endurance limit at the respective p* values. In a similar way, the curves for gear and

bearing RCF are 'shifted' to the right due to the lower torque values. At p* of 10^{-3}, the bearing life is 8500 hours, compared to 440 hours for ASW history.

The material and wear coefficient values are the same in Figure 9.8 and Figure 9.10, so the increase in life is due solely to loading differences; the mean predicted spline life increases by a factor of 2.4 (410 to 980 hours), at p* of 10^{-3}. This indicates that loading is less significant in defining wear lives than are wear coefficient and slip amplitude, see Sections 8.7 and 8.8.

The dominant failure mechanism is that of galvanic corrosion again, since the corrosion rate employed for WE43 is the same as that for AZ91C in Figure 9.8. However, the plain corrosion rate of WE43 is significantly less (0.76 mm/year compared to 6 mm/year). The expected life is therefore increased, by a factor of 7.5 (490 to 3700 hours) at p* of 10^{-3}.

The failure curves all reach a maximum value of 0.1, since the POD is set to 90%, with spline wear being the first to reach this value. The upper and lower bounds of $\mathbf{p_{sys}}$ are close together for significant periods, 40 to 1300 hours. This is more pronounced than in Figure 9.8 since galvanic corrosion predominates over a greater range of life; it is not until 1500 hours that the probability of failure by spline wear begins to influence the upper bound. Thereafter the two bounds diverge as the contributions of spline wear, plain corrosion and bearing contact fatigue assume greater significance.

9.6 System Reliability of Type B gearbox

Results are presented for the Type B gearbox, using two load data files, namely Prototype spectrum and Civil spectrum, both defined in Appendix E. A value of 90% POD has been applied to all failure mechanisms.

9.6.1 Baseline results Type B gearbox - Prototype spectrum

Figure 9.11 shows the increase in failure probability with time for different failure mechanisms in the Type B gearbox with A357 casing and the Prototype spectrum. Results have been calculated using geometrical, material and loading data in Appendix E. The usage rate is 500 hours/year, which has been used in order to plot equivalent time to failure for plain and galvanic corrosion of the gearbox casing. However, the material in this example is A357 aluminium alloy, the plain and galvanic corrosion rates of which are less than 1mm/year.

From initial operation, the system reliability is dominated by RCF for bearing 2, which is predicted to be the most likely component to fail up to 700 hours. This is due to the high loading contained in Prototype spectrum, and the local stresses on this bearing at the gearbox input stage. From initial operation to the 200-hour point, the next most likely failure mechanisms are bearing RCF of bearings 1, 3 and 4 (all close together) followed by gear RCF. These plots have been obtained by extrapolating the two-parameter Weibull equation, and the confidence bounds are likely to be very wide at these low p* values.

The curve for spline wear is noticeably steeper than the curves for fatigue. This is because the distribution of times to failure by wear is based on a probability distribution of slip amplitude; the worn volume is assumed to be directly proportional to slip amplitude in the model.

Tooth root bending fatigue also features on the graph, with a predicted TTF of 500 hours at p* of 10^{-6}, rising to 2300 hours at p* of 10^{-3}. This is a low life for an intermediate gearbox, but is due to the use of an overly conservative torque spectrum, applied for a prototype. This also applies to the over fatigue models, which are highly sensitive to the torque load. A load spectrum that is more representative of in-service loads was used in Section 9.6.2.

The casing of aluminium alloy is less susceptible to corrosion than is magnesium alloy, and does not feature significantly in system reliability calculations. Galvanic corrosion does not feature on the graph until 4000 hours, and the predicted life at p* of 10^{-3} is 9300 hours. The corresponding life for plain corrosion is 12500 hours.

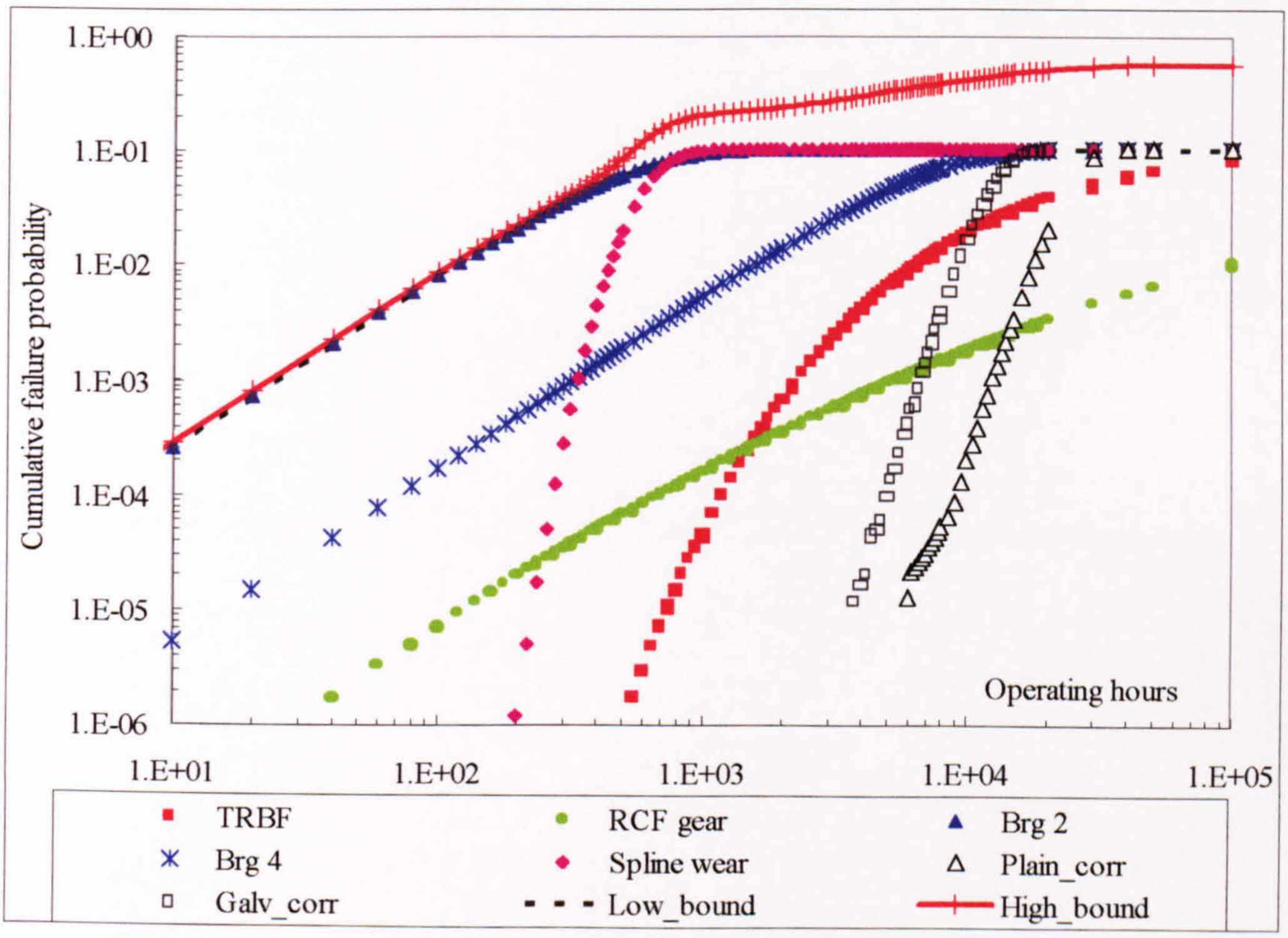

Figure 9.11 : Summary of system failure probability for Type B gearbox, with prototype torque spectrum and A357 casing

The system failure probability (p_{sys}) reaches a maximum of 0.1 at 1200 hours, its lower bound being dictated by the probability of detection. Up to 450 hours, there is little to distinguish the upper and lower bounds, since the values are dominated by bearing 2

RCF. After this point the failure probability of spline wear makes a greater contribution. This, together with the other failure mechanisms, causes the upper bound of $\mathbf{p_{sys}}$ to tend to 0.5, see equation 9.3.

9.6.2 Baseline results Type B gearbox - Civil spectrum

Figure 9.12 shows the increase in failure probability with time for the Type B gearbox with loading taken from the Civil torque spectrum. Results have been calculated using geometrical, material and loading data in Appendix E. The usage rate is 500 hours/year, with corrosion parameters used for the A357 casing.

Compared to the Prototype spectrum, bearing 2 RCF is again the dominant failure mechanism up to 3000 hours, since it is the mostly highly loaded in this particular gearbox design. After this point in time, spline wear becomes the most likely failure mechanism to occur. This is significant when compared to Figure 9.11, since it shows that spline wear assumes a greater significance than fatigue mechanisms when loading is reduced. This other wear parameters, slip amplitude and wear coefficient have been held constant.

Tooth root bending fatigue plays a less significant role in this case compared to Figure 9.11, due to the lower torque levels in Civil spectrum. The other failure mechanisms (bearings 1, 3 and 4 contact fatigue and gear tooth RCF) are still present, but appear later on the graph for the same reason.

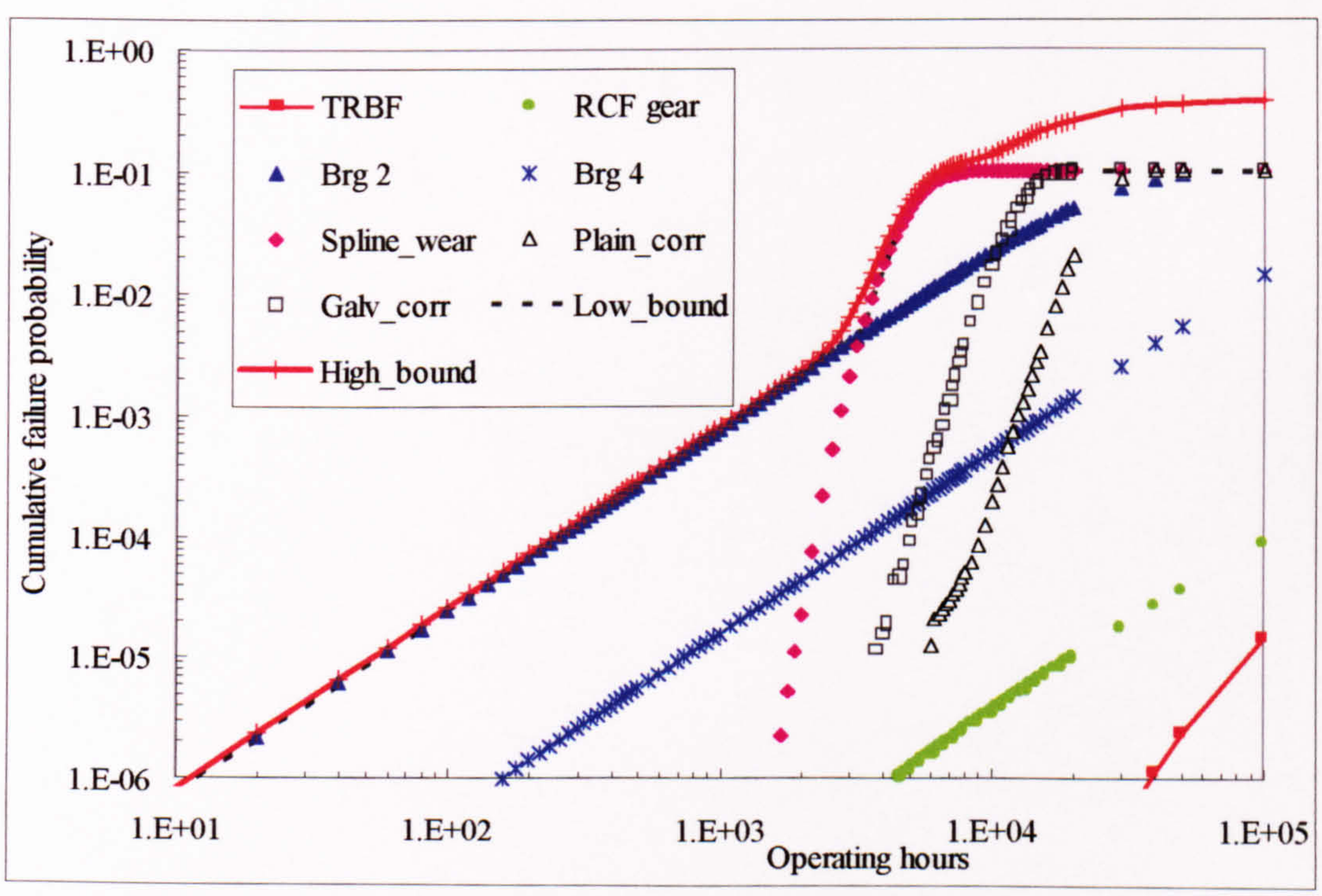

Figure 9.12 : Summary of system failure probability for Type B gearbox, with Civil spectrum and A357 casing

9.7 Comparison of System Reliability Results

Direct comparisons may be made between the system reliability results from the four system graphs. Even with a limited set of results, it is possible to observe characteristics of system reliability that would be common to other gearboxes.

- Type A, ASW history — Figure 9.8
- Type A, Flight 110 — Figure 9.10
- Type B, Prototype spectrum — Figure 9.11
- Type B, Civil Spectrum — Figure 9.12

The corrosion results have been plotted on the same axis as fatigue and wear results, assuming a usage rate of 500 hours per year. This is a good working value for a military helicopter, but is low compared with civil types, e.g. North Sea operations. Hence, the corrosion curves would be shifted to the right if the usage were greater than 500 hours. If p* was 10^{-4} at 100 hours (usage 500 hours), then the same p* will be reached at 200 hours.

For a gearbox with a magnesium alloy casing, it can be seen that the first maintenance priority is the integrity of the protective coating, and the prevention of galvanic action between the casing and the steel bolts used to mount the gearbox to the airframe. In Figure 9.8, the galvanic corrosion is the cause of the steep rise in system failure probability, p_{sys}* to a level of 10^{-3} after just 60 hours. This is particularly noticeable from the results of applying recorded data (Flight 110) to the Type A, Figure 9.10. This load spectrum contains far lower torque levels, so that and tooth root bending fatigue and RCF models do not contribute to system reliability.

The comparison between the two figures for the Type A gearbox shows the relative insensitivity of spline wear to load. The ASW history applied in Figure 9.8 is an overly conservative (i.e. high) set of loads when compared with the recorded data for Flight 110 in Figure 9.10. Despite this fact, the estimated life for spline wear varies by a factor of approximately 2. By comparison, the estimated bearing life increases 20 times. If the wear coefficient, hardness and or slip amplitude were to be changed, this would have a much larger effect on increasing life.

The corresponding pair of graphs for Type B (Figure 9.11 and Figure 9.12) shows the effects of high loading (Prototype design) versus in-service measured loads (Civil spectrum). The fatigue and wear models dominate the system reliability, because the galvanic corrosion rate for the casing material (aluminium alloy) is an order of magnitude less than that for magnesium alloy (Type A). The decrease in load has a larger effect on spline wear than for Type A (a five-fold increase in life) compared to the increase in fatigue life (40 times reduction for bearing RCF. This is purely due to the difference in loads and geometry between the two gearboxes.

The display of the four figures gives an example of how the system model can be used in the analysis of reliability of the transmission system. Changes in material, loading, geometry and environment can all be viewed to determine their inter-relationship.

10 Discussion

10.1 Approach

This thesis has described work to develop and apply techniques to represent the damage mechanisms relevant to a helicopter intermediate gearbox. The models that have been developed and applied are specific to the components of the single-input, single output transmission. Nevertheless, the method could be expanded to encompass additional components and failure mechanisms, depending on the availability of material, load and geometrical data. The results generated by the models have also been used to draw general conclusions relating the mechanical transmission systems in general, rather than the intermediate gearbox in particular.

The approach adopted in this work is an improvement upon existing techniques, which make use of historical data to predict future serviceability; the 'actuarial' approach. The latter assumes that the failure rate is constant with age, and is widely used for Fault Tree and FMECA analyses. The actuarial approach cannot easily account for changes in future use of equipment or newly designed systems. When failure data is available, it rarely includes pertinent information regarding the environmental and load factors that lead to the failure. If failure data were plentiful, this would imply a weakness in design, which should have led to a design change **[Sidaway, 1999].**

The HGBR models developed in this work are reliant on design data for material, loading and geometrical parameters. They are therefore much more useful than FMECA and Fault Tree analyses in showing the key parameters that affect component degradation. It is also possible to estimate the reliability of new designs and the effect on reliability of changes in future use of equipment.

10.2 Definition of System to be modelled

10.2.1 Failure Data and Identification of Failure Mechanisms

The failure mechanisms present in the gearbox have been identified from literature review, in addition to data from manufacturers and maintenance organisations. Useful data are also provided in the work of **[Astridge, 1996b],** who has created a database of all accident and incident records involving the rotor transmission system.

The records kept by maintenance organisations typically list the number of hours accumulated by the components and the types of damage sustained, e.g. pitting, corrosion etc. However, there is no record of the actual extent of damage, e.g. size and number of pits, depth and area of corrosion. Nor was there any information regarding the load or environment, which both play a significant part in damage accumulation rates. It was also found that many maintenance records recorded only the airframe hours, which often differs from component hours due to removal and re-fitting of gearboxes within helicopters.

Further information on the sources and limitations of maintenance data is given by **[Clarke and Lumbard, 1999]**, who have applied Weibull analysis and Monte-carlo simulation to predict failure patterns in a gearbox. The shortcomings of maintenance data are also highlighted by **[Astridge, 1999]**, and this data did not form part of the damage modelling for this reason.

The omission of details regarding the extent of damage restricts the use of failure rate data drawn from data banks kept by various agencies. However, the records are useful in showing the most frequently occurring failure mechanisms. For the specific gearbox studied (Type A), these are fatigue of the gear teeth and bearings, wear of the interconnecting shaft splines and corrosion of the gearbox casing. These failure mechanisms are also found to occur in other types of transmission system.

10.2.2 System Components and Boundaries

The methods used for defining the mechanical system are similar to those employed by **[Martin, 1980]** and **[Warburton, 2000]**. The latter applied a Failure and Degradation Influence Diagram to identify components, failure mechanisms, and their interdependencies.

The boundaries of the system are defined in order to put limits on the scope of the analysis. The components included in the system reliability model were chosen on the basis that they represented the key elements of the transmission system. These are the two meshing gears, the four supporting bearings, the shaft coupling splines and the casing. These components are the most frequently mentioned in maintenance records, as described in Chapter 7. They are also those components responsible for the transmission of torque, resistance of forces and containment, which implies that they are the most highly stressed parts of the gearbox.

Additional complexity in gearbox design will increase the level of analysis required. Typical modern designs of gearboxes include an oil pump, with the oil jets and oil ways to direct oil to and from rotating components. Such additional components could be added to the analysis, provided the loading and material data were available.

The effect of oil leakage has not been included within the system model due to the omission of damage models for the input and output shaft seals. The latter are mentioned frequently in maintenance records, 15% of EDA data, Chapter 7. Despite a substantial body of literature describing the mechanism in detail, e.g. **[Brink et al, 1993]**, this was considered inappropriate to the defining of a model to represent seal wear. The degradation caused by seal wear is particularly hard to examine as the seal is often damaged by the process of removing it from the shaft.

The likelihood of a rubber seal wearing, and thus allowing the oil contained to leak, depends upon a wide range of environmental parameters. Such a model would possess significantly complexity for a helicopter gearbox that is exposed to a variety of operational scenarios. Seals are also susceptible to damage at installation, an event for which no data exist. For the purpose of this work, it has been assumed that oil leakage

is detected during maintenance, such that it will not be considered as a failure mechanism in its own right.

10.2.3 Maintenance

Other failure mechanisms may be caused or exacerbated by errors in assembly and/or maintenance, which could increase the damage accumulation rates of the classical failure mechanisms. An example would be damage incurred to bearings when installed, which could give rise to stress concentrations and lead to premature fatigue and wear damage. Another example is an instantaneous failure mode caused by the accidental reversal of a thrust bearing during assembly **[Astridge, 1996a].**

Without test data, it is very difficult to accurately assess the correlation between the errors introduced by maintenance and resultant changes to model parameters (e.g. fatigue endurance limit). The maintenance errors considered in this work are therefore limited to those that affect, or initiate, spline wear and casing corrosion. This assumption may be justified by considering the rigorous quality procedures in place for the assembly and overhaul of gearbox components, and the accuracy of mechanical tolerances in manufacture.

10.3 Development of Damage Models

A substantial part of the present work was taken up by the development of damage accumulation models to represent fatigue, wear and corrosion. In the case of fatigue, the main part of the work involved adapting existing damage models to be used in the gearbox model. Damage models for wear and corrosion are fewer in number however, and work to build appropriate models took some time to complete.

10.3.1 Tooth root bending fatigue model

The most widely used fatigue damage model, Miner's Law has been used to represent crack initiation in this work. This is partly to allow cross-checks to be made with current life calculations for the example gearboxes quoted. Material data for this failure mechanism has been provided by the manufacturer, as described in Chapter 6.

It would also have been possible to employ a fatigue crack growth model in order to represent the crack growth phase of the failure mechanism. However, this latter phase of the failure is not represented in this work since it forms only a small proportion of the total failure time. This is due to the fast crack growth rate in the highly loaded, high strength gear tooth root and surface **[Drago, 1988]**.

10.3.2 Gear tooth rolling contact fatigue model

Weibull models are generally applied for the failure data from gear RCF. Such data analysis is generally based upon a fixed loading regime, however, which means that any such Weibull probability distributions are of limited value. Due to the lack of experimental data for the gears in question, the industrial standard, AGMA 2003

[AGMA, 1986] was used to develop a rolling contact fatigue-life curve. This has led to the use of a medium to high value of data scatter, COV 15% for the baseline tests. Despite the lack of an explicit damage accumulation model, this did not appear to preclude the use of this technique in calculating system reliability. Clearly it would be better to base these predictions upon actual test data, but the standard employed is itself based upon experience of RCF tests.

10.3.3 Bearing contact fatigue model

Bearing contact fatigue has been represented using the Lundberg-Palmgren model **[Lundberg and Palmgren, 1947]**. The latter model is widely used by bearing manufacturers today. Consideration was given as to whether a two- or three-parameter Weibull distribution should be used to represent bearing RCF. A two-parameter distribution means the minimum life of a bearing is zero, whereas a three-parameter distribution would allow a minimum life to be specified, stated to be 5% of the L_{10} life **[Tallian, 1962]**, from laboratory tests. In this work it was decided to apply a two-parameter distribution; bearings fitted in the transmission system are exposed to a greater variety of adverse conditions that those in laboratory tests. A minimum life is therefore inappropriate in this case.

10.3.4 Wear Damage Model

A number of wear models are in existence, with a good summary provided in **[Halling, 1983]** but the level of confidence in such models does not match that for fatigue. The Archard wear equation employed in this program to model the wear of interconnecting splines has not been confirmed by experimental data. The model assumes that if the shafts are perfectly aligned, and adequately lubricated with no relative movement, there will be no loss of material via wear. This is very difficult to achieve in reality due to the high manufacturing tolerances required and the high loads transmitted by the shaft, factors that are not modelled explicitly.

The confidence limits attached to the model are those representing the state of knowledge about the wear coefficient, which is assumed to be normally distributed. The uncertainty that exists for the wear coefficient, slip amplitude and local loading means that the model results will have wide confidence bands.

The wear of splined couplings is of great interest due to their widespread use throughout industry. Research is ongoing to evaluate the factors affecting wear, by performing laboratory tests of shaft spline couplings **[Olver et al, 1999]**, together with finite element (FE) modelling **[Adey and Taylor, 1999]**. It is considered that this may offer greater insights into the wear damage accumulation process in the future.

10.3.5 Corrosion Damage Model

Few models exist to represent corrosion damage due to the large number of variables that influence the corrosion rate. The modelling of corrosion damage has been conducted using a model with a random initiation (first stage) followed by a linear

damage growth (second stage). The second stage employs corrosion rates published in the open literature based upon the environment in which the gearbox operates, taken as marine (3.5% salt solution in atmosphere) and land.

The use of a linear corrosion growth law may be inaccurate due to the variability of the factors affecting damage growth, particularly for galvanic corrosion. The lack of knowledge of the contact area between the two metals and the amount of moisture present implies that a probabilistic method is more appropriate than a deterministic approach. These are the reasons behind the use of probability distributions to represent the corrosion parameters; the Normal distribution was chosen, but clearly others could be employed if test data became available for the particular materials involved. Despite its apparent simplicity, the relative performance of the corrosion model with different parameters has been assessed satisfactorily.

10.3.6 Uncertainty

The probabilistic approach taken implies that the results should be presented with a quantified measure of confidence. The different types of uncertainty are described below **[Melchers, 1992]** and are described in relation to the reliability model:

a) Physical uncertainty, which is due to a limited knowledge of the physical phenomenon to be modelled. This is present in all three model-types, fatigue, wear and corrosion, but is most significant for the wear model, where research into the exact nature of this failure mechanism is still under conjecture.

b) Physical model uncertainty, which describes the uncertainty caused by the use of simplified models to represent physical failure mechanisms, e.g. Miner's Law to represent fatigue crack initiation.

c) Statistical uncertainty, which is due to the use of simplified probability distributions applied to represent uncertainties of a basic variable, e.g. Normal distribution to represent uncertainty in the corrosion rate.

d) Prediction uncertainty, which is the uncertainty in the ability to predict the future state from existing data. This is considered to be another form of modelling uncertainty.

e) Human factor uncertainty, which describes the uncertainty surrounding human involvement in systems. The clearest example of this is the uncertainty caused by maintenance errors. Limited information is available on the impact of human factors on system reliability, and this has not been examined in detail.

f) Decision uncertainty, which is due to the uncertainty of whether a phenomenon has occurred or not. In the case of a transmission system, this is the probability of detection (POD) of damage. This could be classed as human factor uncertainty if manual inspection of were involved. If condition-monitoring sensors were involved, decision uncertainty would be a function of detection capability.

The above sources of uncertainty will all contribute to the uncertainty of the calculations in this work. However, one of the main purposes of the HGBR model has been to provide a means of comparison between different design and operational factors. It is therefore considered that relative differences between results will still provide a robust means of determining the key parameters of interest.

10.4 Development of System Reliability Model

10.4.1 Combination of diverse failure mechanisms

The novel feature of the system reliability model is the combination of both functional failure and 'non-instantaneous' failure mechanisms, previously referred to as progressive failure mechanisms (PFM). The calculation of system reliability must be based on a consistent definition of the failure condition or 'failure state'. It would not be acceptable to attempt to calculate system reliability using outputs from models having different failure criteria.

The criterion used in the case of the gearbox system reliability is 'functional failure of the gearbox to operate'. This is judged to be the most useful and convenient, since it allows a measure of the effectiveness of damage detection to be included. However the individual failure models use the following damage limits:

a) Tooth root bending fatigue - Miner's sum of unity, the point at which a micro-crack is predicted to develop into a macro-crack, normally about 1mm in length.

b) Gear tooth RCF - Time for first spall to develop, normally with a size threshold 1.58mm diameter by 0.2mm depth **[AGMA, 1986]**.

c) Bearing contact fatigue - Time for first spall to develop, normally with a size threshold 6 mm^2 area **[TIMKEN, 1994]**.

d) Shaft spline wear - Limit of worn material 25 mm^3, an indicative value chosen for this example.

e) Casing corrosion - loss of section of 5mm, an indicative value that depends on the location of the corrosion. The section thickness varies for different areas of the gearbox, so the permissible loss of section will vary.

As stated in (a) above, the output from the TRBF model predicts the time at which the damage sum reaches unity according to Miner's damage summation. This is considered to be the point of functional failure. The other damage models - (b) to (e) above - provide predictions of the time for a threshold of damage to be reached, which could lead to functional failure if left to continue into the future. The times to failure (TTF) and times to first spall (TFS) must therefore be adjusted so that an overall figure for statistical life of the transmission system can be obtained.

In the case of PFM a functional failure could occur if the HM system failed to detect the level of damage present. As described previously, the POD is combined with the probability of degradation occurring:

$$p(FF) = p(\text{damage threshold reached}) \times p(\text{damage undetected})$$

$$= p(PFM) \times (1 - POD) \qquad (10.1)$$

10.4.2 System reliability bounds

The helicopter transmission system under consideration, the intermediate gearbox, is generally agreed to represent a series, single-path, system with no redundancy **[Astridge, 1996; Savage et al, 1988]**. Failure of any one component will cause failure of the system as a whole. However, different results for reliability are obtained depending on the inter-actions between the different components within the system. A series of strictly independent components (Loading Roughness LR = 0) would require the use of the 'product rule' where all the reliability values are multiplied together to find the system reliability.

If the system is subject to infinitely rough loading (LR = 1), when there is a wide range of loads and the strength has one unique value, then the system reliability will equate to that of the least reliable part. With an intermediate value of loading roughness, the system reliability will lie between these two values, as follows:

$$\prod_{i=1}^{k} R_i < R_{sys} < R_{min} \qquad (10.2)$$

where $\prod_{i=1}^{k} R_i = R_1.R_2.R_3...R_k$,

R_i is the individual unit reliability and

R_{min} is the individual reliability of the first unit to fail

This work concurs with the proposition of Astridge **[1996b]** who suggests that the loading roughness (LR) will tend to 1 for a helicopter transmission system. This is because the high manufacturing tolerance implies that the strength distribution will be narrow in comparison to the wide range of loads and manoeuvres that form the stress distribution.

10.4.3 Independence of failure mechansisms

In this work, the models of failure mechanisms operate independently of one another. The prediction of system failure has been based upon the results from individual failure models. This implies that any possible interaction and inter-dependency between failure mechanisms has been ignored. An example of this would be damage caused by debris released due to gear RCF being transported via the lubrication system to one of the bearings, thus causing bearing wear.

Consider T_1 as the time at which the damage limit is reached for one of the mechanisms (e.g. bearing contact fatigue) and Δt as the time between this occurrence and a functional failure due to its influence on another mechanism (e.g. gear teeth RCF). For the purpose of this study it is assumed that

$$T_1 >> \Delta t \qquad (10.3)$$

This is justified because of the rapid progression of failure mechanisms from initiation to functional failure, as in Section 10.4.1 **[AAIB, 1997]**. The proportion of time or cycles spent in the propagation of the failure is considered much less than that spent in the initiation phase.

The overall assumption is that the transmission will fail to function very quickly once the damage threshold has been exceeded. There is little to distinguish between the time to failure (TTF) due to one failure mechanism alone, and the TTF due to the interaction of multiple failure mechanisms. This assumption is appropriate for the reliability prediction for the intermediate gearbox, but may be an over-simplification for larger, more complex transmission systems, e.g. the Main Gearbox (MGB). The larger system would typically have back-up systems, e.g. emergency lubrication **[Astridge, 1996a]**, which could increase Δt in equation 10.3.

10.5 Model Input Data Sources

10.5.1 Material data

The material data provided by the manufacturer has to be considered in relation to each failure mechanism. Material data for tooth root bending fatigue is available in some cases, when manufacturers perform tests to prove the gearbox design. However, such tests are limited to very few samples, due to the high cost of such trials. The scatter (COV) of data is normally estimated from trials with example populations of gearboxes, notably **[Cansdale & Tigwell, 1987]**. These data only relate to one particular gearbox design however; further research is needed to quantify the expected COV for more recently designed gears.

Less data was found for rolling contact fatigue of the gears; test results are normally presented in the form of a Weibull plot, for which the loading is fixed. Most gears and bearings are designed to internationally recognised standards, e.g. AGMA 2003 **[AGMA, 1986]**, which have been developed from experimental data. A S-N curve was taken from the aforementioned standard owing the lack of experimental data specific to the gear. However, the model will operate just as effectively using a curve fitted to experimental data.

Data for the specific bearings studied in this work were supplied by the manufacturer, who specify the dynamic capacity C_1 of each bearing. This is the load that would result in a L_{10} life of 10^6 cycles, and is a function of the bearing geometry, number of balls, rollers etc. The material variability is included in the Weibull slope used in the model, which is 1.5, representing an increasing failure rate, or 'wear-out' failure mechanism.

10.5.2 Loading data

Only fixed torque data were used in the HGBR model, so that the failure results are based on deterministic values. Loading variability has been introduced by changing the proportion of key manoeuvres manually off-line. An alternative approach would be to fit probability functions to the load data, and make use of Monte-Carlo simulation techniques, e.g. **[Moon et al, 1996]**. This has been considered, but considered impractical given the limited sources of measured torque data for this gearbox. Future work could include this activity.

Torque data for the Type A gearbox is extensive, the best being supplied from Operational loads Measurement (OLM) by QinetiQ. However, the torque values recorded were not related to manoeuvres, so restricting the future use of the data for investigating role changes, for example. Such an investigation needs to determine the different loading for a different set of manoeuvres – without torque data for these manoeuvres, it is not possible to assess this.

Data for the Type B was recorded for each manoeuvre, so providing a higher degree of confidence in the use of the loading information for reliability prediction. The Civil Spectrum took the form of 1650 torque values, each with a corresponding percentage occurrence.

10.5.3 Geometrical data

The HGBR developed will accept data for any design of single input-single output gearbox, where each shaft is supported by a pair of bearings. The geometrical parameters were held constant during the testing of the model; two data-sets were used (Type A and B).

The HGBR program does not allow for the consideration of variability in geometrical parameters. This is not considered to be a significant disadvantage, owing the small tolerances permissible in the gearbox. It should also be noted that errors in manufacture would be spotted quickly during assembly. An example is the check of gear mesh patterns which takes place to prevent and misalignment of gears.

10.6 Results from Individual Failure Models

The HGBR program has been developed partly to enable sensitivity studies to be conducted to determine the key parameters within the failure models. The individual failure models were used to measure the influence of:

- Material variability; the choice of alternative materials and alternative manufacturing techniques.
- Loading variability; the difference in loading regime and occurrence of damaging manoeuvres

- Spline wear parameters – wear coefficient and slip amplitude.
- Corrosion model parameters – corrosion rate and time to initiate.

10.6.1 Material Variability Studies

Material variability studies were conducted using the models for tooth root bending fatigue (TRBF) and gear RCF. The results from the TRBF model showed the influence of the endurance limit (T_{inf}) and the scatter factor (COV) of the T-N curve on the predicted TTF.

For a lower p*, reducing the COV gives a proportionately greater improvement in life than increasing mean strength. There is less differential at a higher p* since reducing the COV, or standard deviation of the strength distribution, has a greater effect in the 'tail' of the distribution for lower p*. Depending on the value of p* required, there exists a balance of merit between reducing the coefficient of variation (COV) of the material and increasing its mean strength (T_{inf}). This type of information would allow a designer and manufacturer to decide whether to make improvements to achieve higher levels of material homogeneity or specify a new material or manufacturing process.

Similar conclusions may be drawn from studies of gear tooth RCF. Due to the absence of test data, input parameters have been based on data from industry standards. For this reason, a COV of 15% was used for the baseline tests. Since the material parameters were the same in both cases, the different results are entirely attributable to differences in the load spectra and gear geometry. The results showed that the Civil spectrum produces longer lives at corresponding p* for Type B than the ASW history for Type A. This is attributable to the different loading contained in the ASW history.

Due to the large level of variability on the data scatter (COV), an increase in load results in a significant decrease in TFS at small values of p*, e.g. 10^{-6} as above. This is normally deemed acceptable since gear tooth RCF is a progressive failure mechanism, the evidence of which is detectable using HM techniques. Most useful for gear RCF is oil debris monitoring, although vibration monitoring could aid the detection of degradation of the gear tooth surface.

The gear RCF results indicate the trade-off between the two parameters depending on the p* desired. Due to the large COV of 15% already used in this model, reducing the level of scatter would be the best way to increase predicted TFS for low failure probability.

10.6.2 Results from Spline Wear Studies

The results from the spline wear model were generated by using a log-normal probability distribution for slip amplitude and a Normal distribution for wear coefficient (K). The graphs in Chapter 8 showed the mean time to failure (TTF) where the latter represents the time for a certain volume of material to be lost due to wear. This was set at 25 mm^3, as an example, but could be changed for any future tests. This arbitrary

setting of the failure criterion result in the under or over-estimate of the TTF for spline wear, but the results are useful in showing the relative influence of parameters.

The model based on the assumptions that slip amplitude and wear coefficient K are correlated with TTF in a linear manner. It is suggested that it is easier to reduce K by proper lubrication, rather than reduce the slip amplitude in the same proportion. The slip amplitude is dependent on the geometry of the splines and the accurate assembly and setting-up of the shaft. Due to the small tolerances and accuracy of manufacture it is considered that reductions in slip amplitude are unlikely; reducing the wear coefficient by lubrication and/or increasing the material hardness are more likely strategies for reducing wear.

10.6.3 Results from Loading Variability Studies

To investigate the effect of load variability, the Civil spectrum was utilised since it contains the greatest level of detail regarding torque values, and states recorded manoeuvres against these torques. The proportion of torque values within each manoeuvre was kept constant, and the proportion of manoeuvre within the load spectrum was varied between 0.1% and 2%.

The differences is the fatigue life results may be explained with reference to the Magnitude Occurrence Spectrum (MOS) for manoeuvres 2, 12, 13 and 5, Chapter 8. Manoeuvre 5 (spot turn port) contains torque values in excess of 1900 Nm for more than 20% of the manoeuvre, which explains the large influence on the time to failure by tooth root bending fatigue. Manoeuvres 12 and 13 contain torque values that are above 2000 Nm, but these make up less than 3% of the total spectrum. The effects are highlighted by calculating the actual damage content of each manoeuvre as a proportion of the flight spectrum as a whole.

The analysis of the individual manoeuvres at p* of 10^{-6} (Appendix E.3.5) showed that Manoeuvre 5 contributes 71% of the total tooth root bending damage for the spectrum. This is the reason it has such a large influence on the TTF. Manoeuvres 12 and 13 are responsible for 22.2% and 6.8% of the total tooth root bending damage respectively. The dominance of manoeuvres 5, 12 and 13 for tooth root bending fatigue is due to the fact that these are the only manoeuvres with torque above the endurance limit at p* of 10^{-6} and above. In the case of gear tooth RCF and bearing contact fatigue, all loads cause a finite amount of damage. Manoeuvre 12 is more influential on predicted bearing life than Manoeuvre 5 due to the power law used in the Lundberg-Palmgren model for bearing life.

10.6.4 Over-torque events

The size and occurrence rate of over-torques have a significant effect on the predicted fatigue lives for tooth root bending and gear tooth RCF. The investigation with over-torques showed little effect on bearing RCF and shaft spline wear however; the latter is dominated by the slip amplitude and wear coefficient K.

The variation in the size and occurrence rate of over-torques has a greater proportional effect on TRBF than on gear and bearing RCF. This is because for TRBF, many loads contained in the spectrum will fall beneath the endurance limit (T_{inf}). This is in contrast to RCF, where all loads contribute a finite amount of damage (Chapter 4), since no endurance limit exists. Hence an over-torque will form a larger proportion of the total damaging loads for TRBF, than it would for RCF.

The effect of the over-torque frequency on tooth root bending fatigue has been demonstrated in Chapter 8. A frequency of 0.0056% (one over-torque of two second duration every 10 hours) contributes 65% of the total damage, close to the 71% proportion of damage contributed by spot turn port. The proportional effect of over-torques is far less marked for gear tooth RCF and bearing contact fatigue, for the reason stated above.

Changes in the load on the gearbox were found to have a proportionately smaller effect on wear than on the fatigue models. This is partly because all loads transmitted via the shafts will contribute to wear, given finite slip amplitude and wear coefficient. The addition of short duration, large values of torque to the spectrum have a proportionately smaller effect than they do in the case of fatigue, particularly tooth root bending. In the latter case, many loads are beneath the endurance limit and are therefore non-damaging.

10.6.5 Material variability vs Loading variability

Comparisons have been made between the proportional effect of varying material properties and loading spectrum for each failure mechanism, for a p* of 10^{-6}. The breakdown of the flight load spectrum shows that the relative occurrence of individual manoeuvres is very influential on the TTF or TFS. The role and usage of the helicopter will therefore play a large part in the evaluation of life and emphasise the need for accurate usage monitoring (UM). UM data could be used to determine whether or not the gearbox loading was above or below the design spectrum and thus calculate any extension or curtailment of maintenance checks and/or component replacement. This is particularly true for tooth root bending fatigue, which is highly dependent on loading.

This work was limited to examination of tooth root bending fatigue for Type B gearbox with Civil spectrum, with changes in manoeuvres 5 and 12 being evaluated against material COV increments. It was found that a 2% decrease in material COV has a greater effect on increasing predicted TTF, than a significant reduction in manoeuvre 12 from 2 to 0.1%. However, reducing the proportion of the more damaging manoeuvre 5 from 2 to 0.1% achieved a larger increase in life that decreasing material COV by 2%. This highlights the options available for increasing life, and it is suggested that reducing the load torques is the most achievable option.

10.6.6 Casing Corrosion

The key parameters in the corrosion model have been varied to determine their effect on estimated time to failure. The variation of the proportion of time spent in the marine environment has a larger effect on galvanic corrosion than on plain corrosion. Typically a Magnesium alloy gearbox casing could be expected to last 10 times longer with no

exposure to marine air than with 80% exposure at failure probability of 10^{-3} (Chapter 8). This is to be expected with the high corrosion rates for galvanic corrosion of Magnesium alloy in contact with the steel mounting bolts in the presence of an electrolyte. This emphasises the importance of protective treatments on the casing to prevent the initiation of corrosion.

Other significant parameters are the mean time to initiate corrosion, which is determined by the integrity of the protective coating and any maintenance errors. The MTTI determines when corrosion will begin, after which the time to failure is governed by the (linear) corrosion rate and the maximum allowable corrosion limit.

10.7 System Reliability Results

10.7.1 General

Considering the system as consisting of independent units (product rule – upper bound) and as dependent units (lower bound) enables the plot of the upper and lower bounds of the system failure probability to be drawn. The graphs of the system reliability of the four cases show the advantages of displaying all failure mechanisms together. Although there may be significant confidence bands on certain parameters, the plot shows the relative position of the mechanisms with respect to each other. This could then be used as a design criterion to determine the optimum maintenance interval and to investigate ways to reduce failure probability without increasing other costs.

The accuracy and detection capability of health monitoring is crucial to the combination of the failure mechanisms. The cumulative probability of detection value used was varied in the trials conducted, and could be calculated as in Chapter 5 for current HM techniques. The system reliability calculations were performed with an indicative value of 90% POD. In reality this value will increase as the damage defect increases, however the time from initial detection to functional failure is generally short, so a constant value is a reasonable assumption.

The corrosion results have been plotted on the same timescale as fatigue and wear results by assuming a usage rate of 500 hours per year. This is a good working value for a military helicopter, but is low compared with civil types. Hence, the corrosion curves would be shifted to the right if the usage were greater than 500 hours.

10.7.2 Contribution of fatigue

The output of the fatigue models (gear TRBF and RCF plus bearing contact fatigue) all play a significant part in the value of system reliability. TRBF is particularly dependent on load spectrum; it hardly features in the system reliability graph for Flight 110 and Civil spectrum, but is one of the main contributors when the loads are greater. The POD of 90% was applied to TRBF for the purpose of calculating system reliability. However, this failure mechanism is one the most difficult to detect, since it produces no 'tell-tale' debris during crack initiation **[Collier-Marsh and Astridge, 1985]**. If the POD were to be zero, gear TRBF would play a far greater role in limiting the system

reliability; the failure curve would rise by a decade, i.e. p* of 10^{-4} becomes 10^{-3}, since (1-POD) = 10%.

10.7.3 Contribution of wear

The output of the wear model has demonstrated that the failure probability is largely determined by the wear coefficient and slip amplitude. Large temporary fluctuations in load, e.g. over-torques, do not have a significant effect on the TTF due to wear. However, this is a serious failure mechanism, which makes a large contribution to overall system reliability whenever the slip amplitude is non-zero. Changes in the latter and wear coefficient/ material hardness have a large effect on TTF due to wear.

10.7.4 Contribution of corrosion

The corrosion model set up for the reliability prediction program has shown the large effect that corrosion damage has on gearbox reliability, e.g. for magnesium alloy casing. It is significant that when a lower corrosion rate is used (as for aluminium alloy casing), this almost removes corrosion from contributing to system reliability at all. However, this conclusion is influenced by the usage rate; a usage rate of less than 500 hours per year, although unlikely, would mean that corrosion would play a larger role in system reliability.

10.7.5 Inspection and Overhaul intervals

The results of the system reliability calculation have been obtained without reference to the overhaul of the gearbox. Components such as the bearings are normally replaced upon overhaul whereas the gears are reconditioned and replaced. Due to the lack of information about the effect of this reconditioning on the accumulated damage of the gears, overhaul has not been included in the model.

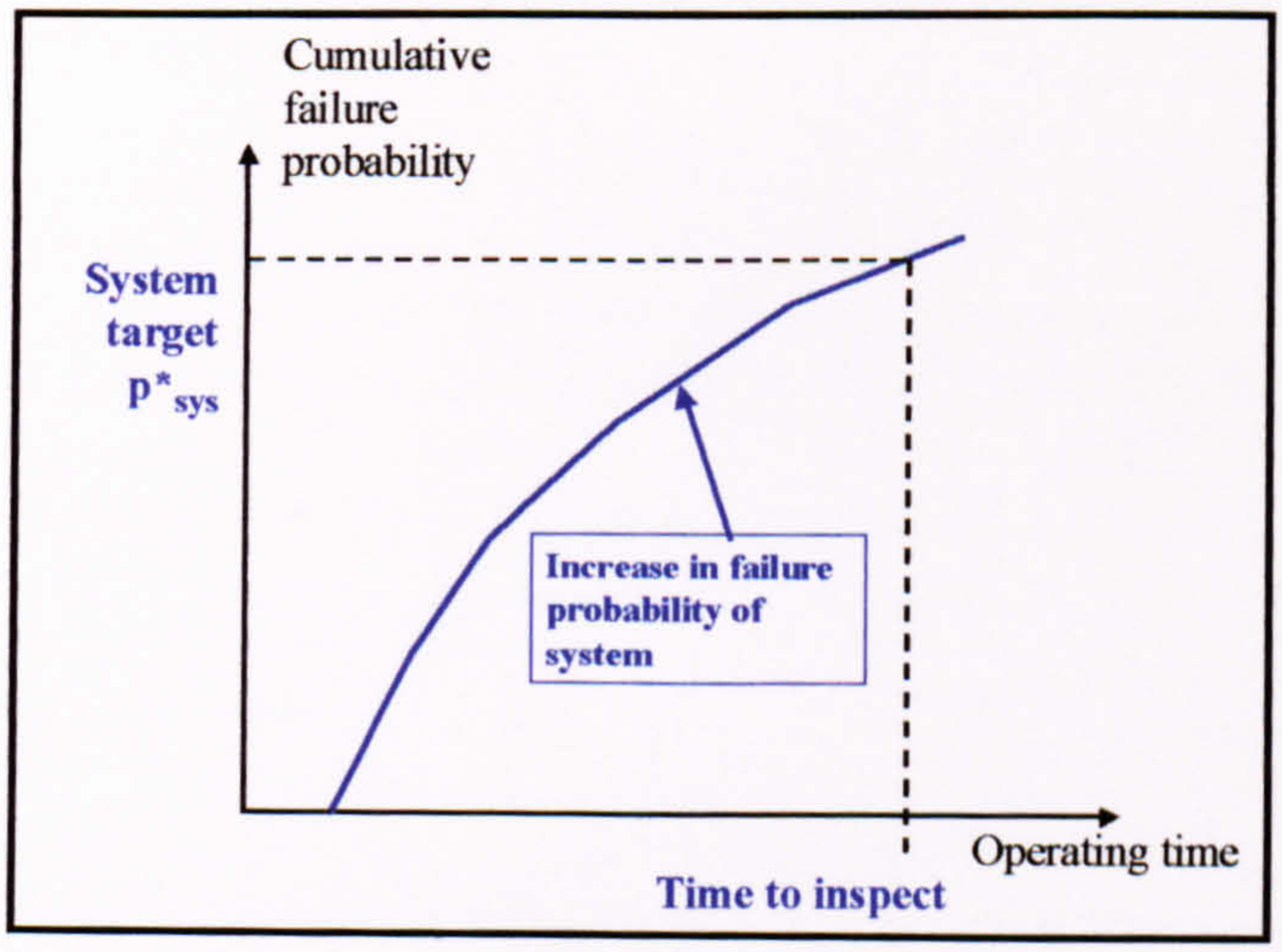

Figure 10.1 : Definition of Inspection interval or TBO based on predicted system reliability

However, another use of the system reliability model developed in this work is the ability to derive a value for a suitable inspection interval or time between overhaul (TBO). The failure probability for the whole system is first calculated, as for the results in Chapter 9. When the upper bound of failure probability exceeds a *system target* for failure probability, the time is noted from the x-axis. This may then be used as a first iteration for setting an inspection interval or TBO (Figure 10.1).

10.8 Achievement of Objectives

The stated aims of this thesis were given in Chapter 1, and these are re-stated to judge the success of the work carried out.

10.8.1 Objective 1

To develop a computer based model to represent physical failure mechanisms in order to predict the reliability of helicopter transmission systems.

A computer program has been developed in Delphi™ language to implement the damage accumulation models proposed. These models represent damage accumulation due to fatigue, wear and corrosion, and calculate separately the predicted time to failure for different values of probability. Individual damage accumulation models were developed for the distinct failure mechanism that most affect gearbox reliability. In some cases these models were widely available, e.g. Miner's Law for fatigue, and in other cases new models were developed, e.g. corrosion. The models used are discussed in Section 10.3. A subsequent set of programs was developed in Microsoft Excel ™ for calculating the upper and lower bounds for system reliability. This procedure could also be incorporated into the same software program if desired.

The estimation of bounds was accomplished by choosing the time to failure and calculating the failure probability for each failure mechanism in turn. The results were then combined to estimate the upper and lower bounds, see Section 10.4.

To facilitate the operation of the model, the failure mechanisms were assumed to be independent. In reality this may not be the case due to the same underlying load, common material and environment, and the different damage mechanisms could interact with one another. An example is the debris from rolling contact fatigue being trapped between the intermeshing gear teeth and causing abrasive wear. The approximations caused by ignoring this interaction are deemed to be negligible for the following reasons:

- The failure criteria are set at a low level.
- Time for damage to initiate is far greater than the time from initiation for functional failure to occur, as discussed in Section 10.4.3.

10.8.2 Objective 2

To apply the model by predicting the reliability of a rotorcraft transmission system to test the methods used.

Chapter 8 gave results from sensitivity studies of the individual models, the purpose of which was to identify key sensitive parameters. The results showed several benefits of developing such models. The user of the program is able to vary geometrical, load and material parameters easily using the gearbox database, and display graphically the results from successive experiments.

The reliability model developed for this work provides a useful tool in the assessment of alternative designs for transmission systems. Alternative loading data can be used as inputs to the model to determine the effect of changing flight patterns, usage and/or manoeuvres on reliability. Alternative material parameters, with attendant values of variability, may also be assessed to view the impact on reliability. Such optimisation can be conducted:

a) For individual failure mechanisms, to determine the mean strength of material, and associated variability to meet the required reliability target.

b) For system reliability, to view the 'system' effect of changing the parameters of an individual failure mechanism.

The model has significant benefits over existing techniques. It allows the analyst to investigate the effect of varying load, material, geometrical and environmental parameters. This is a significant advantage over the method of **[Astridge, 1996b],** which is based upon the interpretation of historical accident data, and also **[Savage et al, 1988],** whose model is based upon the Lundberg-Palmgren model for gears and bearings in a series-chain model.

10.8.3 Objective 3

To investigate means by which condition monitoring information from the gearbox system can be used in the quantification of system reliability.

Data from HM techniques (Chapter 5) is suitable for fault diagnosis, and also, to a limited degree, prognosis, at the current state of development. However, no data were available with which to correlate the output from the various HM monitoring systems to the actual damage state. For this reason, further research is required to provide greater warning time prior to component failure and also to quantify the accuracy with which damage detection is made.

The best way of applying HM data to the system reliability calculation is that of combining the probability of damage occurring with the POD. This then allows the consequence of actual functional failure to be assessed. Results for the system reliability calculation were generated in this way.

The probability of detection by VHM has been estimated using a limited data-set from in-service HM systems **[McColl, 1997].** This produced a figure of 76.3% with a confidence level of 95%. POD values in the range 50 – 99% have been used in this work, Chapter 9.

10.8.4 Objective 4

To investigate the effect on reliability of the variability of material strength and input loading.

The results in Chapter 8 and 9 have been obtained using damage accumulation models that allow the modelling of uncertainty in key parameters to be included in the reliability prediction process. These include the material properties and load spectrum for the fatigue models, wear coefficient and slip amplitude for the spline wear model and all the corrosion model parameters. The insights that have been obtained from this approach are discussed in Sections 10.6 and 10.7.

The overall picture that has emerged is that both material and loading variability have a significant effect on fatigue models. The work conducted in this thesis has indicated that changes in load are generally more achievable than changes in material variability or mean strength. The latter are often determined by weight restrictions and manufacturing technique. However, while changes in helicopter role (e.g. ASW, SAR, North Sea operations), and hence manoeuvre mix, may be unlikely, the accuracy with which loading may be known could significantly increase fatigue life. An example is the use of a conservative load spectrum to calculate life. Once a helicopter is in service, measured loads may be used to replace design loads and thus extend life. An example of this is shown for the Type B gearbox, comparing Prototype spectrum with Civil spectrum.

11 Conclusions and Recommendations for Future Work

On the basis of the evaluation of existing techniques for reliability prediction for a transmission system, the following conclusions have been drawn:

- Existing reliability assessment techniques, e.g. Fault Tree Analysis, Failure Modes and Effects Criticality Analysis, provide good qualitative methods of assessing reliability. However, they may have limited usefulness in assessing reliability quantitatively since most often they assume a constant failure rate. In service failure mechanisms generally lead to failure rates that vary with age and environment.

- Only limited failure data exist for mechanical components for a transmission system. Such information that is available contains little detail of the environment in which the component operated or the exact failure mechanism.

- Statistics of gearbox maintenance data do not generally permit an analyst to pinpoint the exact failure mechanism (or combination of failure mechanisms), thus limiting the usefulness of the failure data recorded.

On the basis of the development of models for reliability prediction for a transmission system, the following conclusions have been drawn:

- The damage mechanisms within a system must be clearly identified before they can be modelled. Certain simplification was required in order to reduce the complexity of such models. This did not detract from the overall results for the quantitative predictions of the reliability.

- The program developed represents the principal failure mechanisms that are present in a transmission system, for a single input, single output shaft configuration. The models of fatigue, wear and corrosion, are generic in nature and could be applied to any mechanical system.

- Damage accumulation models are an effective way of representing the physical failure mechanisms in a gearbox. The mechanisms modelled for the intermediate gearbox are tooth root bending fatigue, gear tooth rolling contact fatigue, bearing contact fatigue, shaft spline coupling wear and casing corrosion.

- The computer-based models developed allow the representation of material, loading and geometrical parameters to predict a time to failure for a certain probability. This has provided a useful 'toolbox', which could be used by a manufacturer to evaluate design changes, a maintainer/operator to determine maintenance regime and a regulatory body to monitor different helicopter fleet reliability.

- Few damage models or data exist for wear and corrosion. There is therefore greater potential for further development of the failure models and understanding of uncertainty surrounding the wear and corrosion models.

- The models developed were based on a probabilistic representation of material variability. The input loading was assumed to be deterministic; load variability was introduced by manually changing values in the torque data set. This proved to be an acceptable approach, since torque data is more likely to be available than material data.

- Only limited qualitative data were found for the modelling of the wear of the radial lip seals. No damage accumulation model was used to represent this mechanism, or the consequential oil leakage. The assumption made was that evidence of this failure mechanism would be detected either before or after each flight, before it has any impact on system reliability or safety.

- Most failure mechanisms result in progressive degradation that could lead to a functional failure if undetected, e.g. rolling contact fatigue. However, tooth root bending fatigue could result in a sudden loss of function soon after a micro-crack has been initiated. The failure probability for tooth root bending fatigue must always be lower than that for rolling contact fatigue to achieve the same level of risk (frequency x consequence).

- Health monitoring of transmission components provides a warning as the point of failure approaches, which may be less than 50 hours. This may be satisfactory for the safety of the helicopter but does not give information as to the life consumed by rotating components.

- The estimation of system reliability has been carried out through the combination of the diverse failure mechanisms by using a common damage limit. This has been achieved by applying the probability of detection (POD) to all failure mechanisms.

- The upper and lower bounds for system reliability have been estimated by consideration of loading roughness, which relates to the ratio of spread of the load and strength distributions. The upper bound was calculated by considering only the weakest link, and the lower bound by considering all components acting independently.

On the basis of the work completed, the following conclusions have been drawn:

- The predicted values of life for tooth root bending fatigue and gear tooth rolling contact fatigue are highly dependent on both the mean and scatter of component strength. The higher the reliability required (smaller p*), the greater the relative merit of reducing the coefficient of variation (COV) compared to increasing the mean strength.

- The load spectra used in the model play a large role in the estimated life of the components and system. In the case of tooth root bending fatigue (TRBF), the presence of an endurance limit means that many loads are non-damaging. The same cannot be said of other failure mechanisms. The magnitude occurrence spectra (MOS) with the highest loads will therefore make a larger difference to TRBF than to other failure mechanisms.

- The largest influence of over-torques is on predicted life for tooth root bending fatigue, followed by gear tooth RCF, bearing contact fatigue, spline wear. This is because most manoeuvres in the spectrum are non-damaging for tooth root bending fatigue, so over-torques have a greater proportional effect than they do for gear tooth RCF, bearing contact fatigue and spline wear.

- The model predictions obtained match the precedence of the different failure mechanisms. At a failure probability of 10^{-3}, the system reliability of the Type A is dominated by galvanic corrosion, followed by spline wear, plain corrosion and bearing fatigue for typical recorded flight data. This similarity to actual in-service results has been achieved despite the lack of confidence in both wear and corrosion models.

- The estimated upper and lower bounds for system reliability lie close together for much of the region of interest. Fatigue failure mechanisms will determine system reliability when the torque loads are high, and are only exceeded by galvanic corrosion if magnesium alloy casing were used. Failure due to spline wear is largely dependent on wear coefficient and slip amplitude; where these parameters are non-zero, wear will feature in all system reliability calculations.

On the basis of this work, the following recommendations for future work have been made:

- Additional trials of the software should be conducted with application to other small mechanical systems. These should then be extended to assess the reliability of a main gearbox (MGB), with a greater number of components.

- Further research should be conducted into the failure models to represent the wear of radial lip shaft seals, and resultant oil leakage. This would then permit this model to be added to complete the gearbox system model.

- Further development of the models for spline wear and corrosion should be carried out to determine the need for additional parameters to be included. It is also essential to directly compare predictions from the model with experimental data for both failure mechanisms.

- Further investigation should be conducted into the transitions between 'benign', or gradual failure mechanisms (e.g. rolling contact fatigue) and the functional failures caused by the release of debris from such mechanisms. This would then allow a re-evaluation of the assumption to treat all models as independent.

- The reliability model should be applied to other mechanical systems, which are affected by wear, corrosion and fatigue or combinations thereof. The techniques adopted may therefore gain more widespread validation.

12. References

Air Accident Investigation Branch (1986). G-BWFC Aircraft Accident Report, DOT/ AAIB/AAR-2/88.

Air Accident Investigation Branch (1997). G-PUMH Aircraft Incident Report 2/98, EW/C95/9/4.

Adey R A, Baynham J W and Taylor J W (1999). Development of Analysis Technology for Spline Couplings. IN: *Institution of Mechanical Engineers Coupling and Shaft Technology for Aerospace Transmissions,* Institution of Mechanical Engineers seminar S676 Solihull.

AGMA (1986). *Rating the Pitting resistance and Bending Strength of generated Straight Bevel, ZEROL Bevel, and Spiral Bevel Gear Teeth.* ANSI/AGMA 2003-A86, American Gear Manufacturers Association.

AgustaWestland (1994). Design Document EA632S01A, Rev B.

AgustaWestland (1997). Type A IGB Reported Defects, MJS/CU.020.

AgustaWestland (1995). Spline Stressing and Wear Research to Develop a Comprehensive Design Capability – Survey of In-service Helicopter Splines Components. Mechanical Research Report MRR 20182.

Allsopp K (1997). Private Communication.

Amer K B (1988). A "New" Philosophy of Structural Reliability, Fail Safe Versus Safe Life – the 1988 Alexander A Nikolsky Lecture. IN: *44th Annual National forum of the American Helicopter Society.*

Ang A H-S & Tang W H (1984). *Probability Concepts in Engineering Planning and Design, Vol 2 - Decision, Risk and Reliability.* John Wiley & Sons

Archard J F (1953). 'Contact and Rubbing of Flat Surfaces'. Journal of Applied Physics Vol 24 No 8 pp 981-988.

Astridge D G (1989). Helicopter transmissions - design for safety and reliability. *Proceedings of Institution of Mechanical Engineers Part G Journal of Aerospace Engineering.* Vol 203 pp 123-138.

Astridge D G (1992). Safety Assessment of Transmission Health and Usage Monitoring Systems. IN: *Institution of Mechanical Engineers Safety Assessment for Transmission Systems Seminar.* Lucas Automotive, Solihull.

Astridge D G (1996a). Rotorcraft transmission design HUM requirements derived from design safety analysis. *Proceedings of Institution of Mechanical Engineers Part G Journal of Aerospace Engineering*, Vol 210 pp 271-279.

Astridge D G (1996b). Design safety analysis of helicopter rotor and transmission systems. *Proceedings of Institution of Mechanical Engineers Part G Journal of Aerospace Engineering*, Vol 210 pp 345-355.

Astridge D G (1997). Rotorcraft Transmission Health Monitoring Performance Matrix. IN: *Institution of Mechanical Engineers Rotorcraft Transmission System Health Monitoring - Experience Update Seminar*, London.

Astridge D G (1999). Current limitations of safety, reliability and maintainability data for aerospace transmission systems. IN: *Safety, Reliability & Maintainability Data for Aerospace Transmission Systems* Institution of Mechanical Engineers Seminar S677, London.

Astridge D G, Montano P and Vaccaro V (1993). Safety assessment of Helicopter Rotor and Transmission Systems. IN: *19th European Rotorcraft Forum*, Italy.

Augustin M J (1998). Specifying HUMS to meet Enhanced Safety and Reduced Operating Cost requirements. IN: *American Helicopter Society 54th Forum*.

Baker R F, Olver A V and Davies D P (1997) The Application of Laboratory Fretting Data to Wear of Splined Couplings. IN: *Advanced materials and processes for Aerospace Transmission systems*, Institution of Mechanical Engineers, Solihull.

Barlow R J (1989). *Statistics - A guide to the use of Statistical Methods in the Physical Sciences*, John Wiley & Sons.

Barraclough T G, Sperring T P, Roylance B J, Nowell T and Hodges D (1999). Generic-based Wear debris identification – the first step towards morphology classification. IN: *Condition Monitoring 99 – Proceedings of the International Conference on Condition Monitoring*, 12-15 April 1999, Swansea.

Bartz W J and Kruger V (1975). Influence of Lubricants on the Pitting Fatigue of Gears IN: *Source Book on Gear Design, Technology and Performance*. American Society for Metals, 1980.

Billinton R and Allan R A (1992). *Reliability Evaluation of Engineering Systems Concepts and Techniques*, 2nd Edition, Plenum Press.

Bogdanoff J L (1985). *Probabilistic models of cumulative damage*. John Wiley & Sons.

Bompas-Smith J H (1973). *Mechanical Survival: The use of reliability data.* McGraw-Hill.

Bompas-Smith J H (1967). The Determination of Distributions that describe the Failures of Mechanical Components. IN: *8th Annals of Reliability and Maintainability* p.343

Brink R V, Czernik D E, Horve L A (1993). *Handbook of Fluid Sealing*. McGraw-Hill.

Bristow J W (1985). 'Structural Integrity of Helicopters in relation to their Airworthiness'. International Journal of Aviation Safety. June 1985.

Bristow J W and Minter R (1999). The Meaning of Life. IN: *CEAS Forum on Life Extension - Aerospace Technology Opportunities*. 23-25 March 1999, Cambridge UK.

BSI (1994). *Reliability of systems, equipment and components Part 2 - Guide to the assessment of reliability* BS 5760: Part 2.

BSI (1991). *Reliability of systems, equipment and components Part 5 - Guide to failure modes, effects and criticality analysis (FMEA and FMECA)* BS 5760: Part 5.

BSI (1995). *Gears - Wear and damage to gear teeth – Terminology*, BS 7848/ISO 10825.

Bury K V (1975). *Statistical Models in Applied Science*, John Wiley & Sons.

Byington C S, Merdes T A and Kozlowski J D (1999). Fusion Techniques for Vibration and Oil Debris/Quality in Gearbox Failure Testing. IN: *Condition Monitoring 99 – Proceedings of the International Conference on Condition Monitoring*. 12-15 April 1999, Swansea.

CAA (1993). Helicopter Health Monitoring Operational Trials Review, CAA Paper 93002, Civil Aviation Authority.

CAA (1984). Report of the Helicopter Airworthiness Review Panel, CAP 491, Civil Aviation Authority.

CAA (1992). Report of the Helicopter Health Monitoring Maintenance Credit Working Group to the 17th Helicopter Health Monitoring Advisory Group, Civil Aviation Authority.

CALCE (1999), Computer Aided Life Cycle Engineering, University of Maryland, http://www.calce.umd.edu/ general/Facilities/failure.html (accessed 12 March 1999).

Calistrat M M (1980). Gear Couplings. IN: *Wear Control Handbook*, Ed Peterson M B and Winer W O, American Society of Mechanical Engineers.

Cameron B G and Stuckey M J (1994), A review of Transmission Vibration Monitoring at Westland Helicopters Ltd. IN: *20th European Rotorcraft Forum* Paper 116.

Cansdale R and Tigwell M G (1987). Fatigue factors as applied to the Testing of Helicopter Gearboxes. IN: *Testing of Aerospace Transmissions* Institution of Mechanical Engineers Seminar, June 1987, Derby.

Cansdale R (1984). A Note on the Derivation of Current UK Fatigue Scatter Factors, Royal Aircraft Establishment.

Carter A D S (1986). *Mechanical Reliability*, 2nd Edition, Macmillan.

Carter A D S (1997). *Mechanical Reliability and Design*, Macmillan.

Clarke P and Lumbard D J (1999). R & M Data Collection, Databases and Correlation with Usage. IN: *Safety, Reliability & Maintainability Data for Aerospace Transmission Systems* S677. Institution of Mechanical Engineers, 16 December 1999, London.

Coleman W (1969). Bevel and Hypoid Gear Surface Durability Pitting and Scoring IN: *Source Book on Gear Design, Technology and Performance*. American Society for Metals (1980).

Collier-Marsh M E and Astridge D G (1985). Operational Experience with the Advanced Transmission Health Monitoring Techniques on the Westland 30 Helicopter. IN: *11th European Rotorcraft Forum*, London.

Cooper P (1989), Rolling Bearing Failure and Wear Debris Detection – Final report NSK-RHP Bearing Research Centre.

Coy J J, Townsend D P and Zaretsky E V (1985). Gearing, NASA RP 1152, p34-40.

Crawford C (1999). HH-60G Mission Usage Spectrum Survey Methodology Overview, IN: *Workshop on Helicopter Health and Usage Monitoring Systems*, DSTO-GD-0197 Forsyth G F (Ed), Melbourne

Danford M D, Mendrek M J, Mitchell M L and Torres P D (1997). The Corrosion Protection of Magnesium Alloy AZ31B, NASA/TP-97-206239.

Davidson J (1994), *The Reliability of Mechanical Systems*, Institution of Mechanical Engineers.

Davies A E (1972). Principles and Practice of Aircraft Powerplant Maintenance. IN: *Transactions of Institute of Marine Engineers*, 14 March 1972, London.

Davies D P, Olver A, Baker R F and Medina S (1999). Fretting and Wear of Splined Couplings, IN: *Coupling and Shaft Technology for Aerospace Transmissions seminar* S676 Solihull, Institution of Mechanical Engineers.

Dawson P H (1965). Further experiments on the effect of Metallic Contact on the pitting of lubricated rolling surfaces, *Proceedings of Institution of Mechanical Engineers* Vol 180 Part 3B.

de la Mare R F(1980). A study of mechanical valve reliability, IN: *Symposium of Mechanical Reliability*, Moss T R (Ed), IPC Science and Technology Press.

Dickson B, Cronkhite J D, Bielefeld S, Killian L and Hayden R (1996). Feasibility Study of a Rotorcraft Health and Usage Monitoring System (HUMS): Usage and Structural Life Monitoring Evaluation, NASA CR-198447, DOT/FAA/AR-95/9.

Ditlevsen O and Madsen H O, *Structural Reliability Methods*, J Wiley & Sons (1996).

Drago R J and Lenski J W (1984). Special Power Train Requirements for the Next Generation of Rotary-wing Aircraft. IN: *AGARD CP 369 Gears and Power Transmission Systems for Helicopter and Turboprops* Paper 5.

Drago R J (1988). *Fundamentals of Gear Design*, Butterworths, USA.

Ebbeler D H, Newlin L E, Sutharshana S, Moore N R, Grigoriu M (1995). Alternative Computational Approaches for Probabilistic Fatigue Analysis. IN: *36th AIAA/ASME/ASCE/AHS/ASC Structures, Structural Dynamics and Materials Conference* AIAA Paper 95-1359, 10-12 April, New Orleans.

Edwards P R and Darts J (1984). Standardised fatigue loading sequences for helicopter rotors (Helix and Felix) - RAE/TR 84084 and 84085, Royal Aircraft Establishment.

Ellingwood B R (1992). Probabilistic Risk Assessment, in *Engineering Safety* (Ed Blockley D), McGraw-Hill.

Everett R A, Bartlett F D and Elber W (1992). 'Probabilistic Fatigue Methodology for Safe Retirement Lives'. Journal of the American Helicopter Society.

Farrant N W (1999). JetSCAN Oil Debris Diagnostic System – An Introductory Overview. IN: *Condition Monitoring 99 – Proceedings of the International Conference on Condition Monitoring*, 12-15 April 1999, Swansea.

Fillion A (1996). *Health Monitoring Systems and Damage Tolerance in Helicopters*, MSc Thesis, Cranfield University.

Fitch J C (1999). Best practices in Maximising Fault detection in Rotating Equipment using Wear Debris Analysis. IN: *Condition Monitoring 99 – Proceedings of the International Conference on Condition Monitoring*, 12-15 April 1999, Swansea.

Freudenthal A M (1947). The safety of structures. IN: Transactions of American Society of Civil Engineers Vol 112, page 125.

Gadd P and Mitchell P J (1984). Condition Monitoring of Helicopter Gearboxes using Automatic Vibration Analysis Techniques, IN: *Gears and Power Transmission Systems for Helicopters and Turboprops* AGARD CP369.

Geary B (1996). Advances in the Application of Magnesium in Helicopter Gearcases. IN: *Proceedings of the Third International Magnesium Conference*, Manchester, Institute of Materials, pp 565-574.

Geary B (1990). Corrosion Resistant Magnesium Casting Alloys. IN: *Advanced Aluminium and Magnesium Alloys*, Proceedings of the International Conference on Light Metals, ASM, Amstersdam.

Goddard K N and MacIsaac B D (1995). 'The use of Oil Borne Debris as a Failure criterion for Rolling Element Bearings'. Lubrication Engineering Vol 51, No 6, 481-487.

Gohar R (1988). *Elastohydrodynamics*, Ellis Horwood.

Goode K B and Roylance B J (1999). Predicting the Time to Failure of Critical Components – A Software Package Strategy. IN: *Condition Monitoring 99 – Proceedings of the International Conference on Condition Monitoring*, 12-15 April 1999, Swansea.

Gunsallus C T, Nagy E, Stennett P G and Flannelly W G, *Investigation of Variation in Fatigue Life Calculated Using Damage Fraction*, in Journal of the American helicopter Society (May 1990).

Hall A D (1976). Helicopter Design Mission Load Spectra. IN: *Specialists Meeting on Helicopter Design Mission Load Spectra* AGARD-CP-206.

Hall P L (2000). Private Communication.

Halling J (1983). 'Toward a Mechanical Wear Equation'. Journal of Lubrication Technology Vol 105.

Harlow D G and Wei R P (1999). 'Probabilities of occurrence and detection of damage in airframe materials'. Fatigue and Fracture Engineering of Materials and Structures Vol 22, pp 427-436.

Harris T A (1991). *Rolling Bearing Analysis*, 3rd Edition, J Wiley & Sons.

Harris T A and McCool J I (1996). 'On the accuracy of Rolling Bearing Fatigue Life Prediction'. Transactions of the American Society of Mechanical Engineers, Journal of Tribology Vol 118 pp 297-310.

Heida J H (1984). Reliability of Non-destructive inspection, National Aerospace Laboratory NLR, The Netherlands, NLR TR 84011 U.

Hess A J, Hardman W and Neubert C (1998). SH-60 Helicopter Integrated Diagnostic System (HIDS) Program Experience and Results of Seeded Fault Testing. IN: *American Helicopter Society 54th Forum.*

Hill R C F (1976). 'Obtaining Hazard Functions from Weibull Plots'. Journal of Naval Science, Vol 3, No 3.

Hodges D and Pearce J (1995). Gearbox Condition Monitoring. IN: *Gearing and Gearbox Practice Today*, Institution of Mechanical Engineers Seminar S 318, London

Hoeprich M R (1998). Private Communication.

Hohn B-R, Winter H, Michaelis K and Vollhuter F (1992). Pitting Resistance and Bending Strength of Bevel and Hypoid Gear Teeth. IN: American Society of Mechanical Engineers International Power Transmission and Gearing Conference, DE-Vol 43-1.

Horve L A (1974). Statistical Interpretation of Shaft Seal Performance. IN: *Society of Automotive Engineers Meeting* 21-25 October 1974, Toronto, Paper 741004.

Howard P L (1987). The application of Quantitative Debris Monitoring to Industrial Gas turbine Monitoring. IN: *Condition monitoring 87*, Ed Jones M H.

Howard P L and Reintjes J (1999). Fusion of Oil Debris and Vibration Technology – The Path to Improved HUMS Performance. IN: 25th European Rotorcraft Forum, 14-16 September 1999, Rome.

Hunter R C (1975). 'Engine Failure Prediction Techniques'. Aircraft Engineering, March 1975.

Ioannides E and Harris T A (1985). 'A new fatigue life model for rolling bearings'. Transactions of American Society of Mechanical Engineers, Journal of Tribology Technology, Vol. 107, No. 3.

Irving P E and Hudson R A (1998). The contribution of Health and Usage Monitoring Systems to calculations of damage state and future life of helicopter components under safe life and damage tolerant designs, Paper 7 in *Exploitation of Structural Loads/Health Data for Reduced Life Cycle Costs,* RTO-MP-7 AC/323(AVT)TP/4, Brussels.

Irving P E, Place S, Strutt J E and Allsopp K (2000). Life prediction, maintenance and failure probabilities in rotorcraft gearboxes equipped with health and usage monitoring systems IN: *Proceedings of Symposium on Condition based maintenance for highly engineered systems*, September 2000, Pisa.

Irving P E, Strutt J E, Hudson R A, Allsopp K and Strathern M (1999). 'The contribution of Fatigue Usage Monitoring Systems to Life Extension in Safe Life and Damage Tolerant Designs'. Aeronautical Journal, Vol 103, pp 589-600.

ISO (1990). Rolling Bearings – Dynamic load ratings and rating life, ISO 281 1990(E) International Organisation for Standardization.

James B, Poon P and Lack L (1998). A new approach to transmission concurrent engineering, IN: *Aerospace Transmission Systems – Concurrent Design and Manufacture*, Institution of Mechanical Engineers S520, Derby.

James S L (1990). The Regulatory Viewpoint. IN: *Helicopter Airworthiness in the 1990s Health and Usage Monitoring Systems – Experience and Applications*, Royal Aeronautical Society Conference.

Joint Aviation Authorities (1993). Large Rotorcraft, JAR-29.

Kececioglu D (1972). 'Reliability Analysis of Mechanical Components and Systems'. Nuclear Engineering and Design Vol 19 p 259-290.

Kececioglu D and Koharcheck A (1983). 'Reliability of Aircraft Splines with or without a wear induction period'. Journal of Vibration, Acoustics, Stress, and reliability in Design, Transactions of American Society of Mechanical Engineers, Vol 105 p 163-170.

Kershner S D, Johnson J B and Gamauf M D (1997). Sikorsky Support to Commercial Health and Usage Monitoring Systems – A summary of forty months of support. IN: *53rd Forum of American Helicopter Society*, Virginia Beach, USA.

Kotorii H (1992). Tooth Surface Fatigue of AISI9310 Steel Spur Gears. IN: *ASME International Power Transmission and Gearing Conference*, DE-Vol43-2.

Ku P M (1980). Gear Failure Modes - Importance of Lubrication and Mechanics. IN: *Source Book on Gear Design, Technology and Performance*, American Society for Metals.

Lorick R R (1970). 'Lubricating gears'. Machine Design, p 108.

Lundberg G and Palmgren A (1947). 'Dynamic Capacity of Rolling Bearings'. Acta Polytechnica Mechanical Engineering Series 1, No 3, Vol 7.

Mansfeld F (1982). 'New Approaches to Atmospheric Corrosion Research'. Corrosion Processes Ed R N Parkins, Applied Science Publishers.

Martin P (1980a). A Systematic Approach to Interactive Failures. IN: *Symposium of Mechanical Reliability*, Moss T R (Ed), IPC Science and Technology Press.

Martin P (1980b). Consequential Failures in Mechanical Systems. IN: *6th Advances in Reliability Technology Seminar.*

Martin P, Strutt J E and Kinkead N (1983). 'A Review of Mechanical Reliability Modelling in Relation to Failure Mechanisms'. IN: Reliability Engineering Vol 6 p 13-42.

McColl J (1997). Overview of Transmissions HUM Performance in UK North Sea Helicopter Operations. IN: *Rotorcraft Transmission System Health Monitoring - Experience Update*, Institution of Mechanical Engineers Seminar S553 London.

Melchers R E (1992). Probabilistic Systems Reliability. IN: *Engineering Safety* (Ed Blockley D), McGraw-Hill.

MOD (1990). Transmission Systems DEF-STAN 00-970, Chapter 705 (1990).

MOD (1989). Health and Usage Monitoring Systems DEF-STAN 00-970, Leaflet 727/1.

Moon S, Menon D and Barndt G (1996). Fatigue Life Reliability based on Measured Usage, Flight Loads and Fatigue Strength Variations. IN: *American Helicopter Society 52nd Forum.*

Moore N R, Ebbeler D H, Newlin L E (1992). An improved approach for flight readiness certification: methodology for failure risk assessment and application examples, NASA/CR-194498, Washington, D.C: NASA.

Moss T R and Strutt J E (1993). 'Data sources for reliability design analysis'. Technical Note in Proceedings of the Institution of Mechanical Engineers Part E Vol 207 pp 13-19.

Moss T R and Andrews J D (1996). 'Reliability assessment of mechanical systems'. Proceedings of the Institution of Mechanical Engineers Part E Vol 210 pp 205-216.

Muir D and Howe B (1997). In-line Oil Debris Monitor (ODM) for Helicopter Gearbox Condition Assessment. IN: *13th International Symposium on Air breathing Engines.*

Newley R A (1978). *The Mechanisms of fretting wear of misaligned splines in the presence of a lubricant*, PhD Thesis, Imperial College London.

Olver A V, Medina S, Baker R F, and Davies D P (1999). Fretting and Wear of Splined Couplings. IN: *Coupling and Shaft Technology for Aerospace Transmissions*, Solihull, Institution of Mechanical Engineers.

Price A L and Roylance B J (1998). Detection and diagnosis of wear through oil and wear debris analysis. IN: *Handbook of Condition Monitoring*, Chapman & Hall.

Qureshi F S and Sheikh A K (1997). 'A Probabilistic Characterization of Adhesive Wear in Metals'. IEEE Transactions on Reliability, p 38-44,Vol 46, No 1.

Rabinowicz E (1980). Wear Coefficients – Metals. IN: *Wear Control Handbook.* (Ed Peterson and Winer). American Society of Mechanical Engineers p 475-506.

Rabinowicz E (1995). *Friction and Wear of Materials*, 2nd Edition, J Wiley and Sons.

Reed J (1998). Bearing Failures – Are we learning from experience? IN: *Rolling bearing Engineering Today*, S596 Institution of Mechanical Engineers.

Savage M and Brikmanis C K (1986). System Life and Reliability Modelling for Helicopter Transmissions, NASA CR 3967.

Savage M, Prasanna M G and Rubadeux K L (1994). TLIFE-A program for Spur, Helical and Spiral Bevel Transmission Life and Reliability Modeling, NASA CR 4622, Army Research Laboratory.

Savage M, Radil K C, Lewicki D G and Coy J J (1988). Computerized Life and Reliability Modelling for Turboprop Transmissions. IN: *AIAA/ASME/SAE/ASEE 24th Joint Propulsion Conference*, Boston AIAA-88-2979.

Schijve J (1990). Fatigue, static tensile strength and stress corrosion of aircraft materials and structures, Parts 1 and 2, Delft University Report LR-630.

Sheikh A K, Ahmed M and Badar M A (1995). 'Fatigue Life prediction of assemblies of rotating parts'. International Journal of Fatigue Vol 17(1), page 35.

Shigley J E (1986). *Mechanical Engineering Design*, First Metric Edition, McGraw Hill.

Sidaway D (1999). Turbomachinery Safety Analysis of Rolls-Royce Civil Aero Engines. IN: *Safety, Reliability & Maintainability Data for Aerospace Transmission Systems,* 16 December 1999, Institution of Mechanical Engineers S677, London

Sims R F and Railton E C (1951). Comparative corrosion tests on magnesium and aluminium parts, RAE Technical Note EL20.

Spigel B S (1991). 'Safe Life Reliability Design for Rotorcraft'. Journal of the American Helicopter Society, Vol 36(1), p 78.

Stagg A M (1976). The Philosophy of Test Factors, RAE TR 76113, Royal Aircraft Establishment.

Strutt J E and Allsopp K (1993). Corrosion risk assessment: at the design stage. IN: *ProcessTech 93*, Paper C446/067, Institution of Mechanical Engineers.

Strutt J E, Allsopp K and Ouchet L (1995). 'Reliability Prediction of Pipes and Valves'. Quality and Reliability Engineering International, Vol 11.

Suresh S (1991). *Fatigue of Metals*, Cambridge University Press.

Tallian T E (1982). 'A unified model for rolling contact life prediction'. Journal of lubrication technology, Transactions of American Society of Mechanical Engineers Vol 104, No 3.

Tallian T E (1962). 'Weibull distribution of rolling contact fatigue life and deviations therefrom'. American Society of Lubrication Engineers Transactions, Vol 5, No 1, pp 183-196.

TIMKEN (1994). *The tapered roller bearing guide*, British Timken.

Venkatesh V C and Krishnamurthy R (1980). On some aspects of metallurgical changes during gear pitting. IN: *Source Book on Gear Design, Technology and Performance*, American Society for Metals.

Viswanathan S P, Tata V, Boorla R, McLeod G and Slack J (1988). 'A Statistical Analysis to Assess the Reliability of a Rotorcraft Component in Fatigue'. IN: Journal of the American Helicopter Society, Vol 33 No 4 pp 55-63.

Warburton D (2000). *Development of a generic methodology for probabilistically predicting the reliability of offshore mechanical components at the design stage*, PhD Thesis, Cranfield University.

Weatherford W D, Valtierra M L and Ku P M (1966). 'Experimental Study of Spline Wear and Lubrication Effects'. American Society of Lubrication Engineers Transactions, Vol 9 pp 171-178.

Wilde R A (1980). Failure in Gears and Related Machine Components. IN: *Source Book on Gear Design, Technology and Performance*, American Society for Metals.

Wilson A J and Cortellini F (1988). The Safety Analysis Approach for the EH-101. IN: *14th European Rotorcraft Forum*, Italy

Wilson A J (1992). Safety Assessment of Helicopter Gearboxes. IN: *Safety Assessment for Transmission Systems*, Lucas Automotive Advanced Engineering Centre, Institution of Mechanical Engineers.

Yang Q J (1996). 'Fatigue test and reliability design of gears'. International Journal of Fatigue Vol 18 No 3 pp 171-177.

Zincone R and Mancini J H (1980). Helicopter Gearbox Testing. IN: *Helicopter Fatigue Life Assessment* AGARD CP-297.

A HGBR Program Description

A.1 Introduction

The HGBR program created for the purpose of this work has been written in Borland Delphi™, an object oriented version of Pascal computer language. The program contains the theoretical models that have been described in Chapter 4, together with loading, geometry and material data for the Type A and Type B gearboxes.

The program is made up of a number of program *units*, each of which has an associated *form*. The forms represent the graphical user interface (GUI), which contain graphs, edit boxes, buttons, tables etc. The units contain the Pascal code to allow the program to run. The pairs of units and associated forms have the same name and are listed in Table A.1.

Unit name	Content/Function
main	General program information, declarations of global variables etc
mathlib	Definitions of functions used to calculate loads, plus procedures for calculating the fatigue life for the gear teeth and bearings. This applies geometrical formulae to calculate component stresses from input torque.
System Modelling	Calculation and output display section of the program. It controls the graphical output and contains the damage models for casing corrosion and shaft spline wear.
Gearbox Parameters DBAccess	Data input section split into three pages for geometry, assembly errors and Overhaul/ HUMS/ Overtorque parameters. This is the part of the program that controls the data file used for each set of experiments.
Torqbands	Gearbox loading section, which controls the load spectrum used by the program. This part of the program is used for selecting the load file or torque spectrum to be used.
ShowBearingLoads	Displays the loads on the gears and bearings for a given input torque. This does not play a direct part in the calculation of stresses or lives.
GBGeneralForm	General view of the gearbox diagram
BrgConfigForm	General view of the bearing configuration

Table A.1 : Names and functions of HGBR units and forms

A.2 Program Unit 'Main'

The following global variables are defined in the program unit **'main'**, and are listed in Table A.2. These contain the torque spectra and calculated loads used throughout the programme, and the calculated times to failure for each failure probability.

Global_Ftime[1..12, 1..26]	Array size 12 rows, 26 columns which contain the times to failure in hours for each failure probability from 10^{-9} and 0.5:	
	Row 1	Input shaft torsion fatigue
	Row 2	Gear tooth root bending fatigue
	Row 3	Output shaft torsion fatigue
	Row 4	Gear tooth rolling contact fatigue
	Rows 5 to 8	Bearing 1 to 4 contact fatigue
	Row 9	Shaft spline wear
	Row 10	Plain corrosion
	Row 11	Galvanic corrosion
	Row 12	Reversal of thrust bearing (initiates functional failure)
Global_logP[1..12, 1..26]	Array size 12 rows, 26 columns that contain the cumulative failure probability corresponding to the rows in Global_Ftime, between 10-9 and 0.5.	
Global_loads [1..2000,1..15]	Array size 2000 rows, 15 columns that contain the cycles, time duration, torque and load for all manoeuvres. The first five columns are read-in from the load file **name_5col.**	
	Column 1	Duration of load state in minutes
	Column 2	Cumulative time in minutes
	Column 3	Duration of load state in cycles
	Column 4	Cumulative cycles
	Column 5	Input torque in Nm
	Column 6	Gear Hertzian contact stress (MPa)
	Columns 7-10	Radial load (kN) for bearings 1 to 4
	Column 11	Input shaft torsion stress
	Column 12	Output shaft torsion stress
	Column 13-15	Not used
Number_of_lines	Number of rows used in **Global_loads**	
TBO_count	Number of overhaul events during lifetime of gearbox	

Table A.2 : Significant global variable names and functions

A.3 Program Unit 'Mathlib'

The formulae for the gear and bearing loads are all in a maths program unit called **'mathlib'**. This includes procedures to calculate:

- Miner damage sum for fatigue models. This procedure uses the model described for fatigue damage accumulation in Chapter 4 and Appendix B.

- Bearing L_{10} life using the formulae in Appendix C, based upon Lundberg-Palmgren model, ISO281.

- All gear and bearing loads using the formulae in Appendix B, given the input torque value. This reads in a five-column load file in the form 'name_5col.txt' and calculates all other stress values for use in the remainder of the program. The combined array is called **'Global_loads'**, with dimensions **'number_of_ lines'** by 12 columns.

A.4 Program Unit 'SystemModelling'

The program unit **'SystemModelling'** is the main display unit for the program. The unit is responsible for calling the procedures that calculate the failure probability due to fatigue of the gears, shaft and bearings (in **mathlib**) and wear (in **SystemModelling**). These results are then displayed in separate graphs – one for fatigue and wear and another for corrosion, before combining them in a system graph (providing the gearbox usage is known). The results are also sent to a text file named **GBdam.txt**.

The unit also calculates the system failure probability by interpolating between points given from the fatigue, wear and corrosion calculations, and applying the probability of detection (POD) that applies to health monitoring (HM) detection capability.

A.4.1 System Definition

The System Definition page (Figure A.1) presents the system and components to be considered in the Reliability Model. Each component is assigned to a type of SN curve or damage model, according to the damage accumulation process to which it is subjected. On the graphical presentation of the system, elements checked (checkbox ticked) are taken into account in the model. Two additional models (1 and 2) are provided, which may be tailored by the user. Model 1 is a fatigue, cycles, based model that calculates damage using an S-N curve, and Model 2 is a random initiation, linear growth-based model similar to the corrosion model.

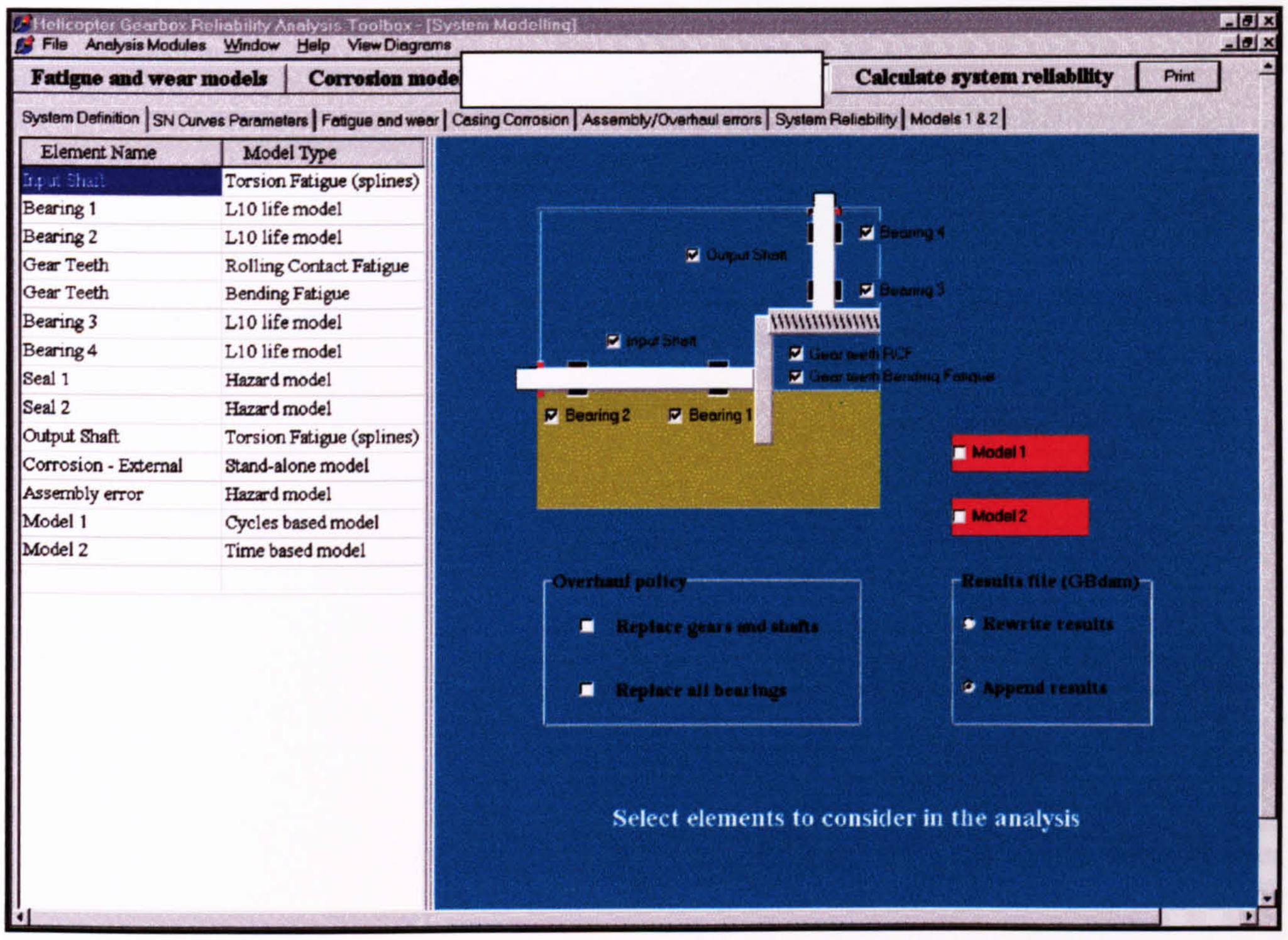

Figure A.1 : System Model and Element Descriptions

A.4.2 S-N Curves Parameters

The system model uses S-N curves to calculate damage on the various components, presented to the analyst as Figure A.2. There are three applicable data sets curves, one each for tooth root bending fatigue of the Type A and Type B gearboxes and one for gear tooth rolling contact fatigue. The parameters for the curves are read in from a text file **SNparameters.txt** and displayed in Figure A.2.

Each curve is shown with the various parameter values used to define the theoretical curve. When available, the experimental data used to define the model curve is also plotted. The parameters of the S-N curves may be changed by the user, and saved to file.

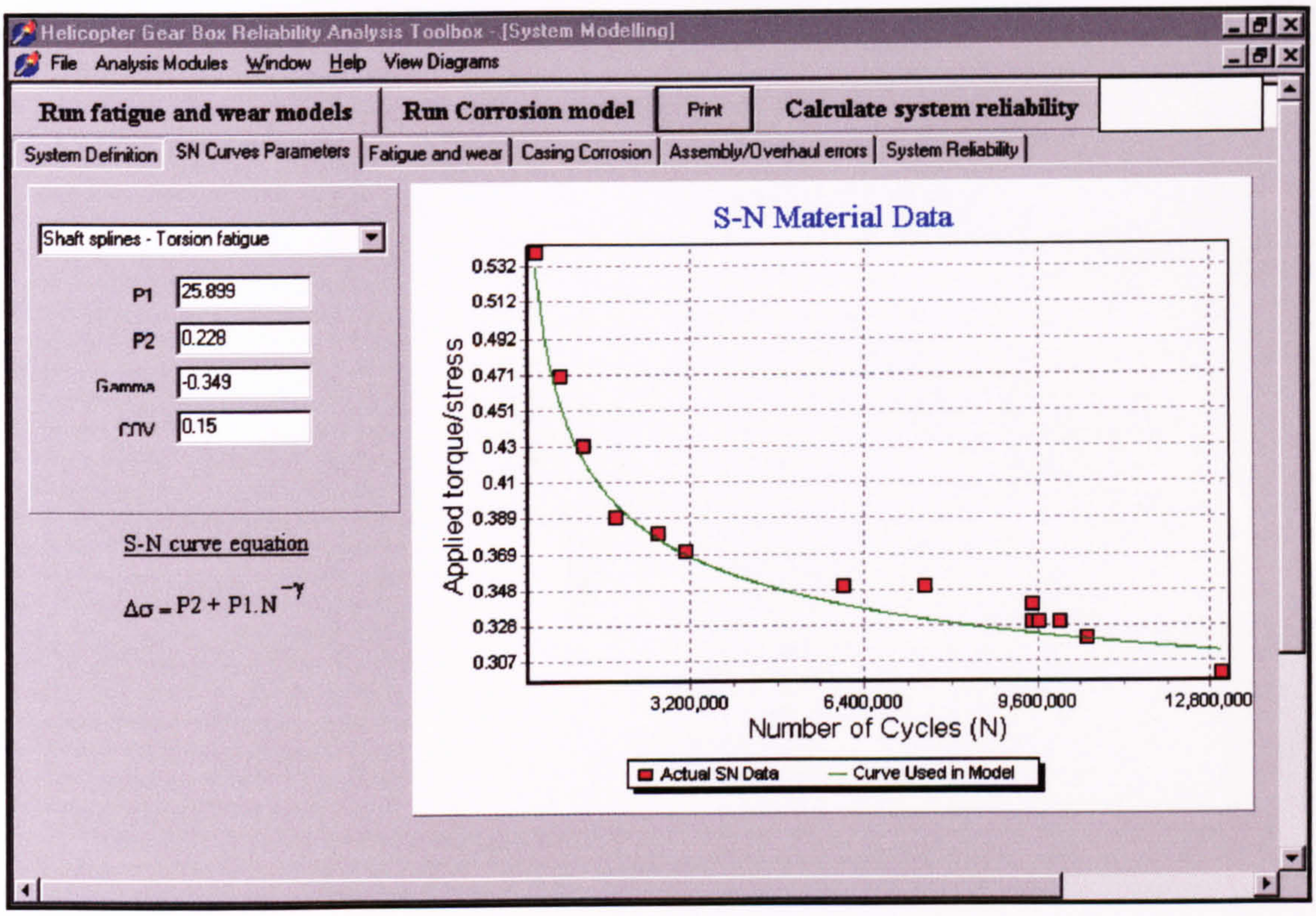

Figure A.2 : S-N Curve Material Parameters

A.4.3 Fatigue and Wear Models

The program calls a procedure in **mathlib**, which implements the equations for tooth root bending, gear rolling contact and bearing contact fatigue, as given in Chapter 4. The wear model is implemented in program unit **'System Modelling'** using equations described in Chapter 4. Outputs from both types of model are displayed to the analyst in the form of Figure A.3.

A.4.4 Casing Corrosion

This calls the procedure to calculate the failure probability due to corrosion (in program unit **'SystemModelling'**). Results are then sent to a text file named **Corr_result.txt**. Different corrosion rates may be applied by changing the material. There are three options set up currently; AZ91C, WE43 (both Mg alloy) and A357 (Al alloy).

The model is run using a Monte Carlo simulation to sample from negative exponential and normal distributions, as described in Chapter 4. A total of 10000 tests are run each time, and the results sorted in order to produce a distribution of failure probabilities, see Figure A.4.

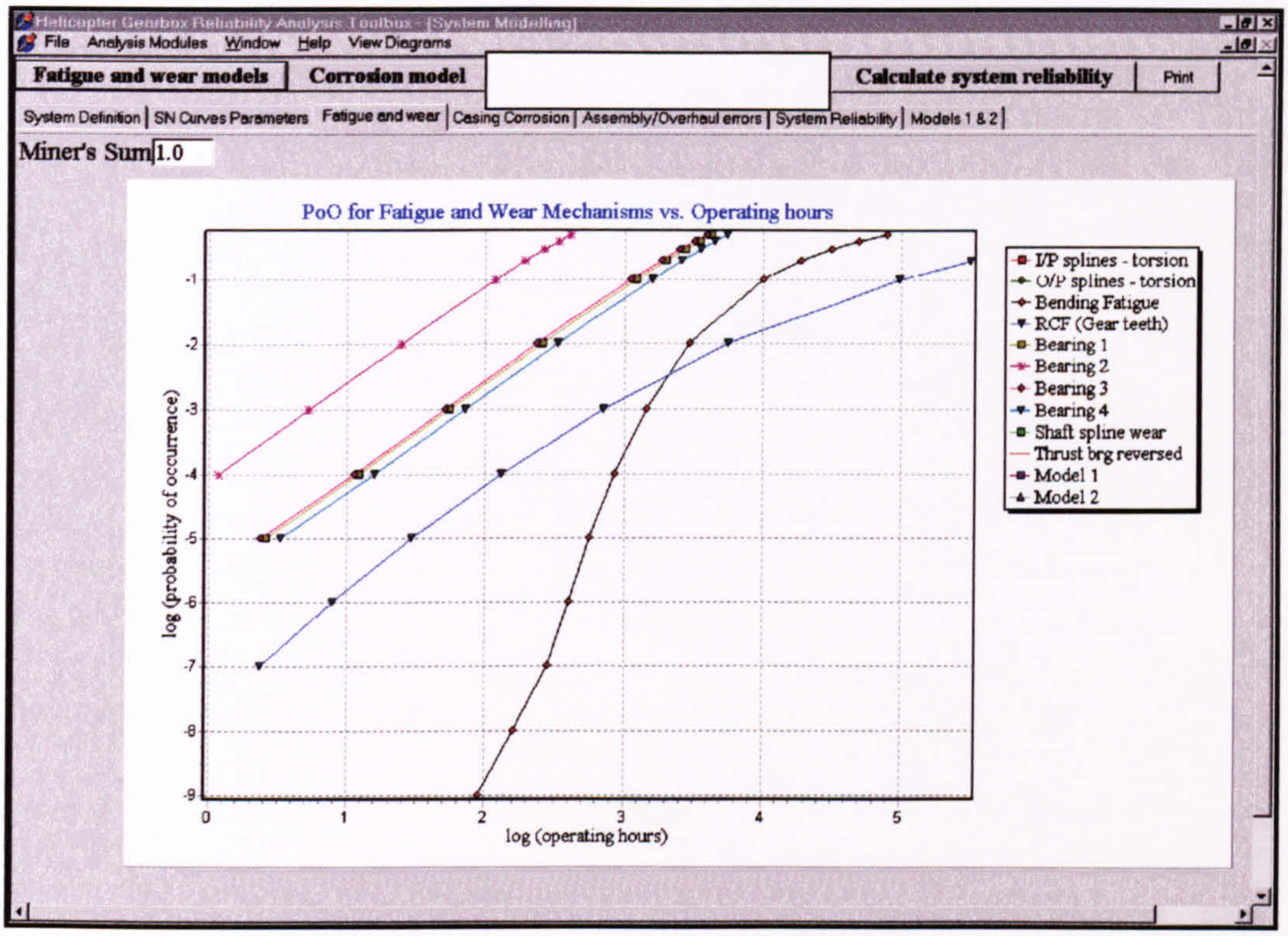

Figure A.3 : Fatigue and Wear Mechanisms – Output page

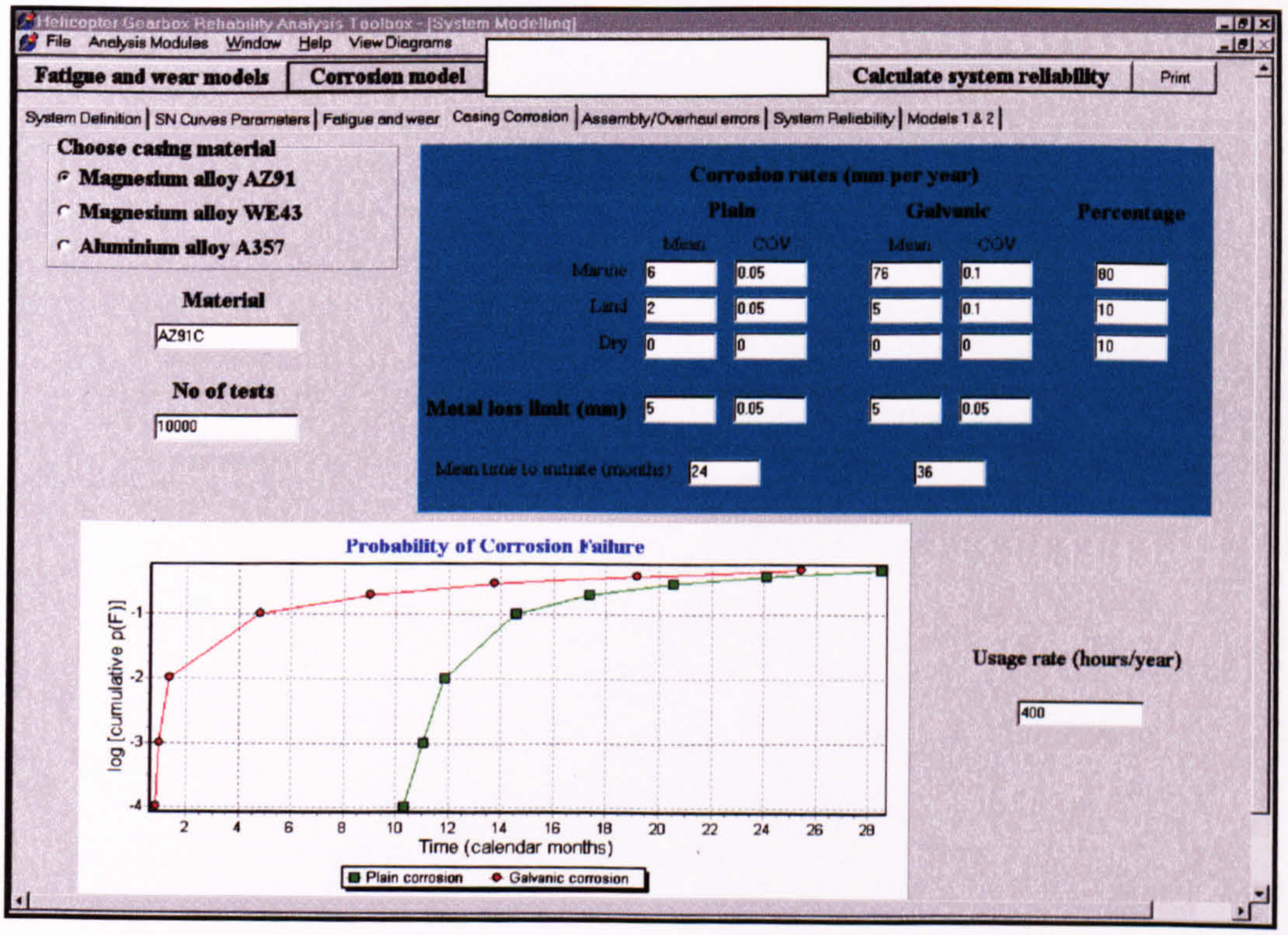

Figure A.4 : Casing Corrosion Model – Output page

A.4.5 System Reliability

This displays the results from the summation of all the failure mechanisms present in the gearbox. The fatigue, wear and corrosion models must have been run in order to provide the input for this output screen (Figure A.5). The program uses the helicopter usage rate (in hours/year) to allow the corrosion failure curve to be plotted on the same axis as the fatigue and wear models that depend on operating hours. Certain curves are modified by a POD factor, depending on the estimated accuracy and reliability of the health monitoring system.

The program also calculates the upper and lower limits for the system failure probability. If it is required to obtain a value for **TBO_output**, this is calculated using the acceptable p*. Results are output to a text file named **Sys_results.txt**.

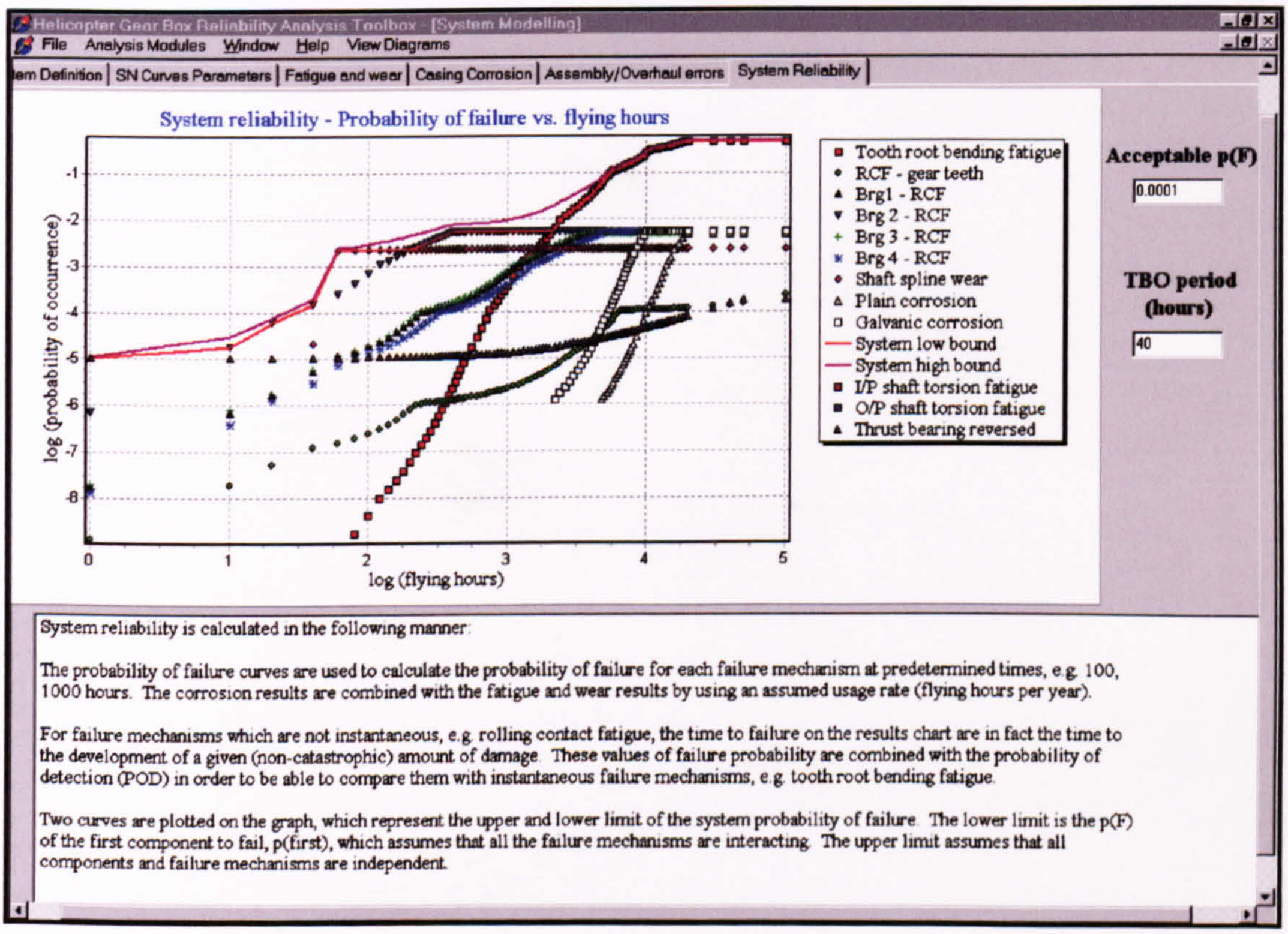

Figure A.5 : System reliability – Results page

A.5 Program Unit 'GearboxParametersDBAccess'

The data entry is via program unit '**GearboxParametersDBAccess'**, which uses text files in the form 'name_data,txt'. Open and save files dialogue boxes are used to choose the text file, and changes may be saved to a new file if desired. An 'Open file' dialogue box appears when the program starts, and also when requested by the user on the

database page. The values in the text file are then loaded into the 74-element array called **'parameters'**. The procedure **Assign_values** sets up all the global variables as required by the program.

Values are read in from the text file, and changes may be saved to the same file, or a file of another name. The types of parameters that can be varied are described in Sections A.5.1 and A.5.2.

A.5.1 Geometry

In order to assess changes to the configuration of the gearbox, the user may alter the geometrical parameters of the gearbox. The number and size of the shaft splines and the specification of the bearings may also be changed (Figure A.6).

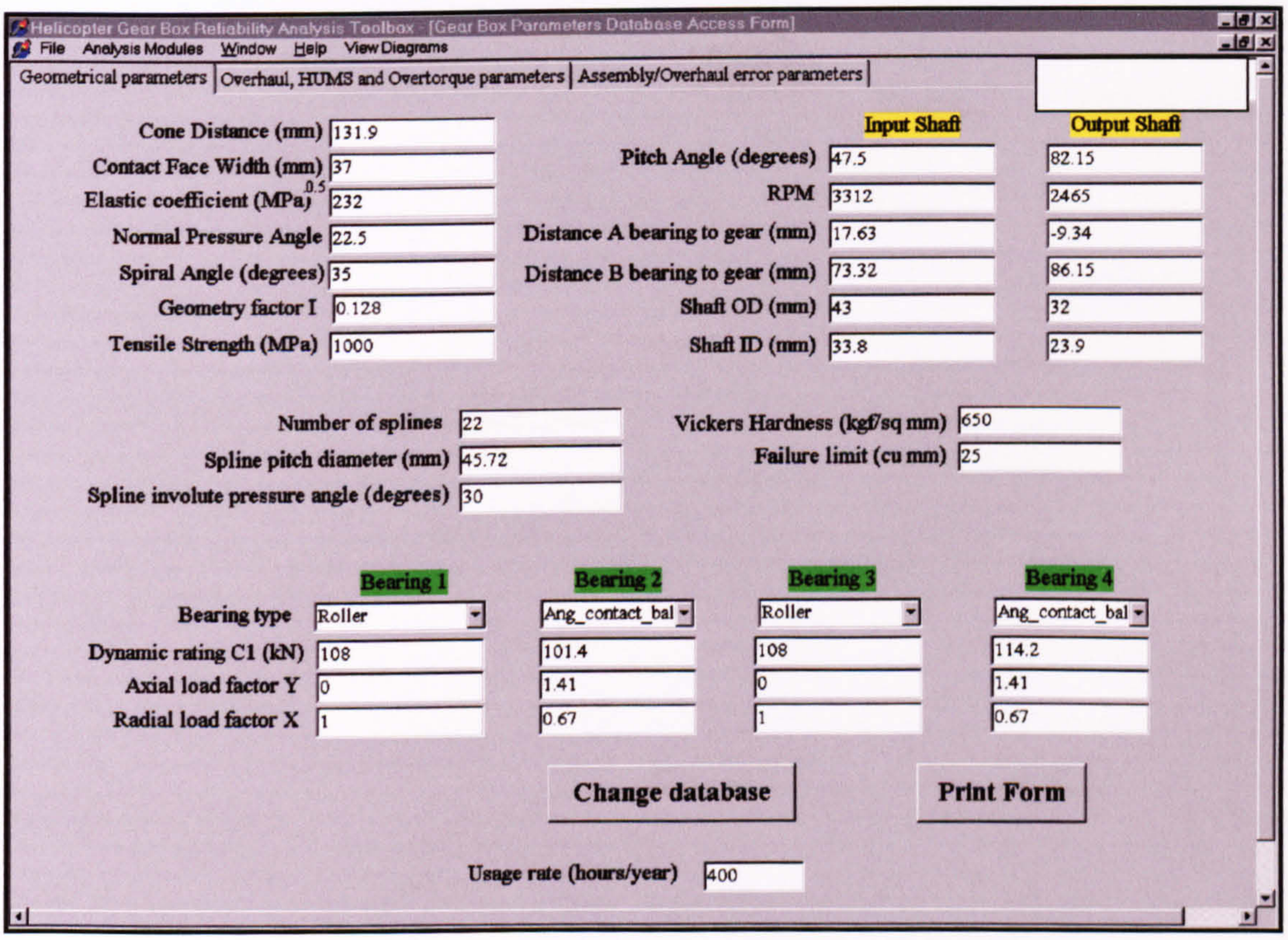

Figure A.6 : Database form for gearbox - geometrical parameters

A.5.2 Overhaul, HUMS and Overtorque parameters

The parameters that may be changed for separate functions (see Figure A.7) within the program are as follows:

a) Probability of detection (POD) – the accuracy and reliability of the HUMS monitoring systems, which is used in unit '**SystemModelling**' to calculate the failure probability of the complete system.

b) Overtorque parameters - the frequency, size and duration of overtorque events can be changed; these are then added to the load spectrum used in the rest of the program, and may be viewed in **torqbands**.

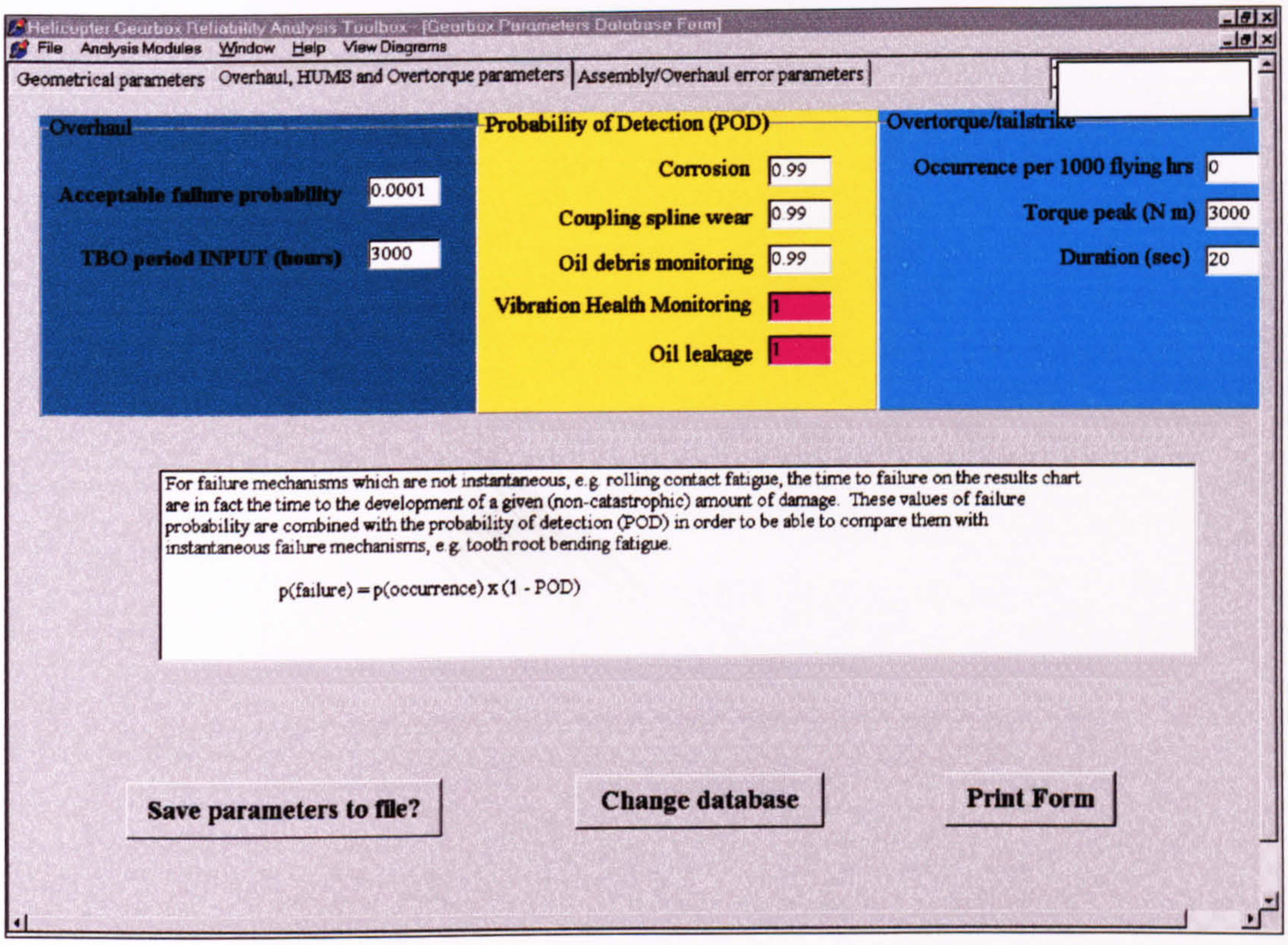

Figure A.7 : Database form for gearbox – Parameters for (a) POD of Health Monitoring techniques and (b) Overtorque

A.6 Torqbands

Unit **torqbands** allows the user to choose the format and content of the manoeuvres contained within a spectrum. It is also possible to changes between the files containing torque data, set-up before running the HGBR program.

This part of the program allows the user to open the file containing the desired load history or spectrum. An Open file dialogue box appears when the program starts, and also when requested by the user. The load file contains the load spectrum or history to be applied to the reliability model, and the values are loaded into the first 5 columns of the 2000 row by 15-column array '**Global_loads**' (Table A.2). The form then displays the values of the transmitted torque, Gear teeth Hertzian contact stress, shaft torsion stress and bearing load, as each varies with time (Figure A.8).

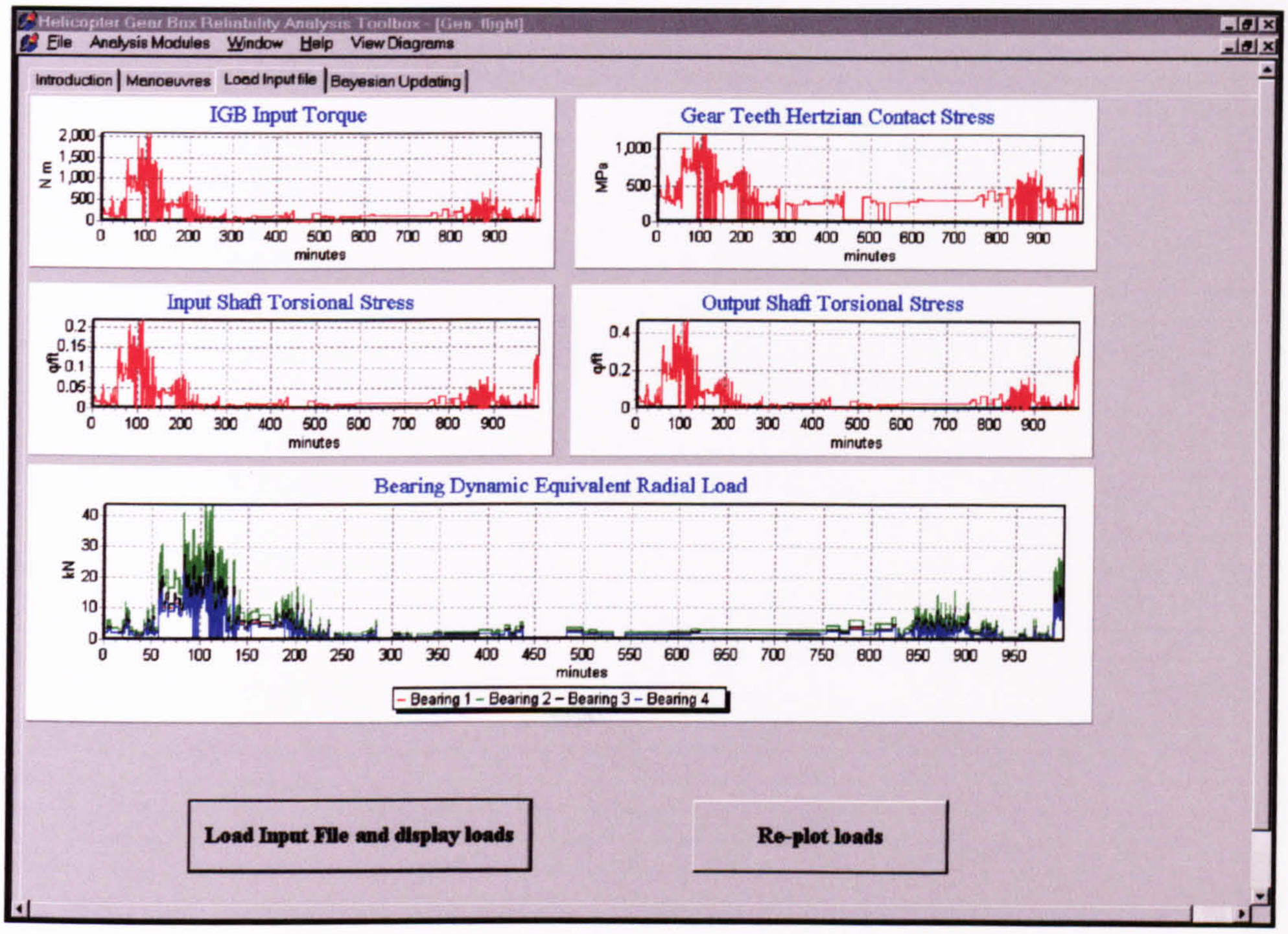

Figure A.8 : Display of Component Loading

A.7 Program Unit 'ShowBearingLoads'

The program unit '**ShowBearingLoads**' reads in values for the input torque from the screen, and then calculates the Hertzian contact stress and bearing loads. These calculated values can then be checked off-line using Excel™, for example.

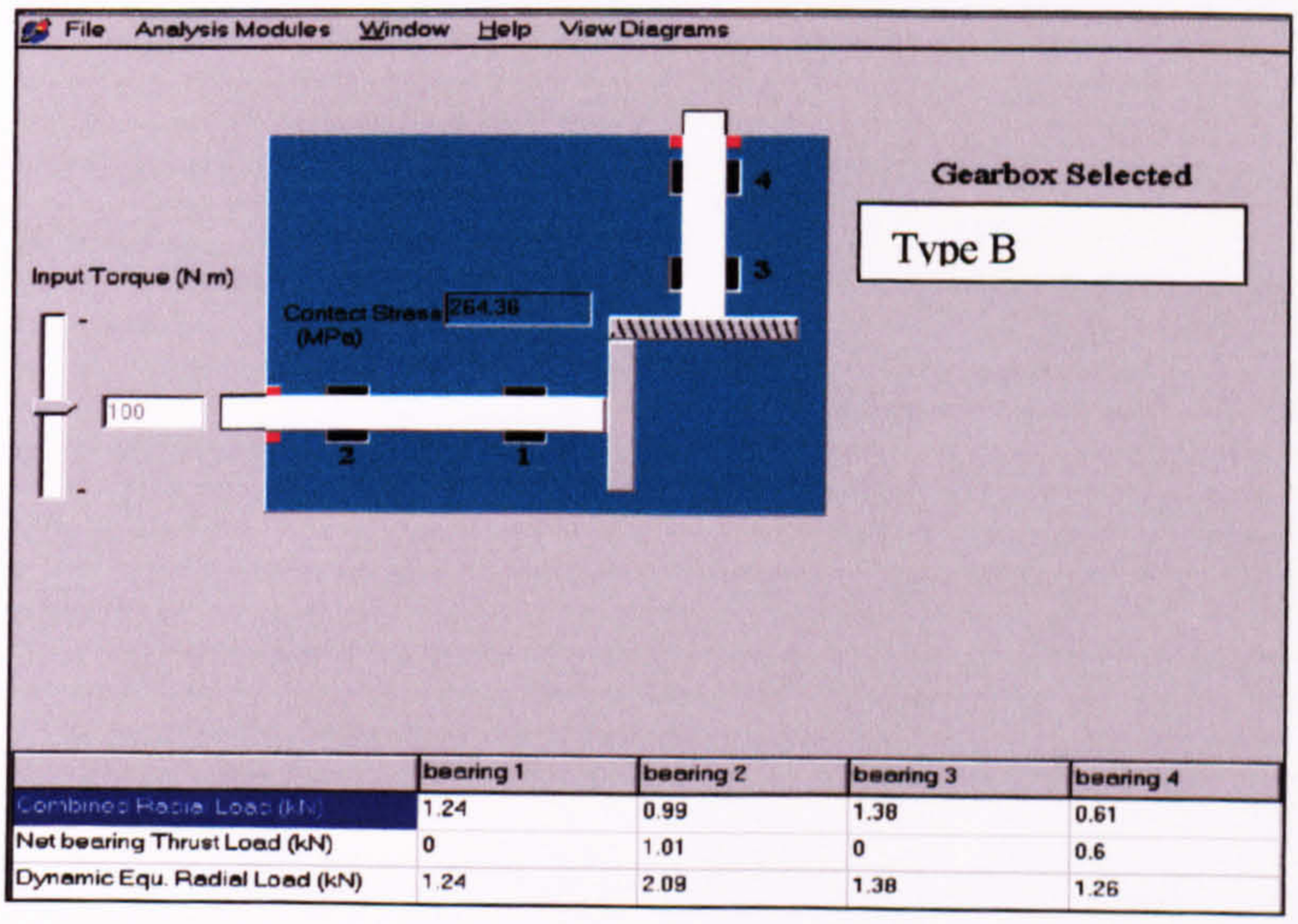

	bearing 1	bearing 2	bearing 3	bearing 4
Combined Radial Load (kN)	1.24	0.99	1.38	0.61
Net bearing Thrust Load (kN)	0	1.01	0	0.6
Dynamic Equ. Radial Load (kN)	1.24	2.09	1.38	1.26

Figure A.9 : Bearing Loads Display Module

B Gearbox Loading and Stress Calculations

B.1 Introduction

The following section describes the technique for using the known tail rotor torque to derive the forces acting on each of the gearbox components. The geometry and configuration are based on a single input and single output shaft (Figure B.1) and can be adapted to most types of intermediate gearbox. The equations are those in general use for gear calculations, and are taken from **[Savage and Brikmanis, 1986; Savage et al, 1994; Drago, 1988; Shigley, 1986; TIMKEN, 1994].**

Using knowledge of the tail rotor torque, the tangential load on the gear teeth may be calculated through knowledge of the gear geometry (section B.2.1). This allows the calculation of the Hertzian Contact Stress (section B.2.2) and the induced radial (section B.2.3) and axial (section B.2.4) loads. The calculation of the radial and axial loads depends on:

(a) whether the gear is driving or being driven,

(b) whether the gear is right- or left-handed, and

(c) the direction of rotation.

The loading experienced by the input and output shafts will be reacted by the bearings, so allowing the loads on the latter to be calculated (section B.3).

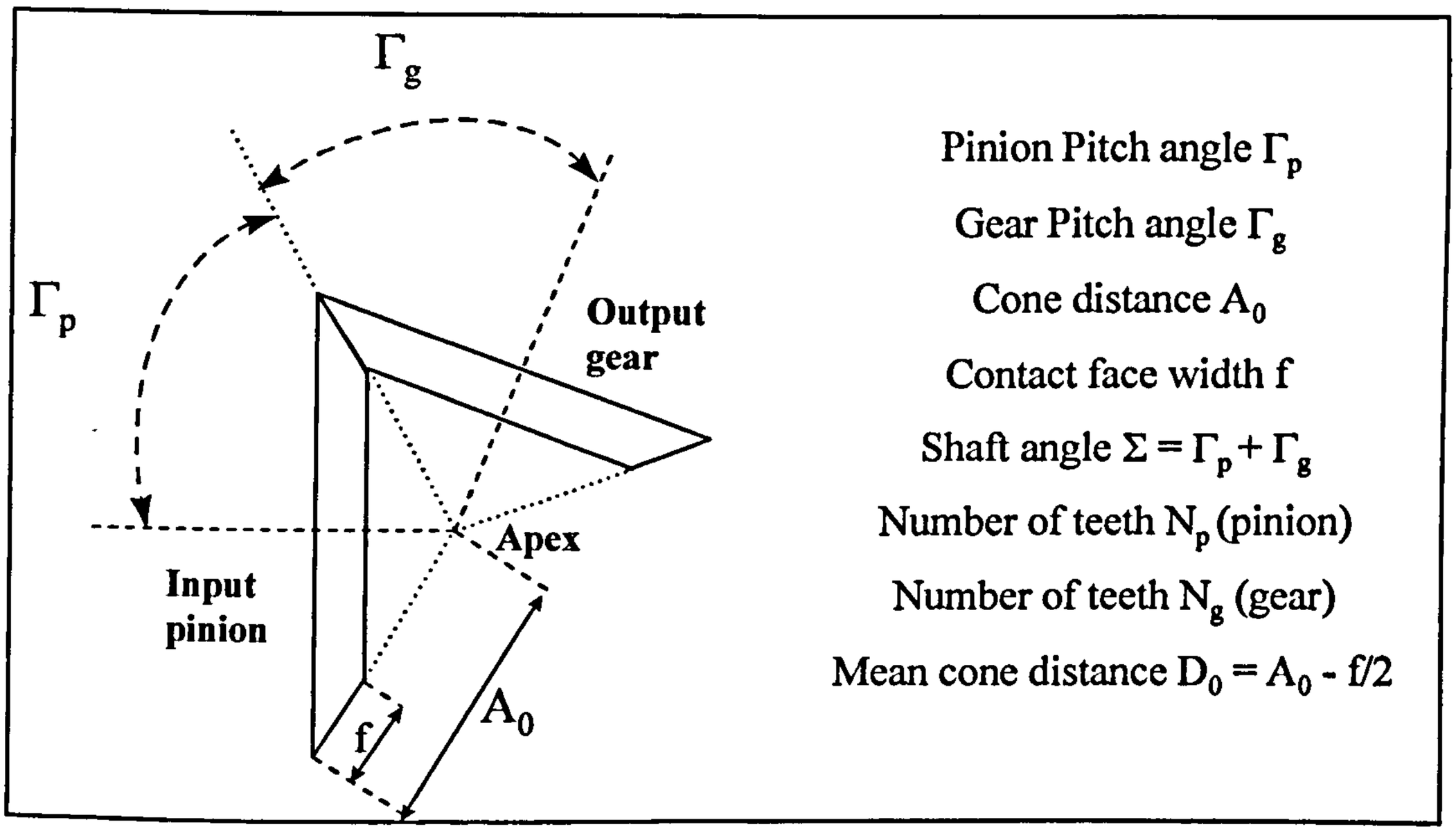

Figure B.1 : Geometry of the Intermediate Gearbox

B.2 Loading on Gear Teeth

B.2.1 Tangential Load on Gear Teeth

Using the same equations as used by **[Savage, 1986]**, the tangential load produced by transmitted torque is the same for the pinion and the gear, W_t:

$$W_t = \frac{T_1}{D_0 \sin\Gamma_p} = \frac{T_2}{D_0 \sin\Gamma_g} \qquad \text{(B.1)}$$

B.2.2 Hertzian Contact Stress produced by Tangential load

The Hertzian Contact Stress produced by the tangential load W_t on the gear teeth is denoted as σ_h. This is the maximum load experienced at the point of contact between the meshing gear teeth, which will only be true at the pitch line between the teeth. Away from the pitch line, sliding of the two surfaces will take place, so altering the contact load. Nevertheless, as a first approximation, the tangential tooth load can be used to calculate the Hertzian Contact stress σ_h, using the AGMA 2003 standard **[AGMA, 1986]**:

$$\sigma_h = C_p \cdot \sqrt{\frac{W_t . C_a}{C_v} \cdot \frac{1}{d_p . f} \cdot \frac{C_m}{I}} \qquad \text{(B.2)}$$

where $C_a = C_m = C_v = 1.0$ **[Agusta Westland, 1994]**

B.2.3 Radial load induced by W_t via the gear geometry

The radial load induced by W_t via the gear geometry is denoted W_r. For a Pinion (driver) with Right-hand spiral, rotating counter-clockwise, the radial load is

$$W_{rp} = \frac{W_t(\tan\phi_n . \cos\Gamma_p - \sin\psi . \sin\Gamma_p)}{\cos\psi} \qquad \text{(B.3)}$$

where ϕ_n is the Normal pressure angle
ψ is the Spiral angle

For a Gear (driven) with Left-hand spiral, rotating clockwise

$$W_{rg} = \frac{W_t(\tan\phi_n . \cos\Gamma_g + \sin\psi . \sin\Gamma_g)}{\cos\psi} \qquad \text{(B.4)}$$

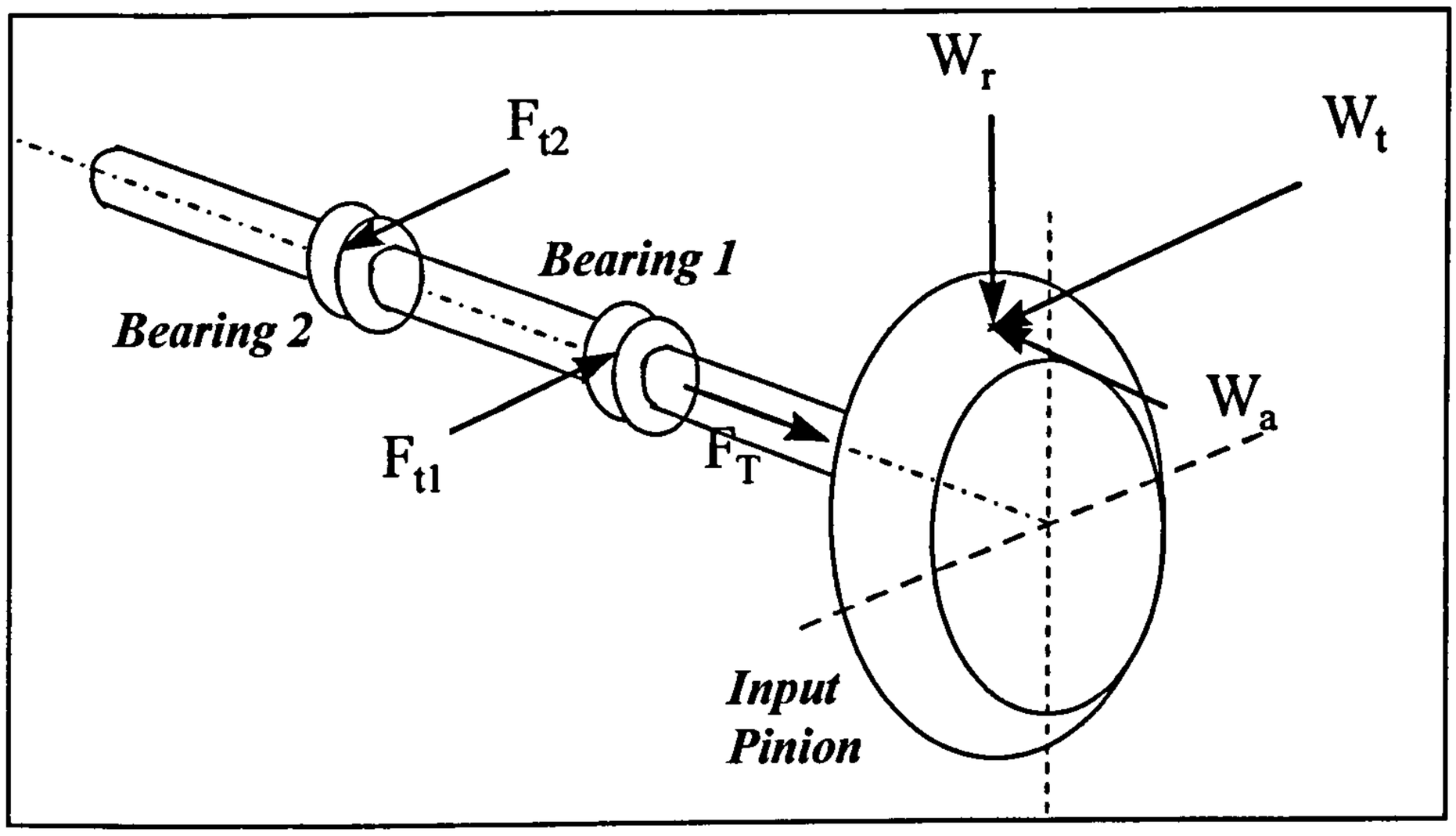

Figure B.2 : Calculation of Gear and Bearing Loads
[Savage and Brikmanis, 1986]

B.2.4 Axial load induced by W_t via the gear geometry

The axial load induced by W_t via the gear geometry is denoted as W_a. For a pinion (driver) with right-hand spiral, rotating counter-clockwise, the axial load is

$$W_{ap} = \frac{W_t(\tan\phi_n . \sin\Gamma_p + \sin\psi . \cos\Gamma_p)}{\cos\psi} \qquad (B.5)$$

For a gear (driven) with left-hand spiral, rotating clockwise

$$W_{ag} = \frac{W_t(\tan\phi_n . \sin\Gamma_g - \sin\psi . \cos\Gamma_g)}{\cos\psi} \qquad (B.6)$$

The total resultant tooth force, W_n, is the same for the pinion and gear,

$$W_n = \sqrt{W_t^2 + W_r^2 + W_a^2} \qquad (B.7)$$

The three force components acting on the gear teeth will cause forces to be transmitted to the bearings. The forces experienced by the thrust bearings will be calculated in Section B.3.

B.3 Bearing Loads

The bearings on the IGB input and output shafts may be mounted in two alternative configurations, either straddle (e.g. Type B) or overhung (e.g. Type A) – see Figure B.3.

The following calculations are valid for both, but for the overhung case, the value for distance **A** is negative.

The loads experienced by the bearings are a combination of axial and radial forces as transmitted from the gear teeth in mesh. The net thrust delivered to the pair of bearings will be equal to the axial load:

$$F_{TI} = W_{ap} \text{ (input shaft)} \qquad \text{(B.8)}$$

$$F_{TO} = W_{ag} \text{ (output shaft)} \qquad \text{(B.9)}$$

The combined radial load acting on the bearings is a combination of the tangential load and the radial load. The *tangential* loads may be calculated from knowledge of the tangential load on the gear/pinion W_t, and the location of the bearings. The *radial* forces may be calculated from knowledge of the radial load on the gear/pinion (W_{rg} and W_{rp}) and the moment produced by the axial load on the gear/pinion (W_{ag} and W_{ap}).

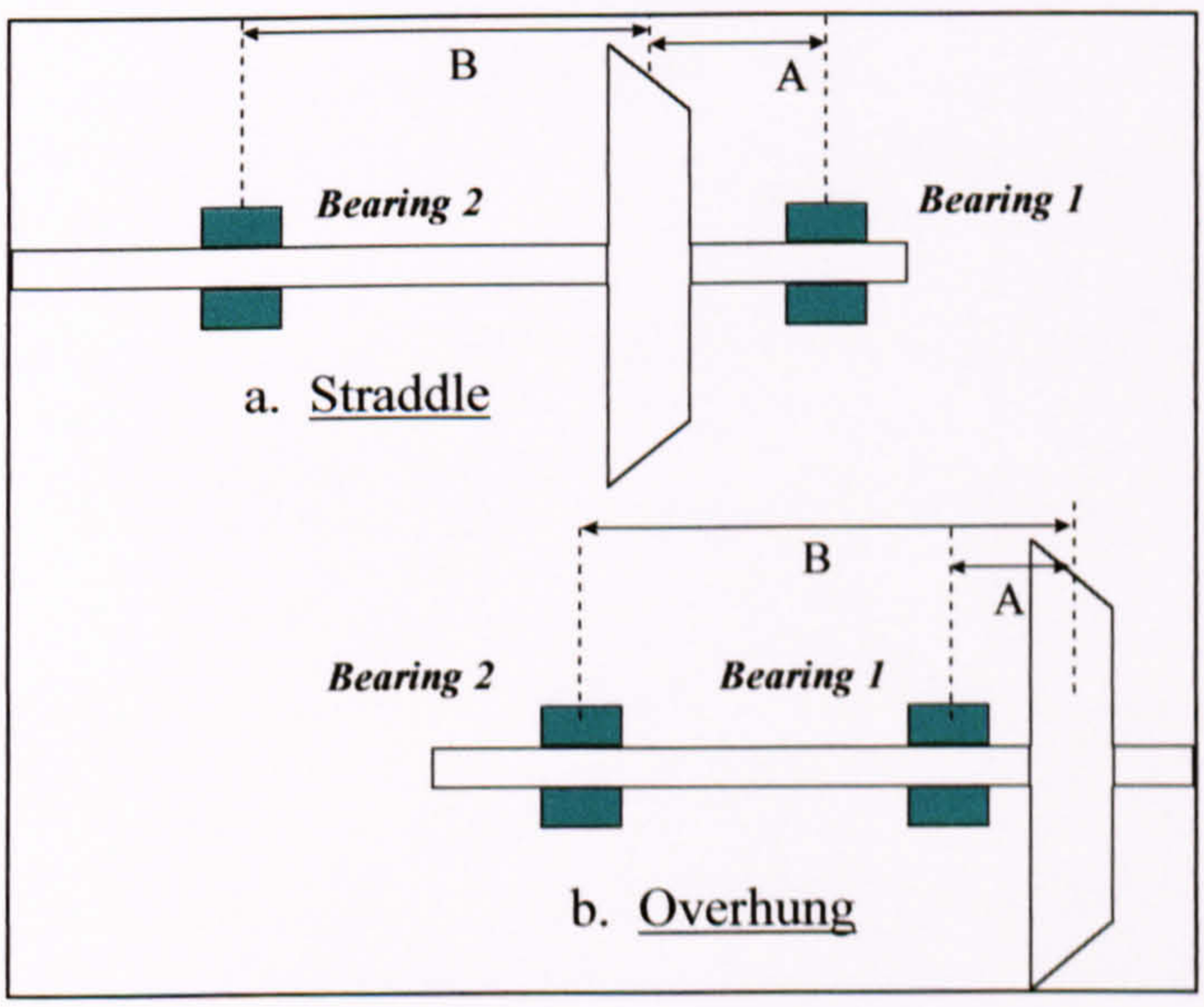

Figure B.3 : Two configurations of bearing and shaft assembly [Savage and Brikmanis, 1986]

B.3.1 Tangential load

Referring to the configurations in Figure B.3, the tangential load experienced by the bearings may be derived using moments. For the input shaft (with bearing spacing A1 and B1):

$$F_{t1} = \frac{W_t . B1}{A1 + B1} \qquad \text{(B.10)}$$

$$F_{t2} = \frac{W_t . A1}{A1 + B1} \tag{B.11}$$

Similarly, for the output shaft (with bearing spacing A2 and B2):

$$F_{t3} = \frac{W_t . B2}{A2 + B2} \tag{B.12}$$

$$F_{t4} = \frac{W_t . A2}{A2 + B2} \tag{B.13}$$

B.3.2 Radial load on bearings

The radial load is derived in a similar manner to the tangential loads, but the moment produced by the axial forces on the pinion and gear, acting at the radius $\mathbf{r_p}$ and $\mathbf{r_g}$ respectively, where

$$r_p = D_0 \, . \, \sin \Gamma_p \tag{B.14}$$

$$r_g = D_0 \, . \, \sin \Gamma_g \tag{B.15}$$

The radial loads on the input shaft bearings are given by the following equations:

$$F_{r1} = \frac{W_{rp} . B1 + W_{ap} . r_p . A1/|A1|}{A1 + B1} \qquad \textbf{Brg 1 (I/P inboard)} \tag{B.16}$$

$$F_{r2} = \frac{W_{rp} . A1 - W_{ap} . r_p . A1/|A1|}{A1 + B1} \qquad \textbf{Brg 2 (I/P outboard)} \tag{B.17}$$

Similar expressions may be derived for the output shaft bearings, substituting W_{rg}, W_{ag}, r_g, A2 and B2 as appropriate.

The *combined radial load* on the input and output bearings are then:

$$F_{R1} = \sqrt{F_{t1}^2 + F_{r1}^2} \tag{B.18}$$

$$F_{R2} = \sqrt{F_{t2}^2 + F_{r2}^2} \qquad \textbf{Input shaft} \tag{B.19}$$

$$F_{R3} = \sqrt{F_{t3}^2 + F_{r3}^2} \tag{B.20}$$

$$F_{R4} = \sqrt{F_{t4}^2 + F_{r4}^2} \qquad \textbf{Output shaft} \tag{B.21}$$

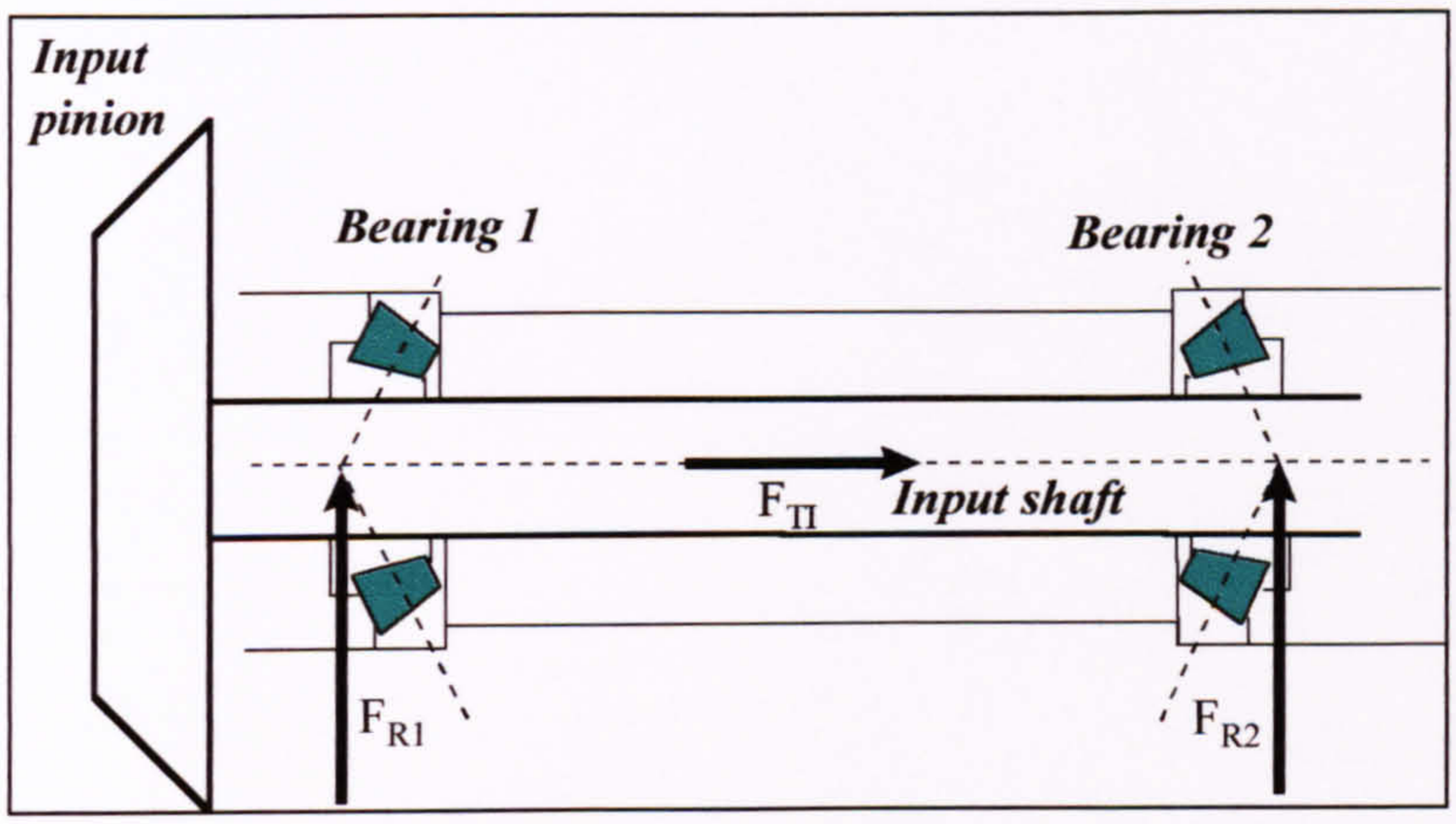

Figure B.4 : Input shaft with tapered roller bearings

B.3.3 Taper roller bearings

From **[TIMKEN, 1994]**, using the loading calculation factor (Y) for each bearing and the combined radial loads, the thrust condition for the Type A IGB is known to be:

$$\frac{0.5F_{R1}}{Y_1} < \frac{0.5F_{R2}}{Y_2} + F_{TI} \qquad \textbf{Input shaft} \qquad (B.22)$$

$$\frac{0.5F_{R3}}{Y_3} > \frac{0.5F_{R4}}{Y_4} + F_{TO} \qquad \textbf{Output shaft} \qquad (B.23)$$

where F_{TI} and F_{TO} are the thrust loads in the input and output shafts respectively.

For bearings 1 and 2 (input shaft), the *Net Bearing Thrust loads* (F_a) may be written as follows **[TIMKEN, 1994]**:

$$F_{a1} = \frac{0.5F_{R2}}{Y_2} + F_{TI} \qquad (B.24)$$

$$F_{a2} = \frac{0.5F_{R2}}{Y_2} \qquad (B.25)$$

For bearings 3 and 4 (output shaft):

$$F_{a4} = \frac{0.5F_{R3}}{Y_3} - F_{TO} \qquad (B.26)$$

$$F_{a3} = \frac{0.5F_{R3}}{Y_3} \qquad (B.27)$$

For the input shaft, the *Dynamic Equivalent Radial loads* (P) are:

$$P1 = X_1 F_{R1} + Y_1 F_{a1} \quad \text{(B.28)}$$

$$P2 = X_2 F_{R2} \quad \text{(B.29)}$$

For the output shaft, the *Dynamic Equivalent Radial loads* (P) are:

$$P3 = X_3 F_{R3} \quad \text{(B.30)}$$

$$P4 = X_4 F_{R4} + Y_4 F_{a4} \quad \text{(B.31)}$$

where $X_1 = X_4 = 0.4$ and $X_2 = X_3 = 1$; for the Type A IGB

B.3.4 Angular contact and roller bearings

In the case of the Type B IGB, bearings 1 and 3 are roller bearings and therefore cannot react against the axial loading from the gears. Hence the axial loads W_{ap} and W_{ag} must be reacted by the angular contact bearings (bearings 2 and 4) alone.

The combined radial loads F_{R1} etc may be calculated as before, Section B.3.2, and the net bearing thrust loads are:

$$F_{a1} = F_{a3} = 0 \quad \text{(B.32)}$$
$$F_{a2} = W_{ap} \quad \text{(B.33)}$$
$$F_{a4} = W_{ag} \quad \text{(B.34)}$$

The D*ynamic Equivalent Radial loads* (P) are:

$$P1 = F_{R1} \quad \text{(B.35)}$$
$$P2 = X_2 F_{R2} + Y_2 F_{a2} \quad \text{(B.36)}$$

$$P3 = F_{R3} \quad \text{(B.37)}$$
$$P4 = X_4 F_{R4} + Y_4 F_{a4} \quad \text{(B.38)}$$

where $X_2 = X_4 = 0.67$ and $Y_2 = Y_4 = 1.41$ for the Type B gearbox

B.4 Wear calculation for shaft splines

The spline wear model described in Chapter 6 uses formulae applied by **[Calistrat, 1980]**, which describes the wear process based on the **[Archard, 1953]** wear equation. This states that the amount of material lost due to the contact of two surfaces in relative motion is directly proportional to the load and the distance moved, and inversely proportional to the hardness of the softer material.

$$\text{Wear volume } \alpha \frac{\text{Load . distance moved}}{\text{hardness}} \qquad \text{(B.39)}$$

$$\text{Wear volume } = \frac{K}{H} \text{Load . distance moved} \qquad \text{(B.40)}$$

where K is the wear coefficient
H is the indentation hardness

The wear may be caused by poor lubrication where there is relative movement between connecting components. This could be due to angular misalignment between the mating shafts, see Figure B.5. For the misalignment case, the relative motion between the interlocking splines can be derived from geometry:

$$\text{Distance moved} = 2L = 2 \frac{PD}{2} \theta \qquad \text{(B.41)}$$

where PD is the pitch diameter of the splines in m
θ is the angle of misalignment in radians

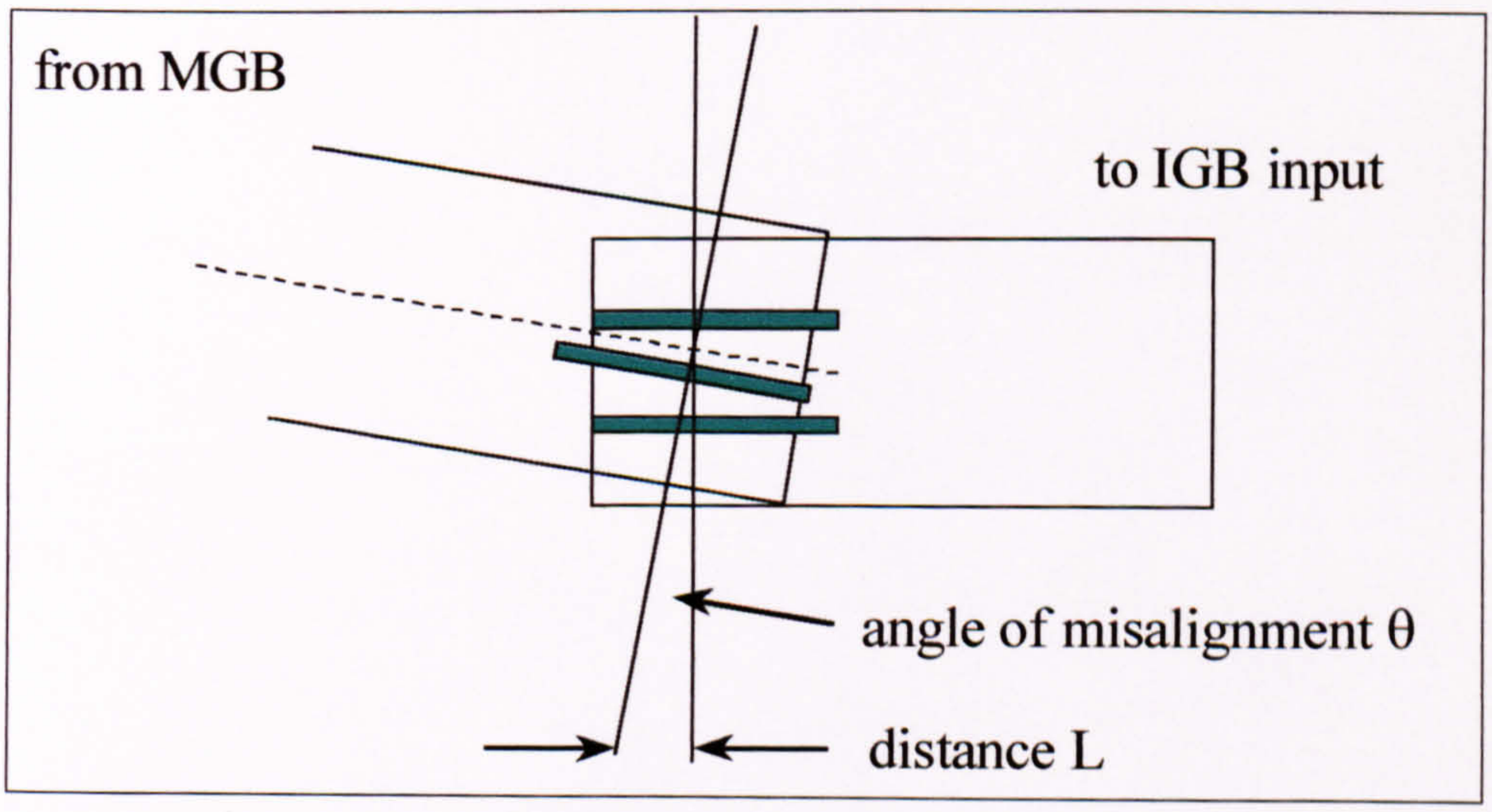

Figure B.5 : View of misalignment of coupling splines [Calistrat, 1980]

The load (in N) applied through the splines may also be derived using knowledge of the geometry, as follows:

$$\text{Load} = \frac{2T}{PDn\tan\varphi} \qquad \text{(B.42)}$$

where T is the transmitted torque in Nm
n is the number of splines
φ is the Involute pressure angle of the splines
PD is the pitch diameter

Finally, Archard's equation for shaft spline wear may be written as **[Calistrat, 1980]**:

$$\text{Wear volume} = \frac{K}{H}.2\frac{PD}{2}\theta \;.\; \frac{2T}{PDn\tan\varphi} \quad \text{per revolution} \qquad \text{(B.43)}$$

where K is the wear coefficient
H is the indentation hardness

C Theoretical Derivations and Analysis

C.1 Probability Distributions

C.1.1 Normal Distribution

The Normal (or Gaussian) distribution is useful for describing the occurrence of any variable that is distributed symmetrically about a mean value μ. A measure of the scatter of the values, or spread of the distribution, is taken from the variance σ^2, which is the square of the standard deviation σ. The shape of the distribution is shown in Figure C.1.

$$f(x) = \frac{1}{\sigma\sqrt{2\pi}} \exp\left[-\frac{(x-\mu)^2}{2\sigma^2}\right] \qquad (C.1)$$

where μ = mean of the distribution
σ = standard deviation of the distribution

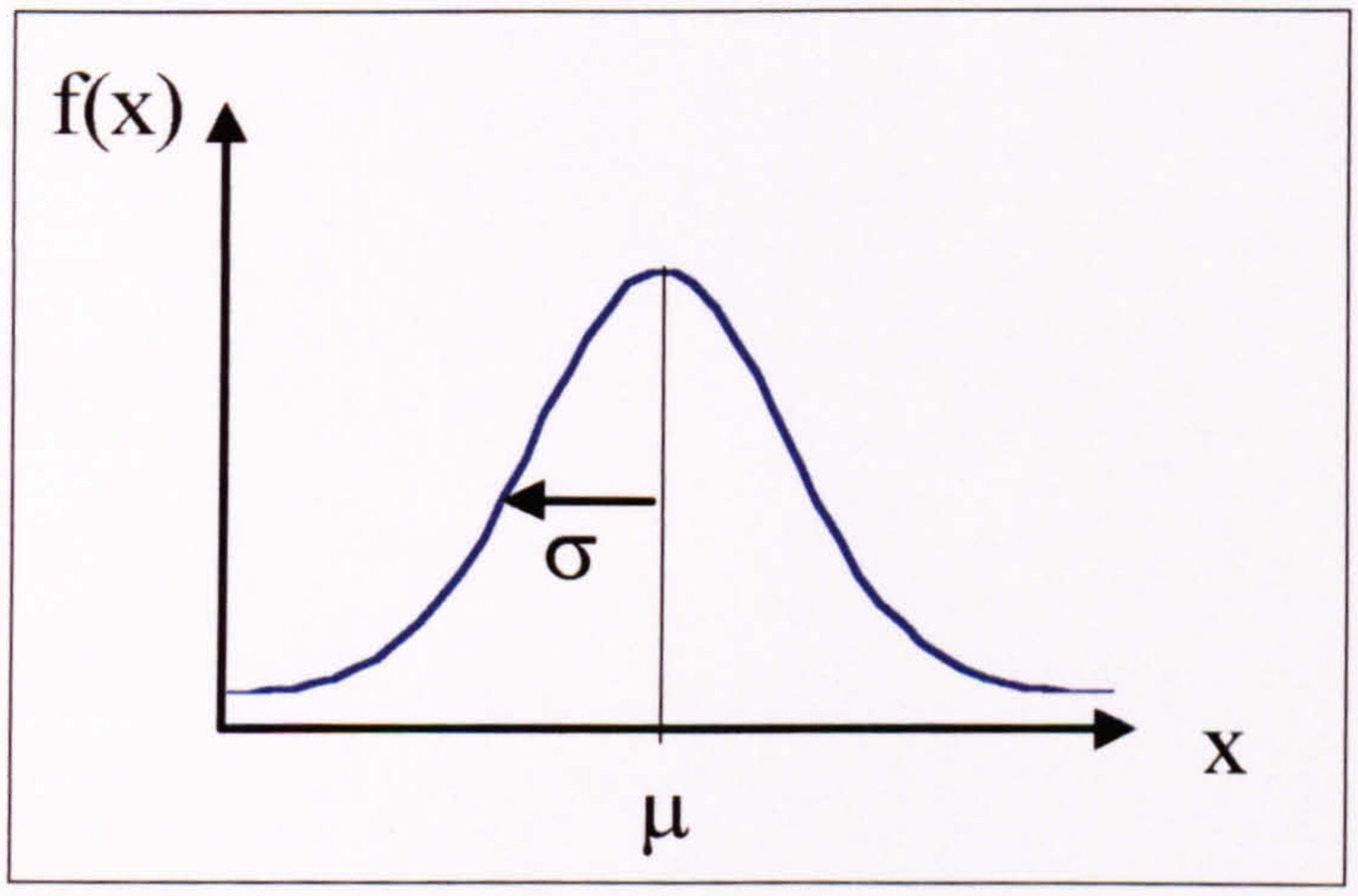

Figure C.1 : Normal distribution with mean μ, standard deviation σ

The coefficient of variation (COV) describes the spread of the distribution (or data scatter) by relating the standard deviation to the mean:

$$COV = \frac{\text{standard deviation}}{\text{mean}} = \frac{\sigma}{\mu} \qquad (C.2)$$

C.1.2 Log-normal Distribution

A variation of the Normal distribution is the log-normal distribution, which is used when the variables appear 'skewed', and have no negative values, e.g. times to repair components. A random variable **t** has a log normal distribution with parameters μ and σ if ln **t** is normally distributed with parameters μ and σ. Parameters μ and σ are the mean and standard deviation of ln **t**.

$$f(t) = \frac{1}{t\sigma\sqrt{2\pi}} \exp\left[-\frac{(\ln t - \mu)^2}{2\sigma^2}\right] \qquad (C.3)$$

where μ = mean of the distribution of ln **t**
σ = standard deviation of the distribution of ln **t**

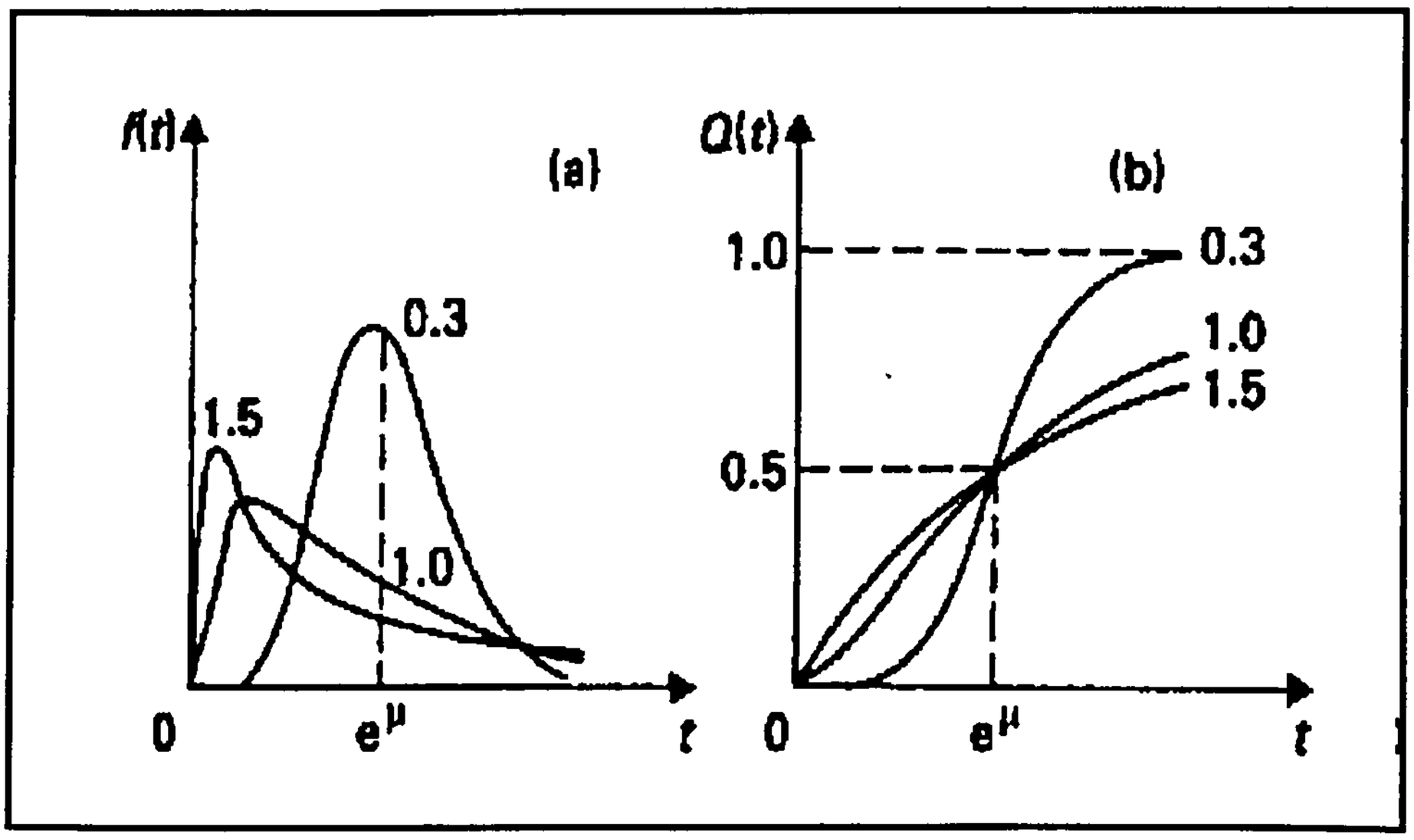

Figure C.2 : PDF and CDF of Log-normal distribution, parameters of σ shown [Billinton and Allan 1992].

The relationship between Normal and Log-normal Distributions allows the following derivations to be made. If Y = ln x is normally distributed with log mean μ_Y and log standard deviation σ_Y, then the mean of the variable x is given by

$$\mu_x = \exp\left(\mu_Y + \frac{\sigma_Y^2}{2}\right) \qquad (C.4)$$

The variance of the variable x is given by

$$\sigma_x^2 = \exp\left(2\mu_Y + \sigma_Y^2\right).\left(\exp\left(\sigma_Y^2\right) - 1\right) \qquad (C.5)$$

The coefficient of variation (COV) of x is defined as

$$\text{COV} = \frac{\text{standard deviation}}{\text{mean}} = \frac{\sigma_x}{\mu_x} \tag{C.6}$$

$$\text{COV} = \frac{\sqrt{\exp\left(2\mu_Y + \sigma_Y^2\right).\left(\exp\left(\sigma_Y^2\right) - 1\right)}}{\exp\left(\mu_Y + \frac{\sigma_Y^2}{2}\right)} \tag{C.7}$$

$$\text{COV} = \frac{\sqrt{\exp\left(2\mu_Y + \sigma_Y^2\right).\left(\exp\left(\sigma_Y^2\right) - 1\right)}}{\sqrt{\exp\left(\mu_Y + \frac{\sigma_Y^2}{2}\right)\exp\left(\mu_Y + \frac{\sigma_Y^2}{2}\right)}}$$

$$= \frac{\sqrt{\exp\left(2\mu_Y + \sigma_Y^2\right).\left(\exp\left(\sigma_Y^2\right) - 1\right)}}{\sqrt{\exp\left(2\mu_Y + \sigma_Y^2\right)}} \tag{C.8}$$

Hence, the coefficient of variation and the standard deviation of the Log-normal distribution may be written:

$$\text{COV} = \sqrt{\exp\left(\sigma_Y^2\right) - 1} \tag{C.9}$$

$$\text{and} \qquad \sigma_Y = \sqrt{\ln(1 + \text{COV}^2)} \tag{C.10}$$

C.1.3 Exponential distribution

The exponential distribution is used to represent events or other data that occur randomly in space or time. When applied to reliability, it may be used to represent a system or component with a constant failure rate λ. If the hazard (or failure) rate is constant, then it can be shown that the reliability, i.e. the probability of no failure, may be written **[Carter, 1986]**:

$$R(t) = e^{-\lambda t} \tag{C.11}$$

The failure function is

$$F(t) = 1 - R(t) = 1 - e^{-\lambda t} \tag{C.12}$$

The probability density function of failure is therefore:

$$f(t) = \frac{dF}{dt} = \lambda e^{-\lambda t} \qquad (C.13)$$

The exponential distribution (Figure C.3), is defined by the failure rate λ, which is the reciprocal of the mean time to failure (MTTF) or mean time between failures (MTBF). The distribution is widely used for modelling the life of components where the underlying damage mechanisms are not known.

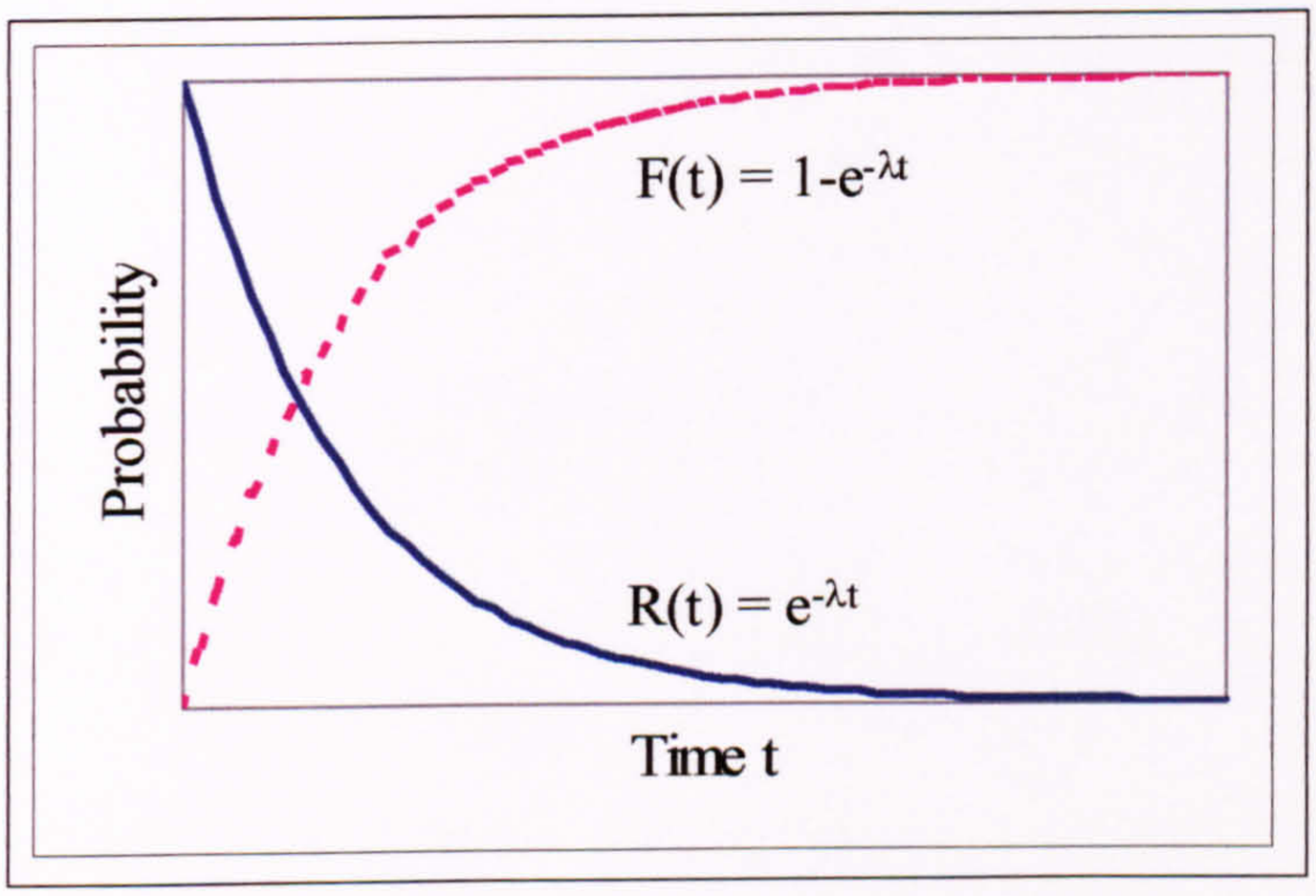

Figure C.3 : Reliability and failure function of Exponential distribution with failure rate λ

C.1.4 Weibull Distribution

The Weibull distribution **[Bompas-Smith, 1973]** is a versatile distribution which allows the failure rate of the component to take different values.. This is a three-parameter distribution, which may be written as:

$$F(t) = 1 - R(t) = 1 - \exp\left[-\left(\frac{t-\gamma}{\eta}\right)^{\beta}\right] \qquad (C.14)$$

where β, Weibull slope, defines the shape of the failure distribution,
η, characteristic life (scale parameter); the life by which 63.2% of the population have failed,
γ, minimum life, or location parameter (hours).

Changes in the slope β affect the failure rate of the system. A value of $\beta < 1$ indicates a decreasing failure rate, $\beta = 1$ indicates a constant failure rate (as in the exponential model Section C.1.3) and $\beta > 1$ indicates an increasing failure rate. These correspond to the three regions of the 'bath-tub' curve where a period of 'wear-in' (decreasing failure rate)

is followed by a constant failure rate, then a period of 'wear-out' (increasing failure rate).

C.2 Distribution of S-N curve

C.2.1 Derivation of Safety Factor for Material Variability

For a population of components upon which a given set of loads is acting, it is required that there should be a predefined probability of failure. Expressed another way, only a certain proportion of components should fail when these loads are applied. If the distribution of the component strength is known, e.g. the mean and standard deviation of a normal distribution, then a factor for calculating the working loads can be specified for a particular failure probability. **[Cansdale, 1984]** explains the rationale of test factors in two parts. The test factor F needs to account for:

1. The difference between the overall population mean and the required minimum strength - factor F_1

2. The difference between the overall population mean and the mean strength obtained from component tests - factor F_2.

For the calculation of F_1, consider a typical failure probability of 10^{-3}, which for a normal distribution equates to 3.09 standard deviations (3σ) below the mean. A strength x_1 must then be found so that the cumulative probability, $F(x_1)$, equals 10^{-3}. In order to find the safe working value of strength, a value of x_1 is found such that

$$x_1 = \mu - 3.09\sigma \qquad \text{(C.15)}$$

F_1 is the factor by which the population mean must be reduced in order to find the working value of x **[Stagg, 1976]**:

$$F_1 = \frac{\mu}{\mu - 3.09\sigma} = \frac{1}{1 - 3.09\upsilon} \qquad \text{(C.16)}$$

where $\upsilon = \frac{\sigma}{\mu}$ = coefficient of variation (COV)

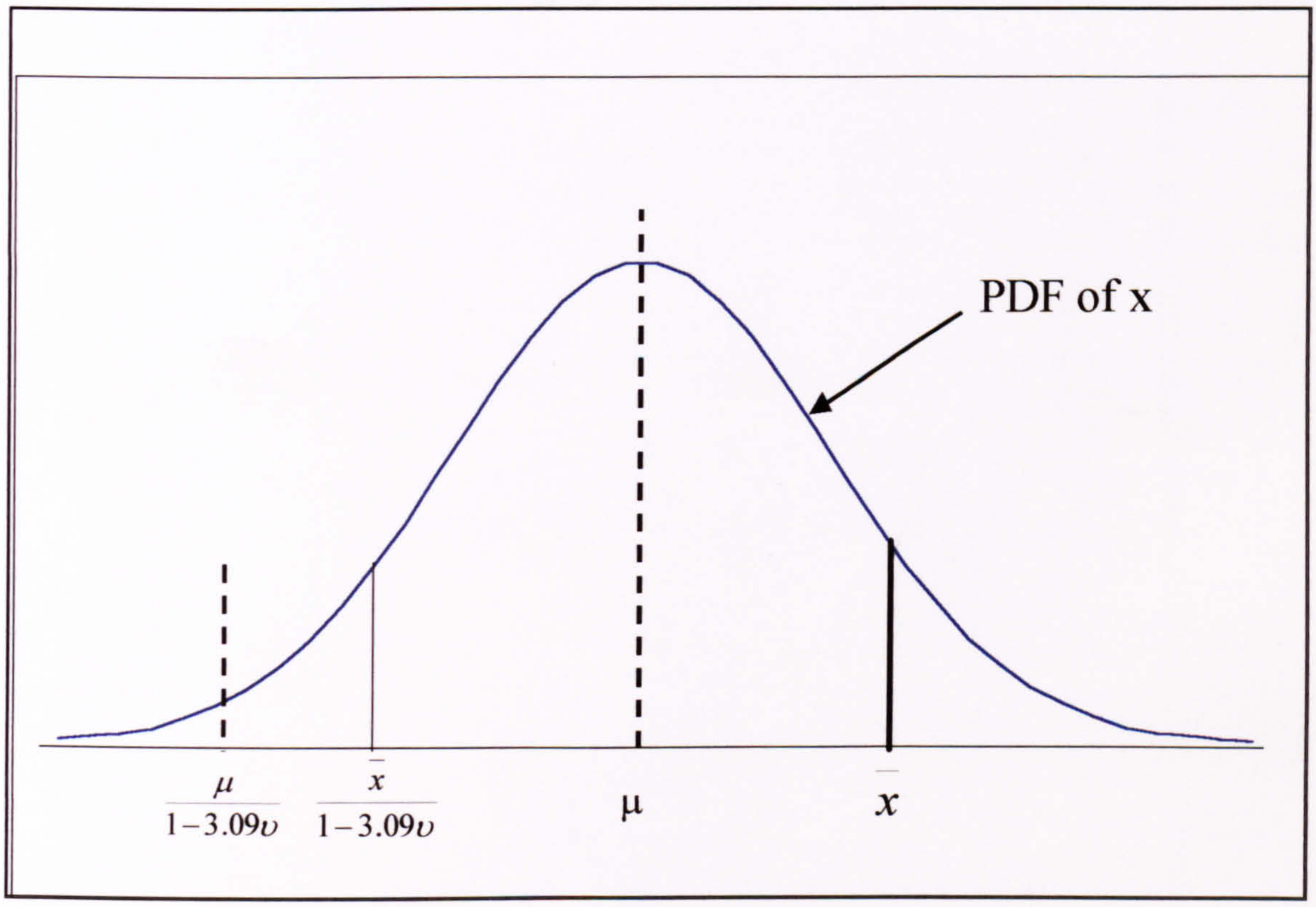

Figure C.4 : Definition of Safety Factor for Normal distribution

If the population shape, mean and standard deviation are known precisely, then F_1 is the only factor that need be applied. In reality, however the details of the parent population are not known precisely. Fatigue tests of the components may be limited to only a small number of test components. This means that the mean strength of the samples tested ($\bar{x}$) may be different to that of a complete population (μ), as presented in Figure C.4.

Figure C.4 shows that if the sample mean is greater than the population mean, then the application of the factor F_1 from equation C.16 would lead to a higher probability of failure for in service components (Figure C.4). The converse would also be true; a sample mean less than that of the population would lead to an overly conservative safety factor F_1.

The second part of the test factor, F_2, must then be derived to take account of this uncertainty, using the Confidence Limit approach **[Stagg, 1976]**. The distribution of sample means will have the same mean μ, but a standard deviation of $\sigma/n^{0.5}$ **[Bury, 1975]**. Therefore for a given confidence limit:

$$\bar{x} = \mu + \frac{C\sigma}{\sqrt{n}} \qquad (C.17)$$

where C is the number of standard deviation from the mean required to give a certain confidence, equals 1.644 for 95%.

Hence factor F_2 is written:

$$F_2 = \frac{\bar{x}}{\mu} = 1 + \frac{C.\upsilon}{\sqrt{n}} \qquad (C.18)$$

where υ is the coefficient of variation = σ / μ

The overall test factor, incorporating F_1 and F_2 is **[Stagg, 1976]**:

$$F = F_1.F_2 = \frac{1 + \frac{C.\upsilon}{\sqrt{n}}}{1 - P.\upsilon} \qquad (C.19)$$

where P is the number of standard deviations required for a level of probability, e.g. 3.09 in equation C.15.

Background tests to investigate gearbox tooth root bending fatigue have been carried out in order to calculate this factor. These tests yielded a COV of 7.2% for ground gears from a sample of 40 intermediate gearboxes and COV of 6% for lapped gears from a sample of 50 tail rotor gearboxes **[Cansdale & Tigwell, 1987]**. Using these values in equation C.19 showed that the required factor for one test (n = 1) was 1.44, and for four tests (n = 4) was 1.36. This is close to the actual factor specified in airworthiness regulations **[JAR, 1993]** to account for the scatter in fatigue strength.

C.2.2 Distribution used for HGBR model

The calculation of the TTF for different values of failure probability is achieved by considering the probability distribution of the S-N curve. Instead of one S-N curve, a family of curves is plotted to give the so-called PNS (probability-cycles-stress) curves **[Bury, 1975]**. The shape of the probability distribution for stress at constant N may be approximated to Log-normal distribution **[Bury, 1975, Yang, 1996]**, which appears as a normal distribution when plotted for ln (S), Figure C.5.

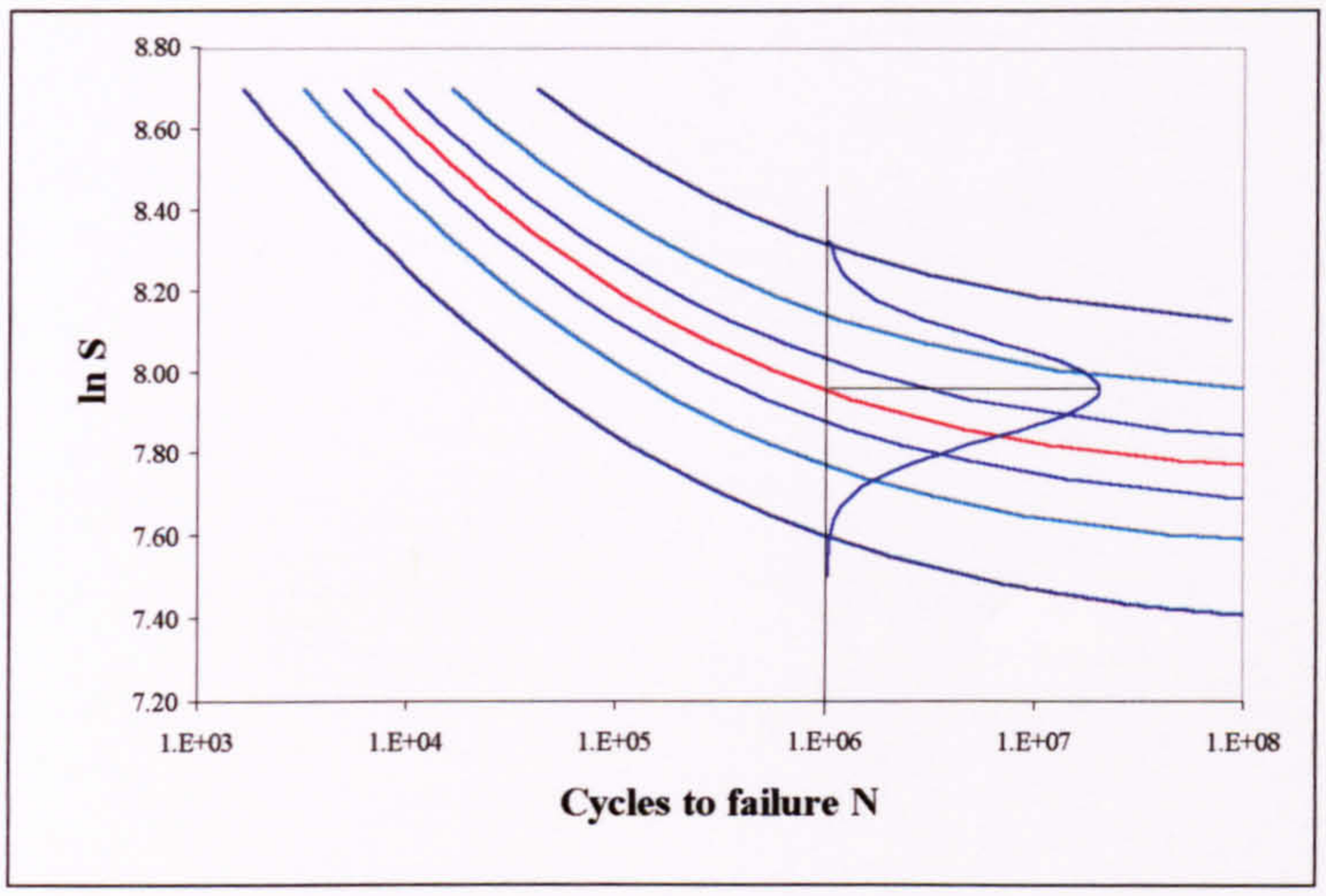

Figure C.5 : Diagram of PNS curves for tooth root bending fatigue

The equation of the mean S-N curve was quoted in Chapter 4 as:

$$\Delta\sigma = S_{inf}\,(1 + A.N_f^{-\gamma}) \qquad (C.20)$$

where $\Delta\sigma$ is the applied stress range
S_{inf} is the endurance limit
A and γ are material constants
N_f is the number of load cycles to failure

For the following mathematical manipulation, equation C.20 has been re-couched in the following manner to ease the implementation in software **[Allsopp, 1997]:**

$$S = P_1 + P_2\,N^{\gamma} \qquad (C.21)$$

where $S = \Delta\sigma$ = applied stress range
$P_1 = S_{inf}$ = endurance limit
$P_2 = S_{inf}$. A = material constant
Exponent γ is negative
N is the number of cycles to failure

Taking logs of both sides

$$\ln S = \ln (P_1 + P_2\,N^{\gamma}) \qquad (C.22)$$

To find the equation of the curve above the mean, an increment δ_{lnS} is added:

$$\ln S = \ln (\,P_1 + P_2\,N^{\gamma}\,) + \delta_{\,lnS} \qquad (C.23)$$

or

$$S = (\,P_1 + P_2\,N^{\gamma}\,)\,.\,e^{\delta} \qquad (C.24)$$

$$Se^{-\delta} = (P_1 + P_2 N^{\gamma}) \qquad (C.25)$$

$$N^{\gamma} = \frac{(Se^{-\delta} - P_1)}{P_2} = \alpha^{-\gamma} \qquad (C.26)$$

The factor δ is used to choose the S-N curve for the respective probability p*. If δ is zero then equation C.24 yields the equation of the median S-N curve. σ_Y is the standard deviation of the Log-normal distribution and n_{stdev} is the number of standard deviations required for the p* required (Table C.1), e.g. 3.09 for p* of 10^{-3}.

$$\delta = \sigma_Y \times n_{stdev} \qquad (C.27)$$

Probability of failure p* required	Number of standard deviations (n_{stdev})
10^{-9}	5.998
10^{-8}	5.612
10^{-7}	5.199
10^{-6}	4.753
10^{-5}	4.265
10^{-4}	3.719
10^{-3}	3.090
10^{-2}	2.326
0.1	1.282
0.2	0.841
0.3	0.525
0.4	0.253
0.5	0

Table C.1 : Number of standard deviations (σ) for p*

C.3 Fitting curve to S-N data

The following section describes a method for fitting a standard S-N type curve to experimental data **[Allsopp, 1997]**. For this purpose, the equation of the mean S-N curve is assumed to take the form:

$$S = P_1 + P_2 N^{\gamma} = P_1 + P_2 e^{\gamma \ln N} \qquad (C.28)$$

where S = applied stress range = $\Delta\sigma$
P_1 = endurance limit
P_2 and γ are material constants

N is the number of cycles to failure

Taking logs of both sides

$$\ln S = \ln (P_1 + P_2 e^{\gamma \ln N}) \qquad (C.29)$$

Choose a point $\overline{\ln S}$ with corresponding $\overline{\ln N}$ by averaging data points:

$$\overline{\ln S} = \frac{1}{N}\sum_{1}^{N}(\ln S_i) \qquad (C.30)$$

$$\text{and} \qquad \overline{\ln N} = \frac{1}{N}\sum_{1}^{N}(\ln N_i) \qquad (C.31)$$

Applying Taylor's theorem around the point chosen above,

$$\ln S - \overline{\ln S} = (\ln N - \overline{\ln N}) \left.\frac{d \ln S}{d \ln N}\right|_{\overline{\ln N}} + \frac{1}{2}(\ln N - \overline{\ln N})^2 \left.\frac{d^2 \ln S}{d(\ln N)^2}\right|_{\overline{\ln N}} + \ldots \qquad (C.32)$$

Next, the experimental data points are fitted to a quadratic around $\overline{\ln S}$, $\overline{\ln N}$ of the form

$$\ln S - \overline{\ln S} = b.(\ln N - \overline{\ln N}) + c.(\ln N - \overline{\ln N})^2 \qquad (C.33)$$

where b and c are constants for a particular curve.

Assuming derivatives are given by differentiating equation C.29:

$$\frac{d \ln S}{d \ln N} = \frac{1}{(P_1 + P_2 e^{\gamma \ln N})}.P_2 \gamma e^{\gamma \ln N} = \frac{P_2}{S}\gamma e^{\gamma \ln N} = \frac{\gamma(S - P_1)}{S} \qquad (C.34)$$

$$\text{and} \qquad \frac{1}{2}\frac{d^2 \ln S}{d(\ln N)^2} = \frac{1}{2}.\left(\frac{P_2 \gamma^2 e^{\gamma \ln N}}{S} - \frac{P_2 \gamma e^{\gamma \ln N}}{S^2} P_2 \gamma e^{\gamma \ln N}\right)$$

$$= \frac{1}{2}.\left(\frac{P_2 \gamma^2}{S}.\frac{(S - P_1)}{P_2} - \frac{(S - P_1)\gamma^2}{S^2}.(S - P_1)\right)$$

$$= \frac{1}{2}\left(\frac{\gamma^2(S - P_1)}{S} - \frac{\gamma^2(S - P_1)^2}{S^2}\right) = \frac{1}{2}.\frac{\gamma^2(S - P_1)}{S}.\frac{P_1}{S} \qquad (C.35)$$

The next step is to equate the derivatives (equations C.7 and C.8) with the coefficients given by the quadratic in equation C.32. Hence

$$b = \frac{\gamma(\bar{S} - P_1)}{\bar{S}} \tag{C.36}$$

and $$b^2 = \frac{\gamma^2(\bar{S} - P_1)^2}{\bar{S}^2} \tag{C.37}$$

$$c = \frac{1}{2}.\frac{\gamma^2(\bar{S} - P_1)}{\bar{S}}.\frac{P_1}{\bar{S}} = \frac{1}{2}.\frac{P_1}{(\bar{S} - P_1)}.\frac{\gamma^2(\bar{S} - P_1)^2}{\bar{S}^2} \tag{C.38}$$

where $\bar{S} = \exp(\overline{\ln S})$

Substituting for b^2 in equation C.37 gives

$$c = \frac{P_1}{(\bar{S} - P_1)}.\frac{b^2}{2} \tag{C.39}$$

$$2(\bar{S} - P_1).c = P_1.b^2 \tag{C.40}$$

$$P_1(b^2 + 2c) = 2\bar{S}c \tag{C.41}$$

Finally, the coefficients of the S-N curve (P1, P2 and γ) may be found by rearranging equations C.28, C.36 and C.41 as follows:

$$P_1 = \frac{2\bar{S}c}{b^2 + 2c} \tag{C.42}$$

$$\gamma = \frac{b\bar{S}}{\bar{S} - P_1} \tag{C.43}$$

$$P_2 = (\bar{S} - P_1).e^{-\gamma\overline{\ln N}} \tag{C.44}$$

An example of the results of using the above procedure is shown in Figure C.6, using data from **[Coleman, 1969]**, where the fitted curve takes the form:

$$\sigma_h = 11.03 \,.\, N^{-0.09} \tag{C.45}$$

where σ_h is the Hertzian Contact Stress in GPa
N is the number of cycles to produce a pit of minimum diameter 1.6 mm

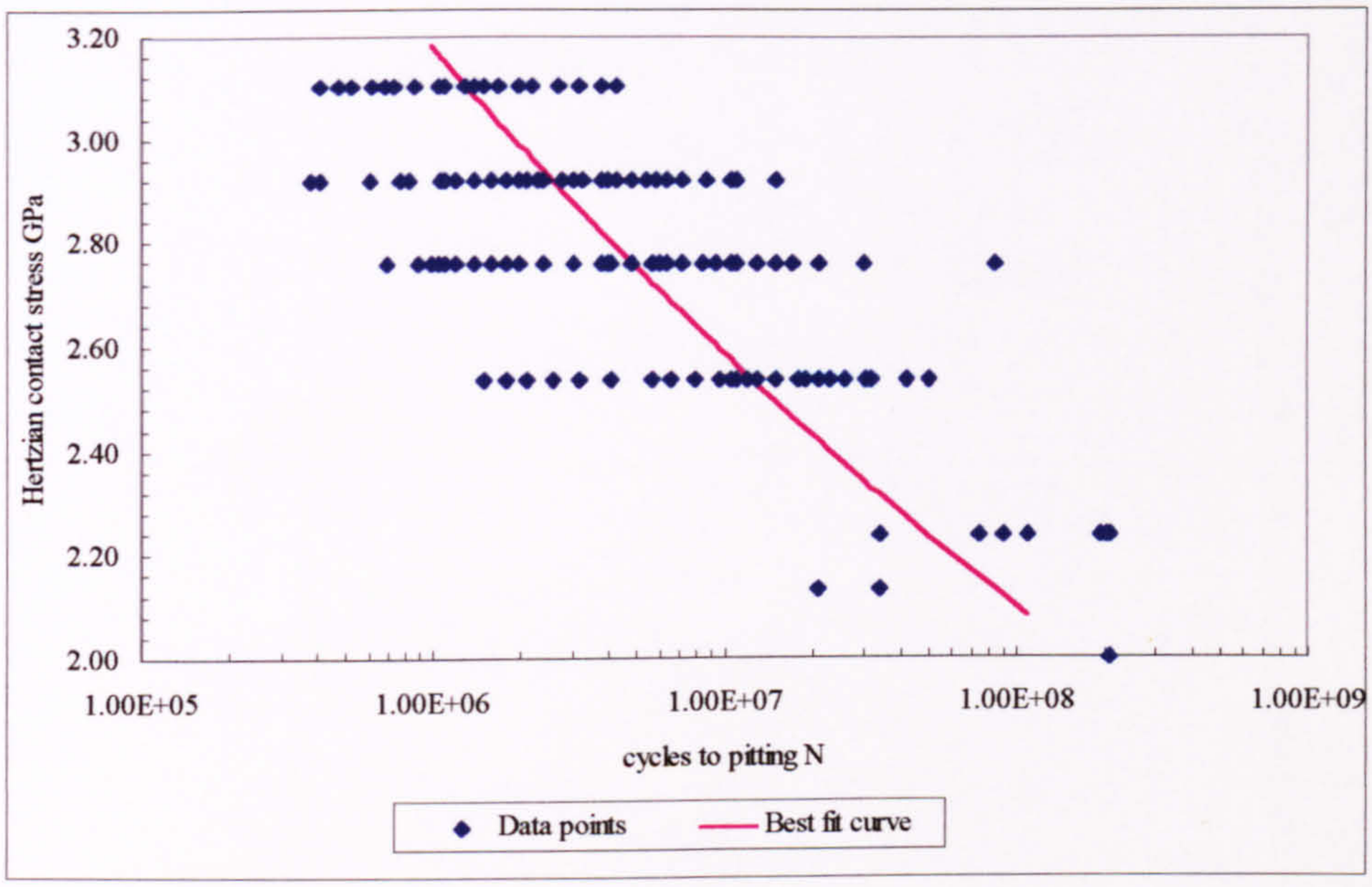

Figure C.6 : Example of Curve Fitting – Data from [Coleman, 1969]

C.4 Calculation of Probability for Fatigue Model TTF

C.4.1 Theory

Section C.2 has given an explanation of how values of N_{fi} are determined from equation C.21. Assuming a Log-normal distribution of stress at constant life, the time to failure is calculated for given values of p(F) by applying equation C.26, re-produced below:

$$N^{\gamma} = \frac{(Se^{-\delta} - P_1)}{P_2} = \alpha^{-\gamma} \qquad (C.46)$$

where δ is the factor used to choose the S-N curve for the respective probability.

The next requirement is to calculate p* from TTF. Starting with the required time to failure (or N_f), the probability of this amount of damage is to be calculated. The equation to be solved is that for Miner's damage sum

$$\sum_{i=1}^{m} \frac{n_i}{N_{fi}} = 1 \qquad (C.47)$$

where m is the number of discrete load states

n_i is the number of cycles of constant stress amplitude $\Delta\sigma_i$ in a sequence of m blocks

N_{fi} is the number of cycles to failure at $\Delta\sigma_i$

Equation C.47 may be re-written as, for the m load states:

$$\sum_{i=1}^{m} n_i (b_i)^{\frac{1}{a}} = C \qquad (C.48)$$

where $b_i = \dfrac{S_i.x - P_1}{P_2}$ etc. and Miner's constant is designated C.

The values for S_i,, n_i, are constant and are known. Values for P_1, P_2 and **a** are all constants, from the S-N curve, and are known.

x is a constant and is unknown - want to solve to find **x**

An iterative (successive approximation) method was applied, which was coded in Visual Basic™. Newton's approximation to the root of an equation was used **[Hall, 2000]**, stating that if the first estimate at a solution to an equation f(x) = 0 is x_0, then a closer approximation will be x_1 where:

$$x_1 = x_0 - \frac{f(x_0)}{f'(x_0)} \qquad (C.49)$$

where $f'(x_0)$ is the first derivative or differential of f(x), df/dx.

In this case equation C.48 is re-arranged to define f(x):

$$f(x) = n_1(S_1x - P_1)^{1/a} + n_2(S_2x - P_1)^{1/a} + ... - CP_2)^{1/a} \qquad (C.50)$$

Differentiating equation C.50:

$$f'(x) = \frac{n_1S_1}{a}(S_1x - P_1)^{1/a-1} + \frac{n_2S_2}{a}(S_2x - P_1)^{1/a-1} + ... \qquad (C.51)$$

The improved estimate of the solution is written (using equation C.49)

$$x_1 = x_0 - \frac{[n_1(S_1x_0 - P_1)^{1/a} + ... - CP_2{}^{1/a}]}{\frac{n_1S_1}{a}(S_1x_0 - P_1)^{1/a-1} + ... + ...} \qquad (C.52)$$

C.4.2 Calculation procedure

The equations given in Section C.4.1 have been coded in Visual Basic™, and are applied in the following sequence:

1. Estimate an approximate solution, x_0, i.e. a value of x for which f(x) is fairly small numerically. The first approximation is that below, which would be the solution if only the first term of the LHS of equation C.48 was present:

$$x_0 = \frac{P_1 + CP_2}{S_1} \qquad (C.53)$$

2. Evaluate f(x) and f'(x) at $x = x_0$, and hence calculate the better approximation x_1 using equation C.52.

3. Having found x_1, an even closer approximation x_2 may be calculated in the same way by evaluating the function and the differential at $x = x_1$:

$$x_2 = x_1 - \frac{[n_1(S_1x_1 - P_1)^{1/a} + ... - CP_2^{1/a}]}{\frac{n_1S_1}{a}(S_1x_1 - P_1)^{1/a-1} + ... + ...} \qquad (C.54)$$

4. The iteration was performed a number of times until the result converged, for a total of 100 separate TTF values, from 1 to 10^5 hours.

C.5 Bearing Life

For the taper roller bearings considered in this analysis, the bearing life may now be calculated using the standard procedure as described in ISO281. Using values for the dynamic loading rating contained in **[TIMKEN, 1994]**, values for the L_{10} life of each bearing may be calculated:

$$L_{10} = \left(\frac{C_1}{P_0}\right)^p .10^6 \text{ revolutions} \qquad (C.55)$$

or
$$L_{10} = \left(\frac{C_1}{P_0}\right)^{\frac{10}{3}} .\frac{10^6}{60n} \text{hours} \qquad (C.56)$$

where n is the rotational speed in rpm
exponent p is 10/3 for roller bearings and 3 for ball bearings.
C_1 is the bearing dynamic rating (kN)
P_0 is the dynamic equivalent radial load, in kN.

Experimental work to evaluate the slope of a Weibull distribution for bearing failures has yielded shape parameter (slope) values in the range 1.1 to 1.5 **[TIMKEN 1994]**. Assuming a minimum life of zero, the two-parameter Weibull distribution may be represented by:

$$F(t) = 1 - R(t) = 1 - \exp\left[-\left(\frac{t}{\eta}\right)^{\beta}\right] \qquad (C.57)$$

For calculating the L_{10} life in terms of the characteristic life (η) at a typical Weibull slope β of 1.5 **[TIMKEN, 1994]**, substitutions are made in equation B.41:

$$0.1 = 1 - \exp\left[-\left(\frac{L_{10}}{\eta}\right)^{1.5}\right]$$

$$\ln(0.9) = -\left(\frac{L_{10}}{\eta}\right)^{1.5}$$

$$\eta = 4.48\, L_{10} \qquad (C.58)$$

Substituting for η back into equation C.57:

$$1 - R(t) = 1 - \exp\left[-\left(\frac{t}{4.48\, L_{10}}\right)^{1.5}\right]$$

$$\ln\left(\frac{1}{R(t)}\right) = \left(\frac{t}{4.48\, L_{10}}\right)^{1.5}$$

$$L_x = 4.48\, L_{10}\left[\ln\left(\frac{1}{R(t)}\right)\right]^{\frac{2}{3}} \qquad (C.59)$$

This may be rewritten as

$$L_x = a_1 \,.\, L_{10} \qquad (C.60)$$

where

$$a_1 = 4.48\left(\ln\frac{100}{R}\right)^{\frac{2}{3}} \qquad (C.61)$$

C.6 Weibull Analysis of Maintenance Data

C.6.1 Bearing failure data from DARA Perth

The following analysis has been performed using data given in Appendix D.1 for the oil debris analysis of the Type A gearbox. A total of 68 records were included, and an indicative population of 140 gearboxes chosen as a typical fleet size.

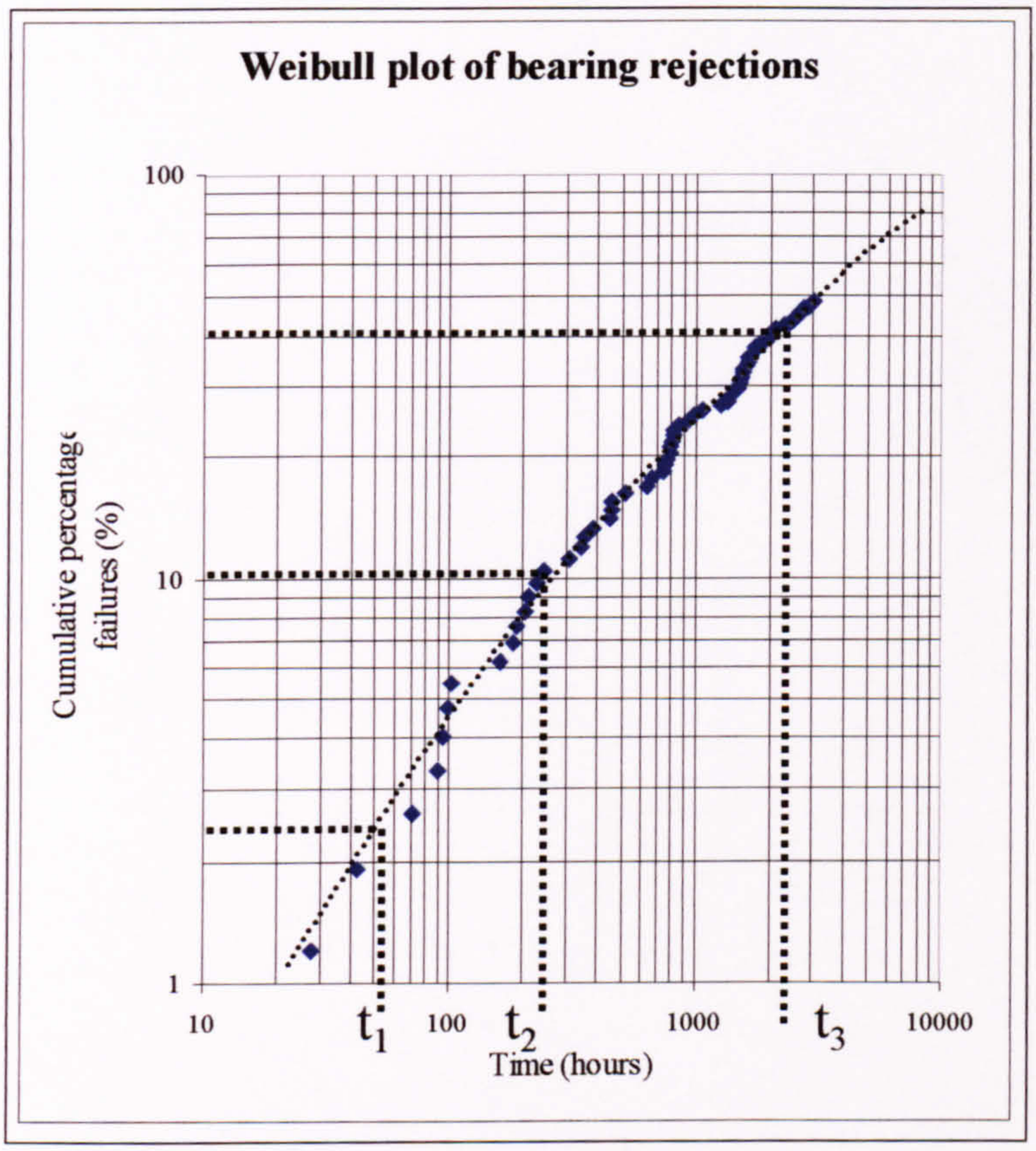

Figure C.7 : Raw data of IGB rejections (NAML data)

The initial data gave a slightly curved line, which indicates that a Weibull distribution could be fitted but with a non-zero minimum life (γ). The latter was determined graphically, as shown in Figure C.7 **[Carter, 1986]**, according to the following equation:

$$\gamma = t_2 - \frac{(t_3 - t_2)(t_2 - t_1)}{(t_3 - t_2) - (t_2 - t_1)} \qquad \text{(C.62)}$$

$$\gamma = 245 - \frac{(2100 - 245)(245 - 56)}{(2100 - 245) - (245 - 56)}$$

$$= 245 - 210 = 35 \text{ hours}$$

Next, the data was re-ranked by subtracting the minimum life (γ), calculated above, and produced a good fit to a straight line, Figure C.8. The slope of this line yielded a Weibull shape parameter (β) of 0.73. If the straight line fitted to the re-ranked data is extrapolated to intercept the x-axis, a value for the characteristic life η can be estimated:

$$\text{Intercept} \qquad \log_e (t - \gamma) = \log_e (\eta - 35) = 8.5$$

$$\text{Characteristic life } \eta = 4950 \text{ hours} \qquad \text{(C.63)}$$

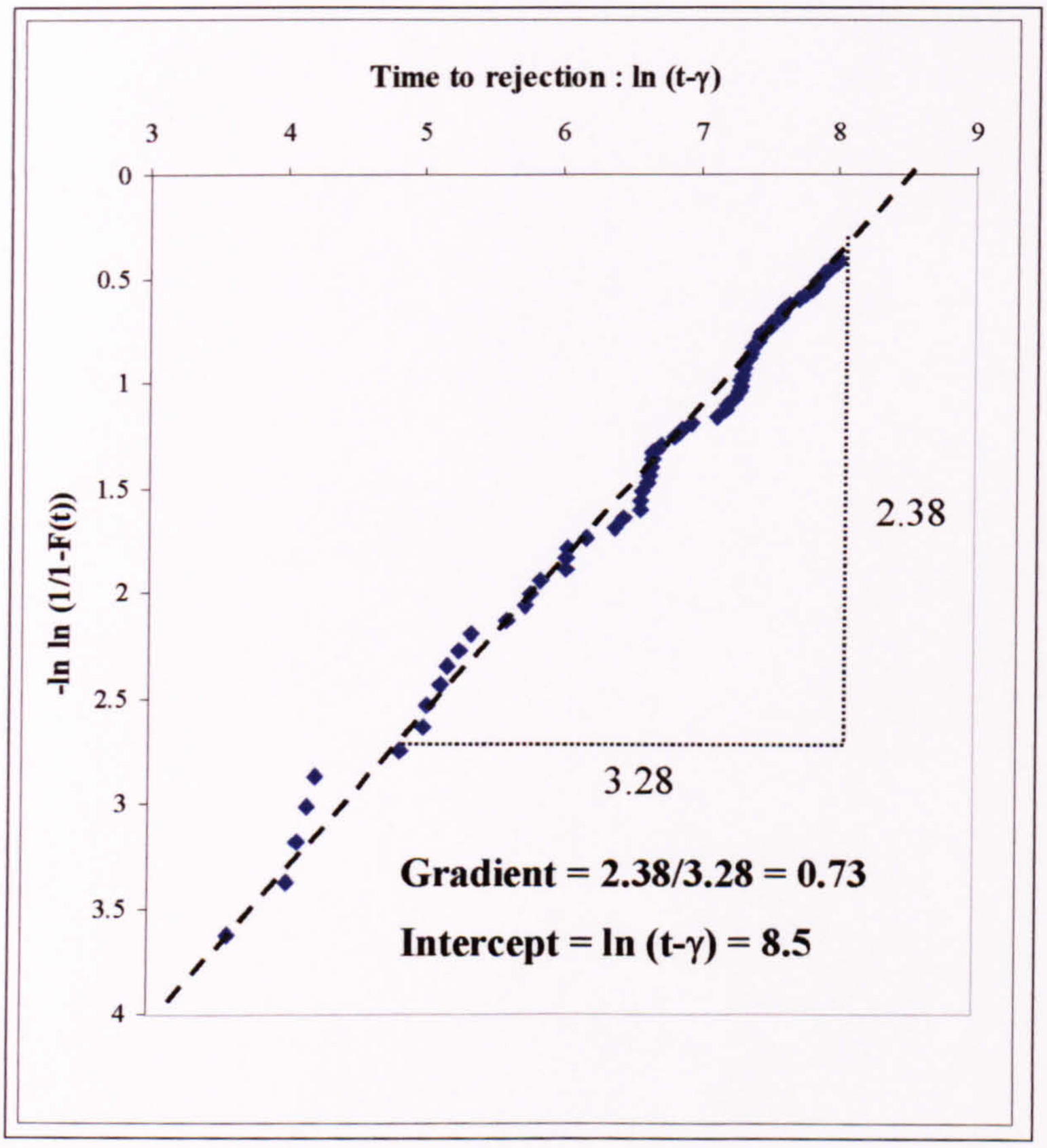

Figure C.8 : Re-ranked Weibull plot of removals of Type A gearbox for bearing wear debris (assumed population of 140 IGB)

Serial No	Hours	Reason(s) for rejection from service	Strip report Investigation results
1	245	High Fe SOA level	Wear to bearing spacer
2	184	Bearing debris	-
3	456	Bearing debris	Badly chipped rollers,output brg suspect
4	992.25	Bearing debris	-
5	1380	Bearing debris	-
6	71.1	Bearing debris	-
7	453.15	Very small flakes bearing debris	-
8	188.3	Bearing debris	-
9	793.5	Bearing debris	Outboard input shaft brg damaged
10		Bearing debris	Defect confirmed - outboard output brg failed
11	1513.15	S135, portions of ball surface	-
12	1275.1	Excessive CD debris	Outboard input shaft brg failed
13	790.1	Excessive debris, Bearing debris material Support sqn rejection.	-
14	1735	Bearing debris	Outer track on O/P shaft brg, cone and rollers spalled
15	1649.05	Excessive bearing debris	Outer brg on I/P shaft had track and rollers damaged, brg rollers extensively spalled
16	2509.1	Bearing debris flakes after 2nd trans chip warning in 25 hrs	Outer roller brg on I/P shaft, cup and rollers spalled
17	309	Excess bearing debris. Reject for investigation. Carry out alignment checks	-
18	103.4	Excess bearing debris. Carry out alignment checks	MSK 333 - spalling failure of I/P shaft outer brg. One roller completely spalled, another partially spalled. Damage appeared to originate from a point contact.
19	1983	Excess bearing debris. Carry out alignment checks	-
20	753.1	Excess bearing debris. Carry out alignment checks	-
21	750.45	Bearing debris. Support sqn rejection.	MSK350 - outboard brg on I/P shaft had suffered a spalling failure. In addition, both I/P and O/P seals had cuts in them caused by displacement and distortion of the expansion rings. Failure due to **misalignment** causing a stress

Appendix D.1 : Type A IGB rejections - source NAML

Serial No	Hours	Reason(s) for rejection from service	Strip report Investigation results
			concentration. Seals not involved in failure.
22	357.1	Bearing debris	MSK421 - failure of O/P outboard brg **Misalignment** resulting in stress concentration Debris blocking oilways may have reduced oil flow
23	1070	Excess Bearing debris	
24	1696.3	Excess PCS and Bearing debris. 4th CD warning	
25	1551	Fragment of bearing debris roller	Confirmed roller brg - O/P inboard brg Rollers brinelled/fatigue spalled
26	1847	Excess bearing debris	
27	1605.35	Persistent generation of bearing debris brg steel	I/P outboard brg rollers badly spalled
28	2106.25	Excess bearing debris	
29	212.35	Excess bearing debris	
30	3007.3	Excess bearing debris - support Sqn rejection	
31	1489	Possible bearing material	4 CD warnings in 2 days
32	2693.1	Sqn rejected g/box for oil condition (black) and excessive debris on CD. Fe rose from 0.1 to 116 ppm	Debris analysed as Bearing debris
33	803.35	Excess bearing debris	
34	1517.3	Some bearing debris post trans-chip (3rd in 50 hrs)	MSK664 - Spalling failures of I/P and O/P brgs (outboard) No misalignment, considered **excessive axial pre-load**
35	2031.55	2nd CD warning - retain oil in case Al/Mg alloy spiral has been damaged 1st CD warning - 8-10 small flakes bearing debris	Reject for F760 action
36	382.55	Large bearing debris flakes - reject for F760 action	
37	2552.55	Excess bearing debris - 2nd CD warning F760 action	
38	4400.3	Bearing debris flakes - F760 action	
39	1362.35	Bearing debris following trans chip	Perth report spalling of all 4 brgs
40	2375.3	Three CD warnings - all PCS, possible wear to brg cage - F760 action	

Appendix D.1 : Type A IGB rejections - source NAML

Serial No	Hours	Reason(s) for rejection from service	Strip report Investigation results
41	4288.1	Bearing debris brg - F760 action	
42	1878.25	Bearing debris flakes - F760 action	
43	42.2	PCS flakes after 3 CD warnings - F760 action	
44	90.2	Mostly small flakes PCS. One typical brg flake: analysis 0.3 Cr : 1.8 Ni	
45	1532.4	Small flakes PCS, bearing debris found following CD warning - F760 action	Defect confirmed - I/P outboard brg failed
46	765.25	Excessive generation of small bearing debris flakes Indicates wear to bearings	Output brg (Perth data)
47	99.35	Excess bearing debris and PCS - reject	
48	2741	Large bearing debris flakes following 2 CD warnings in 3 hrs - support rejection	
49	4450	Persistent generation of bearing debris steel flakes. Sqn rejected g/box after 3rd T/C warning in 2 days	
50	346.55	Excessive generation of bearing debris steel. Rate of debris generation excessive	
51	228	Excessive and persistent high Fe wear metal content	
52	633.25	Fine flakes of bearing debris steel post T/C	I/P inboard brg showed signs of wear to rollers, inside of brg track and taper on brg ring
53	5497	Excessive generation of bearing debris grade steel indicates bearing wear	
54	863.35	Debris ident SAE8719 bearing steel	O/P outboard brg found scored WSB3150-041 (Perth)
55	1448.15	Persistent T/C warnings. Excessive bearing debris steel.	
56	816.35	Debris ident SAE8719 bearing steel	O/P outboard brg found worn WSB3150-041 (Perth)
57	161.3	Sudden and excessive generation of bearing debris (prob SAE8719) and PCS, indicating wear to I/P and O/P bearings - T/C warning	Spalling damage to inner track and rolling elements I/P outboard brg (WSB3206) Suspect **excessive axial preload**

Appendix D.1 : Type A IGB rejections - source NAML

Serial No	Hours	Reason(s) for rejection from service	Strip report Investigation results
58	2018.3	Sample post T/C - several small flakes of bearing debris brg steel	**(see serial 34)**
59	2284.5	Sudden and excessive generation of bearing debris and PCS, indicating wear to bearings	
60	2990.15	Sudden generation of bearing debris flakes (SAE8719), indicating wear to I/P and O/P brgs - T/C warning	
61	1744	Excess debris flakes, indicating wear to bearings	
62	949.25	Sudden and excessive generation of bearing debris steel (SAE8119), indicating wear to bearings	
63	0	Persistent generation of S62 - source unknown Possible internal nut or screw - investigation	**(see serial 47)**
64	2596.25	Debris post T/C warning analysed as particles of debris bearing steel - Indicates wear to bearings	
65	815	PCS with some SAE8019 debris bearing steel on additional final test sample - increase in generation rate. Indicates continuing wear to bearings	Re-strip gearbox **(see serial 56)**
66	95	Sudden and excessive (in ~ 3.30 hrs) generation of PCS - wear to bearing cages	
67	519.2	Sudden and excessive generation of small flakes (30-100μm) of PCS and SAE8019/8119	Fatigue spalling of inner track and rollers WSB3206 - I/P outboard brg
68	1633.55	Three large flakes of PCS T/C warning (2nd in 3 hrs)	
69	4997.1	Excessive amounts debris bearing steel SAE8019/8119/8719	
70	4159.37	Increased generation of SAE8019/8119 and SAE8719 debris bearing steels	Defect confirmed all brgs worn - all done 1733.25hrs since IRAN
71	2875.5	Continued generation of large amounts debris bearing steel (SAE8019/8719) and PCS.	4 T/C in 23 hrs
72	458.2	Sqn rejected g/box after 3 T/C warnings. Debris contained number of debris SAE8019 flakes	Severe fatigue spalling of group of 6 rollers. Damage consistent with application of excessive

Serial No	Hours	Reason(s) for rejection from service	Strip report Investigation results
			axial loading (pre-load?)
73	4749.35	SAE8719, indicates excessive bearing wear	
74	667.5	Bearing debris type brg steel - Indicates wear to I/P or O/P bearings	
75	1558	Sudden generation of bearing debris material Indicates excessive wear to bearings	
76	28	Bearing debris - EFD rejection 3396/N	**Excessive axial pre-load**
77	205	Bearing debris - EFD rejection 3678/N	**Excessive axial pre-load**

Appendix D.1 : Type A IGB rejections - source NAML

Ref No	TSN hours	TSO hours	Pinion hours	Gear hours	Fault	Details/Action taken
1	2322	877			O/P brg siezed onto O/P shaft. Gbox	Oil feed to brg failed. Oil present after
					casting disintegrated around brg hsg	damage = 0.7 pint (50% of normal)
					area : 35mm from end	
					YEO/846/165A/88 refers.	25 hr oil sample - chip wipe 3 hr 10 min
					Report no MSK 565	before damage showed no excessive
					BER	debris
2	3865	540	540	540	LIFEX - High Fe count. Fretting/fatigue spalling	New gears, brgs and seals - RECON
			to 0	to 0	Brg steel	
3	2161	1155	2161	1155	Corr on I/P shaft - spline wear.	New I/P shaft
			to 0		Corr on support assy S6135-66260-2	New supp assy
4	1417	na	1417	1417	I/P seal leaking	RECON
			to 0	to 0	O/P shaft, I/P splines worn - scrapped	Oil contam Source O/P O/B brg,
					O/P flange corroded	I/P I/B brg also damaged
					Spiral corroded	Plug S6135-66238 and oil seal missing
5	5593	1080			Corrosion on refill point (top surface)	Scrapped - BER
6	2553	na	2553	2553	I/P, O/P reject gears	New I/P and O/P gears
			to 0	to 0	I/P splines pitted WD01-68-11211	
					Oil sample - plain carbon steel flakes	Brgs scrapped
7	3187	633			Fe count rising (SOAP rpt 93/128)	Scrapped - BER
					O/P brg heavy corrosion, I/P shaft	
					corrosion on seal face, O/P flange	
					corroded, I/P hsg corroded	

Appendix D.2 : Sample of archived records for Type A IGB - source DARA Perth

Ref No	TSN hours	TSO hours	Pinion hours	Gear hours	Fault	Details/Action taken
8	2196	na	2196 to 0	2196	I/P splines worn	I/P gear replaced
9	5029	2833	2833	5029	I/P splines worn and stepped. Sight glass discoloured. O/B brg scored	BER - Corrosion (splines?)
10	1990	na	1990	1990	Metallic debris on MCD, brg failure	New bearings
11	2893	na	2893	2893	Internal break-up. O/P shaft deeply scored -	New pinion/gear
					rejected. Spiral worn and scored internal	Brg WSB3209-041
					surface of housing. I/P splines worn - rejected.	
					S6135-66231 cover housing corroded.	
12	2876				Corrosion	RECON - Corrosion repaired
13	4667	1791			Salt water contam - brg seized	Scrapped - BER
14	1892	982	1892 to 0	1892	I/P splines worn O/P housing corroded	I/P shaft replaced Replaced
15	2078	186			Salt water immersed - corrosion	Scrapped - BER
16	2474	n/a	2474	2474	Oil seal leaking - output shaft	Replaced seal - bearings serviceable
17	1755	n/a	1755	1755	SOAP reject	Bearings replaced, gears refitted
					WSB3206-041 Cage damaged, rollers spalled	
					WSB3209-041 Race damaged/3253/3150 also	
					damaged - source WSB 3206	

Appendix D.2 : Sample of archived records for Type A IGB - source DARA Perth

Ref No	TSN hours	TSO hours	Pinion hours	Gear hours	Fault	Details/Action taken
18			6852 calc*		*calculated AP100N-0101-Chap 2 para 0203	New I/P, O/P gears
					LIFEX	
19	4065	2262	nk	nk	High Fe count I/P, O/P gears rejected, I/P splines pitted	SAE4340 - all brgs replaced New gears fitted
20	5037	971	971	971	Housing corroded Micropitting on I/P pinion	Scrapped - BER
21		5401	nk	nk	Disconnect splines excessively worn 0.008"	Scrapped - BER
					O/P brg slight scoring	
22	2257	nk	2257	2257	Requires RECON	New I/P pinion fitted
			to 0			
23	3396	28	28	28	High debris count	Stripped - partial IRAN; New bearings Input O/B brg WSB 3206-041
24	4365	997	997	997	Trans chip light. All brgs marked. Centre housing corroded. I/P and O/P gears - pitting and scoring Flange O/P scored and corroded.	Assembly scrapped.
25	2109	n/a	2109	2109	I/P, O/P flanges corroded	Strip O/P housing (rotational drag)
						Strip I/P housing - remove corrosion
						I/P, O/P gears retained
26	1975	nk	nk	nk	nk	nk

Appendix D.2 : Sample of archived records for Type A IGB - source DARA Perth

Ref No	TSN hours	TSO hours	Pinion hours	Gear hours	Fault	Details/Action taken
27	4777	2292	4777	4777	Centre housing corroded around replen points and midway between them.	BER
28		2645			Corrosion around filter plugs	Scrapped
					I/P splines worn	
29	1480		1480 to 0	1480		RECON
30	1788	309	309	1788	Trans chip light	IRAN - bearings repaired
31	3113	1633	1633 to 0	3113 to 0	Excessive metal chips on mag plug O/P gear pitting, I/P splines worn Centre housing corrosion (sight glass area) S6135-66201-2	New pinion/gear
32	2653	na	2653	2653	I/P drive shaft splines worn and stepped.	New I/P shaft/gear
			to 0		O/P brgs damaged	Brgs replaced
33	1121		1121	1121	nk	nk
34	1433	312	1433	1433	Trans chip light (previous history) Spiral damaged	RECON (pinion/gear retained) NAML - excessive fine debris Dirty build (WSB3150 - scrapped) All brgs replaced
35	2088	654	2088 to 0	2088 to 0	I/P shaft worn beyond limits O/P brg scored, I/P brg damaged Spiral corroded	I/P and O/P shafts replaced New brgs

Appendix D.2 : Sample of archived records for Type A IGB - source DARA Perth

Ref No	TSN hours	TSO hours	Pinion hours	Gear hours	Fault	Details/Action taken
36	1000?	na	1000?	1000?	T/R lock shroud loose - disconnect	Replaced I/P, O/P gears
			to 0	to 0	coupling worn	Gearbox idle for 2-3 years - log cards lost
						Hours not known - rejected
37	672				Crashed a/c gearbox Spiral scored - corrosion Shock loaded	I/P, O/P gears scrapped - replaced RECON
38	1488	815	815 to 0	815 to 0	O/P brg worn, cage loose, rollers scored	Gears and brgs replaced NAML brg steel WSB3150
39					IRAN	Re-strip
40	2063	1391	575	575	G/B difficult to turn and noisy when turned Water ingress through O/P seal	New brgs I/P, O/P gears retained RECON
41	2000		2000	2000	Required RECON	New I/P gears and brgs
			to 0	to 0		
42	1895		1895	1895	I/P seal leaking (changed twice before)	New I/P shaft
			to 0		IRAN	
43	3395	na	3395	3395	Required RECON	RECON
44	6880	3485	6880 to 0	6880 to 0	LIFEX pinion and gear Light scoring on rollers (O/P brg) Input splines worn	RECON
45	6978	98	98	98	Sudden/excessive generation of MCD debris	Gear/pinion replaced

Appendix D.2 : Sample of archived records for Type A IGB - source DARA Perth

Ref No	TSN hours	TSO hours	Pinion hours	Gear hours	Fault	Details/Action taken
					Flakes of PCS - brg cages Slight scuffing of gear teeth Scoring on O/P brg	All brg replaced
46	456				3rd chip warning	Cat 4 repair at Fleetlands
47	1575		1575 to 0	1575	High EFD I/P splines worn	RECON - I/P shaft replaced, O/P shaft retained All brgs replaced
48	2361	785	785 to 0	2361 to 0	Input splines worn beyond limits O/P brg good condition	I/P, O/P shafts and all brgs replaced
49	833				nk	Cat 4 repair at Fleetlands
50	898		898 to 0	898	Jaw teeth undersize	RECON
51	3872	2973	2973 to 0	3872 to 0	Input splines worn	New I/P, O/P shaft fitted New brgs
52	2497	na	2497	2497	Slight wear O/P brg Corrosion cover hsg S6135-66231	RECON
53	3812	1315	3812 to 0	3812 to 0	Fretting of splines on I/P shaft and disconnect coupling - pitted	New I/P, O/P shaft RECON
54	2069	na	2069	2069	nk	nk
55	4499	2429			I/P shaft splines stepped	RECON - new I/P, O/P gears

Appendix D.2 : Sample of archived records for Type A IGB - source DARA Perth

Ref No	TSN hours	TSO hours	Pinion hours	Gear hours	Fault	Details/Action taken
					Rollers breaking up - WSB3150 Spiral corroded	
56	2209		2209	2209	O/P flange corroded - pitted IRAN	Flange replaced (only)
57	5564		5564	5564	LIFEX	New I/P, O/P shafts, brgs New housing S6135-66201-C Shot peen O/P flange S6135-66228
58	2055		2055	2055	Input hsg - corroded	RECON - new I/P gear
			to 0		Centre hsg - cracked	
					I/P splines stepped	
59	2307		2307	2307	I/P brg (cage) damage - EFD - IRAN	New I/P, O/P gears
			to 0	to 0	O/P brg good condition	
					I/P, O/P splines worn (corroded)	
60	1987		1987 to 0	1987	nk	RECON
61	5628	3640	3640 to 0	5628 to 0	LIFEX I/P splines worn	New I/P and O/P gears and brgs
62	757		757 to 0	757	Metal flake on MCD - brgs spalled (rollers) All brg damaged - see WSB3206	RECON - I/P shaft replaced O/P shaft retained. All brgs replaced
63	1635	878	878 to 0	1635 to 0	Excessive wear on I/P splines - IRAN Scratches on O/P brg rollers	New I/P, O/P shafts

Appendix D.2 : Sample of archived records for Type A IGB - source DARA Perth

Ref No	TSN hours	TSO hours	Pinion hours	Gear hours	Fault	Details/Action taken
64	2876		2876	2876	Body corroded	New I/P shaft fitted
			to 0		I/P splines worn	
					Brgs worn	
					Cover hsg corrosion S6135-66231	
65	481		481	481	nk	RECON
66	1448	967	1448	1448	Trans chip EFD, I/P inner brg - IRAN O/P rollers breaking up O/P flange corroded I/P splines corroded	New brgs, I/P and O/P shafts fitted Brg steel cone WSB3253A1 (NAML)
67	530	n/a	530 to 0	530 to 0	Shock loaded Cover hsg corroded BER	New I/P, O/P shafts and brgs
68	1312	782	782 to 0	782 to 0	I/P splines worn - IRAN O/P brg scored Cover hsg corroded S6135-66231 O/P flange pitted	New Brgs, I/P and O/P shafts fitted
69	3912	na	3912	3912	Splines worn	New I/P and O/P shafts fitted
			to 0	to 0	Light scoring on O/P brg	
70	3711		3711 to 0	3711 to 0	I/P splines worn beyond limits No visible damage to O/P brg	New I/P, O/P shafts
71	5458	1746	1746	1746	Spiral worn MCD chip light (NAML)	New I/P, O/P shafts
72	2893	n/a	2893	2893	nk	New I/P, O/P shafts

Appendix D.2 : Sample of archived records for Type A IGB - source DARA Perth

Ref No	TSN hours	TSO hours	Pinion hours	Gear hours	Fault	Details/Action taken
			to 0	to 0		
73	5094	2201	2201	2201	I/P, O/P oil seals leaking I/P roller brg damaged on fwd face Slight scoring on O/P brg rollers I/P splines worn O/P shaft corroded	New I/P, O/P shafts
74	5352	674	674	674	Warning Light. O/P outbd brg cage broken up	New I/P, O/P shafts
			to 0	to 0	I/P shaft corrosion	New brgs fitted
75	1077	n/a	1077	1077	Brg wear	I/P and O/P gears serviceable - retained
					Spiral cracked	New brgs and spiral
76	2225	1867	?	?	O/P brg cage damaged during removal of	New I/P and O/P gears
					leaking shaft seal - O/P brg scored and	New brgs
					dented. I/P and O/P splines worn	
77	761	n/a			Suspect brg break-up	nk
78	1235	474	?	?	MCD light: metal particles on plug - IRAN O/P brg good condition. Excessive scoring on WSB3150 (O/P outboard brg) I/P splines worn, corrosion	New I/P, O/P shafts New brgs
79	2990	nk			Rejected - NAML.	New I/P, O/P shafts
					Wear WSB 3253, WSB 3206 (I/P)	New brgs
					I/P splines pitted	
80	3514	nk	3514	3514	Fails rotational wear limits	New I/P, O/P shafts

Appendix D.2 : Sample of archived records for Type A IGB - source DARA Perth

Ref No	TSN hours	TSO hours	Pinion hours	Gear hours	Fault	Details/Action taken
			to 0	to 0	O/P brg - good condition	
					Worn splines - I/P shaft	
81	1379				Chip detector warning	RECON
82	2882	1503	2882 to 0	2882	Chip light in flight - high debris count I/P spline chipped NAML WSB3150 (O/P outboard)	New I/P shaft All brgs replaced
83	1450	n/a	1450	1450	nk	RECON
84	5510	4060	5510 to 0	5510 to 0	Rejected - NAML WSB3209, WSB3150 (Scoring) O/P brg rollers breaking-up I/P splines worn	New I/P, O/P shafts
85	617				Chip detector	RECON
86	1298	212	212 to 0	212	EFD rejection O/P outboard rollers spalled I/P splines worn	New I/P shaft (only)
87	1542	456	244	456	Damaged brg rollers O/P brg (MCD warnings) WSB3150 - O/P outboard	New brgs fitted - only
88	2037	951	739 to 0	951 to 0	Rejected - NAML IRAN	New I/P, O/P shafts New brgs and spiral
89	2055	970	18	18	I/P seal leak	New I/P, O/P hsg and brgs
90	2931	824	2931	2931	nk	

Appendix D.2 : Sample of archived records for Type A IGB - source DARA Perth

Ref No	TSN hours	TSO hours	Pinion hours	Gear hours	Fault	Details/Action taken
91	3596	1489	3596 to 0	3596 to 0	NAML rejection O/P gear pitting	New I/P, O/P shafts NAML - Mag plug debris
92	1066	n/a				RECON
93	5352	4286			Corrosion out of limits on annulus of sight glass fitting O/P bearing satisfactory	BER
94	1005				Oil leak - I/P seal	nk
95	1379				nk	RECON : WHL
96	1719	339	? to 0	? to 0	Excess wear I/P splines - IRAN	New I/P, O/P shafts New brgs
97	3126	1520	1520	1520	nk	RECON
98	4190	1064	? to 0	? to 0	I/P drive pinion scored	New I/P, O/P gears
99	3688		3688 to 0	3688 to 0	I/P splines worn beyond limits	New I/P, O/P gears
100	2128		2128	2128	nk	RECON
101	2128*		2128 to 0	2128	Silica gel contam - I/P pinion pitted	New I/P pinion, I/P hsg, base plate New brgs

Appendix D.2 : Sample of archived records for Type A IGB - source DARA Perth

Ref No	TSN hours	TSO hours	Pinion hours	Gear hours	Fault	Details/Action taken
102	2533	405	405 to 0	2533 to 0	Overtorqued on test - heavy wear on gear teeth	New I/P, O/P gears
103	631		631	631	I/P splines - corrosion and fretting - IRAN	New I/P, O/P gears
			to 0	to 0		New brgs
104	1882	579	1882 to 0	1882	Chip light on shutdown NAML WSB3209 (O/P inboard)	New I/P pinion, O/P retained New brgs fitted
105	1972	90	91	1973	NAML - brg steel in oil	All brgs rejected and replaced
106	4920		4920	4920	Fails wear check on I/P splines	New I/P, O/P shafts
			to 0	to 0		New brgs
107	1857		1857	1857	Corrosion of casing around sight glass	New I/P, O/P shafts
					Excessive wear of I/P splines	
					No visible damage to O/P brg	
108	1003	n/a	1003	1003	nk	RECON
109	2250	1246	2250 to 0	2250 to 0	Debris on MCD NAML WSB3150 (O/P outboard brg)	New I/P, O/P gears All brgs scrapped and replaced
110	1933				nk	RECON
111	4176	1576	4176 to 0	4176	MCD debris (EFD) WSB3209 (O/P inboard) rollers Brinelled/fatigue spalled	New I/P and O/P hsg New I/P gear and brgs

Appendix D.2 : Sample of archived records for Type A IGB - source DARA Perth

Ref No	TSN hours	TSO hours	Pinion hours	Gear hours	Fault	Details/Action taken
112	5680	1504	1504	5680	LIFEX - fault not known Corrosion on all hsgs	BER - Scrapped
113	2181				RECON - Fleetlands	
114	3002	821			RECON - Fleetlands	
115	8306	5303	? to 0	? to 0	I/P splines worn - corroded Cover hsg corroded S6135-66231	
116	1666		1666	1666	Disconnect coupling damaged	Repair to disconnect coupling
117	1783		1783	1783	Loosely assembled at Fleetlands	Repair and tested
118	3230		3230 to 0	3230	EFD	New I/P shaft, I/P and O/P hsgs New O/P flange and brgs
119	3751	521	521	3751	Leaking O/P seal and breather pin broken Scores on rollers (O/P brg)	
120	5092	1862	1862	5092	O/P gear LIFEX	BER - shafts LIFEX Casing corroded

KEY	BER	Beyond Economic Repair		PCS Plain Carbon Steel
	IRAN	Inspect and Repair as Necessary		RECON Reconditioned
	LIFEX	Life expired		TSO Time since overhaul
	MCD	Magnetic Chip Detector		TSN Time since new

Appendix D.2 : Sample of archived records for Type A IGB - source DARA Perth

DATE	Defective item	Symptom	Fault	Action	Removed item	Replaced item	A/F hours
25.05.83	GEARSHAFT		DAMAGED	MOD+RECOND	WARWAU7		0
10.04.86	IGB	WARNINGLIGHTON	CMTNMTSWARF	RECTINSITU	WAK373		4568
19.03.91	WINDOWASSY	DISCOLOURED	DISCOLOURED	RPLLASCRAP	ABD5375	NOTREC	6489
16.09.96	WINDOWASSY	SURVEYOPS-PREPS	DET/PERISHED	RPLLASCRAP	WAH355		7803
16.09.96	SPRINGHELIC	SURVEYOPS-PREPS	CORRODED	RPLLASCRAP	NONE	NONE	7803
02.12.96	IGB	FAILEDTST/CHECK	FAILSBITECHECK	RECTINSITU	WAH355		7803
30.01.97	IGB	SURVEYOPS-PREPS	FAULTFORCATEG	ENTRYDFLOG	WAH355		7821
21.03.97	IGB	FLUIDLEVELHIGH	FLUIDLEVELHIGH	RECTINSITU	WAH355		7859
24.03.97	OUTPUTSEAL	OTHERLQDLEAK	OTHERLQDLEAK	RPLLASCRAP			7864
24.03.97	BREATHER		OTHERLQDLEAK	RPLLASCRAP			0
28.03.97	IGB	WARNINGLIGHTON	FAULTFORCATEG	RECTINSITU	WAH355		7864
28.04.97	IGB	FAILS-EXTINGUISH	FAILSBITECHECK	RECTINSITU	WAH355		7881
30.04.97	IGB	WARNINGLIGHTON	CMTNBYDRT/SAND	RPLLAR2	WAH355		7884
07.02.88	STUD	SHEARED	SHEARED	RPLLAR2	WAX129	WAL383	4631
17.02.88	IGB	WARNINGLIGHTON	SAFEEQNOTKNOW	RECTINSITU		NONE	4635
16.07.91	IGB	SCORED	SCORED	RPLLAR3/4	WAL383	WAH350	6096
27.10.92	IGB	FAILSTOCANCEL	NOFAULTFOUND	NOFAULTFOUND	WAH350		6363
07.10.93	IGB	ROBBED	ROBBED	ROBITEMRPL	WAH350	WAM340	6600
19.02.92	IGB		CORROSIONPITING	RPLLAR2	WAY108	WAH346	6953
12.09.94	IGB	WORN	WORN	RPLLAR2	WAH346	WAA209	7765
14.02.91	JAW, I/P DISCC	OUTOFLIMITS	WORN	RPLLAR2	WAX103	WAA193	0
13.09.91	IGB	ROBBED	ROBBED	ROBITEMRPL	WAA193	WAC278	6950
03.11.94	IGB	CORROSIONPITING	CORROSIONPITING	MITEMSRPLREP			7945
29.02.96	SEALPLAIN	GEARBOXOILLEAK	GEARBOXOILLEAK	RPLLASCRAP	NONE	NONE	8261
21.11.90	SEALPLAIN (INPUT)	HYDOILLEAK	SEALINGLEAKING	RPLLASCRAP	NOTREC	NONE	6715
19.09.86	CHIPDETECTOR	WARNINGLIGHTON	SAFEEQNOTKNOW	RECTINSITU	NONE	NONE	3211
16.12.88	IGB	CMTNBYOIL	CMTNBYOIL	RECTINSITU	WAG332	NONE	3921
15.06.89	IGB	CMTNMTSWARF	CMTNMTSWARF	RPLLAR2	WAG332	WAK368	4035
15.06.89	BEARING		CHIPPED	MOD+RECOND	WAL332		0
24.04.91	IGB	CMTNMTSWARF	CMTNMTSWARF	RPLLAR2	WAK368	WAX71	4802

Appendix D.3 : Records for maintenance for Type A IGB - source EDA

DATE	Defective item	Symptom	Fault	Action	Removed item	Replaced item	A/F hours
17.01.87	BEARING	INDOFFAULT	CHIPPED	MOD+RECOND	WAH340	WAW42	4333
22.07.82	FLANGEOPUT	GEARBOXOILLEAK	LEAKING	RECONDITIOND	WAH340	WAC237	3613
28.03.94	IGB	LIFEEXCOMPONT	LIFEEXCOMPONT	RPLLAR2	WAN44	WAY132	6800
21.12.95	IGB	STI/STUCK	STI/STUCK	RPLLAR3/4	WAY132	ABX0884	7455
03.06.92	IGB	WARNINGLIGHTON	WARNINGLIGHTON	RECTINSITU	WAH343		6670
08.06.92	IGB	WARNINGLIGHTON	WARNINGLIGHTON	RPLLAR2	WAH343	WAD286	6681
13.07.89	SEALPLAIN (INPUT)	LEAKING	WORN	MITEMSRPLREP	NOTREC		5945
11.05.93	IGB	FALEARLYFALDCHK	BEARINGDET	RPLLAR2	AAU3701	WAN389	6799
09.11.95	IGB	ROBBED	ROBBED	ROBITEMRPL	WAN389		7601
09.09.96	SEALPLAIN (INPUT)	OTHERLQDLEAK	OTHERLQDLEAK	RPLLASCRAP	NONE	NONE	7800
29.11.96	IGB	OVERCHARGED	OVERCHARGED	RECTINSITU	WAN389		7949
30.06.92	JAWASSY,DISCCO	OUTOFLIMITS	JOINTWORN	RPLLASCRAP	WAX83	WAY113	6382
21.08.90	IGB	FLUIDLEVELLOW	FLUIDLEVELLOW	RECTINSITU	WAX83		5911
01.12.87	SEALPLAIN (INPUT)	GEARBOXOILLEAK	WORN	RPLLASCRAP	NONE	NONE	4954
08.02.88	SEALPLAIN (INPUT)	LEAKING	WORN	RPLLASCRAP	NONE	NONE	5030
14.09.93	IGB	FLUIDLEVELHIGH	FLUIDLEVELHIGH	RECTINSITU	WAC247		6703
23.07.95	IGB	INTERMITTENT	INTERMITTENT	RECTINSITU	WAC247		7393
22.07.95	IGB	WARNINGLIGHTON	WARNINGLIGHTON	SCHEDSERV	WAC247		7391
06.08.95	IGB	FAILSTOADJUST	OUTOFLIMITS	RPLLAR2	WAC247	WAL382	7408
15.05.96	IGB	ONINSPECTION	CORRODED	RPLLAR2	WAC247	WAC382	7630
29.10.92	IGB	WORN	WORN	RPLLAR2	WAH347	WAU10	7818
07.12.94	IGB	GEARBOXOILLEAK	NOFAULTFOUND	NOFAULTFOUND	WAU10		8433
19.05.95	IGB		LIFEEXCOMPONT	R3/4(R/D)			0
16.10.91	IGB		ROBBED	ROBITEMRPL	WAY132	WAX99	6998
07.01.91	IGB	ROBBED	ROBBED	ROBITEMRPL	WAA209	WAW37	6342
02.04.92	IGB	FLUIDLEVELLOW	FLUIDLEVELLOW	RPLLAR3/4	WAW37	WAX98	6342
02.04.92	IGB		CORRODED	DFNRHAR3/4	WAY132	NOTREC	0
02.04.92	JAW,I/P DISCC		NOTCOMPATIBLE	RPLLAR2		NONE	0
29.09.94	IGB	FLUIDLEVELHIGH	FLUIDLEVELHIGH	RECTINSITU	WAX98		7105
07.08.85	IGB	OUTOFALIGNMENT	OUTOFLIMITS	RPLLAR3/4	WAG337	WAD292	5763

Appendix D.3 : Records for maintenance for Type A IGB - source EDA

DATE	Defective item	Symptom	Fault	Action	Removed item	Replaced item	A/F hours
07.08.85	BEARINGCMPT		CMTNMTSWARF	RECONDITIOND	WAG337		0
01.06.92	SEALPLAIN	GEARBOXOILLEAK	GEARBOXOILLEAK	RPLLASCRAP	WAD292	WAY107	8071
24.04.91	SEALPLAIN (INPUT)	WORN	BUSHWORN	RPLLASCRAP	NOTREC	NONE	7719
30.08.84	IGB		DAMAGED	RPLLAR2	WAW48	WAX25	4321
12.07.90	IGB	WARNINGLIGHTON	SAFEEQNOTKNOW	RECTINSITU	WAX75	1528	5850
03.09.90	IGB	WARNINGLIGHTON	WARNINGLIGHTON	RECTINSITU	WAX75		5876
17.09.90	IGB	SHOCKLOADED	SHOCKLOADED	RPLLAR2	WAX75	WAD309	5899
12.06.91	IGB	WARNINGLIGHTON	WARNINGLIGHTON	RPLLAR2	WAD309	WAD302	6169
14.09.93	IGB	CORRODED	CORRODED	MITEMSRPLREP	WAD302		7089
18.01.95	IGB	DISCOLOURED	DISCOLOURED	RECTINSITU	WAD302		7407
23.04.97	IGB	NOINDICATION	NOFAULTFOUND	NOFAULTFOUND	WAD302		8223
11.06.97	IGB	NOINDICATION	CMTNBYDRT/SAND	ENTRYDFLOG	WAD302		8268
24.06.97	IGB	FAILEDTST/CHECK	WORN	RPLLAR2	WAD302	WAF325	8309
05.07.89	SEAL	HYDOILLEAK	HYDOILLEAK	RPLLAR2	WAW55	WARWAX81	5729
23.01.93	IGB	WORN	WORN	RPLLAR2	WAH344	WAD308	7015
02.02.93	IGB		WORN	RPLLAR3/4	WAH344	NOTREC	0
12.05.95	OUTPUTSEAL	GEARBOXOILLEAK	GEARBOXOILLEAK	RPLLASCRAP			7937
02.08.95	IGB	WARNINGLIGHTON	NOFAULTFOUND	RPLLAR2	WAD308	WAW44	7983
29.05.85	IGB	INDOFFAULT	SAFEEQNOTKNOW	RPLLAR2	NOTREC	NOTREC	3415
03.06.85	IGB	INDOFFAULT	SAFEEQNOTKNOW	RPLLAR3/4	WAW52	WAH352	3422
22.04.82	SPIRAL	WORN	WORN	MITEMSRPLREP	NONE	NONE	2475
05.09.90	IGB	FALEARLYFALDCHK	CMTNMTSWARF	RPLLAR2	WAY126	WAY113	4982
05.09.90	BEARING		BKN/FRACTURED	RECONDITIOND	WAY126		0
25.03.91	IGB - SHAFTINPUT	FAILGAUGECHECK	SPLINEWORN	RPLLAR2 - REPAIREI	WAY113	WAJ360	5369
09.04.92	IGB	WARNINGLIGHTON	CMTNMTSWARF	RECTINSITU	WAJ360		5943
04.03.92	SEALPLAIN (INPUT)	GEARBOXOILLEAK	GEARBOXOILLEAK	RPLLASCRAP	NOTREC	NONE	5882
21.06.86	IGB	INDSUSP/INCOR	SAFEEQNOTKNOW	RECTINSITU	NONE	NONE	4360
04.08.86	IGB	WARNINGLIGHTON	CMTNMTSWARF	MOD+RECOND	WAD281	WAJ362	4381
01.07.92	IGB	CORRODED	CORRODED	RPLLAR2	WAJ362	WAD315	6697
03.11.91	BEARING		SCORED	SCRAPPED	WAW43		0

Appendix D.3 : Records for maintenance for Type A IGB - source EDA

DATE	Defective item	Symptom	Fault	Action	Removed item	Replaced item	A/F hours
14.07.92	IGB	WORN	WORN	RPLLAR2	AAL7163	WAD306	6356
18.06.93	IGB	ROBBED	ROBBED	ROBITEMRPL	WAD30B	AAY0842	6815
04.03.93	SEALPLAIN (INPUT)	GEARBOXOILLEAK	GEARBOXOILLEAK	RPLLAR2	NOTREC	NONE	6676
28.04.97	SEALPLAIN (INPUT)	OTHERLQDLEAK	DET/PERISHED	RPLLASCRAP	NONE	NONE	7616
19.04.82			LIFEEXCOMPONT	MOD+RECOND	WARWAW34		0
21.06.90	IGB	LIFEEXCOMPONT	LIFEEXCOMPONT	RPLLAR2	WAX102	ABRWAW40	7180
27.09.90	IGB	INDICATORSTICK	INDICATORSTICK	RPLLAR3/4	ABRWAW90R1	AAK7958	7270
15.02.95	IGB		CORRODEDSURFACE	R3/4(R/D)			8285
06.06.95	IGB	CORRODED	CORRODED	RPLLAR3/4		WAN390	8285
22.07.97	IGB	SURVEYOPS-PREPS	SURVEYOPS-PREPS	ENTRYDFLOG	WAN390		8941
04.07.89	IGB	OUTOFLIMITS	WORN	MOD+RECOND	WAY107	WAH340	5295
15.05.91	IGB	CORROSIONFRETNG	CORROSIONFRETNG	RPLLAT3/4	WAH340	WAA210	6173
13.07.92	IGB	CMTNMTSWARF	CMTNMTSWARF	RPLLAR2	AAL7163	WAW58	6673
07.07.91	IGB	WARNINGLIGHTON	WARNINGLIGHTON	RPLLAINVEST	AAL7163	NOTREC	6174
16.01.91	IGB	ROBBED	ROBBED	ROBITEMRPL	WAV20	ABX0884	6735
10.11.92	IGB	ROBBED	ROBBED	ROBITEMRPL	WAX87	WAX76	7632
17.02.92	IGB	WORN	WORN	RPLLAR2	WAX72	WAX87	7294
24.02.92	IGB	WORN	WORN	RPLLAR2	WAX72	WAX87	7274
05.05.94	IGB	WORN	WORN	RPLLAT3/4	WAX76	WAX94	7938
27.05.84	SEALPLAIN (INPUT)	LEAKING	LEAKING	RPLLASCRAP	NONE	NONE	4551
01.12.87	IGB		WORN	MOD+RECOND	WAK39		0
23.03.92	IGB		ROBBED	ROBITEMRPL	AAH6913	WAA210	0
16.10.93	IGB	FAILEDTST/CHECK	WORN	RPLLAR2	WAA210	WAL383	6487
07.03.94	IGB	CORRODEDSURFACE	CORRODEDSURFACE	**RECTINSITU**	WAL383	WAY124	6635
27.11.94	OUTPUTSEAL	GEARBOXOILLEAK	SEALINGLEAKING	RPLLASCRAP			7073
04.07.85	IGB	DRY	DRY	RECTINSITU	WAV9	NONE	4126
19.10.94	IGB	CORRODED	CORRODED	RECTINSITU	WAD293		7090
08.10.96	IGB	LIFEEXCOMPONT	LIFEEXCOMPONT	RPLLAR2	WAD293	WAD291	7819
10.03.86	JAW	OUTOFLIMITS	WORN	RPLLASCRAP	NONE	NONE	4000
10.03.86	IGB		OUTOFALIGNMENT	RECTINSITU			4000

Appendix D.3 : Records for maintenance for Type A IGB - source EDA

DATE	Defective item	Symptom	Fault	Action	Removed item	Replaced item	A/F hours
08.01.87	IGB	FALTOOPCORR	NOFAULTFOUND	NOFAULTFOUND	WAX79	NONE	4434
17.05.90	IGB	VIBRATION	OUTOFALIGNMENT	RECTINSITU	WAX79		5805
17.05.90	BEARING		WORN	RPLLASCRAP	NONE	NONE	0
15.10.93	IGB - FITTSUPPORT	WORN	WORN	RPLLAR2	WAX79	WAA202	6856
31.01.96	IGB	STIFF/TIGHT	BEARINGDAMAGED	RPLLAR3/4	WAA202	WAR-WAX-8	7432
23.08.96	IGB	CMTNMTSWARF	CMTNMTSWARF	RECTINSITU	WAR-WAY-6		6411
27.02.84	SEALPLAIN (INPUT)	LEAKING	LEAKING	RPLLASCRAP	NOTREC	NOTREC	3938
07.11.84	SEALPLAIN (INPUT)	DETACHED	DETACHED	RPLLASCRAP	NONE	NONE	4334
09.03.92	IGB	WARNINGLIGHTON	WARNINGLIGHTON	RECTINSITU	WARWAU6		5843
31.03.92	IGB	WARNINGLIGHTON	WARNINGLIGHTON	RECTINSITU	WARWAU6		5872
28.04.92	IGB	FALEARLYFALDCHK	WORN	RPLLAR2	WARWAU6	WAW59	5919
24.01.92	IGB	WARNINGLIGHTON	WARNINGLIGHTON	RECTINSITU	WARWAU6		5749
18.11.93	IGB		ROBBED	ROBITEMRPL	WAW59	WAC244	6687
11.12.85	SEALPLAIN (INPUT)	GEARBOXOILLEAK	SPLIT	MITEMSRPLREP	NONE	NONE	3900
04.07.83	SHIM		DISTORTED	MOD+RECOND	NOTREC		0
21.09.89	SHAFTINPUT		FRETTED	MOD+RECOND	WAD286		0
19.05.92	IGB	ROBBED	ROBBED	ROBITEMRPL	WAD301	WAH349	5455
06.01.94	IGB	WORN	SPLINEWORN	RPLLAR3/4	WAH347	WARWAW35	5851
13.11.85	IGB - FITTSUPPORT	WARNINGLIGHTON	DISTORTED	RPLLAR2	WAK368	WAH344	5007
18.09.96	SEALPLAIN (INPUT)	OTHERLQDLEAK	LEAKRATEWRONG	RECTINSITU	NONE		6998
25.08.92	IGB	ROBBED	ROBBED	SEPJOBCARD	WAH349	NONE	2924
16.03.84	JAW	WORN	WORN	RPLLASCRAP	NOTREC	NOTREC	4203
16.03.84	IGB		WORN	RPLLASCRAP			0
05.02.85	SEALPLAIN	LEAKING	LEAKING	RECTINSITU	NONE	NONE	4760
03.09.85	IGB	WARNINGLIGHTON	CMTNMTSWARF	RECTINSITU	NONE	NONE	4974
05.12.88	WINDOWASSY	CONTAMINATED	CONTAMINATED	RPLLASCRAP	NONE	NONE	5512
19.11.92	IGB	CORROSIONPITING	CORRODED	RECTINSITU	WAD291		7176
10.05.96	JAW,I/P DISCC	WORN	WORN	RPLLAR2	NONE	NONE	8436
10.05.96	IGB		CORRODED	RPLLAR3/4		WAF326	8436
18.03.85	SEALPLAIN (INPUT)	HYDOILLEAK	WORN	RPLLASCRAP	NONE	NONE	4795

Appendix D.3 : Records for maintenance for Type A IGB - source EDA

DATE	Defective item	Symptom	Fault	Action	Removed item	Replaced item	A/F hours
20.09.83	SEALPLAIN	LEAKING	LEAKING	RPLLASCRAP	NONE	NONE	2840
21.05.91	IGB	WORN	SPLINEWORN	RPLHAR2	WAU10	WAA221	5343
21.12.92	IGB - JAW	WORN	WORN	RPLHAR2	WAA221	WAC244	5998
02.10.96	SEALPLAIN (INPUT)	GEARBOXOILLEAK	GEARBOXOILLEAK	RPLLASCRAP	NONE	NONE	7389
26.02.87	IGB	CHAFED/CHAFING	CHAFED/CHAFING	RECTINSITU	WAX89	NONE	5914
02.07.92	IGB	WORN	SPLINEWORN	RPLLAR2	WAX89	WAX78	8079
04.06.97	IGB		WORN	MITEMSRPLREP			0
25.02.91	SEALPLAIN (INPUT)	HYDOILLEAK	HYDOILLEAK	RPLLASCRAP	NOTREC	NONE	7490
06.09.90	IGB	ROBBED	ROBBED	ROBITEMRPL	WAY128	WAC269	5684
01.09.95	IGB	BEARINGBROKEN	FALEARLYFALDCHK	RPLLAR2	WAC269	WARWAU7	7418
14.07.86	IGB	CMTNMTSWARF	WORN	MOD+RECOND	WAJ360	WAV15	4510
07.11.95	IGB	CORRODEDSURFACE	CORROSIONPITING	RECTINSITU	WAK368		7121
25.08.92	IGB	CMTNMTSWARF	CMTNMTSWARF	RPLLAR2	WAH15	WAU9	6799
16.09.82	IGB - CHIPDETECTOR	INDOFFAULT	DAMAGED	MOD+RECOND	WAX98	WAW57	3462
16.12.85	IGB		GEARBOXOILLEAK	MOD+RECOND	WAU13		0
03.09.87	BEARING	CMTNMTSWARF	CHIPPED	REPAIRED	WAG334R1	WAW40R1	5328
15.02.88	IGB	WARNINGLIGHTON	SAFEEQNOTKNOW	RPLLAR3/4	WABRWAW40	ABD5375	5541
13.06.93	SEALPLAIN	GEARBOXOILLEAK	GEARBOXOILLEAK	RPLLASCRAP	AAR2619	NOTREC	7236
30.10.96	IGB	OUTOFADJ	OUTOFLIMITS	RECTINSITU	WAD301		8741
13.07.94	IGB	CORRODED	CORRODED	RPLLAR3/4	AAR2619	WAD301	7623
19.03.85	SEALPLAIN (INPUT)	GEARBOXOILLEAK	WORN	RPLLASCRAP	NONE	NONE	4857
17.11.89	IGB	FAILSTOCANCEL	SAFEEQNOTKNOW	MITEMSRPLREP	WAK366	WAA204	6329
21.05.91	IGB	ROBBED	ROBBED	ROBITEMRPL	WAA210	WAX103	6639
17.02.92	IGB	WARNINGLIGHTON	WARNINGLIGHTON	RECTINSITU	WAJ363		5999
20.03.95	IGB	WORN	WORN	RPLLAR3/4	WAJ363	WAN395	7107
07.11.94	IGB	CORRODED	CORRODED	RECTINSITU			7107
23.09.87	SEALPLAIN (INPUT)	GEARBOXOILLEAK	SEALINGLEAKING	RPLLASCRAP	NONE	NONE	5113
25.01.88	IGB	FALTOOPCORR	LIFEEXCOMPONT	RECONDITIOND	WAH348	WAW59	4661
07.03.89	WINDOWASSY	CRACKED	CRACKED	RPLLASCRAP	NONE	NONE	5243
22.09.95	IGB	CORRODED	CORRODED	RPLLAR2		WAD297	6962

Appendix D.3 : Records for maintenance for Type A IGB - source EDA

DATE	Defective item	Symptom	Fault	Action	Removed item	Replaced item	A/F hours
22.01.92	IGB	GEARBOXOILLEAK	GEARBOXOILLEAK	RPLLAR2	WAX99	WARWAY7	6118
22.01.92	BREATHERPLUG,GE		BKN/FRACTURED	REPAIRED	WAX99		0
24.01.92	IGB	OVERCHARGED	OVERCHARGED	RECTINSITU	NOTREC		6118
02.12.92	IGB	WORN	CMTNMTSWARF	RPLLAR2	WARWAU7	WAW20	6613
15.06.90	IGB	CORRODED	CORRODED	RPLLAR3/4	WARWAW26	WAX99	5597
01.03.96	OUTPUTSEAL	GEARBOXOILLEAK	GEARBOXOILLEAK	RPLLASCRAP			7754
31.07.84	IGB	DETACHED	WORN	RPLLAR2	WAX99	WAX99	3546
02.08.84	SHAFTINPUT	WORN	WORN	RPLLAR2	WAX99	WAD299-R1	3557
28.06.89	WINDOWASSY	DISCOLOURED	DISCOLOURED	RPLLASCRAP	NONE	NONE	5397
05.03.91	JAWSHAFT		CORRODED	SCRAPPED	WAD299R1		0
12.06.91	IGB	CORRODED	CORRODED	MITEMSRPLREP	WAD299R1		6181
05.08.91	IGB	CORRODED	CORRODED	RPLLAR2	WAD299R1	WAC278	6202
18.03.92	IGB	OUTOFLIMITS	WORN	RPLLAT3/4	WAD295	BRWAC273R	6356
07.08.91	IGB		CORRODEDSURFACE	MITEMSRPLREP	WAC278		0
16.10.84	JAW	OUTOFLIMITS	WORN	RPLLASCRAP	NONE	NONE	2600
30.04.85	FLANGEOPUT	CORRODED	CORRODED	REPAIRED	WAD305	WAX66	2814
22.03.88	OUTPUTSEAL	LEAKING	LEAKING	RPLLAR2			2815
07.12.89	IGB	WORN	WORN	RECONDITIOND	WAX66	WAW37	4709
17.02.94	IGB	GEARBOXOILLEAK	GEARBOXOILLEAK	RPLLAR2	WAA209	WARWAU7	5827
30.06.93	SEALPLAIN (INPUT)	HYDOILLEAK	HYDOILLEAK	RPLLASCRAP	NOTREC	NONE	5620
04.09.84	IGB	CMTNMTSWARF	SAFEEQNOTKNOW	RPLLAR2	WAW44	WAW24	2735
30.07.86	IGB	WORN	WORN	RPLLAR3/4	WAH351	WAA193	3530
03.09.87	IGB	FALTOOPCORR	CMTNMTSWARF	RPLLAR3/4	WAW193	WAW56	3847
29.10.87	IGB		SHOCKLOADED	MOD+RECOND	WAW56		0
11.07.91	IGB	OUTOFLIMITS	OUTOFLIMITS	RPLLAR2	WAC244	WAX78	5111
29.10.82	SEALPLAIN (INPUT)	LEAKING	SAFEEQNOTKNOW	RPLLASCRAP	NOTREC	NOTREC	2176
01.03.90	SEALPLAIN (INPUT)	GEARBOXOILLEAK	WORN	RPLLASCRAP	NONE	NONE	4417
07.02.83	SEALPLAIN (INPUT)	GEARBOXOILLEAK	LEAKING - WORN	RPLLASCRAP	NOTREC	NOTREC	2296
30.03.87	IGB	DIRTY	CMTNBYOIL	RPLLASCRAP	WAU20	WAU20	3755
06.11.91	IGB	ROBBED	ROBBED	ROBITEMRPL	WAH346	AAR2620	5571

Appendix D.3 : Records for maintenance for Type A IGB - source EDA

DATE	Defective item	Symptom	Fault	Action	Removed item	Replaced item	A/F hours
21.06.95	IGB	CORROSIONPITING	CORROSIONPITING	RECTINSITU	AAR2620		6599
17.09.88	IGB		SHOCKLOADED	RPLLAR2	WAW45	WAH343	4202
10.01.92	IGB		MOD/STITOBEEMBD	RPLASS+REP	WAW45		0
03.06.93	IGB	WORN	WORN	RPLLAR3/4	WAY116	WAW48	5542
20.05.85	BEARINGCMPT	INDOFFAULT	BRINELLED	RPLLAR2	WAD297	WAY131	2364
17.09.90	IGB	WARNINGLIGHTON	WARNINGLIGHTON	RPLHAR3/4	WAY131	WAY116	3940
01.09.94	OUTPUTSEAL	GEARBOXOILLEAK	SEALINGWORN	RPLLASCRAP			5432
02.09.94	IGB	FAILSTORESET	WARNINGLIGHTON	RECTINSITU	WAG332		5432
14.09.94	IGB	WARNINGLIGHTON	CMTNMTSWARF	MITEMSRPLREP			5447
19.07.90	SEAL	GEARBOXOILLEAK	GEARBOXOILLEAK	RPLLASCRAP	WAY131	NONE	3931
20.08.90	CHIPDETECT	WARNINGLIGHTON	CMTNBYDRT/SAND	RECTINSITU	WAY131		3932
14.09.90	IGB	WARNINGLIGHTON	WARNINGLIGHTON	RECTINSITU	WAY131		3940
30.11.89	SEALPLAIN (INPUT)	GEARBOXOILLEAK	WORN	RPLLASCRAP	NOTREC	NOTREC	3717
20.09.90	IGB	WARNINGLIGHTON	WARNINGLIGHTON	RECTINSITU	WAX88		4166
03.06.96	IGB	FAILEDTST/CHECK	FAILEDTST/CHECK	RPLHAR3/4	WAG334	WAD310	5658
05.10.92	IGB	CRACKED	PANELCRACKED	ENTRYDFLOG			4695
08.08.84	IGB	WARNINGLIGHTON	CMTNMTSWARF	RECTINSITU	WAD281	NONE	2282
15.10.84	IGB	FALEARLYFALDCHK	FALEARLYFALDCHK	RPLLAR3/4	WAD281	WAD314	2356
16.09.92	IGB	INDOFFAULT	FAILEDTST/CHECK	RPLLAR3/4	WAW48	WAU12	4827
17.11.93	IGB	WARNINGLIGHTON	FAILSTOILLUMTE	RPLLAR3/4	WAU12	WAD292	5583
03.09.96	WINDOWASSY	VISIONIMPAIRED	VISIONIMPAIRED	RPLLASCRAP	NONE	NONE	7085
13.08.96	JAW,I/P DISCC	CORROSIONPITING	PITTED	RPLLASCRAP	NONE	NONE	7085
27.05.93	SEALPLAIN (INPUT)	GEARBOXOILLEAK	GEARBOXOILLEAK	RPLLASCRAP	NOTREC	NONE	5148
17.11.93	SEALPLAIN (INPUT)	GEARBOXOILLEAK	SEALINGLEAKING	RPLLASCRAP	NOTREC	NOTREC	5583
22.12.82	IGB	LIFEEXCOMPONT	LIFEEXCOMPONT	ENTRYDFLOG	WAD315		1730
22.12.82	NUT	INCITEMFITTED	DAMAGED	MOD+RECOND	WAD315	NONE	1734
08.02.83	IGB	WARNINGLIGHTON	WARNINGLIGHTON	RECTINSITU	NONE	NONE	1730
26.08.86	IGB	WORN	SPLINEWORN	RPLLAR2	WAH346	WAD312	3927
30.04.90	IGB	OILLEAK	OILLEAK	RPLLAT3/4	WAD312	WAU8	5132
21.08.90	SPIRAL	MISMAT/INCOMPAT	MISMAT/INCOMPAT	RPLLASCRAP	NOTREC	NONE	5164

Appendix D.3 : Records for maintenance for Type A IGB - source EDA

DATE	Defective item	Symptom	Fault	Action	Removed item	Replaced item	A/F hours
06.08.92	IGB	WNGINCATRSHOWN	DEPOSITOFSCALE	RECTINSITU	WAY120		5843
13.12.91	IGB	ROBBED	ROBBED	ROBITEMRPL	WAU13	WAY120	5639
07.08.92	IGB	REMOVED	REMOVED	RPLLAR3/4	WAY120	WAD297	5845
14.12.93	IGB	WORN	SPLINEWORN	RPLLAR3/4	WAD297	WAY106R1	6517
17.02.88	SEALPLAIN (INPUT)	GEARBOXOILLEAK	GEARBOXOILLEAK	RPLLASCRAP	NONE	NONE	4344
11.08.86	WINDOWASSY	DISCOLOURED	DISCOLOURED	RPLLASCRAP	NONE	NONE	1860
01.10.87	SHAFTINPUT	FAILEDTST/CHECK	WORN	MOD+RECOND	WAD304	WAU12	2511
14.11.88	IGB	WARNINGLIGHTON	CMTNMTSWARF	MITEMSRPLREP	WAU12		3014
30.11.88	IGB	CMTNMTSWARF	CMTNMTSWARF	RPLLAR2	WAU12	WAW34	3052
30.11.88	BEARING (O/P OUTBD)		CHIPPED	MOD+RECOND	WAU12		0
07.08.92	IGB	ROBBED	ROBBED	ROBITEMRPL	WAD297	WAL384	5034
17.10.95	IGB	INDOFFAULT	NOFAULTFOUND	NOFAULTFOUND			6725
09.11.95	IGB	LIFEEXCOMPONT	LIFEEXCOMPONT	RPLLAR3/4	WAG331	ADC5371	6779
25.11.93	IGB	READING/SHIGH	CMTNMTSWARF	RPLLAR3/4	WAL384	WAG331	5668
09.02.96	JAW,I/P DISCC	CORROSIONPITING	PITTED	RPLLASCRAP	WA122	WA216	6923
10.01.86	SEALPLAIN (INPUT)	GEARBOXOILLEAK	GEARBOXOILLEAK	RPLLASCRAP	NONE	NONE	1561
31.05.93	SEALPLAIN (INPUT)		GEARBOXOILLEAK	RPLLASCRAP		NONE	0
30.01.98	SEALPLAIN (INPUT)	GEARBOXOILLEAK	GEARBOXOILLEAK	RPLLASCRAP	NONE	NONE	7921
31.10.83	HOUSINGCENTRE	CMTNBYDRT/SAND	NOFAULTFOUND	NOFAULTFOUND	NONE	NONE	2205
30.03.84	IGB	LIFEEXCOMPONT	LIFEEXCOMPONT	RPLLAR3/4	WAD298	AR-A-15705	2451
30.03.84			LIFEEXCOMPONT	RECONDITIOND	NOTREC		0
29.01.88	IGB	FAILSTORESET	CMTNMTSWARF	RPLLAR3/4	WAR-A15705	WAF327	3954
03.03.88	SEAL	GEARBOXOILLEAK	GEARBOXOILLEAK	MOD+RECOND	WAF327	WAG337	3990
26.06.91	IGB	ROBBED	ROBBED	ROBITEMRPL	WAG337	WAU12	5867
16.09.92	IGB	ROBBED	ROBBED	ROBITEMRPL	WAU12	WAY016R	6431
10.03.96	IGB	MISALIGNED	MISALIGNED	RECTINSITU			8370
15.12.93	IGB	ROBBED	ROBBED	ROBITEMRPL	WAY106R1	WAA193	7038
26.03.95	SEALPLAIN (INPUT)	GEARBOXOILLEAK	GEARBOXOILLEAK	RPLLASCRAP	NONE	NONE	7700
22.11.83			LIFEEXCOMPONT	MOD+RECOND	WAD286		0
16.04.90	IGB	FALEARLYFALDCHK	FALEARLYFALDCHK	RPLLAR3/4	WAE317	WAU21	4760

Appendix D.3 : Records for maintenance for Type A IGB - source EDA

DATE	Defective item	Symptom	Fault	Action	Removed item	Replaced item	A/F hours
25.05.90	BEARING		CHIPPED	RECONDITIOND	WAL317		0
05.06.90	IGB	ROBBED	ROBBED	ROBITEMRPL	WAU21	WAU12	4760
26.11.93	IGB	ROBBED	ROBBED	ROBITEMRPL	WAG331	NOTREC	6727
22.06.88	SEALPLAIN (INPUT)	GEARBOXOILLEAK	DAMAGED	RPLLASCRAP	NONE	NONE	3741
06.10.82	IGB	LIFEEXCOMPONT	LIFEEXCOMPONT	RPLLAR3/4	WAD289	WAD283	1975
21.12.82	IGB	CMTNMTSWARF	BEARINGBROKEN	RPLLAR3/4	WAD283	WAD309	2040
21.12.82	BEARING		DAMAGED	RECONDITIOND	WAD283		0
06.02.86	IGB	SEIZED	SEIZED	RPLLAR2	WAD309	WAX98	3661
23.03.89	IGB	GEARBOXOILLEAK	SEALINGLEAKING	MITEMSRPLREP	AAT1525		5142
14.08.97	IGB	ROBBED	ROBBED	ROBITEMRPL		AAK7958	10083
03.11.97	OUTPUTSEAL	GEARBOXOILLEAK	GEARBOXOILLEAK	RPLLASCRAP			10092
16.09.84	SEALPLAIN (INPUT)	GEARBOXOILLEAK	DAMAGED	RPLLASCRAP	NONE	NONE	2932
03.08.84	IGB	CORRODED	RODCORRODED	RECONDITIOND	WAU8	WAD283	2867
25.01.90	SHAFTINPUT	WORN	JOINTWORN	RECONDITIOND	WAD283	WAF326	5841
04.04.95	IGB	LIFEEXCOMPONT	LIFEEXCOMPONT	RPLLAR3/4	WAF326	WAA210	8267
09.06.83	SEALPLAIN (INPUT)	GEARBOXOILLEAK	SEALINGWORN	RPLLASCRAP	NONE	NONE	2410
17.12.90	SEALPLAIN (INPUT)	GEARBOXOILLEAK	SEALINGWORN	MITEMSRPLREP	NOTREC	NONE	6116
09.08.83	IGB	LIFEEXCOMPONT	LIFEEXCOMPONT	RPLLAR3/4	WAB-374	R/WAC275R1	2393
09.08.83	IGB	COVER CORRODED		MOD+RECOND	WAD314		0
25.10.84	BEARING,BALL		DAMAGED	RPLLASCRAP	NONE	NONE	0
01.11.88	COUPLING	WORN	SPLINEWORN	RPLLAR3/4	WAC275R1	WAU13	4970
02.12.88	IGB	WARNINGLIGHTON	CMTNMTSWARF	MITEMSRPLREP	WAU13	WAU13	4970
22.08.91	IGB	ROBBED	ROBBED	ROBITEMRPL	WAG331	WAK39	6190
10.02.92	IGB	ROBBED	ROBBED	ROBITEMRPL	WAK39	AAM4964	6337
29.03.94	OUTPUTSEAL	ENGOILLEAK	DET/PERISHED	RPLLASCRAP			7187
31.05.98	IGB	WARNINGLIGHTON	WARNINGLIGHTON	RECTINSITU	AAM4964		9015
27.10.96	SEALPLAIN (INPUT)	GEARBOXOILLEAK	SEALINGLEAKING	RPLLASCRAP	NONE	NONE	8269
02.04.82	IGB	GLASSPPEXDIRTY	GLASSPPEXDIRTY	MITEMSRPLREP	WAD290	NONE	1834
28.09.82	IGB	LIFEEXCOMPONT	LIFEEXCOMPONT	RPLLAR3/4	WAD290	WAG239	2209
20.12.83	IGB	OUTOFALIGNMENT	OUTOFALIGNMENT	RECTINSITU	NONE	NONE	2640

Appendix D.3 : Records for maintenance for Type A IGB - source EDA

DATE	Defective item	Symptom	Fault	Action	Removed item	Replaced item	A/F hours
30.10.90	IGB	WORN	WORN	RPLLAR3/4	WAX98	AAT1525	6388
10.02.92	IGB	ROBBED	ROBBED	ROBITEMRPL	AAT1525	WAK39	7139
28.10.95	CHIPDETECT	INDOFFAULT	CONTAMINATED	RPLLAR2	NONE	NONE	8537
12.08.97	IGB	FALTOOPCORR	FALTOOPCORR	RPLLAR3/4	ABX0846	WAF323	9644
08.12.82	IGB	LIFEEXCOMPONT	LIFEEXCOMPONT	MOD+RECOND	WAD287	WAG335	2069
09.12.85	SHAFTINPUT	CORRODED	WORN	RPLLAR3/4	WAG335	WAX99	3415
26.11.86	SEALPLAIN	GEARBOXOILLEAK	GEARBOXOILLEAK	RPLLASCRAP	NONE	NONE	3902
05.04.89	CHIPDETECTOR	WARNINGLIGHTON	CONTAMINATED	RPLLAT3/4	WAX99	NOTREC	4940
18.04.89	IGB	CMTNMTSWARF	CMTNMTSWARF	RPLLAR3/4	WAX99	WAF323	4861
18.04.89	BEARING (O/P INBD)		CHIPPED	MOD+RECOND	WAX99		0
03.06.91	IGB	HEAVYLANDING	HEAVYLANDING	RPLLAR3/4	WAF325	WARWAU23	5868
07.05.95	IGB	FAILS-EXTINGUISH	INDOFFAULT	RECTINSITU	AAG1848		7404
23.09.90	IGB		ROBBED	ROBITEMRPL	WAF323	WAF325	0
29.03.95	IGB	INDOFFAULT	INDOFFAULT	ENTYLIMLOG	AAG1848		7336
28.04.95	IGB	INDOFFAULT	INDOFFAULT	RECTINSITU	ADG1848		7379
02.08.95	IGB	INDOFFAULT	INDOFFAULT	RPLLAR3/4	AAG1848	WAX76	7601
12.08.94	IGB	ROBBED	ROBBED	ROBITEMRPL	WAR/WAU23	AAG1848	7039
27.04.87	SEALPLAIN (INPUT)	GEARBOXOILLEAK	LEAKING	RPLLASCRAP	NONE	NONE	3969
23.04.95	SEALPLAIN (INPUT)	GEARBOXOILLEAK	GEARBOXOILLEAK	RPLLASCRAP	NONE	NONE	7375
08.12.82	IGB	LIFEEXCOMPONT	LIFEEXCOMPONT	RECONDITIOND	WAD292	WARWAW34	2115
18.05.84	IGB	DET/PERISHED	CMTNBYOIL	RPLLASCRAP	NONE	NONE	2823
27.07.85	IGB	WARNINGLIGHTON	CMTNMTSWARF	RPLLAR3/4	WA221	VAN367	4280
09.06.87	BEARING	SCORED	OTHERSCRATCHED	MOD+RECOND	WARWAW34	WAA221	4199
27.07.87	IGB	CMTNMTSWARF	CMTNMTSWARF	MOD+RECOND	WAA221	WAN387	4280
25.07.90	IGB	WARNINGLIGHTON	PLUGDIRTY	MITEMSRPLREP	WAN387		5764
10.04.91	IGB	GEARBOXOILLEAK	DAMAGED	RPLLAR3/4	NOTREC	AA69922	6148
23.09.92	IGB	WORN	WORN	RPLLAR3/4	AAG9922	WAU21	6969
09.05.97	IGB	INDSUSP/INCOR	INDSUSP/INCOR	ENTRYDFLOG	WAH347	ABD5375	9684
17.02.95	CHIPDETECT	INDOFFAULT	INDOFFAULT	RPLLAR2	NONE	NONE	8215
07.05.97	IGB	WARNINGLIGHTON	WARNINGLIGHTON	RECTINSITU	WAH347		9679

Appendix D.3 : Records for maintenance for Type A IGB - source EDA

DATE	Defective item	Symptom	Fault	Action	Removed item	Replaced item	A/F hours
07.05.97	SEALPLAIN (INPUT)	OILLEAK	SEALFAULTY	RPLLASCRAP	NONE	NONE	9679
02.08.82			WORN	MOD+RECOND	WAD285		0
19.04.84	IGB	LIFEEXCOMPONT	LIFEEXCOMPONT	RPLLAR3/4	WAD312	WAX95	2962
27.02.87	BEARING	WARNINGLIGHTON	BKN/FRACTURED	MOD+RECOND	WAX95	WAD309	4208
31.01.89	SHAFTINPUT	FRETTED	SPLINEWORN	REPAIRED	WAD309	AAG9922	5087
03.12.91	IGB	WORN	WORN	RPLLAR3/4	WAH345	WAD304	6736
18.04.91	IGB	ROBBED	ROBBED	ROBITEMRPL	AAG9922	WAH345	6435
26.08.93	IGB	CORRODED	CORRODED	RPLLAR3/4	WAD304	WAW29	7484
11.11.95	IGB	FLAGFAILTOCLR	FLAGFAILTOCLR	RECTINSITU	WAW29		7786
24.04.96	IGB	FAILSTORESET	FAILSTORESET	FAULTINLIMIT	WAW29		8058
28.08.96	SEALPLAIN (INPUT)	GEARBOXOILLEAK	GEARBOXOILLEAK	RPLLASCRAP	NONE	NONE	8302
24.08.83	IGB		DAMAGED	RECONDITIOND	WAD293		0
06.08.85	IGB	FLUIDLEVELHIGH	FALTOOPCORR	RPLLAR3/4	WAX82	WAX87	3338
02.06.89	FITTSUPPORT	FAILEDTST/CHECK	WORN	RPLLAR3/4	WAX87	WAX74	5075
15.09.95	IGB	INDOFFAULT	INDOFFAULT	ADJUSTED	WAX74		7991
19.10.82	IGB	LIFEEXCOMPONT	LIFEEXCOMPONT	MOD+RECOND	WAD296	WAG329	2159
16.08.86	IGB	CONTAMINATED	CMTNMTSWARF	MOD+RECOND	WAG329	AAT1525	3968
12.11.86	IGB		ROBBED	ROBITEMRPL	AAT1525	WAX98	4059
02.11.90	IGB	LIFEEXCOMPONT	LIFEEXCOMPONT	RPLLAR3/4	R/WAY106R1	WAD304	5925
03.12.91	IGB	ROBBED	ROBBED	ROBITEMRPL	WAP304	WAC275	6442
24.02.94	IGB	ROBBED	ROBBED	ROBITEMRPL	WAC275	WAJ362	7732
15.11.82	IGB	LIFEEXCOMPONT	LIFEEXCOMPONT	MOD+RECOND	WAE317	WAH345	1803
21.01.84	IGB	WARNINGLIGHTON	SUSPECTUNSVBLTY	RPLLAR2	WAH345	NONE	2470
20.01.95	IGB	GEARBOXOILLEAK	GEARBOXOILLEAK	RPLLAR2	WA6337	AAP0239	6813
03.06.91	IGB	ROBBED	ROBBED	ROBITEMRPL	WAH345	WAG337	5412
19.04.82	CHIPDETECTOR	THREADDAMAGED	THREADDAMAGED	RPLLAR2	NOTREC	NOTREC	495
04.05.89	BEARING	WARNINGLIGHTON	WORN, BRINELLED	REPAIR+MOD	WAD301	WAD281	2200
14.03.91	IGB	CABLEOPENLAY	OUTOFLIMITS	RPLLAR2	WAD281	ACU4696	2986
14.03.91	SHAFTINPUT		WORN	REPAIRED	WAD281		0
12.10.93	IGB	WORN	WORN	RPLLAR2	ACU4696	WAH344	4074

Appendix D.3 : Records for maintenance for Type A IGB - source EDA

DATE	Defective item	Symptom	Fault	Action	Removed item	Replaced item	A/F hours
14.03.91	IGB	CABLEOPENLAY	OUTOFLIMITS	RPLLAR2	WAD281	ACU4696	2986
14.03.91	SHAFTINPUT		WORN	REPAIRED	WAD281		0
04.08.94	IGB	OUTOFALIGNMENT	OUTOFALIGNMENT	RPLLAR2			4326
19.03.85	SEAL	FLUIDLEVELLOW	GEARBOXOILLEAK	RPLLAR2	WAF327	WAD293	1822
27.03.85			OILLEAK	REPAIRED	WAF372		0
01.12.89	IGB	WARNINGLIGHTON	WARNINGLIGHTON	RPLLASCRAP	WAA202	NOTREC	3222
15.09.91	IGB	FALEARLYFALDCHK	FALEARLYFALDCHK	RECTINSITU	WAD289		3603
29.09.94	IGB	CORRODED	CORRODEDSURFACE	RPLLAR2	WAD289	WAG335	4771
28.07.95	IGB	CMTNBYDRT/SAND	CMTNBYDRT/SAND	RECTINSITU	WAG335		4957
03.11.86	IGB	INDSUSP/INCOR	WEAK	RECTINSITU	WAF326	NONE	2832
18.03.87	IGB	VIBRATION	CORRODED	MOD+RECOND	WAF326	WAX82	3007
18.04.91	IGB	TORQLOADGINCOR	TORQLOADGINCOR	RECTINSITU	WAK373		4621
28.09.92	SEAL	GEARBOXOILLEAK	SEALINGDAMAGED, WC	RPLLASCRAP	WAA193	WAV9	5317
05.03.82	SEAL		WORN	REPAIR+MOD	WAD283		0
18.08.82	IGB	WARNINGLIGHTON	WARNINGLIGHTON	MOD+RECOND	WAW52	WAU25	1121
23.06.84			CORRODED	REPAIR+MOD	WAU25		0
19.06.89	IGB	LIFEEXCOMPONT	LIFEEXCOMPONT	MOD+RECOND	WAW41	WAJ361	3581
13.09.88	SEALPLAIN (INPUT)	LEAKING	LEAKING	RECTINSITU	NONE	NONE	3283
20.09.82	CHIPDETECTOR	WNGINCATRSHOWN	CMTNMTSWARF	RPLLAR2	NONE	NONE	914
24.01.83	IGB	WNGINCATRSHOWN	SAFEEQNOTKNOW	RPLLAR2	WAG338	NONE	1349
26.12.84	IGB	LIFEEXCOMPONT	LIFEEXCOMPONT	RECTINSITU	WAG338	NONE	2474
18.01.85	IGB	ENGOILLEAK	ENGOILLEAK	RPLLAR3/4	WAG338	WAD302	2474
18.01.85			SEALINGLEAKING	REPAIRED	WAG338		0
31.05.85	JAW	PLAYEXCESSIVE	WORN	RPLLAR3/4	NONE	NONE	2870
14.05.87	IGB	WORN	FAILEDTST/CHECK	MOD+RECOND	WAD302	WAG335	3880
17.01.92	IGB	FALEARLYFALDCHK	CMTNMTSWARF	RPLLAR3/4	WA6335	WAD308	5748
17.01.92	BOLT		WORN	RPLLASCRAP			0
07.02.92	IGB	CMTNMTSWARF	CMTNMTSWARF	ENTRYDFLOG			5772
23.07.92	SHIM	MISALIGNED	MISALIGNED	RPLLASCRAP	NOTREC	NONE	6030
21.08.92	JAW	OUTOFLIMITS	OUTOFLIMITS	RPLLASCRAP	NOTREC	NONE	6032

Appendix D.3 : Records for maintenance for Type A IGB - source EDA

DATE	Defective item	Symptom	Fault	Action	Removed item	Replaced item	A/F hours
21.03.96	IGB	FAILSTOCANCEL	CMTNMTSWARF	NOTREC-CONSN	AAT1525		7561
10.02.92	IGB	CMTNMTSWARF	CMTNMTSWARF	RPLLAR3/4	WAD308	AAT1525	5777
18.09.85	SHAFTINPUT		WORN	REPAIR+MOD	WAC269		0
23.11.90	BEVELSHAFT	WORN	WORN	RPLHAR3/4	WAU16R1	WAW59	3768
24.03.92	IGB		ROBBED	ROBITEMRPL	WAW59	AAH6913	4168
25.11.92	BEARING	WARNINGLIGHTON	BEARINGFAILED	RPLLAT3/4	AAH6913	-R-WAU16R1	4352
04.08.93	IGB	CORRODEDSURFACE	RODCORRODED	RPLLAR2	WAG335	AAL7163	5976
30.01.96	IGB	ONINSPECTION	CORRODED	RPLLAR2			5598
23.02.84	IGB	INDOFFAULT	SAFEEQNOTKNOW	RECTINSITU	WAH337	WAH337	1833
25.06.90	BEVELSHAFT	WORN	WORN	RECONDITIOND	WAU9	WAH344	4115
27.09.94	IGB	TORQLOADGINCOR	NOFAULTFOUND	NOFAULTFOUND			4732
11.07.95	SEALPLAIN (INPUT)	GEARBOXOILLEAK	GEARBOXOILLEAK	RPLLASCRAP	NONE	NONE	5131
06.01.87	IGB		CORRODED	MOD+RECOND	WAH342		0
14.08.87	IGB		SHOCKLOADED	MOD+RECOND	WAY116		0
03.11.94	IGB	FAILSSEQCORR	FAILSSEQCORR	ADJUSTED	AAG9922		4892
06.05.92	IGB	ROBBED	ROBBED	ROBITEMRPL	WAD302	NOTREC	5601
22.03.93	IGB	BINDING	BEARINGWORN	RPLLAR3/4	WAD301	WAG335	5922
10.08.93	SEAL		OTHERCORRODED	RPLLAR2	WAG335	NOTREC	0
10.08.93	JAW		JOINTCORRODED	RPLLAR2	WAG335	NOTREC	0
08.06.92	IGB	ROBBED	ROBBED	ROBITEMRPL	WAX99	ABX0855	4587
13.01.91	IGB	WORN	WORN	RPLLAR2	WAX72	WAV20	4130
21.06.91	IGB	OUTOFALIGNMENT	OUTOFALIGNMENT	RECTINSITU	WAV20		4341
13.02.92	IGB	WORN	WORN	RPLLAR2	ABX0884	WAX99	4558
13.03.90	IGB	WARNINGLIGHTON	SAFEEQNOTKNOW	RECTINSITU	NONE	NONE	3931
26.02.94	IGB	CMTNMTSWARF	BEARINGWORN	RPLLAR3/4	WAY120	WAD281	4284
04.04.84	IGB	INDOFFAULT	FOD-ORIG-UNKNOWN	RECTINSITU	WAH350		1521
27.06.85	IGB	INDOFFAULT	SAFEEQNOTKNOW	RPLLAR2	WAH350	WAD298	1990
06.03.90	CHIPDETECT	WARNINGLIGHTON	FOD-ORIGIN-A/C	RECTINSITU	WAD298	WAD298	3367
09.03.90	IGB		GEARBOXOILLEAK	OTHAGENCIES	WAD298	WAD298	3367
24.09.90	IGB		WORN	RPLLAR2	WAW52	ACT9837	0

Appendix D.3 : Records for maintenance for Type A IGB - source EDA

DATE	Defective item	Symptom	Fault	Action	Removed item	Replaced item	A/F hours
05.09.90	IGB	WARNINGLIGHTON	CMTNMTSWARF	RPLLAR2	WAD315	WAY128	3069
05.09.90	BEARING		CHIPPED	RECONDITIOND	WAD315		0
17.06.93	FITTSUPPORT	WORN	WORN	RPLLAT3/4	BRWAD282R1	WAD306	3984
28.07.94	IGB	WARNINGLIGHTON	NOFAULTFOUND	NOFAULTFOUND	WAD306		4325
21.08.92	IGB	WORN	OUTOFLIMITS	RPLLAR2	WAY128	BRWAD282R	3770
11.01.94	SEALPLAIN (INPUT)	GEARBOXOILLEAK	GEARBOXOILLEAK	RPLLASCRAP	NOTREC	NOTREC	4136
12.01.83	CHIPDETECTOR	WARNINGLIGHTON	INSULATIONBREAK	RPLLASCRAP	NONE	NONE	954
26.08.83	IGB	WARNINGLIGHTON	CONTAMINATED	RPLLAR2	WAH352	WAW50	1275
11.07.86	IGB	GEARBOXOILLEAK	GEARBOXOILLEAK	RPLLASCRAP	WAW50	WAW50	2317
07.11.91	GEARSHAFT		WORN	GEAR SCRAPPED	WAW50	WAG332	4369
06.05.82	BEARING		BKN/FRACTURED	REPAIR+MOD	BRWAC275R1		0
29.03.84	WINDOWASSY	DISCOLOURED	GLASSPPEXDIRTY	RPLLASCRAP	NOTREC	NOTREC	2237
30.04.92	IGB	WARNINGLIGHTON	WARNINGLIGHTON	RECTINSITU	WAK370		4566
15.06.92	IGB	WORN	WORN	RECTINSITU	WAK370		4703
09.11.92	IGB	WORN	WORN	RPLLAR2	AAP0239	WAX87	4900
17.02.92	IGB	WORN	SPLINEWORN	RPLLAR2	WARWAW35	WAK370	4552
11.04.92	IGB	FAILEDTST/CHECK	TORQLOADGINCOR	RECTINSITU	WAK370		4561
27.04.92	IGB	GEARBOXOILLEAK	GEARBOXOILLEAK	RECTINSITU	WAE284		4557
27.05.92	IGB	WARNINGLIGHTON	WARNINGLIGHTON	RECTINSITU	WAK370		4590
08.07.92	IGB	WARNINGLIGHTON	WARNINGLIGHTON	RECTINSITU	WAK370		4713
13.07.92	IGB	FAILEDTST/CHECK	FAILEDTST/CHECK	RPLLAR2	WAK370	AAP3068	4721
15.12.93	IGB	WORN	SPLINEWORN	RPLHAR3/4	WAX87	ACN3376	5075
27.04.82	IGB		NOFALFORSYMPTOM	MOD+RECOND	WAH351		0
09.02.84	IGB	GEARBOXOILLEAK	SEALINGCORD	RPLLAR3/4	WAU12	WAH351	2297
04.09.87	IGB	INDOFFAULT	CONTAMINATED	RPLLAR3/4	WAW24	WAV25	3319
20.04.88	IGB	INDOFFAULT	SAFEEQNOTKNOW	RECTINSITU	WAV25	NONE	3457
26.04.88	IGB	CMTNMTSWARF	CMTNMTSWARF	MOD+RECOND	WAU25	WAD295	3462
25.01.89	IGB	CCTBRKTRIPPED	SAFEEQNOTKNOW	ADJUSTED	WAD295		3770
08.08.91	IGB		ROBBED	ROBITEMRPL	WAD295	WARWAX81	5271
18.09.91	IGB	CORRODED	CORRODED	RPLLAR2	WAD299R1	WARWAX81	5271

Appendix D.3 : Records for maintenance for Type A IGB - source EDA

DATE	Defective item	Symptom	Fault	Action	Removed item	Replaced item	A/F hours
14.10.94	IGB	OUTOFALIGNMENT	OUTOFALIGNMENT	RPLLAR2	WAH344		6403
05.07.92	SEALPLAIN (INPUT)	HYDOILLEAK	SEALINGLEAKING	RPLLASCRAP	NOTREC	NOTREC	5461
13.12.83	IGB	WARNINGLIGHTON	NOFAULTFOUND	NOFAULTFOUND	NONE		900
02.02.85	IGB	WARNINGLIGHTON	SAFEEQNOTKNOW	RECTINSITU	NOTREC		1296
18.02.85	IGB	WARNINGLIGHTON	SAFEEQNOTKNOW	RPLLAR2	WAJ363	WAD296	1353
18.02.85	BEARING		CHIPPED	REPAIRED	WAJ363		0
23.10.90	IGB	OUTOFLIMITS	WORN	RPLLAR2	WAD296	AAP0238	3493
29.03.96	IGB	GEARBOXOILLEAK	GEARBOXOILLEAK	RECTINSITU	WAK367		5296
08.03.93	SEALPLAIN (INPUT)	GEARBOXOILLEAK	GEARBOXOILLEAK	RPLLASCRAP	NOTREC	NONE	4762
15.06.82	IGB	MISALIGNED	MISALIGNED	RECTINSITU	NOTREC	NOTREC	12
16.05.83	IGB	FAILEDSSTEST	FAILEDSSTEST	RPLLAR3/4	WAJ362	WAX97	789
25.06.86	BEARING		CHIPPED	RECONDITIOND	WAX97	WAX94	2375
11.09.90	IGB	WORN	WORN	RPLLAR2	WAX86	WAW56	3894
01.06.92	IGB		ROBBED	RECTINSITU	WAW56	ACT9738	4429
27.02.92	IGB		CORRODED	RPLLAR2	WAD286	WAN395	0
02.03.92	IGB	WORN	SPLINEWORN	RPLLAR2	WAD287	WAD286	3862
14.09.92	IGB		ROBBED	ROBITEMRPL	WAN395		4036
17.06.87	IGB	WORN	WORN	RPLLAR2	WAX367	WAD289	2100
21.07.89	IGB		WORN	MOD+RECOND	WAK367		0
09.06.92	IGB	CMTNMTSWARF	CMTNMTSWARF	RECTINSITU	WAA202		3460
17.06.92	IGB	WORN	WORN	RPLLAR2	WAA202	WAE317	3469
17.07.95	IGB	CORRODED	CORRODED	SCRAPPED	WAE317	WAU12	4441
28.11.96	IGB	FAILSTORESET	INDICATORPOPPED	RPLLAR2	WAU12	WAW52	4902
03.02.95	SEALPLAIN (INPUT)	GEARBOXOILLEAK	SEALINGLEAKING	RPLLASCRAP	NONE	NONE	4357
27.04.93	IGB	WORN	WORN	RPLLAT3/4	WAX89	WAH340	3944
04.10.91	IGB	ROBBED	ROBBED	ROBITEMRPL	WAW58	WAX78	3375
15.10.84	SEALPLAIN (INPUT)	LEAKING	LEAKING	ENTRYDFLOG	NONE	NONE	1022
07.04.82	RINGRETAIN	DETACHED	SAFEEQNOTKNOW	RECTINSITU	NONE	NONE	1089
14.04.82	IGB	MISSING	WORN	RPLLAR3/4	WAD302	WAC272	1093
20.07.84	IGB	INDOFFAULT	SAFEEQNOTKNOW	RECTINSITU	WAD265		1938

Appendix D.3 : Records for maintenance for Type A IGB - source EDA

DATE	Defective item	Symptom	Fault	Action	Removed item	Replaced item	A/F hours
23.07.84	IGB	INDOFFAULT	SAFEEQNOTKNOW	RPLLAR2	WAD265	WAD286	1938
18.05.90	IGB	GEARBURNT	CORRODED	RPLLAR2	WAD306	AAR2618	3921
18.05.90	CHIPDETECT		INSULATIONBREAK	RPLLASCRAP		NONE	0
22.05.90	HOUSING		WORN	RPLLASCRAP	NONE	NONE	0
05.06.90	HOUSING		CORRODED	RECONDITIOND	WAD306		0
07.07.92	IGB	CORRODED	CORRODED	RECTINSITU	AAR2618		4610
17.10.92	JAW,I/P DISCC	DISTORTED	JOINTDISTORTED	RPLLASCRAP	AAR2618	NOTREC	4732
18.10.93	IGB	CORRODEDSURFACE	CORRODEDSURFACE	RPLLAR3/4	AAR2618	WAW37	5033
18.12.97	SEALPLAIN (INPUT)	ONINSPECTION	OTHERLQDLEAK	RPLLASCRAP	NONE	NONE	5968
17.10.89	SHAFTINPUT	OUTOFLIMITS	WORN	MOD+RECOND	WAD308	WAX95	3366
02.12.92	IGB		ROBBED	ROBITEMRPL	WAX95	WAH345	0
13.06.83	CHIPDETECTOR	INDOFFAULT	CMTNSLUDGE	RECTINSITU	WAG334		1004
15.06.83	CHIPDETECTOR	INDOFFAULT	CMTNMTSWARF	RPLLAR2	WAG334	WAX84	1010
27.04.93	GEARSHAFT,BEVEL	CORRODED	CORRODED	ENTRYDFLOG	WAH348		4448
02.05.95	IGB	GEARBOXOILLEAK	BEARINGDAMAGED	RPLLAR2		ACN9190	5337
04.03.87	SEALPLAIN (INPUT)	GEARBOXOILLEAK	LEAKING	RPLLASCRAP	NONE	NONE	2414
26.04.88	WINDOWASSY	DIRTY	DIRTY	RPLLASCRAP	NONE	NONE	2970
13.06.83	IGB	VIBRATNVERTICAL	MISALIGNED	RECTINSITU	NONE		1337
14.06.95	SEALPLAIN (INPUT)	GEARBOXOILLEAK	GEARBOXOILLEAK	RPLLASCRAP	NONE	NONE	5491
30.04.84	IGB	DAMAGED	SAFEEQNOTKNOW	RPLLAR3/4	WAC279	WAX93	1641
26.11.91	IGB	BRG BRINELLED	BRINELLED	MITEMSRPLREP	2208	3041	0
26.04.91	IGB		ROBBED	ROBITEMRPL	WAX93	WAX72	0
12.07.83	IGB	INDOFFAULT	SAFEEQNOTKNOW	RECTINSITU	WAJ358		787
26.06.90	IGB	CORRODED	CORRODED	RPLLAR2	WAJ358	WAK367	13400
12.12.91	BEARING		BRINELLED	MITEMSRPLREP	2283	2861	0
26.02.93	IGB	INCORRECTLYFIT	INCORRECTLYFIT	RECTINSITU	WAY126		3765
27.02.92	IGB		ROBBED	ROBITEMRPL	WAK367	WAY126	0
27.07.97	IGB	ONINSPECTION	CORRODED	RPLLAR2	WAY126	WAJ357	5580
30.08.90	*IGB*		NOFALFORSYMPTOM	RECONDITIOND	WAJ358		0
29.03.82	IGB	WARNINGLIGHTON	SAFEEQNOTKNOW	RECTINSITU	WAJ357	NONE	209

Appendix D.3 : Records for maintenance for Type A IGB - source EDA

DATE	Defective item	Symptom	Fault	Action	Removed item	Replaced item	A/F hours
17.07.97	IGB	VIBRATION	VIBRATION	RPLLAR2	AAP0238	WAW58	6108
24.11.97	CHIPDETECT	OTHERLQDLEAK	OTHERLQDLEAK	RPLLASCRAP	NONE	NONE	6166
24.11.97	IGB	ONINSPECTION	DISTORTED	RPLLAT3/4		WAW39	6166
22.07.93	SEALPLAIN (INPUT)	GEARBOXOILLEAK	GEARBOXOILLEAK	RPLLASCRAP	NOTREC	NONE	4486
15.11.82	WINDOWASSY	INDSUSP/INCOR	DISCOLOURED	RPLLASCRAP	NONE	NONE	482
29.10.84	IGB	INDOFFAULT	SAFEEQNOTKNOW	RECTINSITU	NOTREC		1267
18.04.86	JAW	WORN	WORN	RPLLAR2	NOTREC	WA516284	1748
17.06.87	WINDOWASSY	DIRTY	DIRTY	RECTINSITU	NONE	NONE	2251
18.01.91	IGB		ROBBED	ROBITEMRPL	WAY104	WAX72	3635
25.04.91	IGB		ROBBED	ROBITEMRPL	WAX72	WAX93	0
08.05.97	SEALPLAIN	ONINSPECTION	OTHERLQDLEAK	RPLLASCRAP	NONE	NONE	5948
21.05.86	CHIPDETECT	INDOFFAULT	CMTNMTSWARF	RECTINSITU	WAJ361	NONE	1676
19.06.86	IGB	FALEARLYFALDCHK	CMTNMTSWARF	MOD+RECOND	WAJ361		0
19.06.86	BEARING		BEARINGFAILED	RPLLAR2	WAJ361	WAD297	1697
31.10.88	IGB	WARNINGLIGHTON	NOFAULTFOUND	NOFAULTFOUND	NONE	NONE	2954
12.03.91	IGB	DISCOLOURED	DISCOLOURED	RECTINSITU	WAY104		3728
20.07.94	IGB	FAILS-EXTINGUISH	FAILS-EXTINGUISH	RPLLAR2	ABRWAX73R1	WAY128	4690
08.03.93	SEALPLAIN (INPUT)	GEARBOXOILLEAK	GEARBOXOILLEAK	RPLLASCRAP	NOTREC	NONE	4398
27.02.97	IGB	WARNINGLIGHTON	CMTNBYDRT/SAND	RECTINSITU	AAL6607		5548
23.06.90	IGB	WARNINGLIGHTON	CMTNMTSWARF	RECTINSITU	WAK370	WARWAU23	2047
13.09.91	IGB	WARNINGLIGHTON	CONTACTDIRTY	RECTINSITU	WARWAU23		2346
27.10.91	IGB	WARNINGLIGHTON	CONTAMINATED	RPLLAR2	WARWAU23	WAJ357	2395
27.10.91	BEARING		BEARINGBROKEN	REPAIRED	WAR-WAU23		0
03.12.91	BEARING x 4	SCORED	SCORED, WORN	RPLLASCRAP	NOTREC	NONE	2444
01.07.93	HOUSINGCENTRE	DISCOLOURED	DISCOLOURED	RECTINSITU	NOTREC		3098
16.09.96	IGB	ROBBED	ROBBED	ROBITEMRPL	WAU8	WAX71	4340
06.08.96	IGB	LIFEEXCOMPONT	LIFEEXCOMPONT	RPLLAR2	WAJ357	WAW8	4330
12.06.96	IGB	HEAVYLANDING	FAILSBITECHECK	RPLLAR2	WAW41	AAX9199	4853
30.09.96	IGB	LIFEEXCOMPONT	LIFEEXCOMPONT	RPLLAR3/4	WAL381	WAY132	5687
28.11.91	SEALPLAIN (INPUT)	SEALINGLEAKING	GEARBOXOILLEAK	RPLLASCRAP	NOTREC	NONE	3357

Appendix D.3 : Records for maintenance for Type A IGB - source EDA

DATE	Defective item	Symptom	Fault	Action	Removed item	Replaced item	A/F hours
28.07.95	SEALPLAIN (INPUT)	HYDOILLEAK	SEALINGLEAKING	RPLLASCRAP	NONE	NONE	5097
11.10.84	IGB	INDOFFAULT	CMTNMTSWARF	RECTINSITU	WAL382	WAL382	198
08.10.86	CHIPDETECTR	WARNINGLIGHTON	INSULATIONBREAK	RPLLASCRAP	NONE	NONE	1175
05.09.90	IGB	CORRODED	CORRODED	RPLLASCRAP	WAL386	WAL388	3008
25.02.93	IGB		ROBBED	ROBITEMRPL	ABRWAW40R1	WAN388	3795
16.09.96	IGB	HUSBANDRY	WORN	RPLLAR2	ABRWAW40R1	NONE	5191
06.07.87	SEALPLAIN (INPUT)	FALTOOPCORR	GEARBOXOILLEAK	RPLLASCRAP	NONE	NONE	1503
23.09.95	SEALPLAIN (INPUT)	GEARBOXOILLEAK	GEARBOXOILLEAK	RPLLASCRAP	NONE	NONE	4778
01.11.96	SEALPLAIN (INPUT)	OTHERLQDLEAK	OTHERLQDLEAK	RPLLASCRAP	NONE	NONE	5287
17.03.98	SEALPLAIN (INPUT)	OTHERLQDLEAK	VIBRATN-HIFREQ	RPLLAR2	NONE	NONE	5947
02.07.86	IGB	CONTAMINATED	WORN	MOD+RECOND	WAL383	WAU17	1077
10.09.88	IGB	SEIZED	SEIZED	RPLLAR2	WAU17	AAR2618	1954
20.09.88	IGB	INDOFFAULT	CMTNMTSWARF	RECTINSITU	AAR2618	AAR2618	1979
02.06.89	IGB	SHOCKLOADED	DAMAGED	RPLLAR2	AAR2618	WARA15705	2374
27.06.90	IGB	CMTNBYWATER	CMTNBYWATER	RECTINSITU	WAR415705		2756
25.07.85	CHIPDETECT	INDOFFAULT	SAFEEQNOTKNOW	RECTINSITU	NONE	NONE	383
09.07.96	IGB	ONINSPECTION	DISTORTED	RPLLAR2	WAL385	WAC269	5131
04.10.93	SEALPLAIN (INPUT)	SEALINGLEAKING	GEARBOXOILLEAK	RPLLASCRAP	NOTREC	NONE	3813
19.06.96	SEALPLAIN (INPUT)	ONINSPECTION	OTHERLQDLEAK	RECTINSITU	NONE	NONE	5131
03.07.85	IGB	WARNINGLIGHTON	SAFEEQNOTKNOW	RECTINSITU	NONE	NONE	321
15.07.89	IGB	FAILSTOOPEN	DIRTY	RECTINSITU	NONE	NONE	2185
17.07.89	IGB	INDICATORPOPPED	SAFEEQNOTKNOW	REPAIRED	WAD297	WAT327	2187
28.07.89	CHIPDETECT	FAILSTORESET	CMTNBYDRT/SAND	RECTINSITU	NONE	NONE	2190
24.08.89	CHIPDETECT	FALTOOPCORR	STI/STUCK	RPLLASCRAP	NONE	NONE	2199
20.09.89	IGB	INDICATORPOPPED	CMTNMTSWARF	RECTINSITU	WAF327		2240
20.09.91	BEARING		BRINELLED	RPLLASCRAP	517	2618	0
07.04.92	SEALPLAIN (INPUT)	OILLEAK	OILLEAK	RPLLASCRAP	WAD305	NOTREC	3110
02.05.86	IGB	VIBRATION	OUTOFALIGNMENT	RPLLAR2	NONE	NONE	632
13.05.86	CHIPDETECTOR	INDOFFAULT	CMTNMTSWARF	RPLLAR2	WAN387	WARWAU7	357
12.09.86	BEARING	INDOFFAULT	CHIPPED	REPAIRED	WAR/WAU/7	ABA6707	569

Appendix D.3 : Records for maintenance for Type A IGB - source EDA

DATE	Defective item	Symptom	Fault	Action	Removed item	Replaced item	A/F hours
06.09.95	SEALPLAIN (INPUT)	GEARBOXOILLEAK	GEARBOXOILLEAK	RPLLAR2	NONE	NONE	4646
19.05.90	IGB	WARNINGLIGHTON	WARNINGLIGHTON	ADJUSTED	NONE	NONE	2521
24.05.90	IGB	WARNINGLIGHTON	SAFEEQNOTKNOW	ADJUSTED	WAN388	NONE	2539
28.09.92	IGB		ROBBED	ROBITEMRPL		WAX66	3434
16.07.93	IGB	DRIVE-DISENGAGED	RODBROKEN	RPLLAR2	WAX66	WAB/T/3	3812
16.03.90	SEALPLAIN (INPUT)	GEARBOXOILLEAK	GEARBOXOILLEAK	RPLLASCRAP	NONE	NONE	2421
31.03.97	SEALPLAIN (INPUT)	OTHERLQDLEAK	OTHERLQDLEAK	RECTINSITU	NONE	NONE	5220
02.10.85	IGB	INDOFFAULT	SAFEEQNOTKNOW	RPLLAR2	WAN389	WABRWAC2	761
16.10.85	CHIPDETECTOR	WARNINGLIGHTON	CMTNMTSWARF	RECTINSITU	NONE	NONE	775
04.02.85	CHIPDETECT	WARNINGLIGHTON	CONTAMINATED	RECTINSITU	NONE	NONE	8
22.05.85	CHIPDETECTOR	INDOFFAULT	SAFEEQNOTKNOW	RECTINSITU	WAN392		220
11.11.94	IGB		CORRODED, WORN	RPLLAR2, RECTINSI	WAN390	AAR2618	3879
22.11.94	IGB	CORRODED	CORRODED	RPLLAR2	WAN390	AAR2618	3879
06.12.94	SEALPLAIN (INPUT)	GEARBOXOILLEAK	GEARBOXOILLEAK	RPLLASCRAP	NONE	NONE	3892
24.10.93	IGB	FAILSTOCANCEL	WARNINGLIGHTON	RECTINSITU	WAW24		3268
12.12.91	SEALPLAIN	GEARBOXOILLEAK	WORN	RPLLASCRAP	WAN395	NONE	2948
23.08.93	IGB	WORN	WORN	RPLLAR3/4	WAN395	WAD287	3414
07.06.92	IGB	ROBBED	ROBBED	ROBITEMRPL	WAD286	WAW395	3072
06.09.90	IGB	WARNINGLIGHTON	WARNINGLIGHTON	RPLLAR3/4	AAG1848	WAX97	2375
06.09.90	JAW,I/P DISCC	WORN	OUTOFLIMITS	RPLLAR2		NONE	0
12.10.90	IGB	TORQLOADGINCOR	TORQLOADGINCOR	RECTINSITU	WAX97		2392
04.09.90	IGB	WARNINGLIGHTON	WARNINGLIGHTON	RECTINSITU	AAG1848		2375
02.03.88	HOUSING	CRACKED	CRACKED	RECONDITIOND	AAG9922	WAH350	1465
23.05.89	CHIPDETECTOR	WARNINGLIGHTON	CMTNMTSWARF	ENTRYDFLOG	WAH350	NONE	2121
24.05.90	BEARING (O/P OUTBI	WARNINGLIGHTON	PITTED	RECONDITIOND	WAH350	WAH351	2634
04.06.90	IGB	WARNINGLIGHTON	FAILURE	RPLLAR2	WAH351	WAU21	2654
14.06.90	IGB	FALEARLYFALDCHK	FALEARLYFALDCHK	RECTINSITU	WAU21		2707
25.06.91	IGB	FLAGFAILTOCLR	CMTNMTSWARF	RPLLAR2	WAU21	WARWAW34	3333
11.08.97	HANPLUG	WORN	HOLED	RPLLASCRAP	NONE	NONE	7174
18.04.91	SEALPLAIN (INPUT)	GEARBOXOILLEAK	LEAKING	RPLLASCRAP	NOTREC	NONE	3191

Appendix D.3 : Records for maintenance for Type A IGB - source EDA

DATE	Defective item	Symptom	Fault	Action	Removed item	Replaced item	A/F hours
08.12.88	SHAFTINPUT	WORN	SPLINEWORN	REPAIRED	AAH6913	WAH355	1866
23.02.91	IGB	FLAGFAILTOCLR	FALEARLYFALDCHK	RPLLAR3/4	WAH355	WAG331	2986
04.12.91	IGB	SMELLOFBURNING	CRACKED	RPLLAR3/4	WAW55	WABRWAC2	3481
09.03.92	IGB	ROBBED	ROBBED	ROBITEMRPL	WAC275	AAG1848	3658
26.04.91	IGB	ROBBED	ROBBED	ROBITEMRPL	WA6331	WAW55	3094
25.06.93	IGB	INDOFFAULT	INDOFFAULT	ENTRYDFLOG	AAG1848		4410
31.10.93	SEALPLAIN (INPUT)	LEAKING	LEAKING	RPLLASCRAP	NOTREC	NONE	4658
19.06.89	IGB	CMTNMTSWARF	CMTNMTSWARF	MOD+RECOND	AAK7958	AAY0841	2289
09.10.90	IGB	VIBRATION	FAILEDTST/CHECK	RPLLAR3/4	HHYD841	WAD304	3059
29.11.90	IGB	ROBBED	ROBBED	ROBITEMRPL	WAD304	WAC275R1	3154
04.12.91	IGB	ROBBED	ROBBED	ROBITEMRPL	WAC-275-R1	WAU13	3693
17.06.94	IGB	WORN	SPLINEWORN	RPLLAR2	WAU13	WAU21	5251
20.07.92	IGB	ROBBED	ROBBED	ROBITEMRPL	APP0239	WAD283	2686
25.10.94	IGB	FLUIDLEVELLOW	GEARFAILED	RPLLAR2	WAD283	ACU4696	3372
10.06.86	IGB	WARNINGLIGHTON	CMTNMTSWARF	RECTINSITU	NONE	NONE	9
02.04.93	IGB	CORRODED	CORRODED	RECTINSITU	WAK366		2545
31.07.93	SEALPLAIN (INPUT)	GEARBOXOILLEAK	SEALINGLEAKING	RPLLASCRAP	NOTREC	NONE	2549
20.09.88	IGB	INDSUSP/INCOR	SAFEEQNOTKNOW	RECTINSITU	AAR2620	NONE	1174
29.05.92	IGB		VIBRATION	RPLLAR2	WAY132	WAW56	2447
14.10.91	IGB		ROBBED	ROBITEMRPL	AAR2620	WAY132	2224
04.06.92	SEALPLAIN (INPUT)	GEARBOXOILLEAK	GEARBOXOILLEAK	RPLLASCRAP	NOTREC	NONE	2456
21.08.88	IGB	INDSUSP/INCOR	CMTNMTSWARF	ADJUSTED	NONE	NONE	1045
27.10.89	IGB	INDICATORSTICK	INDICATORSTICK	RECTINSITU	AAU3701		1661
28.06.95	IGB	CORRODED	CORRODED	RECTINSITU	WAG338		3014
30.03.93	IGB	WORN	SPLINEWORN	RPLHAR2	AAL6607	ACT9736	3142
14.12.88	WAVEGUIDEASY	CCTBRKTRIPPED	CCTBRKTRIPPED	RECTINSITU	AAL7163	NONE	1353
04.05.89	IGB	WORN	SAFEEQNOTKNOW	RPLLAR2	AAL7163	WAH348	1518
17.06.92	IGB	ROBBED	ROBBED	ROBITEMRPL	WAH348	WAX95	2447
16.06.95	SEALPLAIN (INPUT)	GEARBOXOILLEAK	SEALINGLEAKING	RPLLASCRAP	NONE	NONE	3538
21.07.89	WINDOWASSY	DISCOLOURED	DISCOLOURED	RPLLASCRAP	NONE	NONE	1391

Appendix D.3 : Records for maintenance for Type A IGB - source EDA

DATE	Defective item	Symptom	Fault	Action	Removed item	Replaced item	A/F hours
04.08.93	OUTPUTSEAL	GEARBOXOILLEAK	GEARBOXOILLEAK	RPLLASCRAP			2583
26.10.95	IGB	GEARBOXOILLEAK	GEARBOXOILLEAK	RPLLAR3/4	AAX9199	WAX86	3581
06.11.93	SEALPLAIN (INPUT)	GEARBOXOILLEAK	GEARBOXOILLEAK	RPLLASCRAP	NOTREC	NONE	2717
28.02.90	SHAFTINPUT	CORROSIONFRETNG	WORN	REPAIRED	AAP0238	WAR-WAU-7	1493
17.02.91	CHIPDETECTR	FAILSTORESET	INSULSHTCCT	RPLLASCRAP	WAR/WAU/7	NOTREC	1711
03.03.91	IGB	WORN	WARNINGLIGHTON	RPLLAR3/4	WARWAU7	WAD305	1737
03.03.91	BEARING		CMTNMTSWARF	REPAIR+MOD	WAR-WAU7		0
18.11.91	BEARING		BRINELLED	RPLLASCRAP			0
12.02.92	IGB BEARING		BRINELLED	RPLLASCRAP			1828
15.05.92	IGB	FAILSSEQCORR	WORN	RPLLAR2	WAF327	WAD305	1923
22.05.92	IGB	ROBBED	ROBBED	RECTINSITU	WAD305	WAD312	3176
08.06.92	IGB	FAILSSEQCORR	CMTNBYGREASE	RECTINSITU	WAD305		1936
01.04.93	IGB	WORN	WORN	RPLHAR3/4	WAD305	WAF327	2333
16.09.97	IGB	ONINSPECTION	CORRODED	RECTINSITU	WAW63		4089
21.04.98	IGB	OUTOFLIMITS	CORRODED	RPLHAR3/4	WAW63	ACN3376	4298
01.10.90	IGB	CMTNMTSWARF	CMTNMTSWARF	RPLLAR2	AAM4964	WAN63	1628
01.10.90	BEARING		BKN/FRACTURED	RECONDITIOND	AAM4964		0
12.09.91	ARM		SCORED	RPLLASCRAP	WAN2890	AAU0797	0
12.09.91	BEARING		BRINELLED	RPLLASCRAP			0
21.10.92	IGB	FAILSTOLOCKUP	MOVEMENTRESTRTD	RPLLASCRAP	WAW63	NOTREC	2319
16.09.88	BEARING (I/P OUTBD)	WORN	CHIPPED	RPLLAR2	AAY0841	WAH342	803
28.09.88	IGB	INDOFFAULT	INDOFFAULT	RECTINSITU	WAH342		816
27.01.92	BEARING	BRINELLED	BEARINGWORN	RPLLASCRAP	WAD335	NONE	2595
30.06.95	IGB	LIFEEXCOMPONT	LIFEEXCOMPONT	RPLLASCRAP	WAD310	WAH349	4217
30.07.92	SEALPLAIN (INPUT)	GEARBOXOILLEAK	SEALINGLEAKING	RPLLASCRAP	NOTREC	NONE	2800
31.03.87	CHIPDETECT	INDOFFAULT	CONTAMINATED	RECTINSITU	NONE	NONE	10
28.09.90	IGB	CMTNMTSWARF	CMTNMTSWARF	RPLLAR3/4	AAY-0842	WAG-329	1532
15.10.90	IGB	CMTNMTSWARF	NOFAULTFOUND	NOFAULTFOUND	WAG329		1547
04.07.96	SEAL	ONINSPECTION	OTHERLQDLEAK	RPLLASCRAP	NONE	NONE	3900
06.08.96	IGB	ONINSPECTION	CORRODED	RPLLAR3/4		AAR2620	3900

Appendix D.3 : Records for maintenance for Type A IGB - source EDA

DATE	Defective item	Symptom	Fault	Action	Removed item	Replaced item	A/F hours
19.10.89	IGB	READING/SINCOR	SAFEEQNOTKNOW	RECTINSITU	ABA6708		647
13.03.95	IGB	FAILS-EXTINGUISH	FAILS-EXTINGUISH	ADJUSTED			2805
16.06.88	IGB	OUTOFLIMITS	OUTOFALIGNMENT	ADJUSTED	ABE4732	NONE	111
05.09.90	WINDOWASSY	DISCOLOURED	DISCOLOURED	RPLLASCRAP	ABE4732	NOTREC	1105
13.03.96	IGB	OUTOFADJ	OUTOFADJ	RECTINSITU	ABE4732		3191
13.06.88	PLUG	FAILSTOILLUMTE	CIRCUIT-SHORT	RECTINSITU	ABE5201	NONE	113
09.01.95	IGB		VIBRATN-HIFREQ	RPLLAR2	ABX0865	WAY108	0
04.03.92	IGB		ROBBED	ROBITEMRPL	ABG0542	ABX0865	0
17.11.95	SEALPLAIN (INPUT)	GEARBOXOILLEAK	GEARBOXOILLEAK	RPLLASCRAP	NONE	NONE	2925
26.06.96	SEALPLAIN (INPUT)	GEARBOXOILLEAK	GEARBOXOILLEAK	RPLLASCRAP	NONE	NONE	3133
03.01.98	SEALPLAIN (INPUT)	OTHERLQDLEAK	OTHERLQDLEAK	RPLLASCRAP	NONE	NONE	3925
23.05.94	IGB	CRACKED	CRACKED	RPLLAR2	ABD5375	ABD5375	2302
31.03.95	IGB	DISCOLOURED	DISCOLOURED	RECTINSITU	ABD5375		2302
16.05.95	JAW,I/P DISCC	WORN	WORN	RPLLAR2	ABD5375	WAH352	2302
24.06.92	IGB	SPLINEWORN	SPLINEWORN	RPLLAR3/4	ABX0855	WAW45	1002
22.11.90	IGB	WORN	WORN	RPLLAR2	ABX0865	WAW24	348
22.11.93	IGB		CORRODED	RPLLAR2	ABX0869	AAU3701	1561
01.09.94	IGB		CORRODED	R3/4(R/D)		NONE	0
02.03.92	BEARING	BRINELLED	BRINELLED	RPLLASCRAP	NOTREC	NOTREC	882
01.11.93	FITTSUPPORT	LIFEEXCOMPONT	LIFEEXCOMPONT	RPLLAR2	WAB75R2	WAA221	1823
26.04.94	SEALPLAIN (INPUT)	GEARBOXOILLEAK	GEARBOXOILLEAK	RPLLASCRAP	NOTREC	NOTREC	1926
20.10.96	SEALPLAIN (INPUT)	OTHERLQDLEAK	OTHERLQDLEAK	RPLLASCRAP	NONE	NONE	3147
03.12.91	IGB, BEARING x 2		WORN	MITEMSRPLREP			0
25.11.93	FLANGEOPUT	CORRODEDSURFACE	CORRODEDSURFACE	RPLLASCRAP	ABX0880	NONE	1644
25.11.93	FLANGE		CORRODEDSURFACE	RECTINSITU	NONE	NONE	0
25.07.94	SEALPLAIN (INPUT)	GEARBOXOILLEAK	GEARBOXOILLEAK	RECTINSITU	NONE	NONE	1787
06.06.91	IGB	CMTNMTSWARF	CMTNMTSWARF	RPLLAR2	ACT9736	ABRWAW40	341
12.06.91	IGB	CMTNMTSWARF	CMTNMTSWARF	RECTINSITU	-R-WAW40R1		347
21.10.92	IGB	FAILSTOLOCK	FAILSTOLOCK	RPLLASCRAP	R-WAW-40R1	NOTREC	806
22.04.97	IGB	ONINSPECTION	SURVEYOPS-PREPS	MITEMSRPLREP	WAN38C		2612

Appendix D.3 : Records for maintenance for Type A IGB - source EDA

DATE	Defective item	Symptom	Fault	Action	Removed item	Replaced item	A/F hours
29.08.90	IGB	GEARBOXOILLEAK	GEARBOXOILLEAK	RPLLAR2	ABX0884	ACT9736	11
19.04.93	IGB		ROBBED	ROBITEMRPL	WABRWAW40	WAN386	892
14.11.91	BEARING	BEARINGCORRODED	BEARINGCORRODED	RPLLASCRAP	NOTREC	NONE	512
14.11.91	BEARING		BRINELLED	RPLLASCRAP	1560	2629	0
27.02.92	OILOX27	DET/PERISHED	DET/PERISHED	RPLLAR2	ABX0846	WAY124	633
19.05.92	IGB		HEAVYLANDING	RPLLAR3/4	WAY124	WAK370	0
10.10.96	IGB	SURVEYOPS-PREPS	CHAFED/CHAFING	RPLLAR3/4		AJX0865	2338
10.10.91	IGB	CRACKED	CRACKED	RPLLAR2	ACN3376	ABRWABU5I	628
24.04.92	SUPPORT	CORRODED	CORRODED	RPLLASCRAP	ABX0874	NOTREC	827
04.10.93	IGB	CORRODED	CORRODED	RECTINSITU	ABX0874		1466
18.10.93	JAW	OUTOFLIMITS	OUTOFLIMITS	RPLLASCRAP	WY75214	WA873	1466
06.12.93	INTAKE	CORROSIONPITING	CORRODED	RPLLASCRAP	ABX0874	NONE	1466
07.03.94	IGB	WARNINGLIGHTON	CMTNMTSWARF	RPLLAR3/4	ARX0874	WAD314	1514
22.04.97	IGB	OTHERLQDLEAK	NOFAULTFOUND	NOFAULTFOUND	WAD314		3114

Appendix D.3 : Records for maintenance for Type A IGB - source EDA

E Numerical Data and Analysis

E.1 Geometrical Data

E.1.1 Geometrical Gear Data

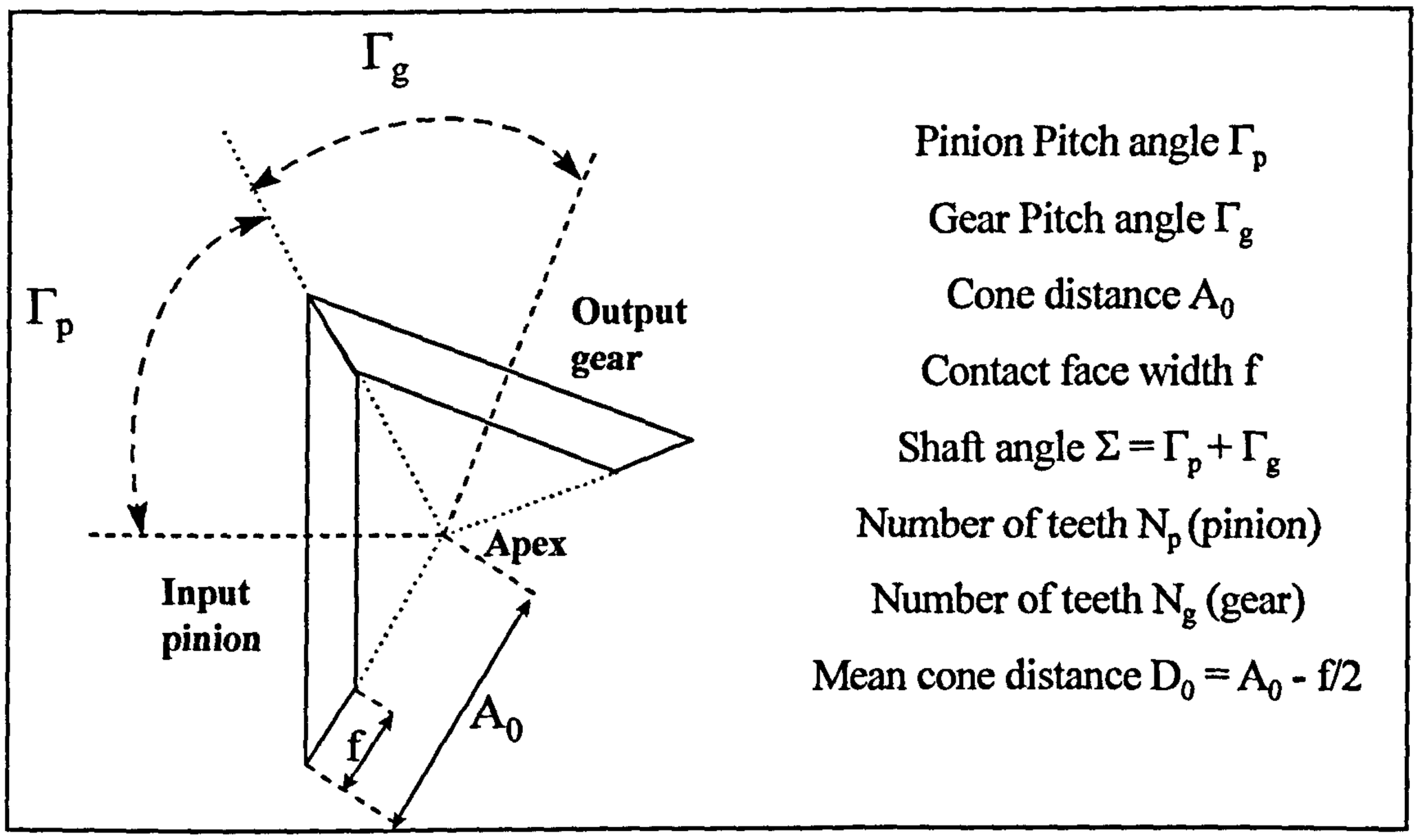

Figure E.1 : Geometry of the IGB Gear-set

Parameter	Units	Type A	Type B
Cone distance	mm	86.3	131.9
Contact face width	mm	25.4	37
CP (Elastic coefficient)	$MPa^{0.5}$	232	232
Normal pressure angle	degrees	20	22.5
Spiral angle	degrees	35	35
Pinion pitch angle	degrees	73.1	47.5
Gear pitch angle	degrees	73.1	82.15
Input rpm	rpm	3121	3312
Output rpm	rpm	3121	2465
I_factor Geometry factor (for Hertzian contact stress)	-	0.106	0.128

Table E.1 : Data for geometrical parameters of gears

E.1.2 Geometrical Shaft Data

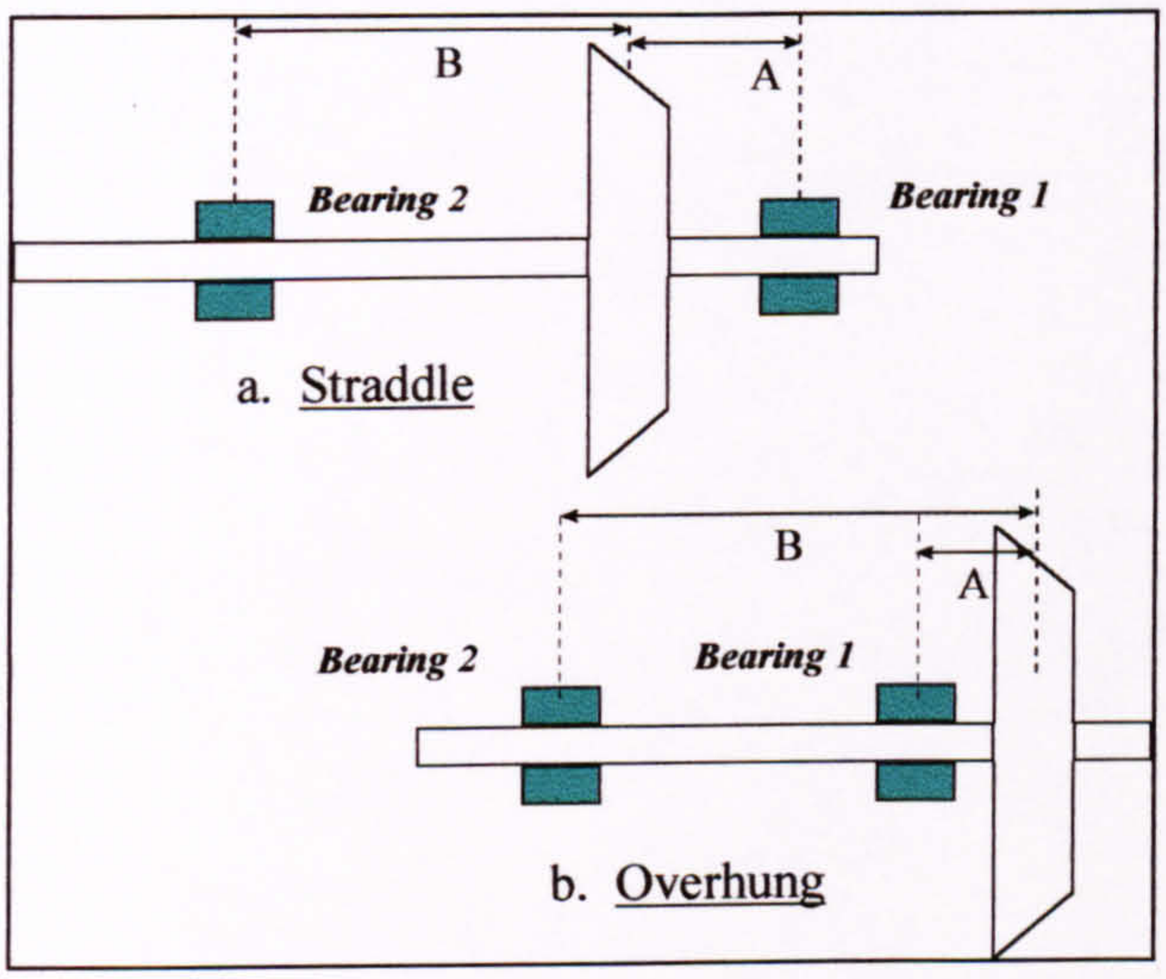

Figure E.2 : Two configurations of bearing and shaft assembly [Savage and Brikmanis, 1986]

Parameter	Units	Type A	Type B
I/P shaft distance A	mm	-28.5 *	17.63
O/P shaft distance A	mm	-28.5 *	-9.34 *
I/P shaft distance B	mm	146.3	73.32
O/P shaft distance B	mm	146.3	86.15
I/P shaft external diameter	mm	43	43
O/P shaft external diameter	mm	32	32
I/P shaft internal diameter	mm	33.8	33.8
O/P shaft internal diameter	mm	23.9	23.9
Dynamic rating (C1) Bearing 1	kN	91.6	108
Dynamic rating (C1) Bearing 2	kN	34.6	101.4
Dynamic rating (C1) Bearing 3	kN	84.2	108
Dynamic rating (C1) Bearing 4	kN	24.1	114.2
Y axial load factor (Bearing 1)	-	1.49	0
Y axial load factor (Bearing 2)	-	1.78	1.41
Y axial load factor (Bearing 3)	-	1.69	0
Y axial load factor (Bearing 4)	-	1.73	1.41
X radial load factor (Bearing 1)	-	0.4	1
X radial load factor (Bearing 2)	-	1	0.67
X radial load factor (Bearing 3)	-	1	1
X radial load factor (Bearing 4)	-	0.4	0.67

Table E.2 : Data for shaft and bearing geometrical parameters[1]

[1] Negative values * refer to position relative to pinion/gear

E.2 Material Baseline Data

Gear tooth root bending fatigue	Type A	Type B	Units
P1	1226	2256	Nm
P2	52385	96344	Nm
Gamma	-0.367	-0.367	
COV	0.06	0.06	
Gear tooth rolling contact fatigue	**Type A**	**Type B**	
P1	4860	4860	MPa
P2	0	0	
Gamma	-0.055	-0.055	
COV	0.15	0.15	
Bearing contact fatigue	**Type A**	**Type B**	
Bearing 1 Dynamic rating C_1	91.6	108	kN
Bearing 2 Dynamic rating C_1	34.6	101.4	kN
Bearing 3 Dynamic rating C_1	84.2	108	kN
Bearing 4 Dynamic rating C_1	24.1	114.2	kN
Slope	1.5	1.5	
Wear (spline)	**Type A I/P**	**Type A O/P**	**Type B I/P, O/P**
Wear coefficient, K	1.00E-06	1.00E-06	1.00E-06
Indentation hardness, H (HV)	650	650	650
Transmitted torque, T (Nm)	Spectrum	Spectrum	Spectrum
Number of splines, n	36	22	35
Involute pressure angle of splines, a (degrees)	30	30	30
Pitch diameter of the splines (mm)	45.72	34.9	74.08
Mean slip amplitude, x (mm)	0.05	0.05	0.05
Slip amplitude COV	0.3	0.3	0.3
Usage rate (operating hours/year)	500		500

Casing Corrosion	AZ91C	WE43	A357
Plain marine corrosion rate – mean (mm/year)	6	0.76	0.125
Plain land corrosion rate – mean (mm/year)	2	0.2	0.05
Plain dry corrosion rate – mean (mm/year)	0	0	0
Plain marine corrosion rate - COV	0.05	0.05	0.1
Plain land corrosion rate - COV	0.05	0.05	0.1
Plain dry corrosion rate - COV	0	0	0
Galvanic marine corrosion rate – mean (mm/year)	76	76	0.25
Galvanic land corrosion rate – mean (mm/year)	5	5	0.1
Galvanic dry corrosion rate – mean (mm/year)	0	0	0
Galvanic marine - COV	0.1	0.1	0.1
Galvanic land - COV	0.1	0.1	0.1
Galvanic dry - COV	0	0	0
Proportion time in marine environment (%)	80	80	80
Proportion time in land environment (%)	10	10	10
Proportion time in dry environment (%)	10	10	10
Plain corrosion limit mean (mm)	5	5	5
Plain corrosion limit COV	0.05	0.05	0.2
Galvanic corrosion limit mean (mm)	5	5	5
Galvanic fail COV	0.05	0.05	0.2
Plain corrosion MTTI (months)	24	24	12
Galvanic corrosion MTTI (months)	36	36	18

Table E.3 : Data for material and corrosion model parameters

E.3 Torque Baseline Data

The load data input for this work is in a standard format of Table E.4, with data of input torque, corresponding with the time at each load state. Load state is defined as a period of time during which the applied torque and load remain constant.

Load state	Time elapsed	Cumulative time	Cycles	Cum cycles	Torque (Nm)
1	T_1	T_1	N_1	N_1	T_1
2	T_2	ΣT_i	N_2	ΣN_i	T_2
3	T_3	ΣT_i	N_3	ΣN_i	T_3
n	T_n	ΣT_i	N_n	ΣN_i	T_n

Table E.4 : Example format of Torque Input Data

Note that manoeuvres may contain different levels of torque/stress and therefore consist of more than one load state.

E.3.1 Torque Loading Data – ASW loading

Data for ASW history was drawn from two sources. Information of the manoeuvres and their percentage occurrence was taken from the HELIX design data **[Edwards and Darts 1984]**. The input torque values for each manoeuvre were themselves estimated from manufacturer's data (Table E.5). The torque data is conservative since it assumes that torque remains constant throughout each manoeuvre.

No	Manoeuvre description	Input torque (Nm)	Percentage for sortie
1	Take off	1108.6	0.12
2	Forward flight 20kt	429.9	2.79
3	Forward flight 30kt	362.0	2.79
4	Forward flight 40kt	316.7	2.79
5	Forward flight 60kt	271.5	5.99
6	Forward flight V_{NO} 103kt	248.9	35.9
7	Maximum power climb 70 kt	972.9	1.2
8	Shallow approach to hover	N/A	-
9	Normal approach to hover	1074.7	1.4
10	Hover	746.6	33.01
11	Bank turn port 30 deg V_{NO}	350.7	5.51
12	Bank turn starboard 30 deg V_{NO}	395.9	5.51
13	Sideways flight to port 30 kt	905.0	0.2
14	Recovery from Manoeuvre 13	837.1	0.08
15	Sideways flight to starboard 30 kt	1730.8	0.2
16	Recovery from Manoeuvre 15	1221.7	0.08
17	Rearwards flight 20 kt	1131.2	0.2
18	Recovery from Manoeuvre 17	1029.4	0.08
19	Spot turn port	1425.4	0.2
20	Spot turn starboard	916.3	0.2
21	Auto-rotation	475.1	0.4
22	Recovery from Manoeuvre 21	610.9	0.03
23	Descent	497.7	1.2
24	Landing	757.9	0.12
	TOTAL		**100**

Table E.5 : Mix of Manoeuvres in Type A ASW Sortie[2] [Edwards and Darts 1984]

[2] Type A torque data supplied by Agusta Westland

E.3.2 Torque Loading Data – Type A Flight 110

Data is presented for shaft speed of 3121 rpm (1 revolution = 1 cycle)

Cycles	Torque (Nm)	Cycles	Torque (Nm)	Cycles	Torque (Nm)	Cycles	Torque (Nm)	Cycles	Torque (Nm)
0	0	455	87.8	4369	150.75	2172	213.7	1860	276.65
416	0	533	89.46	3420	152.41	2081	215.36	1626	278.31
312	1.66	1040	91.11	3628	154.06	3342	217.01	1743	279.97
546	4.97	1847	92.77	3004	155.72	2237	218.67	1639	281.62
8128	6.63	3901	94.43	3823	157.38	2770	220.33	1730	283.28
390	8.28	4877	96.08	2302	159.03	2614	221.98	1300	284.93
26	14.91	4799	97.74	2692	160.69	3511	223.64	1508	286.59
13	16.57	2380	99.4	1691	162.35	2575	225.3	1443	288.25
13	21.54	2029	101.05	2666	164	3394	226.95	1756	289.9
52	23.19	1144	102.71	1756	165.66	3056	228.61	1235	291.56
39	24.85	2159	104.37	1912	167.32	3940	230.27	1417	293.22
26	26.51	1274	106.02	1665	168.97	3667	231.92	1235	294.87
26	29.82	2068	107.68	2042	170.63	3459	233.58	1456	296.53
13	31.48	2159	109.34	1665	172.29	3082	235.24	1066	298.19
39	33.13	2380	110.99	1613	173.94	4213	236.89	1157	299.84
26	41.41	2237	112.65	1443	175.6	3563	238.55	1170	301.5
13	43.07	2484	114.31	1964	177.26	3680	240.21	1561	303.16
26	49.7	2484	115.96	1300	178.91	3108	241.86	1105	304.81
13	51.35	3667	117.62	1482	180.57	3433	243.52	1157	306.47
13	54.67	2991	119.28	1092	182.23	2744	245.18	1248	308.13
13	57.98	4330	120.93	1704	183.88	3485	246.83	1391	309.78
13	59.64	3433	122.59	1352	185.54	2692	248.49	1092	311.44
13	61.29	5085	124.24	1209	187.2	3121	250.15	1235	313.1
13	62.95	4369	125.9	1157	188.85	2510	251.8	1118	314.75
13	64.61	4655	127.56	1639	190.51	2809	253.46	1626	316.41
13	67.92	5605	129.21	1105	192.17	2809	255.12	988	318.07
13	69.58	7217	130.87	1495	193.82	3550	256.77	1092	319.72
78	71.23	5826	132.53	1144	195.48	4031	258.43	1131	321.38
26	72.89	6203	134.18	1613	197.14	6333	260.09	1248	323.04
78	74.55	5696	135.84	1430	198.79	3524	261.74	975	324.69
78	76.2	7113	137.5	1782	200.45	3615	263.4	1300	326.35
130	77.86	5098	139.15	1443	202.11	2120	265.06	845	328.01
117	79.52	5293	140.81	1899	203.76	1899	266.71	1326	329.66
156	81.17	4760	142.47	1508	205.42	1795	268.37	1001	331.32
195	82.83	5852	144.12	1678	207.07	2094	270.03	975	332.98
325	84.49	4825	145.78	1938	208.73	1639	271.68	884	334.63
273	86.14	4473	147.44	3251	210.39	1639	273.34	1053	336.29
455	87.8	4148	149.09	1521	212.04	1717	275	910	337.95

Cycles	Torque (Nm)	Cycles	Torque (Nm)	Cycles	Torque (Nm)	Cycles	Torque (Nm)	Cycles	Torque (Nm)
897	339.6	468	379.36	169	419.12	39	443.97	13	505.26
702	341.26	624	381.02	221	420.78	91	445.62	13	508.58
1300	342.92	676	382.67	208	422.43	39	447.28	26	510.23
1079	344.57	377	384.33	130	424.09	91	448.94	13	511.89
949	346.23	533	385.99	234	425.75	26	450.59	13	513.55
728	347.89	403	387.64	91	427.4	52	452.25	13	515.2
871	349.54	598	389.3	104	429.06	65	453.91	13	516.86
715	351.2	494	390.96	104	430.72	39	455.56	26	518.52
390	352.86	494	392.61	143	432.37	78	457.22	26	520.17
741	354.51	377	394.27	39	468.82	26	458.88	26	521.83
793	356.17	533	395.93	52	470.47	13	460.53	13	523.49
845	357.83	364	397.58	78	472.13	26	462.19	13	526.8
819	359.48	481	399.24	65	475.44	26	467.16	13	528.45
520	361.14	377	400.9	26	478.76	26	487.04	13	535.08
858	362.8	403	402.55	13	480.41	39	488.7	13	538.39
559	364.45	260	404.21	39	482.07	26	490.35	312	0
754	366.11	442	405.87	52	483.73	39	492.01		
598	367.76	351	407.52	39	485.38	52	493.67		
637	369.42	182	409.18	104	434.03	52	495.32		
650	371.08	273	410.84	91	435.69	65	496.98		
650	372.73	260	412.49	91	437.34	52	498.64		
624	374.39	234	414.15	143	439	52	500.29		
741	376.05	156	415.81	39	440.66	13	501.95		
689	377.7	169	417.46	39	442.31	39	503.61		

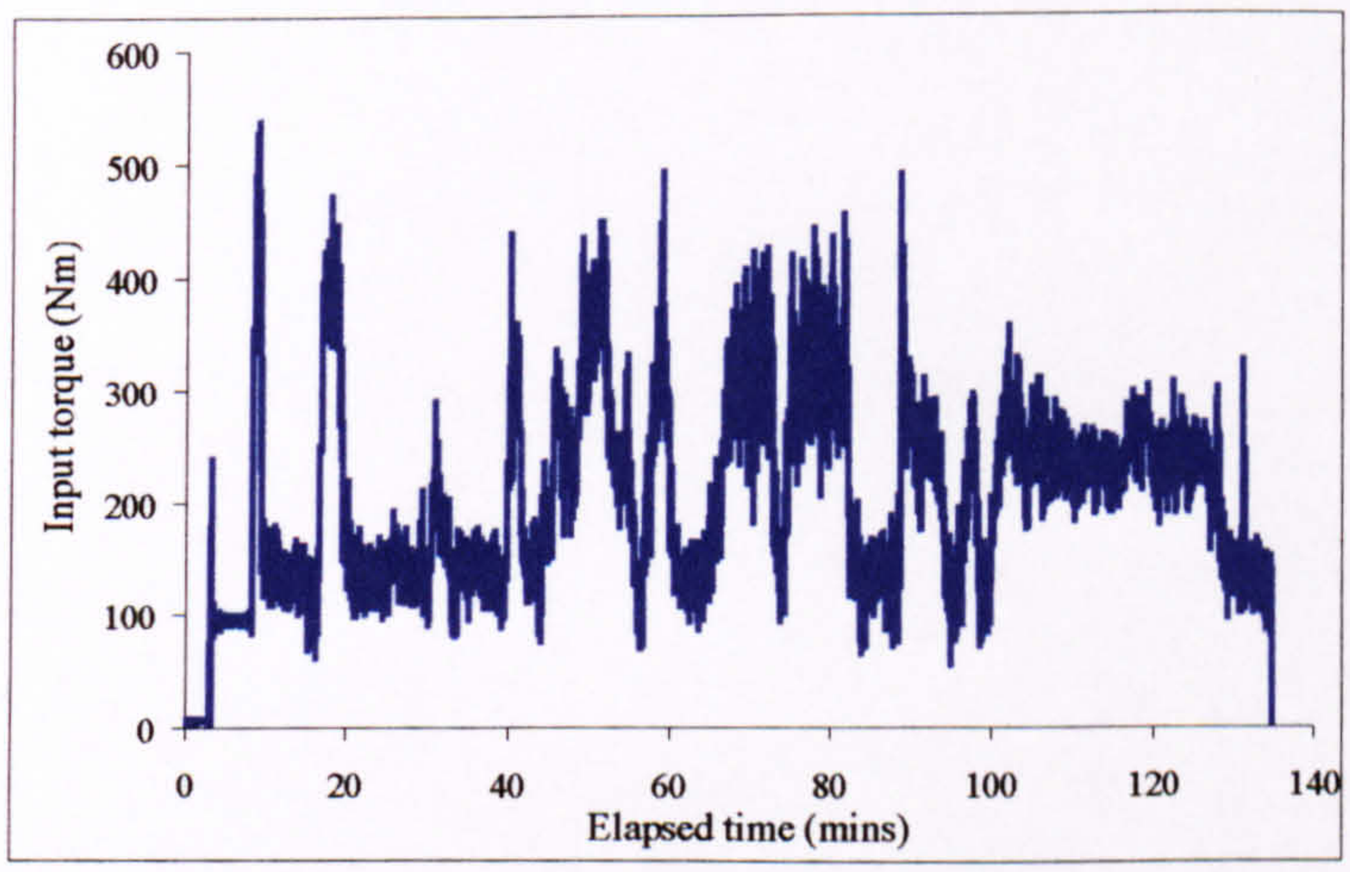

Figure E.3 : Torque Loading Data – Type A Flight 110[3]

[3] Type A torque data supplied by QinetiQ

E.3.3 Torque Loading Data – Type B Prototype Spectrum

Input torque (N m)	% of spectrum	Time (min) in 100 hours
2873	0.0003	0.018
2817	0.0001	0.006
2760	0.0004	0.024
2704	0.001	0.06
2648	0.0019	0.114
2591	0.0036	0.216
2535	0.0074	0.444
2479	0.0157	0.942
2422	0.0394	2.364
2366	0.0629	3.774
2310	0.0921	5.526
2253	0.0986	5.916
2197	0.0918	5.508
2141	0.087	5.22
2084	0.0889	5.334
2028	0.0952	5.712
1972	0.1062	6.372
1915	0.1036	6.216
1859	0.0979	5.874
1803	0.0859	5.154
1746	0.089	5.34
1690	98.83	5929.8
TOTAL	**100**	**6000**

Table E.6 : Type B Prototype Spectrum[4]

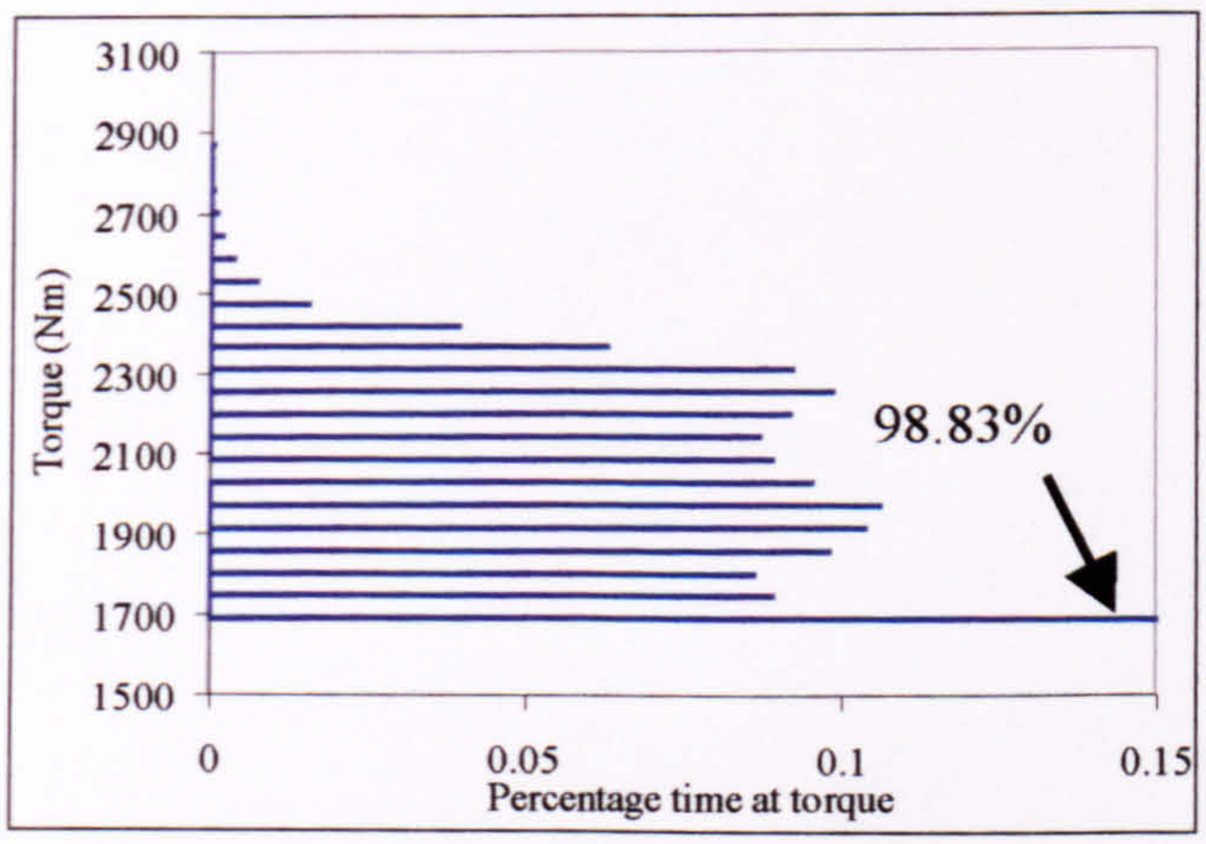

Figure E.4 : Type B gearbox prototype torque spectrum[4]

[4] Type B torque data supplied by Agusta Westland

E.3.4 Torque Loading Data – Type B Civil Spectrum

The data used for the Type B Civil Spectrum is presented in Table E.7 and Table E.8. These give the percentage occurrence of each manoeuvre in the spectrum, and the torque values used, respectively.

No	Manoeuvre description	%	No	Manoeuvre description	%
1	Ground operations	6.05	19	Level Flight 0.4 to 0.6 V_{NE}	2
2	Take Off	0.43	20	Level Flight 0.6 to 0.8 V_{NE}	6
3	Hover in ground effect (IGE)	1.5	21	Level Flight 0.9 V_{NE}	15.2
4	Hover outside ground effect (OGE)	0.5	22	Level Flight 1.0 V_{NE}	37.8
5	Spot turn port (Hover OGE)	0.25	23	Level Flight 1.1 V_{NE}	2
6	Spot turn starboard (Hover OGE)	0.25	24	40 KCAS 30° Bank Turn	0.2
7	Control Reversal (Hover OGE)	0.5	25	0.6 V_{NE} 30° Bank Turn	0.4
8	Transition V_Y to Hover OGE	0.12	26	V_{NE} - 50 kts 45° Bank Turn	0.38
9	Normal Approach to Hover IGE	0.3	27	1.0 V_{NE} 30° Bank Turn	2.06
10	Steep Approach to Hover IGE	0.13	28	1.0 V_{NE} Cyclic and Collective Pull up 1.3G	0.72
11	Transition Hover IGE to V_Y	0.46	29	1.0 V_{NE} Cyclic and Collective Pull up 1.7G	0.01
12	Sideways flight 60°	0.37	30	Control Reversal (Forward Flight)	1.5
13	Sideways flight 90°	0.37	31	Acceleration V_Y to 1.0 V_{NE} level flight	1.5
14	Rearwards flight 180°	0.37	32	Deceleration 1.0 V_{NE} to V_Y level flight	2
15	Sideways flight 270°	0.37	33	Autorotation	1.5
16	Forwards flight 00°	1	34	Descent	6.5
17	Climb	5.5	35	Landing	0.52
18	Level Flight up to 0.4 V_{NE}	1.23		**TOTAL**	**100**

Table E.7 : Summary of 35 different manoeuvres in Civil spectrum

The data for Civil spectrum is given in the form of the percentage of flight spent at a certain torque range, see Table E.8. These ranges have been selected based upon the usage monitoring 'bands' applied in the Type B gearbox. At the highest torque levels, the bands are narrow, but at low levels, where manoeuvres are largely non-damaging (for tooth root bending fatigue) the bands are broad.

Torque range (Nm)		Percentage occurrence
From	To	
2092	2053	0.006
2053	2013	0
2013	1974	0.002
1974	1934	0.064
1934	1896	0.003
1896	1858	0
1858	1820	0.002
1820	1782	0.002
1782	1744	0.013
1744	1705	0.007
1705	1667	0.043
1667	1628	0.056
1628	1590	0.032
1590	1550	0.044
1550	1241	0.939
1241	930	3.171
930	620	2.530
620	310	8.202
<310		84.884
TOTAL		**100**

Table E.8 : Summary of torque data in Civil spectrum, based upon Usage Monitoring bands[4]

E.3.5 Civil Spectrum - Analysis of Damaging Manoeuvres

The following table gives data for the calculation of the tooth root bending fatigue life for damaging manoeuvres at $p^* 10^{-6}$ for Type B gearbox (Civil spectrum).

Percentage of torque	**Cycles**	**Nm**	**Cycles to failure at torque**	**1 / N_f**			
%	**N in 100 hr**	**IP TQ**	**N_f $p^* = 10^{-6}$**	**α**	**Damage in 100 hr**		**Manoeuvre**
0.00068	135	2080	1.540E+06	6.495E-07	8.777E-05		90° AZ. OGE 20 Kts Recovery
0.00501	996	2057	1.810E+06	5.524E-07	5.499E-04		60° AZ. OGE 20 Kts Entry
0.00187	372	1986	3.299E+06	3.031E-07	1.126E-04		90° AZ. OGE 20 Kts Entry
0.00557	1107	1972	3.787E+06	2.641E-07	2.923E-04		60° AZ. OGE 20 Kts Entry
0.05842	11609	1963	4.139E+06	2.416E-07	2.805E-03		Spot Turn Hover OGE 30°/Sec Left
0.00187	372	1910	7.499E+06	1.333E-07	4.955E-05		90° AZ. OGE 20 Kts Entry
0.00068	135	1900	8.638E+06	1.158E-07	1.564E-05		90° AZ. OGE 20 Kts Recovery
0.00203	403	1848	1.912E+07	5.230E-08	2.110E-05		60° AZ. OGE 20 Kts Recovery
0.00024	48	1842	2.140E+07	4.674E-08	2.229E-06		Spot Turn Hover Oge 30°/Sec Left
0.00183	364	1800	5.364E+07	1.864E-08	6.780E-06		60° AZ. OGE 20 Kts Recovery
0.00183	364	1776	1.125E+08	8.889E-09	3.233E-06		60° AZ. OGE 20 Kts Recovery
0.00019	38	1762	1.853E+08	5.397E-09	2.038E-07		Spot Turn Hover Oge 30°/Sec Left
0.00187	372	1762	1.853E+08	5.397E-09	2.006E-06		90° AZ. OGE 20 Kts Entry
0.00203	403	1762	1.892E+08	5.285E-09	2.132E-06		60° AZ. OGE 20 Kts Recovery
0.00734	1459	1744	4.466E+08	2.239E-09	3.266E-06		60° AZ. OGE 20 Kts Recovery
0.00451	896	1713	7.476E+09	1.338E-10	1.199E-07		90° AZ. OGE 20 Kts Entry
0.00010	20	1713	7.719E+09	1.296E-10	2.575E-09		90° AZ. OGE 20 Kts Entry
0.00208	413	1706	3.728E+10	2.683E-11	1.109E-08		Transition Vy To Hover OGE (Normal)
			Damage per 100 hrs		**3.954E-03**		
			Life in hours =		**25292**		**$p^* = 10^{-6}$**

	Damage in 100 hr		$n_i \cdot \alpha_i$		
	Manoeuvre 13		8.777E-05		90° sideways flight OGE 20 Kts
			1.126E-04		
			4.955E-05		
			1.564E-05		
			2.006E-06		
			1.199E-07		
			2.575E-09		
	Damage per 100 hrs		**2.677E-04**	6.77	**percent of total damage**
	Manoeuvre 12		5.499E-04		60° sideways flight OGE 20 Kts
			2.923E-04		
			2.110E-05		
			6.780E-06		
			3.233E-06		
			2.132E-06		
			3.266E-06		
	Damage per 100 hrs		**8.787E-04**	22.22	**percent of total damage**
	Manoeuvre 5		2.805E-03		Spot Turn Hover OGE 30°/Sec Left
			2.229E-06		
			2.038E-07		
	Damage per 100 hrs		**2.807E-03**	71.00	**percent of total damage**
COV 6%	**$p^* = 10^{-6}$**			**100.00**	